UNIVERSITY OF Southampton

Faculty of Engineering and the Environment

Bioengineering Sciences Research Group

A Biomechanical Approach to Improved Fracture Risk Assessment with a Focus on Reference Point Microindentation

Thomas Jenkins

Thesis for the degree of Doctor of Philosophy

January 2015

Supervisory Team: Prof. Philipp J. Thurner and Dr Nicholas C. Harvey

UNIVERSITY OF SOUTHAMPTON

ABSTRACT

FACULTY OF ENGINEERING AND THE ENVIRONMENT

Bioengineering Sciences

Thesis for the degree of Doctor of Philosophy

A BIOMECHANICAL APPROACH TO IMPROVED FRACTURE RISK ASSESSMENT WITH A FOCUS ON REFERENCE POINT MICROINDENTATION

By Thomas Jenkins

Osteoporosis is a bone disease with two primary definitions: 1) the World Health Organisation definition of low Bone Mineral Density (BMD) and 2) the National Institutes of Health definition of increased bone fragility and fracture risk. Though BMD, alongside clinical factors, is the current gold standard for diagnosing osteoporosis, these measures are risk factors that only define a small proportion of individuals who fracture. Changes in the biomechanical properties of the bone may relate to fracture risk and bone disease and, if they can be clinically assessed, could be useful in supplementing existing techniques to improve future diagnosis and treatment. This thesis addresses whether there are biomechanical changes in osteoporotic as well as osteoarthritic bone and whether these can be measured through Reference Point Microindentation (RPI). RPI has previously been applied in vivo with no reported complications and the hypothesis that a higher indentation depth of a needle-like test probe implies increased fracture risk.

Despite emerging implementation of RPI, there is limited research to advise on optimal testing with this technique. Therefore, recommendations are provided to minimise testing variation by studying the variability associated with RPI testing parameters in vitro. Primarily, a best practice would be to: keep maximum load, sample preparation and mode-of-use consistent, fix the device in its stand, remove soft tissue and machine the bone, ensure sufficient cortical thickness and make multiple repeat measurements.

These recommendations then guided the main, clinically focussed, study of this thesis. RPI was applied to femoral neck samples extracted from fractured and osteoarthritic patients, finding the surface measured indentation depth to be increased relative to cadaveric control samples. Furthermore, the measured indentation property had minimal correlation with current existing techniques, supplementing BMD and clinical factors to improve discrimination of fractured from control tissue.

Complementary fracture toughness testing allowed for improved understanding of bone disease and interpretation of the RPI results. This study demonstrated that fracture toughness properties of the inferomedial femoral neck seem largely unaffected by osteoporosis or osteoarthritis. Furthermore, correlation between RPI and fracture properties was minimal, implying that the technique was assessing other properties to discriminate the osteoporotic and osteoarthritic from control bone. Indent imaging, through micro-computed tomography and serial sectioning techniques, confirmed this to be the case with RPI being a multifactorial measure comprised of structural as well as fracture mechanics and elastoplastic properties.

Altogether, this thesis provides insight into the effects of both osteoporosis and osteoarthritis on the biomechanical properties of the femoral neck and presents how these could potential be clinically assessed through RPI, supplementing existing techniques to improve fracture risk assessment.

Table of Contents

List of Tables

List of Figures

Academic Thesis: Declaration of Authorship

I, Thomas Jenkins, declare that this thesis and the work presented in it are my own and has been generated by me as the result of my own original research.

A Biomechanical Approach to Improved Fracture Risk Assessment with a Focus on Reference Point Microindentation

I confirm that:

1. This work was done wholly or mainly while in candidature for a research degree at this University;
2. Where any part of this thesis has previously been submitted for a degree or any other qualification at this University or any other institution, this has been clearly stated;
3. Where I have consulted the published work of others, this is always clearly attributed;
4. Where I have quoted from the work of others, the source is always given. With the exception of such quotations, this thesis is entirely my own work;
5. I have acknowledged all main sources of help;
6. Where the thesis is based on work done by myself jointly with others, I have made clear exactly what was done by others and what I have contributed myself;
7. Either none of this work has been published before submission, or parts of this work have been published as:

   T. Jenkins, L. V. Coutts, D.G. Dunlop, R.O.C. Oreffo, C. Cooper, N.C. Harvey, P.J. Thurner and the OStEO group (N.K. Arden, J.M. Latham, P. Taylor, M. Baxter, N. Moss, C. Ball, K. Chan), *Variability in Reference Point Microindentation and Recommendations for Testing Cortical Bone: Maximum Load, Sample Orientation, Mode of Use, Sample Preparation and Measurement Spacing*, Journal of the Mechanical Behaviour of Biomedical Materials (2015), doi:10.1016/j.jmbbm.2014.09.030

Signed: ……

Date: ……

Acknowledgments

This thesis, to use a slightly forced analogy, has been a marathon. Even in the beginning the difficulties emerged and the expectation of the distance left to cover was daunting. Then the steady plod towards the very distant finish line commenced. Pride at the distance overcome and the overall enjoyment of the challenge helped to spur me on but the final stretch is really where fatigue has started to take its toll. Now in particular the support has been what has kept me going (not to mention the view of the finish).

Where to start? It has to be with my supervisors. Thank you so much to Prof. Philipp Thurner and Dr Nicholas Harvey, who, together with Mr Douglas Dunlop, Prof. Richard Oreffo and Prof. Cyrus Cooper, proposed such an interesting research topic. The clinical nature of the project drove me to apply but, at the same time it is what I found terrifying. I have to thank my supervisors again for their invaluable help in designing the clinical study and going through the nightmarish process of ethical approval with me. Furthermore, there are those that helped to keep the clinical study running (more or less) smoothly. I particularly want to acknowledge Carole Ball, Dr Louise Coutts and Dr Nicole Moss for helping to recruit patients as well as Kitty Chan and individuals at the Bone and Joint Group (particularly May De Andres, Eloise Cook and Tsiloon Li) for collecting samples.

When it comes to the testing, I am very grateful to Philipp for proposing ideas whilst accepting my own. A supervisor moving to Austria sounds disastrous on paper but he has continued to support me throughout. I would like to thank Dr Orestis Andriotis and Dr Orestis Katsamenis for their continued help; allowing me to develop their techniques as well as creating new methods of our own. Thank you again to Louise for working with me through many thousand repetitive indents, which alone might have driven me to insanity.

I would like to express my gratitude towards everyone in the office (particularly those who broke up the day with tea and chat, you know who you are), my friends and family. But particularly, I owe a special thank you to Chloe for her encouragement and listening to my niggles and enthusiastic explanation alike and supporting me through both.

Of course, this research would not be possible without funding from the EPSRC and Mike Russell, to whom I am deeply grateful. Finally, thank you to those who have committed to reading this thesis and for doing so with enough enthusiasm to even read this section! I hope I can maintain your interest through the rest of the ‘marathon’.

Glossary of Acronyms

AFM	Atomic Force Microscope (an imaging technique)
AUC	Area Under the Curve (of ROC)
BMC	Bone Mineral Content
BMD	Bone Mineral Density
BMI	Body Mass Index (Weight/Height^2)
BMU	Basic Multicellular Unit (coupled osteoblasts and osteoclasts)
BSE	Back Scattered Electrons (in SEM)
BSP	Bone Sialoprotein (an NCP)
BUA	Broadband Ultrasound Attenuation (an output of QUS)
CaP	Calcium Phosphate
CID	Creep Indentation Distance (an output of RPI)
COASt	Clinical Outcomes of Arthroplasty Study (an on-going study at UHS)
CTX	Carboxy-terminal collagen crosslinks (a resorption marker)
DEXA	Dual-energy X-ray absorptiometry
DXA	An alternative acronym to DEXA, a means of measuring BMD
DPA	Dual-photon absorptiometry (preceded DEXA)
ED	Energy Dissipated (an output of RPI)
ERGO	Ethics and Research Governance Online (a UoS application system)
FEA	Finite Element Analysis (a computer modelling technique)
FRAX	Fracture Risk Assessment tool
FTIR	Fourier Transform Infrared spectroscopy
HA	Hydroxyapatite (bone mineral crystal)
HBSS	Hanks Balance Salt Solution
HRT	Hormone Replacement Therapy
IIAM	International Institute for the Advancement of Medicine (a tissue bank, now Platinum Training)
IDI	Indentation Distance Increase (an output of RPI)
J	J-Integral, the strain release rate (a measure of fracture toughness)
K	K-value, the stress intensity factor (a measure of fracture toughness)
LEFM	Linear Elastic Fracture Mechanics
µCT	Micro Computed Tomography (an imaging technique)

MHU Measurement Head Unit (of RPI)

MRI Magnetic Resonance Imaging (an imaging technique)

MRTA Mechanical Response Tissue Analyser (a bone assessment)

NCP Noncollagenous Proteins

NIH National Institute of Health

NIHR National Institute for Health Research

OC Osteocalcin (an NCP)

ON Osteonectin (an NCP)

OPN Osteopontin (an NCP)

OStEO Observational Study Examining Osteoporosis (the clinical study)

P1NP Type 1 procollagen (a resorption marker)

PIS Patient Information Sheet

PLM Polarising Light Microscopy (an imaging technique)

pQCT Peripheral Quantative Computed Tomography (an imaging technique)

PLM Polarising Light Microscopy

PTH Parathyroid Hormone

REC Research Ethics Committee

RIR Repetitive Indentation Resistance (the inverse of IDI)

ROC Receiver Operating Characteristic (a statistical measure)

RPI Reference Point Microindentation or Indenter (microindentation)

QUS Quantitative Ultrasound (an imaging technique)

SEM Scanning Electron Microscopy (an imaging technique)

SOS Speed of Sound (an output of QUS)

SPA Single Photon Absorptiometry (preceded DEXA)

SXA Single X-ray Absorptiometry (preceded DEXA)

TDD Touchdown Distance (a RPI output)

TEM Transmission Election Microscopy (an imaging technique)

TID Total Indentation Distance (an output of RPI)

UHS University Hospital Southampton

UoS University of Southampton

US Unloading Slope (an output of RPI)

WHO World Health Organisation

1 Introduction

1.1 Background to Fracture Risk

Bone's mechanical properties make it ideally suited for protecting major organs, acting as a framework to provide support and attaching to muscles to enable movement. The structure, composition and resulting mechanical properties are balanced to form a complex hierarchical material that has developed to ideally perform its major mechanical specification, avoiding fracture. This specification is vital for the skeletal system to provide stability, protection and locomotion to the body.

However, if the integrity of bone is compromised, its ability to perform these vital functions can become limited. Therefore, disorders of the bone can be disastrous, having an extreme detrimental effect for the sufferer. Osteoporosis is one such disorder that may compromise the 'quality' of bone (its material, compositional, structural and ultimately mechanical properties) alongside its currently assessed 'quantity' leading to increased risk of fracture, as defined by The National Institutes of Health [1] and The World Health Organisation [2].

In 2002, there were over 8.9 million osteoporotic fractures worldwide and such fractures cost the US $20 billion and the UK £1.7 billion annually [2-4]. Besides this economic burden, fractures are devastating for an individual, reducing their quality of life and showing this to be a disorder of significant socio-economic impact. Furthermore, with an ageing and increasing population, the numbers affected and healthcare costs are expected to continue to increase with a predicted 5 fold increase in those over 65 leading to a tripling in number of hip fractures by 2050 [2, 3].

Osteoporotic fractures typically affect the femoral neck, vertebrae and the distal radius the consequences of which can be extremely severe. With hip fractures in particular, mortality is increased compared to non-fractured individuals of the same age. Specifically, in the first year post fracture, patients are 20% more likely to die [2, 3]. This is very age dependent, ranging from as low as 3% in under sixties to 50% in the over nineties [5]. Those that do survive are still at risk from pain and disability with 7% of fractured patients having some disability and 8% requiring long-term care [6]. Chronic pain and deformity are common with vertebral fractures and loss of everyday function associated with

fractures of the wrist, however, it is hip fractures in particular that reduce an individual's quality of life with 50% never regaining their pre-fracture status in terms of mobility and levels of pain [2, 3].

Post-menopausal women in particular are affected by osteoporosis with 90% of fractures occurring in people over 50 years with 80% of those in women [6]. Therefore, a simplified explanation might be that fragile bones are just a natural and unavoidable part of ageing. This is far from the case and age does not perfectly correlate with fracture risk but instead osteoporosis is a multifactorial disease. Therefore, measures such as bone quantity (i.e. bone mass) and bone quality (i.e. structure, composition and overall mechanical properties) and clinical factors (e.g. parent fracture, smoking, alcoholism etc.) supply added risk factors for fracture. Though it is generally considered that the material properties of bone contribute to this reduction in bone quality and increase in fracture risk, limited information is currently available. Therefore, though osteoporosis has been shown to be caused by factors beyond ageing alone, further research is required to investigate the biomechanical changes in the tissue with disease.

Lifetime factors such as nutrition, exercise and lifestyle improve bone health and treatments are available that can effectively reduce fracture risk by as much as 50%, indicating the disorder to be avoidable or, at least, with the potential to be delayed [7, 8]. The problem, however, is diagnosis and understanding of the disorder. Diagnosis and fracture risk assessment is historically based on the WHO definition which is centred on 'bone quantity' or bone mineral density. The definition is that bone with a bone mineral density (BMD) of 2.5 standard deviations below the average (based on a young, healthy population – initially 409 Caucasian females aged 20 to 29 from the NHANES III database) is osteoporotic [2]. This definition was initially established to assess prevalence of the bone disease; however, it has been adopted to diagnose and monitor osteoporosis. As intended, the WHO definition is a good predictor of fracture risk in the population and a positive result (BMD < -2.5) identifies a 50% risk of fracture over a lifetime [9]. However, alone, it is not suitable for assessing individuals and a negative result cannot classify someone as healthy, consequently 80% of fractured patients are outside this range [10, 11]. In other words, by this definition, the majority of patients with fragile bones would be considered healthy right up until the point they suffer a fragility fracture. Consequently, there has been a move towards the incorporation of clinical risk factors

alongside BMD, shifting towards fracture risk assessment that is more specific to the individual rather than BMD defined diagnosis of osteoporosis. Algorithms, such as FRAX (the fracture risk assessment tool [12]) created by WHO and the University of Sheffield, combine factors that correlate with fracture risk such as age, sex, patient history and lifestyle with BMD. This algorithm gives an output of 10 year fracture probability with an intervention threshold, however it has been found that the sensitivity (detection rate) is still low and could therefore benefit from the incorporation of further risk factors, perhaps bone quality [2, 13].

The term 'bone quantity' is used within this thesis to define the existing BMD measurements. The term 'bone quality' is used in the literature to define properties intrinsic to the bone that may further contribute to fracture risk. Bone quality is a general term relating to its structural and compositional properties over its hierarchical levels [14] and how these affect the overall mechanical competence, fragility or fracture risk [15-17]. With this broad definition, there are understandably discrepancies in the use of this term but these can largely be split into two classifications [18]: 1) bone quality incorporates all intrinsic properties of the bone relating to fracture risk, including bone quantity (i.e. BMD) or 2) bone quality refers to all intrinsic properties outside those that can be currently measured through existing bone quantity techniques. This study, being clinically focussed, considers the latter definition relating to bone properties that are components of fracture risk but cannot currently be detected clinically.

This thesis primarily assesses aspects of bone quality, whether they are altered with disease and whether there is means for clinical assessment of these measures through the new reference point microindentation (RPI) tool. Reference point microindentation involves a reference probe that can be pushed through the soft tissue and a test probe that cyclically indents into the bone, with higher indentation depth implying more fragile bone (shown in Figure 1). This technique has shown some clinical potential by being applied in vivo with purportedly no discomfort or resulting complications [19-23]. The device also has some potential to assess bone quality showing varying degrees of correlation with bone material properties [19, 24-27] and some discriminative ability between healthy and diseased human bone [19, 21, 28, 29].

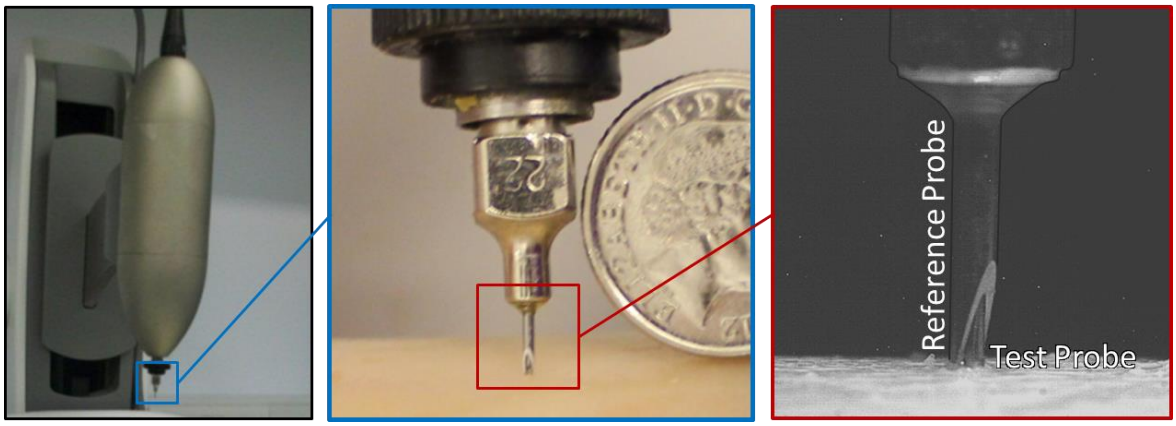

Figure 1 – Images of the Biodent Hfc Reference Point Microindenter at increasing length scales (left to right) showing the outer reference probe that would be pushed through soft tissue and identify the surface of the bone and the test probe that cyclically indents into the bone

In spite of its emerging use, the variability associated with the device is still minimally reported [20, 26, 29-32], giving new users limited points of reference for establishing testing protocols to perform RPI in a repeatable fashion. With such a testing protocol, it is then possible to establish the efficacy of RPI to discriminate between healthy and diseased human bone and whether it is able to supplement existing BMD and FRAX measures to improve fracture risk assessment. Furthermore, the differences in material properties (such as fracture toughness) between diseased and healthy bone is not evident and it remains to be seen whether these properties can measured through RPI or to establish what property the technique is measuring.

This thesis aims to characterise bone by aspects of its 'quality', specifically its biomechanical properties as measured by RPI and fracture toughness, and to establish whether these properties relate to fracture risk. The particular focus is investigating reference point microindentation (RPI) to establish whether there is any clinical potential for the measurement of bone quality and whether this can define a supplementary risk factor for improved fracture risk assessment.

Primary research question

"Are there biomechanical differences between **healthy and diseased bone that can be measured through reference point microindentation and can this complement existing techniques for potential improved fracture risk assessment"**

1.1 Structure of the Thesis

This report is split into a substantive literature review followed by the research findings.

With bone quality being such a general term, following this introduction (Chapter 1) it is important to first consider what is known about bone and its complex structure and the relationship to mechanical properties (Chapter 2 – The Quality of Bone). Equally importantly, bone disease, primarily osteoporosis and increased fracture risk as well as osteoarthritis, a second prominent and deleterious musculoskeletal disease, then need to be defined by their causes, mechanisms and effect on bone (Chapter 3 – Reduce Bone Quantity and Quality). Finally, the methods adopted in this work, will be assessed, discussing their ability to answer the research question and their potential to overcome current limitations in fracture risk assessment (Chapter 4 – Experimental Techniques for the Assessment of Bone).

With this basis, the research question has been addressed through three studies. Due to the emerging nature of the technique, the variability associated with reference point microindentation test parameters first needed to be established. This allows for an optimised testing protocol for applying RPI with known and controllable variability and, hence, more consistent testing (Chapter 5 – Variability Associated with Reference Point Microindentation and Recommendations for Testing of Cortical Bone).

The generated testing protocol is then implemented in the clinical study, examining the potential of RPI to discriminate between fractured and non-fractured tissue in close proximity to the most clinically deleterious fracture site, the femoral neck. Tissue from patients undergoing hip arthroplasty for an osteoporotic hip fracture or for osteoarthritis is compared to cadaveric controls. RPI and clinical techniques were applied to assess their potential to be combined for improved fracture risk assessment (Chapter 6 – The Potential of Reference Point Microindentation for Improved Fracture Risk Assessment).

Biomechanical differences, primarily fracture toughness, are measured in the diseased and control cohorts. This technique, alongside imaging of the indents, was utilised to improve understanding of bone disease and the properties being assessed through RPI (Chapter 7 – Bone Mechanics in Health and Disease: Investigation into the properties assessed by Reference Point Microindentation).

Finally an overall discussion and conclusion summarises the main findings, limitations and the future work implied by this thesis (Chapter 8 – Discussion and Conclusion).

2 The Quality of Bone

Bone is an extremely complex composite material or rather, a family of materials with structure and composition, and hence, properties, that vary widely from bone to bone.

Regardless of this wide variety, the function of any bone, mechanically speaking, is to withstand load. The bone might be plate-like such as the skull, protectively dissipating energy from external impact load. Alternatively, the bones could be long like the radius and acting as a lever, to transmit the internal load of the muscles. The bone might even just be withstanding the compressive load from the constant weight of supporting the body and, accordingly, have a short and stout shape like the vertebrae. Actually, a bone will be suited to a combination of these roles and therefore, in the most basic terms, its overarching aim is simply not to break. Though other functions, such as a compromise against weight to allow for locomotion and avoid drowning or acting as a mineral reservoir are also crucial to bone, from a mechanical perspective it has a hierarchal structure built from the bottom up to be ideally suited not to fracture.

A summary of this seven tier hierarchy (described by Weiner and Wagner [33]) is shown in Figure 2 and described as follows: bone cells lay down collagen, mineral and non-collagenous proteins (Level 1), forming mineralised collagen fibrils (Level 2). These bundle together, forming fibres (Level 3) that layer and stack into lamellae (Level 4). The lamellae form; a mesh of spongy cancellous bone (Level 6) or concentric cylinders, the osteon (Level 5), comprising the dense cortical bone (Level 6). Cancellous bone is held in a cortical shell making the whole bone (Level 7). Starting below the smallest level, with the bone cells, this review explores how each level of the structure is assembled and how this contributes to bone's mechanical function: withstanding load and avoiding fracture.

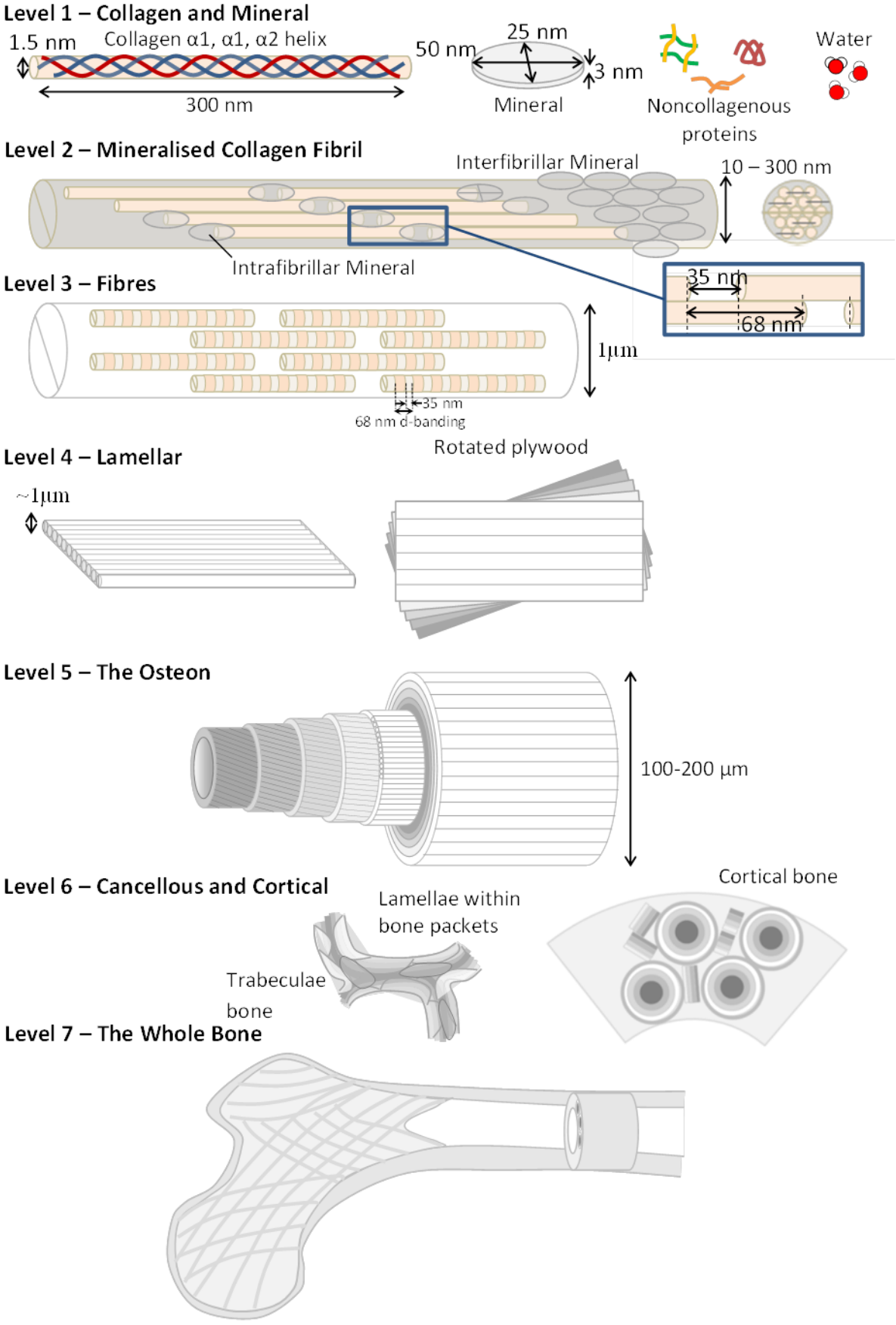

Figure 2 - Bone's hierarchical structure

2.1 The Bone Cells

Though, bone might seem like a stable structure it is actually a dynamic organ that constantly remodels by a partnership of cells; osteoblasts that add on and osteoclasts that take away. This remodelling cycle, pictured in Figure 3 and summarised by Brandi et al [34] who is paraphrased here, keeps bone balanced and optimised to the loads applied to it. The cycle starts when bone is activated from its rest state by recruiting osteoclasts to the bone's surface. The osteoclasts, the bone resorbing cells, secrete an acidic solution and enzymes. The acid dissolves one principal components, the inorganic mineral, while the enzymes breakdown and digest a second component, the organic collagen and proteins [34]. This process, of the osteoclasts eating away at the surface of the bone, creates a concave surface which ends with the programmed death of the cells coupled with the recruitment of osteoblasts, the bone forming cells. Osteoblasts first create the organic matrix then form the mineral crystals [33]. Some osteoblasts stop dividing to become flattened bone-lining cells. Alternatively, once osteoblasts stop dividing they can be built into the bone as it is laid down to fill the recess. These buried osteoblasts become osteocytes that remain within small, liquid filled, voids in the bone, called lacunae. These lacunae are interlinked by channels, the canaliculi, and similarly, the osteocytes are linked together by a network of processes that travel within the canaliculi [14].

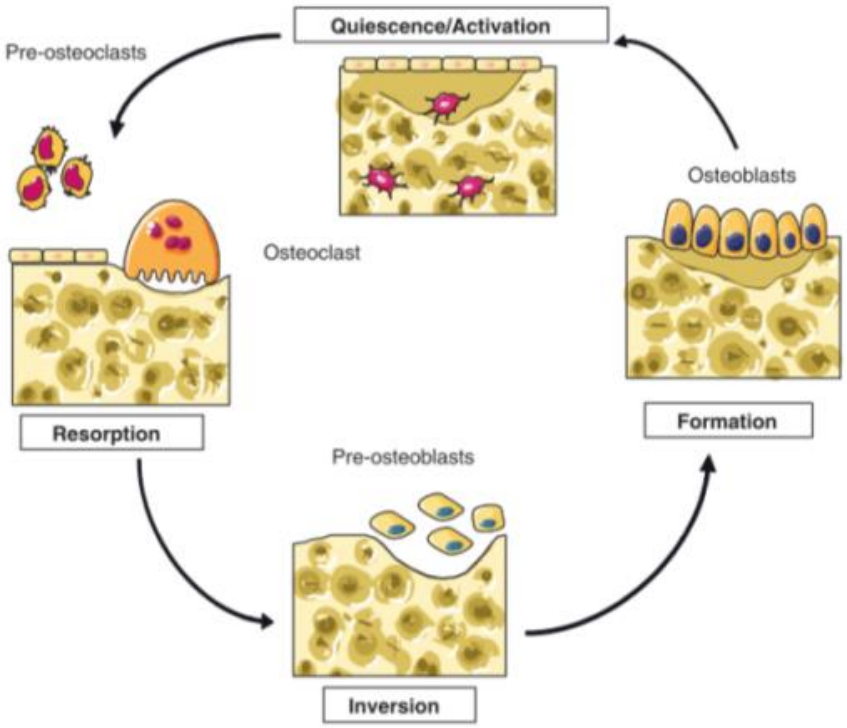

Figure 3 - The bone remodelling cycle. Reproduced from Brandi et al [34] courtesy of the Oxford University Press

It is proposed that osteocytes react to mechanical stimuli to maintain bone at the levels that will withstand load. Initially Wolff's law [35] proposed the structure-function relationship of bone remodelling which was then developed to Frost's mechanostat [36], including responding to load and deformation and perhaps sensing this via the osteocytes. Furthermore, the cellular network responds to microdamage within the bone, repairing cracks to maintain mechanical function.

Adaption and repair is achieved through the action of the osteoblast and osteoclast coupling, the BMU (Basic Multicellular Unit of bone remodelling) that moves through the bone replacing old tissue. Frost's theory [36] states that an increase in strain above approximately 1000 με, such as through exercise, leads to a higher degree of formation (increased osteoblast action within the BMU), increasing the amount of bone and reducing the overall strain. Conversely, a decrease in strain to 50 – 400 με, such as through inactivity or shielding by an implant, leads to a higher degree of resorption (increased osteoclast action within the BMU), increasing the overall strain. In this way, the bone is adapted to maintain a constant level of strain, keeping bone optimised to the loads applied to it.

Jang et al [37], building on FEA modelling by Huiskes et al [38], used this theory of local remodelling to computationally display what happens to the bulk of the tissue. This can be modelled by comparing a loading stimulus to a reference value and adapting the density of individual elements (e.g. if lower than the reference the density is decreased and vice-versa) or the overall topography until the structure converges for a particular loading scenario [37, 39]. Increased load, thickened cortical bone and the trabeculae aligned to transmit this load; and with reduced load, the cortical bone thinned with reduced trabeculae alignment of the trabeculae. This is in line with the clinical observations, supporting mechanosensing and adaptive theories [37]. If the loading is excessively high or through fatigue, microdamage may be produced and, as mentioned, damage repair is also critical in remodelling. McNamara and Prendergast [39], tied the theories together by using separate models that responded to strain and damage separately or in combination. This study predicted that damage sensing (e.g. of microcracks or resorption cavities) was necessary to commence resorption and strain sensing was needed to ensure bone formation and therefore homeostasis.

Though the adaptive nature of bone is well established including the mechanosensing nature of the osteocytes, the exact mechanical stimulus and process of sensing and transmitting this stimulus are still open for discussion. As well as direct strain, the mechanical stimulus has been proposed to be stress, strain energy density (area under stress strain curve [38]) or geometric properties [37].

It is also discussed how this mechanical signal is sensed by the osteocyte and cellular network. The original theories of osteocytes directly sensing the stimulus have been disputed with the 1 – 10% strains required for the bone cell signalling, being substantially greater than the 0.04 – 0.3% in vivo [40, 41]. Theories consequently consider the fluid within the lacunae and canaliculi and how loading causes fluid flow through the network creating shear on the osteocyte processes [40] which would have the added advantage of transporting nutrients and waste to and from the cells [42]. You et al [40], specifically found that an oscillatory fluid flow substantially increased cellular response above direct loading. Furthermore, strain sensing may be amplified through: fluid and network geometry amplify the strain and shear stresses [43, 44], the osteocytes being softer in vivo [41], preferential damage formation around the lacunae stress concentration [45] or specialised microtubes (the primary cilia) extending from the cells to increase their flow sensing abilities [46, 47].

Various chemical processes have then also been proposed [40, 44, 48] for transmitting these sensed mechanical signals to the osteoblasts and osteoclasts. An alternative hypothesis proposes that the osteocytes transfer an inhibitory signal that limits remodelling unless this signal is disrupted such as through high strain or damage [49, 50]. The exact method of mechanosensing and mechanotransduction are still extremely controversial but based on the literature reviewed above, the following opinions have been formed by the author. Firstly, it seems likely that increasing strain energy density is detected by osteocytes alongside canalicular flow amplification (particularly oscillatory) detected through the primary cilia and processes. Secondly, this may result in calcium signalling and the canalicular network transmitting the signal to osteoblasts with a similar mechanism or cell apoptosis due to lack of nutrition through fluid flow also leading to osteoclastic resorption below a certain stimulus threshold. Finally, above a high threshold strain energy density or with presence of damage (amplified by the lacunar-canalicular network stress concentrators) the osteocytes may directly sense this strain or through the

rupture of processes and consequently signal remodelling (or disrupt an inhibitory signal) to repair this damage.

In this way, a constant level of strain aims to be maintained, sensed and controlled alongside a mechanism of damage repair at higher strains, keeping bone constantly suited to function. That is, healthy bone subject to normal loading does not break or, bone that breaks when subject to normal loading is not healthy.

2.2 Level 1: The principal components

At the smallest level, bone is principally made up of mineral crystals and collagen but also noncollagenous proteins (NCPs) and water. These major components are extremely different in structure and properties but each contributes in an essential way to the overall performance of bone.

2.2.1 The inorganic phase

With regards to the mineral crystals, there has previously been some dispute over their size and shape due to the difficulties in measuring such small structures. However, Robinson [51] first suggested, as far back as 1952, that the inorganic components are not needle-like but are instead discrete long flat plates (50 x 25 x 3 nm in size) with hexagonal symmetry. Since this discovery, improved resolution of imaging techniques such as TEM (transmission electron microscopy) has further established this to be the case [33, 51, 52]. These inorganic crystals are composed of a mineral similar to carbonated hydroxyapatite (HA, a ceramic formed of calcium and phosphate) and are stiff (a modulus in the region of 100 GPa) and brittle (maximum extension of 0.1%) giving bone its overall strength [53, 54].

Being a ceramic, it is easy to conjure up the image of an easy to fracture chalk-like material for these mineral crystals. However, their modulus is actually 1 - 2 orders of magnitude higher than would theoretically be expected from bulk HA. Ceramics generally have very low fracture toughness, being intolerant to flaws. This gives them good compressive properties, where the flaws are being pushed closed, and poor tensile properties, where the flaws are pulled open to propagate through the structure. Despite this, mineral crystals are designed to be loaded in tension and are able to resist flaws whereas the thin plate-like structure would be prone to buckling in compression [55]. Gao et al [56] modelled the crystals to explain this (very fortunate) discrepancy by considering the Griffith's criteria for fracture mechanics: that a material can tolerate a crack until it

reaches a critical size. Griffith's criteria is summarised by Equation 1 and explains the discrepancy between theoretical (based on breaking of atomic bonds) and empirical strength of materials by the presence of flaws. That is, above a critical flaw size, the strength of a material is governed by the crack and therefore the material's fracture toughness. The criteria for the critical crack size is given in Equation 1 in terms of fracture toughness, yield strength and elastic modulus. Taking assumption for these values for hydroxyapatite mineral crystals of E = 100 GPa, G_c = 1 J/m^2 and σ = 30 MPa to 300 MPa [56, 57] give an estimate of critical crack size no smaller than 350 nm.

Equation 1 - Griffith's critera to determine the critical crack size (a_c) in terms of the fracture toughness surface energy (Gc), the elastic modulus (E) and strength (σ)

$$a_c = \frac{G_c E}{\pi \sigma^2}$$

These dimensions are larger than those of the crystal themselves (Figure 4 – left). Therefore the nanometre size of the crystals means they can tolerate any possible flaw size and their failure is governed by their high tensile strength and not their low fracture toughness. Gao et al [56] also employ this criteria to give a ballpark figure of tens of nanometres and additionally applying FE models to find that the stiffness of the crystal is achieved by its large aspect ratio and as the thickness of the platelets are reduced they converge on their theoretical strength. So the size and shape of the bone crystals are suited to resisting cracking and therefore give strength and stiffness to the bone as a whole.

Mineral is laid down and matures at different times, meaning bone packets with different degrees of mineralisation form. It is thought that these discontinuities and heterogeneity may also perform an important toughening mechanism [53].

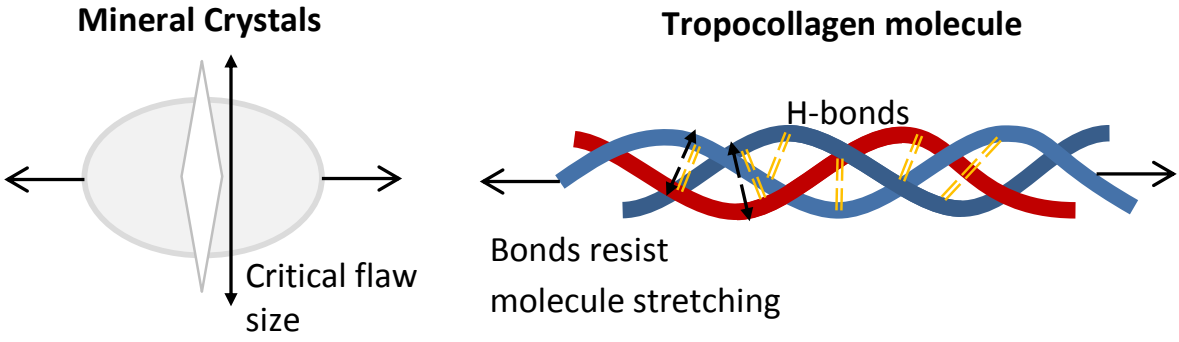

Figure 4 – Flaw tolerance of the mineral (left) and h-bonding resisting the unravelling of collagen (right)

2.2.2 The organic phase

The organic phase of bone is made-up primarily of collagen (80%), a triple helical protein. There are 28 kinds of collagen in the human body such as type II found in cartilage and type VI in muscle but the majority is type I and in bone this makes up 95% of the collagen [58, 59]. Boedtker and Doty [60] unravelled the structure of type I collagen which is structured as 300 nm long molecules [60] that are 1.25 nm in diameter [61]. The collagen fibrils, tropocollagen, can be broken down further, being formed of three protein strands (two the same, α1 and one different, α2) twisted together into a helix [61] (Figure 2 – Level 1). There are additionally small proportions of other collagens in bone (e.g. type III and V [58]) that modulate the fibril size but the predominant type I is unique in having no interruptions in its triple helix while also self-assembling into fibrils [59]. This leads to its stability and suitability for the structural role.

Conversely to the strong and brittle inorganic mineral, the type I collagen is tough, compliant and elastic with a modulus around 1 GPa, a fraction of that of the mineral, but a several fold increased maximum strain of 10% [53]. These properties give bone its resistance to damage and tolerance to deformation.

Thompson et al [62] used an AFM (Atomic Force Microscopy) approach to investigate loading of collagen molecules in tension. The AFM detects the deflection of a cantilever probe with known stiffness to either; image, indent, or in this case pull a sample. The probe was repeatedly pulled away from the collagen molecules which bonded to the probe to resist this movement. Thompson et al [62] found a time dependence in the energy dissipated by the molecules when loaded, attributing this to breaking and reforming of weak sacrificial bonds within (hydrogen or h-bond) and between (crosslinking) the collagen fibrils. With computational modelling at the molecular level, these h-bonds have been found to break at 10-20% of the collagen's maximum strain [63], sacrificially protecting the molecular strands. The breaking and reforming of the intermolecular bonds leads to a stick-slip type resistance to the unravelling of the collagen molecule as the h-bonds try to maintain the helical backbone [64]. This is one of the mechanisms for bone's time and loading-rate dependent response, its viscoelasticity. Additionally, the coiled spring-like structure of the molecules themselves and the existence of the bonds are the source of collagen's excellent elasticity with the helical proteins recoiling and bonds reforming when unloaded (Figure 4 – right)

2.2.3 Noncollagenous Proteins

Making up the other 10 - 20% of the organic phase, there are many noncollagenous proteins (NCPs) including osteocalcin (OC), osteopontin (OPN), osteonectin (ON) and bone sialoprotein (BSP) to name but a few of the greater than two hundred [33]. Hunter et al [65] describe how these proteins aid in regulating mineralisation with, for example, BSP initiating mineralisation but OPN inhibiting nucleation and crystal growth to allow crystals to form and grow but be limited to their all-important nanometre size.

Chen et al [66] suggest that NCPs (OPN and BSP in particular) have another role and hold similar tissues together, cohesion (such as bonding calcium atoms to each other or between mineral crystals) and McKee and Nanci [67] additionally suggest they help to bind dissimilar tissues, adhesion (such as bone mineral to collagen).

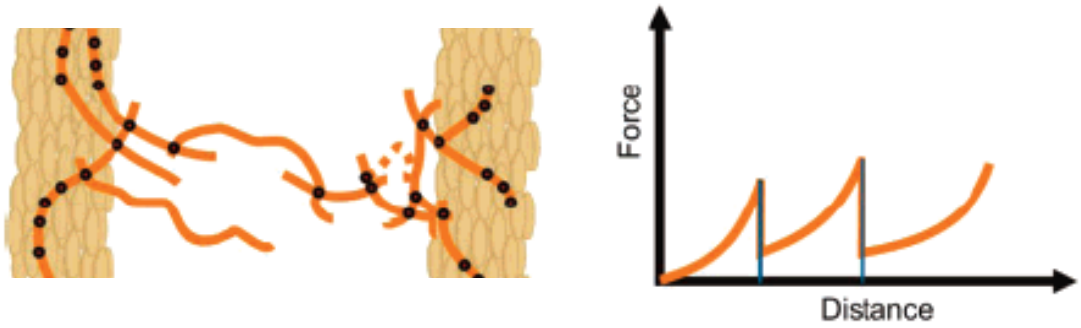

Figure 5 - The hidden length of osteopontin molecules - reprinted from Fantner et al [68], courtesy of American Chemical Society (copyright 2007)

Fantner et al [68] acknowledged that some of the NCP molecules had folding and hidden lengths that unravelled to create resistance to loading but that this was not the case for OPN. Instead, on OPN loading, short molecules link together creating a chain as loading continues as shown in Figure 5. This explains the saw tooth loading curves (with renewed resistance as each new molecule joins the chain) and the resistance up to 2 - 3 µm by 300 nm molecules when loaded within an AFM (atomic force microscope). Zappone et al [69] found a calcium buffer increases this pulling length and maximum force by forming bonds between OPN chains through their positive charge (Ca^{2+}). This adhesion and cohesion is another time dependant mechanism of sacrificial bonds [62].

Thurner et al [70], quantified the deficiency of OPN in mice, showing it to reduce fracture toughness by 30%. Poundarik et al [71] additionally found that in osteocalcin (OC) knockout mice the propagation toughness was reduced to a similar degree as with OPN

and without either the effect was increased. They hypothesised that the OC helps to fix the OPN to the mineral to bond the interfibrillar mineral aggregates to each other. When these bonds were broken, at around 100 nm, voids or 'dilatational bands' form, which dissipate energy and help to resist fracture.

Though NCPs make up a small proportion of the composition, they are invaluable in acting as a glue for both mineral and collagen as well as controlling mineralisation.

2.2.4 Water

Water fills gaps at many of the hierarchical levels to keep the sample hydrated. The majority bonds to the collagen, mediating its internal hydrogen bonds to form an organised network that bridges the protein strands to maintain the helical structure [72]. The control of these bonds aids assembly of the tropocollagen but also help to provide its toughness so is vital to maintain the mechanical performance of bone [33].

For example, Nyman et al [73], when considering bending of cortical bone, showed that a 13% dehydration (in a vacuum oven) can cause a 30% reduction in strength whereas a 5% dehydration (at room temperature) only removes mobile water and not that bound to collagen, increasing strength. The toughness (80% decaying reduction – higher loss of toughness with initial dehydration) and stiffness (40% linear increase) also significantly changed with dehydration. At a smaller scale, considering tension of osteons, Ascenzi et al [74] found wet compared to air dried samples to have an approximately 200% greater elongation at the cost of 50% reduction in strength. With this reduced ability to absorb energy through deformation, damage extends deeper into the bone matrix but with hydrated collagen, the molecules hold together strongly and the toughness is increased.

2.3 Level 2: The mineralised collagen fibril

The two extremely different major components, the stiff mineral plates and the elastic collagen fibres, combine together to form the second level, the main building blocks of bone, the mineralised collagen fibrils. The arrangement of the collagen and mineral is extremely organised with a repeated pattern. The fibrils are laid down by osteoblasts and self assembles into a structured array [63]. Here, individual molecules sit end to end with a 35 nm gap to make long strands that bundle together in parallel with the gaps being offset by 68 nm [33, 61] as shown in Figure 2 (Level 2). These layers stack together to create a three dimensional structure with the same 67 nm offset and 35 nm overlap

maintained between all adjacent fibrils. This repeated offset creates an overall periodicity to the bundled together fibrils known as D - banding [75] (Figure 2 - Level 2 and Level 3). The mineral forms in the gaps but grows out into the overlap with the collagen helping constrain them to their ideal (flaw tolerant) nanometre size [56]. The mineral also coats the fibrils [75] where the collagen network cannot constrain their size so the NCPs alone are likely to be responsible for this. Though the quantities of intrafibrillar and extrafibrillar mineral are disputed [76], Alexander et al [77] used STEM (scanning transmission electron microscopy) to find that 28% of mineral is in the intermolecular overlap, 42% within the gap leaving a minimum of 30% outside of the fibrils. Focusing on the minerals within the matrix: despite having a high aspect ratio themselves, the close packed layout of the collagen fibrils constrains the mineral at its ends and along its length to reduce its susceptibility to buckling [55]. Instead, the staggered layout of the collagen means these are placed in shear when the whole fibril is loaded in tension and transfer tensile load to the plate-like mineral, the loading mode they are ideally suited to (Figure 6 - right) [76, 78].

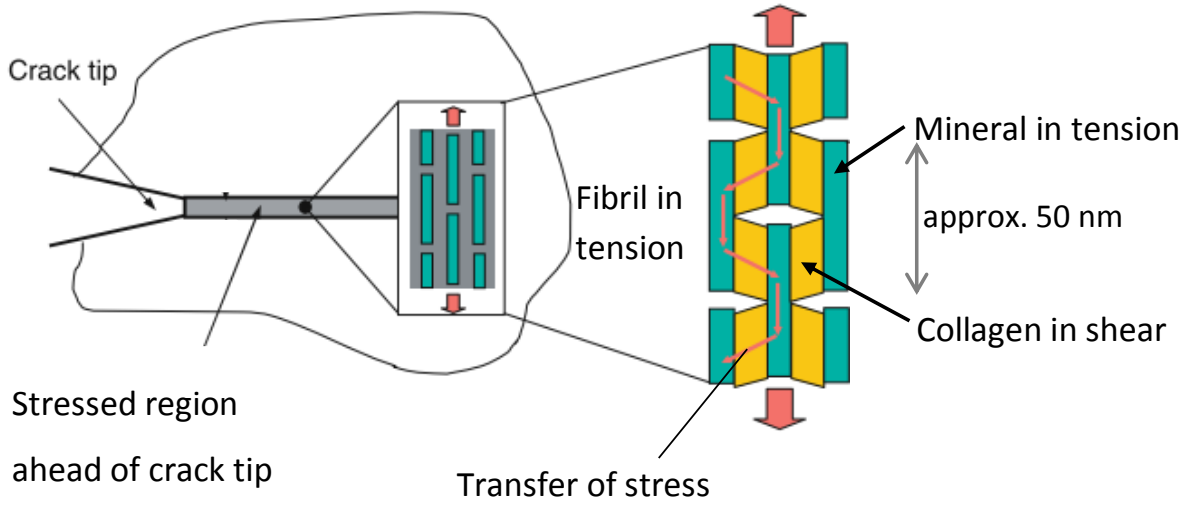

Figure 6 – Transfer of tensile load to shear of collagen and tension of the mineral crystals. Reprinted and annotated from Gao [55], courtesy of Springer

Gao [55] use various mathematical models, that are a useful approach due to the small scale, to answer questions about the collagen fibrils structure-function relationship. The fibrils, with a 1:1 volume ratio (or 1:3 weight ratio [15]), are considered as a mineral reinforced collagen composite rather than a fibre reinforced ceramic. This composite structure is necessary to achieve both the overall strength and the toughness of the bone. It does this through a “strain amplification mechanism” with the elastic collagen allowing large deformation while the mineral only has to withstand a small amount of deformation

but supporting high load. This plays to the advantages of both components with the collagen resisting strain and the mineral resisting stress, optimising bone to its loading conditions. Considering man-made composites, fibres help constrain the composite giving it added strength [79, 80], but in the case of bone it is the mineral crystals that are also adding strength and stiffness by limiting the slip and aiding load transfer between the collagen fibres [55].

Buehler [81], with a two dimensional computational model of the mineralised collagen fibril array, considering undeveloped bone with small crystals, showed the addition of the mineral to the collagen fibril significantly increased both the elastic modulus (to around 6 GPa) and elongation (to around 7%) by about 35% in comparison to unmineralised collagen. Importantly, the post yield behaviour was also substantially improved to double the failure stress. This is reported to correspond well with the experimental results of Gupta et al [82] where modulus and elongation again increase with mineral content. Though this testing relates to mineralised turkey tendon and not bone, at this level, the structure is expected to be comparable. The mechanism proposed by Buehler [81] for increased performance with mineralisation is intermolecular slip that dissipates energy. The staggered layout of the fibrils allows for this slip while the optimised strength of the bonding between collagen and mineral means that there is resistance to the sliding but this is still preferential to overloading of the components themselves. A similar process exists between fibrils where the mineral-mineral bonds or the actual teeth like interlocking of the minerals, offer resistance to interfibrillar sliding, but again being preferable to failure of the fibrils themselves [76]. This interfibrillar mineral bonding is achieved by the NCP cohesion described earlier, the rupture of which creates dilatational bands.

As the collagen develops, crosslinks form to bond adjacent molecules together. A single divalent bond, the immature crosslink forms per fibril, which helps stabilise this newly formed collagen. With age, the number of these immature crosslinks decreases to be replaced by mature crosslinking – the combination of two divalent bonds form a trivalent, mature crosslink (Figure 7) [83]. Both forms of crosslinks enhance the distribution of load and deflection through the collagen and mineral and add stability by forming bonds between and within the fibril [58, 84]. A rat model from Oxlund et al [85] shows animals

with a 45% Lysine and Hydroxylysine (the amino acid base of these enzymatic crosslinks) deficiency have a 20-30% reduction in stiffness, strength and deflection in bending.

A third type of crosslink forms between collagen molecules. Rather than the formation of this molecule being enzyme driven, as with the immature and mature crosslinks, glucose and other sugars produce further links between adjacent molecules (Figure 7). These AGEs (Advanced Glycation End Products) go further than stabilising the collagen and instead limit displacement, stiffening it [83]. This is supported by a computational model from Buehler [86] which shows a small crosslink density to increase pre-yield performance by transmitting load to the molecules to allow them to dissipate energy. However, too many crosslinks over constrains the molecules, reducing energy dissipation through intermolecular sliding and therefore increasing the overall brittleness of the structure.

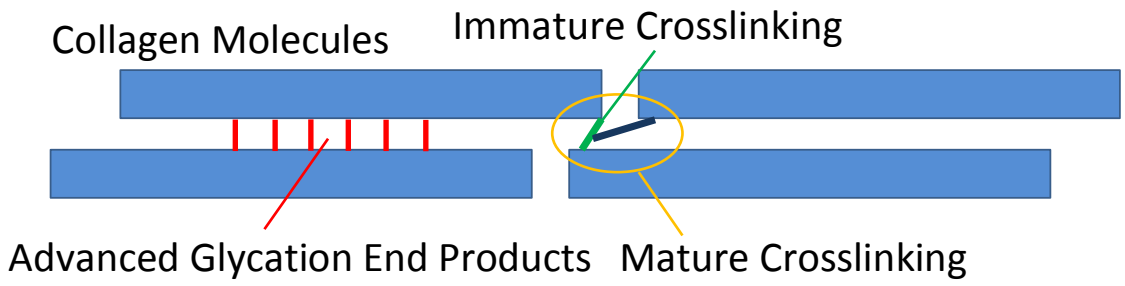

Figure 7 – Crosslinking of collagen molecules

Mineralised collagen fibrils also play a role at the larger scale by spanning cracks to hold the fracturing surfaces together. In this way, energy is dissipated in pulling out or breaking the fibrils, leaving less energy available to propagate the crack tip [87]. Ager et al [88] approximated this mechanism to only have a small contribution to fracture toughness (0.08 $MPam^{1/2}$ out of bone's total 2 - 7 $MPam^{1/2}$) but conceded this bridging may have more of an effect on limiting the propagation of smaller scale cracks.

2.4 Level 3 and 4: Fibres and lamellae

The individual collagen fibrils bundle together into fibres, the third level, which arrange into one of four fibril arrays at the fourth level. Weiner and Wagner [33] recognise four different fibril array patterns but only one of these is found in mature adult bone and this is the lamellar structure.

The fundamental structure (shown in Figure 2 - Level 4), involving stacked layers of collagen fibres, is generally accepted but there is much debate with regards to the orientation of the fibres, the thickness, properties and composition of these layers. Some of these proposed structures are shown in Figure 8 and Figure 9.

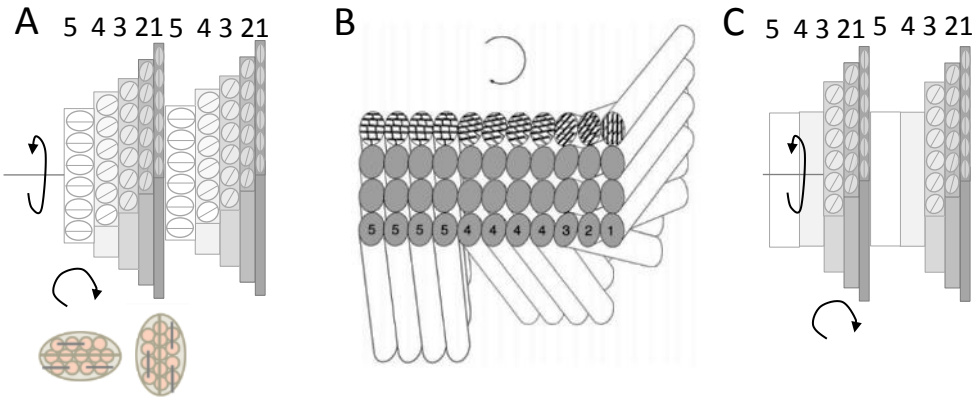

Figure 8 – Possible structures of the lamellar structure (A – Rotated lamellae with thick-thin structure due to fibril rotation [89, 90], B – Rotated plywood with thick-thin structure due to fibril stacking, image adapted from Weiner et al [91], courtesy of Elsevier, C – Rotated plywood structure with thin collagen rich layers and thick collagen poor layers)

A large number of sources (e.g. [75, 89-93]) agree that parallel fibres make up these layers with rotation of this orientation between layers, the 'rotated plywood' model. However, the angle between each layer is disputed. This may be up to 90° and alternating between each layer (i.e. ± 45°) [93] or rotating by 5 - 25° with a greater than 30° jump around every sixth layer creating distinct sub-layers [89] (Figure 2 – Level 4 and Figure 8A).

It seems most likely that both are true and present in different types of lamellae which will be discussed in greater detail in the next section with respect to osteon orientation. The effect of such a 'rotated-plywood' structure would be to create a tortuous path for crack propagation, changing direction as it passes through each layer of the lamella and dissipating energy as it does so, therefore making the layers difficult to break through [76] (Figure 9A).

A thick-thin pattern is also generally considered to exist [76, 91, 94-96] but the arrangement causing this pattern is again uncertain. With mineral plates having a constant orientation within a fibre, Wagermaeir et al [90] used x-ray diffraction to show a rotation of the fibres along their length between layers though with a beam diameter similar to the size of the lamella, 1 µm. The thickness of the plates may give rise to a short axis of the fibre and their width, a long axis, meaning rotation would give rise to different

thicknesses of layers (Figure 8A). Alternatively, thick layers could be made of multiple lamella longitudinal to the bone's axis and thin layers made of single lamella at large angles to the bone's axis [76, 91] (Figure 8B). Marotti [94] suggests these thin layers were 'dense' (collagen rich) and thick layers to be 'loose' (collagen poor).

Between these layers there is additionally variation in mechanical performance with the thick layers having a higher modulus as measured by nanoindentation [95] and the thin layers having a lower modulus [76] .

Varying stiffness between layers would have the effect of stunting the propagation of the crack by altering its direction as it moves through the layers, similar to the effect from varying orientation of the fibrils (Figure 9B).

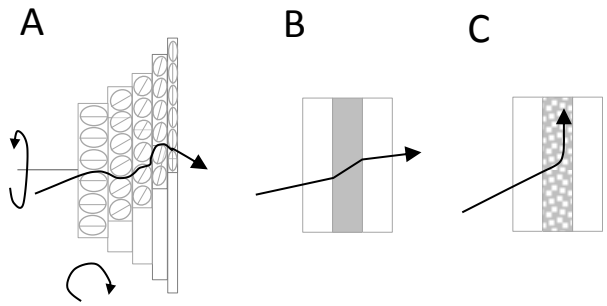

Figure 9 – A: Crack deflection due to rotation of fibrils, B: Crack deflection due to change in mechanical properties between layers, C: Crack deflection due to preferential cracking along a more ductile layer

A suggestion has been made that the thick layers are an isotropic ground substance that hold the thin layers together using the adhesive properties of the NCPs and being similar to the cement lines discussed in the next section [70, 94, 96, 97] (Figure 8C). This would also stand with the variation in mechanical properties between layers. This collagen-poor interlamellar layer would be stiffer but more brittle, allowing for preferential cracking to divert cracks and impede propagation through the lamellae (Figure 9C). Katsamenis et al [98], found the interlamellar layers (equivalent to the 'thin' lamellar) were less stiff (being collagen deficient and NCP rich) than the lamellae and preferentially stiffen on loading to dissipate energy as well as guiding the crack propagation. This crack deflection along cement lines and inter-lamellar layers impedes crack propagation through increasing the crack length and directing it along an NCP rich, preferentially stiffened line with changes in composition and structure. This effectively blunts the crack tip through increasing the quantity of material it must fracture to propagate [98, 99]. Furthermore, being NCP rich,

many bonds must be broken for the cracks to continue and these bonds are readily repairable if the loading is removed [68, 71].

From the literature discussed above, this author's impression is of thin, NCP rich interlamellar layers that join lamella with fibres that rotate about their axis and about their plane through each layer. Though no single theory has been definitively proven, it seems that this model would effectively impede crack propagation through the layers and be optimised, as at the other levels, to resist fracture.

2.5 Level 5 and 6: The Osteon and Cortical/Cancellous bone

The whole bone, level seven of the hierarchical structure, is formed by two types of bone – cortical and cancellous, the sixth levels. Short and flat bones (e.g. the vertebrae or the scapula) are made up of cancellous bone covered in a thin shell of cortical bone. Whereas, long bones (e.g. the femur, ulna etc.) are made of marrow-filled thick cortical tubes with cancellous ends, again with a thin cortical shell.

2.5.1 Cortical bone and the Osteon

Within cortical bone the lamellar forms cylinder made of concentric layers (Figure 2 – Level 5). This cylinder, the fifth level of bone's structure, is called the osteon or Haversian system. Blood vessels run along the centre of the osteon, through the Haversian canal and are connected through the osteons by channels called Volkmann's canals to allow the bone to be vascularised, maintaining the bone cells and creating an active organ that can respond to load and damage.

Ascenzi et al [74, 100-103] used polarising microscopy (PLM) to note three types of osteon dependant on the orientation of the lamellae. This supports the rotating plywood structure of the lamellae and allows for different rotation angles to exist (as hypothesised above). The three osteon types are those with the fibrils directed principally longitudinally along the axis of the osteon (type L), those with fibrils directed principally transversely to this axis (type T) and those whose fibril alignment alternates between longitudinal and transverse through each layer (type A). Martin et al [104] noted that osteons were often a mix of these three types – most commonly with the longitudinal pattern towards the centre and the transverse pattern towards the outer boundary (termed 'hoop' – type O). However, as this study considered equine metacarpus it is unclear which type or

combination of types is most commonly found in human bone. The four types (L, T, A and O) are depicted in Figure 10.

Over a quarter of a century, the Ascenzi group [74, 100-103] developed a catalogue of micro-mechanical testing of individual osteons to compare properties in tension, compression, shear, bending and torsion. The results follow logically: those with the fibres aligned longitudinally (type L) performed optimally in tension and torsion by acting like a tensile spring, those with transverse fibres (type T) resisted compression and shear and those with the alternating pattern (type A) combined these two properties to be suited to bending. This shows that no arrangement or osteon type is optimised to all modes of loading and instead, each is specialised and is present as appropriate e.g. alternate osteons are present in bowed bones to limit further bending [100].

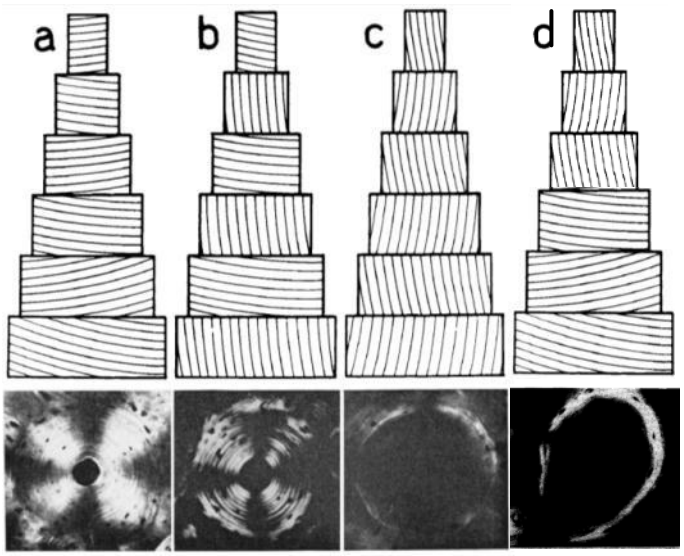

Figure 10 – Osteon patterns: a) type T - Transverse, b) type A - Alternation, c) type L - Longitudinal, d) type O – Hoop. Top: arrangement of the osteons. Bottom: Polarising microscopy (a-c) or photomicrograph (d) image with light patterns showing principally transverse lamellae and dark patterns showing principally longitudinal lamellae. Adapted from Ascenzi and Bonucci [103], courtesy of John Wiley and Sons and from Martin et al [104] courtesy of Elsevier

In human bone, the lamellae is laid down first then is remodelled to form the osteon (therefore termed secondary osteons) by the osteoclasts and osteoblasts. This resorption followed by deposition creates the structure of cortical bone; secondary osteons packed together within original lamellae that fills the gaps (Figure 2 – Level 6), but also leaves remnants named cement lines [67]. These 1 – 5 µm cement lines follow the boundaries of the osteons and Schaffler, Burr et al [105, 106] used SEM imaging and microprobes to find them to be absent of collagen, be less mineralised (less Calcium phosphate but a higher

Ca:P ratio) and contain more sulphur than the surrounding bone. They considered that this was not mature HA but a ground substance that is more ductile than the surrounding bone and it would therefore deform preferentially as with the interlamellar layers [98]. Skedros et al [107] concurred with the low collagen content of the cement lines but disputed their low mineralisation, finding this to be a product of unrecognised artefacts in SEM. Instead, they found cement lines to be highly mineralised.

Regardless of their composition, the mechanical properties of these layers are perhaps more critical. Dong et al [108] measured the performance of the cement lines through osteon push out testing – finding them to be substantially weaker than the surrounding tissue (around 8 MPa compared to 70 MPa). Bigley et al [97], also testing osteon push out, found a less of a marked difference with cement lines having strengths ranging in region of 10 to 50 MPa with the variation relating to the osteon type. Though Bigley measured almost 500 osteons compared to 30 in the study by Dong et al, these were all the metacarpal of a single horse unlike the humeri from four human donors. Regardless, in both cases the cement line was shown to be weaker than the osteon and lamellar layers with Bigley also noting similar weakness of the interlamellar layers. This supports the hypothesis of the lamellar structure that was discussed previously (i.e. NCP-rich interlamellar layers that crack preferentially deflecting and dissipating energy). Additionally, both studies take the view of Burr rather than Skedros that the cement line is less mineralised, supported by its relatively low strength.

With the cement lines and interlamellar layers being weak compared to the surrounding bone as well as the changing orientations and properties between the lamellae - the osteon is a structure designed to be an extremely difficult to penetrate. The relative weakness of the cement line makes this a preferential path for crack propagation as opposed to continuing its path towards the centre of the osteon. The change in direction blunts the tip, reducing the crack driving energy by around 50% [87, 88, 109] and increases the length of the crack path. As mentioned the mechanical properties differ between the thick and thin layers of the lamella (or lamella and interlamellar layers) making cracks deflect as they pass through the structure. In the case of the osteon, the modulus of the thick layers (potentially the interlamellar ground substance) may reduce from the centre (25 GPa) to the outside (20 GPa) whereas the thin layers have a constant modulus (15 GPa) [76, 95]. This means the difference in modulus, and hence the degree

of crack deflection, increases towards the centre of the osteon. That is, the effect in Figure 9B would be more pronounced towards the centre of the osteon.

Koester et al [110] mechanically tested the fracture toughness of bone in two orientations: transverse with the crack attempting to penetrate the osteons ('breaking') and longitudinally, in line with the osteons ('splitting'). 'Clinically appropriate' starter cracks, less than 600 µm in length (in comparison to the 100 µm to 300 µm found in bone [111]), were used to find higher values for the effective stress intensity factor (K_{IC} the fracture toughness) than previously reported and be able to observe the strengthening mechanisms of the osteon. The effects were marked with the samples being five times easier to split than break. This effect, the culmination of the cement line/interlamellar layer deflections and the toughening effects of the lamellae discussed previously, is a very important mechanism. In addition to raising the toughness of bone to avoid fracture, when fracture does occur, this happens preferentially to protect the blood vessels at the centre of the Haversian system (Figure 11– left).

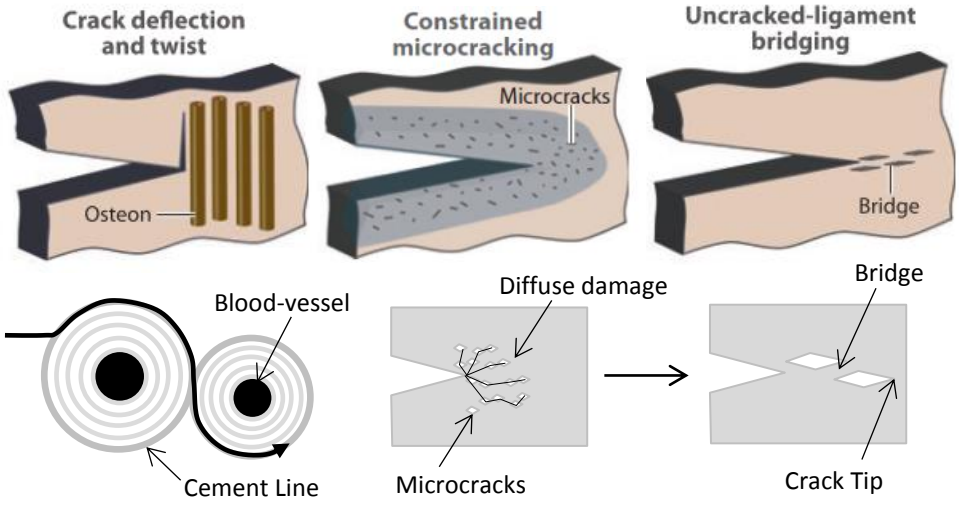

Figure 11 – Strengthening mechanisms at the macroscopic level. Left: crack deflection along osteons, splitting (above) and round/through osteons, breaking (below). Centre: Microcracking creating diffuse damage to dissipate the energy of the crack tip. Right: Uncracked ligament bridging acting behind crack-tip. First line of image adapted from Launey et al [63] courtesy of Annual Reviews

Another strengthening mechanism, microcracks or diffuse damage, form predominantly in the cement line [63, 88]. Though it would seem logical that small cracks within the bone would compromise the structure these can create a low modulus region that cracks preferentially, dispersing the crack tip over an area rather than a single point (Figure 11 - centre). Nalla et al [109, 112] tested the role of microcracking by comparing numerical models with experimental results to find its role in increasing toughness to be minimal

and potentially acting to reduce toughness through a low volume fraction and the alignment of the cracks. This research had limitations in only considering two mechanisms at work, microcracking and crack-bridging (to be discussed later) however, we have seen that there are a large number of mechanisms that alter bone's properties from that predicted by a simplified model. Vashishth [113] also questions the assumption of the low microcrack density, suggesting it to have a larger effect on bone's properties, particularly at a smaller scale.

Regardless of their effect alone at dispersing the crack tip, it is widely believed that microcracks form uncracked ligaments that have a significant effect behind the crack tip, an extrinsic mechanism to limit crack propagation [87, 88] as shown by Figure 11 - right. The microcracks form ahead of the crack tip and grow, progressing the crack with further loading. However, until these 'daughter' cracks coalesce, there is still material (the uncracked ligament) bridging the gap and supporting load [88]. This is estimated numerically to have a 1 - 1.6 $MPam^{1/2}$ contribution to the overall fracture toughness of bone (2 – 7 $MPam^{1/2}$) [88] and, as mentioned, Nalla et al [109, 114] experimentally found crack bridging to have a significant effect in comparison to diffuse damage.

In terms of crack formation, the dilatational banding proposed by Pounderik et al [71] form as gaps between fibrils through extension of the NCP bonds between the mineral aggregates which can reform to repair this nanoscale damage. However, with continued loading these bonds rupture and voids grow through separation of the mineralised collagen fibrils. With repeat overloading the voids develop further into soft areas [71] of interconnected micron sized cracks, the diffuse damage, the microcracking previously described. This diffuse damage may not be repaired through remodelling but by some unknown intrinsic mechanism [115]. Larger 30 - 100 µm linear microcracks can form independently [116] or when these cracks coalesce [88] and grow following the cement lines and interlamellar layers [98]. Up to 100 µm these cracks can be arrested by the osteon cement lines, preventing continued propagation [111]. Beyond this point they begin to activate a remodelling response to heal the cracks [117] but if this is not sufficient in comparison to the magnitude or frequency of the loading they will continue to grow in length, still following the cement lines or interlamellar layers. At 300 µm the remodelling response is increased [117] but the cracks are able to penetrate the osteon

and follow the Haversian canal with the potential to lead to catastrophic failure or rupture of the bloody supply [111].

From the nano-scale up to the sub-millimetre scale, cortical bone has intrinsic mechanisms to impede crack propagation and repair damage that forms. However it appears that the osteonal level is particularly crucial being of the same scale as critical cracks and having many crack resistance mechanisms that greatly contribute to the overall toughness of bone (i.e. crack bridging, deflection and diffuse damage). Therefore, mechanical assessment at this level may be the best means of characterising bone in terms of its fracture resistance.

2.5.2 Cancellous bone

Cancellous or trabecular bone, the other bone type at the sixth level, is formed of plates interconnected by supporting struts that form a network of bone that is, overall, substantially more porous than cortical bone. Wolff, as far back as 1892 [35], considered this type of bone to have a different macro-architecture compared to cortical bone (being porous rather than dense) but to be formed of the same base material. This point has been widely debated but it is now generally believed that there are intrinsic differences between the two types of bone even if they are formed of the same basic building blocks (levels 1 - 4). Despite this is still difficult to draw a line with dense cancellous bone being very similar to low density cortical bone. The distinction tends to lie around 30% porosity or 1.3 gcm^{-3} [118].

Trabecular bone is also formed of lamellae that makes about 40 µm thick arches (the plates and rods, the trabeculae) but it has no osteonal structure. Some, such as Chappard et al [14], consider these thin arched trabeculae to be incomplete osteons to support the similarities between the two bone types with cancellous bone being a younger (more remodelled) form of the bone. These lamellae are differentiated into packets of bone by their age and level of mineralisation (Figure 2 – Level 6) with older bone being more highly mineralised due to crystals reaching 70% of their maturity after a few days but taking years to become fully mineralised [53]. Though trabecular and cortical bone may have similarities, the mechanical properties of the two types (or potentially stages) of bone have generally been found to differ, even at the same size scale.

Carter et al [119] compare large samples to find that cancellous bone can absorb substantially more energy in compression than tension through progressive impaction. At high loading rates, this energy absorption in compression is comparable to cortical bone but at lower loading rates (or in tension) the energy absorption is an order of magnitude lower. Rather than considering large samples where the varying porosity and structure is a confounding factor, Choi et al [120] consider single trabeculae and cortical samples of a comparable size to find the trabeculae to have a 20% reduced bending modulus. Szabo et al [121] also found a single trabeculae to be less stiff than cortical bone with a greater reduction of 43% alongside a 37% higher toughness. This higher reduction is most likely due to the larger dimensions of the cortical bone and the size effect discussed by Choi. Here small cortical sample have a stiffness in the region of 5 GPa but as the size increases, this value tends towards 15 GPa. This is most likely due to the osteonal structure being tested above 100 – 200 μm that is not present in the small scale trabeculae.

Considering the cancellous bone is made up of an interconnected network, it is unlikely to fail by a single crack, making fracture toughness of the whole network a clinically irrelevant parameter [87]. Instead the deformation and yielding mentioned above is more suitable. Particularly, the improved strength in compression reveals the function of the cancellous bone. The network is adapted to follow stress lines, giving a grain direction or general orientation of the trabeculae (e.g. as shown with the femoral head in Figure 2 – Level 7) [14, 122]. This relates to the mechanical stimulus (e.g. strain energy density) sensed by osteocytes to control remodelling by the action of the osteoblasts and osteoclasts, meaning more highly loaded areas have higher formation and less loaded areas have higher resorption [37, 38]. This leads to the aligned porous structure that allows load to be dissipated and transmitted through the trabeculae to the cortical bone.

2.6 Level 7: The whole bone

Single values are occasionally quoted for bone. Perhaps a strength of 100 MPa, a stiffness of 15 GPa or a toughness of 5 $MPam^{0.5}$. But without context such as the direction, location and scale of measurement, these values have little meaning. Instead, bone's properties vary significantly depending on mechanisms from the nano to the macro scale. The single value stiffness could refer to a measurement at the nano-scale and therefore vary wildly between extremely stiff mineral phase and the compliant collagen. But this value would still not consider the flaw-tolerant nature of the mineral or the resistance to

molecular uncoiling from h-bonds. Instead it is these strengthening mechanisms that are important in giving bone its complex and varied mechanical properties and these mechanisms rely heavily on the bone's structure.

To recap (as shown in Figure 2 and Figure 12, [63]): the main components, collagen and mineral are constantly replaced by bone cells depending on mechanical stimulus. The inorganic and organic parts are organised together into mineralised collagen fibrils whose structure ideally loads both components (the collagen giving compliance and the mineral, strength) and NCP bonds resist sliding. These are structured again into bundles then lamellar bone which has a rotated plywood structure and varying thicknesses and properties to deflect crack propagation. The lamellae form cylindrical osteons in cortical bone, with cement lines and their concentric structure again deflecting cracks. At this level microcracks lead to uncracked ligament bridging that dissipates energy, also to increase toughness. As an alternative to the osteon and cortical bone, lamellae forms packets and the trabeculae in cancellous bone that distributes load and dissipates energy through its aligned porous structure. Cancellous bone is surrounded by a cortical shell in varying proportions to form the whole bones.

Alignment such as that of the long axis of collagen fibrils and the mineral plates in lamellae and osteons give direction dependence, anisotropy to the bone. Subtle changes in composition or structure at low length scales (e.g. of the mineral and collagen) or more noticeable variations at higher length scales (e.g. different osteon types and cortical or cancellous bone) mean properties vary throughout the structure, being heterogeneous. These variable properties mean each part of the bone is ideally suited to the mode of loading that they are subjected to. The properties are also time dependant or viscoelastic, in part due to sacrificial bonds from the nano to micro level (e.g. NCP bonds, crosslinking or h-bonds), making bone able to deal with sudden loads. Being dynamic through its remodelling cycle, bone also constantly adapts this structure to be suited to the strains and damage applied to it.

In summary, the complex hierarchical structure described above, creates bone – a structure optimally suited to its mechanical function, to withstand and transmit load or, broadly speaking, not to break.

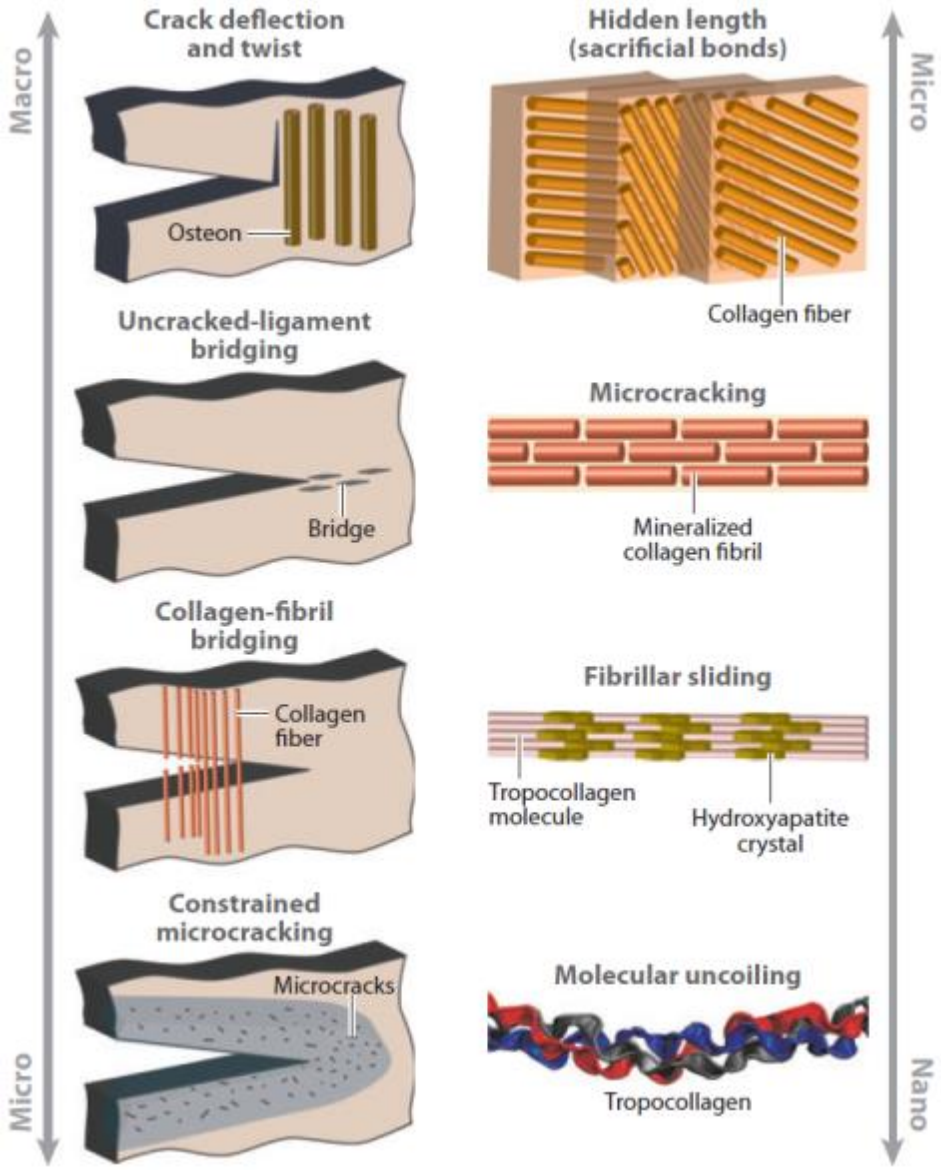

Figure 12 – The nano-scale to macro-scale toughening mechanisms of bone. Image reproduced from Launey et al [63] courtesy of Annual Reviews

3 Bone Disease – Osteoporosis and Osteoarthritis

3.1 Osteoporosis – a disease of bone quantity and quality

The previously made statement 'bones are ideally suited not to break' is contradicted by the fact that they clearly do. This is either through overloading during trauma, where healthy bone would be expected to break, but also through disease that robs bones of their optimal design. Using the NIH definition [1] (as this report will continue to do), osteoporosis is a disorder that compromises bone's mechanical integrity, increasing the risk of fracture to a level where bones can break from minor events such as a low impact fall.

3.1.1 Causes and Risk Factors

Osteoporotic fractures typically occur when bone is overloaded during a fall and therefore the direct cause of an osteoporotic fracture are three fold: Factors extrinsic to the bone: 1) the propensity to fall and 2) the fall mechanics and factors intrinsic to the bone: 3) its quantity and quality.

Likelihood of falling increases with age due to factors including reduced sensory input (i.e. loss of vision), impaired reflexes, movement disorders and muscular disease [2] [123]. The fall mechanics affect the energy, direction and overall severity of the impact and are affected by the above factors (how an individual reacts to the fall) as well as external factors (e.g. trip and slip hazards) [124]. The fall or other low-trauma event is necessary to initiate fracture but despite this, it is thought that less than 5% of falls result in fracture [2] which strongly implies the quantity and quality of the bone (i.e. its mechanical properties) also relates to fracture risk, the NIH [1] and our definition of osteoporosis. Therefore fracture risk is a combination of falls risk and severity and properties of the bone and this thesis is focussing on assessment of the latter and its contribution to fracture risk.

Despite this emerging definition of osteoporosis as increased bone fragility [1], many studies use the WHO operational definition with osteoporosis being considered a condition of low bone mass [2]. This relates well to fracture risk for a population, though not for an individual and therefore gives some idea of fracture risk, if not the whole story. Studies that relate causes to increased fracture risk via BMD therefore give an insight into the effect of this factor and have been included here, but the actual effect on bone could

be increased or diminished compared to that stated. Hence, the trend is shifting towards studies that consider fracture and not BMD as an end point to establish efficacy of diagnosis, treatment and the epidemiology of the disease.

3.1.1.1 Lifetime risks, age related bone loss and the menopause

3.1.1.1.1 Hormones

Bone quality typically reduces in old age, most noticeably in females post-menopausally as approximated by the bone mass trend in Figure 16. Riggs et al [125] considered two sole factors: Sex hormones and Frost's mechanostat. Oestrogen deficiency increases bone turnover and disturbs the BMU – increasing the lifespan of the osteoclasts and reducing that of the osteoblasts. Oestrogen reduces with age in both sexes but, while the regression is linear in men, the menopause induces a significant, non-linear reduction in women. Testosterone, which reduces linearly with age in both sexes but with a higher level always being present in men, accounts for no more than 30% of the effect on bone turnover compared to oestrogen's 70% [125]. The total level of sex hormone does not greatly reduce in men but the amount freely available to act on the bone does decrease due to an increase in SHBG (Sex Hormone Binding Globulin) that joins with the hormone [126]. This leads to significantly reduced bioavailable sex hormone in both sexes as illustrated by Figure 13.

In addition to oestrogen and testosterone changes, parathyroid hormone (PTH) levels increase with age by 84% in men and 64% in women, this increases the calcium content in the bloodstream by increased renal resorption as well as reducing that in bone [126]. Calcium, being a principal constituent of bone, has a significant effect as will be discussed.

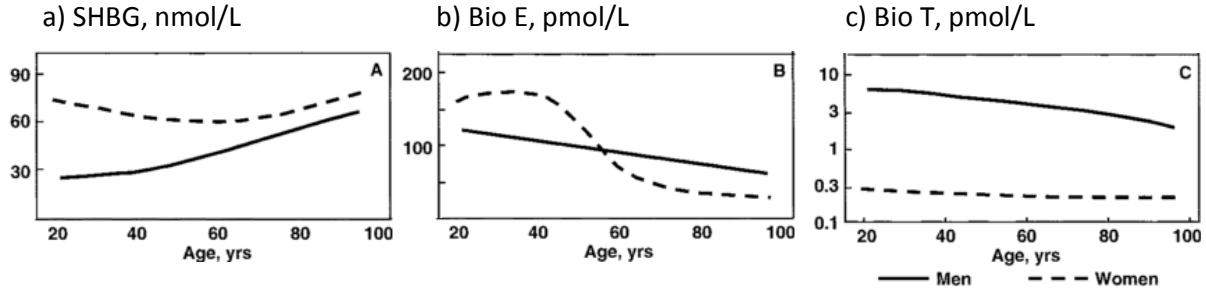

Figure 13 – a) Effects on SHBG (sex hormone binding globulin), B) Bioavailable Oestrogen (E) and c) Testosterone (T) levels with age in men and women. Image reprinted from Riggs et al [125] courtesy of Endocrine Society and data originally from Khosla et al [126]

3.1.1.1.2 Exercise

The mechanostat, where bone senses mechanical stimulus (via the osteocytes [117]), can reduce bone mass through disuse but similarly, the resorption can be fought through exercise [36]. This mechanism was believed to be affected by the reduced oestrogen [125, 127, 128], altering the strain (or strain energy density etc.) level at which bone begins to resorb (moving to disuse mode [36]). This would mean a higher level of loading is required simply to maintain the bone, or the bone becomes suited to a lower level of loading than it is subjected to. There are many other clinical factors that affect bone loss throughout life and in old age. Riggs [125] believes all these factors enact their effect by altering the two core mechanism, sex hormones and the mechanostat. Considering oestrogen deficiency alters the strain threshold, the mechanostat could be thought to be the sole mechanism at work. Whether directly or indirectly, these clinical factors (including exercise and the sex hormones as mentioned as well as nutrition and lifestyle) still have a significant relationship to fracture risk and hence osteoporosis.

3.1.1.1.3 Calcium and Phosphorous

Ilich and Kerstetter [129] give a detailed review of the importance of nutrition to maintain bones and which is summarised as follows. They emphasise the importance of nutrition based on bone's vital role as a mineral reservoir in addition to its mechanical function of supporting load. It is previously discussed that the mineral crystals are made up of calcium and phosphorous which give bone its resistance to stress, but these elements have other vital functions within the body. For example, calcium plays a role in transmitting signals between cells and phosphorous gives structure to DNA and transports cellular energy. So even though the vast majority of both minerals are stored in the bone (99% of all calcium and 85% of the phosphorous [129]) the large store is vital as the body cannot afford to run out. Therefore, if dietary intake is too low (a minimum of 1200 mg/day of calcium and 700 mg/day of phosphorous [129]) the minerals are taken from the bone by the action of PTH to perform other, vital, functions. In such a case, the reinforcing crystals become depleted and bone becomes more susceptible to fracture.

Phosphorous deficiency would rob the bone of one of its structural elements but, being widely available in foodstuffs, this deficiency is relatively uncommon. Instead, an excess consumption relative to that of calcium may also lead to increased bone resorption through elevation in PTH [129]. More relevant, and hence more studied, is the common

calcium deficiency in 20% of individuals. Heaney [130] reviewed a substantial number of papers on the subject to find the vast majority of authors (75 - 99%) found high calcium intake promoted bone health and Cumming and Nevitt [131] quantified this as a 24% fracture risk reduction when at least 1000 mg/day was taken. In old age and post menopause the importance of calcium is increased with oestrogen deficiency and PTH increase necessitating a 60% increase in calcium consumption [130].

Deficiency does not just relate to poor intake in the diet but also malabsorption, such as through intestinal disease, where the mineral might not be able to be metabolised. Levels of absorption have been found to decrease with age and be reduced by around 20% in osteoporotic individuals [132] and weaken bones, having just the same effect as a poor diet. Vitamin D, primarily from sunlight but also in the diet and through supplementation, has a significant effect on absorption and is another major concern due to deficiency being common, particularly in the elderly. Chapuy et al [133], albeit in patients under nursing home care, found those with normal vitamin D (and calcium) to have a 32% lower fracture rate (bone density also increased by 7%), due to reduced bone resorption. Similar to adequate vitamin D reducing fracture risk, LeBoff et al [134] implied that insufficient vitamin D levels also increased fracture. They compared vitamin D, as well as PTH levels, in individuals with a fracture to those with normal and low BMD but no fracture. This group found that vitamin D levels were significantly lower and PTH levels significantly higher in the fractured group, even when compared to the low BMD group. However, the efficacy of vitamin D supplementation is a contentious issue with some studies (e.g. RECORD [135]) finding both vitamin D and calcium supplements to have no effect on reducing fracture. A meta-analysis by Abrahamsen et al [136], having the large number of individuals (almost 70 thousand, including the RECORD study) required to investigate the effect on fracture concludes that vitamin D alone is ineffective (10 µg or 20 µg daily dosage) but when combined with calcium there was a 16% reduction in fracture risk. This is due to low vitamin D reducing the absorption of dietary calcium, meaning less is available for signal transmission in the body and more PTH must act on the bone. This raids the bone store to supply mineral to the blood stream, compensating for the deficiency. Therefore, if there is adequate supply of phosphorous and calcium to the rest of the body it will not need to harvest stocks from the bone and the mechanical function can continue to be carried out.

3.1.1.1.4 Protein and Energy

As with the mineral phase, the other principal constituent of the bone, the protein making up collagen, also needs to be maintained. The consumption of protein is a careful balancing act needing 1 - 1.5 g protein per kg bodyweight a day [129] with both too little and too much being detrimental. Returning to Ilich and Kerstetter [129], it has been found that high protein increases urinary calcium output by around 20% which, as would be expected, increases bone resorption to harvest the mineral for vital functions, therefore increasing fracture risk as above. The opposite, a low protein diet, reduces calcium absorption in the intestine and therefore has a similar effect.

Protein along with fat and carbohydrates make up the majority of the body's energy input which, relative to the energy expended relates directly to the body mass index (BMI = weight/height^2 in kg/m^2). The loss of BMI relates to BMD with a 10% weight loss correlating to a 1 - 2% bone loss [129]. De Laet et al [137] reviewed 60 thousand participants in a meta-analysis to look at the relation between BMI and fracture risk. It is found that on average, per unit reduction in BMI, there is an increase of 7% on hip fracture risk in men as well as women. However, this reduction is non-linear with those less than a BMI of 20 kg/m^2 being at substantially higher risk (Figure 14 and Figure 15), even when the BMD effect is taken into account. With BMD adjustment, high BMI (>35 kg/m^2) also gives some increased risk of fracture as shown in Figure 14. A meta-analysis (almost 400 thousand individuals) by Johansson et al [138] confers that low BMI is a risk factor rather than high BMI being beneficial by some increase in osteoporotic in individuals with high BMI fracture when adjusted for BMD, particularly of the upper arm. Low BMI related fracture risk may be influenced changes in the quality of bone in addition to the reduced weight bearing leading to resorption, poor muscle strength leading to increased fall likelihood and impaired reaction as well a less soft tissue protecting from impact [129, 137]. The effect due to low BMI alone is also more pronounced with age (for fractures in general but not hip fractures), perhaps due to leanness when young indicating physical fitness but when elderly, under nutrition is more likely to be the cause [137]. Though risk is reduced with weight gain, the other aspect to BMI is individual's height that has a separate effect to increase fracture risk, potentially due to the change in fall biomechanics [139].

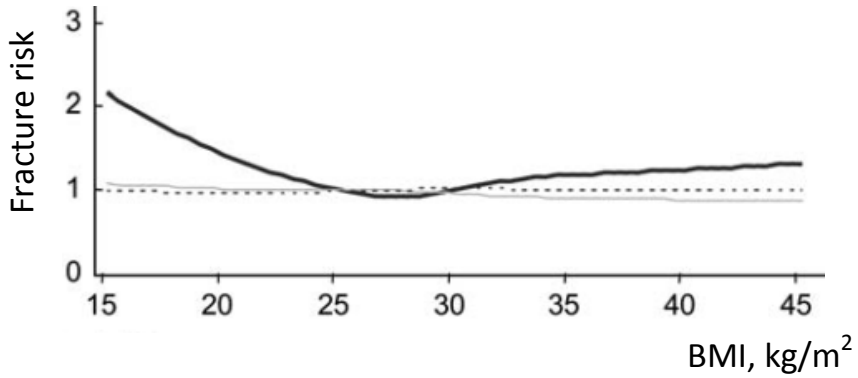

Figure 14 - Relative fracture risk of hip fracture (y-axis) with varying BMI (kg/m^2) (x-axis) with the effect of BMD accounted for and relative to the risk of a BMI of 25kg/m^2. Image reprinted from De Laet et al [137] courtesy of Springer

3.1.1.1.5 Other Nutritional Factors

In Ilich and Kerstetter's detailed review [129], there is also consideration of the need for other minerals that appear in significantly lower quantities than the bulk calcium and phosphorous and this section is a summary of that review. Firstly, magnesium, similar to vitamin D, is necessary for calcium metabolism with deficiency uncoupling resorption and formation, contributing to osteoporosis with reduced bone volume and strength. Magnesium, and similarly, strontium, can substitute the calcium in the mineral crystals, reducing their size. This can reduce their mechanical function and also lead them to become more soluble and therefore easier to resorb. Conversely, a fluoride substitution would increase the crystal size making them more resistant to osteoclasts while also increasing osteoblast activity. This is controversial as the small size of the crystals is essential for their flaw tolerance [56] so growth could lead to increased brittleness of the tissue.

Iron may aid collagen formation but potentially be toxic to bone cells. Copper, a deficiency of which is rare but reduces bone strength, also influences collagen and particularly the formation of crosslinks as does vitamin C. Sodium excess can increase urinary output of calcium increasing fracture risk whereas potassium enhances the incorporation of the calcium into the crystals reducing fracture risk. Vitamin A excess is also detrimental by accelerating resorption while reducing the number of osteoclasts which increases fragility [129].

Therefore, to maintain bone's optimum structure, a finely tuned dietary intake of mineral and protein is required.

3.1.1.1.6 Lifestyle

Other important factors that affect bone quality in old age and over the entire lifetime relate to an individual's lifestyle. In addition to the effects of inactivity and nutrition, caffeine, tobacco and alcohol consumption all have a significant effect as shown by Figure 15.

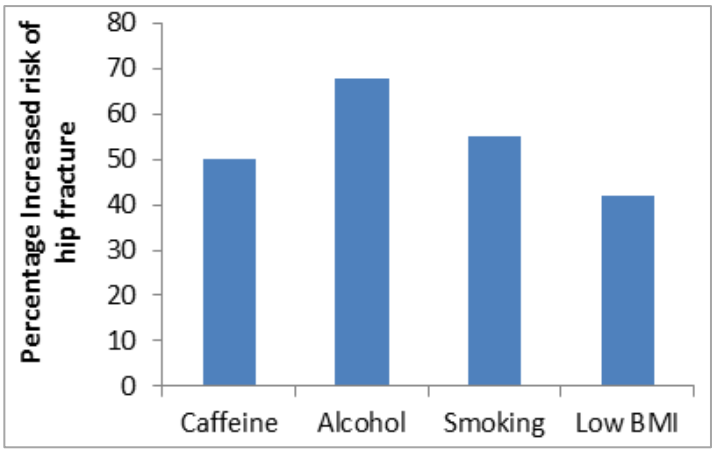

Figure 15 – Life style risk factors for hip fracture: Caffeine >2 units/day, Alcohol >2 units/day, prior or current smoker and BMI of 20kg/m^2. Values from the Kanis group [137, 140, 141] and Kiel et al [142]

Kiel et al [142] considered caffeine in the Framingham study (3000 participants in their mid-seventies over 12 years), finding an increase in consumption to increase fracture risk. A small amount of caffeine intake produced no significant difference but above their threshold of 2 units per day (a unit equates to 1 cup of coffee, 2 cups of tea or 60 - 100 mg of caffeine) showed a greater than 50% increase in fracture risk. This has more of an effect at a younger age (<65), potentially by exacerbating the effect of the menopause.

Ilich and Kerstetter [129] explained that it was once thought that this effect was due to an increased urinary calcium output but, in their review, they found any increased excretion was usually offset by the small amount of milk associated with caffeine consumption. However, they did express that the intake of caffeine is associated with an overall negative correlation to intestinal calcium absorption. This leads to a divide as to whether caffeine intake is deleterious to bone health which can be explained by studies where caffeine is consumed alongside a low calcium intake, finding an increased fracture risk.

Kanis et al [140] conducted a meta-analysis (considering the same large cohorts as De Laet et al [137], belonging to the same group) to assess the effects of smoking and alcohol on fracture risk. Similar to caffeine, alcohol intake has a threshold and again this is given as 2 units/day (i.e. 20 ml or 20 g dependent on country). Below this consumption, there is no significant increase in fracture (and even some suggested benefit to moderate consumption [129, 140]), but above this there is an increase of hip fracture risk of about 7% per unit (or 68% if comparing above threshold consumption with moderate consumption). Additionally, this effect was independent of BMD [140]. It is thought that increased alcohol consumption leads to malabsorption of minerals and is toxic to osteoblasts but other factors, extrinsic to the quality of the bone, could also play a part and affect those significantly above the threshold, with chronic alcoholism. This group are more likely to have lower BMI, have poorer nutrition and are at increased risk of a fall [129, 140].

Smoking is also linked to increased fracture risk, again investigated by Kanis et al [141]. Though age, BMD and BMI are confounding factors making up around 40% of the observed effect, when those factors are accounted for, those who smoke are still 55% more likely to have a hip fracture. The distinction between those who have ever smoked and those who are still smoking was made to find the latter to be at higher risk. The mechanisms hypothesised were co-morbidities such as inactivity with lower BMI but additionally there is higher breakdown of oestrogen, having the effect of early onset menopause [141].

3.1.1.1.7 Disease and drug therapy

There are many diseases that affect the structure of bone directly and others that have an effect through their treatment, both describing conditions of ‘secondary osteoporosis’.

Rheumatoid arthritis is an autoimmune inflammatory disorder of the joint tissue that affects the surrounding cartilage and bone. This increases fracture risk, particularly in the hip where the risk is increased by 76% as found by Kanis et al [143] in another meta-analysis. The treatment of rheumatoid arthritis may involve vitamin D (which has the beneficial effect on the processing of calcium) but also typically involves corticosteroids which further increase the risk of fracture [143]. This increase, independent from BMD and an additional effect from rheumatoid arthritis itself, is in the region of 2 - 4 times

[143]. The drug affects osteoblasts, reducing their lifespan and their capability to create protein as well as having effects on calcium absorption, PTH levels, osteocyte viability and muscle mass (potentially increasing fall likelihood and reaction) [143, 144].

Other disorders of the bone such as Paget's disease [145] (where localised remodelling lays down immature woven and lamellar bone and leads to physical deformity) and cancers [146] (particularly breast and prostate cancers spread to the bone, creating tumours that expand through the tissue) also reduce the quality of bone, increasing fracture risk. Additionally, cancer therapies are associated with fractures that occur at a younger age than would otherwise be expected (around 55 years of age) [147]. Furthermore, hyperparathyroidism (increased production of PTH) leads to the increased calcium in blood (taken from the bone stores), gastrointestinal disorders can lead to malabsorption of the required nutrients, hypergonadism affects the hormone balance in men and organ transplants require corticosteroid treatment [148, 149]. These are just some notable examples but many other disease and treatments can also directly or indirectly affect nutrition, exercise, hormone levels and therefore the bone quality and susceptibility to fracture.

Previous fracture itself increases the likelihood of subsequent fracture. Though, thinking of osteoporosis as a disorder systemically affecting overall bone fragility, this is not surprising. Furthermore, the fracture may additionally weakens the bone and increases the chance of falling [150]. Through another meta-analysis by Kanis et al [150], it is seen that a first fracture makes a second fracture 85% more likely with BMD only explaining 8 - 22% of this effect. The risk does not just apply to one site and the fracture of the distal radius or vertebrae is associated with a substantial (2 – 5 fold) risk of fracture at any location (i.e. hip, spine or radius) [150]. This implies osteoporosis is a disease with an underlying cause (or as discussed above, a wide variety of different causes) that detrimentally affects the overall quality and quantity of bone throughout the skeleton.

3.1.1.2 Development, maternal influences and genetics

Equally important to the stunting and reduction of bone mass and bone quality throughout life (primarily during old age and the menopause in women), is the acquisition of a peak bone mass while young (illustrated by Figure 16).

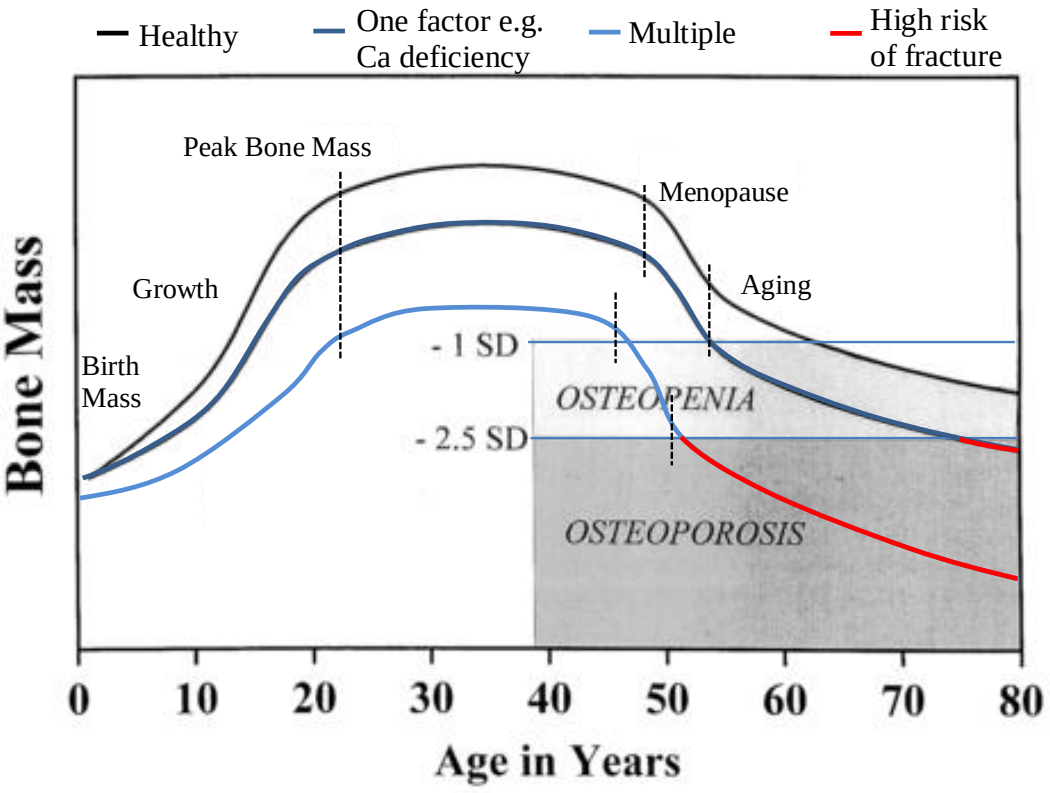

Figure 16 – The bone mass trend with ageing and the effects risk factors. Image adapted from Ilich and Kerstetter [129] courtesy of Routledge

3.1.1.2.1 Childhood development

During childhood and adolescence an individual's bones will grow substantially with the bone mineral content increasing 4 fold during infancy and doubling again during adolescence [151, 152]. The effective development of bones during young age relies on the same factors as their maintenance during life and in old age. That is, those with improved nutrition (vitamin D with calcium being of particular concern [153]), exercise, sex hormone supply (there may also be a benefit from oral contraception) and without over consumption of alcohol, caffeine or tobacco, will better obtain their peak mass [151]. Typically this peak is higher in boys, meaning women's high fracture risk relates both to their lower acquisition of mass and their greater loss due to the menopause. However, Schonau [152] reviews the literature to argue that the gain of a peak bone mass (or even a peak bone quality) is completely reversible with suitable calcium intake and exercise during development, making no difference to a subsequent lifetime of poor nutrition and inactivity. They do concede that improved accrual of bone followed by maintenance of this bone would most likely be the best approach for long-term fracture avoidance. They also stress that currently peak bone mass is not a true measure and this density should

relate to the child's size instead of being an absolute value. That is, bone should suit function and a small child does not require as large or dense bones but is still not osteoporotic. This focus, away from peak bone mass, is alternatively investigated by Cooper et al [154], considering a Finnish cohort (7000 men and women) to find that the rate of childhood growth, not the maximum bone mass, relates to fracture risk. Here it was found that those in the lowest quartile for weight and height acquisition would be twice as likely to fracture in later life.

3.1.1.2.2 Maternal influences

It has been suggested that causes for low quality bone that is likely to fracture go back further than the reduced quality in old age and even before the building of bones in youth. The Barker theory suggests that low birth weight, due to in utero conditions, is associated with health in later life [155]. Tracking 8,000 individuals living in Hertfordshire through their life, a link between high birth weight and reduced mortality from circulatory disease, musculoskeletal disease, pneumonia, diabetes, injury and fall was found [155]. Dennison et al [156] related this specifically to osteoporosis, with birth weight (and weight at 1 year) relating to bone mineral content at 70 years. The reason for low birth weight links to the in utero environment which is again based on factors such as nutrition, exercise and lifestyle but, this time, of the mother. Calcium is important, particularly in the third trimester of pregnancy when the foetus accumulates the majority of its mineral, and vitamin D is again necessary to process this calcium and prevent resorption by PTH. Specifically, Javaid et al [157] found maternal vitamin D deficiency, being common during pregnancy, to relate to reduced childhood BMD with Cockburn et al [158] also finding supplementation of the mothers to reduce hypocalcaemia in their infants. Godfrey et al [159] found maternal smoking to reduce bone mineral content by 11%, leanness to reduce content by 10% and exercise also to have an effect, being beneficial during early pregnancy but detrimental in late pregnancy.

The Barker theory takes the effect further than a detriment due to low birth mass, with the additional effect of 'foetal programming', epigenetics. The environment created by the mother cannot alter which genes are present in her child but may alter their expression, programming the genes which has an effect throughout the individual's life [151].

3.1.1.2.3 Genes

Going back further still, before life in the womb, an individual's genes are inescapable and are thought to contribute to up to 70% of their BMD [151]. Consequently, Godfrey et al [159] found higher maternal and paternal birth weight to increase the bone mineral content of the new born child by around 8% and 14% respectively. This does not mean to say that the factors discussed above can't have a significant effect on the remaining 30% contribution and over the lifetime. Consequently, by old-age, the gene contribution on fracture risk is reduced to a 3% [160]. Nonetheless, in another Kanis et al meta-analysis [161], parental history of any fracture increases risk of hip fracture by 49% and, more significantly, a parental hip fracture increases risk of hip fracture by 127%. This is independent of BMD and has little variation between sexes.

Returning to Figure 16, it can clearly be seen that a single factor, would decrease the peak bone mass, increasing the risk of fracture in old age. However, much more detrimental would be multiple factors at work. For example: 'osteoporotic genes' and poor maternal nutrition would reduce an individual's birth weight, inactivity and poor nutrition would stunt growth then a damaging lifestyle (e.g. smoking) could cause the early onset of menopause. Such a combination would drastically increase the risk of fracture, making an individual at risk early in their life. It can be seen that osteoporosis is multifactorial and care must be taken throughout life to build bone and maintain it, potentially working against the disadvantages of low birth weight or poor genes, in an effort to avoid the consequence of reduced bone quality, bone mass and subsequent fracture. Furthermore, assessment of these factors can help to define those at risk of fracture as will be discussed.

3.1.2 Effects on Bone

Using the NIH definition that osteoporosis is an increased propensity to fracture, the effect on bone is self-evident. As discussed (illustrated by Figure 16), increased fracture risk (that is osteoporosis) is strongly linked to ageing. Though age-related fracture risk also relates to factors extrinsic to the bone (i.e. likelihood and severity of a fall), the ability of the bone to withstand a fall significantly reduces with age due to the changes in hormones, exercise, nutrition and lifestyle as discussed. Burstein et al [162] found the strength of bone to reduce by around 2 - 3% per decade (from twenties to eighties) and the stiffness by 1 - 2% but more marked were the reduction in maximum strain or

ductility (6% per decade) and energy absorption or toughness (9% per decade). The most significant drop in material properties tended to be when individuals were moving into their fifties and sixties, the time of the menopause in women. The fracture toughness, the ability to tolerate cracks (present in all materials and bone is no exception) also significantly reduces by 40% over six decades (age 34 – 99, 6% per decade) with the reduction being greater after middle-age (age 61 - 99) [163]. As well as being the most significant, the toughness and fracture toughness are also the most clinically relevant, relating to how well bone performs under extreme circumstances such as a fall.

As discussed, bone has a complex hierarchical structure that is optimally suited not to break during normal loading. But it can be seen that with age and (by definition) osteoporosis, that bone can become mechanically compromised and have an increased risk of fracturing, beyond that explained by BMD alone. This can be related back to changes that have been measured throughout the hierarchical structure. If it was clinically viable to assess these changes in bone quality, those at risk of fracture could therefore potentially be directly identified.

3.1.2.1 The Bone Cells

In postmenopausal women the bone turnover is accelerated [17]. Additionally, there is thought to be a disconnect between osteoclasts and osteoblasts with increased osteoclastic resorption relative to the osteoblastic formation [164], primarily driven by the changes in oestrogen levels. This disconnect leads to a net loss of bone, as understood by the conventional BMD definition of osteoporosis, but also changes in the structure from the nano to the macroscopic level [14].

The overall mechanosensitivity of bone tissue also reduces with age. This is demonstrated by a reduction in number of lacunae [165] and increase in empty lacunae leading to an overall reduction in osteocyte number [166]. The mechanosensitivity of the osteocytes themselves does not seem to reduce with age alone [167] but reduced number has been suggested to lead to an overall increase in the remodelling threshold at the tissue level [168]. However, with osteoporosis, there is an additional reduction in osteocyte sensitivity, further reducing the adaptive nature of the bone and the ability to repair microcracks [167, 169].

Starting again at the nano-level, this review will consider the changes of bone's structure with osteoporosis and ageing and how this may compromise the important strengthening and toughening mechanisms previously highlighted.

3.1.2.2 The nano-scale: Principal components and the mineralised collagen fibril

With a reduced toughness of bone, changes to the collagen, the component providing bone's resistance to deformation, would be expected to be a major culprit and Nalla et al [163] confirmed this. They observed a change in the collagen composition, as seen through Raman spectroscopy, with age and also observed disorder in the typical banding structure (68 nm overlap, 35 nm gap [61]) of the fibrils. These changes lead to a substantial reduction in the nano indentation modulus in the older bone from 1.22 GPa to 0.22 - 0.78 GPa as shown below in Figure 17.

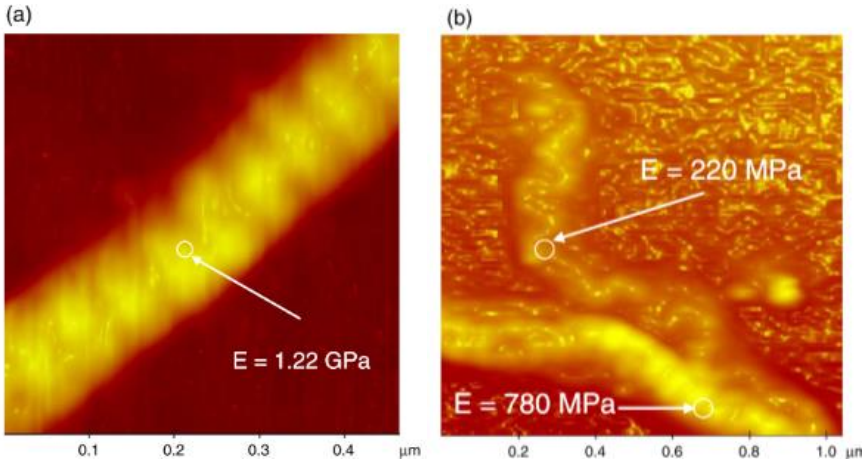

Figure 17 – Image reprinted from Nalla et al [163] courtesy of Elsevier, AFM images of the nanoindentation of collagen fibrils from a) Young (37 years) and b) Aged (99 years) donors

As for the mineral crystals, age is generally thought to increase the overall mineral content (therefore reducing the relative content of the toughening collagen) leading to the more brittle structure. Perhaps more importantly, the shape of the crystal has been seen to change, becoming rounder with size increase [52, 170]. Paschalis et al [171-173] used FTIR (Fourier Transform Infrared Microspectroscopy) to show that the level of crystallinity was increased in bone at the endosteum and centre of the trabeculae (older bone) compared to more recently laid down bone at the periosteum and trabecular surface (younger bone). The large aspect ratio of the crystals is important to allow alignment within the collagen fibrils and give bone its anisotropy and the size of the crystals is critical. An increase in crystal size may shift their dimensions above the tens of nanometre critical crack size for the mineral [55, 56], potentially losing their vital

tolerance to flaws as shown in Figure 18. Though this crystal size has not been measured in old age or osteoporosis, it would have to increase beyond the 100s of nanometres as previously approximated using the Griffith's criteria.

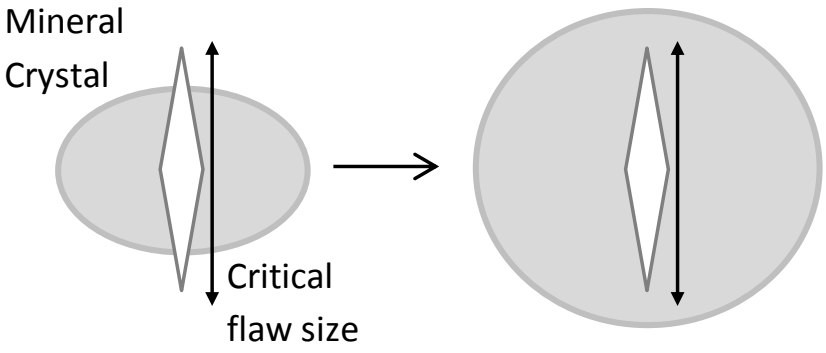

Figure 18 - Increase in mineral size may lose tolerance to flaws

The mineral-mineral as well as the mineral-collagen bonds (NCPs) and inter-collagen bonds (crosslinks) are in a careful balance as to dissipate energy through sliding but not over constrain and stiffen the fibrils [81, 82]. NCP content [70, 174] and, particularly, crosslinking density [175] have been found to shift from this balance with osteoporosis. The NCP content reduces both with age, but even further with osteoporosis when matched for age [174]. The NCPs control mineralisation [65] so their reduction could contribute to the increase in crystal size and, acting as a glue, bonding would be weakened within the mineral, between mineral and collagen, between mineral and mineral and in the cement lines [66, 68, 70]. With age there is an increase in mature crosslinks (up to 60 years) but a reduction in immature crosslinks [63, 170, 175, 176] maintaining the overall level. With osteoporosis this reduces, making the collagen less stable [83]. Additionally, the number of non-enzymatic crosslinks, the AGEs, are increased with osteoporosis and age, leading to an overall stiffening and increase in brittleness that is thought to increase the quantity of microcracks [83, 86].

Nyman et al [73] hypothesised an age-related effect on water content and distribution. They suggest water in the tissue (bound to collagen) would decrease and preferentially pool in the pores that increase in number and size with age. As water is known to be vital to hydrate the tissue for mechanical performance [73, 74] and mediate the h-bonds that give collagen its robust nature [72], this theorised water displacement could be a potential contributor to reducing bone's toughness.

3.1.2.3 The micro-scale: Lamellae and the Osteon

With age, the number of microcracks exponentially increases [177] leading to a reduction in mechanical competence of the whole bone (i.e. a 2 - 3 fold increase in number of microcracks leads to a 20% reduction in fracture toughness) [170, 178]. As mentioned, microcracks, when correctly orientated and in the right quantity, may act to disperse the crack tip but an increase in density or alignment makes it substantially easier for the crack to propagate. Microcracks form in the cement lines and lead to uncracked ligament bridging creating another strengthening mechanism. But with age, this is also compromised. Nalla et al [163] find uncracked ligaments to be present in both young and old specimens but to decrease in size (by 30 - 40%), number and, therefore, implied efficacy with age.

The properties of an individual osteon do not appear to change with age [74], but there is still an extremely important change at this level. The osteon density increases, nearly doubling with age [163], and, therefore, the average diameter decreases and numbers increase [88, 163, 179]. The mechanisms of crack deflection and uncracked ligament bridging relate to the osteons and their cement lines and strongly influence the fracture toughness of bone [88, 109, 112], meaning this increase in osteon density has a significant effect. A reduced osteon size means cracks do not have to deflect as much to follow the cement line and consequently dissipate less energy (Figure 19) [179]. Whereas, the cement line spacing is also reduced, shortening the length of the uncracked ligaments as found by Nalla et al [163] and having a reduced effect in bridging the crack and contributing to fracture toughness (Figure 20).

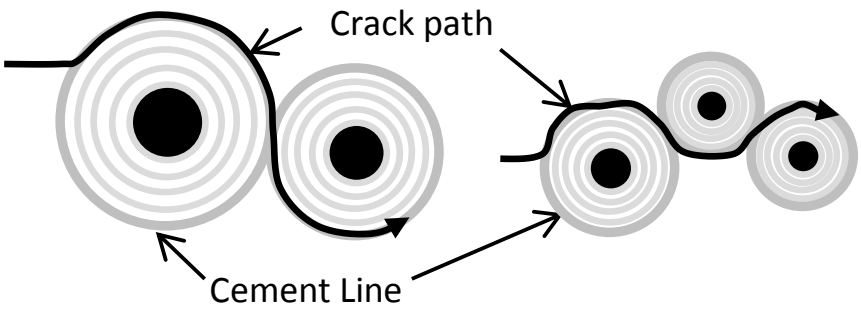

Figure 19 – Left: Osteons in young healthy bone. Right: Increased osteon density in old osteoporotic bone reducing the tortuosity of the crack part

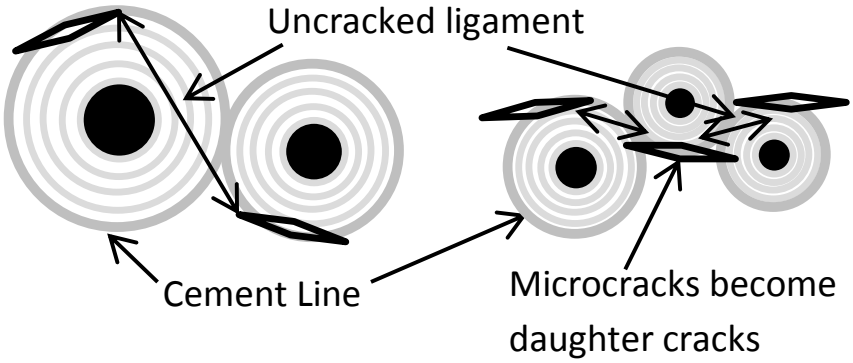

Figure 20 – Left: Osteons in young healthy bone, Right: Increased osteon density/decreased cement line spacing, reduces the size of uncracked ligaments

Recently, Katsamenis et al [24, 180] also found homogeneity between nano-elasticity of the lamellae and interlamellar layers to be positively correlated to fracture toughness ($r = 0.8$) and being more homogenous in elderly bone. This would lead to reduced strain distribution [98] allowing for increased crack initiation and follows with the reduced tortuosity [24].

Again considering the osteonal structure and its alterations to have a significantly large effect on fragility and be altered by disease, assessment of bone quality at this level may best be able to identify aspects of fracture risk.

3.1.2.4 The macro-scale: Cortical and Cancellous bone

At the macroscopic scale there is also a change in the structure of the cortical and cancellous bone.

Remodelling and the formation of new bone, occurs more at the outer (periosteal) rather than inner (endosteal) surface of the cortical bone that forms the central tube of the femur. This leads to a general increase in diameter of the femur with age and also, particularly in women, a thinning of the cortex [34, 88]. Considering basic mechanics principles, a reduction in cross sectional area reduces compressive strength, while thinning significantly reduces the bending strength. At the same time, porosity also increases [176, 181], lending to the reduced toughness. In aged osteoporotic individuals, the cortex preferentially thin in the superolateral region [182]. This is particularly detrimental when loaded in compression during a fall scenario where the thin bone may buckle and initiate fracture, whereas the inferomedial neck that remains loaded in stance, is for the most part protected from thinning or changes in porosity [181, 182].

As for cancellous bone, where remodelling becomes more negative (more osteoclast resorption) on the outer surface of the trabeculae [34], there is a thinning (50 - 70% volume loss from 20 - 90 years [183]) and a loss of connectivity (particular horizontal struts being resorbed [17]). Less load can be supported by the reduced volume and, considering the Euler principal (the load that can be supported is proportional to the inverse of the square of the length) [17] the unsupported length of the trabeculae is increased by the loss of horizontal supports, increasing susceptibility to buckling.

In spite of the general consensus that osteoporosis, as a disease beyond ageing, has a directly detrimental effect on the material properties, in terms of the cortical bone, there is surprisingly limited evidence for this [184] and the majority of the changes discussed above relate to age alone. Investigating the material properties of bone, Dickenson et al [185], compared cadaveric bone from those who had disuse osteoporotic fractures with those who had not sustained a fracture. Samples were machined from the femoral midshaft for testing in tension with the modulus (11.5 GPa compared to 15.6 GPa), strength (95 MPa compared to 117 MPa ultimate strength and 76 MPa compared to 81 MPa yield strength) and plastic energy absorption (0.40 MJm^{-2} compared to 0.98 MJm^{-2}) all being significantly reduced in the disease state. Diez-Perez et al [19] and Milovanovic et al [28] also compared fractured to non-fractured cortical bone finding impaired material properties in terms of reference point microindentation (in vivo and in vitro respectively), the focus of this thesis which will be detailed in later sections. However, though fracture toughness has been demonstrated to reduce with age [24, 163, 179] a putative reduction in osteoporosis is yet to be confirmed. This was evidenced through a review of the literature search for “osteoporosis AND toughness” at the Web of Knowledge database [186] which returned 142 publications, none of which compared the fracture toughness properties of human cortical bone with and without fracture. This may relate to the difficulties in obtaining samples and the clinical lead research focussing on measureable factors such as microarchitecture rather than material properties (e.g. qualitative ultrasound, peripheral quantitative computed tomography and magnetic resonance imaging discussed in ‘9.1 Appendix 1 – Clinical Assessment of Bone Quality’). Regardless, this demonstrates a gap in knowledge with an unexpectedly limited amount of research directly comparing the effects of osteoporosis on the properties of cortical bone.

3.1.3 Diagnosis and Treatments

3.1.3.1 Bone Mineral Density

Fracture risk assessment is currently centred on bone quantity as assessed through bone mineral density via DEXA (or DXA – Dual Energy X-Ray Aborptiometry) techniques. Broadly (detailed in section 4.3), BMD is a measure of bone quantity, how much bone is present i.e. more bone mineral increases the absorption of radiation, increasing the DEXA derived BMD. DEXA gives a good indicator of prevalence of fracture risk for a population [2] and those with reduced BMD are more likely to fracture. Several authors [9, 187-189] report a 1 standard deviation reduction in BMD relating to a doubling or even tripling in fracture risk. A meta-analysis by Marshall et al [189] found BMD prediction was similar to blood pressure for diagnosing stroke and cholesterol for predicting cardiovascular disease but regardless, BMD was not recommended for screening. This is due to a large degree of overlap between BMD for individuals with and without fracture leading to a poor sensitivity (many with the disease are not detected) for a given specificity (rate of incorrect diagnosis). This relates to a low Receiver Operatory Characteristic Area Under the Curve (ROC AUC) for DEXA. The ROC curve is a plot of sensitivity versus specificity for varying thresholds, with an AUC of 0.5 indicating random detection and 1 indicating perfect detection (i.e. 100% sensitivity and 100% specificity) (Figure 21). For DEXA this value is in the region of 0.70 to 0.80 [190, 191].

$$\text{Sensitivity} = \frac{\text{True Positives}}{\text{True Positives} + \text{False Negative}} \qquad \text{Specificity} = \frac{\text{True Negatives}}{\text{False Positives} + \text{True Negatives}}$$

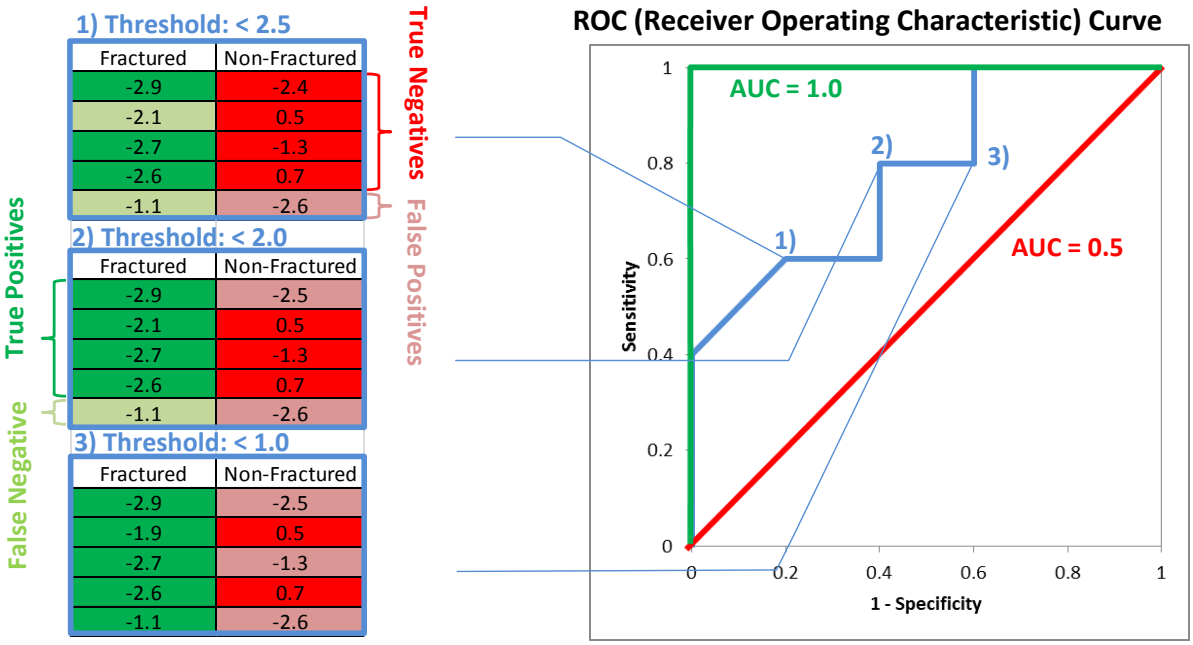

Figure 21 – Demonstration of sensitivity, specificity and the receiver operating characteristic curve

The operational WHO definition that osteoporosis occurs at 2.5 standard deviations below the normal was found to be ineffective for predicting fracture. Schuit et al [11] considered the Rotterdam study with 8000 patients to find that low BMD was most effective at predicting hip fractures in women (64% identified, it's sensitivity) but for any non-vertebral fracture, the majority of women weren't identified (44% identified) and this was worse for men (21% identified). Siris et al [10], considering peripheral forearm measures in the larger NORA observational study (around 150,000 postmenopausal women), found 82% of women who fractured were not osteoporotic by the WHO definition.

3.1.3.2 Clinical Factors

To attempt to improve fracture risk assessment, clinical factors have been combined with BMD. These factors do not directly relate to bone quality (structural and mechanical properties) but relate to the risk factors and causes for the reduction in quality and increased fracture risk.

The previous section (section 3.2.1) discussed the increase in relative risk with a number of clinical risk factors (poor nutrition, inactivity, hazardous lifestyle, disease etc.) showing

presence of these risk factors to have an adverse effect in beyond low BMD. Cummings et al [192] showed the risk of fracture to increase when multiple risk factors (e.g. history of fracture, drug use, high caffeine and low activity) were present or with risk factors alongside low BMD as shown in Figure 22.

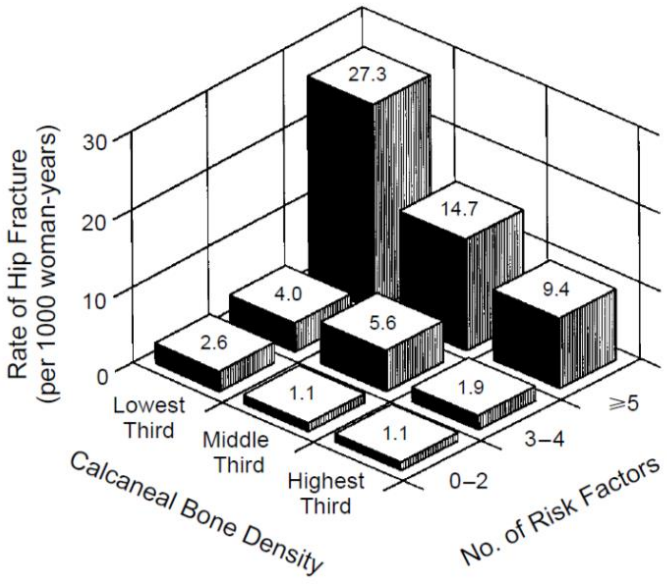

Figure 22 – The effect of multiple risk factors and BMD on the risk of fracture. Image reproduced from Cummings et al [192] with permission from NEJM, Copyright Massachusetts Medical Society

Alone, these clinical factors also have poor specificity and sensitivity, but when combined with BMD the diagnostic power is improved (from ROC AUC of 0.67 with risk factors alone to 0.78 alongside BMD) [9, 193]. Sandhu et al [194] considered the Garvan model (age, sex, body weight, history of prior fracture, history of falls, femoral neck BMD) and FRAX (additionally: height, parent fracture, smoking, glucocorticoids, rheumatoid arthritis, secondary osteoporosis and alcohol but no fall history, further described in 4.4) to find the probability of fracture, assessed by either tool, was increased in fractured individuals (1.6 - 2.2 factor increase). However, the ROC was as low as 0.52 (and a maximum of 0.84) for both models and, similarly, 0.63 for FRAX in a study by Tremollieres et al [13], therefore, requiring combination with BMD for improved clinical fracture risk assessment. Hillier et al [195], reported improved ROC values when FRAX was combined with BMD but still below 0.80 implying further factors could improve fracture risk assessment. With lack of correlation to material properties (toughness) [196], assessment of these aspects of bone quality could therefore complement existing techniques.

Blood and urine samples can be taken to identify further risk factors including vitamin D, calcium levels, hormone (PTH and Oestrogen) and bone turnover markers. However vitamin D and hormone levels were found to be comparable between fractured and non-fractured individuals by Sandhu et al [194]. As osteoporosis is caused by increased bone turnover with increased resorption relative to formation, markers that show the levels of osteoblastic (such as NCP secretion) and osteoclastic (such as phosphatase levels – the acid produced in resorption) activity indicate a doubling in fracture incidence independent of BMD [9, 197]. Chapurlat et al [198] and Ross et al [199] looked at CTX, a resorption marker based on collagen breakdown, finding it to be greater in fractured women, again doubled risk of fracture. However, urinary markers were less effective, depending on the time of day they were taken. These markers provide further information in addition to BMD but only give an indication of turnover at that moment in time, not indicating the lifetime effects on bone. Serum measurements, similar to clinical factors, would also be expected to contribute to fracture risk. However, bone quality is likely also a predominant factor in fracture risk and currently, particularly the material property aspect, cannot be assessed. Any technique, such as RPI investigated here, that purports to measure this element of fracture risk would have to be tested for its efficacy in comparison to existing factors (e.g. BMD, FRAX, blood markers) to assess any supplementary improvement on current techniques.

3.1.3.3 Treatment

Following diagnosis, osteoporosis can be treated with drug therapy. Various different treatments are available and their level of success depends greatly on whether BMD increase or fracture risk reduction is assessed. Deal [8], Cefalu [164], Häuselmann and Rizzoli [7] and Unnanuntana et al [197] review the literature to discuss the effects of osteoporotic drug therapies and the similarities and discrepancies between BMD increase and fracture risk reduction.

Bisphosphonates are a class of drug that are absorbed into the mineral crystals of the bone making it more difficult for osteoclasts to resorb [8]. These are currently widely used in treating osteoporosis with the two most common types, Risedronate and Alendronate acting to increase hip BMD around 6% after 36 months [8] but also reduce the chance of hip fracture by 40 - 60% at 2 - 4 years [7]. This is achieved not just by increasing the BMD, but also preserving the microarchitecture such as cortical shell

thickness and cancellous connectivity [164]. Potentially other microarchitectural features as discussed above are also affected but a reliance on BMD means these are not typically investigated.

Despite having the same trend, BMD only accounts for a maximum of 18% [197] of the fracture risk reduction with these drugs with the microarchitecture and other currently unknown factors making up the difference. Black et al [200] find Alendronate to reduce the risk of subsequent hip fracture in those with an already existing vertebral fracture (50% fracture risk reduction) but be less effective in those who have never fractured (20% reduction). Whereas Cefalu [164] reviews Risedronate to find it proves effective at reducing fracture in both cases (40% to 60% reduction), beginning to show fracture risk reduction after 12 months and increasing up to 3 - 4 years [200].

Alendronate and Risedronate are taken orally at 5 or 10 mg/day (now more commonly 70 mg and 35 mg weekly) [200] but it has been suggested that the regular dosage leads to patient non-compliance [197, 201]. This has led to trials considering bisphosphonates with less frequent doses such as annual infusions of Zoledronate (5 mg for 15 years [202]) or intermittent doses of Ibandronate (20 mg every other day for 12 doses every 3 months [201], now 150 mg/month orally or 3 monthly intravenously). Both found a 40 to 60% reduction in fracture risk after 3 years.

Recently, the FDA (Food and Drug Administration, US) have reviewed the long-term use of bisphosphonates, suggesting that continuation after 5 years may not provide continued fracture risk reduction but have serious adverse events including atypical femoral fractures and osteonecrosis of the jaw [203, 204]. Black et al [205], found that the case of subtrochanteric and diaphyseal fractures were marginally increased with long-term alendronate and zolendronate use but the overall incidence was still low (2.3 fractures per 10,000 patient years).

Cefalu [164] also considered Raloxifene, a drug that affects the oestrogen receptors, to attempt to counter the hormone changes due to the menopause. Again, Raloxifene increases BMD, but by a lower 3%, this time only explaining 4% of the 30 - 50% reduction in fracture risk [164]. Instead of affecting the body's production of oestrogen, oestrogen can be given directly with hormone replacement therapy (HRT). Cefalu [164] found this to have a 7.5% BMD increase and 35% vertebral fracture risk reduction after 6 years. Deal [8]

agrees with the use of oestrogen hormone replacement as an effective therapy but suggesting that it may need to be continued for life to maintain the bone quality and cessation would dramatically increase fracture risk. Despite this, HRT is generally contraindicated due to increased cancer risk, particularly breast cancer. Though mortality is lower in those without HRT therapy and breast cancer risk is only moderately (but significantly) increased, as this is principal cause of death in postmenopausal women, the treatment must be discounted in all but extreme cases [206].

Deal [8] also considers another hormone, calcitonin, that inhibits osteoclasts, reducing resorption and Cefalu [164] finds this to reduce vertebral fracture risk by 30 - 40% but with no effect on the hip and only altering the BMD less than 1%. Girota et al [207] considered PTH which can thicken bone and increase trabecular connectivity in high risk cases. Though, in the long term, PTH reduces formation relative to resorption i.e. catabolism (to reclaim minerals to the bloodstream), in the short term there is an 'anabolic window' where formation is substantially increased above resorption. Therefore, PTH (or a fragment of the molecule, Teriparatide) can be used to intermittently and in low doses if followed up by an antiresorptive therapy for long-term treatment. Nutrition, particularly calcium in combination with other nutrients (e.g. vitamin D and phosphorous) as well as exercise or reduction of caffeine, alcohol and smoking would also have a benefit in treatment as well as being causal as previously discussed [7].

Denosumab, is a human antibody that targets RANKL (a protein involved with bone metabolism) inhibiting osteoclast development and activity. Cummings et al [208] found a 60 mg injection every 6 months reduced the risk of vertebral (70%) and hip (40%) fracture at 3 years. This was also associated with a 6 – 9% increase in BMD as well as an 80% reduction in resorption and formation markers. This therapy has been proposed to be advantageous by affecting osteoclast formation as well as function, having no major reported complications and 6 month injections rather than daily tablets reducing non-compliance [208].

Many other treatments have been considered and new treatments are always being developed but the big question 'what makes an effective treatment?' is still difficult to answer. Though BMD increase is effectively treating WHO defined osteoporosis, is this really an important focus? The devastating clinical event, the fracture, is what is trying to

be avoided, consequently, new osteoporosis therapy trials must consider this as an end point. Fracture can assess treatments efficacy, but when it comes to monitoring intervention in an individual, fracture would be a rather too little too late approach. Therefore, BMD must be relied upon as with diagnosis but, because this only explains a small portion of current treatments effect, supplementary monitoring measures are essential. Sodium fluoride is the case in point, Deal [8] discusses an impressive 35% BMD increase over 4 years but with no fracture risk reduction, Häuselmann and Rizzoli [7] even found an increase in hip fracture incidence despite increased femoral neck BMD. For this reason there is a paradigm shift away from BMD alone towards measures such as clinical factors being utilised for follow-up, similar to diagnosis. However, these suffer from the discussed limitations (3.1.3.2) and assessment of further elements of fracture risk, bone quality measures, would supplement drug development and efficacy monitoring. To establish these bone quality measures it needs to be better established what osteoporosis is. That is, a detailed definition that incorporates not just BMD, but all changes to the bone's hierarchy that lead to its overall increased fragility with ageing and disease. Clinical assessment of these properties is then critical to assess fracture risk.

3.2 Osteoarthritis

Osteoarthritis is not the primary focus of this study, which investigates the assessment of fracture risk and changes in bone with osteoporosis, and therefore is covered in reduced detail. Nonetheless, osteoarthritic bone has been assessed through Reference Point Microindentation and fracture toughness testing because it is a prevalent bone disease that is debilitating for the sufferer.

Like osteoporosis, increasing age and sex are risk factors for osteoarthritis which occurs most commonly in elderly women between 70 and 80 years. There are up 600 newly reported cases of osteoarthritis per 100,000 women per year [209] but it is also prevalent in men with up to 20% of men compared to 25% of women over 80 suffering from the condition [210]. Osteoarthritis is characterised by degradation of synovial joints leading to pain for the individual. Additionally, there is associated loss of mobility and range of motion as well as joint stiffness and inflammation that, together, leads to physical disability in 4-5% of cases [210]. Particularly of the knee, the associated disability is characterised by difficulty in walking and climbing stairs. Annually, this impairments costs over $16 billion in the US (1994 estimate [209]) and approximately £4 billion in the UK

[211]. The main proportion of this cost is lost working hours due to the incapacitating nature of the disease and its incidence increasing from a relatively young age (50-60 years) [209, 210].

Theoretically, any synovial joint can be affected but it is most prevalent in the knee, hip, hand and spine with the osteoarthritis of the knee being most disabling [212].

3.2.1 Risk factors

Age is the biggest risk factor in osteoarthritis as, though it is possible to limit the disease progression or provide temporary relief, it is not reversible so the cumulative number of sufferers increases. This begins from 50 to 60 years and is most elevated at 65 to 75 years, largely contributing to the functional limitations with old age [210]. This age related development primarily relates to changes in cartilage composition and structure through reorganisation of the extracellular matrix structure and composition (i.e. the type II collagen and proteoglycans) and the accumulation of AGEs, stiffening the collagen (as in bone). Also similarly to bone, the ability of the remodelling cells (chondrocytes) to sense and repair damage is reduced by age [212].

Sex also contributes with females being more at risk, even if this sex effect doesn't appear as marked as in osteoporosis. Like osteoporosis, this gender difference may relate to alterations in sex hormones post-menopause. Oestrogen acts on chondrocytes in vitro and, though the evidence is mixed as to whether oestrogen has any direct impact on osteoarthritis, the prevalence does appear to reduce where hormone replacement therapy is taken post-menopausally [213, 214].

There is also a genetic link for osteoarthritis, with a family history in 50% - 70% of cases [212, 213, 215]. Some of these genetic markers, such as those relating to collagen, also relate to osteoporosis, but others relate specifically to cartilage and osteoarthritis [215].

Nutrition additionally plays some influence, with vitamin C and vitamin D perhaps being protective from osteoarthritis due to their relationship to collagen synthesis and in bone metabolism respectively [209, 213]. Poor nutrition may lead to obesity and this leads to increased risk of osteoarthritis, primarily attributed to overloading of the joint resulting in wear of cartilage but potentially linked to metabolic factors associated with increased adiposity [210, 212, 213]. This alteration in biomechanics, as with the increased loading

due to obesity, is a key influencing factor in osteoarthritis. This can additionally be altered through injury, muscle weakness, repetitive overloading and joint deformity.

Acute injury, commonly meniscal or cruciate ligament tears, can increase cartilage shear [209] or, in a similar fashion to muscle weakness, lead to laxity and instability of the joint [213]. As with osteoporosis, where excessive exercise can stimulate the accumulation of microdamage, this can be disadvantageous for the joint. For professional athletes (particularly runners) and those with very manual jobs (e.g. farmers), the excess repeated loading can damage the joint [210, 213]. Finally, joint deformities play a severe role in causing osteoarthritis. Deformities include Legg-Calve-Perthes (a disorder developing during childhood due to vascular restrictions), slipped capital femoral epiphysis (growth plate fracture) and multiple epiphyseal dysplasia (abnormal mineralisation of the epiphysis), and, though rare, lead to osteoarthritis [209, 213, 216]. The review by Ganz et al [216] suggests that even joints not classified as deformed, may still present minor deformities. These include the 'pistol grip' deformity (cam deformity - femoral head tilting relative to the neck) or undeveloped major deformities (e.g. hip dysplasia) with up to 90% of radiographically undetected osteoarthritis relating to these deformities. Though these deformities are minor, the biomechanics can be severely altered causing impingement between the femoral head and acetabular cup, shear of the epiphysis and altered loading of the bone [216].

3.2.2 Relationship to Osteoporosis and Effects on Bone

As discussed, osteoarthritis is typically defined by the degenerative impact it has on cartilage. The articular cartilage thins and stiffens and the efficacy of the chondrocytes is reduced meaning that the tissue becomes more susceptible to damage and less capable of repair [212, 217, 218]. Though this deterioration of cartilage is characteristic of osteoarthritis, subsequent changes to the bone represent advancement of the disease [219]. It can also be argued that changes to the bone such as the described deformities, properties of subchondral bone, trabecular distribution and overall BMD in fact proceed and are causal of cartilage damage [216, 220].

The changes to the properties of the bone tend to be altered in a starkly different manner to osteoporosis and hip fracture is hence reported to be rare in patients with osteoarthritis. In comparison to osteoporosis or non-diseased controls, the trabecular

bone in the osteoarthritic femoral head is reported to be thicker with improved connectivity [221-223] leading to an increased mechanical properties, primarily stiffness [222, 224]. However, this does appear to depend on the progress of the disease and location of the bone. Bone may thin in early osteoarthritis and potentially lead to an over-compensatory bone formation, with increased osteoblastic activity causing the ultimately thicker, stiffer (sclerotic) trabecular bone [220]. Furthermore, Neilson et al [225] observed that there is only an increase in load-bearing regions of the trabecular bone and a diminishing of the number and thickness of trabeculae in the non-weight bearing regions of the inferomedial femoral head.

In terms of the subchondral bone and growth plate, the changes osteoarthritis may cause softening [224] but it is more commonly agreed that the plate thickens and becomes sclerotic [218, 220, 221]. The discrepancies may again relate to the stage of the disease with the increased, and perhaps poorly regulated, remodelling in the later stages of the disease also causing the formation of osteophytes, bony spurs that form along the edges of the joint [212, 213, 219, 221]. These osteophytes, and other changes to the bone such as bone marrow lesions or oedema and subchondral bone defects, [217, 220] due to the innervation of bone, lead to the pain associated with progressed osteoarthritis [226].

This stiffening and increase in trabecular bone volume also increases BMD relative to controls and particular in relation to osteoporotic patients (approximate doubling) [209, 213, 222, 227]. However Rubinacci et al [221], used high resolution quantitative computed tomography, rather than areal BMD, and calculated volumetric BMD, avoiding artefacts such as osteophytes, to find that the cortical and trabecular density actually remained fairly consistent between osteoporosis and osteoarthritis. Even though the increased bone density and stiffening of the trabeculae do not directly transfer to an increase in strength, osteoarthritis may still protect against hip fracture to some extent [227]. It is generally considered that osteoarthritis and osteoporotic fracture in the same individual are rare [209, 210, 220] but they are clearly not completely mutually exclusive. Bobinac et al [218], showed that femoral heads from neck fracture patients had a lower osteoarthritic grading than the osteoarthritic samples but still some fractured samples also had high levels of osteoarthritis. Furthermore, Vestergaard and Rejnmark [227] considered all individuals sustaining a fracture in Denmark (over 100 thousand individuals) against three times as many controls matched for age and sex from the population. The

study found that the risk of hip fracture was increased up to 2 years post diagnosis of osteoarthritis and after this period (particularly after 5 years) the risk of fracture was significantly reduced. Therefore, perhaps early stage osteoarthritis has a weakening effect on the bone, predisposing it to fracture, but as the disease progresses, bone formation and BMD is increased, reducing the risk of fracture but clearly not eliminated.

In terms of this study, and in terms of osteoporotic fracture, the principal site of interest is the cortical bone and the femoral neck. The changes in properties of the neck, due to the focus on the affected cartilage and femoral head, are again under reported. The geometry of the femoral neck appears more elongated in osteoporosis (a larger inferomedial-superolateral to anterior-posterior ratio) but rounder in osteoarthritis [221]. Furthermore, the area or thickness of the cortex is larger in osteoarthritic bone [221, 223, 225, 228]. It may not just be that the thickness of the osteoporotic bone reduces relatively to those with osteoarthritis, but, where the inferomedial region is in compression, the superolateral region preferentially thins [182, 221, 228, 229]. Because the superolateral region is then in compression in a fall scenario, the thin cortex may then buckle and initiate fracture in osteoporotic patients, whereas in osteoarthritis, where the cortical thickness remains more uniform, this may reduce the fracture risk [221, 228]. Li and Aspden [224] carried out the only study that we are aware of to investigate the material properties of the femoral neck in osteoarthritis, comparing the calcar (inferomedial neck) across fractured and osteoarthritic samples with age matched cadaveric controls. The ultrasound derived stiffness (as well as the ash density) were found to be consistent across these three groups. Therefore, due to this limited knowledge of material properties of the femoral neck, further evidence is needed to increase understanding of osteoarthritis.

3.2.3 Diagnosis and Treatments

Osteoarthritis is detected by frequent joint pain alongside radiographic evidence of structural changes. Pain and loss of mobility are the governing symptoms that are initially patient detected but without radiographic identification, this does not necessarily relate to osteoarthritis (e.g. rheumatoid) [213, 217]. Similarly, radiographic evidence alone does not identify osteoarthritis so both features are necessary to define the disease. Radiographic osteoarthritis grading relates to the Kellgren-Lawrence [219] or overall Croft scores [230] with presence of joint space narrowing, osteophytes, cortical sclerosis,

cortical collapse of the femoral head and subchondral cysts all indicating increased levels of the disease. Assessment can be further supplemented through magnetic resonance imaging (MRI) to identify features such as bone marrow oedema and cartilage defects [217, 220] or collagen degradation and cartilage metabolism markers in the serum or urine [212, 220, 231].

The first stage of treatment should always relate to prevention such as controlling the risk factors previously described. Of these, only really over-loading through obesity or during a heavily manual job or excessive physical activity can really be controlled and acted upon, though vitamin C and D may also have some benefit [209, 213]. Once detected through structural changes or pain the disease has progressed and prevention is not possible. The next stage can still relate to changes in these risk factors (e.g. weight loss) and, if the disease has not progressed critically, bracing and orthotics can be considered (more notably for the knee) and pain can be managed through analgesics and inflammation reduced through NSAIDs (non-steroidal anti-inflammatory drugs) [226]. With further progression of the disease, stronger painkillers (i.e. opioid analgesics) and intra-articular steroid injections (reducing inflammation in the short term) can provide relief [226]. However, where the disease is progressing, ultimately surgical intervention will likely be necessary. This can be minimal such as arthroscopy (joint debridement and lavage to remove particles), but may only provide temporary or no relief. Osteotomies can also correct deformities and regain biomechanical loading but arthroplasty is likely to be necessitated. Minimal resurfacing of the damaged articular surface could be taken in the first instance as a conservative approach. However, total hip replacements are often primarily carried out [210](85% of all hip replacements are due to osteoarthritis rather than hip fracture or other conditions) due to their level of success (up to 95% survival at 15 years with regained function and reduced or eliminated pain) [226].

Compared to osteoporosis, osteoarthritis can be effectively diagnosed but, nevertheless, little is understood about the cortical bone that may be affected through alterations in biomechanical loading or remodelling. The assessment of material properties, particularly in comparison to osteoporotic bone due to the reduced osteoarthritic fracture risk, therefore has potential to uncover further knowledge of both bone diseases.

4 Experimental Techniques

The main experimental techniques utilised in this thesis are presented in this chapter. The specific implementation of these techniques is then detailed within each 'Materials and Methods' section of the three results chapters (Chapters 5, 6, and 7).

4.1 Reference Point Microindentation and Indentation Techniques

4.1.1 Indentation Techniques

This study is specifically focussing on a new indentation technique, Reference Point Microindentation, however to interpret this technique, a general understanding of indentation techniques is first important. The following summary of macroscopic, micro and nanoindentation techniques primarily relate to literature reviews by Lewis and Nyman [232], Zhang et al [233] and Zysset [234].

At the macroscopic or tissue level, indentation has historically been applied for the assessment of hardness. A variety of techniques have been used, primarily, Brinell and Rockwell (spherical tipped indenters) and Vickers and Knoop (pyramidal indenters) [234]. Though the indenter geometry varies between these techniques, the core principles remain the same; indentation of a material under a known load and calculation of the resulting imprint area either through direct imaging or extrapolation from indent depth. The hardness value (except for Rockwell hardness using a graded scale) is proportionate to the load applied and the inverse of the indent area. Therefore, lower load required to produce a larger indent implies lower hardness, a softer material. Rather than direct imaging of the indent imprint, the probe depth can be assessed and the indent area extrapolated from the tip geometry [234]. For this to be valid, the geometry of the tip must be known through imaging the tip itself, or more commonly, imaging an imprint left by the tip in a material of known properties. The contact area assessed through direct imaging of the imprint is preferable to that derived by the indentation depth. This is because the elastic response of the material means the indentation depth is a function of unloading as well a loading but only a single value (e.g. max depth) can be used to extrapolate the imprint depth and area. Additionally, sinking in (a curved transition between the imprint edge and slope where the indenter drifts into the material) and pile-up (a bump forming around the edge of the indent due to the elastic response of the

material) lead to underestimations and overestimations of the contact area (and hence elastic modulus or hardness) respectively [234, 235].

An indentation curve (shown in Figure 23) involves loading to a maximum load at a constant rate then unloading at the same rate. A hold period can be included between the loading and unloading period to minimise the effects of creep and thermal drift on the unloading portion of the curve. Based on this curve, an elastic modulus can also be calculated for the material.

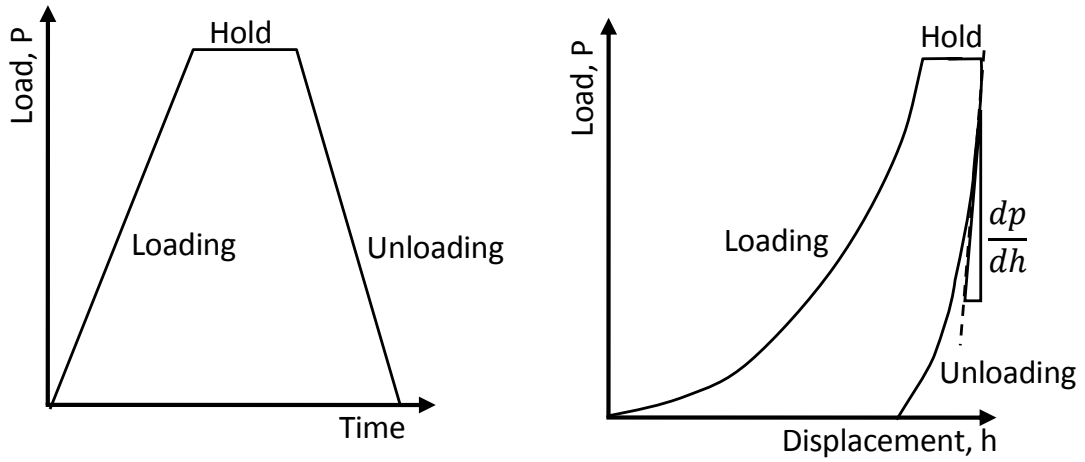

Figure 23 – Typical load-time (left) and load-displacement curves for indentation including a loading (constant rate), hold (constant load) and unloading (constant rate) portion

The Oliver-Pharr [236] method is perhaps the most commonly implemented method for assessing the indentation modulus. This technique uses a Berkovich tip; a triangular pyramid with the same area-depth function as a Vickers tip (square pyramid) and similarities to a conical indenter (contact area is proportional to the depth squared, the point is nominally zero and the load-displacement relationships are non-linear for both) [236]. The indenter is applied to the material with constant monitoring of the load-displacement which is crucial to assess the unloading curve slope and hence the reduced elastic modulus as described by Equation 2.

Equation 2 – Calculation of the reduced elastic modulus (Er) from indentation techniques based on the slope of the load-depth unloading curve (dp/dh) and the indent contact area (A) [236]

$$E_r = \frac{1}{2}\frac{dp}{dh}\sqrt{\frac{\pi}{A}}$$

A power law relationship is applied to the unloading curve with a least-squares fit and the contact area is related to the indent depth by an indenter geometry relationship [232,

236]. Variants on the Oliver-Pharr technique also exist including: the Gong, Miao and Peng method that directly relates reduced modulus to the unloading slope excluding contact area; the Bao, Wang and Zhou method that calculates the reduced modulus directly from the hardness; and the continuous stiffness method that calculates elastic modulus and hardness as a function of indentation depth [232]. Further to these quasistatic techniques, indentation can be performed under dynamically with cyclic loading and the storage and loss moduli calculated over several cycles [232]. In bone tissue, that exhibits viscoelastic properties, the loading rate influences the modulus measured, decreasing from approximately 17 GPa down to approximately 13 GPa with an increasing loading and unloading rate of 100 µN/s to 150,000 µN/s [233]. However, if sufficient to accommodate for creep effects, the hold period duration from 2 s to 15 s has limited influence on the elastic modulus [233].

The tip geometry has a large effect on the properties assessed and a round indenter will reduce stress concentrations and therefore minimise plastic deformation for a more elastic measure [235], whereas the sharp edges of a pyramidal tip can cause non-reversible damage and potentially create localised cracking [237, 238]. Furthermore, pyramidal or conical tips are more scalable, with the constant angle of the faces meaning the relationship between indentation depth and contact area is directly proportionate [235, 239]. Though the same basic principles used in tissue-level indentation are applied at the micro- and nano-level, in bone or other hierarchical inhomogeneous composite structures, the features assessed and, therefore, properties measured, relate to the depth-area relationship and the size of the indenter. This is demonstrate by increased spherical tip diameter, where the contact area-depth relationship is not constant, having a negative relationship with reduced modulus in bone [239].

4.1.2 Measurement parameters and overview of Reference Point Microindentation

The concept behind reference point indentation is to use a conical tipped 350 µm test probe applied in-vivo, broadly using indentation principals to assess the material properties of the bone. In contrast to larger scale indentation (e.g. Vickers hardness) or conventional nanoindentation (e.g. using the Oliver-Pharr method) as discussed above, the indent has been imaged with associated microcracking [19] hypothesising that this

leads to fracture mechanics measurement and therefore can be indicative of fragility and predictive of fracture risk.

The technique, originally described by Hansma et al [240], involves a test probe housed within a cannulated reference probe with a sharp diagonal point (Figure 24b). Due to the presence of soft tissue or irregularities in the surface of the bone, this reference probe is necessary to give a zero-point for testing and to anchor the probe assembly to the surface of the bone through a preload (260 g to 1350 g, equivalent to the maximum test load). In the Biodent Hfc^{TM} system utilized in this study, the test probe indents to a maximum load of 2 N to 10 N in a third of a cycle, holds for a third of a cycle and then unloads for the remaining third. With the probe remaining in place, the probe cyclically repeats this indentation process between 5 and 20 cycles. The displacement of the indentation probe is controlled with a voice coil (as used in speaker systems) based electromagnetic force generator, a coil that induces a magnetic field and hence displaces a permanent magnet secured to the test probe [29, 240].

This indentation technique does not derive an elastic modulus or hardness, in part due to the impracticalities associated with imaging the indent and calculating an indent area in vivo. Though an approximate contact area could be derived through the maximum displacement of the probe, this may not be representative of the actual area due to the discussed microcracking or elastic response [235]. Instead, the indentation depth is used directly as a comparative measure in bone. The main output measures of the device are displayed in Figure 24a [19, 29]. Principally, four points are calculated per cycle: the touchdown point (T) where the probe first contacts the surface of the bone and loading commences, the peak load (P) where the load is first within 3% of the maximum load (i.e. the end of load and the commencement of the hold period), the retraction point (R) where the load is last within 3% of the maximum load (i.e. the end of the hold period and the commencement of the unloading) and lift-off (L) where unloading ends and the probe is at the limit of contact with the bone.

Based on these four points over the cycles a number of measurement parameters are calculated:

- The Total Indentation Distance (TID) – the maximum indent depth, final cycle retraction minus first cycle touchdown
- The Indentation Distance Increase (IDI) – the progressive indentation depth, final cycle peak minus first cycle peak point
- The Creep Indentation Distance (CID) – the indentation depth over the hold period (one third of a cycle), the retraction minus the peak in one cycle: this can be the CID1 (the first cycle CID), the CIDL (the last cycle CID) or avgCID (the CID averaged over all cycles)
- The first cycle Indentation Distance (ID1) – the maximum indent depth of the first cycle, retraction minus the touchdown point for the first cycle
- The average loading slope (avgLS) – the loading stiffness, the gradient of the top 50% of the loading slope averaged (mean) over all the cycles
- The average unloading slope (avgUS) – the unloading stiffness, the gradient of between 95% and 40% of the unloading slope averaged over all the cycles
- The average energy dissipated (ED) – the area under the loading curve minus the area unloading curve averaged over all cycles

Due to their prevalence in the literature, the TID, IDI and CID1 have been focussed upon in this study.

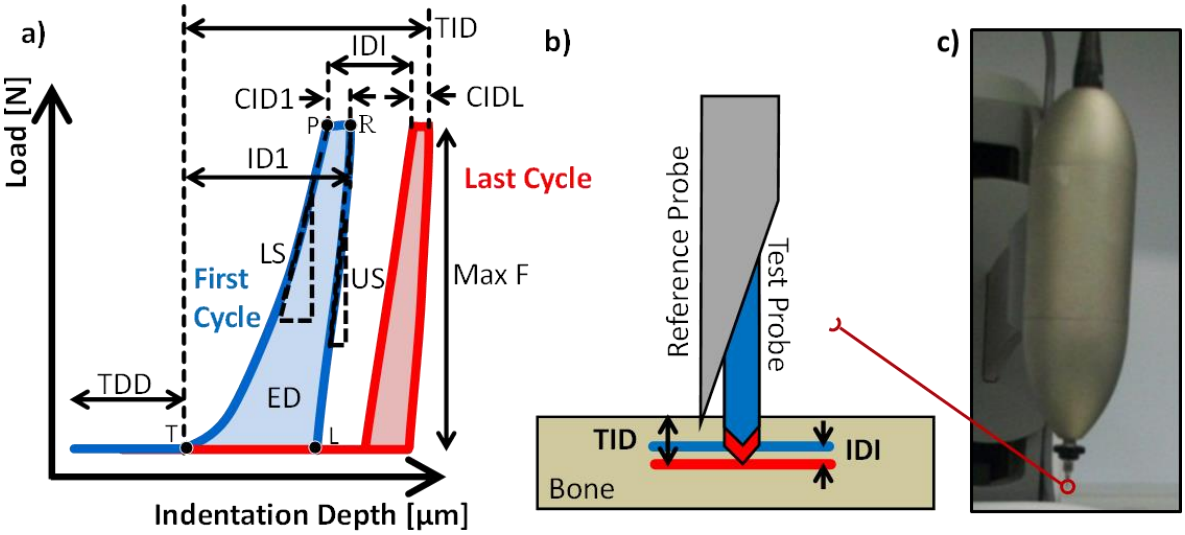

Figure 24 – a) Definition of reference point indentation points (i.e. T- Touchdown, P – Peak load, R – Retraction and L – Lift-off), characteristics (TDD – touchdown distance and Max F – the maximum load) and measures (TID – Total indentation distance, IDI – Indentation distance increase, CID – Creep Indentation Distance, ID1 – first cycle indentation distance, LS – Loading slope, US – Unloading Slope and ED – Energy Dissipated), b) schematic of the device and c) image of the Biodent Hfc Reference Point Microindenter

In addition to the Biodent Hfc™ device used in clinical and laboratory studies, there is a second, somewhat similar, RPI device, the Osteoprobe™. Rather than cyclically indenting the bone, the device, as described by Bridges et al [31], has a single rapid indentation cycle (0.25 ms up to 30 N) that is triggered once a preload (10 N) is achieved. This device does not have a reference probe (instead using the preload alone as a reference point) and is designed for handheld use. This loading rate (120 N/s) is faster than that applied by the Biodent, which typically operates at 2 Hz and therefore loads at a rate of 12 N/s to 60 N/s depending on the maximum load and is therefore towards the upper range typically utilized in indentation [29, 233]. The main output measure of the Osteoprobe™ is the Bone Material Strength (of BMS) that is the ratio between indentation depth measured on PMMA to the indentation depth measured on bone. Therefore a reduced BMS implies impaired material properties i.e. inverse to the Biodent assessed indentation depth (e.g. TID, IDI and CID) [20].

4.1.3 Variability associated with Reference Point Microindentation

Due to the emerging nature of this technique, it is necessary to establish the variability associated with the method and define a protocol for use. To this end, studies have begun to investigate the effects of different testing parameters on indentation results. Bridges et al [31] have considered Osteoprobe™ variability, giving recommendations that the probe is within 10° of normal and that the tip radius is sharper than 10 µm, which are

both directly relevant suggestions to the Biodent Hfc™ RPI device. Hansma et al [29], in one human donor with the Biodent device, suggested that soft tissue removal did not affect indentation depth. Though there was a decrease in indentation depth with removal of the soft tissue (approximately 10%), this was not found to be statistically significant. Randall et al [20] also found that soft tissue did not have an effect on indentation as assessed by the Osteoprobe™ in two human samples. However, the low numbers associated with the investigation of soft tissue still leaves the effect of its presence unclear. This study [20] also recommend 10 repeat measurements in clinical studies using human bone and 20 measurements for horse bone (based on convergence of the coefficient of determination). Rasoulian et al [32] found that the indentation was generally higher on the bone's natural surface in the transverse direction than on a machined surface in the longitudinal direction.

Two recent studies by Setters and Jasiuk [30] and Granke et al [26] have added further recommendations for the improved RPI testing. Granke et al [26] found little variation in RPI around the circumference of cadaveric femora but some anisotropy in the longitudinal and transverse directions in accordance with Rasoulian et al [32]. Due to the anisotropy in terms of elastic [241] and fracture toughness [110] properties of bone as well as the dependence on indentation angle of RPI [31] a higher degree of anisotropy may have been expected through RPI and this parameter requires further investigation still. Setters and Jasiuk [30] tested 6 month old porcine femora and recommended a 4 N - 8 N maximum load (due to a purportedly non-linear relationship in IDI), 15 - 20 cycles should be used and measurements should be taken in the longitudinal direction for improved consistency. Using a conical probe, the relationship between maximum load and indentation depth would additionally be expected to be fairly linear due to the constant depth-contact area relationship of the probe [235, 239] and the relationship with IDI seemed anomalous to the other indentation measures meaning further investigation is required to observe the relationship with maximum load. Additionally, this study [30] also finds that neither the use of preconditioning cycles nor micro-computed tomography prior to testing have a deleterious effect on subsequent RPI.

These six studies give an impression of variability associated with RPI but the list of parameters considered is not exhaustive and there is still need for further systematic research into the measurement parameters associated with the device. In particular,

investigation into the coefficient of variation with various important measurement parameters (e.g. the maximum load applied, whether the device is fixed or held freehand, the preparation of the samples etc.) would allow for recommendations of how to use the device for more repeatable results and, hence, improved discriminative ability.

4.1.4 Clinical Potential of Reference Point Microindentation

Diez-Perez et al [19] describe an in vivo testing procedure applied to the human tibial midshaft: local anaesthetic was applied and a disposable RPI probe was pushed through the soft tissue with a preload applied through the reference probe. The reference probe was scratched against the bone surface to further displace soft tissue and the periosteum. Preconditioning cycles (2.5 N at 4 Hz) were applied to the bone followed by the measurements cycles (up to 11 N at 2 Hz for 20 cycles). Through the same insertion site, 5 measurements were repeated with 2 mm spacing. This study [19], alongside Guerri-Fernandez et al [21], Farr et al [242] and Randall et al [20] reported that the technique is well tolerated by patients, documenting no pain or complication. Aref et al [22], Allen et al [23] and Randall et al [20] also use this technique in vivo for dogs, rats and horses respectively, again finding no clinical complications or apparent discomfort with the technique. Therefore, by successfully being applied in vivo, in this respect, the tool has potential for fracture risk assessment.

Further clinical potential for fracture risk assessment has been identified by the preliminary ability of RPI to discriminate between healthy and diseased tissue. Diez-Perez et al [19] applied the technique in vivo comparing 27 women with osteoporotic fractures with 8 non-fractured controls of comparable ages, finding the TID (46 µm compared to 32 µm), IDI (18.1 µm compared to 12.3 µm) and CID (5.2 µm compared to 3.9 µm) to be higher, implying compromised material properties of the bone, in the fracture patients. Furthermore, the ROC AUCs were high (0.93 for TID, 0.90 for IDI and 0.74 for CID) implying good discriminative ability with high sensitivity and specificity. In these patients Diez Perez et al [19] found no link with age, a risk factor for fracture risk, however Hansma et al [29], found indentation depth in the cadaveric tibial bone of one elderly donor (79 year old female) was high compared to indentation depth in one young donor (17 year old female). Further to this, also in vivo, Guerri-Fernandez et al [21] found the indentation depth to be higher in osteoporotic fractures (38 patients) compared to non-fractures controls (20 post-menopausal women). Similar higher indentation depths were

observed with atypical fractures associated with long-term bisphosphonate usage (6 patients) compared to bisphosphonate use without fracture (6 patients). In vitro, Milovonovic et al [28] compared cadaveric bone from the superolateral femoral neck across 5 fractured individual with 4 donors with no history of fracture. These samples were machined and soaked in ethanol, assumedly altering the indentation properties. Nevertheless, the indentation depth was higher in the fractured donors (e.g. TID was 14.7 µm compared to 13.1 µm and IDI was 1.6 µm compared to 1.3 µm), albeit, due to the low numbers, not significantly so. Type 2 diabetes, also a risk factor for secondary osteoporosis, was compared in 30 post-menopausal women with 30 age matched control by Farr et al [242] using the Osteoprobe^{TM}. This study found lower BMS (by -11.7%) in the disease state, implying impaired material properties. In an in vitro animal model of diabetes, Hammond et al [243], however, observed significantly lower IDI and CID1 using the Biodent device, therefore implying enhanced material properties in diabetic rat tibia. The effects of Raloxifene, an osteoporosis therapy, was assessed on beagles by Aref et al [22] using the Biodent in vivo and finding that 6 month treatment improves the indentation properties, reducing TID, IDI, CID etc.

The presented literature paints the picture of a technique that can be applied in vivo and has shown some potential for discriminating diseased from healthy bone, perhaps improving fracture risk assessment. However, the limited amount of research, particularly comparing fractured to non-fracture tissue (three studies by Diez-Perez et al [19], Guerri-Fernandez [21] et al and Milovanovic et al [28]) demonstrate that this relationship, on which the efficacy of the tool is centered on, needs to be examined in further detail with increased numbers of participants.

4.1.5 Material Properties Assessed by Reference Point Microindentation

Regardless of differences detected between healthy and diseased tissue it is also necessary to understand the property that is being assessed by RPI in order to interpret readings. As discussed, neither reduced modulus nor hardness values are calculated contrary to nanoindentation techniques (e.g. Oliver-Pharr) due to the purported presence of microcracking, instead suggesting fracture mechanics assessment [19]. This relationship with fracture mechanics has been demonstrated by Diez-Perez et al [19] showing strong correlation (r = -0.90) with indentation depth and crack growth toughness in compact tension samples cut from the tibial midshaft, albeit in only five donors (8

samples). Despite this, Katsamenis et el [24] (under review), exhibited a lower correlation between fracture toughness and crack growth toughness calculated from 20 single-edge bend specimens from human cadaveric femora and indentation properties (r = -0.30 to r = -0.50). In terms of IDI and fracture toughness or ED, fracture toughness and crack growth toughness the relationship was not significant. Carriero et al [244] additionally found no correlation (r = 0.00 to 0.03) between indentation depth measurement and whole bone fracture toughness in 35 rat specimens grouped into 5 disease models with different properties (e.g. brittle osteogenesis imperfecta to ductile phosphate impaired). This approach eliminates potentially valuable inter-sample/animal variation but also poses the interesting question of whether interpretation of indentation depth is dependent on the bone type (e.g. healthy or diseased) and therefore has varying contributions of elastoplastic or fracture properties.

Other studies have considered correlation between RPI and elastoplastic properties such as stiffness, strength and toughness. Gallant et al [25] carried out whole bone three-point bending of rat midshafts and beagle ribs and compression of rat lumbar vertebrae. In terms of material properties, the correlation was higher with toughness and post-yield toughness (r = -0.71 to -0.75) than ultimate stress (r = -0.51 to -0.61) and elastic modulus (not significant) in all bone types. The correlation with TID and ID1 (r = -0.37 to -0.53) was also generally lower than in terms of IDI (r = 0.46 to 0.60). Furthermore, Hansma et al [29] showed a similar relationship between age and inverse RPI as that shown in bending toughness in four donors. Granke et al [26] also considered correlation between RPI and material properties machined from the medial quadrant but of human cadaveric bone, finding similar, if lower, correlations as Gallant et al [25](r = -0.5 with toughness and ultimate stress and r = -0.4 with yield stress and post-yield strain). Through combining LS and IDI, the correlations could be improved (r = 0.59) but, as with Gallant et al [25], no measure correlated with flexural stiffness. The reasonably low correlations (i.e. -0.37 to -0.75) imply that RPI is not directly indicative of a single property and may have contributions of both elastoplastic and fracture properties.

Relating these material properties back to the elastic modulus and hardness of conventional indentation methods (e.g. nano-level indentation under the Oliver-Pharr method), discrepancies can be observed. RPI seems to have little influence from elastic modulus properties, rather fracture toughness and plastic properties of bone may, to

some extent influence the measure. This difference likely relates to the indenter geometry and the indentation of bone rather than homogeneous materials. Schwiedrzik and Zysset [235] used FE modelling to consider bone as a damageable elastic spring with an overlying plastic pad dependent on a yielding criterion when indented by a spherical or conical tip. As mentioned previously [239], the spherical tip has an area depth function and therefore the elastic modulus was dependent of the indentation depth but otherwise consistent, whereas the properties assessed by the conical tip were influenced by pile-up, the degree of plasticity and existing damage within the bone [235]. Therefore, in RPI where microcracking has been observed and a conical tip is utilised [19], the elastic modulus is unlikely to be a representative measure. Furthermore, due to the composite nature of bone, plastic deformation and delamination may also occur. In two separate studies, Chen and Bull [245, 246] considered the nanoindentation of engineering ceramics with hardened coatings. These studies predicted a plastic zone (R_p) to form below the indent, for bone this can be approximated as up to 4 times the indentation depth (δ_m) (using a Berkovich geometry, elastic modulus, E_r, of ~15GPa and hardness, H, of 0.5 GPa [234], applied to $R_p/\delta_m = -12.907 \times H/E + 4.5451$ [245]). Adhesion to the probe and presence of layers may also cause buckling of the outer surface, causing cracking and delamination between layers [246]. Therefore fracture mechanics and plastic deformation are likely to play a role in RPI measurement.

Crack growth toughness has previously been related to indentation through the application of cubic or triangular pyramidal tips to initiate cracks within the bone [232, 237, 238]. In particular, Kruzic et al [238] reviewed the use of such techniques principally derived from Equation 3; the Vickers Indentation Fracture technique and derivations thereof. The crack length emanating radially from the stress concentrations of the pyramidal tip edges is imaged and the elastic modulus and hardness are calculated as described above. Mullins et al [237] employed these techniques to calculate fracture toughness values of bone in-line with the literature (i.e. approximately 2 $MPam^{0.5}$). However, a response to this paper by Kruzic and Ritchie [247] and of indentation derived fracture toughness in general [248], questions the applicability of using such techniques to calculate an absolute value in bone. Particularly in terms of fracture toughness, where indentation does not cause a catastrophic failure of the tissue or in terms of crack growth toughness, where the associated crack lengths are minimal (5 µm to 56 µm, [237]), this

technique was not considered valid [247, 248]. Additionally, the unknown constants (alpha in Equation 3) and relationship with maximum load give uncertainty in calculation of absolute, rather than comparative, values [247].

Equation 3 – Derivation of the fracture toughness from indentation where: Kc is the fracture toughness, E is the elastic modulus H is the hardness, c is the crack length, P is the applied load and alpha is a calibration constant based upon comparison to fracture toughness (0.016 ± 0.004 by Kruzic et al [238])

$$K_c = \alpha \sqrt{\frac{E}{H}} \frac{P}{c^{\frac{3}{2}}}$$

One further issue with relating localised material properties to whole bone mechanical properties is the structure of bone. That is, the size of the indent tip and the load applied affects the volume of interaction and hence the structural aspects evaluated. Nanoindentation can be targeted and applied to measure micron and submicron features such as individual lamellae [249] or interlamellar layers [98] that can be built together with FE modelling alongside the structure of the bone to approximate whole bone properties [234]. Whereas, the size of the RPI probe is comparable to the osteons and Haversian canals, combining multiple features of distinct properties which must influence the measures [239]. Therefore the micro- and nano-level structure of bone, due to its composite nature, is also influential in determining indentation depth assessed through RPI. This is exampled by Hardiman et al [79] who modelled the inclusion of fibres within a resin, finding that the volume fraction influenced the Oliver-Pharr derived elastic modulus compared to the bulk properties of the resin. This was attributed to the constraint provided by the fibres, even in large resin pockets indicating the effect of test location. The effect of composite fibres was confirmed experimentally by Gregory et al [80], again considering nanoindentation of composites with fibre inclusion compared to properties of a bulk material showing the fibres to influence the indentation modulus and hardness, adding to heterogeneity of the composite and influencing the force-depth-modulus relationship which would also apply to bone.

Based on this discussion it still is unclear what material properties are assessed through RPI and how this can be related to conventional measures such as modulus or fracture toughness. It seems that post-yield properties may have the greatest relation to the indentation depth but it is also clear, through relation to other indentation techniques, that the hierarchical structure, fracture toughness and elastic properties are also likely to

influence the measures. As yet it remains inconclusive what property or combination of properties the technique is assessing and therefore interpretation of changes in these properties is limited.

4.2 Fracture Mechanics of Bone

All materials contain defects, bone being no exception. The presence of defects means the material properties of bone may not be governed by its strength but rather by its ability to resist propagation of these defects into cracks and, ultimately, fracture. Whether a material is governed by its strength or fracture toughness is defined by an extension of the Griffith's criteria described by Equation 4 [56]. For a crack of length 2a loaded in tension (opening the crack) within an infinite plate, the shape function (Y) can be taken as 1 to give a crude approximation of the critical crack length for bone. This is approximately 250 µm to 1.6 mm (for K_c = 2 - 5 $MPam^{1/2}$ and σ = 100 MPa) and will be more critical for different loading scenarios (e.g. an edge notch with increased Y). Therefore, below this threshold, bone will be governed by its strength but with defects longer than this (comparable to the 100 µm to 500 µm found in bone [250-254]), the failure of bone will be due to its fracture toughness, making this a valuable property to assess.

Equation 4 – relationship between the fracture toughness and material strength for a crack length of 2a and shape function of Y

$$K_c = \sigma\sqrt{\pi a}Y$$

Rather than assessing the propagation of existing microcracks, an artificial notch of known size can be introduced. This can be considered the largest defect within the structure and therefore, the one that will cause failure. Through tracking the failure of this defect, the bone can be characterised by its ability to resist the initiation of crack growth, to impede crack growth extension and finally, to resist fracture. When considering fracture risk, the ability of the tissue to resist fracture seems a particularly pertinent material property to describe the bone properties. The techniques for assessing the fracture mechanics of materials are described by the ASTM standard E1820 [255] and relate the load applied to a specimen of known geometry with a notch of known size to the crack length that propagates from this notch (shown in Equation 5 and Equation 6). The sample geometry is typically either an approximately square plate with the notch opened in tension (the compact tension specimen) or a notched beam placed in bending

to open the notch (a single edge bend specimen) [255]. Due to the thickness and curvature of the cortex, the smaller single edge beam specimens are therefore easier to machine and have been used in this thesis.

The crack propagation can be monitored through knife edge gauges assessing the crack tip opening displacement or through crack propagation imaging. Due to the thickness of the cortex, only small scale samples can be machined from bone, with a thickness in the range of 1 mm to 9 mm as reviewed by Katsamenis et al [256]. This means that assessment of crack propagation at the millimetre and sub-millimetre scale are necessary to characterise the bone, but these small scale are difficult to image optically. Therefore, the Ritchie Group at the Berkeley Lab, University of California [87, 110, 114, 163, 179] employ in situ loading within an environmental SEM to assess this crack propagation. An alternative method was developed by Katsamenis et al [256] specifically crack propagation in small-scale cortical bone samples. This study employs the whitening front tracking method, measuring the whitening effect that is visualised when bone is damaged [121, 257]. This whitening area relates to newly formed microcracks, as confirmed by synchrotron micro-computed tomography [256], which reflect light and allow for visualisation of the damage. This whitening area propagates continuously ahead of the crack tip (as measured in larger rat samples [256] and can therefore be used to assess crack propagation. This whitening effect has been described as similar to the whitening observed in polymers due to ‘crazing’ (a network of fine cracks that dissipate energy) and the increased scatter of reflected light on microcracks forming between the mineral and collagen. However, the effect has additionally been observed in demineralized bone and attributed to increased collagen density when loaded in tension and the changes in optical properties with load induced dehydration [258]. Due to the observations of microcracking in whitening mineralised bone [121, 256, 257] it is likely that both mechanisms are contributory, and, regardless of the cause of the whitening, its link to crack propagation can still be used in fracture mechanics.

Rather than being centred on a single value (i.e. the point of failure being used to calculate the fracture toughness), continuous tracking of the crack extension with loading allows for generation of full crack extension resistance curves (r-curves) which can further describe the material properties by their shape and slope. Conventionally, linear elastic fracture mechanics measures, the stress intensity factor or K-values, are quoted for bone.

This approach makes the assumption that the material can be described as linearly elastic, that is, there is only small scale yielding (i.e. the plastic region is small) around the crack-tip. The size of this plastic region can be stated as: $r_p = K_c^2/\sigma_y^2$, which for bone can be approximated as roughly 2.5 mm (i.e. [5 $MPam^{0.5}$/100 MPa]^2 [255]). Considering the size of the samples being machined in this study (millimetre and sub-millimetre), and in fact any size samples that can feasibly be machined from bone, this plastic zone is large relative to the specimen and therefore the linear elastic approach is inappropriate. The large size of this plastic zone in part explains the whitening visualisation and the difficulties in detecting the crack tip. Instead of the K-value calculation, a non-linear approach should be taken to find the strain energy release rate or J-Integral shown in Equation 6 and Equation 7. The J-integral is a summation of an elastic and plastic component. The elastic component relates directly to the linear elastic K-value by the Poisson ratio and elastic modulus of the bone. The K-value is a continuous function of load, and crack extension combined with geometric measures as shown in Equation 6 and Equation 7. The plastic component relates to the area under the plastic portion of the curve.

Equation 5 – The J integral, J made up of elastic (J_{el}) and plastic (J_{pl}) components. The elastic component is made of the material properties for a linearly elastic material: K is the stress intensity factor (shown in Equation 6), v is the Poisson ratio (v = 0.33) and E is the bending modulus. The plastic component: A_{pl} is the area under the force-displacement curve, B is the specimen's thickness and b is the uncracked ligament (the width minus the notch). From ASTM E1820 [255].

$$J = J_{el} + J_{pl} = \frac{K^2(1-\nu^2)}{E} + \frac{2A_{pl}}{Bb}$$

Equation 6 – The stress intensity factor, K. A function of: P – the load, S – the span, B – the specimen thickness, W – the specimen width and f(a/W) – a shape factor for the single edge bend samples as a function of the crack extension (a) and the width (W). From ASTM E1820 [255].

$$K_{(i)} = \left[\frac{P_i S}{BW^{3/2}}\right] f(a_i/W)$$

Equation 7 – The shape factor, f(a/W), a function of the crack extension (a) and specimen thickness (W). From ASTM E1820 [255].

$$f(a_i/W) = \frac{3(a_i/W)^{1/2}[1.99-(a_i/W)(1-a_i/W)(2.15-3.93(a_i/W)+2.7(a_i/W)^2)]}{2(1+2a_i/W)(1-a_i/W)^{3/2}}$$

Details of the whitening front tracking method utilised in this study are described by Katsamenis et al [256]. Notched single-edge bend specimens are loaded in three-point bending to failure with the loading captured by videography. The videography allows for

the whitening to be tracked and synchronised against the loading. Katsamenis et al [256] developed an algorithm to track this whitening effect which is described by Figure 25. Firstly, the scale is set by selecting a known distance (i.e. the span of the bending rig) from the initial frame. The videography is then cropped by manual selection of the region of interest, the notch and surrounding bone where the whitening develops. Next the image is adjusted using gamma correction to improve the contrast of the whitening area. A sub-pixel cross-correlation technique is used to register the initial frame against all following frames, accommodating for the displacement of the bone relative to the region of interest during loading. The initial frame, a baseline where no whitening is visualised, is then subtracted from each subsequent frame with the difference image indicating the whitening. The difference image is binarised through thresholding and the user is asked to manually select the whitening area from each of these binary images. An automated procedure is then applied to find the extreme points of the whitening area, the farthest of these points from the manually selected notch tip is recorded as the whitening displacement (Δa). Through synchronising against the load-displacement-time data via the videography frame rate and input of the measured sample geometries, the crack extension resistance curve can then be generated as described (Equation 5, Equation 6 and Equation 7).

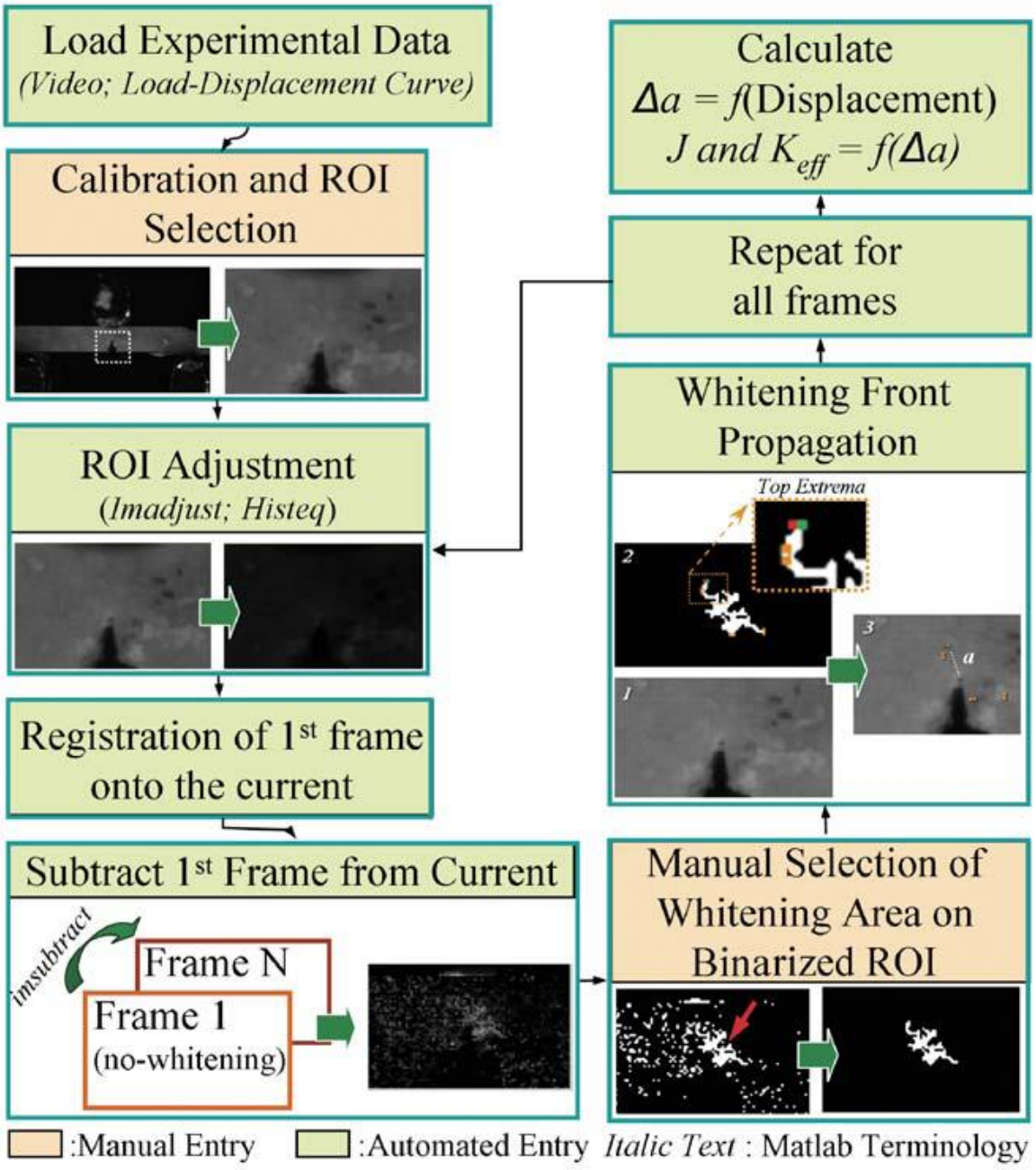

Figure 25 – Whitening front algorithm as described by Katsamenis et al [256]. Image reproduced from Katsamenis et al [256] courtesy of PLOS ONE.

The samples analysed by Katsamenis et al [256] were machined in the 'longitudinal antiplane' orientation. In this orientation, the crack propagates around the osteons in the 'separating' mode rather than through them, in the 'breaking' mode of the transverse orientation or propagating along the length of the osteons in the 'splitting' mode of the longitudinal orientation as described by Koester et al [110] and shown in Figure 26. The breaking mode is the most resistant to crack propagation, having a 5 fold increase in fracture toughness relative to the splitting mode and would therefore be expected to exhibit the largest plastic response and whitening area. The toughness of bone in the

separating mode lies between the two of these, being more similar to the splitting mode with the cracks driven along the cement lines in both techniques. Therefore the breaking mode would theoretically be preferable for whitening visualisation though transverse specimens require a larger quantity of bone which is infeasible with the curvature and thickness of the femoral neck. Therefore, the longitudinal antiplane separating specimens are the most resistant to fracture, theoretically with the clearest whitening, that can be applied to this study.

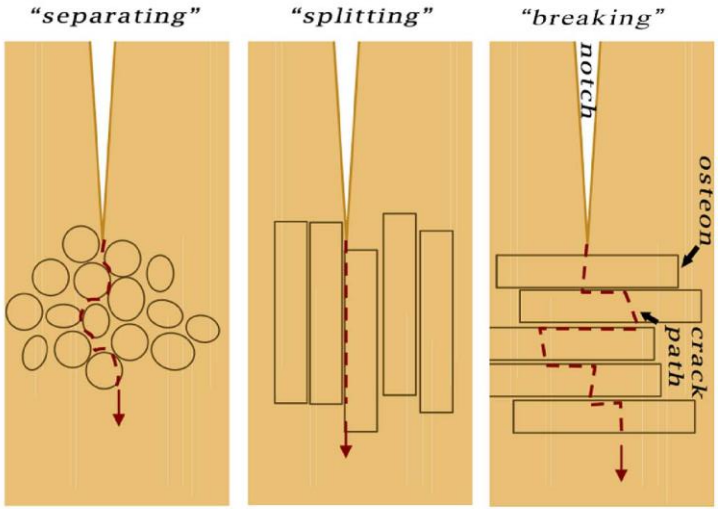

Figure 26 – Different notching orientation with respect to the osteonal direction. Adapted from Katsamenis et al [256] courtesy of PLOS ONE.

The whitening front tracking method has since been shown to find a decrease in toughness with a minimal correlation to RPI measures [24] albeit in only four donors (20 samples). The technique therefore shows potential for assessing the correlation between indentation and conventional material properties in small bone samples machined from human cortical bone. Though the technique has shown differences with age and is therefore in-line with other fracture toughness studies that find a decrease in material properties with age [24, 163, 179, 259], there is surprisingly little evidence for the decrease in material properties with disease. Therefore, though it is generally assumed that fracture mechanics properties, due to their implication of resistance to cracking and hence fragility, would strongly relate to fracture risk, but this remains to be shown. Furthermore, little is known about the material properties of other conditions, including osteoarthritis and this has not been examined in the literature. This unreported effect may relate to the difficulties of fracture toughness in small bone specimens that has only recently been addressed through the whitening front tracking method [24, 256] and

environmental SEM [87, 110, 114, 163, 179] or the difficulties associated with obtaining both healthy and diseased human tissue.

4.3 Details of Densitometry Techniques

Currently, bone mineral density (BMD) as measured by DEXA, often with the addition of FRAX (as will be discussed), is the gold standard for assessing osteoporosis and increased fracture risk [8, 14, 260]. The term density is used though this is actually a measure of how the tissue affects a beam of radiation, not a physical property. Single Photon Absorptiometry (SPA) was initially used with a gamma radiation source coupled to a detector [188, 191]. Single X-ray Absorptiometry (SXA) and Dual Photon Absorptiometry (DPA) provided advancements on this technique. The use of an X-Ray source in SXA increased the photon flux, allowing for a narrower beam with higher resolution and improved scanning time, whereas the dual-energies used in DPA eliminated the need for calibration against an equivalent material to eliminate soft tissue effects [188, 261]. These improvements were combined to create DEXA or DXA (Dual Energy X-Ray Absorptiometry), which uses an x-ray beam at two energies (e.g. 100 keV and 140 keV) to asses BMD [188]. The effect on the patient is low with minimal radiation dose (in the order of tens of µSv, less than a day's background radiation) and a quick scan time (around 5 minutes) and the device is effective with a reasonable resolution (~ 1 mm), accuracy ($r < 0.96$) and precision (around 1% coefficient of variation) [188, 262].

The following understanding of the technical principals behind DEXA and absorptiometry has gathered from the review by Blake and Fogelman [262]. Bone mineral density is defined as the integral of the mass of the bone being imaged over its area and has been calculated for various areas of the body but is typically applied to the proximal femora or lumbar vertebrae. An x-ray beam from a radiation tube (i.e. an electron gun accelerated into a heavy metal target to release x-ray radiation) is used. The beam is filtered to remove lower energies from the spectrum and minimise beam hardening effects (i.e. filtering of the beam as it passes through the sample) then is passed through the patient and an x-ray detector measures the resulting intensity [262].

It is essential to perform the measurement at two energies to calculate the density of two tissue types: bone and soft tissue. The intensity for hard and soft tissue can be related to the intensity of the original beam through modification of the Beer-Lambert law as shown

in the two equations (Equation 8) for the high (140 keV) and low (100 keV) energy scans [262] (e.g. Figure 27 left).

Equation 8 - Beer-Lambert equations relating the beam intensity measured by the detector (I for high energy and I' for low energy) to the intensity of the beam emitted by the source (I_0 for high energy and I'_0 for low energy) via the energy absorbed by the bone of mass (M_B) and mass attenuation coefficient (μ_B for high energy and μ_B' for low energy) and by the soft tissue of mass (M_S) and mass attenuation coefficient (μ_S for high energy and μ_S' for low energy)

$$I' = I'_0 e^{-(\mu'_S M_S + \mu'_B M_B)}$$

$$I = I_0 e^{-(\mu_S M_S + \mu_B M_B)}$$

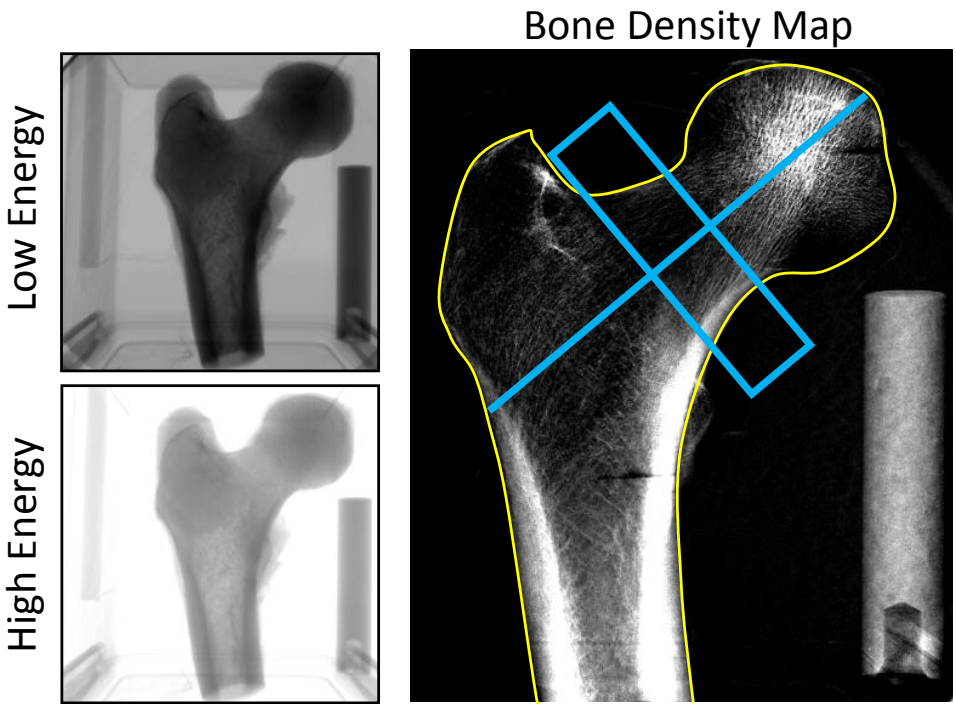

Figure 27 – Densitometry, combining the low and high intensity images to calculate the bone mass (right) based on the Beer-Lambert equations (Equation 8) and assumed mass attenuation coefficients. The segmentation of the bone (yellow) and a possible region of interest (blue) are shown in the right hand image

These equations can be simplified by defining the ratio of the negative natural log of the detected to emitted intensities (i.e. $J = -\ln[I/I_0]$ and $J' = -\ln[I'/I_0']$) and rearranging the equations to calculate the mass of the bone as shown in equation (Equation 9). In this equation the intensities are measured by the detector (I and I') or known as the input (I_0 and I_0') and the mass attenuation coefficients are assumed from standard calculation of bone with known mass [263].

Equation 9 - Simplification of Equation 8 for calculation of the mass of the bone (M_B) via the ratio of the detected and emitted energies at the high (J) and low (J') energy scans and, the mass attenuation coefficients for the soft tissue (μ_S for high energy and μ_S' for low energy converted to a constant, $k = \mu_S'/\mu_S$) and the bone (μ_B for high energy and μ_B' for low energy) at the two energies.

$$M_B = \frac{J' - kJ}{\mu'_B - k\mu_B}$$

Bone mass (Equation 9) is calculated on a pixel per pixel basis (i.e. Figure 27 - right) but can be summated over the area of the bone (defined by thresholding and edge detection) to define the bone mineral content or BMC. This can then be divided by the area of the segmented bone to give the bone mineral density (BMD). As mentioned, BMD is typically calculated at the proximal femora or lumbar vertebrae and, within this, the scans can further be segmented in terms of the femoral neck, total femoral head or individual vertebrae.

The BMD values are converted to t-scores through a linear relationship (dependent on sex) or less commonly used z-scores (dependent on age and sex). The t-score is defined by WHO [2] relative to the average BMD of a young healthy individual (set as a t-score of 0) and the standard deviation of BMD across the population (1 standard deviation being equivalent to a unit change in t-score). Based on this, WHO defines osteopenia as a t-score below -1.0 and osteoporosis, the intervention threshold, as a t-score of -2.5.

As discussed, BMD is limited in terms of its sensitivity for the fracture risk assessment of individuals, requiring new complimentary techniques to improve diagnosis.

4.4 Fracture Risk Assessment Tool

FRAX™ - the fracture risk assessment algorithm (the online tool is shown in Figure 28) is intended as a complementary tool to make up for some of the limitations of BMD assessed fracture risk. The literature review ('3.1.1 Causes and Risk Factors') discussed the increase in relative risk with a number of clinical factors (poor nutrition, inactivity, hazardous lifestyle, disease etc) showing presence of these risk factors to have an adverse effect beyond low BMD. In particular, the meta-analyses by Kanis et al [137, 140, 141, 143, 150, 161] highlighted the contribution of several risk factors: age, sex, body mass index (weight/height^2), previous fracture, parent hip fracture, current tobacco smoking, ever long-term use of oral glucocorticoids, rheumatoid arthritis, daily alcohol consumption (greater than 3 units daily) and secondary osteoporosis (hypogonadism, inflammatory bowel disease, chronic malnutrition, type I diabetes, hypothyroidism or hyperparathyroidism) [264].

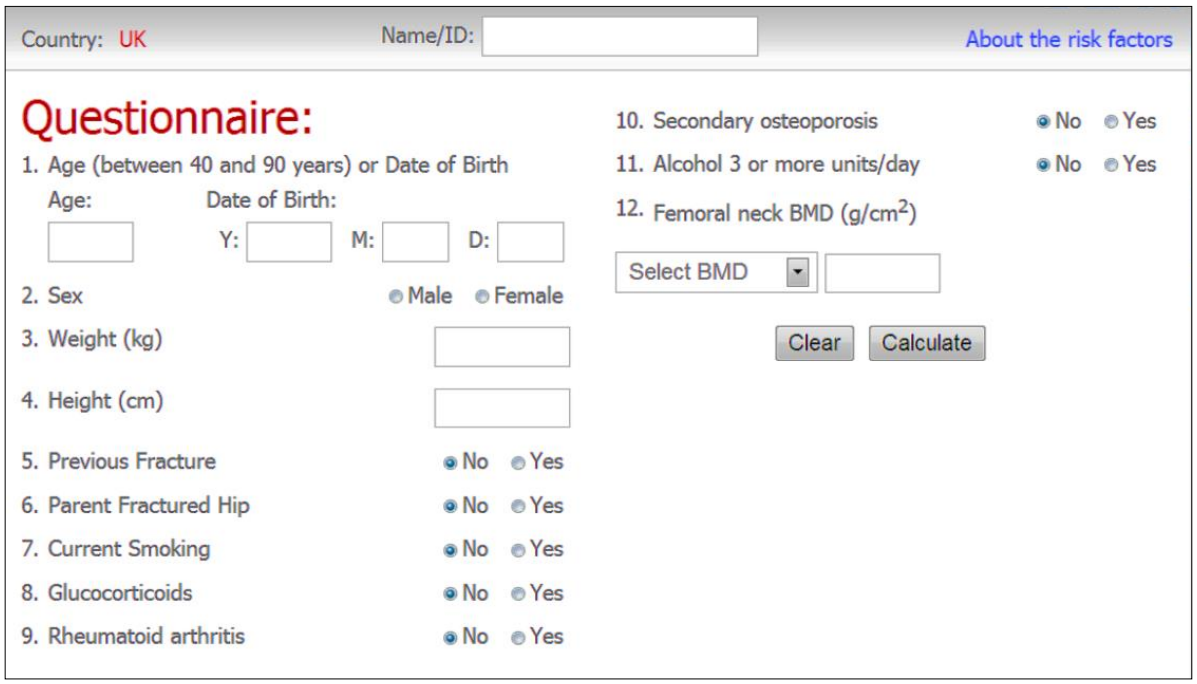

Figure 28 – FRAX questionnaire for calculation of 10 year fracture risk. Reproduced from the FRAX website [12] and Kanis et al [265] courtesy of Springer

Based on these clinical risk factors, alone or combined with BMD, the FRAX score was developed. Through 9 large-scale prospective studies (a total of 46 thousand individuals with 4000 osteoporotic fractures including 850 hip fractures) spanning multiple countries, the relationship between each of these factors was established [193]. Using a Poisson regression model within each cohort the contribution of each factor to the overall risk

was established with adjustment for the other factors. The regression beta-coefficients (equivalent to the gradient of the regression line) for each variable were then used to weight that variable within the fracture probability score; the exponent of the sum of these weighted variable [264]. Four models exist based on this analysis, giving four output measures to the FRAX^{TM} tool, the 10 year percentage probability of fracture in terms of hip fracture and major osteoporotic fracture as the end-points for models based on clinical risk factors alone and also combined with BMD [193]. It should be noted that fracture is not the only outcome measure concerned with these models and total probability of fracture also incorporates probability of death. This algorithm was then applied to 11 different cohorts (a total of 230 thousand individuals) for validation, finding the predictive power was similar within these cohorts to the primary cohorts [193].

Through the epidemiological incidence of fracture and the death rate in a specific country, the tool can be re-calibrated for fracture risk assessment in that country. This has been applied to a few countries (USA, Japan, China, Switzerland, Belgium and Poland) including the UK [264]. The hazard function (the exponential sum of the weighted risk factors) is calculated and then equated to the combined probability of fracture and death in that particular country through a calibration constant [264].

With each country specific model, a guideline threshold was then established based on the cost effectiveness of the tool [265]. The cost of assessment (the cost of 3 minutes of GP admin, a DEXA scan and a 10 minute GP consultation) and resulting cost of treatment (five year alendronate treatment) can then be weighed against the efficacy of assessment and treatment and the 'willingness to pay' based on the GDP per capita of a nation and the effect of successful treatment on quality of life [265]. This threshold, for the UK can be seen to be a minimum risk of fracture of greater than 7% (when alendronate treatment is cost-effective), but this is age dependent so the threshold can be increased at higher ages as described by Figure 29. Furthermore, for the clinical risk factors alone, a lower threshold can also be considered. That is, with a high risk based on clinical factors alone, treatment should be considered but for an intermediate risk, BMD should first be assessed prior to considering whether treatment is necessary.

As discussed previously, the inclusion of clinical risk factors offers some improvement on the sensitivity of BMD alone but does not consider all fracture risk factors or identify all

individuals who go on to fracture. This is not necessarily a limitation of FRAX which gives a probability of fracture and a threshold where treatment becomes cost-effective so does not purport to identify all who will fracture just those at greater risk of doing so. Nonetheless, supplementary measures could improve the tool further. Kanis et al [264] suggest; bone turnover markers, BMD at other sites, ultrasonography or pQCT, but the assessment of material properties of bone may also be a starkly different and therefore a useful contributing risk factor.

Additionally, the efficacy of a new measure, perhaps RPI assessed material properties, should be compared against FRAX and BMD, the current gold standards for fracture prediction, to establish ability to improve fracture risk assessment through supplementing existing techniques.

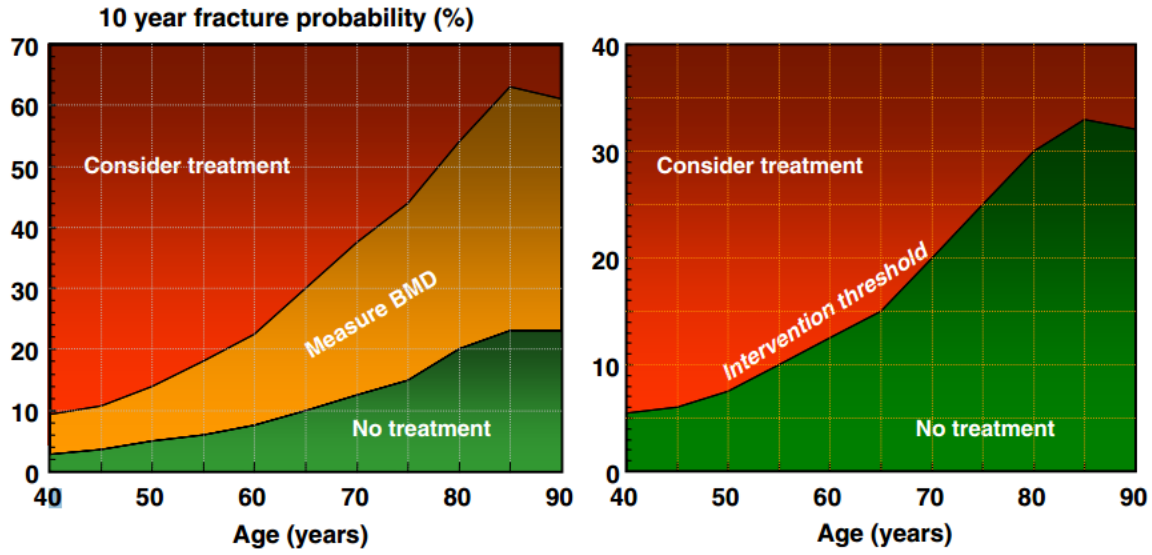

Figure 29 – Age dependent threshold for the 10 year risk of fracture (y-axis) when considering the potential combination with BMD (left) or when only considering clinical risk factors (right). Reproduced from the FRAX website [12] and Kanis et al [265] courtesy of Springer

4.5 Fluorescence Microscopy and Staining of Bone

Microcracks exist within bone and develop in number and length with age and fatigue loading to increase fragility and reduce fracture toughness with age [250, 251, 266]. The assessment of these cracks can provide information about the fracture mechanics of bone and techniques have therefore been developed for their assessment. Contrast agents, primarily basic fuchsin stain, can fill the voids of the microcracks and improve discrimination from the surrounding bone. Cracks can therefore be discriminated from bone porosity by their intermediate size (200 µm to 500 µm in length, approximately 100 µm in width and around 10 µm or less in thickness [250-254], between canaliculi/lacunae and vascular channels) as well as their sharp rather than rounded borders [266].

Lee et al [251] describe the principles of fluorescence microscopy for the imaging of bone microcracking. By applying light of a specific energy to the basic fuchsin stain, the electrons are excited and shifted to a higher energy level (indicated in Figure 30). On returning to their lower, more stable level, energy is emitted in the form of photons of light at a lower energy and longer wavelength than the exciting light. For fuchsin, the excitation wavelength is green light (545 nm wavelength) and the emission is therefore of a longer wavelength and appears red/orange (640 nm wavelength) [251]. Without staining, the structure of bone can also be visualised by the auto-fluorescence of collagen. The bone is excited with light at a wavelength of 450 nm to 490 nm (i.e. blue) with emission wavelength shifted to around 515 nm to 565 nm (i.e. green).

The staining technique involves fixation of the samples in 70% ethanol followed by repeat bulk staining with fuchsin. First, the bone is stained with 1% basic fuchsin in 80% ethanol for two 2 hour periods with intermediate change of solution. Then repeating this step with 90% ethanol and 100% ethanol prior to rinsing for 1 hour in ethanol to remove surface stain and the stain that has not penetrated microcracks [266-268] (demonstrated in Figure 30). The staining processes can be performed within a vacuum desiccator for more complete penetration of the stain [252, 266].

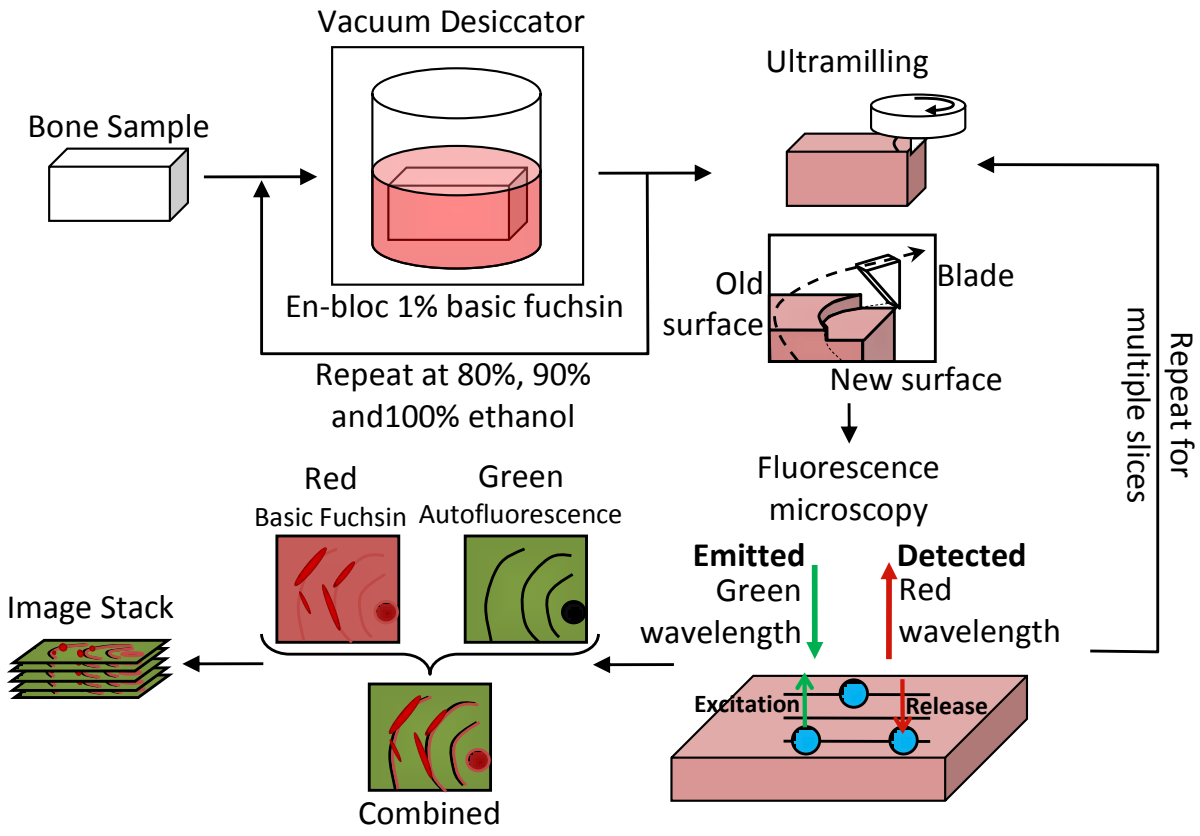

Figure 30 – Schematic of the bone staining technique that can be included with serial sectioning through ultramilling and fluorescence imaging at the red and/or green wavelength for visualisation of cracking and the structure of the bone

This technique has been used to effectively label two dimensional microdamage in vitro and allow the measurement of length and orientation (typically following the osteonal long axis - the vast majority within 25° and a median of 4° [253]). An advancement of the technique involves serial sectioning for three dimensional imaging of the microcracks [252, 254, 268]. This method utilises, an ultra-miller or microtome, a hard and sharp blade drawn across the surface of the bone to remove small slices of material from the surface or machine thin specimens as used in traditional histology. These techniques can create surface roughness comparable to repeat polishing down to 1 µm diamond solution and remove materials or produce samples in the order of micron thickness [269]. Serial sectioning, in combination with fluorescence microscopy allows for observations of the width as well as length of the microcracks and observation of the crack propagation and bone structure in three dimensions [252, 268].

Basic fuchsin staining, serial sectioning and fluorescence microscopy is therefore suitable for the two dimensional or even three dimensional observation of microcracks, features describing the fracture mechanics of the bone, and therefore useful in assessing the purported microcracking associated with RPI [19, 270].

4.6 Micro Computed Tomography

As an extension of the principles applied in radiographic densitometry (i.e. DEXA and BMD, 4.3) and a non-destructive alternative to serial-sectioning, micro computed tomography (μCT) allows for 3D visualisation and quantification of the structure and density of bone. Reviews by Landis and Keane [271] and Ketcham and Carlson [272] give a good overview of computed tomography. As mentioned, CT is based on radiographic principles with electrons directed from a cathode to impact a heavy metal anode, causing the release of x-ray radiation that is directed through a sample to a scintillator that converts the x-ray radiation to visible light which is then received by a photodetector [271](Figure 31). Using the same Beer-Lambert equations as DEXA (Equation 8, [262]) at one energy, the absorption of each pixel within the sample can be calculated to form a two dimensional shadow of the sample, the radiographic projection. Through the full 360° (often only 180° due to symmetry) of relative rotation (in clinical CT this is of the source and detector relative to the patient but in the laboratory it is typically easier to rotate the specimen) a number of radiographic projections are created for the sample. Each pixel in these projections can be considered as the integral of all the voxels in the sample that it has passed through on the line between the detector and source. Working backwards from this, the absorption value of each voxel in the sample can be reconstructed based on the grey-values as a function of x, y and θ (the sample angle of rotation) of the pixels in the projections [271, 272].

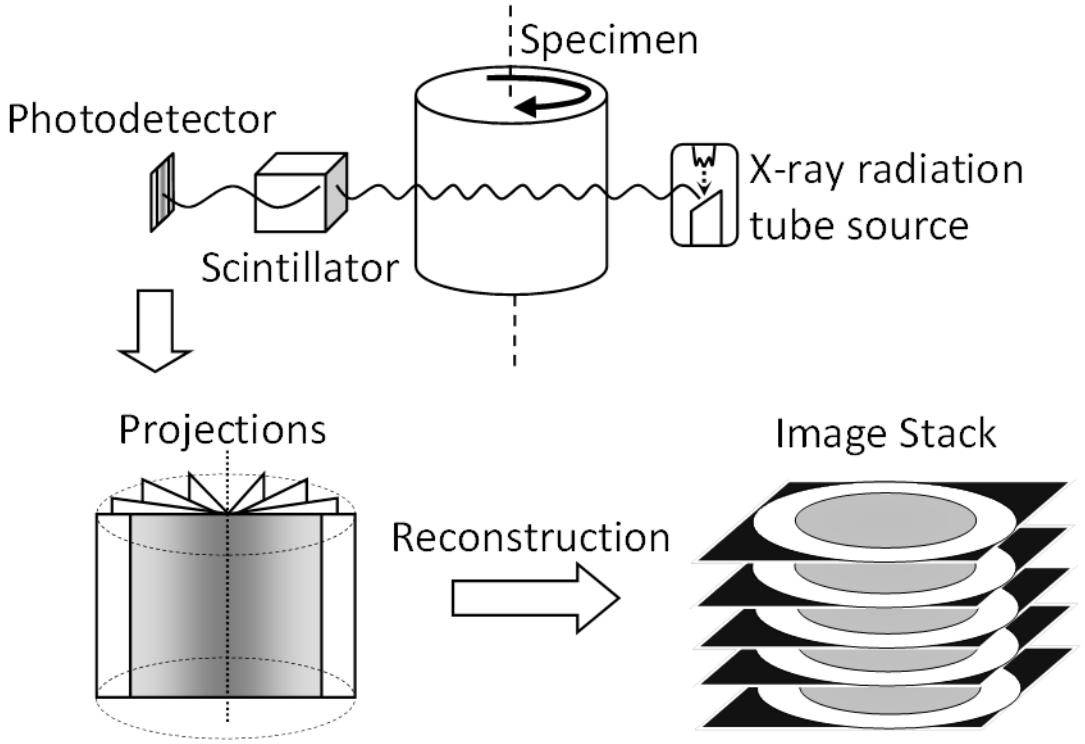

Figure 31 – Schematic of the computed tomography technique with the acquisition of 2D projections and their conversion to an image stack through reconstruction

During test set-up, considerations need to be made to the overall quality of this reconstructed 3D image or image-stack to minimised artefacts. The beam hardening effect (discussed briefly in section 4.3) causes a gradient in grey-values from the inner to outer of the sample, defects in individual pixels of the detector or unknown responses to heat or radiation intensity can lead to ring artefacts and limitations in resolution and region of interest can lead to partial volume effects. These effects can be minimised through calibration with a wedge shaped phantom (to observe the effect of thickness on beam hardening), through filtering the beam to pre-harden it, through shuttling the sample to mean the same detector pixels are not always recording the same point in x-y space and through selection of appropriate resolution [272].

From the sub-millimetre resolution of clinical scanners, micro-computed tomography is now able to achieve sub-micrometre resolution. The improvements relate principally to the ability to apply x-ray radiation of higher flux in vitro than in vivo, the machining of smaller samples that can therefore be closer to the source and the increase in detector resolution relative to the spot size of the beam [271]. These micron resolutions allow for visualisation and quantification of features including the cortical porosity [273], trabecular thickness [274] and, with higher submicron resolution systems, indent

associated bone microcracks [270], lacunae and canaliculae [275]. The visualisation of particularly small features such as bone microcracks can be enhanced using a contrast agent (such as barium sulphate) that is taken-up by the cracks and pores (similar to basic fuchsin for fluorescence microscopy 4.5) [276, 277]. Furthermore, synchrotron radiation micro computed tomography, where powerful magnets are used to accelerate electrons around a torus to a high flux can, in the same way as described, be used to excite the release of x-ray radiation allowing for high contrast, substantially faster scans with the ability to discriminate microdamage [275].

Micro-computed tomography is therefore also a valid technique for imaging of the indent (in the order of a few hundred microns length [19]) and its surrounding microcracks [270] for the assessment of the material properties assessed by RPI.

4.7 Atomic Force Microscopy

Meyer et al [278] describe Atomic Force Microscopy (AFM) for surface imaging as depicted by Figure 32. To overcome the limitations of scanning tunnelling microscopy (i.e. sample conductivity effects) AFM uses physical interaction between the sample surface and a sharp scanning probe. The interaction between the surface of the sample and the probe relate to van der Waals, electrostatic, magnetic and capillary force which deflect the probe and allow for sensing of the sample surface height. When the probe is brought closer to the sample surface (in the sub-nanometre scale) it can be considered to be in contact mode and, by drawing this probe over the sample surface and measuring its deflection, the surface topography can be generated (Figure 32).

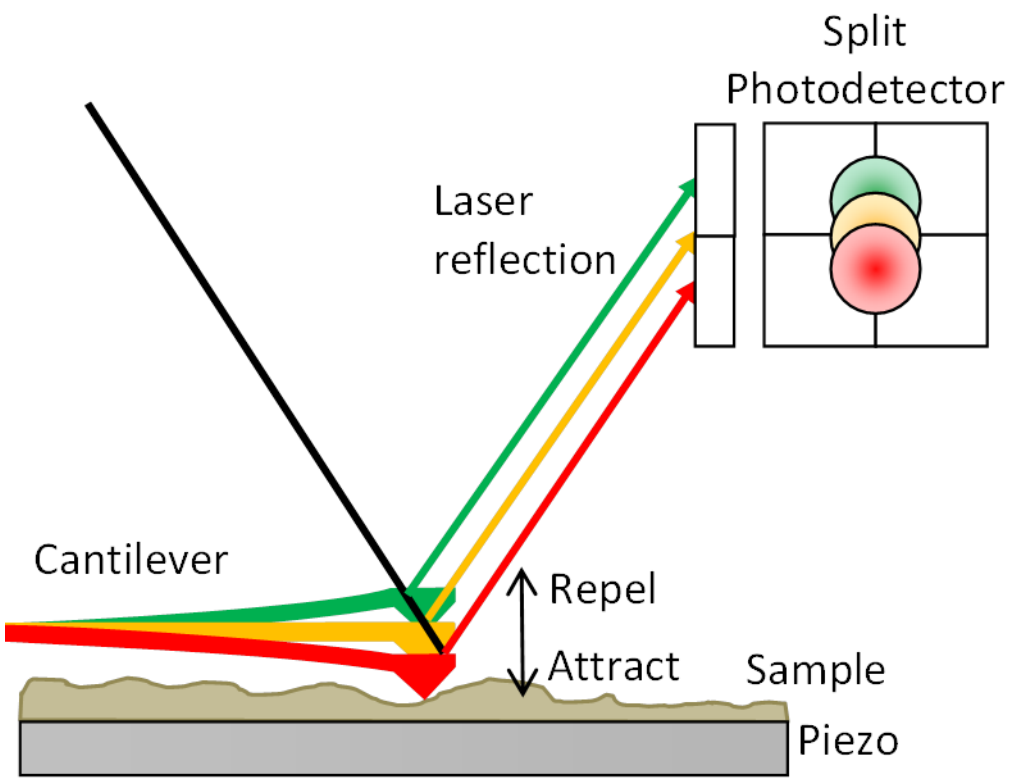

Figure 32 - Atomic Force Microscopy for imaging of surface topography by deflection of a cantilever and measurement of the result deflection using laser light reflection onto a photodetector and measurement of the load using a piezo-sensor

The probe is a sharp tip attached to a cantilever, the deflection of which can be sensed by the location of a reflected laser beam onto a split photodetector. That is, upward deflection of the cantilever causes the laser spot reflected off of the cantilever to also move upwards and therefore have a larger proportion of this spot on the upper section of the photodetector (Figure 32). The compression of a piezo crystal on the sample stage is also used to assess the low loads applied by the probe (0.01 nN to 1 mN), which, via Hooke's law and a cantilever of known stiffness (in the order of 0.001 N/m to 100 N/m), can also be related to the deflection of the cantilever and close the control loop with a feedback signal, maintaining surface contact [278]. This technique can be applied to image the surface topography at nanometre (or in the z-direction, sub nanometre) resolutions. The resolution is primarily dependent on the sharpness of the probe and its hardness relative to the sample and the resolution of the photodetector and has therefore been used to image small scale features in bone tissue (e.g. the mineral crystals and periodic fibril banding [163]). Therefore, this technique is also suitable for the imaging of small scale features within the bone and indent associated microcracks.

5 Variability associated with Reference Point Microindentation and Recommendations for In Vitro Testing

5.1 Introduction

Despite the emerging use of the RPI technique, there has been little published work characterising the variability associated with the device and establishing recommendations for optimally carrying out measurements. Hence, new users of the RPI device have limited point of reference for selecting optimal parameters and establishing a test protocol. This chapter therefore considers testing parameters associated with RPI to supply recommendations for reduced variability to advise future studies and the following chapters of this thesis (Chapter 6 and 7).

This work has been published as a journal article which this chapter is based upon [279] and reproduced here with permission from Elsevier:

- T. Jenkins, L. V. Coutts, D.G. Dunlop, R.O.C. Oreffo, C. Cooper, N.C. Harvey, P.J. Thurner and the OStEO group (N.K. Arden, J.M. Latham, P. Taylor, M. Baxter, N. Moss, C. Ball, K. Chan), *Variability in Reference Point Microindentation and Recommendations for Testing Cortical Bone: Maximum Load, Sample Orientation, Mode of Use, Sample Preparation and Measurement Spacing*, Journal of the Mechanical Behaviour of Biomedical Materials, Volume 42, doi:10.1016/j.jmbbm.2014.09.030, 2013

Additionally, preliminary results of this study have been presented at the following internal and external conferences

- T. Jenkins, L.V. Coutts, N.C. Harvey, R.O.C. Oreffo, D.G. Dunlop, C. Cooper, P.J. Thurner, *Reference Point Indentation Trends of the Human Femoral Neck,* Poster at European Society of Biomechanics, August 2013
- T. Jenkins, L.V. Coutts, O.L. Katsamenis, N.C. Harvey, P.J. Thurner, *Validation of Reference Point Indentation for Improved Fracture Risk Assessment*, Podium at University of Southampton postgraduate conference, November 2012
- T. Jenkins, L.V. Coutts, O.L. Katsamenis, N.C. Harvey, P.J. Thurner, *Validation of Reference Point Indentation for Bone Fragility Assessment*, Podium at Bath Biomechanics Symposium,

To form recommendations this study considered five parameters, central to RPI testing:

1. The maximum load applied can be varied between 2 N and 10 N but further work is required to investigate the variability with this parameter. Specifically, investigating further species (bovine and human), a larger number of samples (five) and the variation on both periosteal and machined bone that has not previously been addressed. Furthermore, investigating the relationship between coefficient of variation and maximum load is required to establish whether a specific maximum load is optimal.
2. If un-machined, the sample surface will be irregular (e.g. testing the uneven surface of the human femoral neck, Chapter 6) and in this case it may be useful to use the device freehand rather than fixed in its stand, the suitability of which is currently unclear.
3. Bone samples have soft tissue attached and irregular surfaces. Though, for ease or to remain minimally invasive, it would be preferable to leave these in place, it should be established if there is benefit in preparing a test surfaces for reduced variability. If machining the sample surface, the depth of material removed and the resulting thickness of the sample may also introduce confounding effects.
4. In machining a bone sample, it is still not completely clear whether the orientation of the cut and direction of indentation will alter results due to the anisotropic mechanical behaviour of bone. Specifically, investigating further species (bovine as well as human) and locations (the human femoral neck), that have not previously been addressed.
5. In areas with a limited quantity of tissue, measurement spacing is a key factor to maximise the number of measurements. Yet it is unclear which minimum spacing should be used to avoid artefacts from neighbouring indents.

Though some of these parameters have, to some extent, been investigated previously (e.g. maximum load [30], sample orientation [26, 30, 32], sample machining/polishing [30] and soft tissue removal [20, 29]) this study furthers understanding through: a larger number of animals (five compared to typically one or two [29, 30]) and different species/locations (bovine femoral midshaft and human femoral neck/head compared to the previous porcine and human femoral midshaft). Furthermore, parameters that have previously not been investigated (coefficient of variation with maximum load, orientation and sample preparation as well as maximum load on machined and un-machined surfaces, mode of use, sample thickness and measurement spacing) are explored to form a more comprehensive assessment of the variability associated with RPI.

5.2 Materials and Methods

5.2.1 Reference Point Microindentation

The Biodent Hfc^{TM} (Active Life Scientific, Inc, Santa Barbara, California) reference point micro-indenter, as described in section 4.1, was applied to bone investigate the five test parameters. A custom Matlab (Mathworks, Natick, Massachusetts) code (9.5 Appendix 4 – Matlab Algorithms) was used to identify the IDI, TID and CID (first cycle) as defined in section 4.1.2. The three indentation depth parameters tend to indicate similar relationships so only IDI has been presented in this chapter and TID and CID figures shown in '9.3 Appendix 2 – Additional Figures for alternate RPI measures'. Unless stated otherwise, all samples were tested with 3 – 5 repeat measurements (typically limited by the area of the bone sample being tested and the measurement spacing), a 10 N maximum load, the fixed mode of use, a greater than 1 mm sample thickness, in the transverse direction and greater than 2 mm spacing.

5.2.2 Bovine Bone Samples

5.2.2.1 Bovine Sample Preparation

Five whole bovine femora (aged 30 to 36 months and hence expected to have both osteonal and plexiform bone present [280]) were obtained from a local butcher (Uptons of Bassett, Southampton) and sectioned using a band-saw (BG 200, Medoc, Logroño). Firstly, the midshaft (approximately the central 50% of the femur where the cross section was approximately constant and there was no cancellous bone present) was sectioned by removing the proximal and distal epiphyses (Figure 33a). Secondly, three 20 mm-thick slices were removed from the proximal end of this midshaft section. Finally, these three proximal midshaft slices were sectioned into anterior, posteromedial and posterolateral thirds with the anterior and posterolateral samples being used in this study (Figure 33b). The testing of each anterior and posterolateral sections is summarised in Figure 33c and as follows (5.2.2.1 to 5.2.2.8), each being carried out on samples from the five separate animals. Prior to testing samples were stored at -80 °C in Hanks Balance Salt Solution (HBSS) and defrosted in HBSS overnight (over 15 hours). During indentation a syringe was used periodically to apply HBSS to the surface of the bone to maintain hydration.

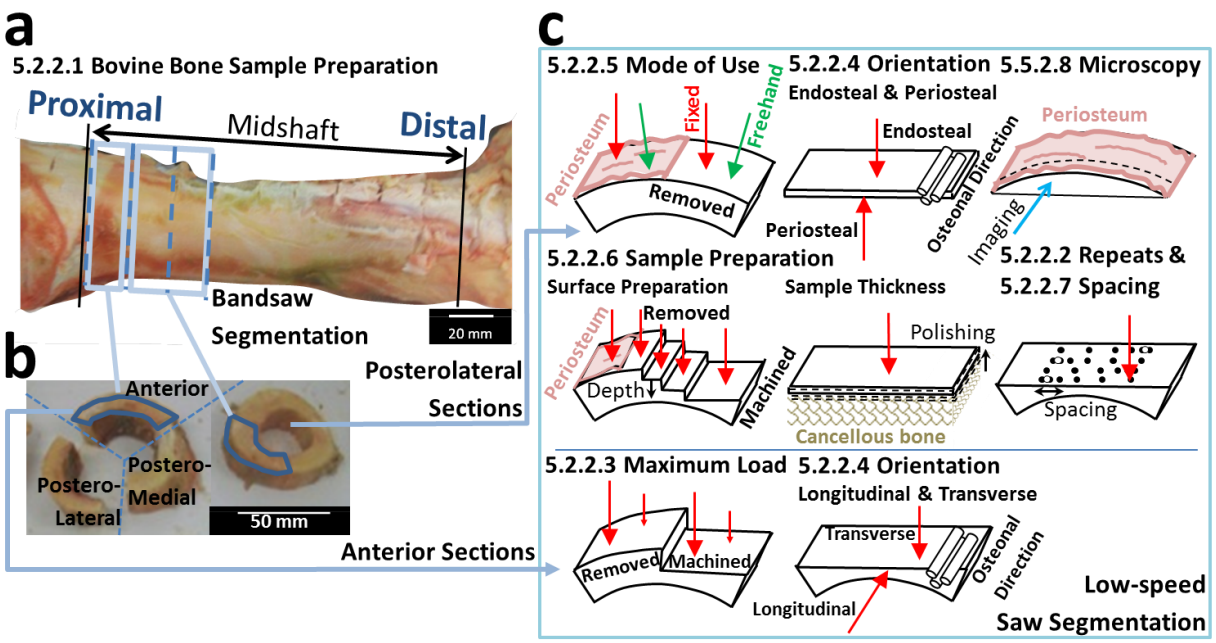

Figure 33 : Bovine Bone Sample Preparation displaying: a) sectioning of the whole bovine bone into approximately 20 mm thick slices, b) sectioning of the bone slices into anterior, posterior-lateral and posterior-medial thirds and c) subsequent Reference Point Indentation testing and fluorescence microscopy imaging.

5.2.2.2 Variation of Repeat Measurements

The surface was removed from posterolateral sections using the band-saw followed by polishing of the surface with 600 grit sandpaper. Twenty-eight repeat measurements were performed over a 15 mm by 15 mm area in the transverse direction on samples from all five animals. These same measurements were used later to consider measurement spacing meaning that 8 of these measurements had a less than 2 mm spacing as indicated in '5.2.2.7 Variation of Measurement Spacing'.

5.2.2.3 Variation of Maximum Load

The maximum load of the Biodent Hfc^{TM} system can be varied between 2 N and 10 N at 1 N intervals. RPI was performed at 2 N (260 g to 310 g preload), 4 N (520 g to 570 g preload), 6 N (780 g to 830 g preload), 8 N (1040 g to 1090 g preload) and 10 N (1300 g to 1350 g preload) on the anterior cortical bone samples in the transverse direction with the periosteum removed using a scalpel and rat-tooth tissue tweezers. Measurements were then repeated at the same loads with the surface removed using a band-saw and polishing with 600 grit sandpaper.

5.2.2.4 Variation of Orientation

The surfaces of the anterior cortical bone samples were removed using a band-saw and polishing using 600 grit sandpaper. Following this sample preparation, the two perpendicular faces were indented to allow for measurement in the longitudinal

(indenting roughly parallel to the direction of the osteons) and transverse (approximately perpendicular to the osteons) directions.

Posterolateral cortical bone samples were cut to a thickness between 1.0 mm and 1.6 mm using a diamond wafering blade on a low-speed saw (IsoMet, Buehler, Lake Bluff, Illinois) and indented in opposite transverse directions on these two parallel faces (i.e. towards the inner surface, endosteally and towards the outer surface, periosteally).

5.2.2.5 Variation of Mode of Use

Indentation was carried out in both the 'fixed' mode (where the RPI device is supported vertically in its stand, Figure 34) and 'freehand' mode (where the device is held by hand, Figure 34) on the posterolateral bone samples. Initially, RPI was performed with the periosteum in place by inserting the probe with a preload and scratching side-to-side with the aim to displace the soft tissue. This allowed for comparison of the two modes with the soft tissue in place. The periosteum was then removed using a scalpel and rat-tooth tissue tweezers and the fixed and freehand indentations repeated to allow for investigation into mode of use with the soft tissue removed.

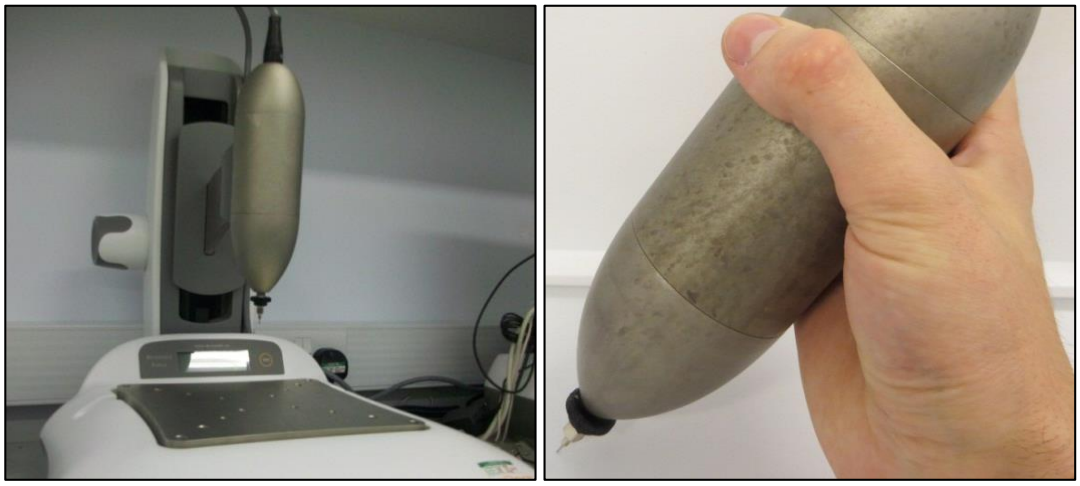

Figure 34 – Example image of the RPI device in fixed and freehand mode of use

5.2.2.6 Variation of Sample Preparation

5.2.2.6.1 Surface preparation

As in the mode of use study (5.2.2.5), the native periosteal surface of each posterolateral bone sample was indented followed by removal of the periosteum using a scalpel and rat-tooth tissue tweezers and repetition of the indentation. Following this, the sample surface was removed using the low-speed saw with multiple cuts. Initially, to a sufficient

depth to remove the curvature of the bone, creating an approximately 20 mm by 20 mm even surface (1.6 mm - 2.6 mm removed, depending on the sample, this is labelled depth 1). Following this, two subsequent cuts first removed 1.0 mm - 1.6 mm (depth 2) and then a further 0.3 mm to 1.9 mm (depth 3), as allowed by the total specimen thickness. Each newly created surface, three in total (depth 1, depth 2 and depth 3), was indented.

5.2.2.6.2 Sample thickness

The surface was removed from the posterolateral bone samples with a second, parallel cut to create 1.2 mm to 1.9 mm thick plates. For indentation, these samples were placed on a section of cancellous bone taken from the distal femur. The purpose of this was to more clearly observe the effects of sample thickness by using a substrate that could support the sample but could not support the indentation probe and, further, as an analogue to the thickness of cortical bone surrounding cancellous bone in the epiphysis as shown in Figure 35. Bone was then removed using 180 grit sandpaper to reduce the thickness of the plates to approximately 1.0 mm before repeat indentation, then again to 0.4 – 0.6 mm and finally to 0.2 - 0.4 mm depending on the sample. The bone was indented on the periosteal side and polished from the endosteal side of this thin sample to allow for the same surface to continue to be indented, avoiding potential confounding factors from heterogeneity in depth. Hydration of the samples was also ensured by keeping the samples submerged in HBSS, prior to and after polishing, keeping the time spent polishing short (approximately 1 to 2 minutes) and periodically applying HBSS via syringe to lubricate the sample as it was polished. For analysis, the results across the five samples were pooled to provide a larger range of sample thicknesses.

This process was repeated on posterolateral samples from two bones for both 2 N and 6 N maximum loads with eight thicknesses ranging from 0.08 mm to 2.25 mm. Again, for the analysis, the results were pooled across the two samples.

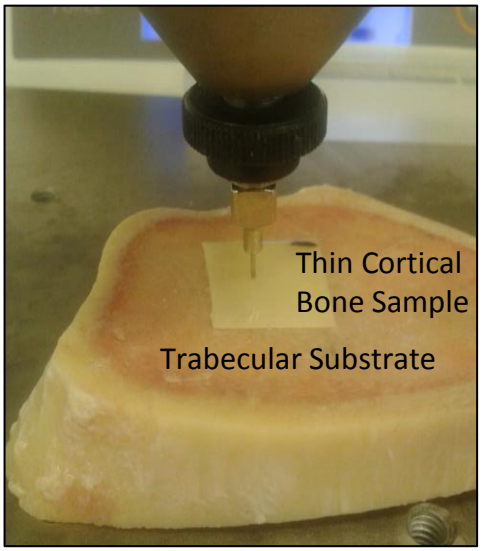

Figure 35 – Variation of sample thickness test set-up

5.2.2.7 Variation of Measurement Spacing

To investigate measurement spacing, RPI was performed on posterolateral sections, varying the distance to the next nearest measurement: greater than 10 mm (Si), 5 mm, 4 mm, 3 mm, 2 mm, 1 mm (S5 etc.) and less than 1 mm with two neighbouring measurements (Sm). This measurement spacing was achieved by following the grid shown in Figure 49. First, creating four indents with at least 10 mm spacing (Si, Figure 49a), then, continuing through the remaining indent spacings in descending order of proximity (S5, S4, S3 etc., Figure 49b). On the same specimens, outside this grid, a further four indents were taken without moving the probe assembly, that is, directly on top of a previous indent.

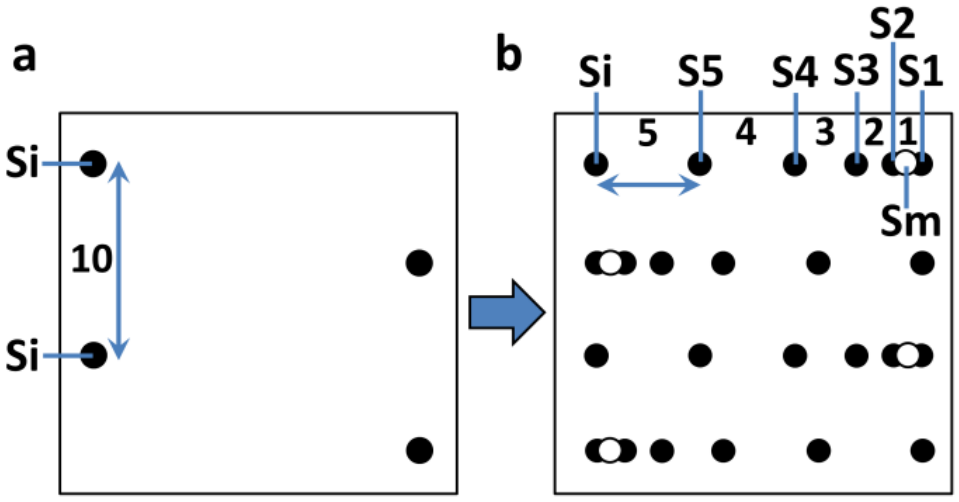

Figure 36 : Measurement Spacing Grid – The grid was followed to allow for measurements with varying spacings. a) First, four indents were made at a greater than 10 mm spacing (Si). b) This was followed by four indents at 5 mm (S5), 4 mm (S4), 3 mm (S3), 2 mm (S2) and 1 mm (S1) spacing. A final indent was made at less than 1 mm spacing between two adjacent measurements (Sm).

5.2.2.8 Fluorescent Light Microscopy Imaging

Samples that had not previously been indented were stained and imaged with the intention of visualising the structure of the bone at the periosteum and further from the surface of the bone. Samples were sectioned from the posterolateral bone and had 1 mm - 2 mm of their outer surface removed using the low-speed saw. These 1 mm – 2 mm surface samples were then polished with 1200 grit sandpaper, 6 µm, 3 µm, 1 µm and then 0.25 µm diamond solutions with rinsing in water and cleaning in an ultrasonic bath (3 minutes) between each successive polish. These 1 mm - 2 mm samples, including the periosteal surface of the bone, were left in 80% ethanol overnight prior to staining in 1% basic fuchsin for 2 hours with a final 5 minute rinsing in 80% ethanol. Imaging of the external structure of the bone was completed with reflectance imaging at the blue wavelength (447 nm, DAPI – 4', 6-Diamidino-2-phenylindole setting) of the epi-fluorescence microscopy (EVOS FL, Life Technologies, Paisley). This process has previously been used by Lee et al [266] and Burr and Hooser [267] for the imaging of microdamage in bone, but here it is used for the improved visualisation of structure and pores towards the periosteal surface of the bone.

5.2.3 Human Bone Samples

5.2.3.1 Source of Human Samples

Human femoral head and neck samples were excised as part of hip replacement surgery (5 donors for investigating maximum load variation in the femoral head and 5 separate donors for investigating variation with orientation and machining) and tested at the University of Southampton under full ethical approval (12/SC/0325 - Southampton A REC and 10/H0604/91 – Oxford A REC). Sectioning and testing of the femoral head and neck samples is summarised in Figure 37 and the subsequent sections (5.2.3.2 to 5.2.3.4).

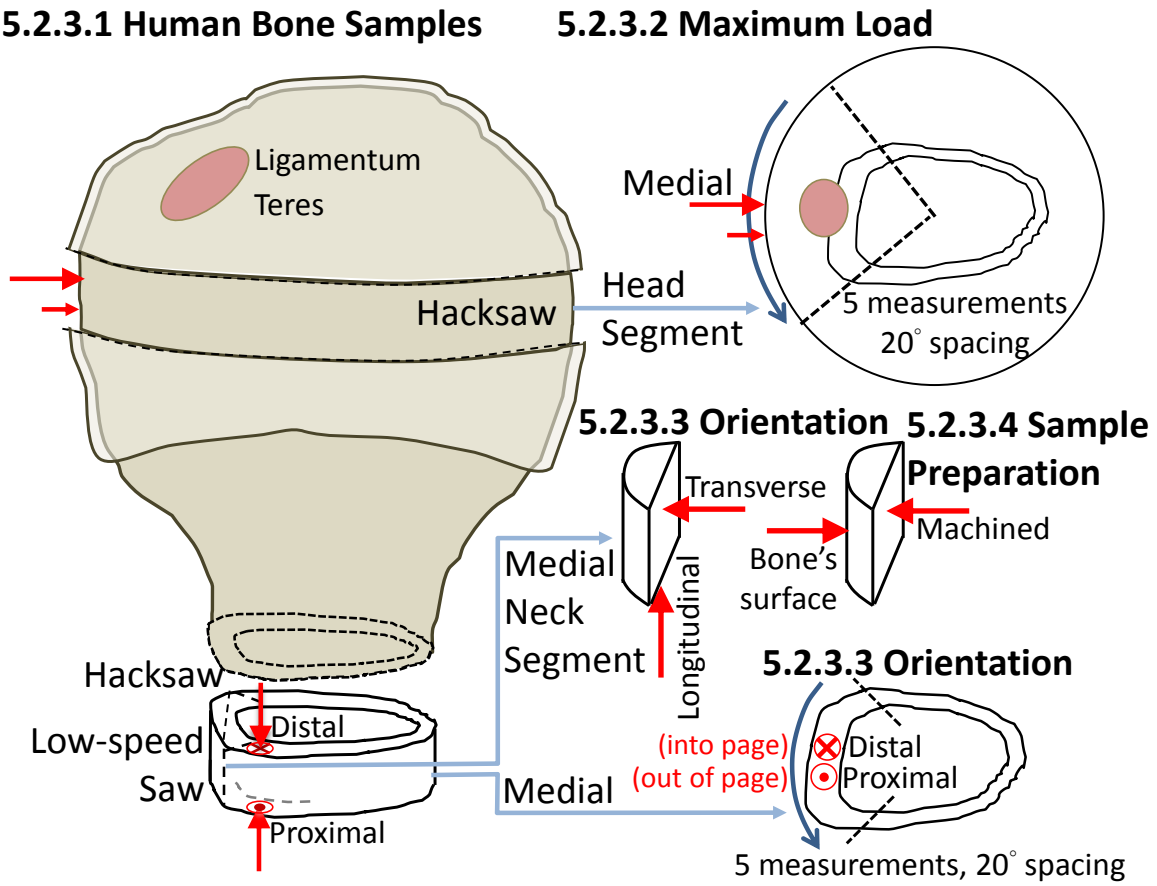

Figure 37 : Human Bone Sample Preparation. Sectioning of the femoral head and femoral neck for subsequent Reference Point Indentation testing.

5.2.3.2 Variation of Maximum Load

A junior hacksaw was used to make two parallel cuts transversely through five femoral heads (two males: aged 67 and 71 and three females aged: 79, 86 and 89) to create a disc-like section. The cartilage was removed using a scalpel prior to testing at 5 test locations (20 degree spacing) in the inferomedial quadrant, using the freehand mode of use. The thickness and porosity of the femoral head made measurement of the femoral head difficult and limited the number of measurements hence RPI was only performed at the minimum (2 N) and maximum (10 N) possible maximum loads.

5.2.3.3 Variation of Orientation

A junior hacksaw was used to remove a 5 mm - 10 mm section from the distal neck of five samples (three males: aged 56, 64 and 79 and two females aged: 58 and 77) by making a cut approximately parallel to the surgeon's cut. Both sides of this section were indented (i.e. on the surgeon's cut in the proximal direction and on the hacksaw cut in the proximal directions) at 5 locations in the inferomedial quadrant (20 degree spacing). The junior hacksaw was again used to section the neck slice in quarters. The inferomedial quarter

was then machined further using a diamond wafering blade and low-speed saw to make a longitudinal cut and remove the periosteal surface of the bone. RPI was carried out in the fixed mode of use on the removed surface in the outwards/periosteal direction for comparison of indentation in the transverse direction (approximately normal to the osteonal direction) with the previously measured proximal/distal longitudinal directions (approximately parallel to the osteonal direction).

5.2.3.4 Variation of Sample Preparation

RPI was performed on the natural outer surface of the inferomedial neck (the five samples investigated in section 5.2.3.3) with the small amount of soft tissue present first being removed. The samples were then machined using a low speed saw and tested in the outwards/periosteal direction as described above (5.2.3.3 Variation of Orientation) for comparison of indentation on a machined surface with that on the surface of the bone.

5.2.4 Statistical Analysis

Initially, 22 measurements were made on the surface of one bovine bone (this is distinct from the 28 repeat measurements performed upon samples from five bovine bones, 5.2.2.2). For these repeat measurements IDI was tested and found to be approximately normally distributed. The histograms had an approximate bell curve shape, the mean and median were similar (within 10%), the mean ± 0.675 x the standard deviation was similar to the upper and lower quartiles (within 10%), 1.35 x the standard deviation was approximately equal to the interquartile range (within 10%) and over 95% of the data was within the range mean ± 1.96 x the standard deviation (indicated by Figure 38). Extrapolating from this, it has been assumed that repeat measurements under the same test conditions can therefore be combined using the mean.

Parametric	Non-parametric
mean	median
mean ± 0.675 x standard deviation	upper/lower quartiles
1.35 x standard deviation	interquartile range

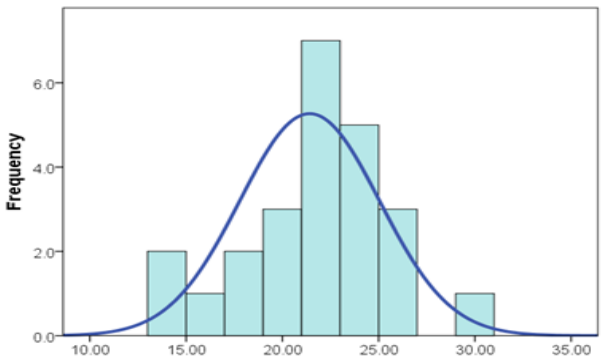

Figure 38 – Indicators of a normal distribution with normality test parameters (left) and the bell-shaped histogram plot (right)

Between the five samples (n = 5) in both the human and bovine testing, the low numbers meant a normal distribution was not observed. Therefore, non-parametric tests were used: the Wilcoxon Signed Rank paired test, the Friedman paired test for multiple comparisons, the Mann-Whitney U-Test for independent samples, the Kruskal-Wallis for multiple independent samples and Spearman's Rank Correlation Coefficient as appropriate. Similarly, the five data points (different markers denote the 5 different samples), the median and the upper/lower quartiles were displayed on the figures. A level of significance of $p < 0.05$ was used and this is displayed on the figures with an asterisk (*). Owing to the small number of samples, any p-values below 0.1 was also noted as close to significance and displayed on the figures with a hash (#).

5.3 Results

5.3.1 Variation of Repeat Measurements

Repeat measurements on one sample are approximately normally distributed as shown by the distribution in Figure 39a on five different samples. However, all the conditions for normality (as discussed above in 5.2.4 Statistical Analysis) are not met, notably 1.35 x the standard deviation tends to be larger than the interquartile range. There are no significant differences between samples ($p = 0.08$ comparing sample 1 and 4, and $p = 0.17$ to 0.88 for all other relationships using the Mann-Whitney U test for comparing pairs of samples and $p = 0.41$ using the Kruskal-Wallis test to compare all samples) and the coefficient of variation is consistently 22.5% to 36.2% (30.7% if considering all samples). This is higher than when considering measurements on PMMA where the coefficient of variation is 5.3% (based on 10 repeat measurements).

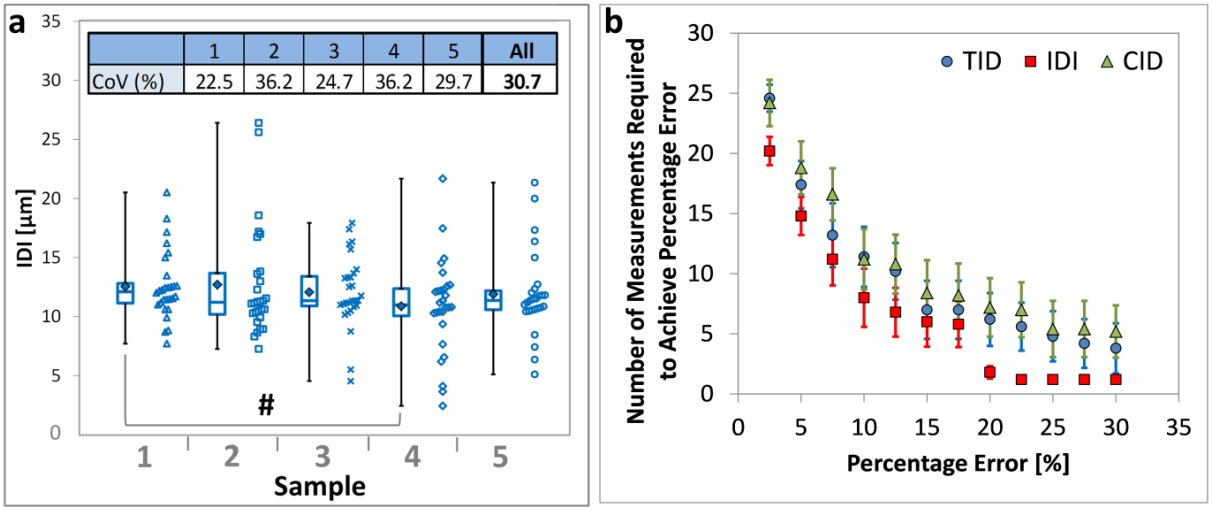

Figure 39 : Variation in Repeat Measurements: a) the coefficient of variation (CoV) and distribution of repeat measurements in five samples. The graphs display the individual measurements, a box plot (the median, upper quartile, lower quartile and range) and the mean (diamond). Differences between samples are displayed as significant (* $p < 0.05$, not applicable) or close to significance (# $p < 0.1$) using the Mann-Whitney U-Test. b) the number of measurements required to achieve a given percentage error from the 'true' value with the error bars showing the standard error. The error bars indicate the standard error across the five samples.

The number of measurements required to obtain a mean value that is representative of the sample is also considered in Figure 39b. Here a cumulative mean was found for 1 to 28 measurements then the percentage error of that mean from the 'true' mean (the mean after 28 measurements) was found. Figure 39b plots the number of measurement required to achieve a certain percentage error for TID, IDI and CID. This shows, in terms of IDI, that to achieve a 10% error, 8 measurements are required or to achieve a 5% error, 15 measurements are required and so on. Conversely, it can be seen that with just 1

measurement the error is 29.4% (in line with the coefficient of variation) and with the 3 to 5 measurements used in this study, the error is between 15% and 20%.

5.3.2 Maximum Load

Figure 40a shows a strong linear relationship between IDI and increasing maximum load on a machined surface ($r = 0.94$, $p < 0.001$). With the natural surface of the bone in place (i.e. without machining) and only the periosteum removed, this relationship can still be seen though with a weaker relationship ($r = 0.45$, $p = 0.025$). Additionally, on the natural surface of the bone, there is no significant increase in IDI above 4 N ($p = 0.14$ to 0.69) perhaps representing a plateau above 4 N. However, the median values do continue to increase (14.4 µm, 16.1 µm, 18.6 µm, 20.0 µm and 20.7 µm at 2 N, 4 N, 6 N, 8 N and 10 N respectively) perhaps only deviating away from the linearly increasing relationship in IDI above 6 N or 8 N. Indenting the human femoral head samples also show an increase in IDI (close to significance, $p < 0.1$) from a 2 N to a 10 N maximum load (Figure 40b), however the thickness of the cortices at this site may add confounding. Though IDI varies with maximum load on both the periosteal and machine surfaces (Friedman's test $p < 0.05$), the difference between the coefficients of variation at various loads is also not statistically significant for human or bovine bone ($p > 0.05$, graph not shown).

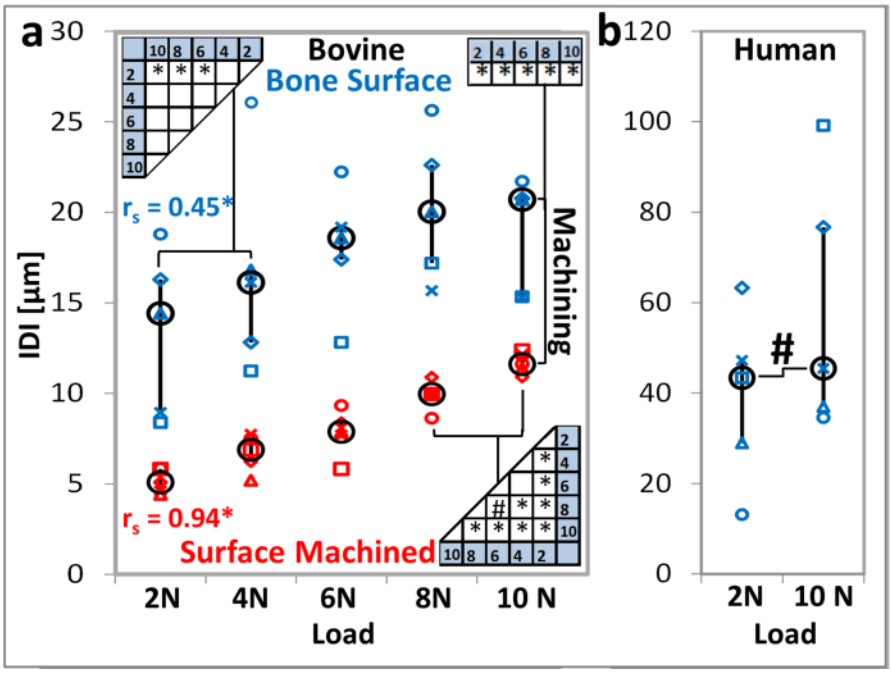

Figure 40 : Variation of IDI with maximum load on the periosteal and machined surfaces of: a) bovine bone and b) human medial femoral head with the cartilage removed. Results are displayed as significant (* $p < 0.05$) or close to significance (# $p < 0.1$) and display mean values for each sample (each marker representing a different sample) as well as the median and interquartile range across the five samples. a) r_s is the Spearman's correlation. The rectangular table displays the level of significance between the non-machined and machined bone at each different load. The triangular tables display the level of significance between the different loads for the bone's surface (a - top left) and machined surface (a - bottom right).

5.3.3 Orientation

Within bovine bone (Figure 41a), indentation is not significantly different in the longitudinal compared to the transverse direction in terms of IDI, nor when comparing the endosteal (transversely inwards) and periosteal (transversely outwards) directions (the p value is greater than 0.5 in all cases). When indenting human femoral neck (Figure 41b), again there are no significant differences between IDI in the longitudinal compared to transverse directions and also when indenting longitudinally in the distal compared to proximal directions (again, the minimum p value is 0.5). It should be noted that when comparing the proximal and distal directions there may be an effect from measurement location (i.e. there is a 5 mm to 10 mm gap between these samples, the thickness of the neck slice) that has not be investigated here.

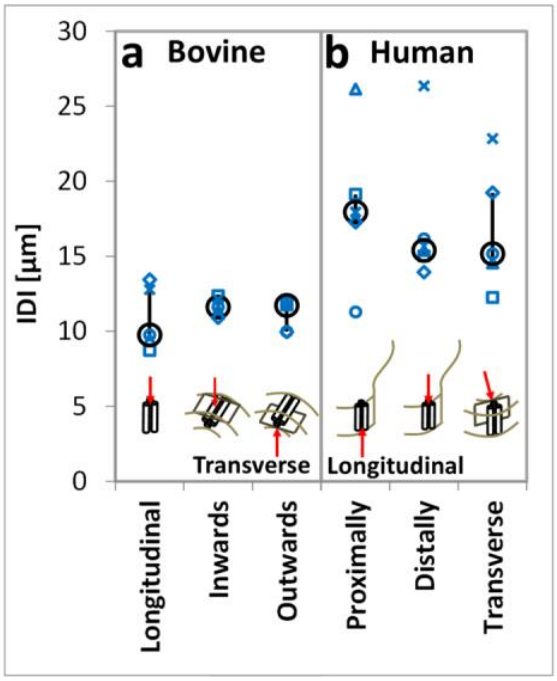

Figure 41: Variation of IDI with orientation on bovine bone with in the longitudinal and transverse endosteal (inwards)/periosteal (outwards) directions (a) and on the human medial femoral neck in the transverse and distal/proximal longitudinal directions (b). The graphs display mean values for each sample (each marker representing a different sample) as well as the median and interquartile range across the five samples

5.3.4 Mode of Use

When working with the 'fixed' mode of use on an unprepared bone surface (i.e. periosteum in place), the IDI is significantly higher (p = 0.04) compared to the 'freehand' mode (Figure 42a). However, though this difference is large in one sample (30.8 µm compared to 19.6 µm, 57% higher), it is marginal in the other four samples (1% to 9% higher). With the periosteum removed, there is no difference between the modes of use in terms of IDI (p = 0.23). Despite these similarities between the modes, the 'freehand' mode is more variable in terms of IDI, having a higher coefficient of variation, when the periosteum is in place (p = 0.04), and likely also when it is removed (p = 0.08, close to significance, Figure 42b).

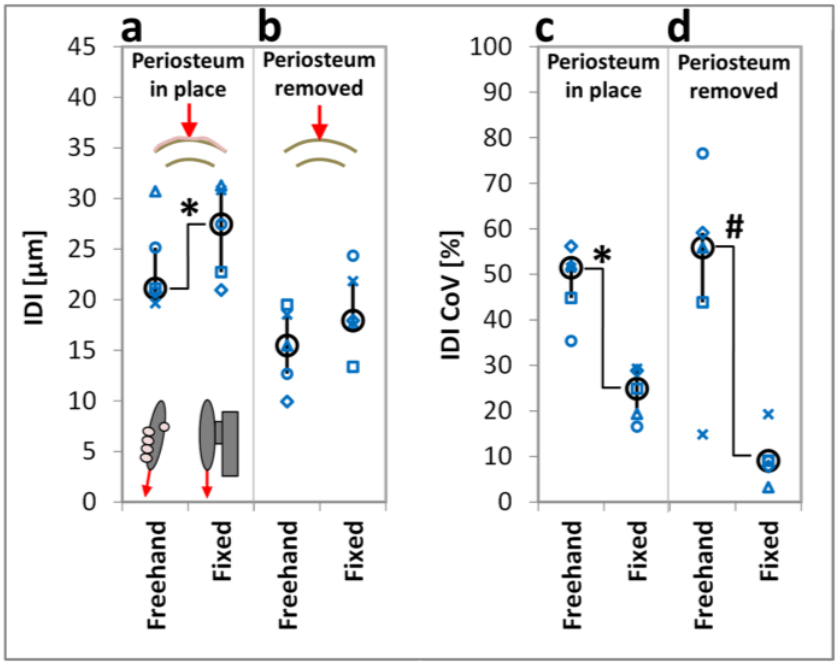

Figure 42: Variation of IDI with mode of use (a) and the coefficient of variation (CoV) of these measurements (b). Results are displayed as significant (* p < 0.05) or close to significance (# p < 0.1) and the graphs display mean values for each sample (each marker representing a different sample) as well as the median and interquartile range across the five samples

5.3.5 Sample Preparation

Figure 43a shows that surface preparation affects the IDI (Friedman test p = 0.004) with removal of the soft tissue reducing the IDI (p = 0.04), doing this also significantly reduces the coefficient of variation (p = 0.04, graph not shown). Machining the bone's surface further reduces the IDI (Figure 43a) regardless of maximum load used (Figure 40a, p = 0.04) and there is also a possible reduction in coefficient of variation (p = 0.08, close to significance - graph not shown). In the human samples (Figure 43d), the same reduction with machining of the surface is again seen (p = 0.04). However, it should be noted that in this case the natural surface is indented endosteally (inwards) whereas the

machined surface is indented periosteally (outwards) (cf. Figure 43d), though these two orientations were found to be similar in bovine bone (Figure 43a). When testing bovine bone, increasing the amount of the bone's surface removed, i.e. indenting deeper from the periosteal surface, has no further effect on the IDI (Figure 43a, $p > 0.5$). Additionally, by plotting depth as a continuous variable, there is also no significant correlation with IDI ($p = 0.64$, Figure 43b).

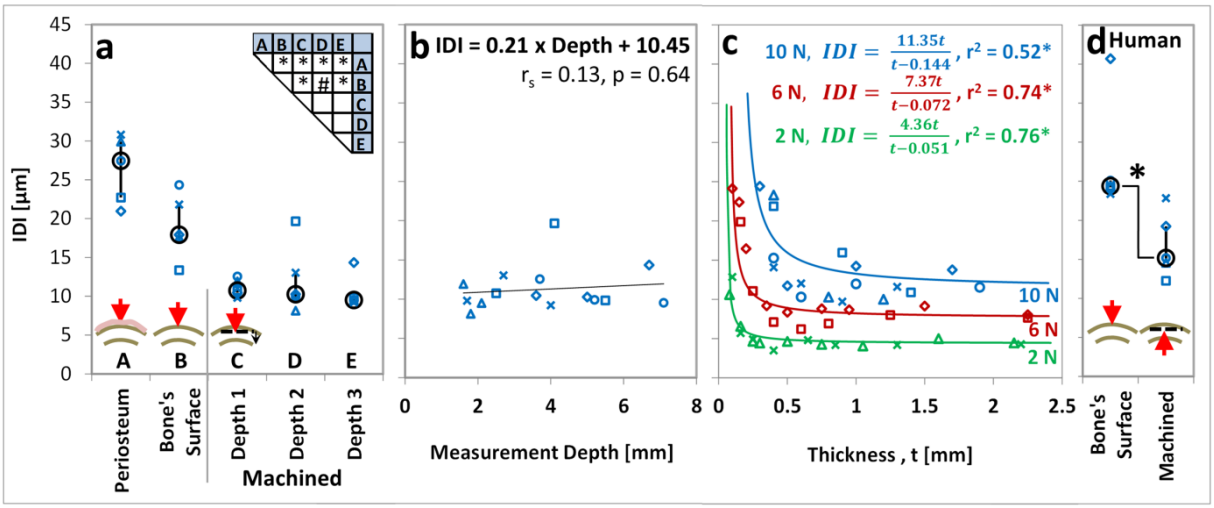

Figure 43: Variation of IDI with sample preparation considering the removal of the periosteum and bone's surface (a), the depth the surface removed (b), the thickness of the sample (c) on bovine bone and the removal of the surface on human bone (d). All figures display the mean values for each sample (each marker representing a different sample). (a) and (d) additionally show the median and interquartile range across the five samples and (b) and (c) display the Spearman's correlation (r_s) and adjusted correlation (r^2). Results are displayed as significant (* $p < 0.05$) or close to significance (# $p < 0.1$). The triangular table in (a) displays the level of significance between the different sample preparations. The equation in (b) is of the form IDI = m x Depth + C where IDI is in µm, depth is in mm, m is the gradient [µm/mm] and C is the y-intercept [µm]. The equations in (c) are of the form IDI = P_1 x thickness/(thickness-P_2) where IDI is in µm, thickness is in mm, P_1 represents the horizontal asymptote [µm] and P_2 represents the vertical asymptote [mm].

The sample thickness exhibits an approximately hyperbolic relationship with IDI (IDI = P_1 x thickness/(thickness - P_2), $p < 0.001$) (Figure 43c). The horizontal asymptote (P_1) represents the "true" IDI - that of an infinitely thick sample. The mean of the "thick" samples (8 to 10 measurements on a greater than 2 mm thick sample) was found and the horizontal asymptote constrained to this value (P_1 = 11.35 µm, 7.37 µm and 4.36 µm for 10 N, 6 N and 2 N respectively). The vertical asymptote (P_2) represents an infinite IDI, which is approximately the minimum possible thickness that can be indented (P_2 = 0.144 mm, 0.072 mm and 0.051 mm for 10 N, 6 N and 2 N respectively). It should be noted that measurements at this "minimum" thickness were not possible as the probe began to punch through the cortical bone sample into the underlying trabecular bone at approximately 0.30 mm, 0.10 mm and 0.08 mm for 10 N, 6 N and 2 N respectively.

To achieve an IDI within two standard deviations of the mean for a "thick" sample (11.35 ± 2 x 2.14 µm, 7.63 ± 2 x 1.14 µm and 4.36 ± 2 x 0.57 µm for 10 N, 6 N and 2 N respectively, again based on 8 to 10 measurements on a greater than 2 mm thick sample), the range in which 95% of normally distributed data will lie, the minimum thickness should be selected as 0.53 mm, 0.31 mm and 0.25 mm for 10 N, 6 N and 2 N respectively. Using a more conservative, one standard deviation limit, the minimum required thickness is increased by to 0.91 mm, 0.55 mm and 0.44 mm.

5.3.6 Measurement Spacing

Measurement spacing from greater than 10 mm and down to multiple measurements within less than 1 mm of each other does not significantly alter the IDI ($p > 0.05$, Wilcoxon and Friedman tests). One possible exception to this is a slightly elevated measurement at 3 mm spacing ($p = 0.08$, Figure 44a), which is close to significance.

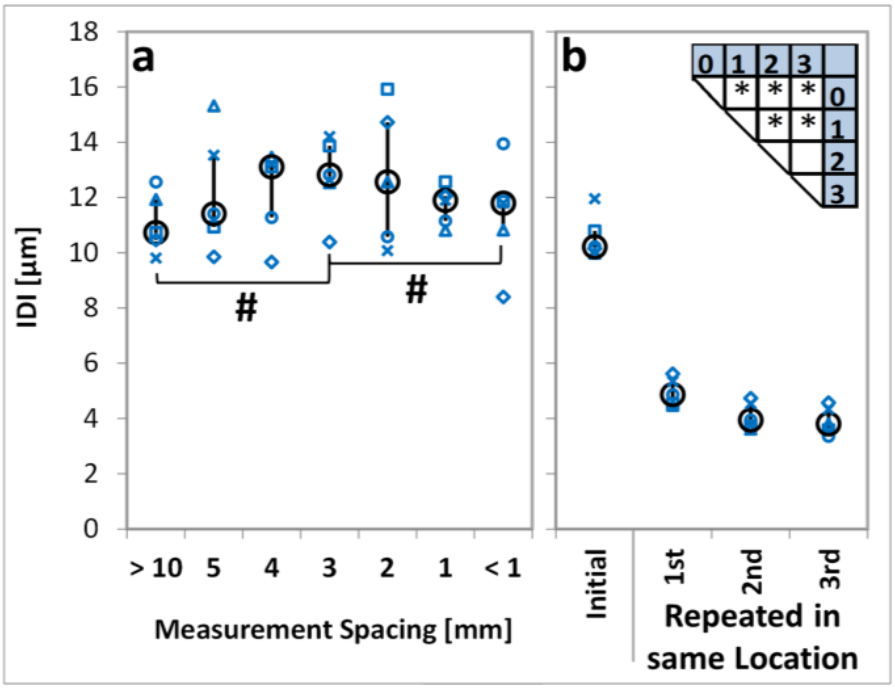

Figure 44: Variation of IDI with measurement spacing (a) and indentation repeated on the same location (b) in bovine bone. Results are displayed as significant (* $p < 0.05$) or close to significance (# $p < 0.1$) and the graphs display mean values for each sample (each marker representing a different sample) as well as the median and interquartile range across the five samples. b) The triangular table displays the level of significance between the different numbers of repeat measurements (with 0 representing the initial measurement, 1 the 1st repeat etc.)

Measuring in exactly the same location does reduce the IDI (Figure 44b, Friedman test, $p = 0.003$) from 10.0 µm - 12.0 µm for the initial indentation down to between 4.5 µm - 5.6 µm for the first repeat indent ($p = 0.04$). A second indentation without moving the probe reduces the IDI further still (down to 3.6 µm - 4.7 µm, $p = 0.04$) but this plateaus and is consistent for a third repeat indentation (3.4 µm - 4.6 µm, $p = 0.23$).

5.3.7 Total Indentation Distance and Creep Indentation Distance

Table 1 and '9.3 Appendix 2 – Additional Figures for alternate RPI measures' shows the RPI results in terms of TID and CID. In comparison to IDI, similar relationships are seen in terms of variation with load, orientation, mode-of-use, sample preparation and measurement spacing, however, there are some minor exceptions.

TID is significantly higher in the outward transverse orientation compared to the inward transverse and longitudinal orientations ($p = 0.04$), which is not seen in IDI ($p = 0.50$) or CID ($p = 0.23$). No significant differences are seen between the fixed and freehand mode of use in terms of TID ($p = 0.69$) or CID ($p = 0.14$) or their coefficients of variation (minimum $p = 0.14$) whereas marginal, though significant differences are observed for IDI ($p = 0.04$). Repeat measurements in the same location seem to have minimal effect on TID ($p = 0.23$), though even the initial measurement does appear lower than at other spacings. Contrary to this, both IDI and CID both show a large initial reduction with the first repeat and similar measurements with the first, second and third repeats. The coefficient of variation (Figure 39) is comparable for IDI and CID (30.7% and 33.3% respectively) though higher for TID (44.5%) with IDI needing fewest measurements to achieve a given error.

Table 1 - Summary of results showing the measurement parameters investigated in terms of IDI, TID and CID. Results are in microns apart from the coefficients of variation (CoV), which are given as a percentage. Significance is shown through p-values based on the Wilcoxon Signed Rank or Spearman's rank correlation (r_s) and shown in black if significant or close to significance ($p < 0.1$) or grey otherwise ($p > 0.1$). The superscript letters given with the p-values indicates the comparison being made (given in superscript next to the appropriate median values). (F-H: Freehand Mode of Use).

Parameter				IDI [µm]		TID [µm]		CID [µm]	
Repeat	Bovine Machined		CoV across all samples	30.7%		44.5%		33.3%	
Maximum Load	Bovine Bone Surface		2 N	14.4	$r_s = 0.45$ $p = 0.046$	93.4	$r_s = 0.75$ $p = 0.0001$	9.8	$r_s = 0.45$ $p = 0.046$
			4 N	16.1		127.5		8.6	
			6 N	18.6		150.6		13.1	
			8 N	20.0		171.0		13.0	
			10 N	20.7		167.3		12.1	
	Bovine Machined		2 N	5.1	$r_s = 0.94$ $p < 0.0001$	37.4	$r_s = 0.98$ $p < 0.0001$	3.4	$r_s = 0.78$ $p < 0.0001$
			4 N	6.9		53.2		4.1	
			6 N	7.9		72.4		6.2	
			8 N	10.0		89.6		6.7	
			10 N	11.6		101.0		6.4	
	Human (Fem. Head)		2 N	43.4	p = 0.08	128.1	p = 0.04	9.1	p = 0.04
			10 N	45.4		299.0		19.6	
Orientation	Bovine		Long.	9.8	$p_{min} = 0.50$	97.6^{a}	$p^{a, b} = 0.04$	6.8	$p_{min} = 0.35$
			Inwards	11.6		101.0^{b}		6.4	
			Outwards	11.7		236.7^{ab}		5.6	
	Human (Fem. Neck)		Prox.	17.9	$p_{min} = 0.50$	170.7	$p_{min} = 0.23$	8.7	$p_{min} = 0.23$
			Dist.	15.4		125.7		8.9	
			Trans.	15.2		117.7		8.2	
Mode of Use	Bovine	Peri-osteum	F-H	21.1	p = 0.04	281.7	*p = 0.69*	11.2	*p = 0.14*
			Fixed	27.5		268.9		14.4	
		Bone Surface	F-H	15.5	*p = 0.23*	188.9	*p = 0.89*	9.6	*p = 0.50*
			Fixed	17.9		187.0		9.4	
		Peri-osteum	CoV F-H	51.5%	p = 0.04	21.3%	*p = 0.14*	45.4%	*p = 0.23*
			CoV Fixed	24.9%		11.5%		36.4%	
		Bone Surface	CoV F-H	55.9%	p = 0.08	26.6%	*p = 0.23*	27.0%	*p = 0.89*
			CoV Fixed	9.1%		14.9%		18.9%	
Sample Prep.	Bovine		Tissue	27.5^{a}	$p^{a} = 0.04$ $p^{b} = 0.04$ $p_{min}{}^{c} = 0.50$	267.5^{a}	$p^{a} = 0.14$ $p^{b} = 0.23$ $p_{min}{}^{c} = 0.69$	14.4^{a}	$p^{a} = 0.04$ $p^{b} = 0.08$ $p_{min}{}^{c} = 0.14$
			Surface	17.9^{ab}		187.0^{ab}		9.4^{ab}	
			Depth 1	10.7^{bc}		134.0^{bc}		5.8^{bc}	
			Depth 2	10.3^{c}		153.9^{c}		5.2^{c}	
			Depth 3	9.5^{c}		130.4^{c}		4.7^{c}	
	Human (Fem. Neck)		Surface	24.4	p = 0.04	214.7	p = 0.04	11.3	*p = 0.14*
			Machined	15.2		117.7		8.2	
Measurement Spacing	Bovine		> 10 mm	10.7^{a}	$p^{a, b} = 0.08$ *else, p = 0.14 to 0.89*	134.0	$p^{a} = 0.08$ *else, p = 0.14 to 0.89*	5.8^{a}	$p^{a,b} = 0.08$ $p^{c} = 0.04$ *else, p = 0.23 to 0.89*
			5 mm	11.4		128.2^{a}		6.1^{c}	
			4 mm	13.1		140.0^{a}		6.2	
			3 mm	12.8^{ab}		141.8		6.3^{ab}	
			2 mm	12.6		140.6		5.5	
			1 mm	11.9		121.8		4.8^{c}	
			< 1 mm	11.8^{b}		122.9		6.4^{b}	
			First	10.2	p = 0.04 *p^{a} = 0.23*	90.6	*p_{min} = 0.23*	5.9	p = 0.04 $p^{a} = 0.08$
			Repeat 1	4.9		95.5		3.3	
			Repeat 2	3.9^{a}		98.2		2.7^{a}	
			Repeat 3	3.8^{a}		100.2		2.8^{a}	

5.4 Discussion

Based on these results, recommendations can be made to optimise future testing through the investigation of variability in reference point indentation across five different parameters: i) maximum load, ii) orientation of the bone, iii) mode of use of the device, iv) sample preparation and, v) measurement spacing.

5.4.1 Variation of Repeat Measurements

The inherent variability associated with the device appears to be low (i.e. 5.3% coefficient of variation on heterogeneous PMMA with 10 repeat measurements at 10 cycles and 10 N – graph not shown). However, factors associated with the bone (e.g. location of measurements relative to Haversian canals, lamellar structure, local density variation etc.) increase this variability to around 30%. Therefore, it is clear that further repeat measurements are necessary to discern smaller changes. The number of measurements here (3 to 5) allows for detection of a 15-20% change in IDI, with repeats in five donors improving this further. This current study highlights that further measurements, beyond the 3 to 5 used here, would be able to detect a smaller effect size, however we were previously limited by the area being tested (typically 20 mm by 20 mm bovine bone sections) and the previously unknown effect of measurement spacing in this study. Therefore, smaller effects or need for greater precision would require further repeats i.e. 8 to 15 measurements for a 5% to 10% error. This is similar to the 10 measurements recommended for human bone or the 20 measurements in horse bone in the clinical study by Randall et al [20].

5.4.2 Maximum Load

As might be expected, the IDI increases with maximum indentation load meaning this parameter should be kept consistent throughout testing. Consistency with coefficient of variation implies there is no preferred load and that the load most suitable for the sample should be selected. This linear relationship appears similar to that published by Setters and Jasiuk [30] in porcine bone for all parameters except for IDI where they show a cubic relationship.

As well as being observed on the machined surface, this increase in IDI with load is still present when testing the natural surface of the bone, but with a no significant increase in IDI above 2 N. Though this is similar to the trend found by Setters and Jasiuk [30] for IDI,

their study observes polished bone rather than the natural surface here. Instead, we hypothesise that this relationship may relate to the TID compared to the variation in bone structure and properties with depth. At low loads (e.g. 2 N to 4 N) the TID ranges between 50 µm and 150 µm. This is below the thickness of the circumferential lamellae and plexiform bone that make up the outer surface of the bone [91, 195, 281, 282]. However, at higher loads (e.g. 6 N to 10 N), the probe indents up to a depth of 200 µm, which is in the region of the 200 µm thick outer layers measured from the fluorescence microscopy (Figure 45) or the 400 µm thick circumferential layers previously reported [282, 283]. Therefore, at lower loads the indentation depth may be influenced by these outer layers alone, whereas at higher loads it may also be impacted by the underlying osteonal structure (depicted in Figure 45).

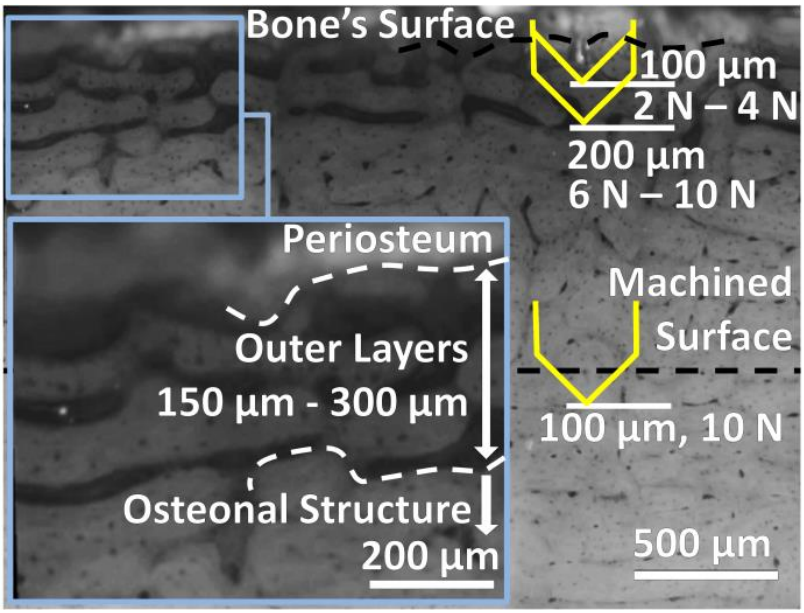

Figure 45: Fluorescence Microscopy Image of a Cross Section of Bovine Bone. The diagram indicates thickness of the outer layers and the total indentation distance with low (2 N – 4 N) and high (6 N – 10 N) load on the natural and machined surfaces.

The increase in IDI also appears apparent on the femoral head of human bone, though this was not quite significant ($p = 0.08$) with thickness perhaps also influencing the indentation depth, particularly at higher loads. The thin bone also created difficulties in indenting the femoral head and limited the number of measurements. Hence, only the maximum (10 N) and minimum (2 N) loads were used and it would be of further interest to investigate other load increments (i.e. 4 N to 8 N) in thicker human cortical bone.

5.4.3 Sample Preparation

5.4.3.1 Machining

The presence of a structurally distinct outer surface also explains differences seen with sample preparation, where the removal of these outer layers significantly reduces the IDI in both bovine and human bone. Indenting the surface would therefore be measuring the indentation properties of these outer layers but indenting a machined surface would be measuring the properties of the seemingly more resistant underlying osteonal structure. Setters and Jasiuk [30] observe similar changes when comparing polished and unpolished surfaces in one porcine femur. With further machining, removing the surface to greater depths, the IDI is unchanged, representing the lack of change in structure through the depth beyond the initial outer layers.

5.4.3.2 Soft Tissue

Contrary to the studies by Hansma et al [29] and Randall et al [20], presence of the periosteum also increases the IDI beyond indentation of the natural surface alone. Instead of the not significant 10% increase seen by Hansma et al [29], a significant increase in IDI with soft tissue in place was noted with both the fixed mode (13% to 78% depending on sample) and freehand mode of use (6% to 100%). This disparity may relate to a number of differences in the studies: the number of samples (one [20, 29] rather than five tested here), the species (human [20, 29] rather than bovine tested here), the indenter model (Osteoprobe II™ [20, 29] rather than the Biodent Hfc™ used here) and bone's heterogeneity (two locations 10 cm apart [20] rather than in the same 2 cm section used here). Based on our findings, we believe the presence of soft tissue influences RPI and thus, do not recommend comparing results with the periosteum removed with those where it is left in place. Additionally, the coefficient of variation reduces with removal of the periosteum and machining of the surface, so this sample preparation is recommended where possible.

5.4.3.3 Sample Thickness

The hyperbolic relationship between IDI and sample thickness means that samples should be kept thicker than 0.25 mm for a 2 N maximum load, 0.31 mm for 6 N and 0.53 mm for 10 N. The indentation depth (TID) represents 11% to 19% of these threshold thicknesses, recommending a thickness of 10 times the indentation depth, in line with the general rule

of thumb for other indentation techniques. By keeping samples above this threshold, thickness should have a minimal effect on the indentation to improve measurement consistency. Additionally, at higher thicknesses any deformation caused by the preload applied by the reference probe will also be minimised. Conversely, where sample thickness is the limiting factor (e.g. the cortical thickness towards the epiphysis or of small animal bones), the maximum load should be limited to allow no greater than 10% of the sample thickness to be indented. Particularly, the 2 N, 6 N and 10 N maximum loads should only be used for samples thicker than 0.25 mm, 0.31 mm and 0.53 mm respectively.

It should be considered that this study investigates bovine bone on a relatively dense cancellous sample from the bovine distal condyle. With poorly supported samples (for example osteoporotic femoral heads or the midsection of small animal bones) the thickness of the sample will be more critical and, therefore, lower maximum loads are likely to be necessitated.

5.4.4 Orientation

Similar to the consistency of RPI with machining depth, the technique did not detect any changes between structurally identical orientations, the periosteal (outwards) and endosteal (inwards) directions in bovine bone and the proximal and distal directions in human bone. However, mechanical differences in structurally distinct orientations, the longitudinal and transverse directions, also were also not detected by RPI in either bovine or human bone. Despite this, Rasoulian et al [32], Setters et al [30] and Granke et al [26] did report a difference in indentation parameters between the transverse and longitudinal directions. In the case of Setters and Jasiuk [30], the IDI was significantly higher in the transverse direction. Whereas, though Granke et al [26] found average CID and average energy dissipated (also TID and CID1 of the lateral and medial quadrants) were higher in the transverse direction and loading/unloading slope parameter were higher in the longitudinal direction, IDI showed no significant differences between the two orientations. Additionally, where the difference between the two orientations was found to be significant, the magnitude of this difference is similar to the not-significant increase in the transverse direction seen here in bovine bone. Rasoulian et al [32] compared machined bone in the longitudinal direction with the natural bone's surface in the transverse direction, therefore, the higher magnitude of this difference most likely

relates to the removal of the periosteal surface as described above rather than orientation alone.

The anisotropy of bone relative to the direction of the osteons leads to a fivefold increase in fracture toughness when comparing the transverse direction (i.e. breaking mode) to the longitudinal direction (i.e. splitting mode), where cracks must propagate through the osteons rather than along their length [110]. Conversely, the tensile and compressive elastic moduli and yield strength are about two-fold greater in the longitudinal compared to transverse direction [241]. As RPI has previously demonstrated some correlation with both fracture toughness [19] and elastoplastic properties [25, 26] it may be that these counter-orientated anisotropies, to some extent, have a cancelling effect. This highlights that it is still not entirely clear what mechanical property, or combination of properties, is being assessed by RPI. Though, the two orientations appear similar, this study, alongside the literature [26, 30, 32], implies that the transverse direction yields a marginally higher IDI and care should still be taken when combining results from these two structurally distinct orientations. It should also be noted that the direction of the osteons has not been imaged and the 'transverse' and 'longitudinal' orientations instead relate to the long axis of the bone, from which the osteonal axis may have some discrepancy.

5.4.5 Measurement Spacing

The sample spacing seems to have little effect on IDI from a spacing of greater than 10 mm down to sub-millimetre spacing. However, measuring in exactly the same location does reduce the IDI noticeably (greater than 50%) implying previous indentations can affect subsequent measurements in close proximity. Therefore, providing the spacing is greater than the indent diameter, which could theoretically be as large as the probe diameter of 350 µm, the previous indent should have little to no effect on subsequent measurements. To accommodate the reference probe (750 µm diameter) a conservative minimum spacing of 500 µm is recommended. If there are difficulties in locating the precise location of a subsequent indent relative to a previous indent (i.e. particularly in the freehand mode of use where positioning may be more variable), a larger minimum spacing may be required to accommodate for this uncertainty. Additionally, areas that have previously been heavily indented should be avoided for further testing. Alongside the need for repeat measurements, this recommendation is particularly important as it allows for a large number of measurements to be carried out in a relatively small area.

5.4.6 Mode of Use

Considering the mode of use, comparing the device being fixed in its stand to being held freehand, a significant difference between the two modes could be seen. IDI using the fixed mode of use, though significant, is only marginally higher when the periosteum was in place (median 8% higher) and on removal of the periosteum this difference is not significant. Though the results were similar with both modes of use, the coefficient of variation is significantly and substantially higher (a median of 2 fold increase with the periosteum in place and 8 fold when removed) using the freehand rather than fixed mode of use. This variability with the freehand mode is likely to relate to the difficulty in achieving a consistent preload as well as keeping the probe angle constant and within 10° of normal as recommended by Bridges et al [31]. The similarities in IDI values between the two modes means the freehand mode can be used where practical, such as with particularly irregular samples (for example the human femoral neck samples tested within Chapter 6) or in clinical studies where the device must be angled to achieve indentation normal to the bone's surface. However, with this freehand mode there is a higher variation, requiring a greater number of measurements and therefore the fixed mode of use is preferred where suitable. Furthermore, confounding factors presented by the different modes of use should be avoided through consistently using fixed or freehand modes throughout a study.

5.4.7 Measurement Parameter

Based on their variability, IDI and CID are preferable measures compared to the TID. The increased variability associated with TID is likely to relate to difficulties in detecting the touchdown point. Particularly where soft tissue or even the outer surface of bone is in place, there is initial variation in the stiffness rather than a clear transition between moving in air and loading of bone as demonstrated by Figure 46. Other parameters associated with the device such as first cycle indentation distance and energy dissipated (area under the curve) are also likely to be affected in a similar way. However, both IDI and CID only rely on the peak and retraction points, which are typically straightforward and clear to identify, making these parameters more robust and recommended for use. Hence, IDI and CID typically tend to agree on the relationships observed whereas there is some discrepancy when using TID.

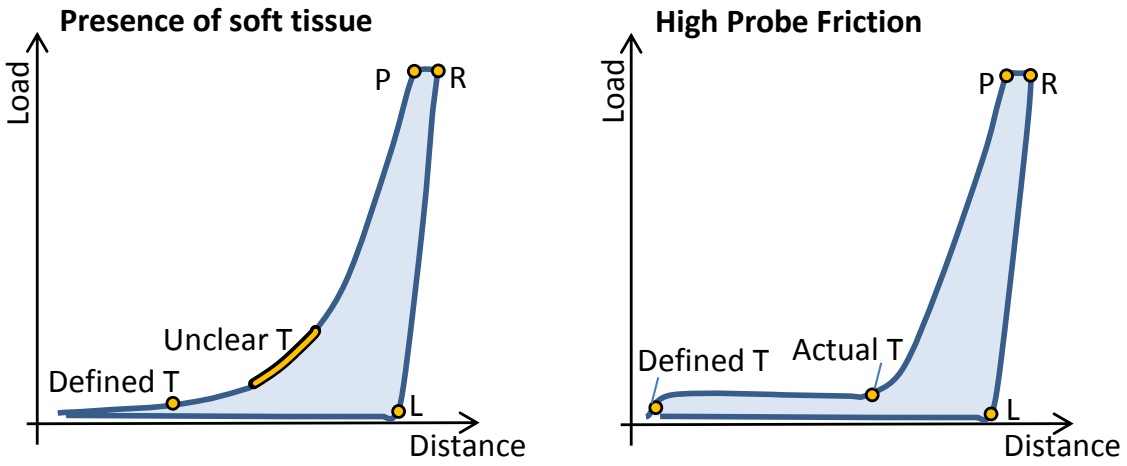

Figure 46 – Examples of "incorrect" first cycle loading leading to incorrect selection of the touchdown point (T) and hence touchdown distance but correct section of the Peak Load (P), Retraction (R) and Lift-off (L). This could potentially be due to: Left: presence of soft tissue or Right: high friction of the test probe

5.4.8 Species of Bone

Though the IDI is typically higher for human bone in comparison to bovine bone, the test parameters investigated in both models yields similar results. That is, in both human and bovine bone IDI: increases with load, is minimally affected by structurally distinct or different orientations and decreases with machining of the sample surface. Additionally, this study concurs with the findings of Setters and Jasiuk in porcine bone [30], particularly in terms of the relationship with load. This implies that many of the recommendations and optimisation for reduction of variability derived in bovine bone can be directly applied when testing human bone or other animal models. However, differences in mechanical [284], compositional [285] and structural properties [195] between different types of bone may require further adaptation of the bovine testing protocol when applied to human or other animal bone. Therefore, though these relationships do appear applicable in different animals, due to the considerable range in properties of bone, care should still be taken when applying the recommendations established here directly to other animal models.

5.5 Conclusions

By considering five measurement parameters associated with RPI, recommendations have been established for the maximum load, mode of use, sample orientation, sample preparation and measurement spacing. In summary, the best practice for such measurements is:

1) Repeat measurements to reduce variability in line with the effect size being observed (8 to 15 measurements recommended for a 5% to 10% error).

2) Keep maximum load, sample orientation, mode of use and surface preparation consistent throughout testing.

3) Use the fixed mode of use when possible.

4) Remove the periosteum and machine the surface of the bone when possible.

5) Ensure a sample thickness 10 fold greater than the maximum indentation depth.

6) Select a suitable maximum load for the sample thickness with a 2 N, 6 N and 10 N only being appropriate above 0.25 mm, 0.31 mm or 0.53 mm respectively.

7) Ensure a minimum measurement spacing of 500 µm and avoid previously tested areas.

8) Focus on the IDI and CID measures rather than TID unless the touchdown point is clearly discernable.

Furthermore, it should be noted that there does not appear to be an optimal maximum load, orientation or machining depth (or indeed thickness or measurement spacing above the given thresholds). Therefore, no recommendation has been given for these parameters and they should instead be selected as suitable to the specific testing. These recommendations are illustrated by Figure 47.

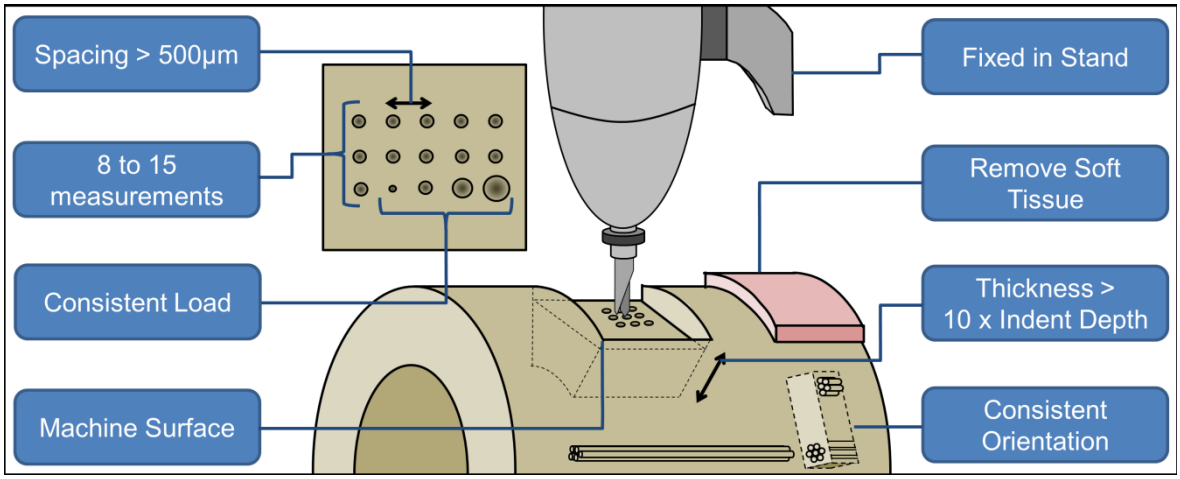

Figure 47 – Illustrative figure of the recommendations for consistent RPI testing

It is understood that these recommendations will not always be practical (e.g. considering in vivo RPI where it may be infeasible to prepare the surface of the bone and the uneven surface of the bone may necessitate the freehand mode) but where alternative approaches are employed, the experimenter should be aware of the additional variability being introduced as discussed here.

Prior to applying these recommendations to other studies, it is necessary to scrutinise their applicability in terms of the model being used and the properties of the bone being tested.

These recommendations are by no means all-encompassing and further investigation, beyond that previously reported, is necessary. Notably, the effects of; measurement location relative to the heterogeneity of the bone (investigated in a collaborative publication by Coutts et al [229], under review and Chapter 6) and patient specific parameters (e.g. age, sex, height and BMD investigated in Chapter 7) are important for clinical applications. Importantly, this study provides guidelines for use of the novel emerging RPI technique where few currently exist in the literature and advises the following chapters of this thesis (Chapter 6 and 7).

6 The Potential of Reference Point Microindentation for Improved Fracture Risk Assessment

6.1 Introduction

The presented clinical study aimed to further examine the potential of reference point microindentation for assessing fracture risk. With the optimised recommendations from Chapter 5, RPI was applied to investigate the discriminative ability between both osteoporotic and, the previously unreported, osteoarthritic diseased tissue to a cadaveric control.

A journal publication is currently in preparation with joint first authorship between this author and Dr Louise Coutts who has contributed equally to this work. Additionally, preliminary results of the study presented in this chapter have been presented at the following internal and external conferences:

- T. Jenkins, L.V. Coutts, R.O.C. Oreffo, D.G. Dunlop, C. Cooper, N.C. Harvey, P.J. Thurner, *The Potential of Reference Point Microindentation for Fracture Risk Assessment*, Podium at Bath Biomechanics Symposium, September 2014
- T. Jenkins, L.V. Coutts, R.O.C. Oreffo, D.G. Dunlop, C. Cooper, N.C. Harvey, P.J. Thurner, *The Potential of Reference Point Microindentation as a Fracture Risk Assessment Tool*, Poster at the University of Southampton Postgraduate Conference, Awarded Best Poster, November 2013
- T. Jenkins, L.V. Coutts, R.O.C. Oreffo, D.G. Dunlop, C. Cooper, N.C. Harvey, P.J. Thurner, *Reference Point Microindentation: Investigation of a Novel Fracture Risk Assessment Tool*, Poster at the University of Southampton Ageing USRG Exhibition, September 2013
- T. Jenkins, L.V. Coutts, N.C. Harvey, R.O.C. Oreffo, D.G. Dunlop, C. Cooper, P.J. Thurner, *Reference Point Indentation Trends of the Human Femoral Neck*, Poster at European Society of Biomechanics, August 2013
- L.V. Coutts, T. Jenkins, N.C. Harvey, R.O.C. Oreffo, D.G. Dunlop, C. Cooper, P.J. Thurner, *Regional Variation in Reference Point Indentation in Healthy And Diseased Cortical Bone*, Poster at European Society of Biomechanics, August 2013

Diez-Perez et al [19], Guerri-Fernandez et al [21] and Milovonovic et al [28] have, to varying extents, found increased indentation depth in the bone of individuals with osteoporotic fracture. However, these studies have been limited in number (from 5 to 38 fracture cases) and further research is necessary to establish the ability of RPI to discriminate diseased from control bone, relating to its potential for clinical fracture risk assessment. The most clinically relevant fracture site, the femoral neck, is of principal interest yet this has only been investigated to a limited extent (5 fractured compared to 4 non-fractured samples [28]). The presented study applies RPI to the femoral neck which is in close proximity to; the hip fracture of 46 donors in the osteoporotic group and the deteriorated femoral head and joint of 47 donors in the osteoarthritic patients in comparison to 16 cadaveric donors with no evidence of bone disease.

Lack of correlation with BMD has, previously been reported within 14 individuals by Diez-Perez et al [19], but comparison between RPI and existing clinical tools needs to be investigated further. This chapter considers BMD correlation in a larger population (70 donors across osteoporotic, osteoarthritic and control groups) and investigates other clinical measures that have yet to be compared to RPI including: clinical factors as part of the pre-existing FRAX tool, vitamin D and calcium blood levels in osteoporosis and the radiographic disease grade in osteoarthritis. Furthermore, a new approach was taken to analyse the complementary diagnostic potential of RPI by quantifying the discriminative ability of RPI, current clinical techniques and a combined RPI-BMD-FRAX tool.

6.2 Materials and Methods

6.2.1 Human Bone Samples

Human femoral neck samples were collected to form three groups: 1) the osteoporotic (OP) group (46 samples), 2) the osteoarthritic (OA) group (47 samples) and 3) the control group (16 samples). A clinical study was specifically designed for the collection of osteoporotic samples, patient information and bone mineral density scans. Whereas, samples and data for the osteoarthritic group were obtained through collaboration with the COASt (Clinical Outcomes in Arthroplasty Study) research team. Cadaveric control samples were obtained from tissue banks and were provided alongside data.

6.2.1.1 Osteoporotic Group

The osteoporotic group was formed of resected proximal femora from patients undergoing a hip arthroplasty at University Hospital Southampton NHS Foundation Trust (UHS) for a fracture of the femoral neck. These samples were collected specifically as part of OStEO (Observational Study Examining Osteoporosis), the clinical study created for this thesis and sponsored by UHS (T&O0149). Surgeons at UHS retained and temporarily stored these samples; first in a fridge outside theatres and then a member of the Bone and Joint Group (University of Southampton, UoS) collected the samples in a linked-anonymised form. Following a mean duration of 1.5 days, samples were then frozen, wrapped in Hank's Balanced Salt Solution (HBSS) soaked gauze at -80°C for 0 to 4 months prior to testing (if the patient was consented to the study).

Patients who had capacity were approached between 1 day and 8 days (mean 5 days) post-operatively depending on their speed of recovery and general health as assessed by the clinicians on the ward. Due to the emergency nature of the operations (patients operated upon within 36 hours of admission) it was not feasible to approach or consent patients pre-operatively. A researcher on this study or specialist registrar (Dr Nicole Moss) discussed the study with the patient and provided them with a Patient Information Sheet (PIS) to consider for a minimum of 24 hours (9.4 Appendix 3 – Clinical Paperwork). A researcher or research nurse (Carole Ball) then consented patients that were willing and able to participate in study, allowing for: use of their retained femoral sample in a non-anonymised form, collection of relevant information from their medical notes and through an interviewer led questionnaire and returning to UHS for a DEXA scans.

Collection of the samples was approved under the ethical approval obtained by the Bone and Joint Group (LREC 194/99/1 & LREC 210/01 - Southampton and South West Hampshire Research Ethics Committee) and recruitment of participant and the testing of the samples was approved under the ethical approval submitted specifically for this study, OStEO (12/SC/0325 - Southampton REC A).

6.2.1.2 Osteoarthritic Group

The osteoarthritic group was formed of resected proximal femora from patients undergoing an elective hip arthroplasty at UHS, and were collected through collaboration with the COASt (Clinical Outcomes of Arthroplasty Study) research team. These samples were collected directly from surgery and snap-frozen then stored dry (i.e. no gauze or HBSS) at -80°C and then tested in two batches either: transferred directly from UHS after 0 to 8 months or transferred first to Oxford Musculoskeletal Biobank then to UoS after 19 to 29 months of storage.

Patients were consented to COASt pre-operatively by completing a self-assessment questionnaire. Patients were officially consented at an assessment session including DEXA scans.

Samples were collected under the COASt ethical approval (10/H0604/91 – Oxford REC A) and transferred to this study for testing under the OStEO approval (12/SC/0325 - Southampton REC A).

6.2.1.3 Control Group

Innoved Institute LLC (Besenville, Illinois – 15 samples) and IIAM (International Institute for the Advancement of Medicine, Edison, New Jersey – 1 sample) provided the control group samples. Samples consisted of the proximal third, cut from the whole femora that had been removed from cadaveric donors with no known history of fracture or bone disease.

Dr Louise Coutts obtained samples from Innoved and Prof. Philipp Thurner obtained the sample from IIAM. The time from death of the donor to procurement (and hence freezing) of the femora varied between 4 days and 21 days. During this time, bodies were stored at 4 °C from a few hours of death then at approximately 0 °C at the procurement facility. Here, the samples were denuded, wrapped in cotton wool and blue plastic wrap and

frozen at -20 °C. These samples were stored for 3 to 19 months except for one sample that was stored for 68 months (primarily, 53 months of which were at the UoS at -80 °C) prior to testing. During transfer to UoS the temperature of the samples were maintained through packaging in dry-ice within a polystyrene container and on arrival, they were frozen at -80 °C.

The tissue bank provided data on the samples through a 'donor summary', created by a clinician from the donors' medical notes. Older donors were preferentially selected based on this information, aiming to be in-line with the osteoporotic group. Additionally, this procurement process aimed to limit unsuitable samples using the information available to attempt to avoid samples from donors with: osteoporosis or other metabolic bone disease, previous long bone or spinal fracture, osteoarthritis, rheumatoid arthritis, bone or joint surgery, glucocorticoid use, malnutrition or chronic liver disease, hysterectomy or secondary osteoporosis (i.e. hyperthyroidism, hyperparathyroidism, type I diabetes, hypogonadism or early menopause before 45).

6.2.2 Reference Point Micro-Indentation

RPI was performed using the Biodent Hfc^{TM} device (Active Life Scientific, Santa Barbara, California). The methods chapter (section 4.1) and other authors [19, 29] have previously described this tool in detail and it was applied in this chapter with the reference probe applying 1300 g to 1350 g preload and the test probe indenting up to a 10 N maximum load with 10 repeat cycles at 2 Hz.

Our previous chapter (Chapter 5 [279]), consistent with the study by Setters and Jasiuk [30], found that there is an increasing relationship between indentation depth and maximum load. However, the coefficient of variation was independent of maximum load, so, for this reason, we have selected a 10 N maximum load, with the rationale that it gives a more representative measure of the bulk properties of the bone with a reduced influence from the outer circumferential layers (Chapter 5 [279]). As the cortical thickness is estimated to be above 1 mm in thickness [182, 229], this 10 N maximum load is appropriate (Chapter 5 [279]).

Though Setters and Jasiuk [30] report a plateau in indentation measures above 15 cycles, the indentation depth is relatively consistent above 10 cycles [26, 30] which has therefore

been selected in this study. Furthermore, Setters and Jasiuk [30] found no effect of including preconditioning cycles, and therefore these have not been utilised here.

As described in the methods chapter (4.1.2), three indentation depth measurements: the IDI, TID and CID have been used in this study.

6.2.3 Femoral Neck Testing Procedure

The proximal femoral samples were defrosted overnight (for more than 15 hours at room temperature) while submerged in Hank's Balanced Salt Solution (HBSS) for rehydration. Hydration was maintained throughout testing through periodic application of HBSS to the femoral neck using a syringe, typically after every four or five measurements or if no surface moisture was visible. Throughout testing the RPI device was held freehand which is likely to give marginally higher values (typically less than 10% higher) but also have an increased coefficient of variation (Chapter 5 [279]). Due to the curved and irregular geometry of the femoral neck and the requirement to achieve an indentation angle within 10° of the normal [31], this freehand mode was necessary. The sample itself was supported using a tray with a recessed cup and padding with paper towel in conjunction with securing the femoral head with concave tongs and, where necessary, by hand.

The site of femoral neck testing was standardised by measuring a set distance (Test Location, T - Figure 48), equal to the radial diameter of the femoral head (Head Diameter, Ø - Figure 48). However, this proximal-distal test location was not always achievable, particularly in the presence of bone deformities in the osteoarthritic group and the location of the fracture in the osteoporotic group.

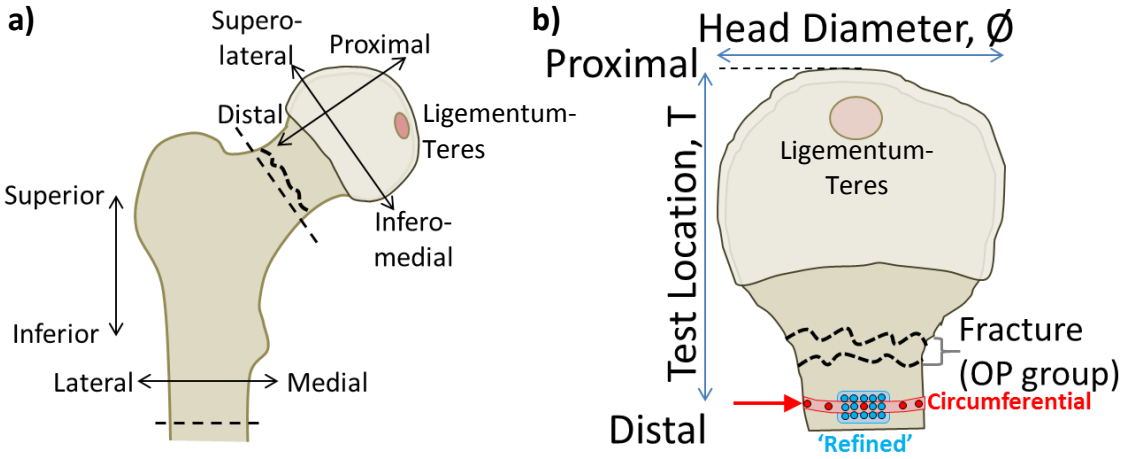

Figure 48 – Reference Point Indentation of the femoral neck a) A depiction of the proximal third of the femora showing the location of the osteoporotic and osteoarthritic femoral head and neck samples. b) 'Refined' and 'Circumferential' indentation showing the proximal-distal test location.

The orientation of the samples was established through identification of the inferomedial point, where the cortex was thickest, through the geometry of the femoral neck and through the location of the ligamentum teres (that stabilises the femoral head to the acetabulum) as shown in Figure 48.

A scalpel was use to remove the soft tissue of the periosteum and the probe was scratched along the indentation surface prior to testing, intending to minimize the effect of soft tissue and reduce the coefficient of variation associated with testing (Chapter 5 [279]). However, the surface of the bone was not machined, intending to mimic clinical testing where feasible, so there is a potential increased coefficient of variation associated with the natural surface of the bone (Chapter 5 [279]).

With the freehand technique requiring two individuals to perform the indentation testing, all experiments were carried out with Dr Louise Coutts.

6.2.3.1 Circumferential testing of the femoral neck excluding the superolateral region

The probe was applied to 13 test locations around the femoral neck, indenting every 20° but excluding the superolateral quadrant (as shown in Figure 49a) where thickness and porosity made indentation unreliable (Chapter 5 [181, 182, 229, 279]).

Furthermore, presence of deformities in the osteoarthritic group and the location of the fracture in the osteoporotic group limited testing and therefore the full 13 measurements per donor could not always be achieved. It was intended to include many repeat

measurement for reduced variability, with the 13 to 15 measurements used here giving a 5% to 7% error from the 'true' value (Chapter 5 [279]).

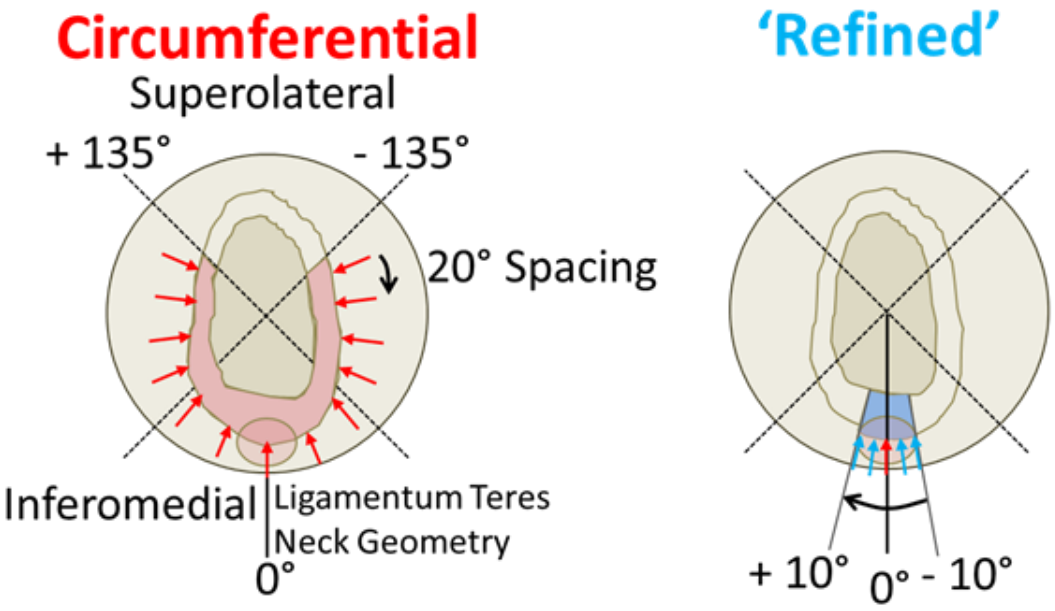

Figure 49 –Circumferential and 'Refined' test locations: a) the 'Circumferential' method with 20° spacing in the inferomedial three quarters and b) the'Refined' method with 15 measurements in the inferomedial section (within ±10° of inferomedial),

6.2.3.2 'Refined' testing of the inferomedial neck

Due to the circumferential heterogeneity of the femoral neck [229], the requirement for repeat measurements (Chapter 5 [279]) and to further focus on the thickest and least porous region [181, 182, 229], a 'refined' testing protocol was established (as shown in Figure 49b). RPI measurements were made within a 20° section of the inferomedial neck with three rows of five measurements (i.e. 15 measurements with approximately 1 mm to 2 mm spacing, greater than the recommended 0.5 mm spacing, Chapter 5 [279]). This testing aimed for a more representative assessment of the material properties of the bone by reducing the variability associated with circumferential heterogeneity, porosity and thickness.

6.2.4 Bone Mineral Densitometry

For the two clinical groups (osteoporotic and osteoarthritic), patients underwent bone mineral density DEXA (Dual-Energy X-Ray Absorptiometry) scans of their femur and lumbar spine at the Osteoporosis Centre, UHS using a Hologic Discovery A instrument (x-ray energies 100 keV and 140 keV, 30 s maximum exposure, 10 mA maximum current - Hologic Inc, Bedford, Massachusetts). Being elective procedures, the osteoarthritic group

could be consented to COASt pre-operatively and 35 of these participants were scanned a mean of 2.5 months prior to their hip arthroplasty. In the majority of these participants (32 of 35) the contralateral hip was scanned whereas the ipsilateral hip was scanned in the remaining 3 cases. 18 participants were able to attend the Osteoporosis Centre, UHS one to two months post-operatively, for a DEXA scan of their contralateral hip. A further 1 participant had a DEXA scan of their contralateral hip 7 months pre-operatively and this was accessed through their medical notes. DEXA scans were carried out by clinical scientist (Pat Taylor) and technologists (Alison Beaumont and Claire Burvill) at the Osteoporosis Centre, UHS.

For the control group, the distal third of the proximal femora were scanned at the μ-VIS computed tomography centre, UoS using a 225kV X-TEK/Nikon Metrology HMX ST system. The methodology behind the densitometry techniques are described in detail in the methods chapter (4.3).

To simulate the clinical DEXA scanner, dual energy radiography principles were applied to dual images of the femoral samples acquired with the following settings: voltages 100 kV and 140 kV, exposure time of 1415 ms and current of 50 μA. A 1 mm Cu filter was used to reduce beam-hardening effects in the sample and the setup resulted in a resolution of 50 μm/pixel. An 8 mm diameter aluminium cylindrical rod was also imaged for calibration.

A cylindrical rod was chosen because the local thickness varies across its curved face, providing a range of known thickness values, from the thinnest part at the edge of the curved face, to the thickest part at the centre. The attenuation was averaged along the length of the rod and symmetrically through this varying thickness giving the average measured intensity in Figure 50a.

The overall density and mass attenuation coefficients of the rod were known, and therefore, expected local areal density (density x thickness) could be calculated for each point across the radius (Figure 50a, expected intensity). This provided multiple points for the calibration to adjust the areal density calculated from the dual energy radiography technique (4.3).

A validation was performed by comparing the total mass (total bone mineral, lean and fat content) of the sample with the physical mass of the sample showing them to be in good agreement (Figure 50b).

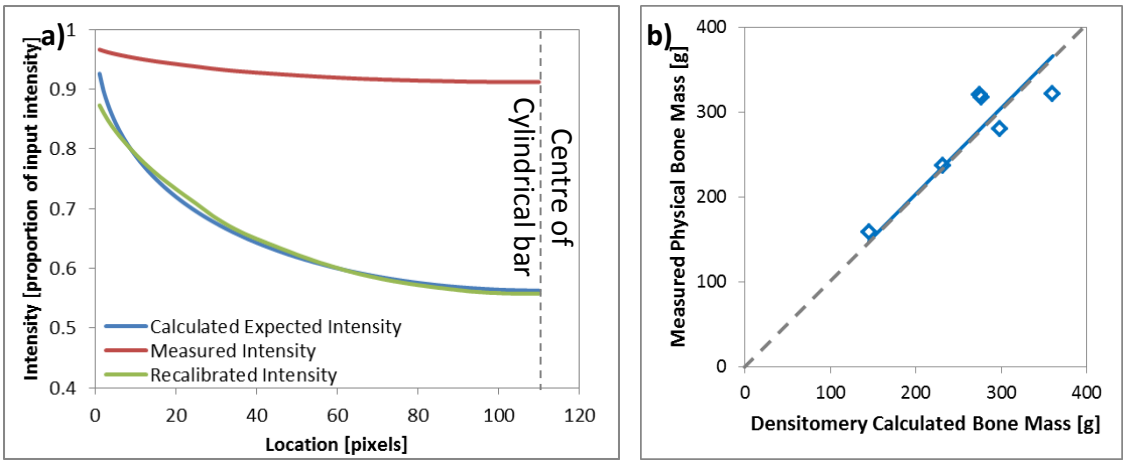

Figure 50 – Calibration and Validation of the in vitro Bone Mineral Density Assessment: a) Correction against a phantom of known density as a continuous function of its thickness and b) Comparison between physical densities and those assessed through the densitometry technique

Segmentation of the femoral neck was performed through selecting the hip angle (manually selecting the most proximal point of the femoral head then bisecting the femoral neck) then selecting a 10 mm thick slice that is normal to the hip angle and proximal of the greater trochanter (indicated in 4.3, Figure 27). This segmentation is based on the Hologic system to give a comparable femoral neck BMD. These scans were performed with Dr Orestis Katsamenis and Dr Louise Coutts and the development of the technique and subsequent analysis of the scans for calculation of BMD was undertaken completely by Dr Louise Coutts.

6.2.5 Clinical Factors

Clinical information including relevant medical conditions (diabetes, thyroid disease, hyperparathyroidism, avascular necrosis, Paget's disease, hypogonadism, osteogenesis imperfect, chronic malnutrition, rheumatoid arthritis, osteoporosis and osteoarthritis), medical history (fracture history and hysterectomy), medication (antiresorptives, steroid use and hormone replacement therapy), lifestyle factors (current smoking, units of daily alcohol consumption) and other factors relevant to bone health (height, weight and familial osteoporosis for all groups and calcium and vitamin D levels for the osteoporotic group) were collected where possible. For the two clinical groups this data was collected through researcher-led questionnaires, self-assessment questionnaires (osteoarthritic

group only) and access to the participants' medical notes. For the control group, these data were provided by the tissue bank through the 'donor summary'. The control and osteoarthritic patient information were supplied to this study alongside the samples, whereas the information for the osteoporotic group was collected specifically for this study with aid of Carole Ball (9.4 Appendix 3 – Clinical Paperwork).

Using this patient information it was possible to generate a FRAX score^{TM} using the online fracture risk assessment tool to predict 10 year fracture probability for the hip or any major osteoporotic fracture [12, 264, 265]. The tool was used with clinical factors alone (age, sex, height, weight and binary responses to the following: previous hip fracture, parent hip fracture, rheumatoid arthritis, glucocorticoid use, current smoker, greater than 3 units of alcohol per day and secondary osteoporosis) and in combination with the femoral neck BMD as described in the methods (04.3).

6.2.6 Assessment of Clinical Radiographs

The pre-operative radiographs of the ipsilateral hip were used to grade the level of osteoarthritis for the osteoarthritic group. For the cadaveric control samples, no preoperative radiographs were available and the radiographer advised that assessment of the DEXA mimic scans was not possible. Therefore, as no THR had been performed, it was assumed that the level of osteoarthritis was low for this group (i.e. a Croft Score less than 3). Additionally, as the level of osteoarthritis is only of principal interest in the osteoarthritic group, the osteoporotic group were also not assessed and are not considered in this comparison. The osteoarthritic hips were graded in terms of the severity of the osteophytes (0 to 3), the level of joint space narrowing (0 to 3) and the presence or absence of: cortical collapse of the femoral head, subchondral cysts and sclerosis of the cortical bone. The assessment of these features were combined for calculation of the Kellgren-Lawrence Score (0 to 4) and Overall Croft Score (0 to 5) [219, 230] as defined in Table 2. The osteoarthritic grading of the clinical radiographs was performed by Janet Cushnaghan, Lifecourse Epidemiology Unit.

Table 2 – Radiographic osteoarthritis grading classification based on the Kellgren-Lawrence score [219] and Overall Croft Score [230]

Kellgren-Lawrence	Overall Croft Score
0 – No indicators of osteoarthritis	0 – No indicators of osteoarthritis
1 – Presence of small osteophytes	1 – Presence of osteophytes only
2 – Presence of severe osteophytes	2 – Joint space narrowing only
3 – Moderate narrowing of the joint space	3 – Two indicators of osteoarthritis including: osteophytes, joint space narrowing, subchondral sclerosis or cyst formation
4 – Severe joint space narrowing with sclerosis of the subchondral bone	4 – As with grade 3 but with three indicators of osteoarthritis
	5 – As with grade 4 but with deformity of the femoral head

6.2.7 Statistical Analysis

Considering the shape of the distribution, normality was not observed in the repeat RPI measurements made on each sample due to the relatively small number of measurements and the presence of outliers (e.g. indentations in close proximity to pores). For this reason, a median of the repeat measurements was calculated to give a single measurement per donor.

When comparing groups, the normality of each measure was established by plotting the histogram and assessing if the curve was approximately bell-shaped. The median and interquartile range were displayed for all skewed variables (e.g. 'refined' TID) whereas the mean and standard deviation were displayed for all normally distributed parameters (e.g. IDI, CID). The statistical comparisons were then made as appropriate. In the case where comparing two groups (i.e. osteoporotic vs. control, osteoarthritic vs. control and osteoporotic vs. osteoarthritic), a t-test was used where normally distributed and a Mann-Whitney U-Test was used otherwise. The non-normally distributed variables were then transformed using the Fisher Yates z-scores to reach normality.

Multivariable linear regression was used to examine the association between exposure (the three groups: osteoporotic, osteoarthritic and control) and outcome (e.g. TID, IDI and CID). To take into account the effect of possible confounders after the initial unadjusted analysis (Model 0), the associations between exposure and outcome were adjusted for patient related factors; age, sex, BMI and height (Model 1). Secondly, testing related variables were further adjusted to add the time stored, the proximal-distal test location

and the number of repeat measurements to the model (Model 2 that is inclusive of Model 1).

The β coefficients and 95% confidence intervals (95% CI) are displayed for these adjusted models, and for normally distributed outcome are interpreted as the difference between groups. For not normally distributed outcomes (previously transformed using Fisher Yates- z-scores), the β coefficients indicate the number of standard deviation difference between groups.

When considering multiple groups (i.e. comparing between the three levels of Croft Score); Kruskall-Wallis test (non-normally distributed) and ANOVA (normally distributed) were used. Spearman's (non-normally distributed) and Pearson's (normally distributed) correlation coefficients were calculated when comparing two continuous variables. To compare two categorical variables (i.e. group and sex) the Pearson's Chi-Squared (and where lower than 5 donors in any sub-group, the Fisher's Exact) statistical test was used. A level of significance of $p < 0.05$ has been used throughout.

To assess the sensitivity and specificity of the RPI tool in comparison to existing clinical factors, ROC (Receiver Operator Characteristic) as described in section 3.1.3.1. These curves plot the sensitivity (true positive rate – those correctly identified as having the disease state) against its 1 - specificity (false positive rate – healthy individuals incorrectly identified as having the disease) across a range of threshold values. The area under these curves indicates a technique's discriminative ability between two groups: i.e. for an area of 0.5, the tool is no better than random chance but for an area of 1.0, there is a threshold value that can perfectly discriminate the two groups (i.e. 100% sensitivity and 100% specificity).

Statistical analysis was completed using SPSS v20 (IBM, Portsmouth), or by Stefania D'Angelo, statistician at the Lifecourse Epidemiology Unit, using the Stata software v13.1 (StataCorp LP, Texas).

6.3 Results

6.3.1 Baseline Characteristics and Potential Confounding Factors

The clinical study, OStEO, recruited 53 patients into the osteoporotic groups, however, the femoral neck sample for 7 of these participants was not suitable for indentation, resulting in 46 samples in this group tested with the 'circumferential' method. Additionally, 47 osteoarthritic samples were obtained from COASt and 16 cadaveric control samples were obtained from tissue banks, all of which were suitable for testing with the 'circumferential' method. Due to the 'refined' method being implemented later in the study, after some samples had been segmented, it was possible to test all 16 control samples but only 34 osteoporotic and 32 osteoarthritic samples.

Table 3 indicates some potential confounding factors associated with the groups. Notably, the osteoporotic group were older ($p < 0.001$), have a seemingly higher proportion of females (not significant, Pearson's Chi-square $p > 0.05$), have lower body mass ($p < 0.05$) and hence lower BMI ($p < 0.05$ compared to osteoarthritic but not control). Due to the presence of the fracture resulting in absent tissue, there are also fewer measurements per donor ($p < 0.05$) in the fractured compared to both the osteoarthritic and control groups.

Additionally, though the osteoporotic samples were frozen for a similar duration compared to the first batch of osteoarthritic samples ($p > 0.05$) this storage duration was significantly shorter than both the control group and the second batch of osteoarthritic samples ($p < 0.05$).

The influence of each of these factors is investigated in the following section (6.3.2).

Table 3 – Comparison of baseline characteristics and potential confounding factors between groups showing mean (SD) for the normally distributed parameters and median (IQR) for non-normally distributed variables (additionally highlighted with a *). For the categorical variable, sex, the ratio between male and female donors is shown.

	Osteoporotic	Osteoarthritic	Control
Circumferential (excluding superolateral)			
Number of donors	46	47	16
Male : Female ratio	17:29 (1:1.71)	20:27 (1:1.35)	7:9 (1:1.29)
Age*	83 (77 - 87)	68 (61 - 78)	64.5 (61 - 74)
Height (m)	1.63 (0.10)	1.67 (0.10)	1.70 (0.11)
Weight (kg)	68.4 (13.0)	82.6 (23.9)	85.6 (26.0)
BMI (kg/m^2)	25.6 (4.5)	29.4 (7.6)	29.5 (8.5)
Length of Storage (months)	1.6 (0.9)	B1: 2.1 (1.8) B2: 21.7 (4.0)	13.6 (15.8)
Test location (T/Ø)	1.07 (0.17)	1.02 (0.11)	1.00 (0.00)
Number of measurements*	10 (7 – 12)	13 (12 – 13)	13 (all)
'Refined' Inferomedial			
Number of donors	34	32	All
Male : Female ratio	12:22 (1:1.83)	12:20 (1:1.67)	
Length of Storage (months)	4.8 (4.7)	B1: 7.4 (3.8) B2: 20.5 (9.9)	
Number of measurements*	15	15	15

6.3.2 Investigation into Potential Confounding Factors

6.3.2.1 Clinical Factors and Co-morbidities

Though the study was selective in obtaining tissue as discussed in section 6.2.1.3, this exclusion was not always possible. Selection of older cadaveric tissue that had no bone disease or associated risk factors proved, as might be expected, problematic i.e. older donors are predisposed to osteoporosis and osteoarthritis and deceased donors are likely to have associated co-morbidities. Similarly, the osteoporotic group, being older, had associated comorbidities and conditions related to osteoporosis and osteoarthritis. The distribution of these clinical risk factors is shown in Table 4. The number of donors with associated conditions was generally too low for statistical analysis or to be considered as subgroups. However, these donors did not present as outliers when plotted in terms of indentation depth, nor were they grouped in terms of their associated conditions. For this reason, where indentation was practical, no donor was excluded from any of the groups.

Table 4 – Summary of clinical factors based on the donors medical history. The group specific parameters show the diagnosis of young OA (< 50 years) in the OA group, cases of 'high trauma' fracture (fall from greater than standing height i.e. bike or stairs) and cases of OA or OP outside their respective groups.

	Medical History							Medications			Group Specific				Lifestyle	
											OA	OP Cont	OA Cont	OP		
	Diabetes	Thyroid Disease	Hyperparathyroidism	Avascular Necrosis	Rheumatoid Arthritis	Hysterectomy	Previous fracture	Steroid Use	Bisphosphonate	HRT	Young OA	OA diagnosis	OP diagnosis	'Traumatic' fracture	Current smoker	Alcohol (>3 units/day)
OP	10	6	2	0	4	8	5	4	5	6		6		3	4	6
OA	2	5	0	1	4	2	2	9	1	4	5		6		6	3
Control	2	0	0	0	0	1	0	0	0	0		1	1		7	1

6.3.2.2 Age and Sex

The mean age of the osteoporotic donors is significantly higher than the mean donor age of the other two groups ($p < 0.05$, Table 3). However, considering the age ranges, there is considerable overlap between the three groups (osteoporotic aged 54 to 97, osteoarthritic aged 26 to 84 and control aged 57 to 92 as shown in Figure 51a). This is because, though younger osteoporotic donors and older control donors were preferentially selected, osteoporotic fractures still occur more commonly in elderly

women and 'healthy' (e.g. without history of bone disease) elderly cadaveric tissue is rarely available. There appears to be no significant relationship between age and IDI ($p > 0.05$) for any of the three groups (Figure 51a and Table 5), though TID and CID appear to decrease with age in the control group alone (Pearson's $r = -0.57$ and -0.51 respectively, $p < 0.05$).

When comparing femoral neck bone from male and female donors there is considerable overlap in IDI for all cases and indentation values for the two sexes appear identical in the control group ($p > 0.05$). However, for the osteoarthritic group, the RPI values are seemingly higher in bone from male participants ($p < 0.05$ for IDI and TID) and lower for those in the osteoporotic group ($p < 0.05$ for CID).

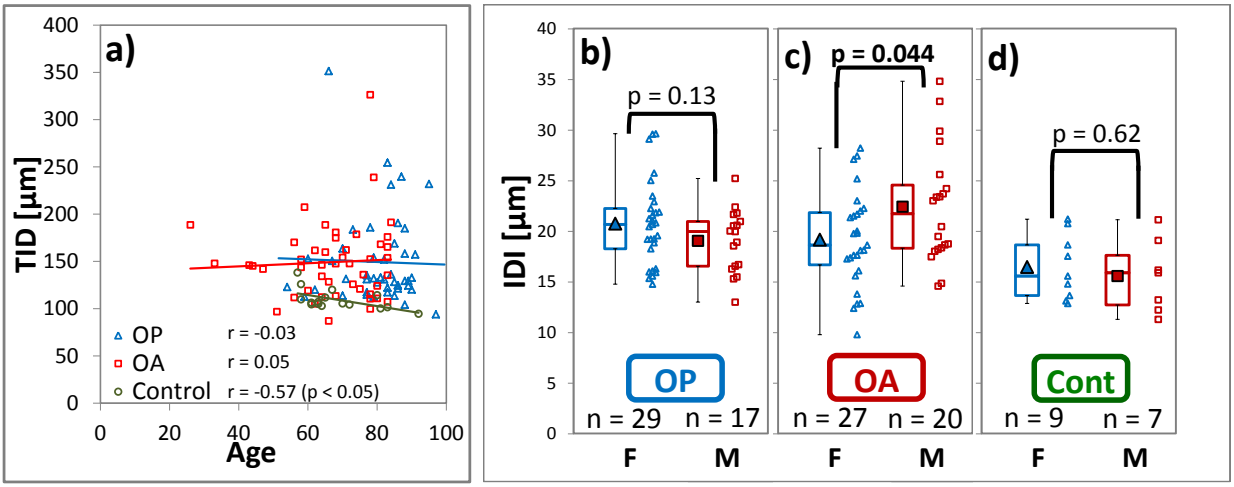

Figure 51 – Correlation of circumferential TID with age (a) and comparison of IDI between sexes (b) alongside comparison between the groups (osteoporotic – OP, osteoarthritic – OA and Control – Cont)

Table 5 – Statistical summary of Figure 51: correlation and comparison of age and sex across the groups. The column Fig. relates to the panels labelled in Figure 51. The correlations (Pearson's) and comparisons of means (t-tests) are shown in bold and highlighted in grey where significant ($p < 0.05$)

			Fig.		TID	IDI	CID1
Age	OP	r-val	a		-0.03	0.11	0.16
	OA				0.05	-0.10	-0.08
	Control				**-0.57**	-0.06	**-0.51**
Sex	OP	Mean	b	F	154.4	20.8	**10.0**
				M	140.7	19.1	**8.5**
	OA	Mean	c	F	**136.8**	**19.2**	9.0
				M	**166.1**	**22.4**	9.5
	Control	Mean	d	F	111.5	16.5	7.30
				M	106.8	15.6	6.99

6.3.2.3 Height and Body Mass Index

Again, though the osteoporotic group appear shorter ($p > 0.05$) and of lower body mass (BMI, $p < 0.05$) than the other two cohorts, there is considerable overlap between all three groups (Figure 52, Table 6). Furthermore, the correlation between indentation depth and both height and BMI is either non-significant ($p > 0.05$) as for IDI and TID in all groups or minimal (Pearson's r = -0.38 height, r = 0.35 BMI, $p < 0.05$) as for CID for the osteoporotic group.

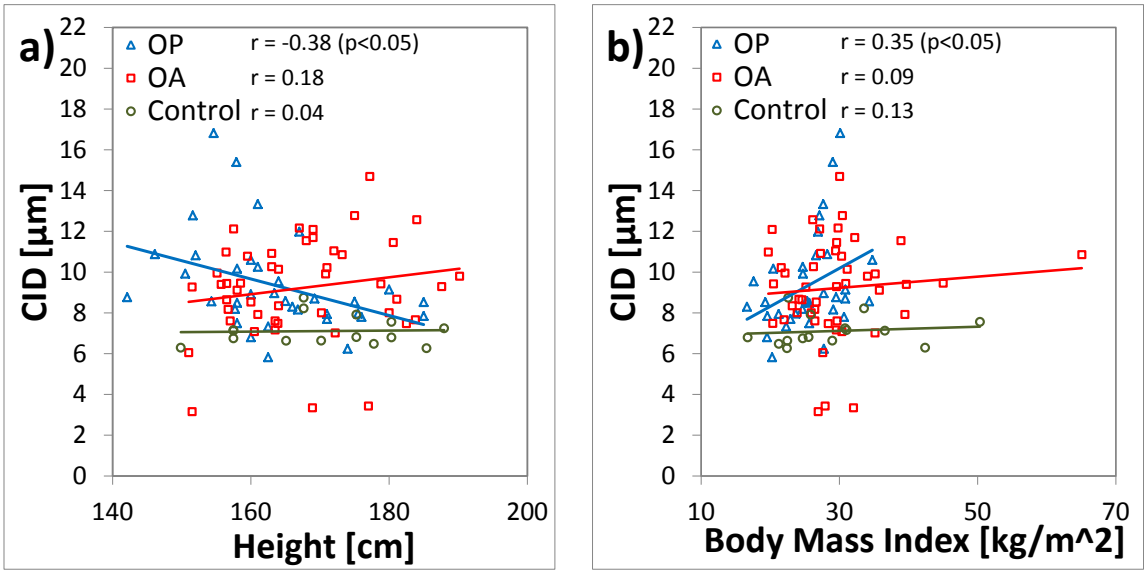

Figure 52 - Correlation of circumferential CID with height (a) and Body Mass Index (b) and comparison between the groups

Table 6 – Statistical summary of Figure 52: correlation and comparison of height and Body Mass Index across the groups. The column Fig. relates to the panels labelled in Figure 52. The correlations (Pearson's) are shown in bold and highlighted in grey where significant (p <0.05)

			Fig.	TID	IDI	CID1
Height	OP	r-val	a	-0.32	-0.33	**-0.38**
	OA			0.27	0.16	0.18
	Control			0.14	0.05	0.04
BMI	OP	r-val	b	0.20	0.22	**0.35**
	OA			-0.06	-0.13	0.09
	Control			-0.04	-0.11	0.13

6.3.2.4 Storage Conditions

Figure 53a and Table 7 show that there is no correlation (r = 0.27 maximum, p > 0.05) between freezer storage duration and indentation depth in any of the individual groups, except for the OA group, which can be separated into two distinct batches (Figure 53b); those directly transferred from UHS with a short storage period (0 to 8 months, Batch 1) and those that were first transferred to the Oxford Musculoskeletal Biobank (OMB) and tested after a longer period of storage (19 to 29 months, Batch 2). The samples in Batch 1 have a significantly higher indentation depth than Batch 2 in terms of IDI and TID (Figure 53b and Table 7).

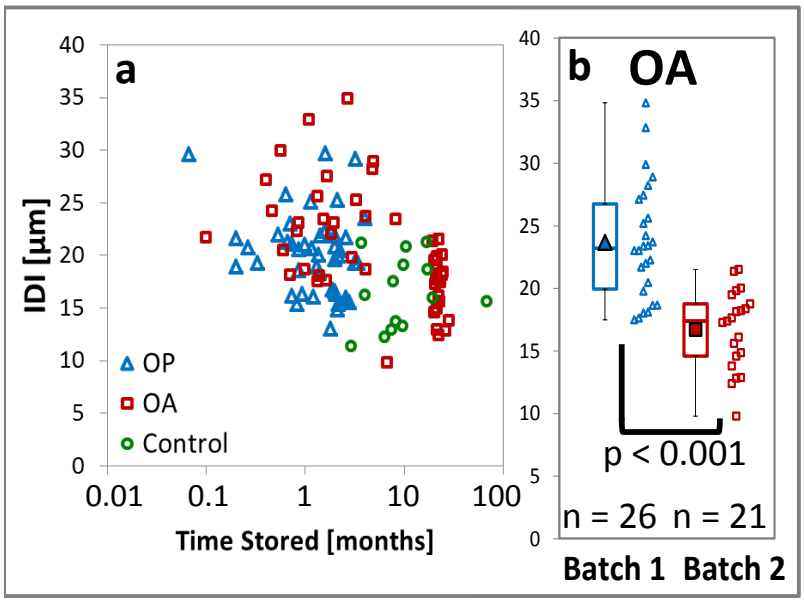

Figure 53 – The effect of storage conditions on circumferential IDI in terms of time frozen. a) The correlation with time stored for the three groups indicating two batches of OA testing – Batch 1 within a short period similar to the OP group and Batch 2 within a longer period similar to the Control group. b) Compares the indentation depth (IDI) between the two osteoarthritic batched

Table 7 – Statistical summary of Figure 53: correlation with time stored with circumferential measures of the indentation depth and the differences in circumferential indentation depth between the two batches of osteoarthritic samples. The column Fig. relates to the panels labelled in Figure 53. The correlations (Pearson's) and comparisons of means (t-tests) are shown in bold and highlighted in grey where significant (p < 0.05)

			Fig.		TID	IDI	CID1
Time Stored	OP	r-val	a		0.06	-0.11	0.12
	OA Batch 1				-0.08	0.23	0.08
	OA Batch 2				0.24	0.27	0.27
	Control				-0.09	0.05	0.10
Batch 1 - Batch 2		mean	b	1	**168.2**	**23.7**	9.51
				2	**125.7**	**16.7**	8.85

Figure 54 demonstrates other differences between these two batches that may lead to the decreased indentation depth with time. It can be seen that age (Figure 54a) and BMD (Figure 54b) are similar between the two batches (p = 0.71). However, the first batch includes a greater proportion of donors with a higher Croft Score (i.e. level of osteoarthritis are further progressed, p = 0.078 - Figure 54c) and this batch also has a higher proportion of male donors (p = 0.081 - Figure 54d). These difference (as described in section 6.3.2.2 for sex and section 6.2.6 for osteoarthritis grading), could perhaps result in the higher indentation depth in the first batch compared to the second batch, rather than directly being an effect of differences in storage duration.

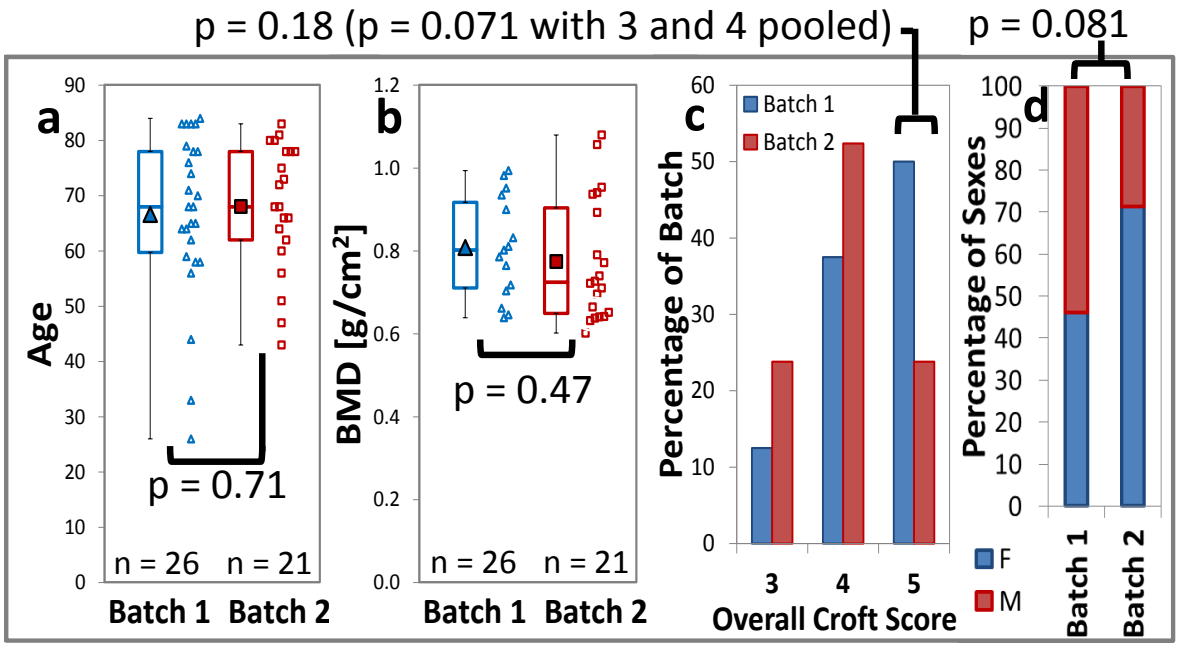

Figure 54 – Potential differences between the first (frozen for 0 to 8 months) and second batch (frozen 19 to 29 months) of osteoarthritic bones in terms of: a) age, b) Bone mineral Density, c) Overall Croft Score distribution and d) proportion of male and female donors. The difference in mean values is assessed through t-tests and (a and b) and the proportion of samples between groups is compared using the Chi-squared and Fisher's exact test (c and d)

To investigate the effects of storage duration further, RPI measurements were conducted on the same sample at two different storage durations: (1) between 3 days and 4 months, a mean of 1.1 months and (2) between 5.6 months and 15.8 months, a mean of 9.5 months, for 7 osteoporotic and 8 osteoarthritic samples (Figure 55 and Table 8). This comparison showed a significant reduction in TID for the increased storage duration (paired t-tests, $p < 0.05$), but this was not significant for IDI or CID.

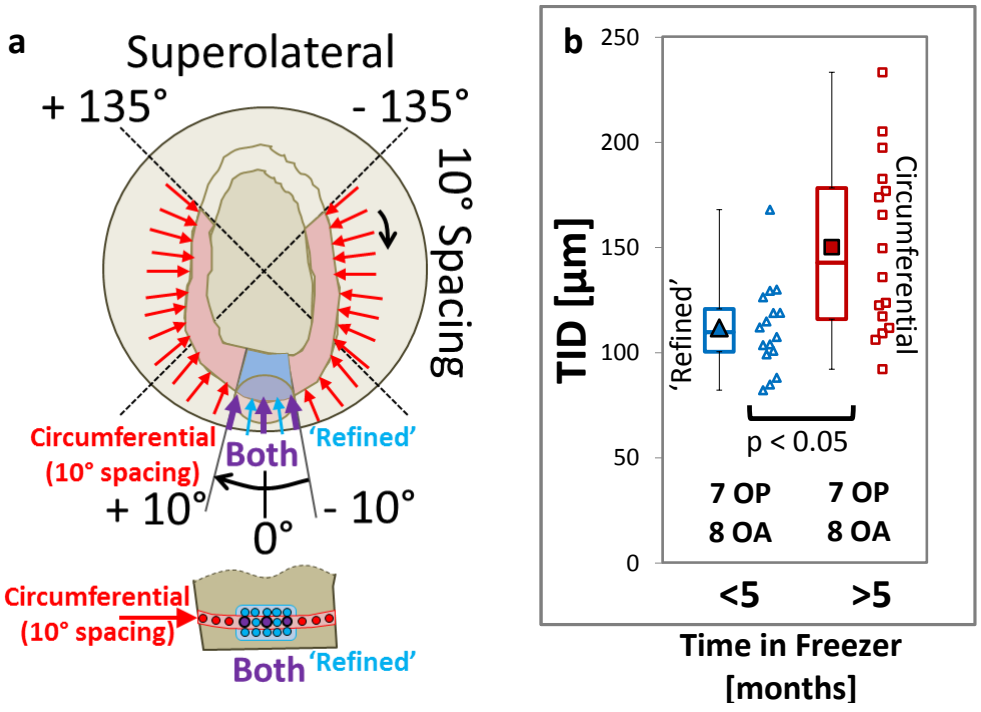

Figure 55 – Effect of storage duration on IDI in paired samples with 3 measurements from the circumferential protocol after a short time of storage (< 5 months) and an equivalent 3 measurements from the refined protocol on the same samples after a longer period of storage (> 5 months). a) shows a schematic of these measurements and c) shows the difference between the two storage durations

Table 8 – Statistical summary of Figure 55 indicating the effect of a short (< 5 month) and long (> 5 month) storage durations on paired samples. The differences between the paired groups (paired t-tests) are shown in bold and highlighted in grey where significant ($p < 0.05$)

			TID	IDI	CID1
Time Stored	mean	<5	**154.0**	22.8	10.4
		>5	**113.2**	17.1	7.8

The osteoarthritic samples are from elective arthroplasties and therefore their collection from surgery and subsequent freezing could be planned and the time to freezing is therefore negligible. The osteoporotic samples are first stored in a fridge for up to 5 days (mean 1-2 days), however, this storage period does not have any significant effect on the indentation properties (Figure 56a and Table 9, $p > 0.05$). Similarly, the control samples are initially stored at close to freezing for 4 to 21 days (mean 9.7 days), which again does not appear to affect the indentation depth (Figure 56b and Table 9, $r > -0.2$, $p > 0.05$).

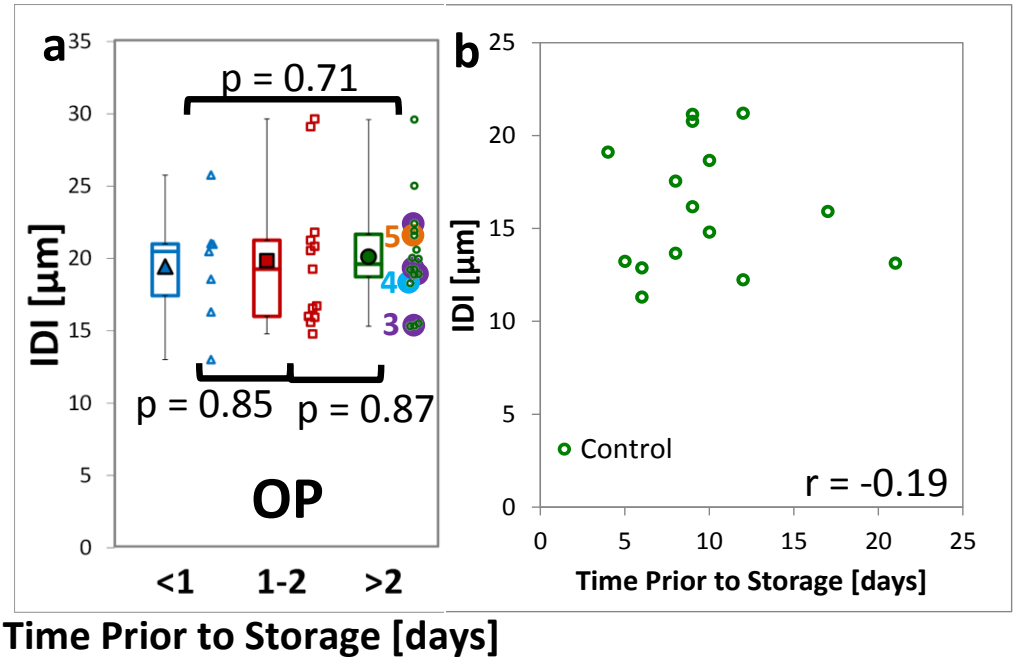

Figure 56 – The effect of time prior to freezing on circumferential IDI. a) for the osteoporotic samples and b) for the control samples.

Table 9 – Statistical summary of Figure 56: correlation with time prior to freezing. The column Fig. relates to the panels labelled in Figure 56. The correlations (Pearson's) and comparisons of means (t-tests) are shown in bold and highlighted in grey where significant ($p < 0.05$)

		Fig.		TID	IDI	CID1
Time Prior to Storage	mean	a	<1	126.5	19.5	8.82
			<2	144.4	19.9	9.06
			>2	153.6	20.1	9.23
	r-val	b		-0.19	-0.05	-0.10

6.3.2.5 Measurement Location

The proximal-distal RPI measurement location (defined in Figure 48) has a minimal, though significant, relationship with indentation depth in the osteoporotic group ($r = -0.31$ to -0.38, $p < 0.05$ as shown in Figure 57a and Table 10). In the osteoarthritic group, there is no relationship with test location ($r = -0.02$ to 0.08) and the ample quantity of control cortical bone meant a consistent proximal-distal test location was achievable (T/Ø = 1).

This weak correlation between indentation depth and test location in the osteoporotic group is likely to relate to variations in thickness and potential differences in material properties in the femoral neck. However, the presence of the fracture also has some effect. Figure 57b and Table 10 show that there is a higher indentation depth in the femoral neck proximal rather than distal to the fracture ($p < 0.05$).

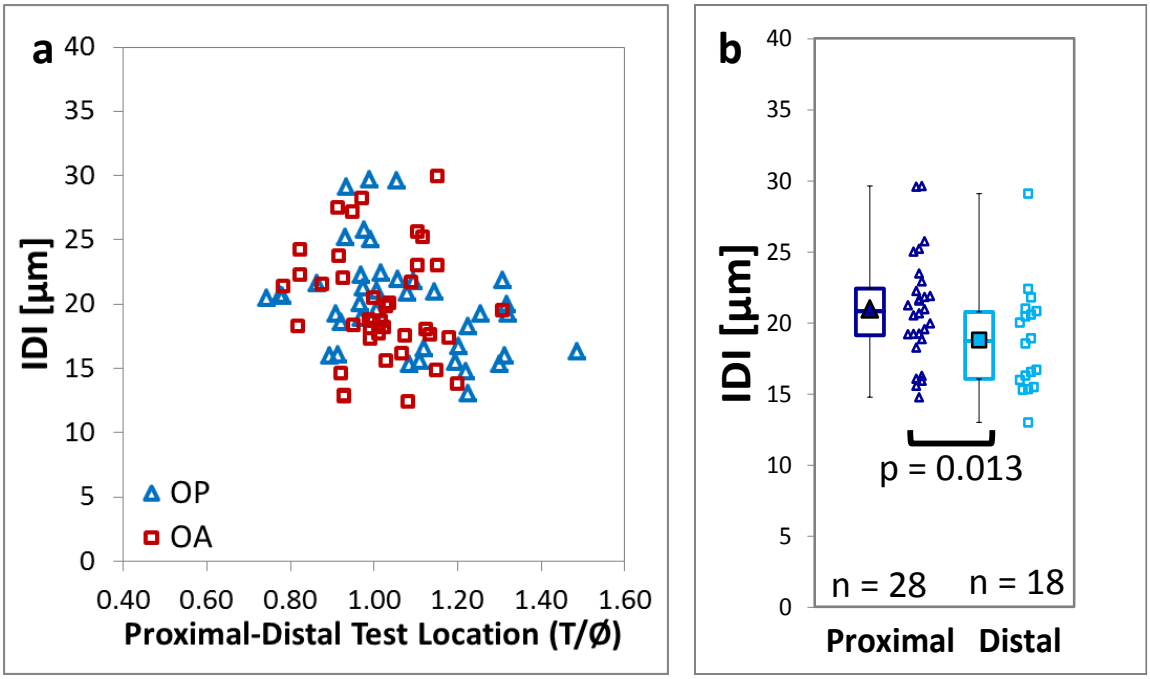

Figure 57 - Correlation of circumferential IDI and test location as defined in Figure 48d (a) comparison between indentation proximally and distally of the fracture site in the osteoporotic group (b)

Table 10 – Statistical summary of Figure 57: correlation between indentation depth and test location. The column Fig. relates to the panels labelled in Figure 57. The correlations (Pearson's) are shown in bold and highlighted in grey where significant ($p < 0.05$)

			Fig.		TID	IDI	CID1
T/Ø	OP	r-val	a		**-0.31**	**-0.38**	**-0.35**
	OA				0.08	0.01	-0.02
prox-dist	OP	mean	b	P	**164.3**	**21.2**	**10.1**
				D	**126.0**	**18.5**	**8.4**

6.3.2.6 Number of Measurements

The osteoarthritic and control samples had ample cortical bone to allow for sufficient number of measurements. However, in the osteoporotic group, the location of the fracture limited the number of measurements that could be performed on the femoral neck in some cases (median 10 measurements). Despite this, there does not appear to be a great association between number of measurements and indentation depth as shown in Figure 58a and Table 11 ($r = -0.41$ for TID, $p < 0.05$ but $r < -0.2$ for IDI and CID, $p > 0.05$). The measurements that were missing in the osteoporotic group were typically in the posterior and anterior quadrants, towards the superolateral region, with indentation of the inferomedial quadrant tending to be possible (Figure 58b).

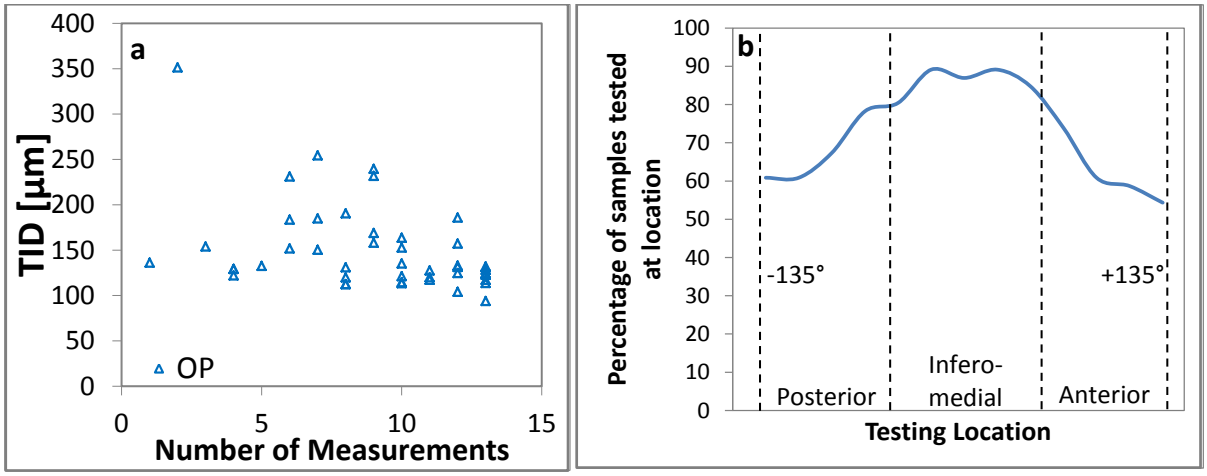

Figure 58 - a) Correlation of circumferential TID with number of repeat measurements and b) the percentage of measurements at test location

Table 11 - Statistical summary of Figure 58: correlation between indentation depth and number of repeat measurements. The correlation (Pearson's) is shown in bold and highlighted in grey where significant ($p < 0.05$)

			TID	IDI	CID1
No.	OP	mean	**-0.41**	-0.18	-0.16

6.3.2.7 Justification of Statistical Adjustment

Based on the above sections it can be seen that there is some, minimal relationship between indentation depth and age, sex, height and weight. However, as there is some correlation and these patient related factors have previously been related to fracture risk [129, 137, 139, 192], these factors were included in Model 1.

Testing related parameters: number of measurements, measurement location and, most significantly, duration of storage, appear to have a greater influence though the correlation is still minimal ($r < 0.6$ in all cases and generally $r < 0.4$ and $p > 0.05$). These factors have therefore been included, along with the patient factors (Model 1), in a further adjusted model (Model 2).

The influence of measuring proximally or distally of the fracture only relates to testing the osteoporotic group and was therefore not included in the adjustment, rather the proximal-distal test location was included instead. Although the differences between storage conditions could relate to other factors (discussed in further detail in section 6.4.1), this factor is dependent on groups and correlates with the outcome measure, therefore, it meets the requirements of a confounding factor and has been adjusted for. Time to freezing, however, does not relate to outcome measure and the times given are not comparable between groups (i.e. temperature and conditions of storage differ), so has not been included.

6.3.2.8 Variability of Repeat Measurements

The coefficient of variation for repeat measurements are shown in Figure 59 for IDI and summarised in Table 12 for IDI, TID and CID. There is a large degree of variation between donors with the CoV ranging between as little as 6% and as much as 90% but generally the mean intra-sample variation is a rather high 30% to 50% regardless of measurement (TID, IDI or CID), group (OA, OP or control) or test method ('circumferential' or 'refined').

The CoV is reasonably consistent across groups using the 'circumferential' method ($p > 0.05$, Figure 59a) but in 'refined' testing, the control group has a significantly lower CoV compared to the other two groups ($p < 0.05$, ANOVA, Figure 59b). Following on from this, as intended, the 'refined' method is less variable than the 'circumferential' method ($p < 0.05$, paired t-tests, Table 12). Finally, the IDI is the most variable measure and TID has the lowest ($p < 0.001$, paired t-tests, Table 12).

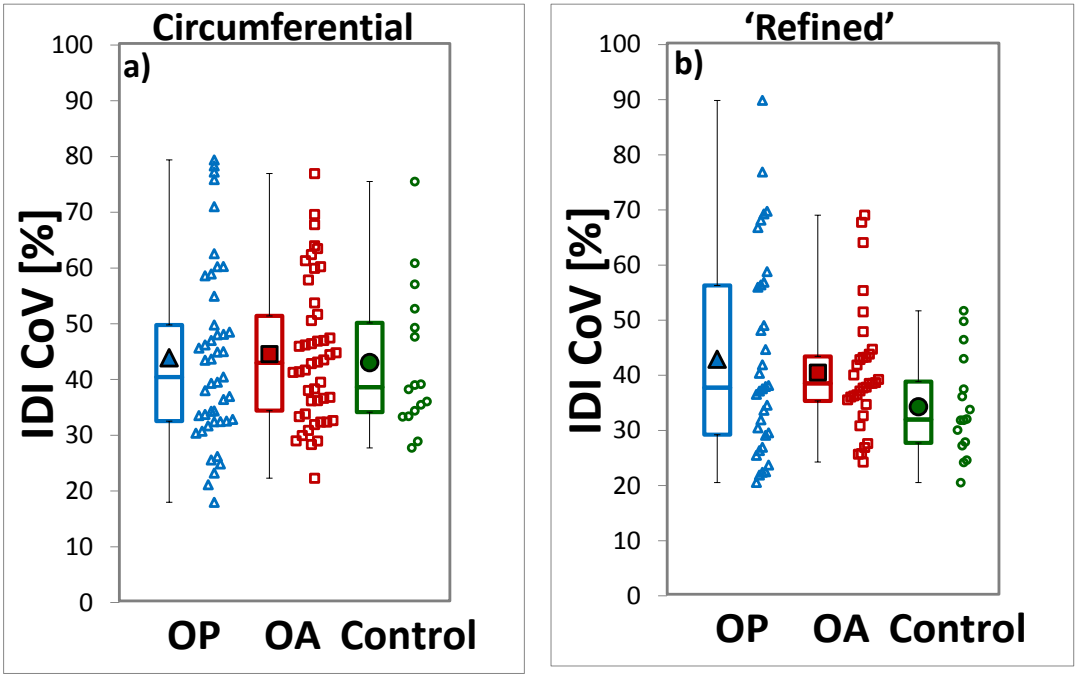

Figure 59 – Coefficient of Variation (CoV) in terms of the IDI across the three groups based on repeat measurements in a) the 'Circumferential' method of testing and b) the 'Refined' method of testing.

Table 12 – Statistical Summary of Figure 59: summary of the coefficient of variation across groups (osteoporotic, osteoarthritic and control), parameters (TID, IDI and CID) and methods of testing ('Circumferential' and 'Refined')

		TID	IDI	CID1
Circumferential	OP	0.33	0.44	0.42
	OA	0.29	0.45	0.38
	Control	0.28	0.43	0.41
Refined	OP	0.25	0.43	0.38
	OA	0.26	0.41	0.36
	Control	0.18	0.34	0.28

6.3.3 Reference Point Microindentation of the Femoral Neck

With the above confounding factors and variability in mind, the osteoporotic, osteoarthritic and control groups are compared when indenting circumferentially around the femoral neck (at 20° spacing excluding the superolateral quadrant, 'circumferential' testing – Figure 60a) and the 'refined' testing (within ±10° of the inferomedial neck – Figure 60b). These groups are compared in terms of the IDI (Figure 60) as well as the TID and CID (Table 13 and Table 14).

With the circumferential method, both the osteoporotic and osteoarthritic disease states have higher indentation distance (IDI, TID and CID, $p < 0.005$, Figure 60a) compared to the control group. The osteoporotic and osteoarthritic groups, however, appear similar in terms of indentation depth ($p \sim 0.6$).

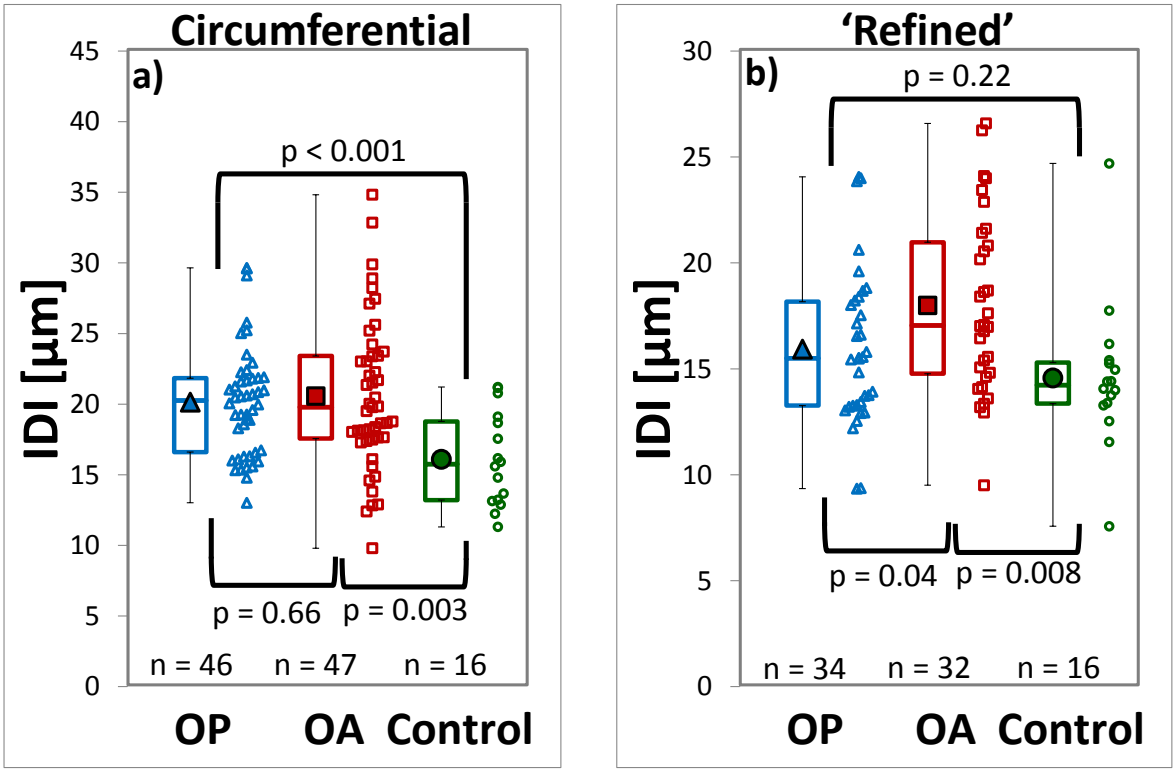

Figure 60 – Comparison of the three groups (osteoarthritic, osteoporotic and control) using reference point indentation (IDI displayed). a) Measurements made around the circumference of the femoral neck at 20° spacing and excluding the superolateral quadrant. b) 'Refined' measurements made within ±10° of the inferomedial region. The level of significance (p value) is shown for the unadjusted comparisons using t-tests.

Table 13 –Summary of indentation measurements (TID, IDI and CID) of the femoral neck using the 'circumferential' and 'refined' testing protocols between the osteoporotic, osteoarthritic and control groups. The averages are shown as mean (standard deviation) for the normally distributed variables (IDI and CID) and median (lower quartile – upper quartile) for non-normally distributed variables (Circumferential TID – marked with *)

	Osteoporotic	Osteoarthritic	Control
Circumferential (excluding superolateral)			
TID (μm) *	131.3 (121.3 – 158.2)	146.4 (119.1 – 168.2)	105.9 (103.6 – 113.0)
IDI (μm)	20.1 (3.9)	20.6 (5.4)	16.1 (3.3)
CID1 (μm)	9.5 (2.4)	9.2 (2.4)	7.2 (0.7)
'Refined' Inferomedial			
TID (μm)	119.8 (20.9)	131.1 (26.6)	107.8 (13.6)
IDI (μm)	15.9 (3.7)	18.0 (1.2)	14.6 (3.5)
CID1 (μm)	7.6 (1.5)	9.3 (2.0)	6.6 (0.7)

Considering the 'refined' method, there is a similar higher indentation depth in the osteoporotic group, which is only significant in terms of TID and CID ($p < 0.05$, Figure 60b) and not IDI ($p = 0.22$). As well as remaining higher relative to the control ($p < 0.05$), using the 'refined' method the osteoarthritic group is also easier to indent than the osteoporotic group (IDI and CID, $p < 0.05$ and for TID, $p = 0.06$).

The previous section (6.3.2) demonstrates the relationship between RPI and other potential confounding factors. When these factors are included in Model 1 (minimally adjusted model including patient related factors: age, sex, height and BMI) using linear regression, the same trends persist for the circumferential indentation with IDI, TID and CID being higher in the osteoporotic and osteoarthritic groups compared to the control ($p < 0.01$) and similar in both disease states ($p > 0.05$). In the 'refined', method, the minimally adjusted Model 1 leads to the osteoporotic group no longer being significantly higher than the control ($p > 0.05$) but indentation in the osteoarthritic group remains significant when compared to either the osteoporotic or control groups ($p < 0.05$).

When the comparisons are further adjusted for testing related factors: proximal-distal test location, number of measurements and freezing duration in Model 2, the differences are generally less significant. When comparing the osteoporotic and control group and indenting circumferentially; though indentation depth is still higher in the osteoporotic group it is no longer significant in terms of IDI ($p = 0.298$) but close to significance when considering CID and TID ($p = 0.081$ and $p = 0.051$ respectively). When applying the 'refined' inferomedial testing, the osteoporotic and control groups no longer appear different using the further adjusted Model 2 ($p > 0.05$). Despite this, the osteoarthritic

group is still easier to indent than the control group ($p < 0.02$) in both circumferential and 'refined' testing (except for the 'refined' IDI, $p = 0.097$). Furthermore, with this increased adjustment, the osteoarthritic is easier to indent than the osteoporotic group in terms of IDI (close to significant, $p = 0.052$ circumferentially, $p = 0.015$ 'refined') but not TID or CID in either test methods.

Dissecting these models, it can be seen which variables are having a significant contribution and therefore the largest confounding effect. In the osteoporotic and control comparison, age has minimal effect ($p = 0.037$ for circumferential TID but otherwise $p > 0.05$) and all other variables (i.e. sex, BMI and height) do not have a significant influence in the patient specific variables of Model 1. In Model 2, the time stored and number of measurements has no significant confounding effect ($p > 0.05$) whereas the proximal-distal test location has a significant contribution in terms of 'circumferential' testing ($p = 0.013$, $p = 0.081$ and $p = 0.030$ for TID, IDI and CID respectively) but not the 'refined' measurements.

When comparing the osteoarthritic and control group, the patient specific variables of Model 1 again have no significant confounding effect and neither do proximal-distal test location or number of measurements in Model 2. However, the length of storage does influence this model for the circumferential indentation measurements (TID and IDI, $p < 0.01$ but for CID, $p > 0.05$).

Finally, comparing the osteoporotic and osteoarthritic groups, age ($p = 0.015$ for 'refined' CID), sex ($p = 0.006$ for 'circumferential' TID and $p = 0.01$ for 'refined' IDI) and height ($p = 0.038$ for 'circumferential' TID and $p = 0.007$ for 'refined' IDI) all have some influence on Model 1, but generally the effect of these variables is not significant. Considering the additional variables of Model 2, time stored again influences the circumferential measurements (TID and IDI, $p < 0.005$ but CID, $p > 0.05$) but proximal-distal test location ($p = 0.021$ for 'circumferential' TID, $p > 0.05$ otherwise) and number of measurements ($p = 0.029$ for 'refined' TID, $p > 0.05$ otherwise) have minimal effect.

Table 14 – Comparison between the osteoporotic, osteoarthritic and control groups in terms of the indentation depth (TID, IDI and CID) when measuring circumferentially around the femoral neck at 20° spacing (excluding the superolateral quadrant) and 15 'refined' measurements within ±10° of the inferomedial point. Model 0 shows the unadjusted comparisons with the t-test for normally distributed variables and the Mann-Whitney U-test for non-normally distributed variables (* Circumferential TID). Model 1 shows the comparisons minimally adjusted for age, sex, height and BMI. Model 2 shows the comparisons further adjusted for length of storage, proximal-distal test location and number of measurements. For Model 1 and Model 2, a linear regression comparison is used with non-normally distributed variables being transformed using the Fisher Yates z score to reach normality. The β coefficient (difference between the median or, where normally distributed, mean values) are shown alongside the 95% confidence intervals. Significant comparisons are displayed in bold and highlighted in grey.

		Circumferential			'Refined' Inferomedial		
		TID*	IDI	CID1	TID	IDI	CID1
OP - Cont	Model 0	**1.21** **0.74, 1.68**	**4.05** **1.88, 6.22**	**2.30** **1.09, 3.52**	**12.01** **0.49, 23.53**	1.36 -0.85, 3.57	**1.04** **0.23, 1.86**
	Model 1	**1.31** **0.70, 1.91**	**3.97** **1.21, 6.73**	**2.24** **0.78, 3.70**	5.06 -10.21, 20.34	-0.01 -2.79, 2.77	0.65 -0.38, 1.68
	Model 2	0.95 -0.01, 1.91	2.56 -2.36, 7.49	1.94 -0.25, 4.14	10.99 -15.68, 37.65	-0.70 -5.45, 4.04	0.31 -1.49, 2.11
OA - Cont	Model 0	**1.22** **0.72, 1.72**	**4.48** **1.63, 7.33**	**2.05** **0.82, 3.27**	**23.30** **9.01, 37.58**	**3.42** **0.95, 5.89**	**2.72** **1.65, 3.78**
	Model 1	**1.20** **0.68, 1.71**	**4.13** **1.24, 7.02**	**2.01** **0.80, 3.22**	**22.57** **7.45, 37.69**	**3.14** **0.63, 5.66**	**2.75** **1.67, 3.84**
	Model 2	**1.08** **0.56, 1.60**	**3.22** **0.56, 5.87**	**2.20** **1.17, 3.24**	**20.86** **4.11, 37.60**	2.31 -0.44, 5.05	**2.63** **1.46, 3.80**
OA - OP	Model 0	0.01 -0.37, 0.38	0.43 -1.49, 2.36	-0.26 -1.24, 0.73	11.29 -0.43, 23.01	**2.06** **0.11, 4.01**	**1.67** **0.78, 2.56**
	Model 1	-0.05 -0.52, 0.43	0.05 -2.37, 2.46	-0.55 -1.75, 0.65	**19.58** **4.61, 34.56**	**3.93** **1.66, 6.20**	**2.62** **1.56, 3.68**
	Model 2	0.52 -0.11, 1.14	2.81 -0.02, 5.65	0.44 -0.98, 1.86	8.59 -14.44, 31.62	**4.39** **0.90, 7.88**	1.51 -0.05, 3.07

6.3.4 Osteoarthritis Grading

The indentation depth appears to be higher with increased levels of osteoarthritis, though in general this difference is not significant. In terms of the individual radiographic measures of osteoarthritis (Figure 61a and Table 15), there appears to be an elevation in indentation depth with increased osteophyte severity, narrowing severity and with presence of cortical collapse. This difference is clearer in the 'circumferential' compared to 'refined' testing but is only significant in terms of osteophyte severity and narrowing severity for TID ($p = 0.01$). Similarly, using the 'circumferential' testing, the indentation depth appears to increase with osteoarthritic grading (Figure 61b and Table 15) as evaluated by the Overall Croft Score, though, again this is not quite significant ($p = 0.09$, $p = 0.08$ and $p = 0.08$ for TID, IDI and CID respectively) except comparing the highest Croft score (5) with the lowest (3) (IDI and CID, $p < 0.05$).

Also interestingly, the lower levels of osteoarthritis (i.e. osteophyte severity of 0 or 1, narrowing severity of 2, no cortical collapse and an overall croft score of 3) appear more similar to the control group in terms of indentation depth. Despite this, the low level osteoarthritis subgroup is still significantly elevated above the control except for in terms of osteophyte severity (circumferential IDI, $p > 0.05$) and Overall Croft Score (circumferential IDI, CID and 'refined' IDI, $p > 0.05$). The other side to this is that the increased levels of osteoarthritis (i.e. osteophyte severity of 2 or 3, narrowing severity of 3, cortical collapse present and an overall croft score of 5), appear more greatly elevated above the control group and are all statistically significantly higher ($p < 0.05$ with the exception of 'refined' IDI and Overall Croft Score).

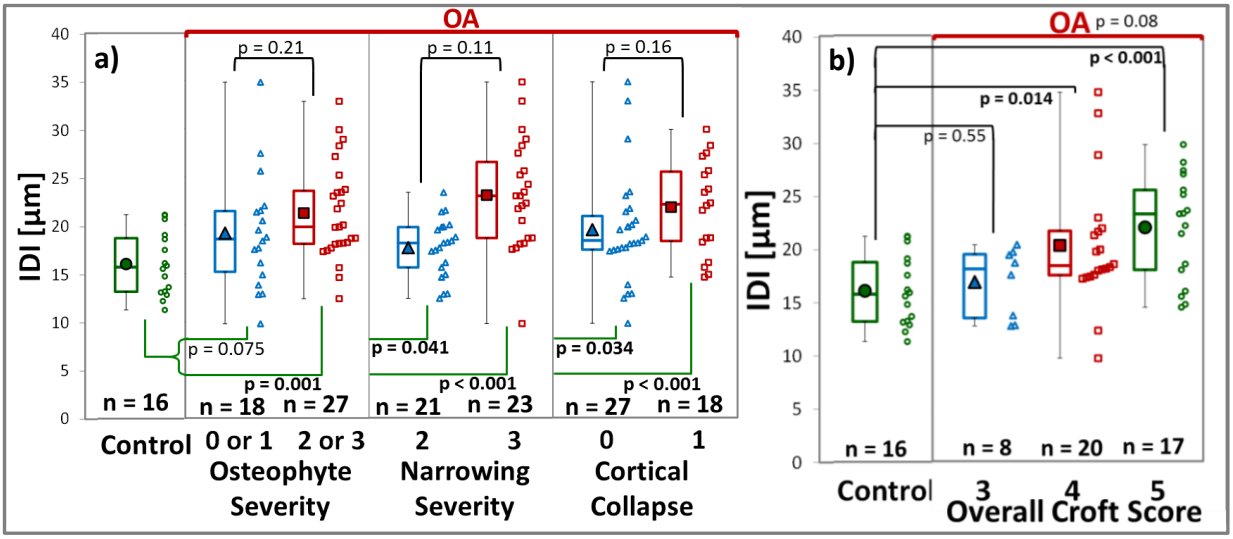

Figure 61 – Demonstration of the relationship between indentation measurements (IDI) and radiographic osteoarthritic grading of the osteoarthritic group compared to the control in terms of a) the individual measures indicating level of osteoarthritis (osteophyte severity, narrowing severity and presence of subchondral cortical collapse) and b) the measures combined into an overall croft score

Table 15 – Statistical summary of Figure 61 showing the relationship between radiographic osteoarthritis grading and indentation depth. The osteoarthritic group is split into subgroups based on the individual parameters indicating osteoarthritis (osteophyte severity, narrowing severity and presence of subchondral cortical collapse) and these parameters combined as an overall croft score. The p-values indicate the level of statistical difference between the grades (e.g. between absence and presence of cortical collapse) and the highlighted (grey and bold) values indicate a significant difference between the osteoarthritic sub-group and the control group. The mean and (standard deviation) is shown for normally distributed parameters (t-test and ANOVA for statistical comparisons) and the median and (interquartile range) is shown for non-parametric variables (Mann-Whitney U test and Kruskall Wallis for statistical comparison *)

		Circumferential			'Refined' Inferomedial		
		TID*	IDI	CID1	TID	IDI	CID1
Control		105.9 (103.6 – 113.0)	16.1 (3.3)	7.2 (0.7)	107.8 (13.6)	14.6 (3.5)	6.6 (0.7)
Osteophyte severity	0 or 1	**122.5 (111.8 – 152.1)**	19.2 (6.0)	**8.6 (2.1)**	**126.2 (16.6)**	**17.3 (3.2)**	**9.2 (1.4)**
	2 or 3	**148.0 (135.4 – 178.7)**	**21.3 (5.0)**	**9.4 (2.5)**	**136.3 (31.6)**	**18.1 (4.8)**	**9.5 (2.4)**
	p value	**0.01**	0.21	0.23	0.31	0.60	0.69
Narrowing severity	2	**134.3 (112.3 – 146.4)**	**19.2 (5.2)**	**9.0 (2.4)**	**133.6 (28.9)**	**17.7 (3.8)**	**9.9 (2.3)**
	3	**154.3 (136.1 – 175.9)**	**21.9 (5.4)**	**9.3 (2.4)**	**130.8 (25.7)**	**18.1 (4.6)**	**8.9 (1.7)**
	p value	**0.01**	0.11	0.69	0.78	0.82	0.19
Cortical Collapse	Absent	**136.1 (111.8 – 165.3)**	**19.5 (5.7)**	**8.6 (2.7)**	**131.9 (26.4)**	**17.8 (3.7)**	**9.6 (2.1)**
	Present	**150.9 (120.9 – 162.2)**	**21.8 (4.9)**	**9.8 (1.6)**	**132.3 (27.8)**	17.8 (4.9)	**9.0 (1.9)**
	p value	0.19	0.16	0.11	0.97	0.97	0.40
Overall Croft Score	3	**120.4 (111.4 – 155.3)**	17.0 (3.3)	8.0 (2.4)	**123.3 (12.3)**	16.0 (1.9)	**9.0 (1.3)**
	4	**138.7 (114.4 – 156.2)**	**20.4 (6.0)**	**8.7 (2.7)**	**138.8 (31.9)**	**18.7 (4.1)**	**10.0 (2.3)**
	5	**153.9 (143.8 – 170.2)**	**22.1 (5.0)**	**10.0 (1.6)**	**128.3 (24.2)**	17.7 (5.0)	**8.7 (1.9)**
	p value	0.09	0.08	0.08	0.43	0.43	0.25

6.3.5 Comparison with Clinical Techniques

The clinical fracture risk assessment measures are significantly different between the three groups ($p < 0.001$, Kruskall-Wallis for these skewed variables). That is, the femoral neck BMD is lowest in the osteoporotic group, higher in the osteoarthritic group and higher still in the control group. Furthermore, the 10 year probability of hip fracture as assessed by the FRAX tool is highest in the osteoporotic group and lowest in the control group when using clinical fracture risk factors alone (i.e. age, sex, previous fracture etc.) and when these are combined with BMD. These differences remain in terms of BMD and FRAX including BMD when adjusted for the patient related factors (Model 1 – age, sex, height and BMI). Adjustment of the FRAX scores with using Model 1 is not suitable as these factors are already incorporated within the score.

Table 16 – Comparison between clinical measurements (FN BMD – Femoral Neck Bone Mineral Density) across the three groups showing the median value and (lower – upper quartile) per group

	Osteoporotic	Osteoarthritic	Control
Clinical Measurements			
FN BMD (g/cm^2)	0.60 (0.54 – 0.66)	0.77 (0.66 – 0.94)	1.15 (0.77 – 1.36)
FRAX hip fracture risk (%)	11.0 (4.6 – 17.0)	2.8 (0.7 – 4.5)	1.3 (0.7 – 3.8)
FRAX with BMD (%)	7.8 (4.5 – 17.0)	1.1 (0.3 – 3.3)	0.1 (0.0 – 1.3)

Despite the clinical disease states being distinct in terms of BMD and FRAX scores, the sensitivity of the tools to discriminate those that have fractured from the non-fractured control is still poor in terms of existing clinical threshold. This is demonstrated in Table 17 and Figure 63a and b (y-axis) by some overlap between the osteoporotic and control group and a low proportion of the osteoporotic group being below the clinical thresholds (a t-score of -2.5 for BMD and an age dependent threshold for FRAX as shown in Figure 62 [265]). Using a lower threshold for BMD, e.g. a t-score of -1.0 as used to denote osteopenia, does improve the sensitivity of the tool.

Comparing the osteoarthritic to control group, the sensitivity is further reduced (0% to 13%) but, considering BMD and FRAX are intended to identify those at risk of fracture, this comparison is not of great value.

Table 17 – Sensitivity and specificity of the clinical measures between the osteoporotic and control groups with the FRAX thresholds based on Figure 62 and the recommendations by Kanis et al [265]

Clinical Measurements	OP: Control	Threshold	Osteoporotic vs. Control (%)	
			Sensitivity	Specificity
FN BMD (g/cm^2)	19:16	t-score < -1.0	95	81
FN BMD (g/cm^2)		t-score < -2.5	37	94
FRAX hip fracture risk (%)	37:16	Treat or BMD	54	75
FRAX hip fracture risk (%)		Treat	14	100
FRAX with BMD (%)	20:16	Treat	40	94

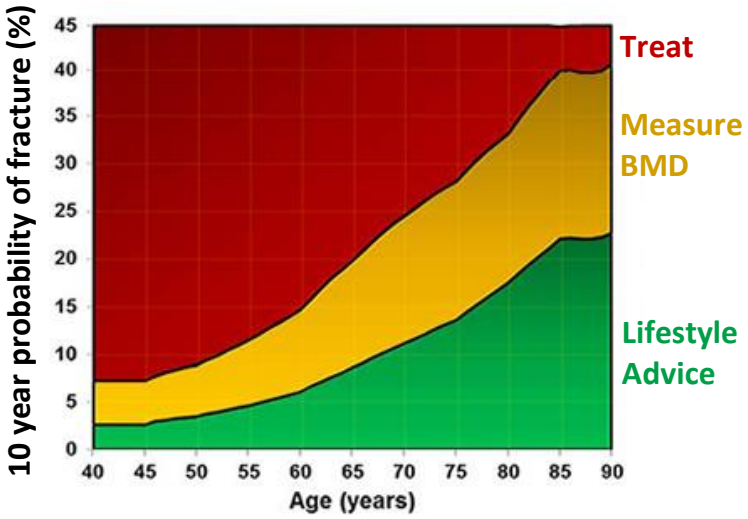

Figure 62 – Clinical threshold for FRAX with and without BMD based on the age dependent UK threshold established by Kanis et al [265] and the National Osteoporosis Guideline Group. Image adapted from FRAX website [12] and Kanis et al [265] courtesy of Springer

Figure 63 and Table 18 compare clinical measures to RPI measures, generally finding no correlation between the two, therefore implying indentation is measuring a property distinct from those assessed by existing tools. In terms of BMD, there is no significant correlation between the indentation depth (TID, IDI and CID) when testing circumferentially or in the 'refined' method ($r = -0.39$ to 0.34, $p > 0.05$). Generally, there is also no relationship between FRAX and indentation depth except for CID and FRAX (without BMD) with 'refined' testing ($r = -0.52$, $p < 0.05$) and 'circumferential' TID and CID with FRAX including BMD ($r = -0.62$ and $r = -0.51$ respectively). Furthermore, comparing indentation with calcium and vitamin D blood levels (Figure 63c and Table 18) in the osteoporotic group there is only minimal correlation between circumferential TID and adjusted calcium level ($r = -0.31$, $p < 0.05$) but otherwise the correlations are low and non-significant ($r = -0.30$ to 0.32, $p > 0.05$).

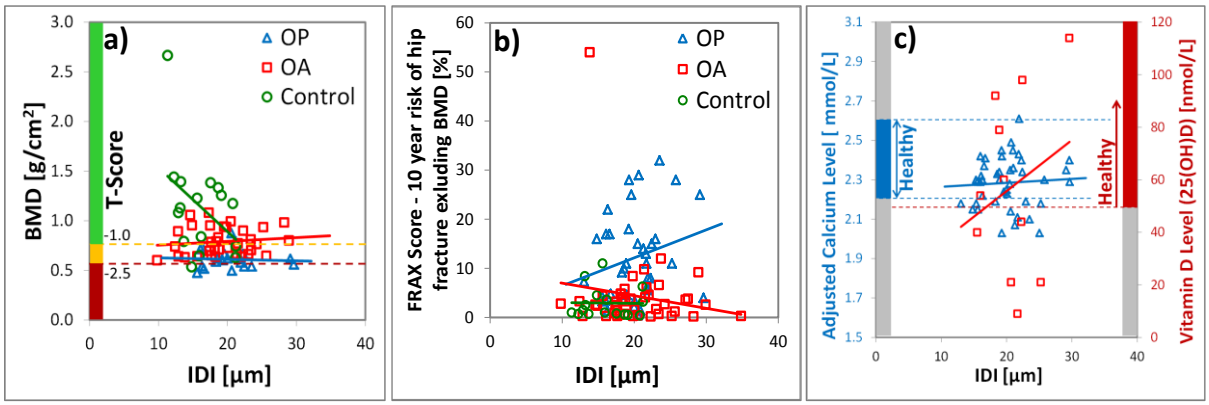

Figure 63 – Comparison between indentation distance increase (IDI) and clinical factors: a) Bone Mineral Density (BMD), b) FRAX hip fracture risk assessment and c) Calcium and Vitamin D levels

Table 18 – Statistical summary of Figure 63: Spearman's correlation coefficient (r value) for comparison between indentation depth and clinical factors across the three groups (significant correlations shown in bold and highlighted in grey)

		Circumferential			'Refined' Inferomedial		
		TID	IDI	CID1	TID	IDI	CID1
OP	BMD	0.06	-0.09	0.14	0.04	0.02	0.08
	FRAX	0.18	0.21	0.29	0.22	0.10	0.11
	FRAX (BMD)	0.19	0.28	0.39	0.09	-0.03	0.01
	Calcium	**-0.31**	0.09	-0.08	-0.30	-0.06	-0.06
	Vit D	0.32	0.11	0.22	0.26	0.14	0.14
OA	BMD	0.23	0.13	0.01	0.34	0.11	0.02
	FRAX	-0.02	0.03	0.07	-0.12	0.14	0.08
	FRAX (BMD)	0.06	0.01	-0.03	-0.33	0.11	-0.04
Control	BMD	0.11	-0.39	0.20	-0.10	-0.34	0.21
	FRAX	-0.31	0.25	-0.37	-0.31	0.11	**-0.52**
	FRAX (BMD)	**-0.62**	-0.12	**-0.51**	0.01	0.34	-0.42

6.3.6 Discriminative Ability of Indentation, Clinical and Combined Tools

When comparing the discriminative ability of the indentation and clinical tools between the osteoporotic and control groups (with the main focus of RPI, BMD and FRAX being fracture risk assessments making the osteoarthritic comparison less relevant), Receiver Operator Characteristic (ROC) curves can be plotted and the Area Under the Curve (AUC) calculated.

By plotting ROC curves, it can be seen that the AUC of both FRAX and BMD are extremely high (0.86 and 0.90), which relates to the statistical difference between the two groups discussed above (Section 6.3.3) and the minimal overlap as shown in Figure 63a and b. This indicates a possible sensitivity and specificity of 95% and 81% respectively for BMD if a t-score of -1.0 were used (i.e. osteopenic or a BMD below 0.75 g/cm^2). The AUC is

improved further to 0.95 (a theoretical sensitivity of 91% and sensitivity of 94% if a threshold of fracture risk above 3% were used) when BMD is added into the FRAX tool. It is very important to note that these thresholds are less strict than the established t-scores below -2.5 and FRAX risk above 7% (and rising with age, Figure 62) [265] and these ROC curves are therefore not representative and the sensitivity and specificity are actually lower as discussed and indicated by Table 17.

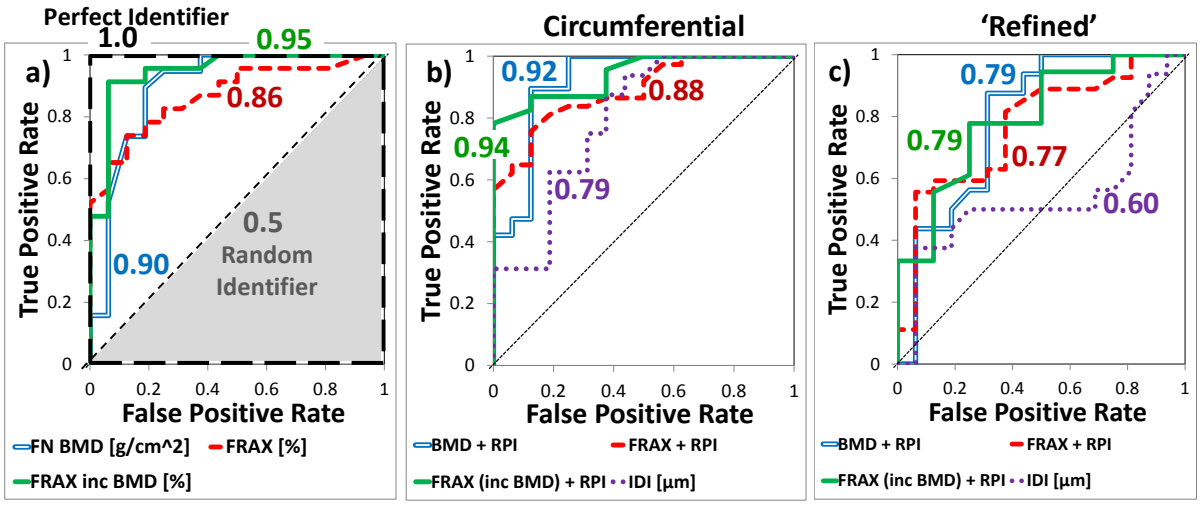

Figure 64 – Receiver Operator Characteristic Curves comparing the osteoporotic and control groups in terms of: a) clinical factors (Femoral Neck Bone Mineral Density, FRAX 10-year hip fracture risk based on risk factors alone and combined with BMD), b) Indentation testing circumferentially and combined with clinical factors, c) Indentation testing in the 'refined' method and combined with clinical factors

Indentation measurements have a lower AUC when using the 'refined' method and a further improved discriminative ability when considering TID or CID rather than IDI. Using TID or CID in the circumferential testing method, the AUC is comparable to that of the FRAX or BMD tools alone (0.88 – 0.89), but with IDI and the 'refined' method this is reduced relative to existing clinical techniques (AUC = 0.60 – 0.79). If only the donors with BMD are considered (i.e. equivalent to the BMD comparison and, next, the combined BMD and RPI comparison) the ROC values are marginally increase for 'circumferential' indentation and marginally decreased for 'refined' indentation, indicating these values are representative and not due to differences in sampling (Table 19).

By combining BMD and RPI measures the discriminative ability can be improved. This is true of the FRAX tool and BMD alone when combined with circumferential RPI, increasing the AUCs from 0.90 to 0.92 up to 0.99 for BMD and from 0.86 to 0.88 up to 0.95 for FRAX (without BMD), again with TID and CID being more effective than IDI. The 'refined' method, however, does not contribute to the tool with AUCs of 0.77 to 0.93, similar to

the clinical measures alone. Furthermore, the discriminative ability of the combined FRAX and BMD tool is already close to perfect (0.95) and the addition of indentation measures does little to affect this (0.94-0.96).

Evaluating the tool's ability to differentiate the osteoarthritic group from the healthy control (Table 19), it can be seen that this is similar to the osteoporotic-control ROC AUC (0.76 to 0.87 compared to 0.79 to 0.89) in the circumferential testing. Rather than being less effective, here, the 'refined' testing is similar (0.75 to 0.91) to the circumferential testing. In comparing the osteoarthritic group to the control, the ROC AUC of the clinical factors is low (0.54 to 0.75) and again improved by the addition of indentation measures (0.65 to 0.93). However, the clinical measures are only intended for fracture risk assessment and, therefore, this comparison is again not particularly appropriate.

Table 19 – Summary of the Receiver Operator Characteristic Curves shown in Figure 64 indicating the Area Under the Curve and Confidence Intervals for clinical measures, indentation measures and combined clinical and indentation measures

Osteoporotic vs. Control ROC AUC						
FN BMD [g/cm^2]	0.90 0.79 – 1.00					
FRAX [%]	0.86 0.76 – 0.97					
FRAX (BMD) [%]	0.95 0.88 – 1.00					
	Circumferential			'Refined'		
	TID	IDI	CID1	TID	IDI	CID1
RPI [µm] (all donors)	0.89 0.79 – 0.99	0.79 0.65 – 0.92	0.88 0.78 – 0.97	0.67 0.51 – 0.83	0.60 0.44 – 0.77	0.73 0.59 – 0.87
(limited to donors with corresponding BMD)	0.93 0.84 – 1.00	0.81 0.66 – 0.95	0.91 0.81 – 1.00	0.63 0.43 – 0.83	0.55 0.33 – 0.76	0.78 0.61 – 0.95
FN BMD + RPI	0.99 0.98 – 1.00	0.92 0.81 – 1.00	0.98 0.95 – 1.00	0.87 0.74 – 1.00	0.79 0.63 – 0.96	0.93 0.85 – 1.00
FRAX + RPI	0.95 0.89 – 1.00	0.88 0.79 – 0.97	0.93 0.87 – 1.00	0.81 0.68 – 0.94	0.77 0.62 – 0.92	0.87 0.76 – 0.98
FRAX (BMD) + RPI	0.96 0.88 – 1.00	0.94 0.87 – 1.00	0.95 0.87 – 1.00	0.86 0.71 – 1.00	0.79 0.60 – 0.98	0.93 0.82 – 1.00
Osteoarthritic vs. Control ROC AUC						
RPI [µm]	0.87 0.78 – 0.96	0.76 0.63 – 0.89	0.84 0.74 – 0.94	0.80 0.67 – 0.93	0.75 0.60 – 0.90	0.91 0.82 – 0.99
Key	< 0.65	> 0.65	> 0.75	> 0.85	> 0.90	> 0.95

To further investigate the potential of combining RPI and existing clinical measures (FRAX and BMD), ROC curves can be plotted for RPI for individuals who would not currently be

detected by the existing clinical thresholds (with a t-score of > -2.5 or an age dependent FRAX threshold, Figure 62). Though this limits the numbers further (e.g. 12 osteoporotic donors undetected by BMD) and therefore findings are more speculative, this can still provide some insight into the complementary nature of the techniques. The ROC curve in Figure 65and summary of the AUC values in Table 20 indicate that RPI, primarily circumferential TID or CID, can be beneficial in supplementing existing clinical measures.

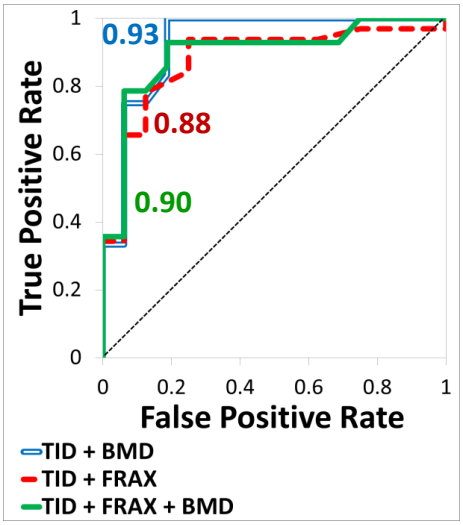

Figure 65 – The Receiver Operator Characteristic Curve for circumferential TID for three subgroups those undetected by: BMD (TID + BMD) i.e. with a t-score of > -2.5, FRAX (TID + FRAX) i.e. with a 10 year fracture risk > 7% and increasing (Figure 62) and the combined FRAX and BMD tool (TID + FRAX + BMD).

Table 20 – Summary of ROC AUC values and confidence intervals based on the indentation parameters (TID, IDI, CID) for those above the clinical thresholds for osteoporosis or treatment

Osteoporotic vs. Control ROC AUC						
	Circumferential			'Refined'		
	TID	IDI	CID1	TID	IDI	CID1
FN BMD + RPI	0.93 0.84 – 1.00	0.82 0.66 – 0.97	0.94 0.86 – 1.00	0.60 0.38 – 0.83	0.52 0.27 – 0.76	0.78 0.58 – 0.97
FRAX + RPI	0.88 0.77 – 0.99	0.78 0.65 – 0.92	0.85 0.74 – 0.96	0.65 0.48 – 0.83	0.60 0.41 – 0.78	0.70 0.54 – 0.87
FRAX (BMD) + RPI	0.90 0.77 – 1.00	0.82 0.67 – 0.97	0.91 0.81 – 1.00	0.70 0.50 – 0.90	0.67 0.45 – 0.89	0.88 0.75 – 1.00
Key	< 0.65	> 0.65	> 0.75	> 0.85	> 0.90	> 0.95

Furthermore, a sensitivity and specificity for a given threshold can be read off the ROC curves as exampled by Figure 65. Due to the cross-sectional retrospective nature of this study, the small numbers of patients and therefore the elevated 'prevalence' of the disease in our cohort, the estimation of this threshold and given sensitivity are also speculative and much larger longitudinal prospective studies would be needed to

establish this. Nevertheless, Table 21 indicates the minimum required RPI threshold to give the maximum sensitivity if the specificity is set at 80% (i.e. allowing 20% false positives). For example, a TID above 115 µm would identify all individuals that are not currently detected by a t-score of less than -2.5.

Table 21 – Potential thresholds (based on a >80% specificity) for the three RPI measures (TID, IDI and CID) and their sensitivity based on those not currently detected by BMD or FRAX

	Osteoporotic vs. Control		Threshold	Sensitivity (%)
	Clinical Measurements	No.		
TID	All Samples	46:16	> 115 µm	85
	FN BMD (g/cm^2) < -2.5	12:15		100
	FRAX hip fracture risk (%) – Treat			81
	FRAX with BMD (%) - Treat			93
IDI	All Samples	46:16	> 19 µm	63
	FN BMD (g/cm^2) < -2.5	32:16		67
	FRAX hip fracture risk (%) – Treat			59
	FRAX with BMD (%) - Treat			64
CID	All Samples	46:16	> 8 µm	76
	FN BMD (g/cm^2) < -2.5	13:15		100
	FRAX hip fracture risk (%) – Treat			75
	FRAX with BMD (%) - Treat			86

6.4 Discussion

The results of this study further assess the clinical potential of RPI to discriminate between those at higher risk of fracture and non-fractured controls. The broad picture is that indentation depth is increased in osteoporotic hip fracture patients relative to a cadaveric control and that, in measuring a parameter distinct from currently available clinical techniques, the RPI tool may be able act as a complementary measure for improved fracture risk assessment. In this respect, this study is supportive of the previous in vivo studies by Diez-Perez et al [19] and Guerri-Fernandez et al [21] and the in vitro study by Milovonovic et al [28] where indentation depth is higher in osteoporotic fracture patients relative to non-fracture controls. Additionally, it is supplementary by evaluating the combination of RPI with existing techniques, considering a larger number of fracture cases, investigating osteoarthritis and studying the minimally tested femoral neck.

6.4.1 Effect of Confounding Factors

To be confident with these results we have thoroughly investigated potential confounding factors associated with these groups. However, some potentially influential factors could not be included in the analysis such as physical activity levels, vitamin D and calcium serum levels due to the limitations of the data available for the cadaveric control and osteoarthritic group.

Though the osteoporotic group is significantly older than the control group and, as there appears to be minimal correlation between age and indentation depth (shown here and previously by Diez-Perez et al [19]), this does not have a significant confounding effect. This minimal correlation with age, and in fact a significant negative correlation with TID and CID in the control group, does not support RPIs ability to assess this aspect of fracture risk (with 50% of fractures occurring in those over 80 years [192]). However, this is only one risk factor associated with fracture and indeed, one that can clearly already be assessed, so RPI may still be of some contributory benefit. Additionally, the osteoporotic group has a higher proportion of females, and because women have an increased risk of fracture (a 2 fold risk of fracture with 80% of fractures occurring in women [192]), this variable might be expected to have a significant confounding effect. Despite there being some increase in indentation depth in the osteoporotic group (CID, $p < 0.05$) implying, to some extent, that this aspect of fracture risk may be assessed by RPI, this variable does not have a significant influence on the osteoporotic-control comparison.

The relationship with indentation depth and standing height is minimal and, where significant, it is negative ($r = -0.31$, $p < 0.05$). This negative correlation is contrary to the study by Gunnes et al [139] that found increased height to be indicative of increased risk of hip or spinal fracture. However, height loss (indicating vertebral crush fractures) was also indicative of increased fracture risk [139] and this has not been recorded here. Increased height, rather than affecting the material properties of the bone itself, has been suggested to relate to the increased impact during the fall. Therefore, this may be a completely separate aspect of fracture risk which would support the minimal relationship observed here.

Increased BMI, has been indicated to be protective of hip fracture [129, 137, 139], particularly with a low BMI (below 20 kg/m^2) being indicative of hip and spinal fracture. This is again contrary to the potentially positive correlation ($r = 0.35$, $p = 0.04$ for CID) seen in our three groups. Though the link between BMI and fracture risk has been suggested to affect the fall risk (i.e. reduced muscle strength or reduced protection from soft tissue), there is also likely to be an effect from decreased weight bearing and poor nutrition, which would affect the bone itself. This aspect of fracture risk is therefore not assessed by RPI but, again, a separate currently clinically undetectable bone quality related risk factor may be being measured. For this reason, height and BMI do not influence indentation and do not act as confounding factors in this study.

When considering the testing related parameters of number of measurements, proximal-distal indentation location and freezer storage duration it is only the test location that significantly affects the comparison. The lack of influence from the number of measurements made on the samples can be attributed to this tending to be fairly high, even for the osteoporotic group (median of 10 out of 13). Therefore, this gives a reasonably representative measure of the bone as discussed in the previous chapter (it would expect approximately 10% error from the 'true' value - Chapter 5 [279]). Furthermore, where measurements were missed in this group, this would typically be towards the superolateral region where the fracture had occurred (Figure 58b) and also where the indentation distance would be increased [229]. Therefore, by having fewer measurements in the osteoporotic group the superolateral measurements with higher indentation depth are excluded and the average indentation depth is reduced. To conclude, if the reduced number of measurements has any effect on the osteoporotic

group, it would be to reduce the differences observed between the groups and not be artificially enhancing it.

The storage conditions appear to present a larger confounding effect by the control samples being stored for longer and a potential negative relationship between indentation depth and length of storage being presented by the two batches of the osteoarthritic group. Despite this, the storage conditions do not present as a significant confounding factor in the adjusted model. It is most likely that length of storage does not influence indentation depth because: 1) there is no significant relationship between indentation depth and length of storage in any of the three groups when the two batches of osteoarthritic samples are taken into account, 2) the reduction with indentation depth seen with the longer storage period of the second batch of osteoarthritic samples can perhaps partly be explained by a lower proportion of severe radiographic osteoarthritis and more male donors, 3) though there is a some reduction in indentation depth in paired samples that have been stored for varying degrees of time, this is only significant in terms of TID and the difference is small (around 25%) when compared to the large variability associated with only 3 repeat measurements (around 20% Chapter 5 [279]) and could perhaps be attributed to retesting of a previously tested area, 4) a previous study by Kaye et al [286] showed no relationship between time stored and indentation depth, albeit considering shorter periods of storage, with freezing also being indicated to have no measureable effect on other material properties, primarily stiffness [287, 288]. Furthermore, the shorter duration of storage, alongside; being stored hydrated with HBSS and gauze to minimise freezer burn, being stored at -80°C rather than -20°C and being transported from patient to freezer in a shorter period of time would imply the improved preservation of the material properties of osteoporotic bone. The effects of storage duration, as with number of measurements, would therefore act to minimise rather than exaggerating the elevation in osteoporotic relative to control samples.

The influence of proximal-distant test location on indentation of the osteoporotic group relates in part to a minimal relationship between indentation depth and test location ($r = -0.31$ to -0.38, $p < 0.05$). However, the test location relative to the fracture site (with lower indentation testing distally of the fracture rather than proximally, $p < 0.05$) is perhaps more influential. This effectively splits the osteoporotic cohort into two groups, those with elevated indentation depth correlating to testing proximally of the fracture

and those with reduced indentation distance correlating to testing distally of the fracture. However, due to the mean test location of the osteoporotic group being more distal than the control group, the overall effect is a reduced indentation depth, again minimizing rather than exaggerating the observed differences between groups. It is additionally possible that bone with compromised material properties, fractures more distally, with a more distal fracture encouraging indentation proximal to the fracture and increasing the indentation depth. However, testing along the femoral neck in different locations of both control and fractured tissue would be necessary to confirm this hypothesis.

Therefore, the considered potential confounding factors either appear to have minimal effect (i.e. age, sex, height and BMI), a potentially artificial effect (i.e. storage duration) or an effect that is diminishing rather than exaggerating the difference (i.e. number of measurements, storage duration and test location).

6.4.2 Discriminative ability of RPI and potential as a complementary fracture risk assessment tool

With these factors in mind, despite the model adjusted for patient and testing parameters (Model 2) not being significant ($p = 0.30$ for IDI and a significance level of $p < 0.05$) or close to significance ($p = 0.051$ and $p = 0.081$ for TID and CID respectively), we believe that the differences observed between the fractured osteoporotic group and the control group can be attributed to differences in the properties of the bone rather than patient or testing specific confounding effects. In addition to the cumulative effect of the, generally not significant or interpretable confounding factors, the reduced significance with adjustment may relate to the reduced number of samples in consideration (i.e. 12 osteoporotic samples do not have information available for all adjusted factors). This further indicates that the difference between cohorts that is observed in the unadjusted model is representative (i.e. higher indentation depth in the osteoporotic and osteoarthritic groups relative to the control). Indentation in the circumferential method is more effective for differentiating fractured from control bone in comparison to the 'refined' method (discussed in section 6.4.4) and therefore the following discussion focuses on the circumferential testing results unless stated otherwise.

Accepting that the difference in indentation relate to differences in the properties of the bone, the difference observed here (24% to 32%) lies between that found by Milovanovic

et al [28] (3% to 20%) and that of Diez-Perez et al [19] (33% to 47%). Though the differences between these two groups (osteoporotic fractured and healthy control) is statistically significant, it is also comparable to the 28% to 44% coefficient of variation seen within repeat measurements.

The discriminative ability of the tool relates to its ROC AUC, which describes its sensitivity and specificity. For RPI this value is high (0.79 to 0.89) and comparable to the previous study by Diez-Perez et al (0.74 to 0.93) indicating a good discriminative ability of the technique. In comparison to these values, the existing clinical factors (FRAX and BMD), have higher ROC AUC values (0.86 to 0.95). However, this is not characteristic of these tools that typically have a low ability to identify individuals at risk of fracture with BMD being reported to have an ROC of 0.66 to 0.80 [13, 190, 191] and FRAX having an ROC between 0.62 and 0.78 [13, 195]. Indeed, when the existing clinical thresholds are considered, the sensitivity is shown to be low (14% to 39%), in-line with the literature (18% to 64% for BMD [10, 11] and 29% to 56% for clinical risk factors [289]), indicating that these high ROC AUC values are not representative. It should be noted that the predictive ability of both the clinical and RPI techniques discussed in this study are dependent on the population that has been considered. As this is a retrospective study considering those who have fractured, the fracture incidence is understandably high (74%). Whereas, for a population, the prevalence of osteoporosis is in the region of 10-20% [2]. Therefore, if the prevalence was reduced for this study (indicated in Table 22) in line with the general population but the sensitivity maintained, then the specificity must reduce. To demonstrate the efficacy in a larger population, assumptions must be made. Table 22 assumes that the total proportion of individuals above and below the threshold would remain the same regardless of population size. Therefore, to maintain a given specificity (depending on the cost-effectiveness of the technique), the threshold would have to be made substantially more strict. That is, the RPI threshold would need to be increased and the t-score reduced (i.e. from the optimum -1.0 towards the conventional -2.5 threshold). The model in Table 22 may make quite strict assumptions and, for example, it is possible that with reduced incidence of fracture (particularly if the device is assessing an aspect of fracture risk) the proportion of those above the indentation threshold might similarly reduce. Regardless, the sensitivity and specificity for

a larger population are likely to relate to the incidence of fracture which is artificially elevated in this retrospective study.

Table 22 – Sensitivity and specificity in the population of this study and adjusted for a population with a representative prevalence of osteoporosis. To approximate the adjusted specificity, the sensitivity (proportion of those detected) is maintained (green), the prevalence is adjusted (blue) and the resulting specificity (orange)

Population in this study

	Fractured	Non-Fractured	
>115 µm	39	3	42 (68%)
<115 µm	7	13	20 (32%)
	46 (74%)	16 (26%)	62

Sensitivity	Specificity
85%	81%

Overall Population

	Fractured	Non-Fractured	
>115 µm	17	119	136 (68%)
<115 µm	3	61	64 (32%)
	20 (10%)	180 (90%)	200

Sensitivity	Specificity
85%	34%

The RPI measures have weak correlation with BMD (r = -0.39 to 0.23) which is similar to the low and not significant (r = -0.35 to -0.51, p > 0.05) correlation indicated by Diez-Perez et al [19]. We show, for the first time, that RPI additionally has a low correlation with FRAX (r = -0.62 to 0.39). Perhaps unexpectedly, the only significant correlation between clinical and indentation measures is a negative correlation between FRAX including BMD and TID or CID (-0.62 and -0.51 respectively) in the control group. Though increased FRAX score and increased indentation both imply increased fracture risk so a positive correlation would be expected, in the control group the FRAX scores are extremely low and over a short range (0.0% to 1.3%) so the regression gradient is low and there is still minimal relationship between these variables. Furthermore, there is limited correlation with calcium and vitamin D levels in the osteoporotic group implying RPI does not assess this (already measurable) aspect of fracture risk [130, 133]. Where significant, the correlation with indentation depth and calcium levels is negative, with low levels of calcium and high indentation depth implying increased fracture risk, therefore these factors may perhaps be minimally related [19, 130].

The lack of relationship between indentation and clinical measures leads to the two techniques measuring distinct properties and being complementary of each other. That is, when combining indentation parameters with BMD or FRAX (based on clinical risk factors alone), the discriminative ability of the tools is improved with an AUC of 0.88 to 0.94 for

IDI and a close to perfect AUC of 0.93 to 0.99 tor TID and CID. Furthermore, when considering a subset of samples that are not currently detected by BMD or FRAX, the AUC values for TID and CID range from 0.85 to 0.94 implying that the addition of RPI to a combined tool could detect the majority of those who fracture.

Speculatively assigning thresholds to RPI (and using the established clinical thresholds for BMD and FRAX), further indicates the complementary nature of the measures as further demonstrated by Figure 66. The Venn diagram in Figure 66 shows the proportion of fractured individuals in our study that would be identified by RPI and clinical tools, which when combined could define the majority of osteoporotic participant (95%). This implies that indentation measurements could complement current techniques and improve the fracture risk assessment but the methodology of Figure 66 would have to be applied to a substantially larger longitudinal prospective study to verify this speculation.

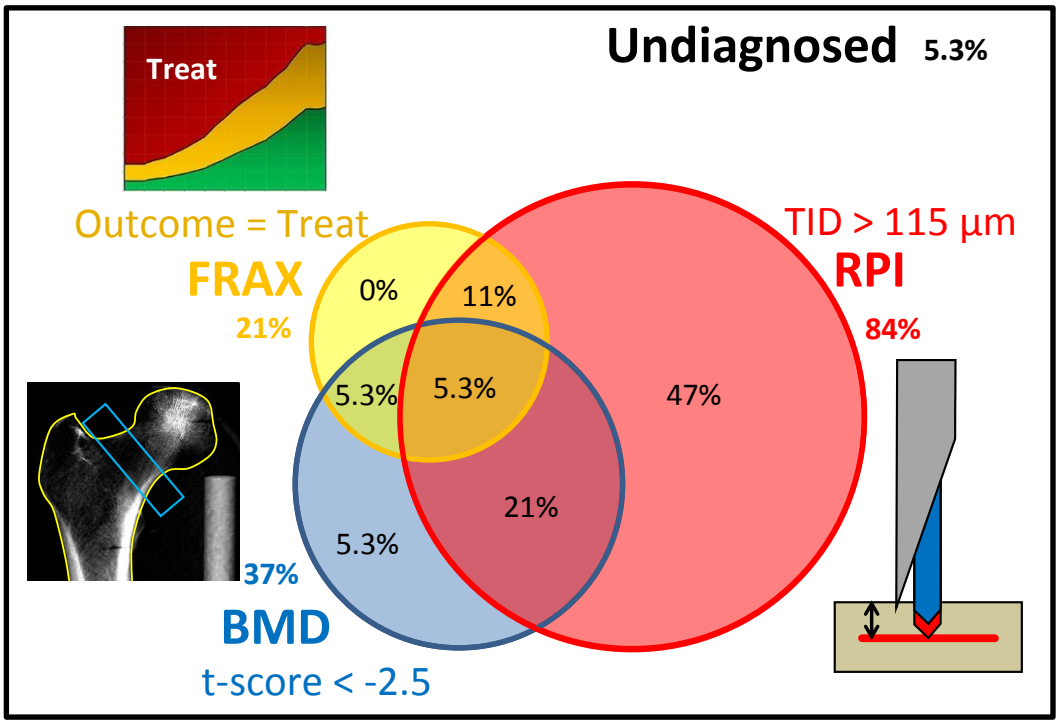

Figure 66 – Speculative contribution of existing clinical tools (FRAX and BMD) with the combination of RPI (TID) in identifying those who fracture. The percentages indicate those identified by each area indicating the sensitivity of the tool alone and in combination.

6.4.3 Investigation of the osteoarthritic disease state

Though there is some evidence for increased stiffness of the trabecular bone and changes in stiffness of the subchondral bone [222, 224, 290], little is really known about the material properties of cortical bone in the osteoarthritic femoral neck. Therefore, the findings here provide new knowledge about the effects of the disease on the properties

of the bone. There is a higher indentation depth relative to the control group that remains significant with the adjusting of the models for patient and testing specific parameters ($p < 0.05$, except for 'refined' IDI where $p = 0.063$). The confounding factors have little effect on this comparison with none of the patient related factors having a significant effect, due to the similarity in age, sex, height and BMI between the two groups. The number of measurements and test location is again similar between the osteoarthritic and control groups, both having ample quantity of bone as not to restrict testing in this way. The storage duration (shorter in the first batch but longer in the second batch of osteoarthritic samples compared to the control) does have some influence on circumferential TID and IDI ($p < 0.01$), but as stated previously in section 6.4.1, we do not believe that freezing duration has an effect on indentation depth.

A further indicator that the measured differences between the two groups relates to the disease state is the higher indentation depth with more severe radiographic osteoarthritis grading. Though this is not significant (except for osteophyte severity and degree of joint space narrowing in terms of TID, $p < 0.01$), particularly in the circumferential testing, there is a consistently higher median indentation depth with osteophyte severity, narrowing severity, presence of subchondral cortical collapse and higher Overall Croft score (Figure 61). Furthermore, when comparing these osteoarthritic subgroups to the healthy control, the difference between the groups is more pronounced at higher levels of osteoarthritis. Most notably, in terms of the osteophyte severity and Overall Croft score, only the osteoarthritic sub-groups that have a further progressed disease state (i.e. osteophyte severity of 2 or 3 and a Croft score of 4 or 5) are significantly different from the control in terms of IDI. For the Croft score, this similarity between controls and lower grade osteoarthritis (a Croft score of 3) is also seen in terms of CID. This implies that the higher indentation depth in osteoarthritis is a function of the disease, with further progressed osteoarthritis making the bone less resistant to indentation relative to the control.

As well as being higher relative to the control group, the osteoarthritic indentation depth is higher still than the osteoporotic group, although not significantly in circumferential testing. Therefore, the mean indentation depth is 28% to 38% higher in the osteoarthritic compared to control in comparison to 24% to 32% when comparing the osteoporotic group to the control. This difference between the osteoarthritic and osteoporotic groups

(2% to 22%) is less pronounced than the comparison with the control and is only significant when considering the 'refined' method.

With the current interpretation of the RPI technique [19, 21], this would imply that the osteoarthritic group are at elevated risk of fracture, even more so than the osteoporotic group. However, it is considered that presence of osteoarthritis is protective of hip fracture [222, 224] and, though there is evidence of increased fracture risk within 2 years of osteoarthritis diagnosis, after this period the fracture risk is reduced with time [227]. In our group with progressed osteoarthritis (Overall Croft scores greater than 3) surgical intervention has been necessitated. Therefore, though the period since diagnosis is unknown, it can be assumed that the donors have been suffering with the disease for long enough to indicate reduced fracture risk. This is further indicated by a low incidence of osteoporotic fracture (2 individuals with wrist fracture, hip and spinal fractures were excluded) or diagnosis of osteoporosis (6 donors based on their self-assessment questionnaire) in the osteoarthritic group.

The higher indentation depth in these osteoarthritic donors but reduced fracture incidence therefore further shines a light on the fact that it is not entirely clear what parameter RPI is measuring. Previously, correlations (and indeed contrary lack of correlations) have been shown between indentation depth and different measures from; elastoplastic [25, 26] to fracture toughness [19, 24, 244] properties. This current lack of understanding of the properties assessed by indentation would therefore make it difficult to interpret a higher measurement as indicative of osteoporosis or osteoarthritis, i.e. if the bone had purported changes in fracture toughness or elastoplastic properties. Furthermore, in different types of bone, the properties assessed through RPI may differ with the elevated indentation depth in osteoarthritic bone not necessarily indicating increased fracture risk. Furthermore, osteoarthritis is a disease localized to the joint (and here, it appears, the cortical bone) whereas osteoporosis may be a systemic condition affecting the bone as a whole, with the fracture location potentially more influenced by the biomechanics. Therefore, even if the bone quality is similarly reduced in both osteoarthritic and osteoporotic bone, other factors such as falls risk and biomechanics during loading and fall may be more significant factors in determining fracture risk in these two bone types. Regardless, the similar indentation properties of the two types of

bone can be discriminated clinically through higher osteoarthritic grading and BMD in osteoarthritis [209, 213, 219, 222, 227, 230].

6.4.4 'Refined' compared to 'Circumferential' testing

The rationale behind the 'refined' testing was to reduce the variability associated with RPI by reducing the influence of; cortical thickness, porosity (more repeat measurements in the thick, less porous inferomedial quadrant [181, 182, 229]) and circumferential heterogeneity (testing in a smaller, 20°, region [229]). Though this may have been effective, and the CoV does reduce, any improvement in variation is incidental because with the 'refined' testing, the discriminative ability of the tool is also reduced. Using the 'refined' testing, the difference between the osteoporotic and healthy control is reduced (9% to 15% compared to 24% to 32% in the circumferential method), the level of significance diminished and the ROC AUC reduced (0.60 to 0.73 compared to 0.79 to 0.89). The reduced discriminative ability between fracture and non-fractured tissue when taking more indents in the thicker, less porous inferomedial neck can therefore likely be attributed to the exclusion of factors that relate to fracture risk such as porosity [181, 185], cortical thickness [182] and heterogeneity of the bone [181, 182, 229].Therefore, the 'refined' method is likely to give a more repeatable measure that is more representative of the bone material properties, yet in doing so, is eliminating factors that relate to fracture risk and reducing the efficacy of the tool.

When considering the osteoarthritic group, the 'refined' method is similarly effective as the circumferential method for discriminating from the control and more effective when comparing to the osteoporotic group. This follows with the circumferential measurement including aspects of thickness, porosity and heterogeneity, factors that are likely to be influential in osteoporotic group [181, 182, 185] and, therefore, their exclusion have the greatest effect on this group. In terms of IDI and CID, if not TID, the difference between the circumferential and 'refined' measurements appears more apparent for the osteoporotic (20% and 21% reduction using the 'refined' method) than for the osteoarthritic (1% increase and 13% reduction) or control groups (8% and 9%) (Table 13).

Based on the effect of circumferential and 'refined' testing, and the knowledge that low thicknesses (Chapter 5 [229, 279]) and elastoplastic/fracture toughness properties [19, 24-26, 244] influence indentation depth, it is apparent that RPI is assessing both

structural and material properties. With this speculation in mind, it could therefore be hypothesised that the higher indentation with circumferential but not 'refined' testing seen in the osteoporotic relative to control group primarily relates to structural differences (i.e. thickness and porosity). Furthermore, the higher indentation depth in the osteoarthritic relative to control group that persists with both circumferential and 'refined' testing may well primarily relate to differences in material properties of the tissue, with the structure having a reduced effect.

6.4.5 Summary of study limitations and translation to clinical use

The primary limitations have been discussed above and relate to confounding factors between the groups. With a high proportion of fractures occurring in elderly women [291], this group is intrinsically older with a higher proportion of females. However, though these patient related factors (alongside height and BMI) relate to fracture risk [129, 137, 139, 192], they do not influence RPI or present confounding in our analysis. This additionally implies that RPI cannot detect these already measureable elements of fracture risk.

The intrinsic differences in testing (i.e. number of measurements and proximal-distal test location being limited by the quantity of bone in the osteoporotic group and limited control of the storage conditions for the cadaveric tissue) presents a confounding effect in the statistical analysis though with further analysis (6.3.2), the healthy-disease comparisons may still be considered valid.

Furthermore, there are comorbidities such as secondary osteoporosis and fracture risk factors that lead to overlap between the osteoporotic, osteoarthritic and control groups. This links to the difficulties associated with obtaining tissue that is representative of healthy (with no associated comorbidities) and diseased (purely osteoarthritic or osteoporotic with no risk factors for the other disease) states whilst being otherwise similar to the other two groups. This difficulty in obtaining tissue entirely free from confounding comorbidities whilst also aiming to be matched to the other two cohorts (primarily in terms of age and sex), lead to some compromise in selection, introducing confound effect and, particularly in terms of the control group, acted to limit the numbers.

A secondary limitation that has been discussed is the inherent variability associated with indenting bone (i.e. localised heterogeneity [181, 182, 185, 229]) as well as variability

within the experimental method and equipment (Chapter 5 [279]). Combined, these leads to a high coefficient of variation with repeat measurements relative to the differences observed. Some of the variability associated with the indentation here relates to the necessity to use the freehand mode of use due to the irregular samples and reluctance to machine the surface of the bone which would decrease the clinical equivalence. If the device could be fixed in its stand, the surface of the bone was instead machined and further repeat measurements were performed the coefficient of variation could be reduced (Chapter 5 [279]). Additionally, differences in indentation properties between the three groups relative to the inter-donor variation, limits the maximum sensitivity and specificity (and hence the ROC AUC values) of RPI.

Finally, interpretation of the RPI results is still difficult, with it being unclear what material properties are being assessed [19, 24-26, 244]. We suggest above that in addition to the assessment of material properties, structural features such as porosity and cortical thickness also affect the technique [181, 182, 229]. Following on from this, higher indentation depth in both osteoporotic and osteoarthritic bone would lead to confusion when assessing an individual patient. For example, by indenting a patient it could perhaps be established that the bone was diseased but, without further analysis (i.e. radiographic assessment, functional or hip pain score etc.), it may not be clear whether their bone was osteoporotic or osteoarthritic.

Translating this study to a clinical setting, clear differences between the in vivo and in vitro use of RPI must be considered. In this in vitro study, there is; limited soft tissue in place, a clinically inaccessible test site has been selected, the tissue has been extracted (and hence frozen, potentially dehydrated and body temperature not maintained) and the number of measurements did not have to be limited to maintain a minimally invasive technique. The effect of freezing has been discussed and rehydration of the samples was ensured, though, for the osteoarthritic and control groups their initial dehydration could not be controlled. Reducing the number of measurements would further increase the coefficient of variation so the repeat measurements used here may further damage the patient's bone (albeit with small approximately 100 μm indents that could be repeated in close proximity - Chapter 5 [279]). In Chapter 5 [279], we previously showed the presence of soft tissue influences the indentation depth and increases the coefficient of variation,

contrary to other studies with limited numbers [20, 29]. Perhaps most importantly, though testing close to the site of fracture discerns important differences in the material properties of the bone, the presence of soft tissue and the joint capsule makes this site infeasible for clinical testing. In vivo, the tool is applied to the anterior tibia [19, 21, 242] and it is not yet clear if indentation at the femoral neck is representative of these clinical measures. Though, differences between fractured and healthy bone are similar to those found in the tibia by Diez-Perez et al [19], the values for indentation depth (TID, IDI and CID) are substantially higher at the femoral neck. Furthermore, indentation depth has been found to vary with proximal-distal test location along the length of the femur [229], so it stands to reason there would be a further deviation when testing the femoral neck relative to the tibia. Therefore, though the tool discriminates healthy from diseased tissue, supplementing existing techniques, further work is necessary to establish if this can translate to clinically detectable differences between these groups.

6.5 Conclusion

From a scientific perspective, this chapter provides novel insights into the differences in the properties of bone with health and disease. In this study, it is established that the properties of the femoral neck are different not only in osteoporotic, but also in osteoarthritic bone as a function of radiographic severity. Furthermore, these differences are site dependent, being less prominent in the inferomedial region than when considering a larger proportion of the femoral neck. Additionally, in a similar vein to Chapter 5, variation with testing and patient related parameters (age, sex, height, BMI, test location, storage conditions and number of measurements) indicates how these influence RPI and where it is necessary to control these factors for improved repeatability.

From a clinical perspective, RPI assesses a property distinct from that currently measured by BMD or FRAX and can successfully supplement these techniques to form a complementary tool for improved fracture risk assessment. However, the high variability associated with repeat measurements and the difficulty interpreting these measurements calls for further development into the design and knowledge associated with the device. Regardless of the direct clinical potential, this study investigates the most relevant fracture site, the femoral neck, in substantially more detail than previously presented and, for the first time, demonstrates the differences in indentation properties with osteoarthritis.

7 Bone mechanics in health and disease: Investigation into the property assessed by Reference Point Microindentation

7.1 Introduction

Chapter 6 demonstrates that RPI has some potential for discriminating diseased osteoporotic and osteoarthritic bone from cadaveric controls but interpretation of these measurements is limited without further understanding of the property that is being assessed by the technique. Furthermore, though we have demonstrated higher indentation depth in osteoporotic and osteoarthritic bone (Chapter 6) it is still poorly understood how the material properties, especially fracture mechanics, of bone are altered by disease rather than ageing alone. Overlapping techniques, principally material property assessment of cortical bone through fracture mechanics and indentation, can be applied to answer these two research questions.

Diez-Perez et al [19] initially proposed that RPI assesses fracture mechanics properties by the indentation propagating microcracks within the bone. Based on this, a strong correlation with crack growth resistance, was found [19], however, Katsamenis et al [24] have since found significantly lower correlations between RPI and crack growth resistance parameters and Carriero et al [244] found no significant relationship when considering murine specimens. Furthermore, some correlation has also been found between the RPI technique and elastoplastic properties including yield strength and toughness [25, 26]. This correlation would be attributed to the local deformation of the bone in line with other more conventional microindentation techniques. Finally, in Chapters 5 and 6 we suggest structural features, thickness and porosity, affect RPI. Therefore there is current uncertainty as to what property is being assessed by the technique.

For this reason, it was decided to investigate the correlation between RPI and fracture toughness in a substantially larger number of human bone specimens (i.e. $n > 90$ compared to previous maximum $n = 20$ [24]) to further the understanding of the technique. Furthermore, imaging of indentation imprints aimed to assess the contribution of associated microdamage, indent volume and porosity and hence the relation to fracture, elastoplastic and structural properties of the bone respectively. Multiple imaging techniques were applied including staining with serial sectioning and fluorescence microscopy, micro computed-tomography and atomic force microscopy to allow for

visualisation of indents and porosity and associated diffuse damage and linear microcracks. For our research, this aimed to clarify what a higher indentation depth in the osteoporotic and osteoarthritic bone (Chapter 6) actually reveals about the properties of the bone tissue in these groups as well as improving interpretation of the RPI technique for the field in general.

The same techniques applied to further investigate RPI; fracture toughness experiments and indentation, also allow for improved understanding of the material properties of the bone. Though research into bone disease can enhance diagnosis and treatment of these conditions, the literature presents limited evidence of the effects of osteoporosis and osteoarthritis on the material properties of the bone. A handful of studies have directly compared bone disease against non-diseased control [19, 21, 28, 185, 224, 290] and there has also been much research into the reduced fracture resistance properties with age [114, 162, 163, 179, 259]. However, though fracture resistance properties have been implied to relate to fracture risk, and this also seems intuitive, a link has yet to be presented. For this reason, samples have been prepared from osteoporotic as well as osteoarthritic bone for comparison to 'healthy' cadaveric controls using the fracture toughness and RPI techniques.

The utilisation of multiple groups of samples (i.e. osteoporotic, osteoarthritic and control) also furthers the investigation of 'what property is being assessed by RPI?'. It is possible that the correlation between RPI and fracture toughness (or the crack extent, indent size and pore proximity assessed by imaging) may be dependent on the properties of the bone itself. For example, if the osteoporotic bone were to have a lower fracture resistance an indent may cause a higher degree of cracking, the RPI measured indentation depth may be more greatly governed by the fracture properties of the bone. Whereas, in another example, if osteoarthritic bone was less susceptible to localised cracking but was stiffer, the elastoplastic properties may have a greater influence on RPI depth. That is, the material property being assessed by the RPI technique may be affected by the properties of the bone being indented. An extreme example of this would be substantially different interpretation of a high indentation depth in a rubber sample (i.e. low stiffness) to that in glass (i.e. low fracture toughness). This material dependent relationship will be established by measuring RPI, fracture mechanics properties and imaging indents in different types of bone (i.e. osteoporotic, osteoarthritic and control).

The research in this chapter is yet to be published as a journal paper but it is based on an adaptation of the whitening front tracking technique which has previously been described:

- O.L. Katsamenis, T. Jenkins, F. Quinci, S. Michopoulou, I. Sinclair, P.J. Thurner (2013), *A Novel Videography Method for Generating Crack-Extension Resistance Curves in Small Bone Samples,* 2003, PLoS ONE, 8(2): e55641
- T. Jenkins, O.L. Katsamenis, N.C. Harvey, S. Michopoulou, I. Sinclair, P.J. Thurner, *Whitening Front Tracking: A High-Speed Videography Method for Assessing Fracture Toughness of Small Bone Samples*, Poster at Orthopaedic Research Society, January 2013
- O.L. Katsamenis, T. Jenkins, S. Michopoulou, I. Sinclair, P.J. Thurner, *A Novel Method for Generating Crack Extension Resistance Curves in Small Bone Samples using High-Speed Videography*, Podium at European Orthopaedic Research Society, September 2012

The whitening front tracking technique has also been utilised for the comparison with RPI and lamellar heterogeneity and is currently under review as a journal publication:

- O.L. Katsamenis, T. Jenkins, P.J. Thurner, *Toughness and Damage Susceptibility in Human Cortical Bone is Proportional to Mechanical Inhomogeneity at the Osteonal Level*, under review
- O.L. Katsamenis, T. Jenkins, S. Michopoulou, I. Sinclair, P.J. Thurner, *Multiscale Experimental Analysis of Human Bone Fracture Toughness: From the Osteonal up to the Tissue Leve*l, Podium at Orthopaedic Research Society, January 2013

7.2 Materials and Methods

7.2.1 Machining of Regular Human Bone Samples

For mechanical testing and imaging of the indents it was necessary to machine regular sections of cortical bone from the proximal femora. Osteoporotic and cadaveric control bone was machined for imaging and fracture toughness testing and further osteoarthritic samples were also machined for fracture toughness testing as demonstrated by Figure 67. These samples are a subset of those obtained from UHS and a tissue bank (Innoved Institute LLC, Besenville, Illinois) as described in Chapter 6.

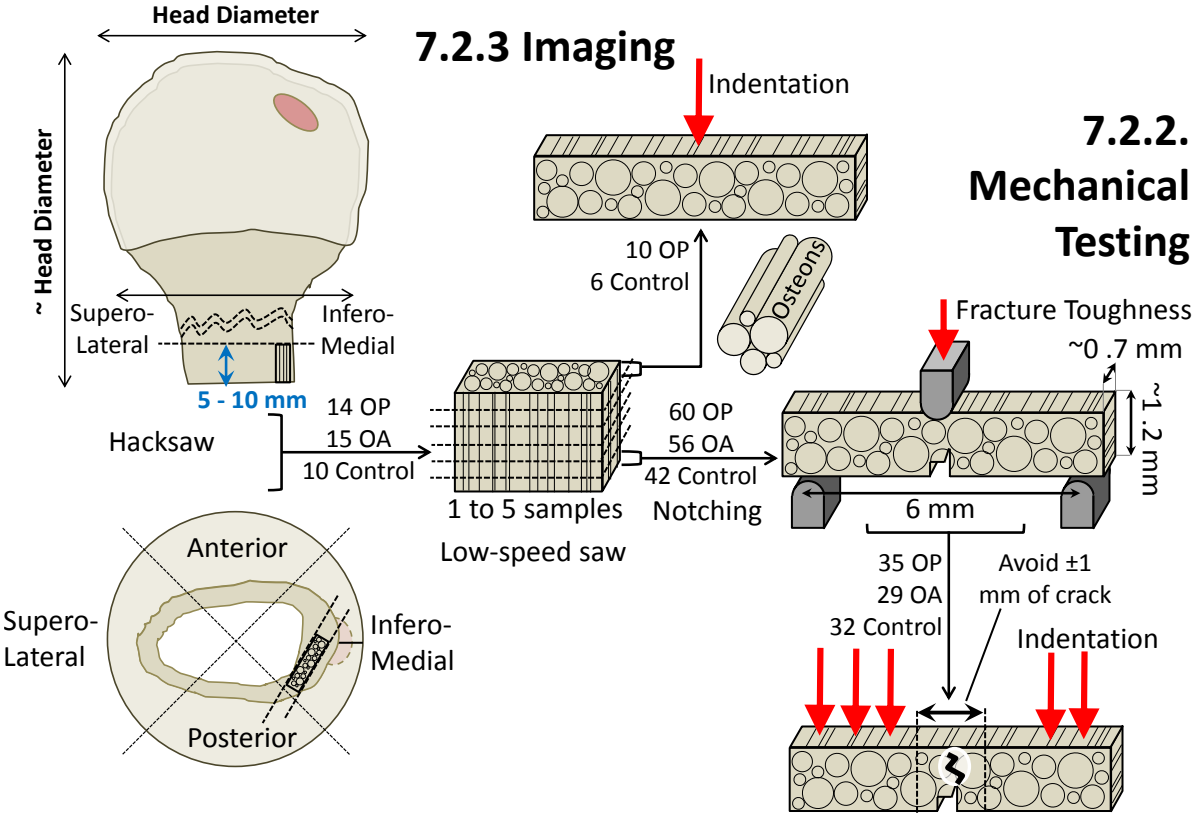

Figure 67 – Machining of regular cortical specimens from the human femoral neck of osteoporotic (OP), osteoarthritis (OA) and healthy control donors. These samples are subsequently imaged (as described in section 7.2.3) and mechanically tested with fracture toughness and indentation (section 7.2.2)

From the osteoarthritic group samples were taken from 15 donors by making a 5 mm to 10 mm proximal cut approximately parallel to the surgeon's cut. For 10 of the cadaveric control samples, a junior hack saw cut was first made at a proximal-distal distance equivalent to the femoral head diameter with a second cut being made a further 5 mm to 10 mm distally of this original cut. Therefore, for these two groups, an approximately disk shaped slice of femoral neck was prepared. For the osteoporotic group, however, the cortical bone sectioned by the patient's fracture and the surgeon's cut was taken from 14 donors.

The cortical neck segments were sectioned into quadrants using the junior hacksaw with the inferomedial quadrant being used to machine regular samples. This quadrant was selected due to its thickness [182, 229] allowing for thicker and longer samples to be machined whilst minimising inclusion of trabecular or transitional trabecular-cortical bone. This inferomedial quadrant was sectioned in half, taking the thickest and least curved side (eighth). At this point, the osteoporotic samples were cut transversely to remove the bone closest to the fracture and create an approximately parallel slice comparable to the other two groups.

Parallel longitudinal plates were then machined using a low-speed saw and diamond wafering blade (Buehler, Germany). Samples were secured with a small clamp before the periosteal surface was removed (sufficiently to remove the curvature of the bone ~ 1 mm to 2 mm) with a second cut being made to section an approximately 1 mm to 1.5 mm thick plate (sample width, *w*). The low-speed saw includes a water bath for constant irrigation. In cases where the thickness or angle of the cortex made clamping and machining impossible, 600 grit sandpaper was used instead of the low-speed saw. In a similar manner to the above machining, the periosteal surface was polished until the curvature of the bone was removed to produce a flat surface. For these samples, the majority of the trabecular bone usually broke away during previous sectioning. Any remaining trabeculae were then cut away using a scalpel followed by polishing of the endosteal surface, again with 600 grit sandpaper, until a smooth, non-porous, regular thickness cortical bone sample was machined. The thickness of these samples was measured periodically at different sites (the four corners and across the width and length of the plates) using callipers and polishing was adjusted to achieve a consistently (< 0.05 mm variation) thick sample, in the region of 1 mm to 1.5 mm (sample width, *w*). Water was applied to the samples periodically as a lubricant for the polishing and to maintain sample hydration.

Bone plates were again clamped in the low-speed saw with parallel cuts being made to produce approximately 0.7 mm to 1 mm thick samples (sample thickness, *t*). These samples were wrapped in gauze and HBSS and frozen at -80°C until use.

7.2.2 Fracture Toughness of Human cortical Bone

Fracture toughness experiments were undertaken on the three cohorts (osteoporotic, osteoarthritic and control) for two purposes: to investigate the differences in this material property with disease and to investigate the extent to which RPI is representative of fracture toughness. These experiments utilised an adapted version of the 'Whitening Front Tracking Method' developed by Katsamenis et al [256] as described below (7.2.2.4) and the methods chapter (4.2).

7.2.2.1 Sample Preparation

For the fracture toughness experiments, samples were machined as described above (7.2.1) to approximately 1.25 mm width (*w*) and 0.75 mm thickness (*t*) with the individual sample measurements recorded using Vernier callipers (RS Component Ltd, Corby, Northamptonshire). Whilst frozen, these samples were notched using the low-speed saw, approximately in the 'longitudinal antiplane' direction though the osteonal direction was not directly imaged. The sample was clamped close to a marked central point and rested on the saw for a set time (35 turns of the saw at a set speed), and load (with the support arm in balance just above the saw blade) aiming to produce a repeatable pre-notch. The pre-notch was sharpened using 1 µm diamond solution and a scalpel blade, polishing the rectangular saw notch until the scalpel blade moved freely. This technique has been reported by Kruzic et al [292] to produce a less than 5 µm diameter sharp notch. A digital microscope (S02 USB Digital Microscope, HOT Technology Co., Shenzhen, China) was used to capture the notch length (*a0*). A water-jet followed by ultrasonic cleaning for 3 minutes (USC1200D 12 L Ultrasonic Cleaner, VWR Symphony, Radnor, Pennsylvania) was used to clean any residual diamond solution from the notch. 158 samples were machined in this way from 39 donors from the osteoporotic (60 samples, 14 donors), osteoarthritic (56 samples, 15 donors) and control (42 samples, 10 donors) groups.

7.2.2.2 Mechanical Testing

Samples were defrosted in HBSS overnight (approximately 15 hours). Each sample was placed on a three-point bending rig with a 6 mm span, submerged in HBSS within a water-bath as depicted in Figure 68. The notch was placed downwards to be in tension during loading and to drive crack propagation in the longitudinal anti-plane or 'separating' direction [256]. In this orientation the crack is driven to propagate around the osteons

and was selected to maximise the observable whitening through selecting the most resistant orientation feasible (Section 4.2 [110, 256]).

The samples were placed in the Electroforce 3200 mechanical tester (Bose, Eden Prairie, Minnesota) with a preload being applied by the central plunger (0.02 N to 0.05 N). The samples were then loaded to failure (a reduction of greater than 50% after the peak load) at a quasi-static rate of 0.001 mm/s.

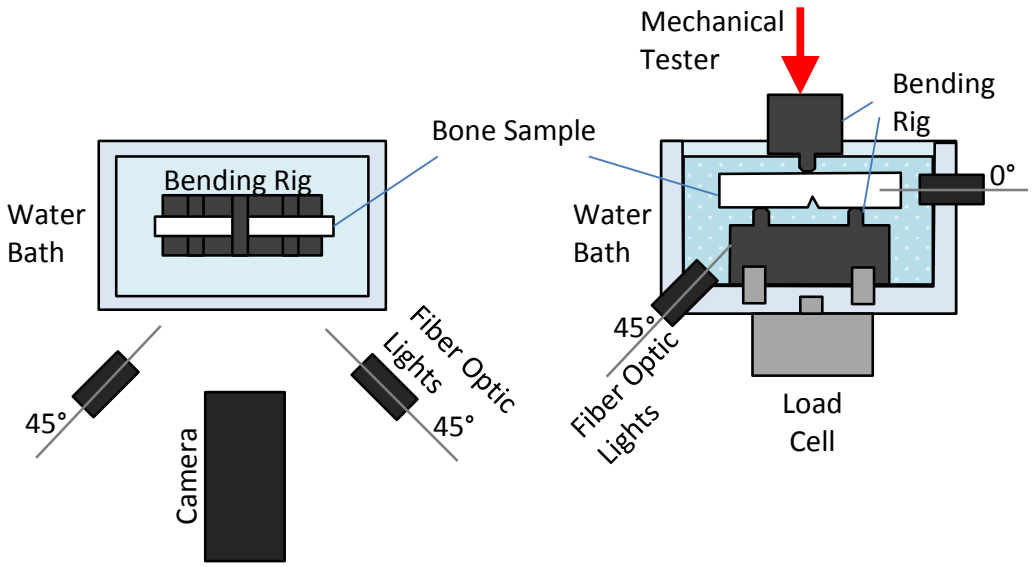

Figure 68 – Set-up of the mechanical testing rig for three point single-edge bending fracture toughness testing demonstrating the rig assembly and optic positioning

7.2.2.3 Videography

Two fibre-optic lights (KL 1500 LCD, Schott, Mainz, Germany and DC950H Fiber-Lite, Dolan Jenner, Boxborough, Massachusetts) were positioned at approximately ±45° as viewed from above and 0° and 45° as viewed in plane (shown in Figure 68). This positioning aimed to scatter light reflected from microcrack surfaces that form during crack propagation [121, 256, 257] and hence observe the whitening effect. The loading and whitening were captured using a single 2 MPixel camera from a 3 dimensional digital image correlation system (Q-400-3D, Limess, Krefeld, Germany) with a macro lens (28 - 105 mm Nikkor zoom lens, Nikon, Tokyo) at 1 frame per second. The low loading rate meant that any discrepancy between videography and loading initiation would be minimal. Additionally, by starting loading directly after commencing the videography, any discrepancy would also be visualised and the load-videography synchronisation could be

offset by the number of frames where the plunger appeared static - this discrepancy was not observed.

7.2.2.4 Crack Extension Resistance Curve Generation using Whitening Front Tracking

Further to the previously discussed 'Whitening Front Tracking' technique (4.2)[256], modifications were made to the algorithm for increased automation (code in 9.5 Appendix 4 – Matlab Algorithms). This was necessitated by the increased number of samples being processed here compared to those by Katsamenis et al [256] (158 compared to 20 samples). The algorithm was adapted as depicted in Figure 69 (with the following number relating to the figure labels):

1. As with the published algorithm (discussed in 4.2 [256]), the videography and force-displacement-time data was first loaded and the sample dimensions entered.
2. A linear fit was applied between 10% and 60% of the maximum load (a good initial approximation of the linear portion from multiple force-displacement curves) and where there was a greater than 10% error from this fitted slope, the end of the linear region was defined.
3. The selection of the span (the known width of bending rig posts used for calibration) was used to define the region of interest. This was 1 mm wide with a height equivalent to the known sample width (w) and centred between the two posts.
4. All samples were cropped to this region of interest and a gamma correction was applied to improve the whitening visualisation (unchanged from original algorithm).
5. An option to translate the region of interest by the constant (0.001 mm/s) displacement rate was included for initial frame registration secondary to the sub-pixel cross-correlation algorithm described by Katsamenis et al [256].
6. The registered initial frame was subtracted from each subsequent frame to produce a difference image which was binarised with a threshold value (unchanged).
7. This binary image was morphologically opened to disconnect background whitening and remove specks. A smaller disk size (6 compared to 9 pixel octagon) was used to increase whitening connectivity and to remove fewer binary elements.
8. The main increase in automation from the previous algorithm related to the selection of the whitening area. Starting at the final frame (i.e. maximum load where the whitening was best visualised), the largest binary area was selected and

its centroid calculated. Looping backwards through the remaining frames, the whitening area with a centroid in close proximity (10% of the region of interest, i.e. within approximately 100 μm) to the previous whitening centroid was selected. If there was no whitening area in close proximity and of a large enough area (50 pixels area) no whitening was recorded.

9. The point of the pre-notch was manually selected based on two guidelines: one based on the microscopy measured notch size and one based on the uppermost point of a binarised notch from the videography. The manual selection was made between these two guidelines, typically towards the microscopy identified point where the notch was typically clearer.
10. The most extreme points of the whitening area were found and the vertical distance between the furthest of these points and the pre-notch denoted the crack extension (Δa) (unchanged).
11. The whitening area and crack extension were plotted against actuator displacement and the minimum (when the whitening area begins to expand) and maximum (the maximum load) were automatically selected as the limits.
12. The J-integral and $K_{effective}$ were calculated as a function of crack extension, geometry and loading to generate crack extension resistance curves (r-curves) for each sample (unchanged).

The results of the automatic selection were reviewed for each step by the user, and, where this was unsuccessful, a manual selection could alternatively be made (steps 2, 3, 5, 9 and 11). The various threshold were selected based on the existing algorithm [256] and adaptations based on the ease of visualisation and accurate selection in multiple datasets.

The adaptations to the whitening algorithm, specifically; automatic whitening selection (8), automatic linear region selection (2) and whitening opening (7), were compared to the published algorithm with 10 samples being run using the manual method by Dr Orestis Katsamenis.

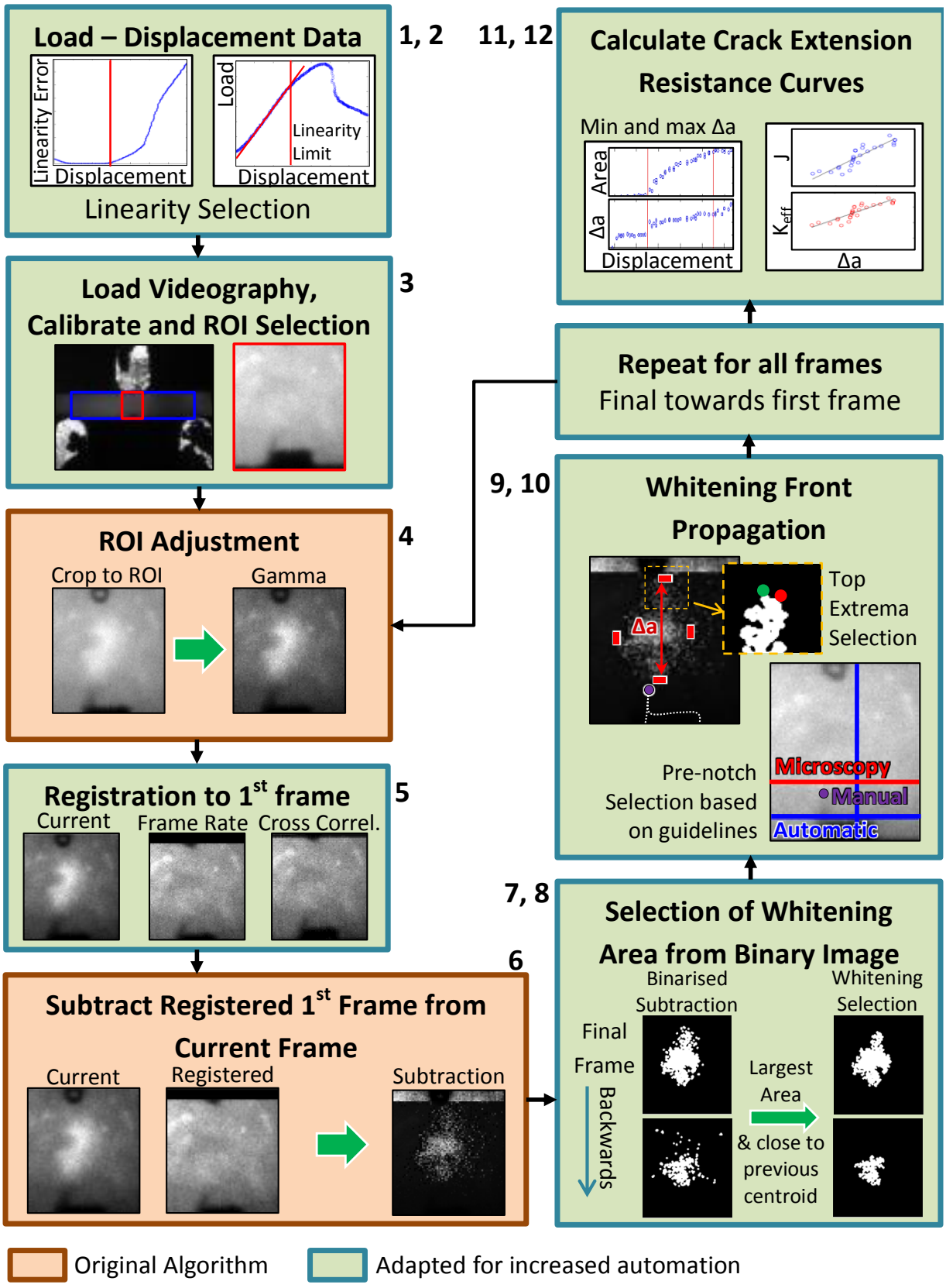

Figure 69 – Summary of the Whitening front tracking method algorithm, stylised for comparison between this adapted algorithm and the original algorithm developed by Katsamenis et al [256]

7.2.2.5 Indentation of fracture toughness specimens

Unmachined human femoral neck samples were indented in the inferomedial 'refined' region and circumferentially around the femoral neck as described in Chapter 6. This allowed for correlation between fracture toughness measures and surface indentation measures on a donor-by-donor basis. Following fracture toughness testing, the individual samples were also indented. Five indents were made in the endosteal (inwards) transverse direction on the machined samples. Longitudinal measurements were not made in this study due to the reduced clinical relevance of the direction and the utilisation of transverse measurements previously applied to the surface of the bone (Chapter 6). Furthermore, though longitudinal indentation may uncover alternate relationships with fracture toughness (orientation utilised by Katsamenis et al [256]) the lack of anisotropy found in human bone (Chapter 5), implies that the relationship would be similar in the two orientations. These indents were made at least 1 mm from the central notch to minimise impact of the previous fracture and associated microdamage on the subsequent reference point indentation as depicted in Figure 67. Indentation was performed at a 10 N maximum load, at 2 Hz and with 10 cycles. This individual sample indentation allowed for correlation between fracture toughness measures and RPI of machined samples on a and sample-by-sample as well as donor-by-donor basis

7.2.3 Imaging of Indents

To gain further understanding of the property being assessed through RPI, the indent imprints and their surrounding microdamage were imaged. The imaging of these samples intended to assess the contribution of the indent volume (elastoplastic properties), surrounding microcracks (fracture mechanics properties) and proximity to pores (structural properties) to the measurements made by the device (TID, IDI and CID). The principal imaging modalities used were serial sectioning and micro-computed tomography. The proportion of osteoporotic and control samples used in each technique is described by Figure 70.

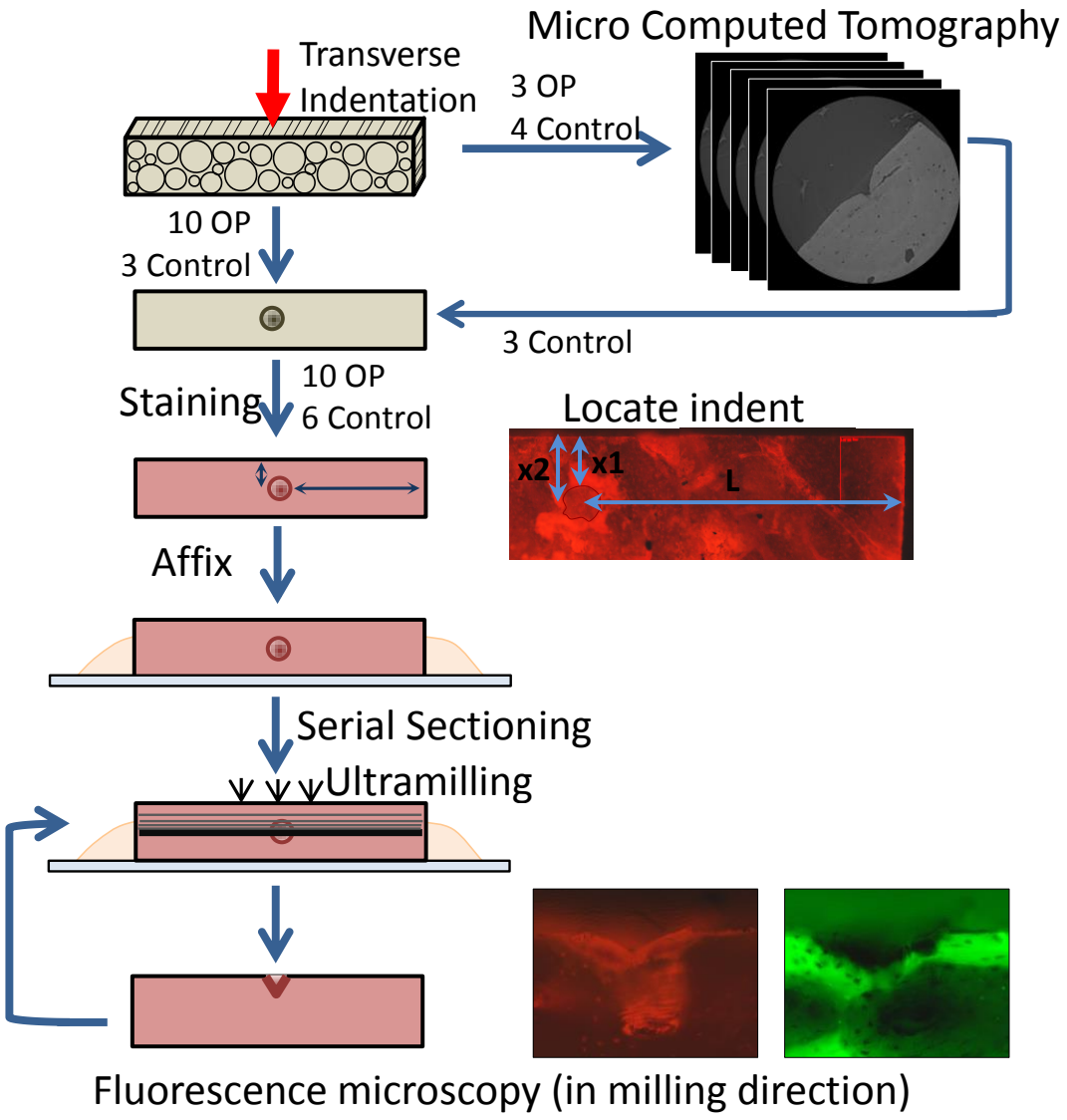

Figure 70 – Imaging of indent imprints using computed tomography and serial sectioning with fluorescence microscopy. Flowchart indicating numbers of osteoporotic and control samples used for each imaging technique

7.2.3.1 Indentation of Human Bone Samples

From the osteoporotic group, 10 samples from 8 donors, and from the control group, 6 samples from 6 donors, were machined to a 0.7 mm to 1.1 mm thickness and 1.0 mm to 1.3 mm width using the technique described above (7.2.1). These samples were fully defrosted overnight (over 15 hours) in HBSS prior to indentation in the transverse direction approximately 1 mm from the end of the sample. The Biodent RPI system was applied to the samples at 10 N, 2 Hz and 10 cycles to produce a single indent.

7.2.3.2 Micro Computed Tomography

Three osteoporotic and four control indented cortical bone samples were imaged using micro computed tomography (µCT) (detailed in section 4.6) which has previously been

described for imaging indents and their surrounding microcracking in a conference abstract by Schneider et al [270]. The μCT system (Zeiss Xradia Versa 510, Carl Zeiss X-ray Microscopy Inc, Pleasanton, California) at the μ-VIS computed tomography suite, UoS, operated by Dr Orestis Katsamenis was used to image the indents. Low resolution (9.5 μm - 11.6 μm) fast scans (0.4 times objective, 0.4 s exposure and 550 projections giving approximately 16 min scans) first identified the location of the indent. The objective was increased (4 times objective) and the detector brought closer to the sample to reduce the field of view and give an increased resolution (0.826 μm with 2 x binning). The seven samples were scanned at a voltage of 110 kV, a current of 91 μA and a power of 10 W with 2201 projections and 13 s exposure (approximately 9 hours per scan). A 150 μm SiO_2 filter was used to minimise beam-hardening effects.

These datasets were reconstructed, again by Dr Orestis Katsamenis, using the XMreconstructor software (Xradia, Carl Zeiss X-ray Microscopy Inc, Pleasanton, California) to select the centre of rotation and adjust for beam hardening effects, converting the series of radiographs into a 16-bit image stack. From this stack, the indent, Haversian canals and microcracks were segmented as indicated in Figure 71 (with the numbering indicating the steps in Figure 71).

1. The image stack was first re-aligned using Fiji (open source software) by correcting the x-y orientation (rotation of the image stack) and x-z or y-z orientation (shifting the image stack).

The following segmentation used Avizo Fire software (version 8.0, FEI, Hillsboro, Oregon):

2. The dataset was cropped to the region of interest (approximately 500 x 500 x 150 voxels) based on the surface of the bone and indent location.
3. A threshold value (the lowest 60% of the intensity range) was then applied to segment the air (indent, microcracks, Haversian canals and lacunae, identified as blue or 1 in Figure 71) from the bone (identified as black or 0). This value (slightly above the local minimum) was selected by interactively adjusting the threshold in multiple image stacks until the microcracks were visually segmented.
4. a) The small unconnected elements (less than 5000 voxels in volume which was selected as intermediate between the lacunae and microcrack volume in multiple

image stacks) were removed from the thresholded image (3) to remove small particles, principally the lacunae.

4. b) Morphological opening (a three dimensional 6 voxel radius ball used to erode and then dilate the pores, cracks and indents) was applied to the thresholded image (3). The size of the erosion was increased in multiple image stacks until all small particles and thin sections (i.e. the lacunae and microcracking) were removed to leave only the large connected components, the indent and the canals. Dilation (the second part of the opening procedure) ensured the volume of the indent and canals were mostly maintained.
5. The indent and canals were discriminated from each other in this opened image (4.b) through manual selection
6. A dilated (5 voxel radius) version of the morphologically opened image (4.a) was subtracted from the greater than 5000 voxel elements (4.b) to remove the indent and canals (the dilation also removes any voxels in very close proximity to the indent and canals). This primarily left only the microcracking.
7. Some of the microcracking was close to the resolution of the scan, being only a few voxels in size and therefore these small microcracks needed to be selected manually using the Avizo blowout and paintbrush tools. The network of microcracks was also manually segmented into individual microcracks (e.g. red, green and blue Figure 71-7)
8. Once the microcracks had been selected they were morphologically closed (1 voxel radius ball, dilation followed by erosion shown in Figure 71-8) to reconnect any small elements. The microcracks were then eroded (1 voxel ball) to remove any specks that had remained unconnected after the closing step and to thin the microcracks (with the manual selection potentially overestimating their size).
9. The microcracks (8) were added to the indent and canal image (5) for visualisation (microcracks in red, canals in green and the indent in blue, Figure 71-9).

Measurements were made on the crack length, crack volume, indent volume and porosity using the built-in label measuring in Avizo. Further measurements of the indent diameter, proximity to the closest pore, and central slice indent area/depth were made using a custom made Matlab algorithm (Mathworks, Natick, Massachusetts) applied to the segmented image stack.

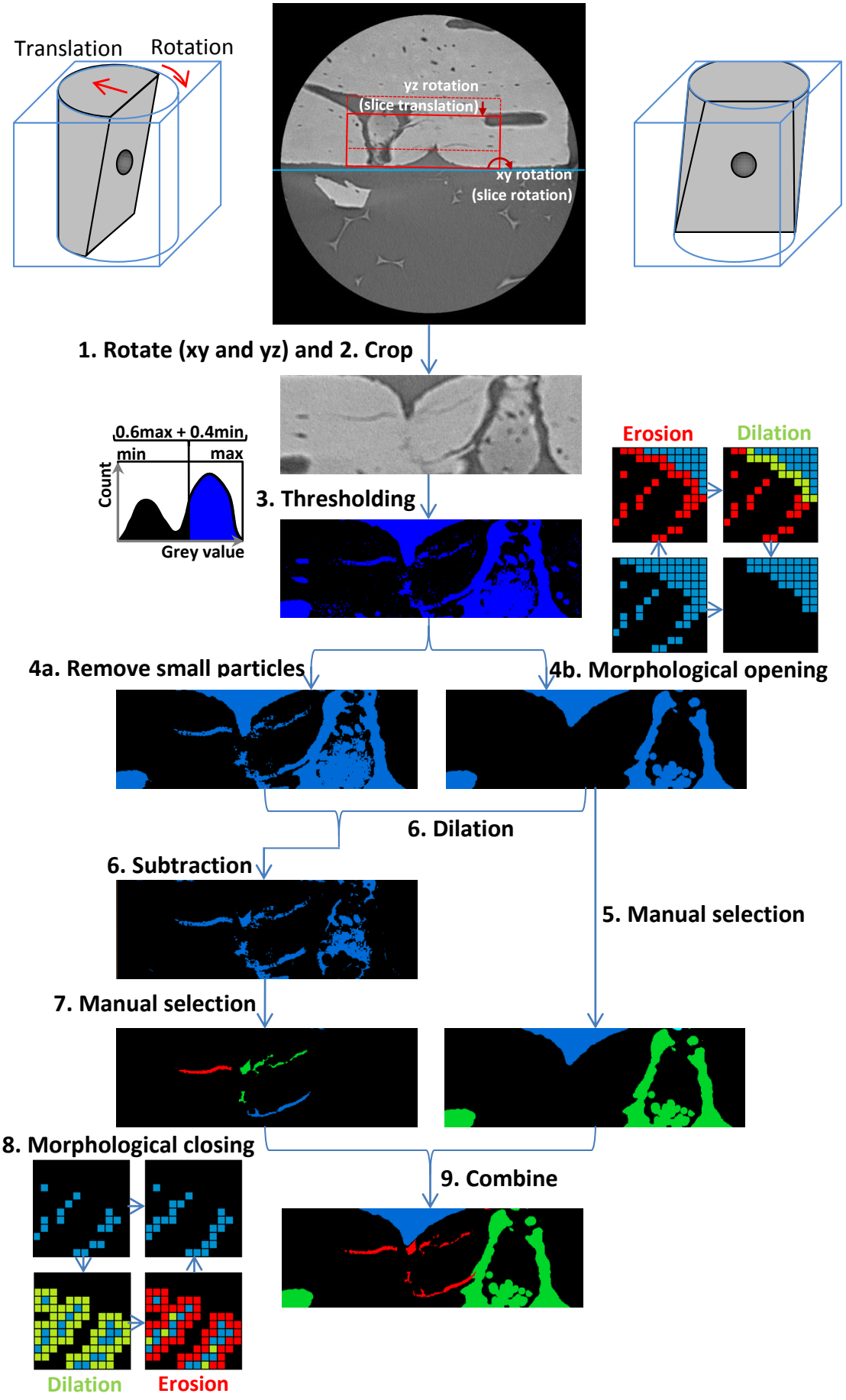

Figure 71 – Segmentation of the indent, adjacent microdamage and Haversian canals, blue, red and green respectively in the final image. Apart from the top image (using Fiji), all segmentation was performed using Avizo Fire.

7.2.3.3 Staining, Serial Sectioning and Fluorescence Imaging

Following µCT, three of the cadaveric control samples, and a further 10 osteoporotic and three control samples that had also been machined and indented were stained with basic fuchsin (shown in Figure 70). For staining, these samples were first dehydrated in 80% ethanol overnight (approximately 15 hours) followed by submersion in basic fuchsin stain (1% basic fuchsin, 80% ethanol) for 3 hours. Samples were then rinsed in 80% ethanol for 5 minutes. This technique has previously been described by Lee et al [251], Burr and Hooser [267] and in the methods chapter (4.5) for the imaging of microdamage. A protocol has been developed by Dr Louise Coutts and Benjamin Carter in our laboratory, being applied to visualising whitening area and the surface of the indent.

At the Institute of Lightweight Design and Structural Biomechanics, Vienna University of Technology (ILSB, TUWien) with the aid of Dr Orestis Andriotis, these indents were imaged using fluorescence microscopy and serial sectioning. First, the indented surface of the samples were imaged using fluorescence microscopy (Zeiss Axio Imager.Z1m, Carl Zeiss Microscopy Inc, Oberkochen, Germany) to identify the location of the indent on the surface by measuring the distance of the indent from the end (*L*) and edge (*x*) of the sample (Figure 70). The samples were then mounted on a glass slide using epoxy resin so that the indented face was perpendicular to the slide and would be sectioned through ultramilling. The samples were loaded into the ultramiller (SM250, Leica Microsystems, Solms, Germany) with a feed rate of 4 mm/s and a cutting speed of 1000 rpm. The samples were fed into the rotating blade to remove 10 µm of material per cut until the surface of the bone began to be removed (initial cuts only removed epoxy). The surface of the bone was again imaged using the fluorescence microscope, centring at the predefined distance (*L*) from the end of the sample. The stage of the microscope was locked in place in terms of *x*, *y* and rotation. The samples were returned to the ultramiller to remove a set depth (the previously measured x, Figure 70) from the sample at 10 µm slices.

The initial damage of the indent was then imaged on the microscope at red (Rhodamine, emission wavelength 575 nm - 640 nm) and green (FITC, emission wavelength of 515 nm - 565 nm, collagen auto-fluorescence) wavelengths using the 10 times objective with 10 µm slices being made through the indent between further successive images (described in 4.5). When the shape of the indent was clearly visible and it appeared to be close to its central point, 5 µm slices were taken between imaging steps to ensure the

deepest point, the centre of the indent, was captured. At this central point, a 20 times objective was used with median averaging over 20 images to give a sharper, higher resolution image. Once this central point was past, the ultramilling reverted to 10 µm steps until the indent, and then associated microdamage, were no longer visible.

The serial sectioning image stacks were semi-automatically segmented using a custom Matlab algorithm (9.5 Appendix 4 – Matlab Algorithms) as described in Figure 72 (the following numbering relates to the labelling of the figure).

The indent was segmented as follows:

1. For the central slice of the image stack, the red and green images were loaded and combined into a single RGB image (the blue channel is populated by 0s).
2. The bottom left, bottom right and uppermost (the point of the indents) points were manually selected to define the region of interest (described by the rectangle 150 pixels outside these three points).
3. The green channel was subtracted from the red channel to create a 16 bit image. Because the stain appeared bright in the red channel but dark in the green channel and the indent appeared dark in both channels, this subtraction allowed for clearer visualisation of the stain and indent.
4. The combined image was cropped to the region of interest.
5. The user manually drew around the indent to give the 'initial' outline.
6. The initial outline was split into three overlapping outlines: the left and right (splitting the initial outline either side of its point i.e. the uppermost row) and the upper (a variable range around the uppermost point). The range of the upper section (i.e. the columns from uppermost point – range to uppermost point + range) was approximately between the 7% and 40% of the indent width dependent on the indent shape. A function was established to accommodate for the aspect ratio of the indent (width/depth) in each slice (range = (1/12)x(width/depth)$^{0.75}$). This function meant the upper section outline included the tip of the indent whether it was a sharp point or a shallower curve and was established through multiple image stacks.
7. The algorithm searched the combined image (3) near the outlines (6) for the largest steps in intensity. For the left and right outlines this involved looping

through the rows and plotting the image intensity ±20 columns either side of the initial outline. The largest step is where the intensity is first above an intensity threshold (0.7 min + 0.3 max). For the upper outline, the columns were looped through and the largest step within ±20 rows of the outline was selected in the same way. These thresholds (±20 pixels and the intensity threshold) were selected by their ability to successfully identify the indent outline in multiple image stacks.

8. Selecting the largest step in intensity gave three 'refined' outlines for the left, right and upper outlines. These outlines were smoothed with a 20-point moving average to remove sudden jumps and give outlines that more closely followed the indent as observed in multiple image stacks.
9. The three outlines overlapped and intersected or came close to intersection in all cases. The three outlines were combined to a single 'refined' outline using a weighted average where they overlapped e.g. at 70% between the left overlap and the uppermost point of the initial outline, the refined outline would be 30% left outline and 70% upper outline etc.
10. The subsequent (i.e. central slice plus 1) RGB image (1) was loaded and registered against the previous image (i.e. central slice) using a built-in Matlab function. The combined image (3) was cropped to the region of interest using the previously defined points (4). The refined outline from the previous slice (i.e. central slice) was then used as the initial outline to repeat the outline selection (6, 7, 8 and 9).
11. This process (1, 3, 4, 6, 7, 8 and 9) was repeated, moving forwards (i.e. increasing slice number/depth) through the rest of the stack with each selection being reviewed by the user. If the automatic selection visually began to move away from the indent, another manual initial selection was made (5) to guide the automatic selection. This continued until the enclosed area was considered small (fewer than 1000 pixels in area or 6 pixels in height) and, hence, the indent was no longer visible i.e. the far edge of the indent.
12. The other half of the indent was then segmented. The refined outline from the central slice was used as the initial outline on the previous slice (i.e. central slice minus 1). The steps (1, 3, 4, 6, 7, 8, 9 and 10) were then repeated, moving backwards (i.e. decreasing slice number/depth) through the slices until the indent was again no longer detectable i.e. the near edge of the indent.

Following the segmentation of the indent, the indent associated damage was segmented:

1. An initial threshold was defined as the mean (over the whole image stack) upper quartile of the pixel intensities per image.
2. A baseline threshold was then calculated per image by taking a mean value of all the pixel intensities between 25% and 75% of this initial threshold. This accommodated for the large number of pixels with a close to zero intensity as well as adjusting for variation in the baseline intensity of different images.
3. Each image was binarised using its specific threshold.
4. This binary area was dilated by 1 pixel to reconnect the small specks into large interconnected areas.
5. The binary area was morphologically opened (5 pixel erosion followed by dilation) to remove smaller areas that were not connected following the dilation step (4).
6. Interconnected binary areas that overlapped the segmented indent were selected as 'indent associated damage' and the indent was also subtracted from this area.

The background thresholds and dilation/erosion sizes were established for the visually most effective segmentation of multiple image stacks. An attempt was made to segment the pore associated stain in close proximity to the indent to that directly associated with the indent. However, due to the overlap between these two sources of stain, this differentiation was not consistently possible so has not been applied to the analysis.

The closest pore was segmented as follows:

1. The first and final slices in the stack were displayed and the centres of the pore closest to the indent were manually selected. Due to the orientation of the indent and the serial sectioning being approximately transverse to the long axis of the osteons, the same Haversian canal could be visualised throughout the image stack.
2. Linear extrapolation approximated the pore location of each intermediary slice.
3. A mean of the intensities within ±25 pixels of the approximate pore location gave a threshold to binarise each slice in the stack.
4. The largest binary area close to the approximate pore location (within 200 pixels) was selected as the nearest pore.
5. This selection was reviewed by the user for each slice and, where incorrectly selected, the closest edge of the pore was selected manually.

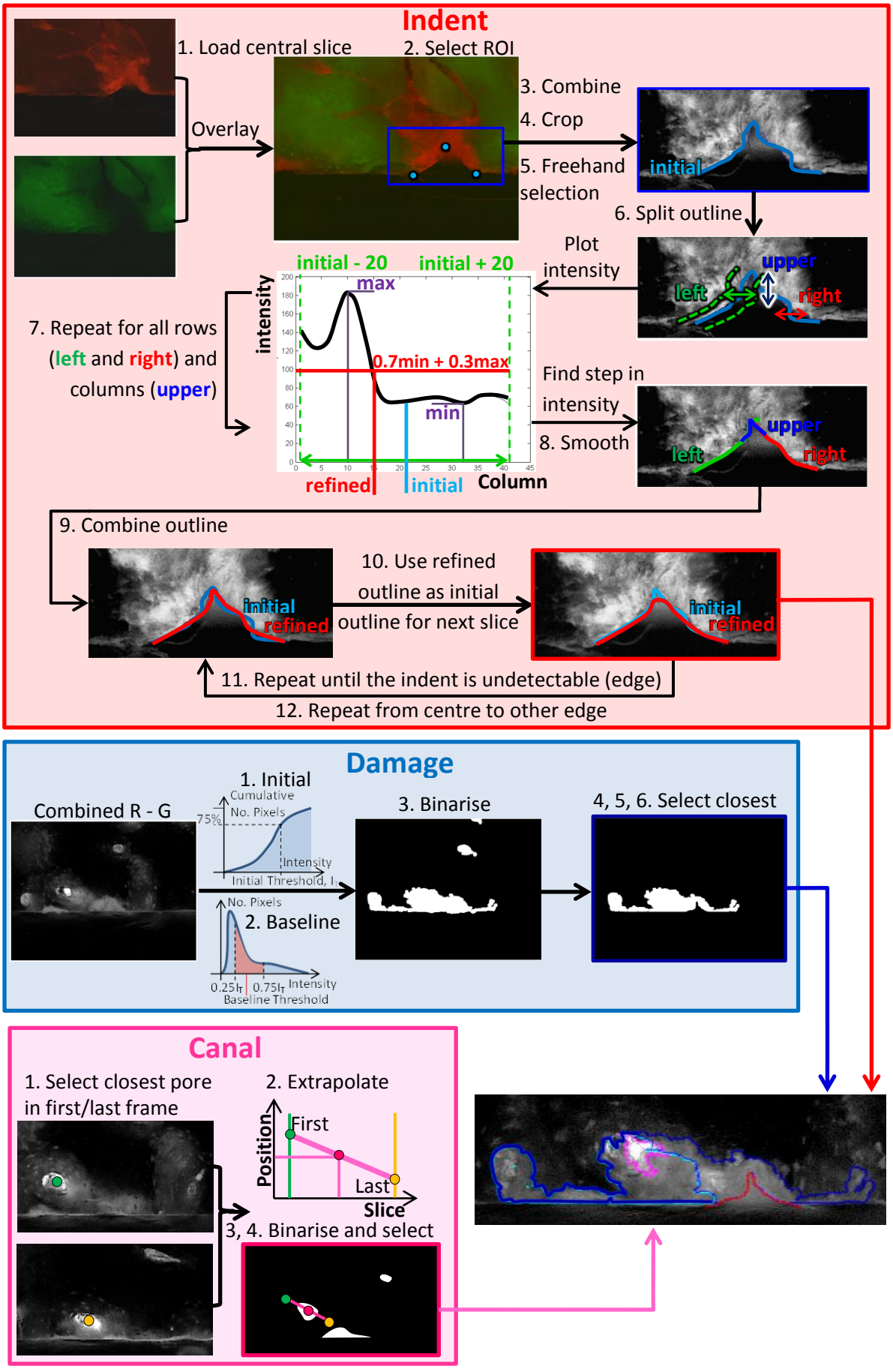

Figure 72 – The custom Matlab segmentation algorithm for the fluorescence microscopy and serial sectioning image stack with the indent segmentation highlighted in red, the damage in blue and the canal in pink

7.2.3.4 Atomic Force Microscopy and Polarised Light Microscopy

For one osteoporotic sample, at the central point (selected through ultramilling and fluorescence microscopy), the indent and associated microcracks were imaged using atomic force microscopy (AFM – described in 4.7) by Dr Orestis Andriotis at ILSB, TUWien. This was performed in air using the NanoWizard ULTRA Speed A system (JPK instruments, Berlin) in contact mode with a 0.32 N/m nominal spring constant, V-shaped AFM cantilever (PNP-DB NanoWorld AG, Neuchâtel, Switzerland). Image size was 10 µm by 10 µm with a 512 pixel x 512 pixel resolution (hence a 19.5 nm pixel resolution) with a scanning frequency of 0.8 Hz and multiple images forming an approximately 50 µm by 50 µm image area. Further to this, an image was also taken of this surface with polarized light microscopy (with a 20x and 50x objective) and the microscope described for fluorescence microscopy (Zeiss Axio Imager.Z1m).

7.2.4 Statistical Analysis

The relatively small number of fracture toughness samples per donor (1 to 6), led to the use of the arithmetic mean to incorporate measurements from all samples. Similarly, the mean was used to combine the 5 repeat RPI measures on fracture toughness samples.

When comparing the fracture toughness between groups, the normality of each group was assessed through plotting the histogram. This generally leads to a non-normal distribution, perhaps due to the relatively small number of donors (i.e. $n < 14$), a small number of potential outlying samples skewing otherwise normally distributed data (e.g. Figure 76a) or due to a skewed distribution towards higher fracture toughness measurements (e.g. Figure 75). For normally distribute parameters, the mean and standard deviation were displayed and t-tests were performed (only 'refined' CID). For skewed variables, the median and upper and lower quartiles were displayed and Mann-Whitney U-tests were performed. The level of significance of $p < 0.05$ was shown but, due to the limited significant comparisons within this section, p values less than 0.1 are also displayed to add some descriptive value even where correlations or differences are not significant. The Spearman's rank correlation coefficient is used to investigate the relationship between fracture toughness and RPI and, similarly, for the correlation between RPI measures and indent imaging parameters. Considering the indent imaging, the correlation between RPI measures and indent imaging measures is discussed for each modality (i.e. µCT and serial section). However, due to the low number of samples (a

maximum of 10 osteoporotic and 6 control samples), the different modalities are also combined for statistical analysis, also using Spearman's correlation.

7.3 Results

7.3.1 Fracture Toughness of Human Bone

7.3.1.1 Validation against published technique

Full crack extension resistance curves (R-curves) could successfully be generated in 158 samples. Further samples were also machined (19 osteoporotic, 17 osteoarthritic and 6 control) but were fractured during notching and handling or the whitening was not sufficiently clear. Of these, a further 29 samples were excluded because there were too few data points ($n < 10$), or there was a very low correlation between crack extension and crack extension resistance (i.e. not a clearly rising R-curve, $r < 0.3$ or $p > 0.05$). Therefore, in these remaining 129 samples, the whitening could clearly be visualised and rising r-curves were generated.

A proportion of these curves displayed lower correlations (i.e. 14 of 129 curves with r-values less than 0.6 and a further 7 with r-values less than 0.7) and some outliers as indicated by the example in Figure 73b. It was unclear whether these data points were outliers or representative of the whitening propagation so the videography was reviewed and this technique compared to the published 'whitening front tracking method' [256].

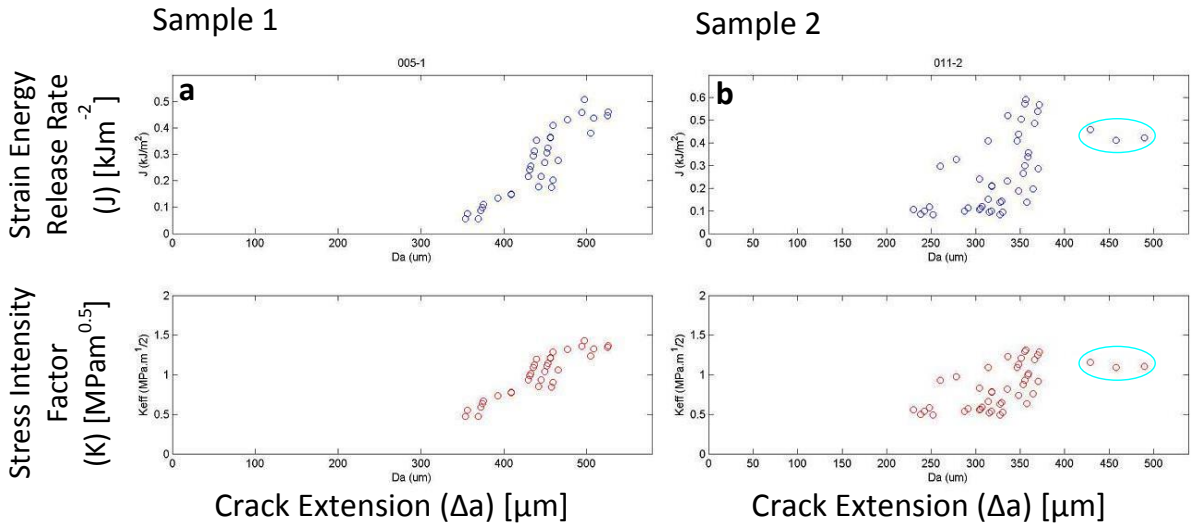

Figure 73 – Crack extension resistance curves (R-curves) for two samples a) an ideal curve with good correlation between crack extension and crack extension resistance (K and J) and b) a curve with examples of outliers (highlighted in light blue)

Ten samples were evaluated with the adapted whitening front tracking algorithm used here and using the aspects of the original algorithm that were believed to effect the

selection of the whitening area. Firstly, manual selection of the linear portion of the force-displacement curve (rather than automatic selection in the adapted algorithm) alongside an larger disk-size for morphologically opening the binary whitening area was compared to the adapted algorithm. Figure 74a and Table 23 (row 1) show that these two aspects; the disk size used for morphological opening of the binary area (i.e. how interconnected the individual areas were) and linearity selection, had minimal effect and the correlation was extremely high between the two algorithms.

Secondly, Dr Orestis Katsamenis (who developed and published the original algorithm [256]), compared the manual selection of the whitening area from the binary image in-line with the published algorithm [256] to the automatic selection used here. Figure 74b and Table 23 (row 2) show the whitening selection aspect of the adapted algorithm to be representative of the original algorithm. There is a marginal discrepancy between the two techniques in terms of the whitening front selection which leads to slight differences in the slope of the R-curve (the crack growth resistance, $r = 0.79$ to 0.82, $p < 0.05$) but the two techniques appear to produce identical fracture toughness values ($r = 0.99$, $p < 0.05$).

Furthermore, Dr Orestis Katsamenis and myself visually examined the videography and compared the automatic whitening selection to the raw images, concluding that the algorithm correctly identifies the whitening front. Therefore, we can be confident that the ‘outliers’ shown in Figure 73b are still representative and that all the r-curves and fracture toughness values generated here are representative of the material properties of the sample in accordance with the previously published technique [256].

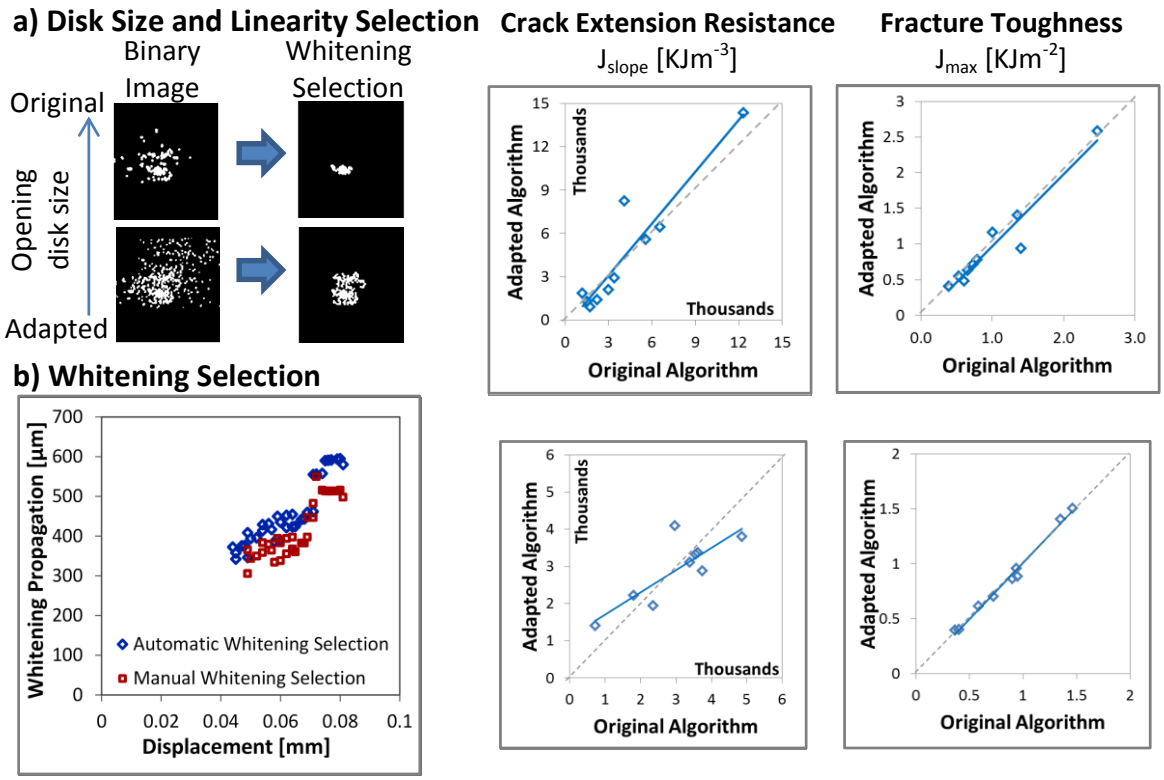

Figure 74 – Comparison between the r-curve generation algorithm used here (adapted algorithm) and the published whitening front tracking method (original algorithm) [256]. The techniques were compared in terms of: a) the disk size used in dilating the binary whitening area and the selection of the linear portion of the force-displacement curve and b) automatic compared to manual selection of the whitening front

Table 23 – Statistical summary of Figure 74 displaying the correlation coefficient (r-value) and the level of significance (highlighted in grey for p < 0.05)

	Kslope	Kmax	Jslope	Jmax	E
Disk Size and Linearity Selection	0.92	0.97	0.94	0.96	0.93
Whitening Area Selection	0.79	0.99	0.82	0.99	NA

7.3.1.2 Differences in material properties of the bone with disease

7.3.1.2.1 Individual measurements per sample

The inferomedial machined fracture toughness samples are compared across the three groups (osteoporotic, osteoarthritic and control) to compare the crack extension resistance measures and indentation on machined specimens in 'health' and disease states. A further 5 specimens were excluded from this analysis because they appeared as outliers (Figure 76) and were samples that belonged to an atypically young osteoarthritic donor (26 years) or were otherwise anomalous (e.g. unclear whitening or visible porosity).

Of the remaining samples, the difference between the three groups is extremely minimal in terms of fracture toughness and indentation measurements as shown in Figure 75 and Table 24. There is a large degree of overlap between the groups and the difference

between the groups is less than 20% in the majority of cases. The most pronounced difference between the group medians is strain energy release rate fracture toughness (J max - Figure 75b), where the control (0.698 kJm^{-2}, 22%) and osteoarthritic (0.693 kJm^{-2}, 21%) groups appears tougher than the osteoporotic group (0.574 kJm^{-2}) but this is not significant (p = 0.34). Therefore, all three groups appear identical in terms of fracture resistance.

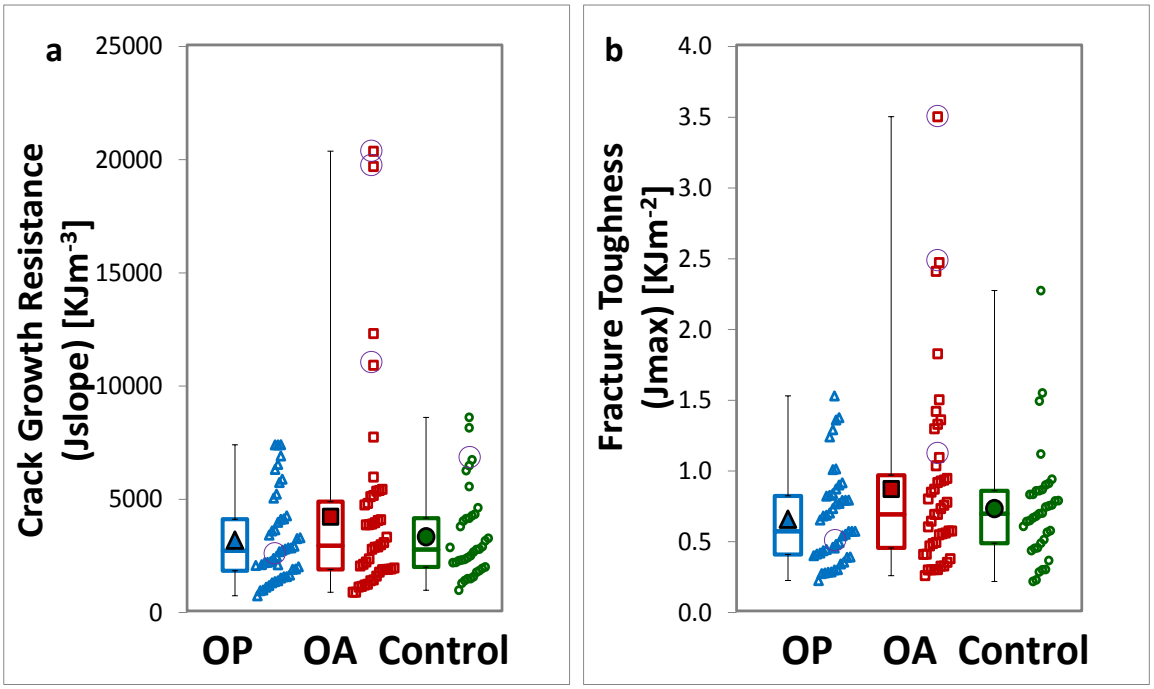

Figure 75 - Example figures comparing crack extension resistance measures for individual samples across the three groups (osteoporotic, osteoarthritic and control) in terms of a) Crack growth resistance (J slope), b) fracture toughness (J max). The excluded samples are indicated by a purple circle.

In terms of approximated elastic modulus (derived from the notched specimens [256] - Figure 76a), the osteoporotic group is significantly stiffer than the control (8.92 GPa compared to 7.52 GPa, 19% higher stiffness). Moreover, in terms of indentation measurements (Figure 76b), the osteoarthritic samples are easier to indent than the osteoporotic samples (TID, p = 0.020 and CID, p = 0.074, less than 15% higher). However, in terms of indentation and elastic modulus, much like fracture resistance, the difference between the three groups is still marginal compared to the degree of variation and therefore, these groups are generally comparable in terms of material properties.

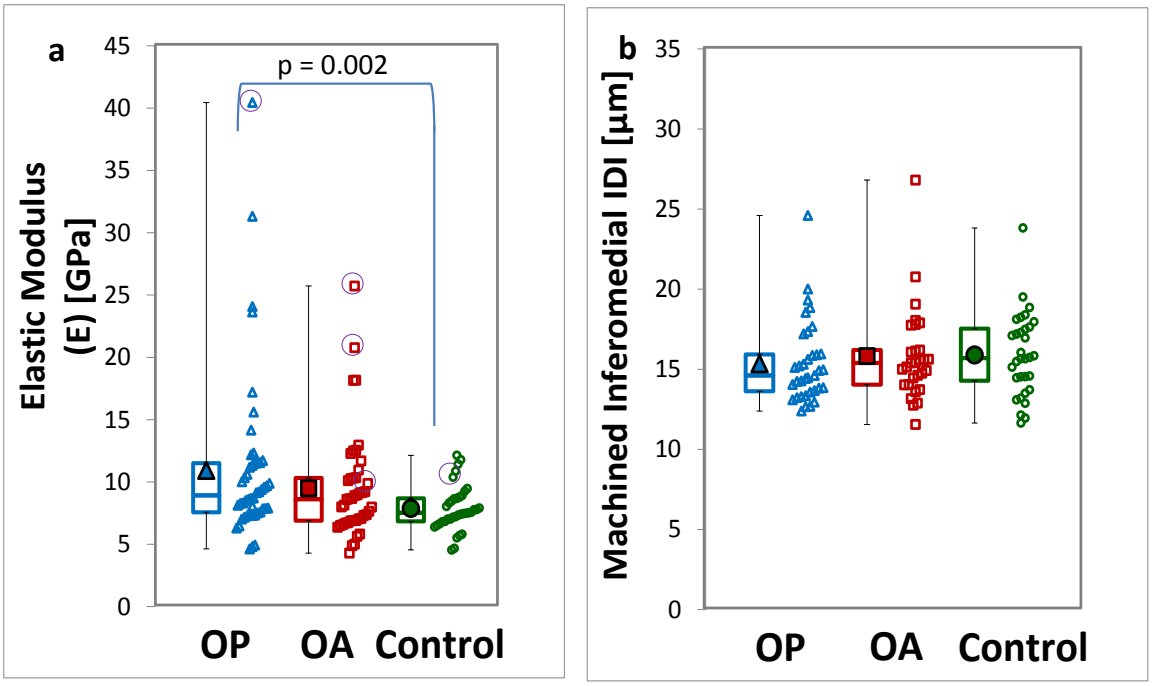

Figure 76 – Example figures comparing elastic and indentation measures for individual samples across the three groups (osteoporotic, osteoarthritic and control) in terms of a) elastic modulus and b) Indentation distance increase of the individual fracture toughness samples. The excluded samples are indicated by a purple circle.

Table 24 – Statistical comparison between osteoporotic (OP), osteoarthritic (OA) and control groups as exampled by Figure 76. The groups are compared against the other two groups using a Mann-Whitney U-Test (no variables are normally distributed) and the median and interquartile ranges are displayed. The light grey italicised shows a comparison is 'close to' significance ($p < 0.1$) and the dark grey bold highlighting shows a significant difference ($p < 0.05$). Fracture mechanics properties are shown in terms of the crack growth resistance (K slope and J slope) and the fracture toughness (K max and J max).

		Osteoporotic (n = 48)		Osteoarthritic (n = 40)	Control (n = 36)	
K slope, [MPa.m$^{-0.5}$]		7587.7 (5091.8 – 10378.0)	OA	6855.4 (4721.2 – 12274.3)	6323.7 (4820.5 – 11579.0)	OP OA
K max, [MPa.m$^{0.5}$]		2.49 (1.87 – 2.96)	OA	2.53 (2.03 – 3.08)	2.39 (1.94 – 2.77)	OP OA
J slope [kJ.m^{-3}]		2718.9 (1844.9 – 4120.1)	OA	2947.6 (1901.6 – 4895.8)	2782.3 (2009.4 – 4167.8)	OP OA
J max [kJ.m^{-2}]		0.574 (0.410 – 0.824)	OA	0.693 (0.456 – 0.971)	0.698 (0.490 – 0.860)	OP OA
Elastic Modulus [GPa]		8.92 (7.57 – 11.51)	OA	8.62 (6.90 – 10.32)	7.52 (6.83 – 8.68)	**OP** OA
Individual (per sample) [µm]	TID	110.1 (106.1 – 116.5)	**OA**	119.3 (110.5 – 129.3)	112.8 (108.3 – 117.8)	OP OA
	IDI	14.61 (13.92 – 15.93)	OA	15.39 (14.04 – 16.20)	15.70 (14.28 – 17.53)	OP OA
	CID	7.36 (7.13 – 8.20)	*OA*	7.93 (7.30 – 8.92)	8.37 (7.34 – 8.94)	*OP* OA

7.3.1.2.2 Measurements averaged over donors

When the individual samples are grouped in terms of donors (1 to 6 samples per donor, a median of 4 samples) by taking a mean value per donor, the crack extension resistance, indentation and elastic modulus results are again comparable. The young osteoarthritic donor still appears as an outlier and has been excluded from the analysis (Figure 77). The fracture mechanics properties of the groups are still not significantly different (Figure 77 and Table 25), with less than 15% difference between the median values. The exception is the stress intensity factor crack growth resistance (Kslope) that appears to be higher (hence tougher) in the osteoporotic compared to control group (34%, 8915 $MPam^{-0.5}$ compared to 6641 $MPam^{-0.5}$, p = 0.30, Figure 77a) but this is not significant.

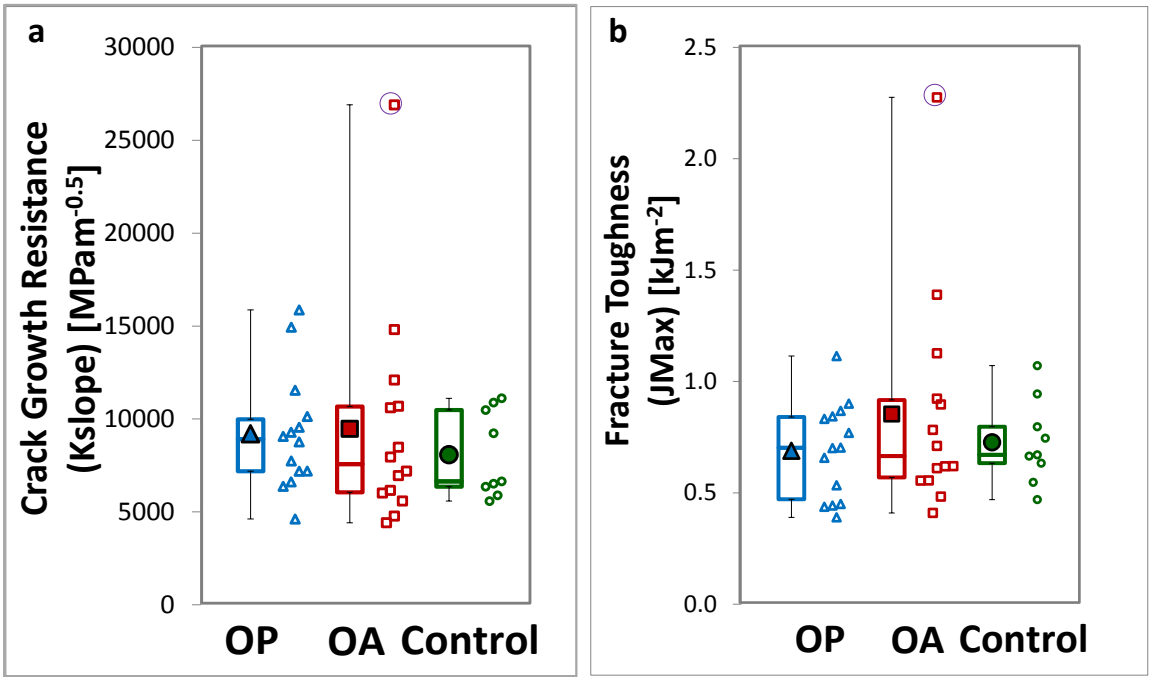

Figure 77 – Example figures comparing crack extension resistance measures for mean measurements per donor across the three groups (osteoporotic, osteoarthritic and control) in terms of a) Crack growth resistance (J slope) and b) fracture toughness (J max). The excluded sample is indicated by a purple circle.

When grouped per donor, the osteoporotic group remains significantly but minimally stiffer than control group (Figure 78a, 9.00 GPa compared to 8.22 GPa, 9.5% p = 0.013).

With the indentation measures on the individual fracture toughness samples grouped in terms of donors, the difference between groups is still marginal (less than 10%, though p = 0.006 for TID and p = 0.063 for CID comparing the osteoporotic to control group and p = 0.061 for TID comparing the osteoarthritic to control group, data not shown). This implies that the indentation, elastic and fracture mechanics properties are fairly

consistent even in presence of disease when considering the bulk properties of the inferomedial femoral neck.

Nevertheless, when these three groups are compared in terms of the inferomedial 'refined' measurements and circumferential measurements around the surface of the femoral neck, similar relationships are observed as presented in Chapter 6. That is, when indenting the inferomedial surface of the femoral neck ('refined' method, Table 25), the indentation depth is elevated in the osteoarthritic group relative to the control (31%, $p = 0.043$ for IDI and 52%, $p = 0.008$ for IDI and CID) and not significantly higher comparing the osteoporotic to control (14% in terms of IDI, $p = 0.077$). In the circumferential measurements (Figure 78b and Table 25), the differences are more pronounced with the osteoporotic group having a higher indentation depth relative to the control (20% to 43%, $p < 0.05$) and the osteoarthritic group having a yet higher indentation depth still (47% to 71% compared to the control group, $p < 0.05$). This implies that these donors are a representative sample of the larger group measured in Chapter 6 and that there are differences in the properties of the femoral neck with osteoporosis and osteoarthritis but that these do not translate to difference in the material properties of the bulk inferomedial cortical bone.

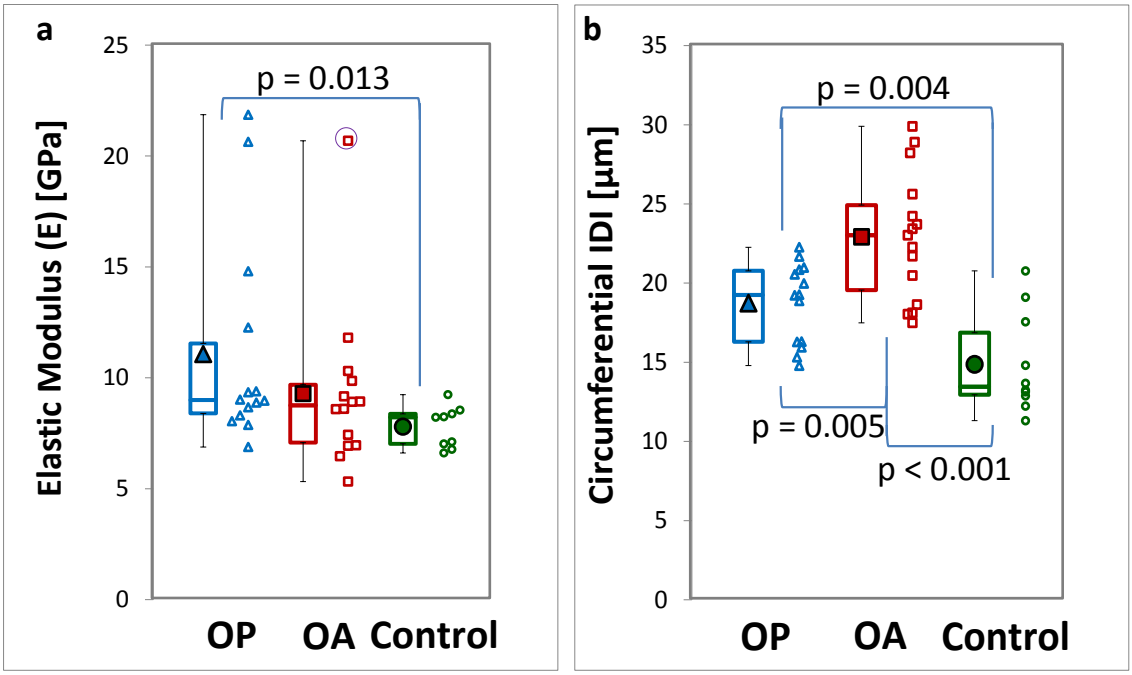

Figure 78 – Example figures comparing elastic modulus and surface indentation measures for mean measurements per donor across the three groups (osteoporotic, osteoarthritic and control) in terms of a) elastic modulus and b) Indentation distance increase of the femoral neck. The excluded sample is indicated by a purple circle.

Table 25 – Statistical comparison between osteoporotic, osteoarthritic and control groups as exampled by Figure 78. The groups are compared against the other two groups using a Mann-Whitney U-Test (not normally distributed) or t-test (normally distributed 'Refined' CID*) the median and interquartile ranges are displayed where not normally distributed and the mean and standard deviation are displayed where normally distributed ('Refined' Creep Indentation Distance – CID*). The light grey italicised cells indicate a comparison is 'close to' significance ($p < 0.1$) and the dark grey bold highlighting shows a significant difference ($p < 0.05$). Fracture mechanics properties are shown in terms of the crack growth resistance (K slope and J slope) and the fracture toughness (K max and J max).

		Osteoporotic (n = 14)		Osteoarthritic (n = 13)	Control (n = 9)	
Age [years]		78 (70 – 83)	OA	68 (60 – 79)	63 (61 – 65)	**OP** OA
K slope, [MPa.m$^{-0.5}$]		8914.9 (7190.4 – 9984.3)	OA	7574.0 (6053.4 – 10665.8)	6640.6 (6357.1 – 10482.3)	OP OA
K max, [MPa.m$^{0.5}$]		2.57 (2.27 – 2.88)	OA	2.37 (2.23 – 2.95)	2.30 (2.10 – 2.58)	OP OA
J slope [kJ.m^{-3}]		3011.9 (2637.9 – 4255.9)	OA	3237.9 (2734.9 – 4477.9)	3399.5 (2612.7 – 3789.9)	OP OA
J max [kJ.m^{-2}]		0.702 (0.471 – 0.841)	OA	0.665 (0.569 – 0.917)	0.671 (0.633 – 0.797)	OP OA
Elastic Modulus [GPa]		9.00 (8.40 – 11.55)	OA	8.76 (7.08 – 9.69)	8.22 (7.03 – 8.37)	**OP** OA
'Refined' RPI [µm]	TID	112.3 (99.2 – 120.0)	OA	122.4 (104.8 – 132.8)	106.3 (97.8 – 115.1)	OP OA
	IDI	15.48 (13.20 – 17.53)	*OA*	20.69 (14.30 – 23.72)	13.57 (12.72 – 14.32)	*OP* **OA**
	CID*	7.24 (1.28)	*OA*	8.53 (2.07)	6.52 (0.53)	OP **OA**
Circumferential RPI [µm]	TID	128.0 (117.3 – 132.0)	**OA**	159.9 (144.5 – 184.7)	105.7 (104.3 – 109.1)	**OP** **OA**
	IDI	19.25 (16.29 – 20.77)	**OA**	23.03 (19.56 – 24.93)	13.45 (12.95 – 16.87)	**OP** **OA**
	CID	8.37 (7.94 – 9.00)	**OA**	10.23 (9.54 – 12.13)	6.97 (6.66 – 7.48)	**OP** **OA**

7.3.1.3 Correlation with reference point microindentation

7.3.1.3.1 Individual measurements per sample

Of the 124 fracture toughness samples included in the above analysis, 92 of these samples were indented at least 1 mm away from the notch/fracture site post testing. Figure 79 and Table 26 show the correlation between these indentation measures on individual samples and fracture mechanics measurements to be low. Comparing the total indentation depth to the stress intensity factor crack growth resistance (Kslope), there is a significant negative correlation in the osteoarthritic group, but this is nonetheless minimal (r = -0.40) and does not persist across other groups, the samples as a whole or any other measures. In fact, for all other relationships, the correlation is similarly low (-0.4 < r < 0.4) and is also not statistically significant (p > 0.05).

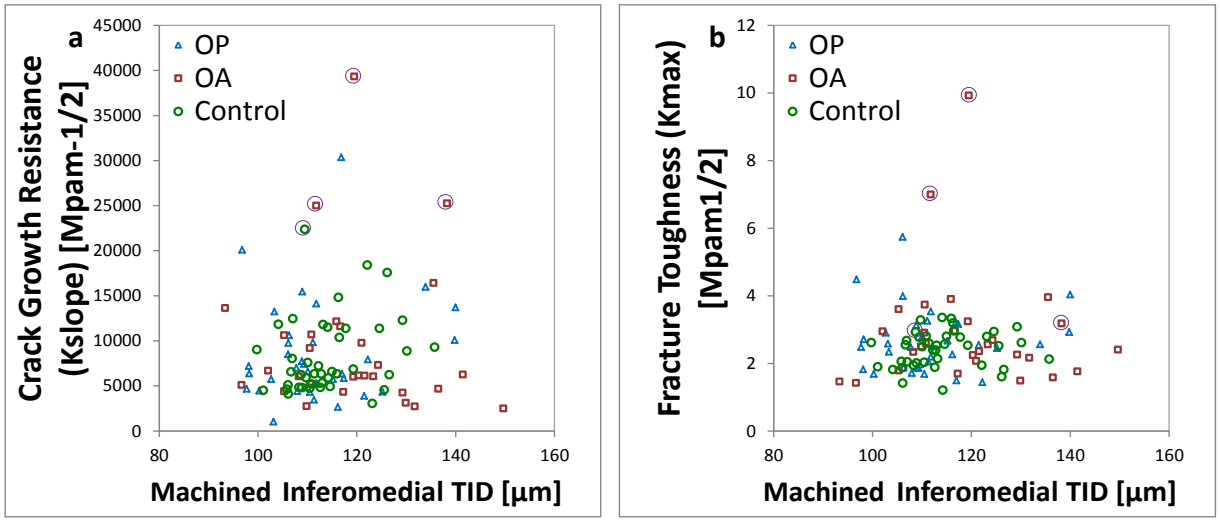

Figure 79 – Correlation between reference point indentation and fracture mechanics measures on an individual sample basis. Example curves in terms of a) crack growth resistance and b) fracture toughness. The purple circle indicates excluded samples

Table 26 – Summary of the spearman's correlation (no two variables in correlations are both normally distributed) between reference point indentation measures and fracture mechanics measures (statistical summary of Figure 79). Correlations are highlighted in pink if r < -0.2 or in light green if r > 0.2 but not statistically significant (p > 0.05). Where significant (p < 0.05), the cell is highlighted in red where negative, green where positive and displayed with an asterisk (*). If the relationship only relates to one of the three indentation measures (TID, IDI or CID) this is indicated in brackets otherwise the range relates to more than one measure. All other comparisons have extremely low correlation (-0.2 < r < 0.2) that are not significant (p > 0.05) and are not shown.

	Stress Intensity Factor (K)		Strain Energy Release Rate (J)		Elastic Modulus
	K slope	K max	J slope	J max	
All (n = 92)					-0.23 (IDI)
OP (n = 35)			0.24 to 0.26		
OA (n = 25)	**-0.40* (TID)**		-0.25 to -0.38		-0.23 (TID)
Cont. (n = 32)	0.22 (TID)				-0.23 to -0.30

7.3.1.3.2 Measurements averaged over donors

By grouping the individual measurements per donor, the correlation between mean indentation and fracture mechanics measurements across multiple samples can be observed. This is displayed in Figure 80 and Table 27 and, similar to the measurements on individual samples, the correlations between indentation and fracture mechanics measures remains low and, generally, not significant.

The comparison (across all groups) between fracture toughness (K-max) and indentation depth is significant and negative in terms of IDI (r = -0.40) and CID (r = -0.36) (Figure 80b and Table 27). This low, though not significant, negative correlation (r ~ -0.2 to -0.6) appears to remain across other fracture toughness measures (K-slope, J-slope and J-max) and within the two diseased groups (osteoporosis and osteoarthritis). This finding leads to the assumption that higher indentation depth relates, albeit weakly, to decreased toughness in these donors (Figure 80a). When considering the control group, however, these correlations are generally positive (r ~ 0.2 to 0.6), though not significant, implying a higher indentation depth would actually relate to an higher toughness in these donors.

The derived elastic modulus is similarly negatively correlated with indentation depth across all samples (r = -0.40 for IDI and r = -0.35 for CID, $p < 0.05$) and notably in the osteoporotic group (r = -0.64 for IDI and r = -0.56 for CID, $p < 0.05$). This negative correlation with elastic modulus and RPI may persist in the osteoarthritic group but, in this case, the correlations are not significant (Figure 80c).

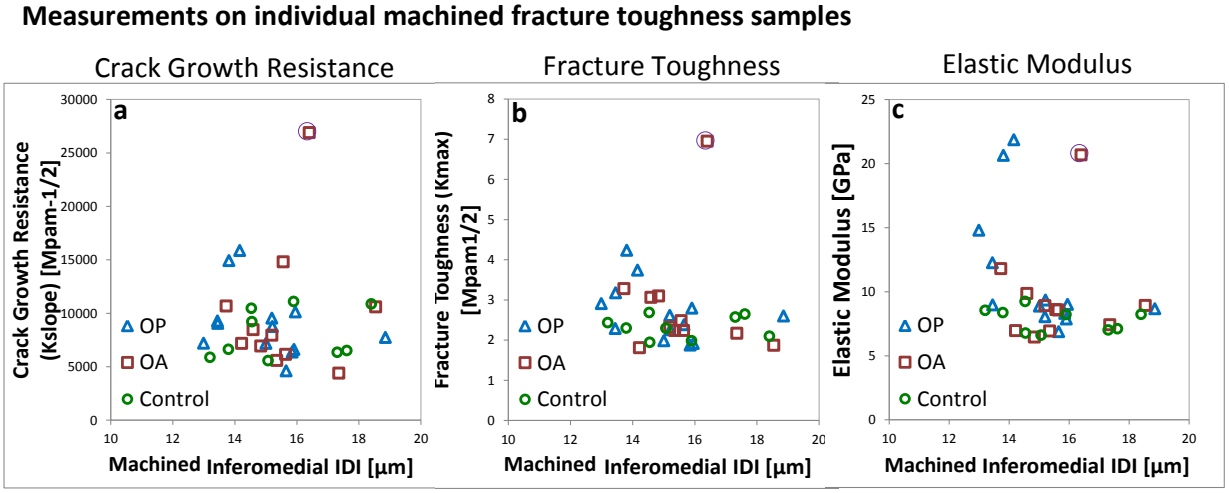

Figure 80 - Correlation between reference point indentation, age and fracture mechanics measures grouped per donor. Example curves in terms of indentation on the machined fracture toughness samples against: a) crack growth resistance, b) fracture toughness, c) elastic modulus. The purple circle indicates excluded samples

When considering the indentation measurements on the surface of the bone using the 'refined' and circumferential measurements, there is no significant correlation with the fracture mechanics measures of the bulk of the inferomedial cortical bone (Figure 81a and b and Table 27). With this lack of significance in mind, there does still appear to be a low positive correlation in the osteoporotic group ($r = 0.21$ to 0.44, $p > 0.05$) and a low negative correlation in the control group ($r = -0.20$ to -0.35, $p > 0.05$). The elastic modulus remains significantly correlated with indentation measures (Figure 81c) when indenting circumferentially around the femoral neck. However, the correlation is positive both over the three groups ($r = 0.33$ for CID, $p < 0.05$) and in the osteoporotic ($r = 0.53$ for CID, $p < 0.05$) and osteoarthritic ($r = 0.54$ for TID, $p < 0.05$) groups.

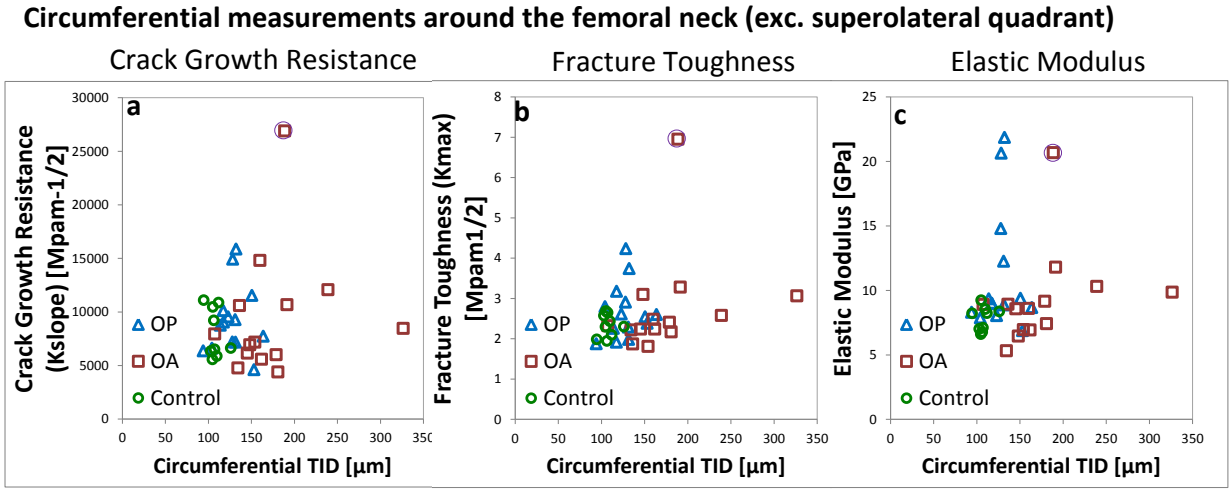

Figure 81 - Correlation between reference point indentation, age and fracture mechanics measures grouped per donor. Example curves in terms of indentation of the whole femoral neck against a) crack growth resistance, b) fracture toughness and c) elastic modulus. The purple circle indicates excluded samples

Fracture toughness and elastic modulus also are, to some extent, correlated with age within these samples (Figure 82). Toughness decreases with age ($r = -0.36$ for J-max, $p < 0.05$), except for the control group where the toughness actually increases with age ($r = 0.77$ for J-slope, $p < 0.05$), and the elastic modulus increases with age ($r = 0.40$ across the three groups combined, $p < 0.05$).

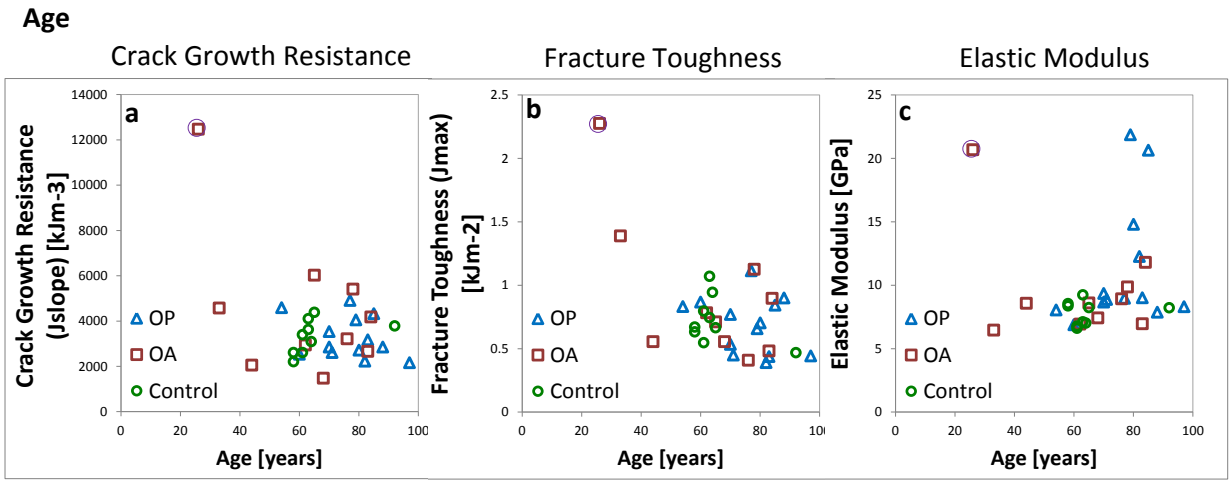

Figure 82 - Correlation between reference point indentation, age and fracture mechanics measures grouped per donor. Example curves in terms of age correlated to a) crack growth resistance, b) fracture toughness and c) elastic modulus. The purple circle indicates excluded samples

Table 27 – Summary of the spearman's correlation (no two variables in correlations are both normally distributed) between reference point indentation measures and fracture mechanics measures (statistical summary of Figure 81). Correlations are highlighted in pink if r < -0.2 or in light green if r > 0.2 but not statistically significant (p > 0.05). Where significant (p < 0.05), the cell is highlighted in red where negative, green where positive and displayed with an asterisk (*). If the relationship only relates to one of the three indentation measures (TID, IDI or CID) this is indicated in brackets otherwise the range relates to more than one measure. All other comparisons have extremely low correlation (-0.2 < r < 0.2) that are not significant (p > 0.05) and are not shown.

		Stress Intensity Factor (K)		Strain Energy Release Rate (J)		Elastic Modulus
		K slope	K max	J slope	J max	
All	Age (n = 37)	0.29			**-0.36***	**0.40***
	Mach. (n = 32)	-0.23 (TID)	-0.21 (TID) **-0.40* (IDI)** **-0.36* (CID)**			-0.27 (TID) **-0.40* (IDI)** **-0.35* (CID)**
	Ref. (n = 31)	0.24 to 0.26				0.22 to 0.23
	Circ. (n = 36)					0.23 to 0.24 **0.33* (CID)**
Osteoporotic	Age (n = 14)			-0.36	-0.25	0.22
	Mach. (n = 13)	-0.30 to -0.52	-0.25 to -0.50	-0.34 (TID)		-0.29 (TID) **-0.64* (IDI)** **-0.56* (CID)**
	Ref. (n = 13)	0.28 to 0.39	0.28 to 0.42	0.29 to 0.40		0.41 (CID)
	Circ. (n = 14)	0.44 (CID)	0.21 to 0.35	0.28 (CID)		0.20 (IDI) **0.53* (CID)**
Osteoarthritic	Age (n = 14)	0.20			-0.40	0.34
	Mach. (n = 10)	-0.26 to -0.46	-0.45 to -0.52	-0.32 to -0.41	-0.43 to -0.55	-0.45 (TID)
	Ref. (n = 9)	0.60 (TID)	-0.34 to -0.38	0.28 (TID) -0.27 (IDI)	-0.26 to -0.39	0.24 (TID)
	Circ. (n = 13)	0.22	0.29 to 0.48			**0.54* (TID)** 0.27 to 0.47
Control	Age (n = 9)	0.62		**0.77***		
	Mach. (n = 9)	0.23 to 0.27	0.37 (TID)	0.47 to 0.58	0.29 to 0.39	0.41 (TID) -0.29 to -0.46
	Ref. (n = 9)		-0.29 to -0.35	-0.20 (TID)	-0.33 (TID)	0.29 (IDI) -0.39 (CID)
	Circ. (n = 9)		-0.25 (CID)	-0.32 (IDI)	-0.23 (IDI)	0.27 to 0.38

7.3.2 Imaging of indentations

7.3.2.1 Micro-computed Tomography and Serial Sectioning for Imaging and Quantifying the Indent and Associated Damage

Both computed tomography (µCT) and serial section were effective at imaging the Haversian canals, the indent and surrounding microdamage as displayed in Figure 83. The clear visualisation of the cracking, particularly using µCT, also allowed for observation of crack resistance mechanisms. Preferential propagation of cracks along cement lines and inter-lamellar layers leading to delamination, crack deflection along the length (Figure 83a and d) and around the osteon (Figure 83c and e-h) and crack bridging (Figure 83a-c) were observed. Though the resolution was not sufficient to observe lamellae, interlamellar layers or cement lines directly, the cracks did follow the shape of the osteon, curving

around the canals and it has previously been shown that cracks do preferentially propagate through these areas [98] so it has been assumed to also be the case here.

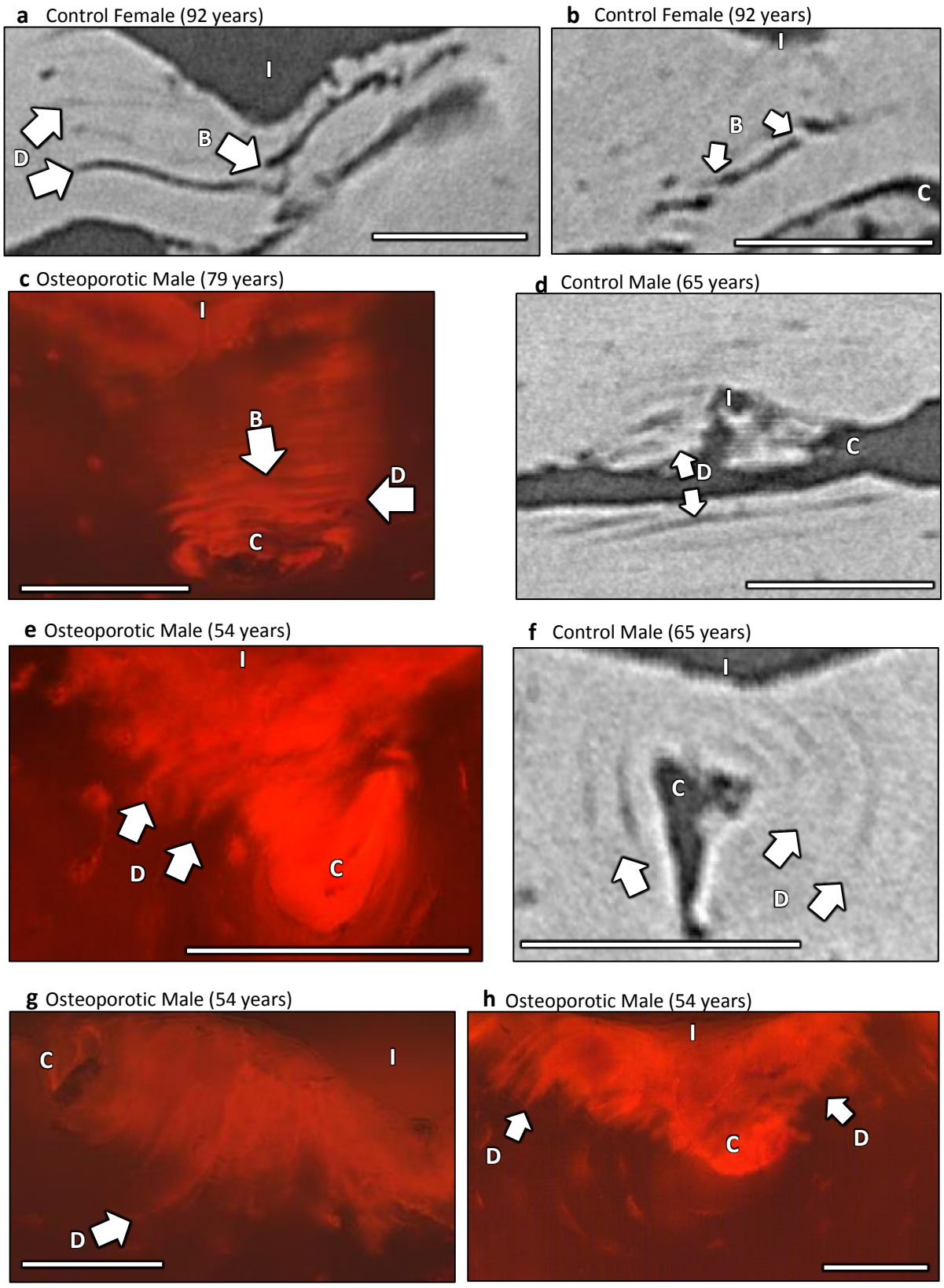

Figure 83 – Examples of cracking and fracture resistance mechanisms surrounding the indents imaged using high-resolution micro computed tomography (a, b, d, and f) and serial sectioning with fluorescence microscopy (c, e , g and h). The scale bars are 100 µm and the arrows indicate the cracking resistance: B – crack bridging and D – delamination and crack deflection. I shows the indent and C shows a Haversian canal

The seven (3 osteoporotic and 4 control) µCT samples were all successfully segmented for quantification of the indent, canals and microdamage with varying degrees of manual selection. In all samples, the pores and indent could be automatically segmented from the surrounding bone, with manual selection used to differentiate between the two. The segmentation of the smaller cracks was typically (five of seven samples) utilising a semi-automatic procedure (Figure 84b) in which the previously described algorithm (7.2.3.2) successfully identified the majority of larger cracks but manual segmentation was required to select these, differentiate from some lacunae and to segment the smaller damage. In the further two samples (both osteoporotic), the microcracks were not clearly visible and had to be segmented manually (Figure 84a). In this case, the small size of these cracks, close to the resolution of the scan, meant there were difficulties in identification and segmentation and it is even possible that these were artefacts relating to lacunae or imaging rather than the cracks themselves. Even if the inclusion of these features lead to an overestimation in the two cracking associated measures; the mean crack length was still lowest in these two samples and the crack volume was, at least, an order of magnitude lower than the other five samples.

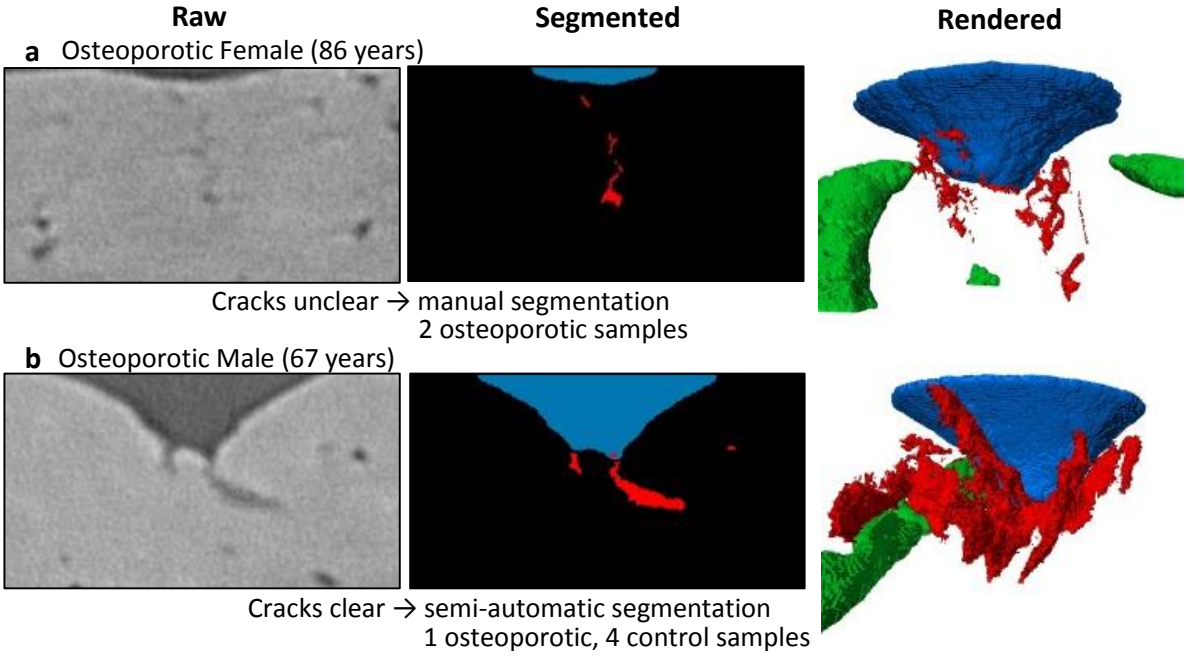

Figure 84 – Segmentation of micro-computed tomography image stacks using a) predominantly manual segmentation of the cracks and b) predominantly automatic segmentation of the cracks and the resulting 3D volume rendering. The indent is indicated in blue, the Haversian canals in green and the cracking in red.

In the serial sectioning and fluorescence microscopy of the nine samples (5 control and 4 osteoporotic) the indent was successfully segmented in all of the samples using the described semi-automatic procedure (7.2.3.3) as shown in Figure 85. The segmentation of

the microdamage surrounding the indent presented difficulties in discriminating the baseline stain/damage (i.e. associated with pores and the surface rather than the indent alone, light blue Figure 85) from that associated solely with the indent (Figure 85 dark blue). Therefore both sources of damage were included in the analysis. This segmented area across the whole stack was used to derive the damage volume and 'damage extent' (where damage extent = $(3/(2\pi) \times \text{damage volume})^{1/3}$, assuming a hemispherical volume, to be compared with the µCT crack length, shown later in Figure 89) which can be considered an overestimate.

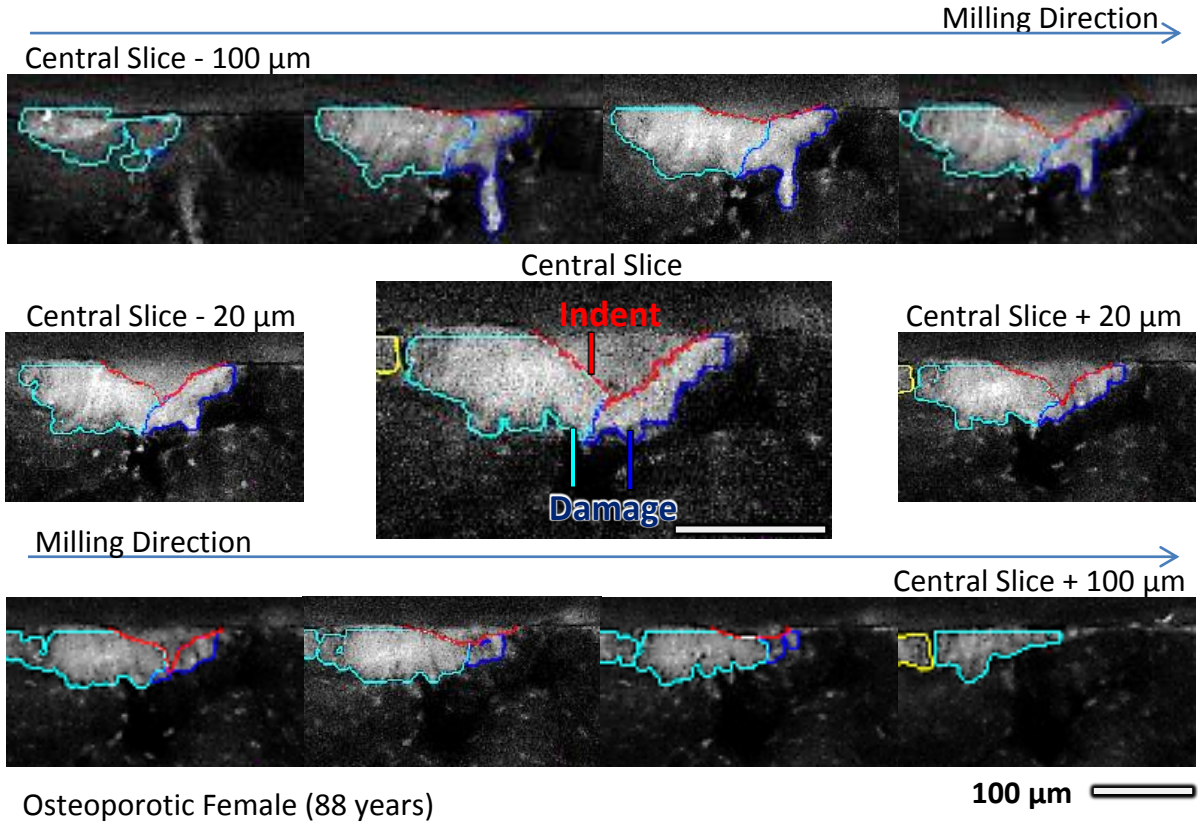

Figure 85 – Segmentation of the serial section fluorescence microscopy images with eleven sample slices from the image stack of one osteoporotic donor. The light blue indicates an attempt to separate background/pore associated damage from that associated with the indent alone (dark blue). This was generally unsuccessful and both have been combined to quantify the damage.

7.3.2.2 Damage visualisation through AFM and PLM

Validation of the staining and fluorescence microscopy technique is shown in Figure 86. Polarised light microscopy (PLM) and higher resolution confirms the fluorescence microscopy defined damage area relates to microdamage in the form of linear microcracks. Atomic Force Microscopy, at yet higher resolution still, further confirms the presence of linear microcracks and also displays smaller, less than 2 µm cracks that relate to diffuse damage. As well as the damage area identified by staining being visualised to

contain diffuse damage, other crack resistance mechanisms can also be observed, crack bridging and deflection, using the higher resolution imaging (Figure 86).

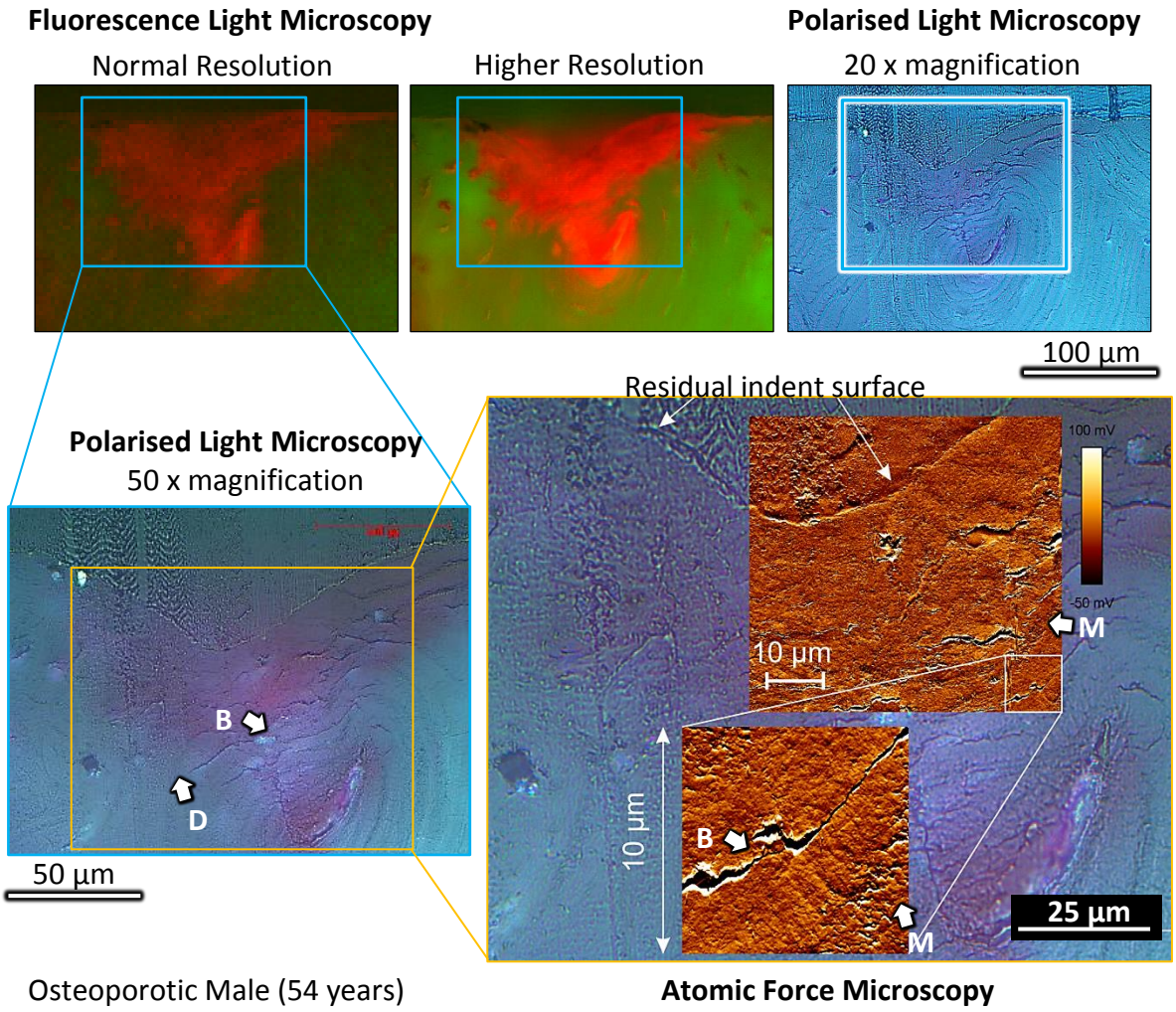

Figure 86 – Imaging of microdamage surrounding an indent at its deepest point. Imaging with fluorescence microscopy at normal resolution (10 times objective of a single image, 680 nm resolution) and high resolution (20 times objective averaged over 20 images, 340 nm resolution). Polarised Light Microscopy (PLM) at this same resolution and at higher magnification (50 times objective averaged over 50 images, 136 nm resolution). Atomic Force Microscopy image overlaid on the higher resolution PLM image with the scale bar showing vertical deflection of the cantilever (-50 mV to 100 mV, 20 nm resolution). Crack resistance mechanisms labelled D (deflection), M (Diffuse Microdamage) and B (Un-cracked ligament, crack bridging)

7.3.2.3 Comparison between imaging modalities

Figure 87 shows good congruence between the indent imaging with the µCT and serial sectioning techniques. The indent can be similarly visualised with both techniques, though the better contrast using µCT leads to clearer segmentation, particularly around the tip of the indent. This improved contrast also leads to the ease of segmenting the canals and larger microcracks. Despite this, the smaller diffuse microcracks (i.e. the majority of the red stain, Figure 87 relating to AFM imaged microdamage, Figure 86) cannot be clearly visualised with the µCT technique whereas this is clear using serial sectioning and fluorescence microscopy. Diffuse damage visualisation relates to the

higher resolution in the *x* and *y* direction (0.34 µm/pixel with the 20 times objective and 0.68 µm/pixel with the 20 times objective compared to the 0.83 µm/pixel for µCT) despite being significant lower in the *z* direction (i.e. 5 µm or 10 µm slices compared to the same 0.83 µm/pixel) and the contrast provided by the fuchsin stain. Therefore, both techniques have their merits for imaging different kinds of indent associated damage.

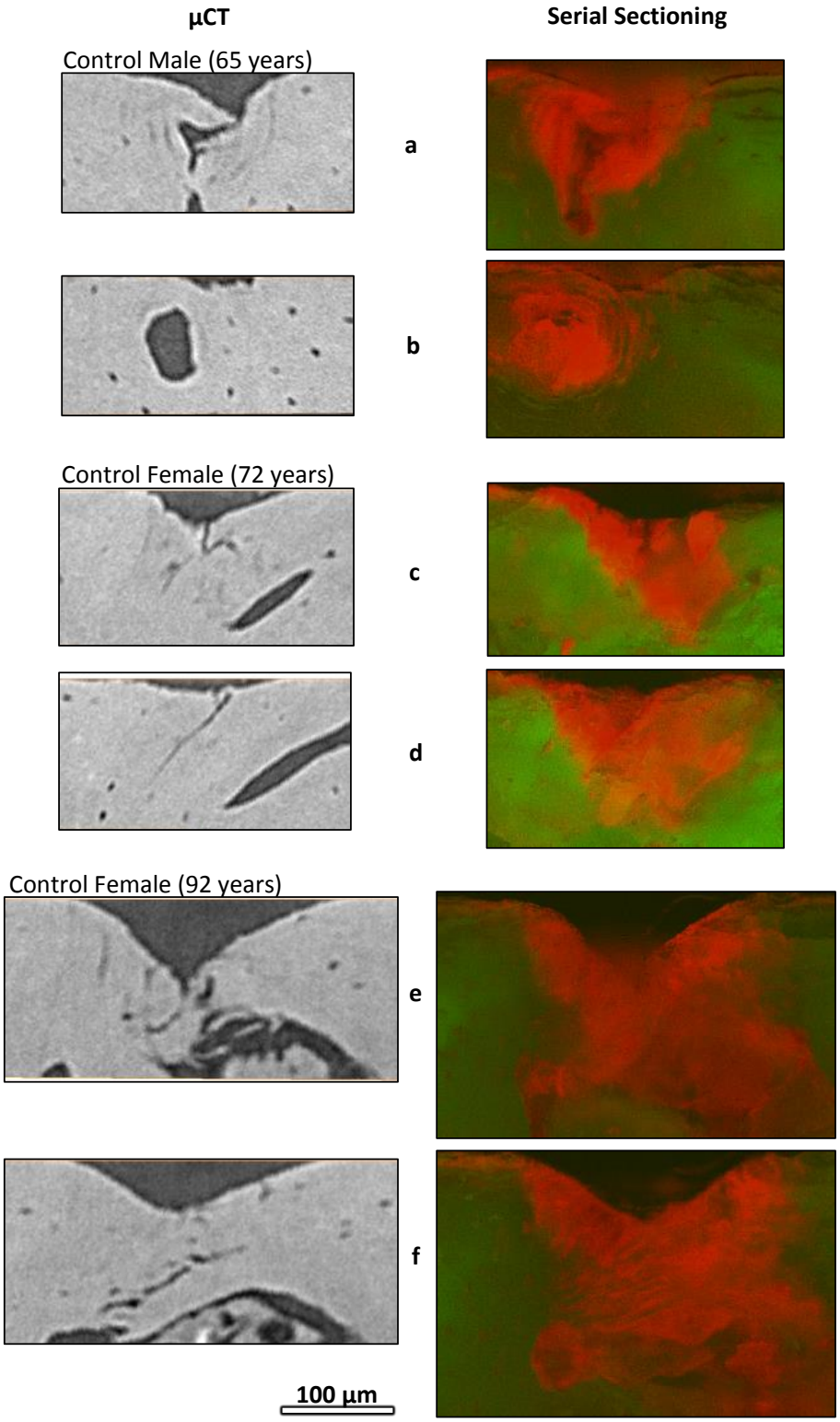

Figure 87 – Comparison between the two imaging techniques (micro computed tomography and serial section with fluorescence microscopy) across the three donors common to both techniques (all control donors)

A complete image stack was not available for a further three of the serial sectioning samples and therefore only the manually segmented central slice was used in the analysis (total 12 samples exampled in Figure 88b and c). These central slices were imaged at lower resolution (a single image with 10x objective, all samples, Figure 88b) and higher resolution (20x objective averaged over 20 repeat images for 9 samples, Figure 88c). There was excellent correlation between these techniques ($r = 0.86$ to 0.99, $p < 0.05$, not shown) so the samples were pooled (i.e. 9 samples using the higher resolution and the remaining 3 using the normal resolution).

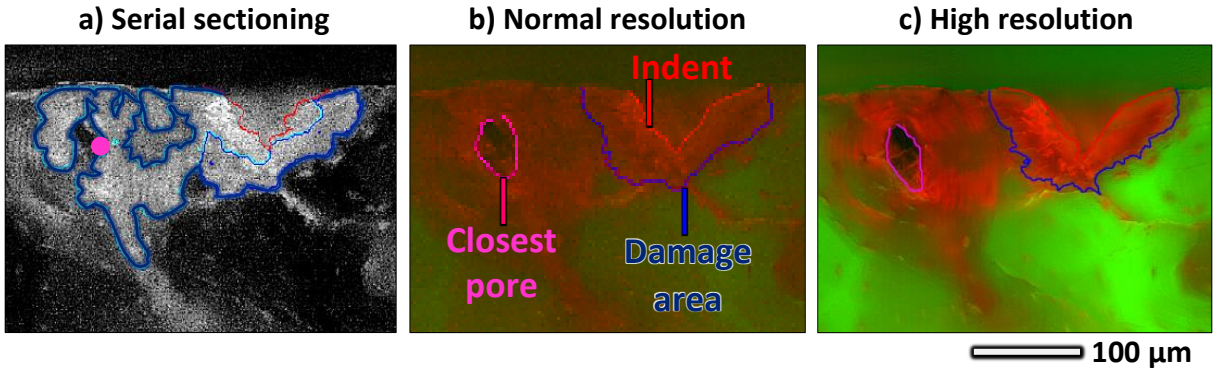

Figure 88 – Comparison between: a) semi-automatic segmentation of the image stack (greyscale image shown), b) normal resolution image of the central slice (i.e. 10 times magnification of a single image) with manual segmentation and c) higher resolution image of the central slice (i.e. 20 times magnification averaged over 20 slices) with manual segmentation (red-green-blue image).

When compared to the volumetric measures of the full stacks (Figure 88, Figure 90 and Table 28), the central slice produced similar results in terms of the indent measures (indent volume, diameter and depth $r = 0.88$, $r = 0.86$ and $r = 0.81$ respectively, $p < 0.05$). The quantification of the damage is overestimated in the automatic sectioning of the image stack. This leads to a not significant, correlation between the 'crack extent' of the two techniques (Figure 90c, discrepancy of the purple points from dotted diagonal line, $r = 0.37$, $p = 0.33$). Crack extent for the central slice is based on a semi-circle area (extent = $(2/\pi \times \text{damage area})^{1/2}$ shown in Figure 89) in a similar way to crack extent being based on a hemi-sphere for the complete image stack. The pore proximity is again similar ($r = 0.62$, $p = 0.069$) across the two methods but, due to only having one slice to represent the three-dimensional stack, the central slice overestimates the distance to the closest pore (Figure 90b discrepancy of the purple points from dotted diagonal line).

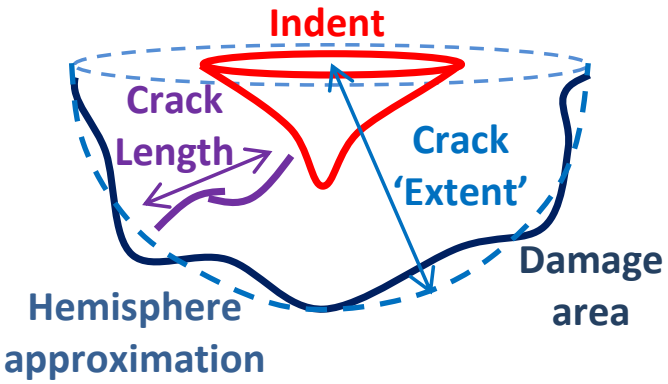

Figure 89 - Comparison of the micro computed tomography calculated crack length and the serial sectioning based fluorescence imaging to calculate the crack extent based on equating the damaged area to a semicircle or damage volume to a hemisphere

The quantification of the indent, damage and pores through fluorescence microscopy can be directly compared to µCT based measurements, which are assumed to be the more representative measures due to the clearer visualization of the indent, pores and linear microcracks leading to ease and reliability of segmentation and quantification. Because there is only overlap of three samples between the µCT and both the automatic serial sectioning and manual central slice techniques, statistical comparison between the techniques would be meaningless. However, observations can still be made about the similarity or differences between the techniques. By observing the approximate correlations in Figure 90 and calculating a paired sample t-statistic (the mean difference between the paired samples divided by the standard error of this difference, as would be used to assess the significance in a paired t-test), comparisons can be made between techniques. Based on these comparisons it can be scrutinized whether the central slice or complete stack are more representative of µCT for combining the techniques across all samples. Again, it should be noted that this approach is limited due to the existence of only 3 comparable samples.

Because the central slice only provides areal measurements, the indent volume can only be combined with serial sectioning and µCT. This combination is valid as both measured give similar values (11% to 23% higher in the serial sectioning than µCT). The other indent measures (depth and diameter) are also similar across the central slice, complete stack and µCT (2% to 13% difference) as indicated by the close vertical proximity of the red to purple points in Figure 90a.

Having the full stack available leads to similarities between serial sectioning and µCT in terms of the pore proximity measures (the vertical proximity between the purple and red

points in Figure 90b). There is still discrepancy between these two techniques (between 3 µm and as high as 30 µm, a 60% underestimation by serial sectioning), though this is minimal compared to the consistent overestimation in pore proximity when only using the central slice (difference between the red points and diagonal line, Figure 90b).

Due to the overestimation of the damage in the automatic selection, the crack extent in the central slice is more representative of the mean crack length of the µCT (Figure 90c). The central slice has a lower t-statistic and difference between groups, though this still represents a reasonably large (67%) underestimation (difference between red points and diagonal line, Figure 90c).

Therefore, when considering correlation with RPI measures across all 16 samples, the techniques were combined based on their similarity to µCT measures. That is, µCT measures were used where available, else preferentially combining with serial sectioning measures for indent (i.e. volume, depth and diameter) and pore (proximity) assessment. Whereas for damage assessment (crack extent), the central slice is used preferentially. This combination is indicated by black circles in Figure 91 and the 'Technique' column in Table 29. The author acknowledges that, where there are discrepancies between the two techniques (e.g. the quantification of linear microcracks in µCT rather than an area containing diffuse damage and linear microcracks in fluorescence microscopy), this combination of techniques is not entirely appropriate. However, though the measurements based on each technique alone are also discussed, these are typically not statistically significant due to lower number, and therefore this combination of techniques is necessary to draw conclusions.

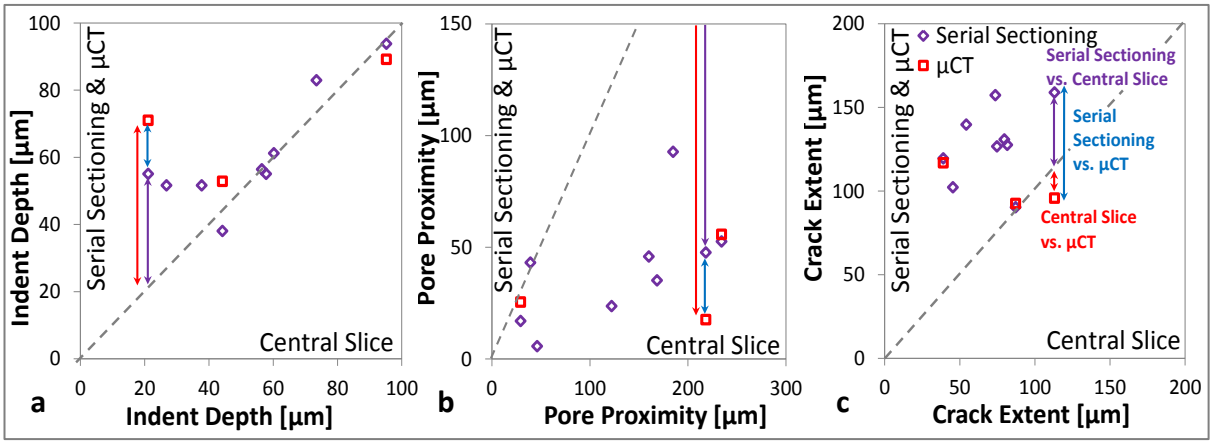

Figure 90 – Comparison between the serial sectioning technique of the whole image stack, the central slice alone and micro computed-tomography measures of: a) indent depth, b) Pore Proximity and c) Crack Exten

Table 28 – Statistical summary of the correlations shown in Figure 91 with the correlations between serial sectioning of the whole stack (i.e. volumetric measures) and their equivalent based on the central slice alone (i.e. areal measures). Significant comparisons are shown in bold and dark grey (p < 0.05) and those 'close to' significance are highlighted in italics and light grey

	Semi-automatic Serial Sectioning					
	Indent Volume	Indent Diameter	Indent Depth	Damage Volume	Crack Extent	Pore Proximity
Manual Central Slice Equivalent	**0.88**	**0.86**	**0.81**	*0.60*	0.37	*0.63*

7.3.2.4 Comparison between indent imaging and RPI measurement parameters

The individual measures of the Biodent Hfc^{TM} RPI device, principally (TID, IDI and CID used in this report) can be compared with the measures from imaging of these indents to better discern the property being assessed by the technique.

The indent volume positively correlates with the indentation depth both when measured by µCT ($r = 0.46$ to 0.57, $p > 0.05$, $n = 7$) and serial sectioning of the full image stack ($r = 0.33$ to 0.63, $p > 0.05$, $n = 9$) but these comparisons only have the numbers required to gain significance when techniques are combined (IDI $r = 0.63$, $p = 0.021$, $n = 13$). Similarly, the indent cross-sectional area, depth and diameter are significantly positively correlated with RPI measures ($r = 0.56$ to $r = 0.82$, $p < 0.05$) as shown in Figure 91a and Table 29. This positive correlation between indent size and RPI assessed indent depth persists across imaging modalities and also when considering the osteoporotic and control groups separately.

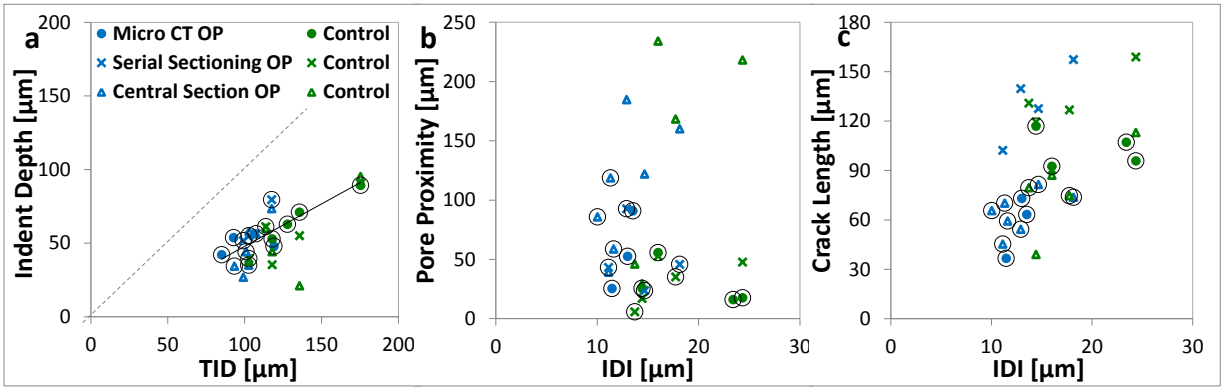

Figure 91 – Comparison between RPI measurements and indent imaging measures: a) maximum indent depth, b) proximity to the nearest pore and c) "crack length" or "damage extent" based on micro computed tomography, fluorescence microscopy of serial sectioning transversely through the entire indent and sectioning of the central slice only. The black circles indicate which of these three imaging modalities has been used for the correlation in Table 29 based on the discussion in 7.3.2.2 and the similarities between techniques.

When considering the damage extent and the mean crack length (Figure 91c), this is again positively correlated with indentation measures. Using μCT, the crack length is significantly positively correlated with RPI ($r = 0.79$, $p = 0.036$ for TID and $r = 0.71$, $p = 0.071$ for IDI). This is also the case when using the crack extent for central slice ($r = 0.64$, $p = 0.024$ for IDI and $r = 0.50$, $p = 0.095$ for CID, as for damage area, Table 29) and when all techniques are combined ($r = 0.55$ and $p = 0.028$ for TID and $r = 0.54$ and $p = 0.029$ for IDI, Figure 91c, Table 29). However, when using the serial sectioning stack and the overestimated damage volume/crack extent the correlation does not persist ($r = 0.07$ to 0.42, $p > 0.05$). Furthermore, the positive correlation with μCT crack volume is additionally not significant ($r = 0.14$ to 0.54, Table 29). This implies that initiation and propagation of microcracks from the indent also influences the RPI measures but, perhaps, to a lesser extent than the deformation of the bone and resulting indent size.

The proximity to the closest pore as overestimated by manual selection of the central slice gives positive correlation with indentation measures ($r = 0.59$ to 0.62, $p < 0.05$). However, the overall trend across the three imaging techniques is a negative correlation ($r = -0.33$ and -0.19 for TID and CID respectively, $p > 0.05$ and $r = -0.55$ for IDI, $p = 0.027$, Figure 91b, Table 29). The porosity (based on the Haversian canals and not including the lacunae) as assessed by μCT, is also significantly positively correlated with indentation measures (IDI, $r = 0.93$, $p = 0.003$, CID, $r = 0.75$, $p = 0.050$ and TID, $r = 0.68$, $p = 0.094$). Finally, as well as indent size and damage extent, porosity and proximity to pores also affects the RPI assessed indentation measurements.

Table 29 – Spearman's correlation between indentation measurements (TID, IDI and CID) and measures from indent imaging. The column No. indicates the number of samples included in the correlation with the column 'Modality' indicating how these measures are made up of CT (computed tomography), SS (serial sectioning and fluorescence microscopy of the full stack) and CS (the central slice from the serial sectioning stack). The correlations are highlighted as significant in bold and dark grey or 'close to' significance in italics and light grey.

Combined		Technique	No.	TID [µm]	IDI [µm]	CID [µm]
Indent	Indent Volume [μm^3]	7 CT + 6 SS	13	0.29	**0.63**	0.32
	Indent Area [μm^2]	7 CT + 1 SS + 8 CS	16	**0.58**	**0.66**	**0.56**
	Indent Depth [µm]	7 CT + 6 SS + 3 CS	16	**0.71**	**0.78**	**0.65**
	Indent Diameter [µm]	7 CT + 6 SS + 3 CS	16	**0.76**	**0.82**	**0.75**
Damage	Crack Volume [μm^3]	7 CT	7	0.43	0.54	0.14
	Crack Length [µm]	7 CT	7	**0.79**	*0.71*	0.21
	Damage Volume [μm^3]	9 SS	9	0.07	0.42	0.37
	Damage Area [μm^2]	12 CS	12	0.46	**0.64**	*0.50*
	Damage "Extent" [µm]	7 CT + 9 CS	16	**0.55**	**0.54**	0.41
Pore	Proximity to Pore [µm]	7 CT + 6 SS + 3 CS	16	-0.33	**-0.55**	-0.19
	Macro Porosity [%]	7 CT	7	*0.68*	**0.93**	**0.75**

7.3.2.5 Indent Imaging in Osteoporotic and Control Bone

The RPI indentation depth of the individual imprints is significantly higher ($p < 0.05$) in the osteoporotic (n = 10) than the control (n = 6) samples as demonstrated by the x-axis of Figure 91, Figure 93 and the statistical summary in Table 31. It appears that the higher porosity of the bone (7.89% in the control, n = 4, compared to 1.26% in the osteoporotic group, n = 3, p = 0.11, not significant due to the small numbers, Table 30) leads to a substantially decreased proximity to the closest pore (61% decreased from 55.7 µm to 21.6 µm, p = 0.022, Table 30, Figure 93c). Though pore proximity seems to have the largest influence on the apparent differences in RPI between these two groups, indent size (particularly indent depth 24.5% higher in the control group, p = 0.12 and indent diameter 16.1% higher, p = 0.056, close to significance, Table 30, Figure 93a) and damage extent (particularly µCT crack length 60.3% higher, p = 0.057, close to significance, Table 30, Figure 93b) also affect the higher indentation depth in these samples.

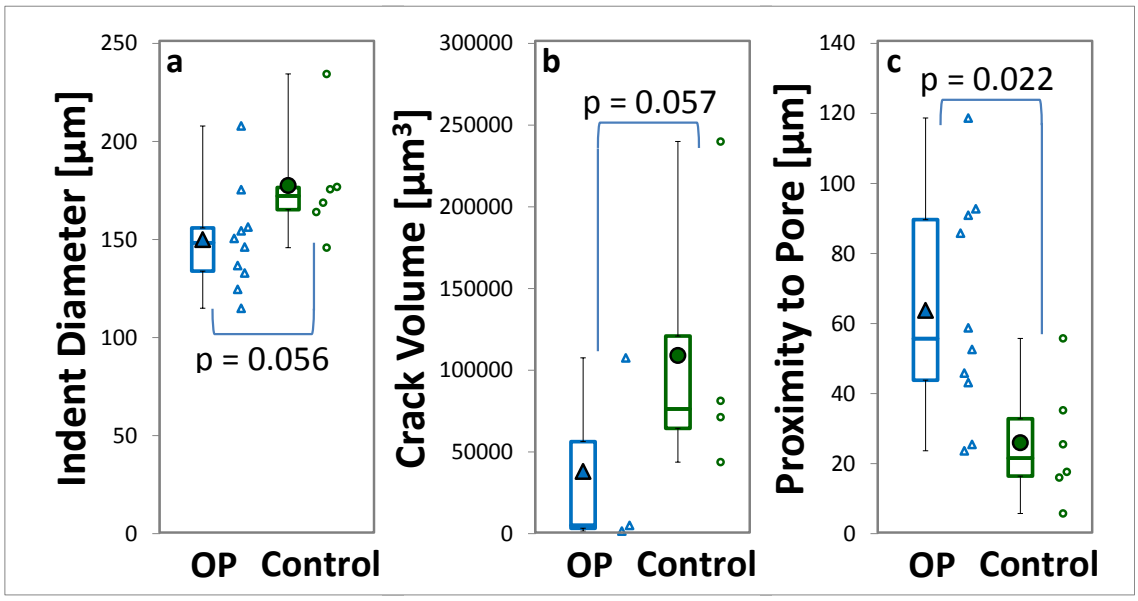

Figure 92 – Comparison between the osteoporotic and control group in terms of imaging measurements: a) the indent diameter, b) the µCT measured crack volume and c) the proximity to the closest pore

Table 30 – Comparison between the osteoporotic and control group using the Mann-Whitney U-test in terms of imaging measurements. The contribution of micro computed tomography, serial sectioning and central slice fluorescence microscopy are as indicated in Figure 91. The median and interquartile range (lower quartile to upper quartile) are shown, alongside the number of measures [n] where the full 10 osteoporotic and 6 control samples were not assessed. The level of significance (p) is highlighted in bold and dark grey where significant (p < 0.05) or in light grey and italics where 'close to' significance (p < 0.1).

Combined		Osteoporotic (n = 10)	Control (n = 6)	p
Indent	Indent Volume [µm³] x 1000	311.6 [7] (214.0 – 554.0)	330.9 (239.4 – 497.7)	0.63
	Indent Area [µm²]	3048.5 (2314.5 – 4176.3)	3759.0 (2684.8 – 5825.3)	0.37
	Indent Depth [µm]	49.8 (40.3 – 55.4)	62.0 (49.5 – 75.6)	0.12
	Indent Diameter [µm]	148.3 (130.8 – 161.1)	172.2 (159.5 – 191.2)	*0.056*
Damage	Crack Volume [µm³] x 1000	5.05 [3] (1.53 – 5.05)	76.29 [4] (50.64 – 200.27)	0.40
	Crack Length [µm]	63.3 [3] (36.6 – 63.3)	101.5 [4] (93.4 -114.5)	*0.057*
	Damage Volume [µm³] x 1000	5032.3 [4] (2768.0 – 7548.4)	4266.0 [5] (2562.5 – 6555.9)	0.73
	Damage Area [µm²]	6767.5 [7] (4627.7 – 8528.9)	9948.4 [5] (5571.7 – 16006.9)	0.20
	Damage "Extent" [µm]	113.6 (70.6 – 142.2)	112.0 (95.0 – 151.8)	0.64
Pore	Proximity to Pore [µm]	55.7 (38.7 – 91.4)	21.6 (13.5 – 40.4)	**0.022**
	Macro Porosity [%]	1.26 [3] (0.86 – 1.26)	7.89 [4] (2.66 – 11.88)	0.11

Though the samples used in imaging with singular indentation measurements have a significantly higher RPI indentation depth in the control relative to osteoporotic group, this is contrary to the results discussed in the Chapter 6 and section 7.3.1.2. Furthermore, when multiple measurements are taken on these same donors, the measurements are representative of our previous findings (Chapter 6 and section 7.3.1.2) (Figure 93c and d and Table 31). Specifically, the indentation depth is higher in the osteoporotic group when indenting the surface of the inferomedial neck (by 1.8% in terms of TID, $p > 0.05$ and 9.3% to 10.2% in terms of IDI and CID, $p < 0.05$, Figure 93d and Table 31) or the circumferential measurements of the femoral neck (15.4% to 22.8%, $p < 0.05$ for CID, Figure 93d and Table 31). Additionally, the two groups are identical in terms of measurement on the machined samples as discussed for the indentation of fracture toughness samples in section 7.3.1.2.1 (0.8% to 1.9%, $p > 0.05$, Figure 93b and Table 31).

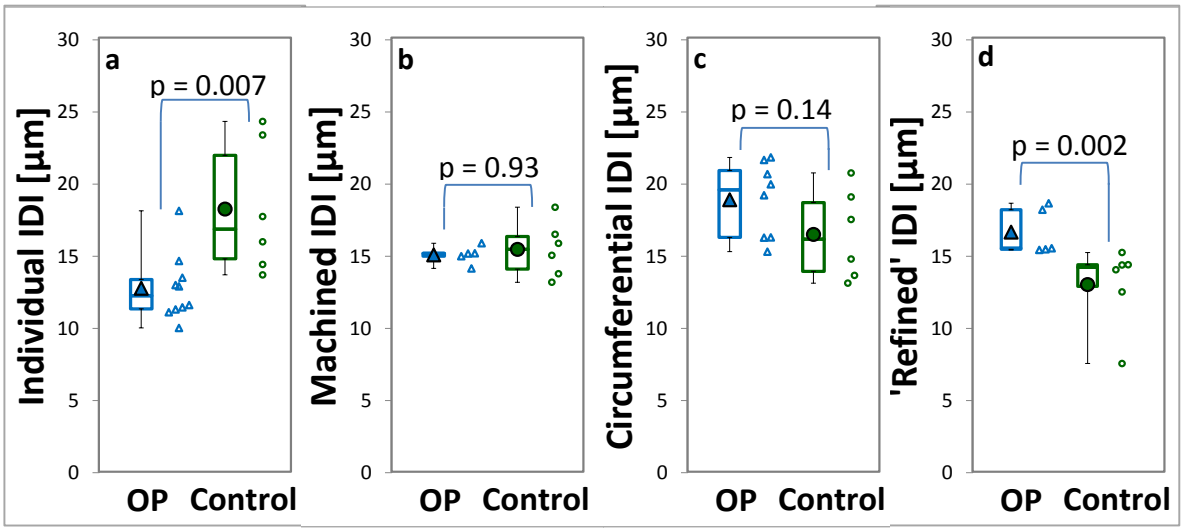

Figure 93 – Indentation distance in the imaged samples: a) the individual imaged indents, b) the mean indent measurements on the machined fracture toughness samples, c) the circumferential (excluding the superolateral quadrant) measurements around the Unmachined femoral neck and d) the 'refined' measurements in the unmachined inferomedial femoral neck

Table 31 – Statistical summary of Figure 93, comparison between RPI assessed indentation depth in image samples in terms of the individual (imaged) measurements and the measurements averaged over multiple indents (machined, circumferential measurements around the femoral neck and 'refined' measurements on the inferomedial femoral neck)

RPI Measures		Osteoporotic	Control	p
Individual	TID [µm]	101.8 (93.2 – 110.0)	122.9 (111.0 – 145.6)	**0.011**
	IDI [µm]	12.3 (11.3 – 13.8)	16.9 (14.3 – 23.6)	**0.007**
	CID [µm]	6.26 (5.68 – 7.28)	8.38 (7.57 – 10.61)	**0.042**
Machined	TID [µm]	111.1 (110.1 – 111.5)	110.1 (107.1 -113.7)	0.79
	IDI [µm]	15.2 (15.0 – 15.2)	15.5 (14.1 – 16.4)	0.93
	CID [µm]	7.69 (7.30 – 7.75)	7.61 (7.44 – 7.77)	1.00
Circ.	TID [µm]	123.7 (114.5 – 131.7)	107.2 (104.3 – 111.2)	*0.059*
	IDI [µm]	19.6 (16.3 – 20.9)	16.2 (14.0 – 18.7)	*0.14*
	CID [µm]	8.52 (7.82 – 8.92)	6.94 (6.66 – 7.45)	**0.013**
'Refined'	TID [µm]	112.3 (110.5 – 117.8)	110.3 (100.5 – 120.6)	0.54
	IDI [µm]	15.6 (15.5 – 18.2)	14.2 (12.9 – 14.4)	**0.002**
	CID [µm]	7.19 (7.18 – 7.46)	6.53 (6.40 – 7.01)	*0.052*

7.4 Discussion

7.4.1 Validity of mechanical testing and imaging techniques

To address the question of which property of the bone is being assessed via RPI, fracture toughness experiments and indent imaging techniques were applied. Due to the use of novel approaches, specifically advanced automation of the whitening front tracking method [256] and serial sectioning of indentations, validations against existing techniques was necessary.

The comparison with micro-computed tomography indicates that the indent volume was successfully identified and segmented using the serial sectioning technique. Though this staining technique was developed for the imaging of microdamage [251, 267], its use in identifying the damage associated with indentation has not previously been reported. The AFM imaging, PLM, µCT together highlight that the area identified by the stain contains both linear microcracks and diffuse microdamage associated with the indent. Though this microdamage was visually identifiable as indicated by the manual segmentation of the central slice, there were difficulties in discriminating this damage from the staining associated with pores in an automated fashion.

To assess the correlation with fracture toughness, the large number of samples analysed required increased automation of the whitening front tracking method developed by Katsamenis et al [256]. This technique was necessary to image the small, sub-millimetre, crack propagation and is a simpler method the alternative environmental SEM method [87, 110, 114, 163, 179]. The adaptations made to this technique increased automation for improved throughput and made the analysis of the 158 samples feasible. Through comparison with the published method [256] applied to 10 representative specimens, the two techniques significantly correlated and were able to produce similar, and in case of the fracture toughness values, verging on identical, results. Moreover, the fracture toughness and crack growth toughness assessed here, though at a different site, are within the range of properties previously identified for human cortical bone [24, 87, 110, 114, 163, 179, 256]. In particular, the values are similar to the results by Katsamenis et al [256] who used the same fracture orientation and whitening front tracking method to give fracture toughness values between 1.77 $MPa^{0.5}$ and 3.41 $MPa^{0.5}$ (compared to 2.39 $MPa^{0.5}$ to 2.49 $MPa^{0.5}$ median derived here) and crack growth resistance values of

0.007 $MPa^{0.5}$/µm to 0.015 $MPa^{0.5}$/µm (compared to 0.0063 $MPa^{0.5}$/µm to 0.0076 $MPa^{0.5}$/µm).

With these validations, the imaging and mechanical testing techniques were appropriate for assessing; the properties of RPI and differences between cohorts.

7.4.2 Interpretation of reference point indentation measurements

7.4.2.1 Crack propagation

The indentation transverse to the direction of the osteons appears to cause compression of the lamellar layers and therefore relative movement between these layers. We believe this leads to delamination, failure of the interfaces or interlamellar layers, which is visualised as linear cracks that follow the shape of the osteon both longitudinally (visualised using µCT) and circumferentially (µCT, AFM, PLM and fluorescence microscopy). The deflection of the linear microcracks by osteons acts to impede crack propagation [110] by increasing the tortuosity of the crack path [24]. The preferential formation of microcracks within the cement lines [63] and interlamellar layers, as can be visualised by periodic spacing between the cracking, means their propagation is further impeded by variation in material properties (whether relating to variation in mineral content and/or collagen orientation [33, 89, 91, 98]) between these layers.

Other crack extension resistance mechanisms can also be visualised surrounding the indent, principally crack bridging and the presence of diffuse damage. Crack bridging is associated with uncracked ligaments, bone material that spans the crack and provides resistance to its propagation [88]. Nalla et al [109], numerically estimate that this mechanism alone has a significant contribution (1 – 1.6 $MPam^{1/2}$) to the overall fracture toughness of bone (2 – 7 $MPam^{1/2}$). The crack bridging mechanism can clearly be visualized through µCT, PLM and AFM.

The AFM, being the technique with the highest resolution utilised here (20 nm compared to down to 136 nm of the fluorescence and PLM and the 826 nm of the µCT) clearly shows the small, less than 2 µm microcracks within the stained area of the fluorescence imaging. The relative contribution of these small microcracks or diffuse damage as a crack resistance mechanism for dissipating and blunting the crack tip has been debated [109, 113, 165]. However, it is clear that diffuse damage has at least some relation to the material properties of the bone and it has hence been quantified through the whitening

effect and used to assess the extent of post-yield damage and crack propagation as utilised in this study [24, 121, 256, 257, 293].

The presence of crack extension resistance mechanisms (crack deflection, bridging and diffuse damage) that impede the propagation of microdamage from the indent into the surrounding bone implies that RPI is to some extent measuring the crack initiation and crack growth resistance of the bone as previously hypothesised [19].

Quantifying the presence of microdamage, as imaged through fluorescence microscopy and μCT, shows that the higher linear crack length leads to higher indentation depth. The correlation is reasonably high (r = 0.50 to 0.79) but non-perfect, additionally not correlating with crack volume or damage volume and therefore implying that the cracking extent is not the only property being assessed by the indentation technique. The crack length measures may, to some extent, be influenced by the two osteoporotic samples for which the extent of cracking was minimal and therefore required manual segmentation. This minimal damage surrounding the indent could relate to a reduction in microcrack formation in these two samples but there is also potential that this relates to the storage period of the samples. Post indentation, these samples were stored dry for a long period of time (approximately one year) and it is possible that an intrinsic repair mechanism exists within the bone, with Seref-Ferlengez et al [115] reporting repair of microdamage in vivo with no cellular response or remodelling. The two samples have not been imaged using any other techniques or time-points meaning that this repair cannot be verified. Furthermore, a large degree of linear microcracking could be visualised in the third osteoporotic sample also stored under similar conditions. Additionally, Schneider et al [270] used μCT to image two indents, finding the degree of microcracking to be reduced in the sample with a larger indentation depth, perhaps implying these osteoporotic samples are softer and deform rather than dissipate energy through microcracking.

The relationship between crack length and RPI indent depth translates to a minimal, generally not significant correlation with fracture toughness measurements (r = -0.23 to -0.55) in the osteoporotic and osteoarthritic groups but not in the individual (per sample) fracture toughness measurements or when considering the control group. This is in line with the minimal, generally not significant, negative correlation by Katsamenis et al [24](r = -0.35 to -0.50) and the recent study by Carriero et al [244](r = 0.00 to 0.03) but

contrary to the strong negative correlation (r = -0.90) observed by Diez-Perez et al [19]. The difference in correlation found by Diez-Perez et al [19], may relate to indentation of the surface of the tibial midshaft compared to the machined femoral neck indented here. However, it is most likely that the differences relate to the samples size with only eight specimens from five donors (correlation primarily due to one donor with high IDI and low crack growth toughness) compared to the 92 specimens and 37 donors measured here.

Indentation has been directly related to fracture mechanics measurements previously by using a cubic or triangular pyramid tip to initiate cracks within bone and directly measuring the crack length using the Vickers Indentation Fracture technique [232, 237, 238]. This technique relates the measured crack length, tip geometry, load and derived reduced modulus and hardness to find a fracture toughness value that has been reported to be comparable to that of the reported bulk properties of bone [237]. However, the suitability of this technique to derive a fracture toughness value has been called into question. This is principally due to the short crack lengths relative to sample failure meaning that 'fracture' toughness is potentially invalid and, furthermore, the dehydration required for imaging may create artefacts and exaggerate the crack length [247, 248]. These limitations apply directly to the RPI techniques here and, additionally, the fact that ten rather that one indentation cycles have been applied is a further barrier to deriving a fracture toughness value from measured RPI crack lengths. The limitations in fracture toughness calculation from indentation may in part explain the limited correlation between the two techniques found here. Due to the nature of the indents forcing damage to form, it is possible that crack initiation may be a more suitable comparison than fracture or growth toughness. However, due to the nature of the whitening front tracking method, 'crack' initiation occurs at a non-zero crack length (i.e. the whitening forms ahead of the crack tip) and hence, the crack initiation values calculated here were extremely low (due to the curve fitting, also in places negative) and were not considered valid.

7.4.2.2 Elastoplastic properties

Considering that crack propagation is only one aspect and potentially only contributes in a small proportion to the RPI measured indentation depth, other properties have been considered. Conventionally, microcracking would not be considered in indentation and instead, the output measure would be related to reduced elastic modulus and hardness

through the Oliver-Pharr method [236]. The Oliver-Pharr method relates the contact depth, projected contact area and loading/unloading slope stiffness to calculate an elastoplastic property [294]. Larger scale indentation techniques, such as Vicker's hardness testing, are also reliant on similar measures [294]. Therefore, despite the presence of microcracking, it is fair to assume that these factors influence the indentation depth measured by RPI but despite this, the focus has been on crack formation and the assessment of fracture mechanics properties [19].

When correlating indent volume, cross sectional area, diameter and depth to the indentation measures, there is indeed a high correlation ($r = 0.54$ to 0.93 where significant, $p < 0.05$). The indent diameter and depth, relating to the Oliver-Pharr reduced modulus and the Vicker's hardness [234], have the highest correlation with RPI implying that elastoplastic properties of the bone influence its indentation depth, perhaps to a greater degree than fracture mechanics properties. The non-unity regression between TID and imaged indentation depth (indent depth approximately 50% of the TID) relates to the elastic nature of the technique. The curved shape of the indent (described in Figure 94) and potential presence of pile-up and sink-in show that the indentation is not purely plastic and that there is a degree of elastic resilience of the bone. Pile-up could be visualized at the edge of the central indent (Figure 94) but was also a means of identifying the indent location during serial section, where a bump on the surface was often observed prior to the imprint itself. Elastic resilience leads to the curved rather than perfectly conical shape of the indent and the RPI measured maximum indentation depth (TID) being larger than the visualized residual imprint depth.

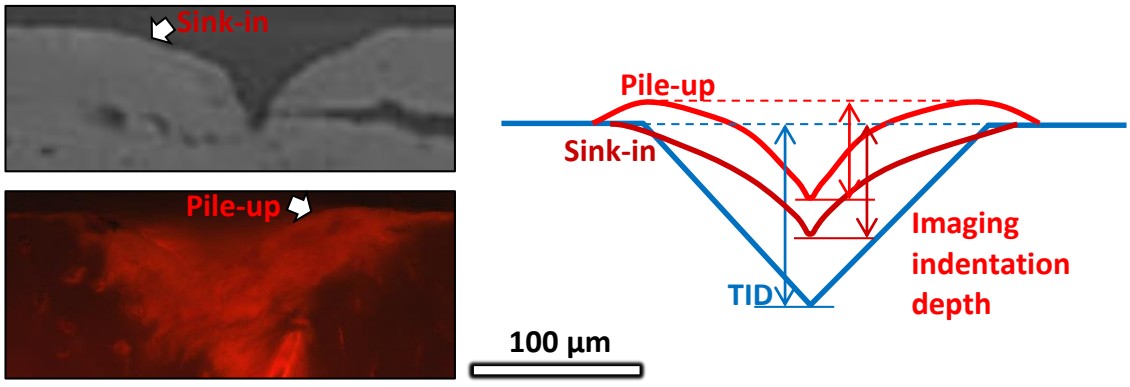

Figure 94 – Indent depth comparison between the perfectly plastic (blue) indentation depth that would be described by the TID and the elastoplastic indentation depth (red) imaged with µCT and fluorescence microscopy

The relationship with elastoplastic properties is highlighted by a minimal correlation between the indentation depth and the elastic modulus ($r = -0.35$ to -0.64 where $p < 0.05$). This negative correlation is in line with conventional nanoindentation techniques such as the Oliver-Pharr method, in which the reduced modulus is proportional to the inverse of the indentation depth [232, 294]. As mentioned, the unloading slope is also used to calculate the reduced elastic modulus in the Oliver-Pharr method [236] and this is also an RPI output measure (4.1.2). However, this author has generally not found this to be a useful measure in determining differences between cohorts and also, this does not have a significant correlation with elastic modulus ($r = 0.35$, $p > 0.05$ in osteoporotic donors, else $r < 0.2$). This measure therefore hasn't been presented in this thesis and is unlikely to be suitable for deriving a material elastic modulus. Additionally, due to the presence of cracking, elastic response, pile up or sink in, a contact area extrapolated from the probe geometry and a reference material would have discrepancies from an absolute value. Rather, to obtain an absolute material property, the indent imprint should always be directly imaged, which is not clinically feasible. Furthermore, having ten rather than one repeat cycles means that there would be further uncertainties relating the unloading slope and measured load/depth to the visualized imprint. Therefore, it is unclear whether a comparative reduced modulus would be any more useful than the comparative indentation depth measurements currently measured using RPI.

The low correlation seen here with elastic modulus, relates to the non-significant correlation with stiffness measured by Gallant et al in murine femora [25] and Granke et al [26] in human bone. Additionally, the implication that elastoplastic rather than purely elastic properties are being assessed is also supported by Gallant et al [25] and Granke et al [26] who found negative correlations between indentation depth and post-yield stress, ultimate stress and toughness ($r = -0.37$ to $r = -0.75$).

7.4.2.3 Structural properties

An influence of structural features on indentation depth was alluded to in Chapter 5 and Chapter 6 with the reduced porosity [181] and increased thickness [182, 229] of the inferomedial femoral neck leading to reduced discrimination between the fractured and non-fractured groups. This is again demonstrated with the sample of specimens investigated in this chapter. The indentation depth is higher in the osteoporotic and osteoarthritic groups relative to the control when including; the more porous [181], thinner [182, 229] anterior and posterior sections (circumferential testing) or including the circumferential lamellar and surface porosity (Chapter 6 [279, 282, 283]) of the surface of the bone ('refined' testing). However, when indenting samples machined from the inferomedial cortex the indentation properties are consistent across groups.

The effect of the structure of the cortical bone, namely porosity, on indentation depth are observed through negative correlation ($r = -0.55$ for IDI, $p < 0.05$) with proximity to the closest pore and a positive correlation with macro-porosity (i.e. relating to Haversian canals in the µCT samples $r = 0.75$ to 0.93 where significant, $n = 7$). This should be expected, with the porosity of cortical bone being up to 30% and the Haversian canal diameter being approximately 100 µm to 300 µm [181], which is comparable, typically larger, than the indent dimensions (mean diameter of 160 µm and mean depth of 55 µm). Therefore, the likelihood of indenting close to a pore and of this influencing the indentation depth are high and account, to some extent, for the high variability (30% to 50% from Chapter 5 and Chapter 6) in the technique.

Though porosity also influences the bulk properties of the bone such as fracture mechanics and elastoplastic properties, it would be expected to be more critical in terms of indentation. This is because the volume of interaction is small for RPI (approximately 4 times the indentation depth i.e. 300 µm to 600 µm calculated in the methods chapter (4.1.5) based on the work by Chen and Bull [245]). Furthermore, the comparability to pore size means the effect of structural properties on RPI is more critical compared to the larger volume of interaction in whole sample testing.

As discussed in Chapter 5 and our recent publication [279], below a threshold thickness (0.55 mm, thinner than the cortical bone indented here), the indentation depth

exponentially increases with decreasing thickness. With this, and the influence of porosity and surface structure in mind, it seems clear that bone structure also influences RPI.

Altogether, RPI is a multifactorial measure with influence from elastoplastic, fracture mechanics and structural properties as pictorially represented in Figure 95. The advantage to this combined measure is a potential to assess many aspects of the bone simultaneously with the possibility of detecting variations in each. The disadvantage, however, is direct interpretation of the measure and equivalence to conventional mechanical testing technique with difficulties distinguishing the contributions of the multiple properties being assessed.

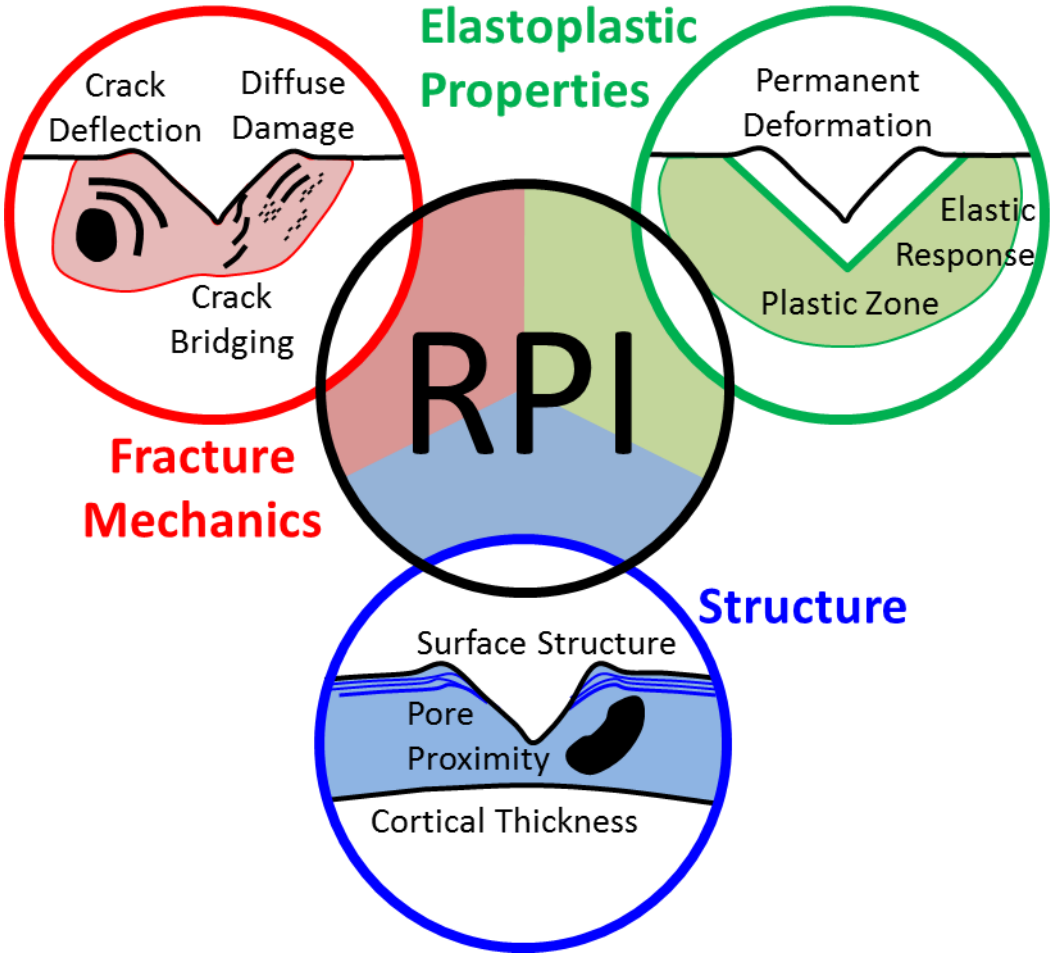

Figure 95 – Contribution of elastoplastic, fracture and structural properties to the RPI measured indentation depth

7.4.3 Properties of healthy and diseased bone

Though the material properties of bone have been measured to deteriorate with age (i.e. strength, stiffness, toughness, and fracture toughness reduce by 1% to 9% per decade [118, 162, 163, 179, 295]), there is surprisingly little evidence of changes in material properties with disease. In terms of osteoporosis and fracture, Dickenson et al [185] showed a lower elastic modulus, strength and plastic energy absorption with disuse osteoporosis through tensile testing of samples machined from the femoral midshaft of cadaveric bone. Additionally, Milovanovic et al [28] showed a higher (though not significant) RPI indentation depth in fractured than non-fractured cadaveric tissue from the superolateral femoral neck. In terms of fracture toughness, we are not aware of any publication that directly compares osteoporotic bone to healthy controls.

There is similarly limited report of changes in material properties of osteoarthritic cortical bone, again particularly in terms of fracture toughness. Li and Aspden [224] find the calcar of the femoral neck to have similar ultrasound assessed stiffness in osteoarthritic, osteoporotic and healthy tissue but the study of the material properties in osteoarthritic bone principally concern subchondral or trabecular and not non-epiphyseal cortical bone [222, 224, 290].

Here, we show correlation with decreasing material properties, the strain energy release rate or J-integral, of the inferomedial femoral neck (growth toughness reduces by 1.0% per decade, not significant and fracture toughness by 7.0% per decade, $p < 0.05$) with increasing age from 33 to 97 years. This reduction in fracture mechanics properties is comparable to the 14% reduction in growth toughness and the 43% reduction in initiation toughness from 25 to 74 years (equivalent to 2.9% and 8.8% per decade) observed by Koester et al [179] and higher than the 3.0% to 4.1% reduction per decade measured by Zioupos and Currey [296]. Discrepancies, in part, may relate to the orientation of the bone with our study utilising the longitudinal ‘separating’ mode (crack propagation around osteons) which has been shown by Katsamenis et al [256] to be more comparable to the longitudinal ‘splitting’ mode (crack propagation along osteons) utilised by Nalla et al [163] rather than the transverse ‘breaking’ mode (crack propagation through osteons) utilised by Koester et al [110, 179] or Zioupos and Currey [296]. As a result, our findings are also similar to the 40% reduction in initiation and growth toughness observed by Nalla et al [163] over a 34 to 99 year age range (i.e. 6.1% per decade).

Furthermore, the sample location is likely to have an influence on this age-fracture toughness relationship with this study considering the femoral neck rather than the midshaft of the humerus [163, 179], femur [296] or tibia [179]. Brown et al [297] found that the femoral neck had a higher fracture toughness but that there was only a significant correlation with age in the tibial and femoral diaphysis. The fracture toughness results of our study are more comparable to the measurements at the midshaft than femoral neck by Brown et al [297]. However, there is limited research into the fracture toughness of the femoral neck and our presented results are additionally within the range shown by Yeni and Norman [298]. Discrepancies may relate to sample geometry (using single edge bend here rather than compact tension), location (inferomedial only rather than posterior and inferomedial) or crack direction ('separating' used here rather than 'splitting'). Though the gradient of this slope is similar between our study and the literature, the correlation with age is somewhat reduced ($r = -0.36$ here, albeit in a larger number of samples, compared to -0.87 to -0.92 [163]) implying other clinical risk factors (e.g. fracture risk factors such as sex, height, smoking etc.) are additionally influencing the fracture toughness.

Despite the reduction in fracture toughness with age over the three groups, we also present an increase in crack growth toughness when the control group is presented alone (stress intensity toughness increases by a not significant 18.1% per decade and strain energy release rate toughness increases by a significant 9.6% per decade). Though this is contrary to the reduction in fracture toughness with age discussed above [24, 163, 179], this most likely relates to the majority of these donors being over a short age range with 8 of the 10 donors aged between 58 and 65 years. That is, in these younger donors there is a two fold increase in crack growth toughness 'per decade' but this is only over a 7 year range implying the trend does not really relate to the age, which remains relatively constant across these donors.

Furthermore, there is a stiffening of the bone with age, represented as an 18.3% increase in elastic modulus per decade. Though this is contrary to the 1% to 2% reduction in stiffness per decade reported by Burstein et al [162] or Zioupos and Currey [296], the correlation is again reasonably low in this study ($r = 0.40$) implying other fracture risk factors are also influencing this correlation. Additionally, the stiffness calculated by Burstein et al [162] is a tensile modulus of the tibial and femoral midshaft whereas this

study extrapolates a bending modulus from notched samples in the femoral neck (as described by Katsamenis et al [256]). Though Zioupos and Currey [296] do calculate a flexural modulus, this is still based on the femoral midshaft. Therefore, either the notched samples are not suitable to derive an elastic modulus or this region of the femoral neck may indeed preferentially stiffen with age, perhaps contributing to increased brittleness and fracture risk.

The minimal correlation between fracture toughness and age may relate to confounding factors (e.g. variability in storage condition, test location or clinical fracture risk factors) as discussed in Chapter 6 but may also relate directly to the site being investigated, the inferomedial femoral neck. As far as we are aware, no study has previously presented the alterations in fracture toughness properties in this site with age or disease and it is possible that the bulk properties of this section of cortical bone is therefore mostly unaffected by differences in the overall fracture risk of the bone. This consideration is further supported by limited differences between the osteoporotic, osteoarthritic and control groups, both in terms of indentation depth and fracture toughness properties. Specifically, the differences between the crack growth toughness, fracture toughness and indentation depth across the osteoporotic, osteoarthritic and control groups are generally not significant (a marginally higher osteoarthritic TID being the exception) and in all cases are minimal (less than 20%).

Milanovic et al [28] found a not significant 12.0% higher TID and 20.5% higher IDI in the superolateral neck in hip-fracture donors and Koester et al [179] found a 30% reduction in initiation toughness but no significant difference in crack growth toughness with diabetes in the tibial and humeral midshaft. With limited number of findings in mind, it is possible that the bulk material properties of the cortical bone in the inferomedial femoral neck are not different in disease. Supporting this, Poole et al [182] found the cortical thickness and BMD of the superoposterior and superoanterior femoral neck (a 76.2% and 60.9% reduction in thickness and a 36.4% and 23.4% reduction in BMD respectively) to be more greatly affected by age than the inferoanterior and inferoposterior regions (a 15.4% and 40.5% reduction in thickness and a 0.7% and 16.7% reduction in BMD respectively). Furthermore, Bell et al [181] showed that the porosity of the anterior quadrant and not any other region was higher in fracture patients. So in addition to the material properties of the inferomedial neck appearing constant with disease, the structural properties are

also maintained. Rather, the structure, and therefore perhaps the material properties, of other regions of the neck are different with bone disease.

Furthermore, the volume of interaction is still small for fracture toughness relative to the pore size (relating to the 1 mm to 1.5 mm cross section less the 0.3 mm to 0.6 mm pre-notch, i.e. sub-millimeter). Therefore, the pre-notch may not be the largest defect and the porosity may also have a greater effect on the crack initiation and resulting fracture mechanics than anticipated. This would increase the non-linearity of the samples, already greatly influenced by the large plastic zone (250 μm to 1.6 mm calculated in the methods chapter (4.2) based on Gao et al [56] and the ASTM standard [255]). Therefore, it is possible that the fracture toughness is not the driving property in these small samples or indeed in the thin cortex of the femoral neck (approximately 0.5 mm on the superolateral side to 4 mm on the inferomedial side [182, 229]) where porosity and the plastic zone will likely be influential.

The exception to the constant material properties of the femoral neck is a higher stiffness in the osteoporotic relative to control group (from 7.52 GPa to 8.92 GPa, 18.6% higher based on individual measurements and from 8.22 GPa to 9.0 GPa, 9.5% higher based on donor measurements). This may relate to two donors with higher elastic moduli (20.6 GPa and 21.9 GPa), but, apart from one donor having had a hysterectomy and only having two test specimens included in their analysis, there is no clear reason to exclude these donors as outliers. Though we are again not aware of research into the differences in elastic modulus measurements of the femoral neck with health and disease, due to the previously reported reduction in stiffness with age [162], a lower stiffness of the osteoporotic group would perhaps be expected. However, it is possible that stiffer bone is consequently more brittle or inhomogeneities and variation in the properties of other areas of the femoral neck contribute to the increased fracture risk associated with this group.

Furthermore, the variation in the derived elastic modulus across specific samples supports the need to calculate an elastic modulus per sample through the technique used here (an FE derived approximation by Katsamenis et al [256]) or nanoindentation [110, 179] rather than using a constant value for conversion of a J-Integral to K-effective values.

Despite the similarities in material properties of the bulk inferomedial cortex with 'health', ageing and disease, the indentation depth of the surface of the inferomedial cortical bone and the total femoral neck are still elevated in the osteoporotic group and further still in the osteoarthritic group as presented in Chapter 6. This implies that there are differences in the structural or material properties of the anterior/posterior regions and differences in the outer surface of the bone that are not apparent in the bulk material properties of the inferomedial cortex. Again, this corresponds well with the increased porosity [181] and reduction in thickness [182] with age and disease away from the inferomedial femoral neck as well as our previous finding that machining of the bone's surface significantly influences indentation depth (Chapter 5 [279]). If surface indentation or indentation in a close proximity site is not representative of the bulk material properties of the bone, this again raises the question of what property RPI is really assessing and how representative this measure can be of the whole bone and fracture risk. Interpreting the higher indentation depth in osteoporotic and osteoarthritic bone in Chapter 6 may therefore relate more to structural and surface properties than bulk material properties.

The property being assessed by RPI also appears to be influenced by disease. There is negative, in places significant, correlation with elastic and fracture mechanics properties in both osteoporotic and osteoarthritic disease states ($r = -0.25$ to -0.56), which is in contrast to a generally positive, albeit not significant correlation in the control group ($r = 0.23$ to 0.58). Though the positive correlation with indent size during indent imaging (i.e. volume, area, depth and diameter) is consistent across both osteoporotic and the control group, the number of samples is generally too low to assess whether the contribution of cracking and pore proximity to indent depth is group dependent. Therefore, it is possible that in diseased bone with a greater extent of cracking, the fracture toughness is more influential than in fracture-resistant control bone. In this case, relating RPI indentation depth to a material property would again be difficult as the relationship would vary with health and disease.

Further difficulties in interpreting the RPI measurements stem from the variation in repeat indents and a single measure not being representative of the bone. This is demonstrated by the reverse trend comparing the groups (higher indentation depth in the control group) with the individual imaged indents compared to the surface measures (higher indentation depth in the osteoporotic group) or machined samples (equal

indentation depth in both the osteoporotic and control groups). This evidence further supports our results from the previous chapter and publication (Chapter 5 [279]) along with recommendations from Randall et al [20], that a single indentation measurement is not representative and repeat measurements are essential. The factors that appear to be influencing the difference between osteoporotic and control group in these individual indentation measurements is a higher porosity in the control group and hence a lower proximity to the nearest pore. Furthermore, this appears to lead to a higher crack length and indent diameter, hence explaining the higher RPI measured indentation depth. The higher porosity in the control group is also contrary to previous evidence of increased porosity with osteoporosis [181] and may relate to the inclusion of only macro-porosity (Haversian canals and not lacunae) or the small sample area selected (approximately 400 µm x 400 µm x 120 µm) considered.

Finally, as we have discussed, bulk material properties are not altered with disease in the inferomedial femoral neck, and though an individual indentation may detect differences between osteoporotic and control bone, this single measurement is not representative.

7.4.4 Limitations of Reference Point Microindentation

The main limitations associated with this study are similar to the confounding factors discussed extensively in Chapter 6. The osteoporotic sample are still from significantly older samples with a higher proportion of female donors but the effects of age and sex between groups have not been considered in this chapter. This is because the number of donors in this chapter is reduced and therefore linear regression to adjust for confounding factors would be applying severe scrutiny, to already generally not-significant differences between cohorts. The effects of freezing and storage conditions are likely to be reduced in this study because only 'batch 1' osteoarthritic samples have been included and these have comparatively similar storage durations to the osteoporotic group. The difference between the diseased (short-term) and cadaveric control (long-term) sample storage has been discussed to have minimal influence (Chapter 6). However, though freezing has minimal effect on stiffness [287, 288], the effect on fracture toughness is unknown. It may be possible that fracture toughness has been artificially reduced in longer-term storage of the control group, leading to the not-significant differences observed here. This is speculative as these factors have not been considered in the analysis.

Sample location is likely to be the largest confounding factor, effecting indentation depth of the femoral neck (discussed in Chapter 6) and with properties varying circumferentially around the neck [181, 182, 229]. Though consistency in specimen location was the target, the necessity to machine regular samples from cortical bone limited the location to the thickest, least curved area of inferomedial femoral neck. Particularly, as differences in the material properties of the femoral neck are minimal, but the indentation properties of the anterior and posterior regions appear to be higher with disease, fracture toughness and its differences with disease may additionally vary with site. Therefore, perhaps the material properties of anterior, posterior or superolateral region may be more greatly affected by disease, but our ability to prepare specimens from these sites precluded their analysis in this study.

When imaging individual indents, as mentioned, it is possible that the μCT measures are affected by the time between indentation and imaging and a potential intrinsic repair mechanism within the bone [115]. Additionally, all the imaging techniques involved dehydration of the bone, either in air or ethanol. This dehydration could enhance the effect of cracking seen here and cause new cracks to appear.

Though the area highlighted by the staining technique was shown to be extremely indicative of cracking through comparison with μCT, PLM and AFM, the automatic segmentation of the image stack overestimated this damage extent, including staining areas associated with structural features other than the indent (i.e. canals and porosity). Therefore, this technique would benefit from further development (or manual segmentation of the whole image stack) to ensure the relationship with RPI assessed indentation depth and microdamage extent is valid. Furthermore, the small number of indents imaged required combination of the μCT and fluorescence microscopy techniques that, in places are not completely comparable (i.e. assessing length of linear microcracks compared to approximate radius of a damage volume). Therefore, further indent imaging would improve the conclusions drawn.

7.5 Conclusion

This chapter can be summarised in terms of two main findings relating to investigation of: the properties assessed by RPI and differences in material properties of the femoral neck.

It has been found that RPI is not directly indicative of fracture mechanics properties or indeed any one material property as previously suggested but rather this contributes a small proportion to the measured indentation depth. Consequently, a single RPI measurement is not indicative of the properties of the bone. Instead, the indent size (i.e. elastoplastic properties), the proximity to pores (i.e. structural properties) as well as the extent of cracking (i.e. fracture mechanics properties) all contribute approximately equally to RPI measures. This mixed-mode measurement would therefore require further developments (e.g. consideration of the different indentation parameters, different probe tip geometries or combination with high resolution imaging), to disentangle the different contributing properties. If this were possible, RPI could be an extremely useful technique for probing elastic, plastic, fracture mechanics and structural properties of bone but in its current form, interpretation is difficult.

There is some reduction in the fracture toughness and increase in stiffness of the bone with age. However, even though the surface indentation properties of the inferomedial neck and femoral neck as a whole are higher with disease (Chapter 6) this does not generally translate to the bulk properties of the inferomedial cortical bone which are not different in osteoporosis or osteoarthritis. This consistency in material properties across the diseased and healthy cohorts is confirmed through RPI, fracture mechanics and derived elastic properties. Even though this location appears unaffected by disease, this is a significant contribution to understanding osteoporosis and osteoarthritis where, primarily, only age related effects have been investigated.

Though this thesis raises many further questions (e.g. ‘how can multifactorial RPI results be interpreted?’ or ‘what properties of the bone are altered by disease?’) a large step has been made towards understanding both RPI and the effects of osteoporosis and osteoarthritis on cortical bone.

8 Discussion and Conclusion

8.1 Summary of Thesis Outcomes

The main aim of this thesis was to improve the understanding of biomechanical differences in bone quality, as assessed through reference point microindentation and fracture resistance measures, with disease. Further, the aim was to establish whether these measures, assessed by RPI, can contribute to an improvement in fracture risk assessment.

Because RPI is an emerging technique with limited associated validation, the starting point for this thesis was to establish a protocol for use of the tool. By varying different indentation testing parameters (primarily: maximum load, mode of use, sample orientation, sample preparation and measurement spacing) the effect on indentation depth and its coefficient of variation was observed. Based upon this variation, an optimised testing protocol was established to advise other users and our subsequent experimentation for consistent testing and awareness of variability.

This optimum protocol was then applied to the main clinical study; indenting cortical bone of the human femoral neck, the core of this thesis. Reference Point Microindentation discriminated well between both osteoporotic fractured and osteoarthritic bone from 'healthy' cadaveric control with no history of bone disease. Furthermore, RPI was shown to be distinct and complementary to existing BMD and clinical risk factors and we demonstrated a potential to improve fracture risk assessment by supplementing current techniques. However, there were difficulties in interpreting the RPI results due to; reduced discriminative ability in the inferomedial neck, general similarities between osteoporotic and osteoarthritic bone and high variability.

To overcome uncertainties due to the novelty of RPI, the material properties in osteoporotic, osteoarthritic and cadaveric control bone were further examined through fracture toughness testing of the inferomedial femoral neck (where the thickness was sufficient to machine samples). The elastic, fracture and indentation properties demonstrated similarities between osteoporotic, osteoarthritic and cadaveric control bone. Though it is widely assumed that material properties of the bone are compromised by osteoporosis, the literature only demonstrates an age effect. Therefore, we conclude

that bone disease actually has minimal impact on the bulk material properties of the inferomedial neck whereas other locations may exhibit greater differences. Additionally, to better interpret RPI results, they were compared to the fracture mechanics properties and individual indents were imaged. Through this, it was found that fracture, elastoplastic and structural properties all contribute to RPI to a similar extent, with the technique not being directly indicative of any one measure. This makes the technique promising for assessing bone quality properties but currently compromised in terms of directly understanding the properties assessed.

A detailed summary of the main outcomes of each results chapter are highlighted as follows:

8.1.1 Variability associated with Reference Point Microindentation and Recommendations for In Vitro Testing

The variability associated with RPI could be established to provide recommendations for optimised testing with reduced variability as follows.

- The chapter recommends a best practice of: repeating measurements, using the fixed mode of use, removing the periosteum, machining the bone's surface, ensuring sufficient thickness (10 times indentation depth), keeping spacing above 500 μm and avoiding previously indented areas.
- A relationship with indentation depth was found between: maximum load, mode of use and surface preparation and so these were recommended to be kept consistent throughout testing.
- There did not appear to be a relationship between indentation depth with: sample orientation, machining depth, or thickness and measurement spacing above the given thresholds so no recommendation was given for these measures.

8.1.2 The Potential of Reference Point Microindentation for Improved Fracture Risk Assessment

The clinical potential of reference point microindentation could be established through comparison between cortical bone tissue of the femoral neck with and without bone disease (osteoporosis and osteoarthritis).

- RPI can discriminate between healthy and diseased bone when testing the femoral neck inclusive of the inferomedial, anterior and posterior regions. The mean indentation properties in this region of the femoral neck are different in both osteoporosis and osteoarthritis compared to cadaveric controls.
- RPI measures a property distinct from current fracture risk assessment tools in terms of vitamin D, calcium, BMD and FRAX
- RPI can supplement existing BMD and FRAX measures for improved discriminative ability between tissue with and without bone disease and hence has potential for complementary fracture risk assessment.
- The discriminative ability of the tool is site dependent. In the fractured group, the indentation depth is higher than controls when incorporating the inferomedial, anterior and posterior femoral neck but not when focussing on the inferomedial region alone. In contrast, the higher indentation depth in the osteoarthritic group is relatively independent of site implying the changes in bone properties with osteoarthritis are more homogeneous.
- There are no apparent differences between osteoporotic and osteoarthritic bone except in the inferomedial neck where osteoarthritic bone displays deteriorated properties
- Higher indentation depth in osteoarthritic bone is a function of the disease, being elevated further in bone with more severe radiographic osteoarthritic grading

8.1.3 Bone mechanics in health and disease: Investigation into the property assessed by Reference Point Microindentation

Comparison between osteoporotic, osteoarthritic and control bone could be further made alongside assessment of the property measured by reference point indentation through crack growth resistance experiments and direct imaging of the indents.

- The fracture toughness and indentation depth of the bulk cortical bone of the inferomedial femoral neck is consistent in ‘health’ and disease. The osteoporotic fracture bone shows a higher stiffness, albeit marginal. The material properties of this region are therefore largely unaffected by osteoporosis or osteoarthritis.

- The correlation between reference point microindentation and conventional mechanical testing properties is minimal indicating only a slight contribution from fracture mechanics and elastic properties on indentation depth.
- Indent imaging suggests approximately equal contribution of elastoplastic, fracture mechanics and structural properties of bone on RPI measured indentation depth

Overall, the presented research furthers understanding into how RPI should be applied, its efficacy for fracture risk assessment and what properties are being assessed. This greatly adds to the knowledge of an emerging, yet currently limited field through larger studies and systematic investigation into more unreported test variables that have previously not been considered. Furthermore, the efficacy of the technique at the primary fracture site (the femoral neck) and for assessing osteoarthritic bone is established which has not been investigated elsewhere. For the first time, the complementary nature of RPI to BMD and FRAX has been observed through a combined tool with improved fracture risk assessment potential. Understanding of the technique has been enhanced through fluorescence microscopy and AFM imaging that haven't previously been applied to RPI-related microdamage, alongside micro-computed tomography and correlation with conventional mechanical testing. This demonstrates that, though contributory, neither fracture mechanics nor elastic properties are directly represented by RPI and the higher indentation depth in diseased bone may be influenced greatly by surface and structural properties.

Importantly, this study also directly compares diseased (osteoporotic and osteoarthritic) bone to non-diseased cadaveric controls to assess the differences in material properties with disease. The finding that the properties of the inferomedial femoral neck are actually fairly consistent despite disease is a large step to assessing how bone quality is affected with osteoporosis and osteoarthritis where predominantly only age related effects have been previously measured. The discovery highlights that perhaps the assessment of the material properties of the inferomedial femoral neck are not critical and other locations within the bone or aspects of bone quality (e.g. structure or composition) should instead be investigated to improve understanding of bone disease.

8.2 Dissemination of Work

Chapter 5 (Variability associated with Reference Point Microindentation and Recommendations for In Vitro Testing) of this thesis has been published in the Journal of the Mechanical Behaviour of Biomedical Materials. A joint first author article is currently in preparation with Dr Louise Coutts based on the findings of Chapter 6 (The Potential of Reference Point Microindentation for Improved Fracture Risk Assessment) and Chapter 7 (Bone mechanics in health and disease: Investigation into the property assessed by Reference Point Microindentation) is also being prepared for publication. Furthermore, the core work of this thesis has also been disseminated by myself at conferences and symposia internally, nationally and internationally in the form of three podium and three poster presentations.

In addition to the work presented in this thesis, over the duration of the doctorate, collaborative work and parallel research efforts has produced four journal publications (one published and three presently under review for publication). At least a further three articles will additionally be prepared based on this parallel and collaborative work. This work has also been accepted as conference abstracts in the form of four podium and four poster presentations, primarily presented by the collaborating authors.

‘9.6 Appendix 5 – List of Publications’ details these publications.

8.3 Experimental Limitations

The main limitations associated with the study relate to confounding factors between the three cohorts. Individuals who fracture are primarily more elderly with a generally reduced quality of life whereas to be selected for elective hip arthroplasty the patient must be healthier, typically younger. Furthermore, obtaining cadaveric tissue from donors that have progressed to an older age without developing confounding comorbidities is inherently difficult. Additionally, the storage conditions of the cadaveric tissue and the osteoarthritic tissue from the COASt collaboration could not be as tightly controlled and information on these samples was not as complete as that of the osteoporotic group. The tissue from the osteoporotic group was limited due to the fracture and the tissue retained by the surgeon, typically limiting the test location and number of measurements with porosity and thickness likely to have a greater confounding effect. In the main clinical study (Chapter 6), comparing indentation between osteoporotic, osteoarthritic and cadaveric controls these factors have been adjusted for as best as possible but the inherent differences between groups is still a factor and, additionally, complete information for adjustment of the samples was not necessarily available for all samples. For the comparison of machined samples, no adjustment was performed due to the already limited significance in this study, meaning these factors are also likely to affect the results of Chapter 7.

A second general limitation is the coefficient of variation associated with repeat measurements using RPI (30% to 50%) which is very high in comparison to the conclusions drawn, even where these are found to be significant.

Further specific limitations associated with each study are highlighted below:

8.3.1 Variability associated with Reference Point Microindentation and Recommendations for In Vitro Testing

- The number of samples considered with respect to the variability of the tool. We discussed that more indentation measurements could reduce variability (i.e. 8 to 15 measurements for a 5% to 10% error) but typically only used 3 to 5 measurements (15% to 20% error) were performed on 5 repeat samples. Therefore, some non-significant comparisons (e.g. effect of orientation or coefficient of variation with maximum load) would benefit from further investigation.
- Indentation of the femoral head was used to compare the effects of maximum load in human cortical bone but, due to its thickness, we have recommended against using this site.
- As well as inter-species variability, there are some limitations in terms of directly applying the findings of this chapter to the clinical study:
    - The load-thickness relationship is likely to be influenced by the poor-quality (e.g. osteoporotic) human bone and porosity of the underlying cancellous substrate, implying that a greater thickness (than the 0.55 mm recommended) is required for the 10 N loading.
    - The freehand mode of use when indenting a clamped specimen is not directly comparable with clinical study where the femoral head/neck is also held freehand meaning there could be added variability than that considered

8.3.2 The Potential of Reference Point Microindentation for Improved Fracture Risk Assessment

- The direct clinical relevance of this technique is limited by differences to in vivo testing protocol. The femoral neck is not an accessible site for in vivo indentation testing, indentation would be through soft tissue and repeat measurements and testing area may be limited. Furthermore, the RPI device implemented here (the Biodent) is unlikely to be applied clinically, rather the Osteoprobe II is in development for clinical use. This reduces the translational strength of this study yet does not completely negate it.
- The study is retrospective and cross-sectional with a much higher incidence of fracture than in the general population and speculated RPI thresholds are specialised to the relatively limited number of donors in this study. This acts to artificially improve the discriminative ability described which is likely to be considerably lower for a larger prospective population.
- The number of clinical BMD measurements was limited for the osteoporotic group due to the age and frailty of this group meaning a return hospital visit was not possible in over half of the cases. Furthermore, the comparison between clinical BMD measurements at different time points (pre-operatively in the osteoarthritic group and post-operatively in the osteoporotic group) and their relation to the laboratory derived BMD measures has not been explicitly considered.
- For the most part, the clinical information collected from the osteoporotic and osteoarthritic group (e.g. to derive FRAX score) was based on the information provided by the patient. Though this was supplemented and verified by their medical notes where possible, patient recollection may influence clinical factors.
- Some confounding clinical factors could not be considered such as caffeine consumption, falls risk, vitamin D levels, calcium levels, level of activity and exercise as, though these could be collected for the osteoporotic group, differences in study design of the osteoarthritic group and limited data collection of the cadaveric control, meant these could not be considered in this study.
- The thickness and porosity of each sample and measurement site has, at this stage, not been considered though these are parameters that have been considered to influence RPI.

8.3.3 Bone mechanics in health and disease: Investigation into the property assessed by Reference Point Microindentation

- The location of the machined samples was in the inferomedial femoral neck, taken at a proximal-distal location approximately equivalent to the diameter of the femoral head. However, the effect of the exact proximal-distal, circumferential and cortical depth location has not been considered.
- An elastic modulus value was derived from notched samples meaning this is not necessarily an absolute value and is likely to be influenced by stress concentrations and fracture mechanics of the notch.
- Porosity information was generally not available for the machined fracture specimens (except the seven indented in the μCT study).
- Based on indentation measurements, the material properties are expected to vary circumferentially. Additionally, fractures initiate superolaterally and the thickness of the inferomedial site is maintained with osteoporosis. Therefore, the inferomedial quadrant may not have been the optimal location to observe differences in material properties. Similarly, other orientations (i.e. the transverse breaking mode) may exhibit more difference with disease. However, due to the thickness and curvature of the cortex, other test locations and orientations were infeasible for machining regular notched specimens.
- Some donors only had a small number of samples tested (less than 3 in a number of cases, 1 sample for a single donor) and there was variation between repeat fracture experiments which could introduce anomalous results
- The limited numbers of indents imaged meant that micro-computed tomography and fluorescence imaging technique were, perhaps inappropriately, combined for statistical analysis.
- The automatic damage segmentation of the serial section fluorescence imaging was not optimal and overestimated the extent of the damage compared to manual segmentation.

8.4 Open Questions and Future Work

The findings of this thesis and some of their associated limitations give rise to new research questions to direct future studies and the continued development of bone mechanics and the reference point microindentation technique.

In terms of establishing testing protocols for reference point microindentation, this study goes a long way but further research in a larger number of samples, with increased repeat measurements and in different species (primarily more investigation of human bone) would better establish how the technique should be applied. Of primary interest would be the effects of test location (this has been considered though a parallel research effort), testing of different bones (i.e. the clinical tibial site compared to the femoral neck), sample storage/hydration and the translation to clinical practice.

The clinical study results indicate that the tool can supplement existing clinical factors to improve discrimination between fractured and non-fractured tissue. However, concerns relating to the variability of the device and the risk versus benefit of this minimally invasive tool limit its current clinical potential. Therefore, further examination into influencing factors to reduce the tools variability would be extremely beneficial or potential examination into modification of the device (e.g. effects of tip size and shape). Ultimately, if this tool is to continue its trajectory towards clinical use, a series of large (10s to 100s of thousands of participants to accommodate for the low incidence of fracture in the population) prospective clinical trials are necessary alongside BMD, FRAX and other available fracture risk assessment technique to; establish whether RPI has any ability to predict fracture, establish a clinical threshold, discover potential rare side effects and conclude whether this offers an advantage over current techniques. Certainly prior to testing such a large number of individuals, any detrimental effect of the technique has to be investigated through further imaging of indentation and assessment of the effect of these defects on the mechanical integrity of bone. Furthermore, repeat studies, similar to the one described here but with increased focus on reducing variability, are necessary to establish whether the technique should be continued to the larger clinical trials.

Regardless of the clinical potential, RPI may still be of use in a laboratory environment but this does lead to an increased focus on interpreting the property assessed by the tool and validation of the technique. The study presented here implies that indentation is

multifactorial so further work is necessary to establish how to discriminate between these different contributing properties. For example: Can multiple indents with different shaped probes establish the contribution of fracture, plastic and elastic properties? Can combination with imaging of the indent, damage and surrounding bone be used to calculate representative absolute material properties? Is there a possibility to guide indentation, avoiding pores or targeting bone features to give a more representative measure of the material properties? If such factors could also be applied clinically, the discriminative ability of the tool may be further improved but from a laboratory point of view, this may also detract from the simplicity of the tool, making conventional techniques more appealing.

In terms of assessment of material properties of bone with disease, this study highlights a significant limitation of the existing research and, therefore, substantially more work should be undertaken to understand how disease, and not ageing alone, affects material properties and the mechanisms that lead to fracture. As our research found consistent bulk properties with disease of the inferomedial neck, this asks the question whether surface properties of the bone, as assessed by RPI, are altered rather than the bulk. Additionally, it should be questioned whether other locations rather than the inferomedial neck are affected by disease. Principally, the superolateral neck where fracture initiates and the thickness and porosity of which are more greatly affected by osteoporosis may provide better understanding of the disease if fracture mechanics or other micro-mechanical testing specimens can feasibly be machined. It may even be possible, and needs to be investigated, that increased fracture risk is not governed by changes in material properties of the femoral neck at all and structural or compositional properties may have a greater effect on the overall fragility.

8.5 Epilogue

With an ageing population, bone diseases such as osteoporosis and osteoarthritis are a growing problem. Particularly, the definition of osteoporosis as a disease of impaired quantity and low bone mineral density will need to change. Supplementary factors are necessary to allow for screening and identification of those at risk, as well as improvement in current medication, if the number of individuals sustaining fracture is to be reduced. To this end, the improved understanding of changes in bone quality at the early stage of disease is an essential development alongside clinically viable means of assessing these properties for early detection of disease.

This thesis highlights that the tissue level fracture mechanics and bulk indentation properties of the inferomedial femoral neck may well not be important aspects of bone quality in the progression of disease. However, indentation properties of other locations on the surface of the femoral neck have been shown, for the first time, to be deteriorated in both osteoporosis and osteoarthritis. This technique has also been demonstrated to be, in some part, related to elastoplastic, fracture resistance and structural aspects of bone quality. These bone quality measures have been found to be distinct from current fracture risk assessment techniques with the potential to complement these measures for improved fracture risk assessment.

Even though this thesis has highlighted some limitations with the current embodiment of reference point microindentation for assessing fracture risk, it does highlight the need for improved understanding of bone disease and bone quality and raises some potential of assessing aspects of this in vivo. It is now the role of the bone research community to further the extensive task of systematically reviewing all the multi-scale changes in bone quality with disease and not just ageing alone and to establish means of clinically assessing these for improved fracture risk assessment and diagnosis of bone disease.

9 Appendices

9.1 Appendix 1 – Clinical Assessment of Bone Quality

Returning to our initial definition, bone quality is a measure of any aspect of bone fragility that cannot be assessed by bone quantity (i.e. BMD). Bone's fragility depends on its composition and structure and how these elements work together to provide its mechanical competence over its entire length scale. These properties are not conventionally assessed clinically but the following sections will address novel technique for the assessment of the structural, compositional and mechanical properties – bone quality.

There are many extremely effective laboratory based tools that can assess structural, mechanical and compositional changes in bone from the tissue level right down to the nanometre scale. However, a requirement for sample preparation, a destructive nature, high radiation doses and/or a long scan times are just some of the reasons that preclude these extremely effective measures of bone quality from currently having clinical relevance. Nevertheless, the focus towards clinical fracture risk assessment of bone quality to overcome current limitations, has led to the emergence of some techniques with the clinical potential to assess bone's structural, compositional and mechanical properties in vivo.

9.1.1 Structural Assessment of Bone Quality

Bone quantity as measured by BMD is essentially a measure of structural bone quality at the tissue level. However, in terms of our definition and clinical assessment, it should be thought of distinctly to allow for current techniques to be built on and supplemented. Assessment of bone's structure at this and lower hierarchical levels is being investigated with emerging technologies with clinical potential for assessing bone quality.

9.1.1.1 Peripheral Quantitative Computed Tomography

There is some interest in taking measurements of the peripheries (i.e. radius, tibia or calcaneus) as opposed to the core (hip and spine) as this can provide a solution that is less expensive, more mobile and supplying a lower dose of radiation. These peripheral measurements can give some indication of general susceptibility to fracture with a low BMD measurement at the radius indicating a 80% increased risk of hip fracture, however,

the site of interest is a better predictor and a low BMD measurement at the hip indicates a 160% increased risk of hip fracture [9, 189].

As BMD measures a density per area, not accounting for the volumetric loss of bone, pQCT (peripheral Quantitative Computed-Tomography) has been employed to measure the volumetric BMD, particularly of the radius or tibia. pQCT involves a coupled source and detector that rotate to image a 1 - 2.5 mm slice [188] but supplies a higher dose of radiation (30 – 100 μSv), though this is at a peripheral rather than core site. The resolution is improved with pQCT but the precision and accuracy are marginally less than DEXA with some correlation between BMD values measured by the two ($r = 0.75$) [188]. Though pQCT also measures other characteristics of bone which will be discussed later, its volumetric BMD (vBMD) measure alone is less effective than the areal BMD (aBMD) for diagnosis, relating to the size effect. For a given vBMD, bones with a larger cross sectional area will have a higher aBMD and, for the hip, aBMD also relates to height and hence femoral neck length whereas vBMD does not [299].

The size effect explains the reduced ability to differentiate fractured and non-fractured bone found by the BMD value of pQCT compared with DEXA. Therefore, vBMD may give a truer representation of BMD but excludes parameters associated with the size of the bone and hence relating to fracture risk. Formica et al [191] compared the techniques to find the ROC is lower for pQCT (0.81) than DEXA of the radius (0.89) for predicting hip fracture. These ROC values were site dependent with Formica also giving values of 0.69 (pQCT) and 0.79 (DEXA) when considering any fracture and Majumda et al [190] similarly finding 0.69 for pQCT compared to 0.73 for DEXA. These low values for DEXA relate to the large number of unpredicted hip fractures found by Schuit [11] and Siris [10] so pQCT would be expected to have an poorer detection rate still. Therefore, BMD calculated by either means, DEXA or pQCT (areal or peripheral volumetric), is insufficient as a sole parameter to predict fracture.

The typical clinical assessment of bone quality relates to histomorphometry, the observation of structure and how this varies. Bone turnover markers, discussed above, aim to observe this at the cellular level looking at cell number, but through observation or computer analysis of imaging techniques (or alternatively biopsied samples), observations can also be made at the tissue level [300]. As these parameters, such as bone volume,

trabecular number, wall thickness etc., vary with age and disease, they can be useful parameters to measure [183, 300]. pQCT, in addition to its BMD measurement, can be used to create a three dimensional image of the bone allowing for differentiation between the cortex and trabeculae, measurement of geometry and structural properties, histomorphometry at the tissue level [188, 260]. Additionally, these parameters can be used to approximate mechanical properties of the material, the stress strain index correlates extremely highly (r = 0.99) with stiffness values found through mechanical testing (though only of eight rabbit humeri) [301]. Despite this measurement of mechanical properties and structure, the specificity is still poor, most likely relating to stiffness not correlating as strongly to fracture risk as other mechanical properties [162] and measurement only being able to be made peripherally (due to the radiation doses) and not at the hip. Additionally, only structural properties of the tissue level bone are being assessed whereas the overall mechanical properties will also rely on structural and compositional changes at lower levels. Nevertheless, pQCT can measure both bone quantity and quality so is promising as an osteoporotic diagnostic tool if improvements can be made.

9.1.1.2 Quantitative Ultrasound

Though the doses of ionising radiation to the core are relatively low in both DEXA and pQCT, radiation free alternatives are being considered. One such alternative is quantitative ultrasound (QUS), which, like QCT is typically a peripheral measure but, in this case, of the calcaneus rather than radius or tibia. Though the propagation of the sound wave is affected by other material properties as well [260], this is also thought to depend in part on the density of the bone and is therefore compared with the x-ray propagation of DEXA. Hans et al [187] and also Pluijm et al [302] found that the output measures of QUS, the broadband ultrasound attenuation (BUA) and the speed of sound (SOS) both have an approximate doubling in fracture risk with every standard deviation reduction, similar to DEXA. Hans [187] found that the effect on fracture risk was eliminated for SOS when controlled for BMD but still apparent for BUA. This implies SOS to be related to density but BUA to be an additional measure.

A review by Gregg et al [303] agreed with Hans that there was some correlation between DEXA and QUS but this was minimal (r = 0.4 - 0.7). Nonetheless, QUS was still no better at

discriminating fractured and non-fractured, still with a ROC value between 0.72 and 0.85. Gregg's review [303] also found the precision of QUS to be reduced relative to DEXA.

As well as calculating a BMD type value, QUS directly assesses aspects of bone quality. QUS (shown in Figure 96) uses ultrasound that, unlike the x-ray radiation with DEXA, mechanically interacts with the tissue. As well as being absorbed it also scatters due to the microarchitecture and inhomogeneity [303] and therefore may relate to the strength and elasticity [260, 303]. Cook et al [196] found correlation between the parameters measured at the calcaneus by QUS (e.g. BUA and SOS) to have some correlation with toughness and strength (r = 0.46 to 0.84). Additionally, Qin et al [304] found correlation between BUA and the strength and modulus (r = 0.67 - 0.80) and structural properties of the trabeculae (r = 0.61 - 0.88). Though this means of measurement is no more able than DEXA for differentiating between fractured and non-fractured bone (having similar ROC values) by incorporating both parameters together, 30% of individual's risk level was reclassified and the ROC level was increased, albeit only by 2 - 3% [305]. Therefore, QUS seems to measure some structural and mechanical properties of bone and hence marginally improves the definition based on quantity alone. However, a measurement with better correlation with bone quality through more direct assessment of the mechanical properties might be expected to further improve this definition.

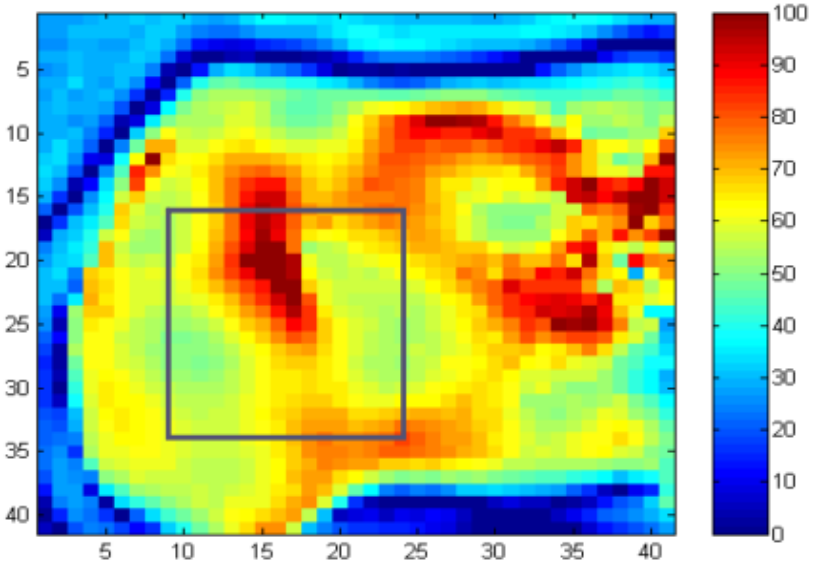

Figure 96 - The distribution of ultrasound signal attenuation (BUA) when transmitted through human cadaveric calcaneus. Image reproduced from Qin et al [304] courtesy of Springer

9.1.1.3 Magnetic Resonance Imaging

Another clinical imaging technique, MRI (magnetic resonance imaging) does not use radiation but strong magnetic fields to orientate the atoms within the body then release them back to their natural state. Atoms in different tissues take different times to revert and, in this way, the type and structure of the tissue can be identified at extremely high (0.1 mm) resolutions [260, 306]. Such an accurate model can then be loaded into FEA (Finite Element Analysis) software and mechanical testing can be computationally simulated [14]. Majumdar et al [190], using MRI, measured structural properties finding trabecular number, trabecular spacing and bone volume to be the best differentiators of fractured and non-fractured tissue. On their own, the ROC value of the histomorphometric parameters wasn't particular high (0.62 to 0.78), in-line with DEXA (0.73) but when combined with BMD as measured by DEXA, this increased (up to 0.80 to 0.87).

Though this is an expensive and timely means of assessing bone quality, the structural properties measured by MRI do prove useful showing histomorphometry, as a measure of bone quality, to be beneficial in osteoporotic diagnosis.

The data from MRI scan, as well as other high resolution volumetric imaging techniques including HR-pQCT (high resolution peripheral quantitative ultrasound with resolution of 300-500 μm) can also be directly fed into finite element models [306]. This allows for the simulated application of a variety of in vivo loading conditions to predict the response of the bone's structure to loading, its stiffness and strength. This modelling improves the ability to detect bone strength showing some ability to discriminate between vertebrae in fractured and non-fractured individuals (Figure 97) [307].

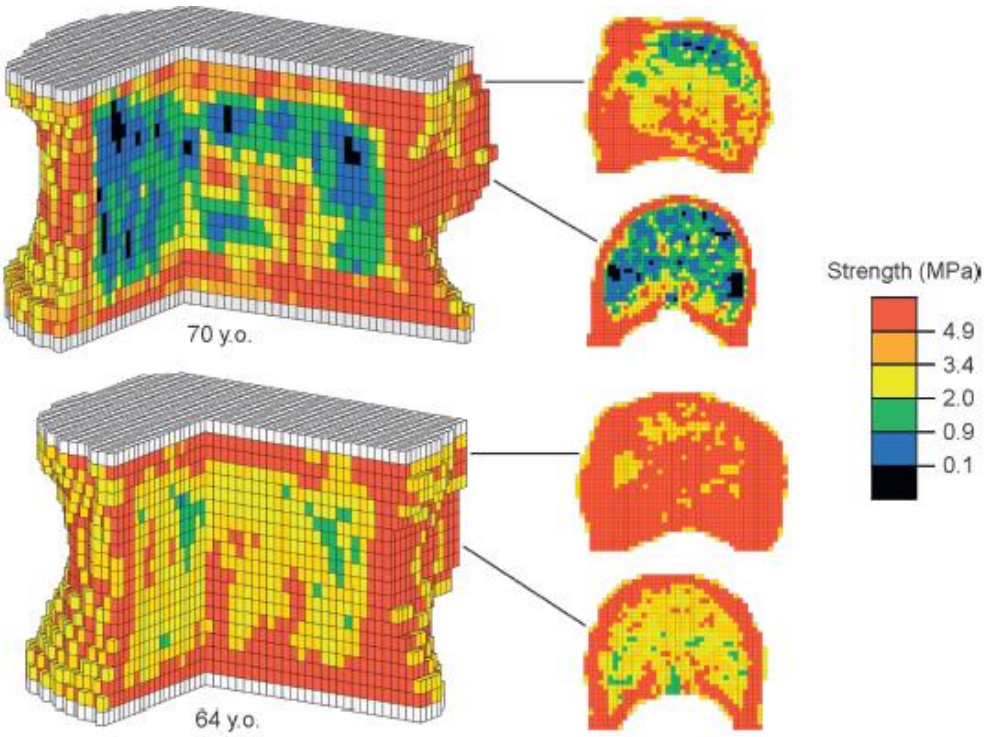

Figure 97 – Voxel based Finite Element Model of the lumbar vertebrae based on quantitative computed tomography imaging. Image reproduced from Melton et al [307] courtesy of John Wiley and Sons

9.1.2 Compositional Assessment of Bone Quality

Assessing the structure of bone is an important aspect of bone quality and this can be used as a predictor of mechanical properties. Even an infinitely detailed model of the bone's structure would still not be able to completely predict the mechanical properties of bone as it would be lacking this compositional element.

9.1.2.1 Raman and FTIR Spectroscopy

FTIR (Fourier Transform Infrared) and Raman spectroscopy are vibrational techniques used at the mineral and crystal level. A light beam is emitted (from an infrared diode in FTIR and laser in Raman), the energy of which excites the sample's surface. Each different molecule present has a unique vibrational mode depending on their atoms and bonding which shifts the energy of the beam, indicating which molecules are present by peaks at different frequencies [14]. These techniques can therefore unravel the composition of the bone at the molecular level as shown in Figure 98 [163, 171-173].

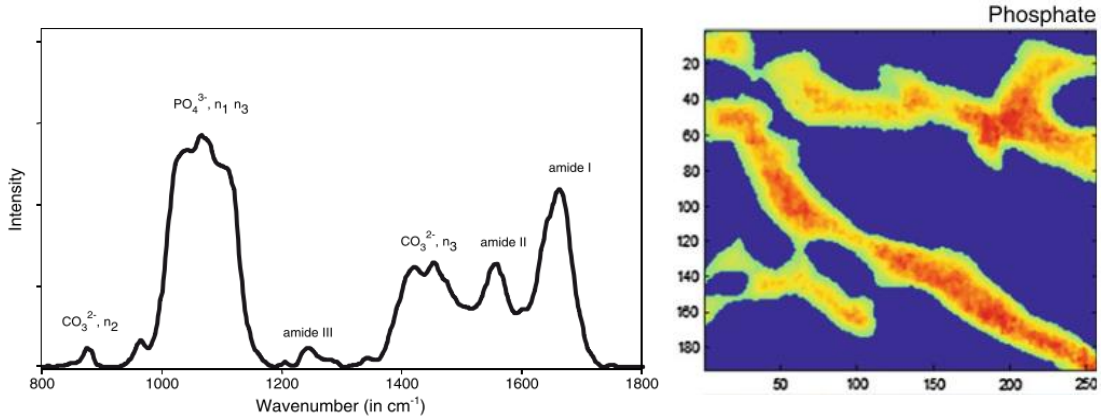

Figure 98 –FTIR spectroscopy showing: Left - The atoms and bonds present (corresponding to the organic and inorganic composition) and Right – The distribution of one of these peaks (Phosphate) in cancellous bone. Image reproduced from Chappard et al [14] courtesy of Springer

Both FTIR and Raman spectroscopy have shown the ability to detect age and osteoporosis related changes in bone including changes in the mineral to matrix ratio, mineral crystallinity, carbonate to phosphate ratio and collagen quality [308, 309]. However, it is only Raman spectroscopy that has shown clinical potential with the ability to test sub-surface tissue. Through use of a fiber-optic Raman probe that is spatially offset from the laser point, SORS (Spatially Offset Raman Spectroscopy) is able to vary the relative contribution of the surface and subsurface tissue [310]. Though there is still background noise from the soft tissue, this can be largely negated giving a measure of the compositional properties millimetres below the surface of the sample. This can allow for measurements through soft tissue in areas where bone is close to the surface and can be achieved with a clinically safe low intensity beam (2 mW) with a 200 second scan (for 1 measurement point).

This technique therefore shows the potential for clinical assessment of the bone's composition and hence the measurement of factors that vary with age and osteoporosis.

9.1.3 Mechanical Assessment of Bone Quality

Bone quality is certainly dependent on compositional and structural properties of bone but these are not truly of concern when considering fracture risk. It is how these aspects affect the mechanical properties of the bone that is of principal importance. Essentially this is what the term 'bone quality' really refers to. The composition and structural properties make up the mechanical properties at each level of bone's hierarchy and these in turn make up the overall quality of the tissue. There are limited (two) tools that have been proposed for the assessment of bone's mechanical properties in vivo.

9.1.3.1 Mechanical Response Tissue Analysis

Djokoto et al [311] looked at MRTA (Mechanical Response Tissue Analyser), a tool that was initially developed by NASA to measure bone loss in astronauts (shown in Figure 99). This uses an electromagnetic oscillator to apply low frequency vibrations to the body (typically at a site with little soft tissue, i.e. the forearm) to measure its mechanical response. This was found to correlate with DEXA measures (r = 0.6 - 0.8) but not QUS. Like pQCT, this measures bending stiffness but, unlike pQCT, this measurement is done by direct mechanical testing rather than approximations made based on the structure. Even in this case, stiffness is not the most useful mechanical measurement and a predictor of fracture resistance would be more useful for assessing the bone quality and fracture risk.

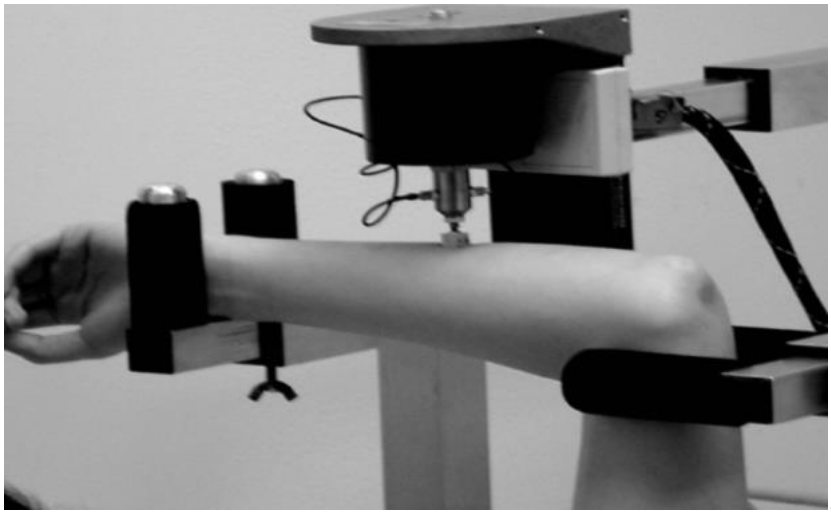

Figure 99 - Mechanical Response Tissue Analyser testing of the ulna. Image reproduced from Djokoto et al [311] courtesy of Elsevier

9.3 Appendix 2 – Additional Figures for alternate RPI measures

This appendices has been published as part of a journal article by the author (Jenkins et al [279]) and reproduced here with permission from Elsevier

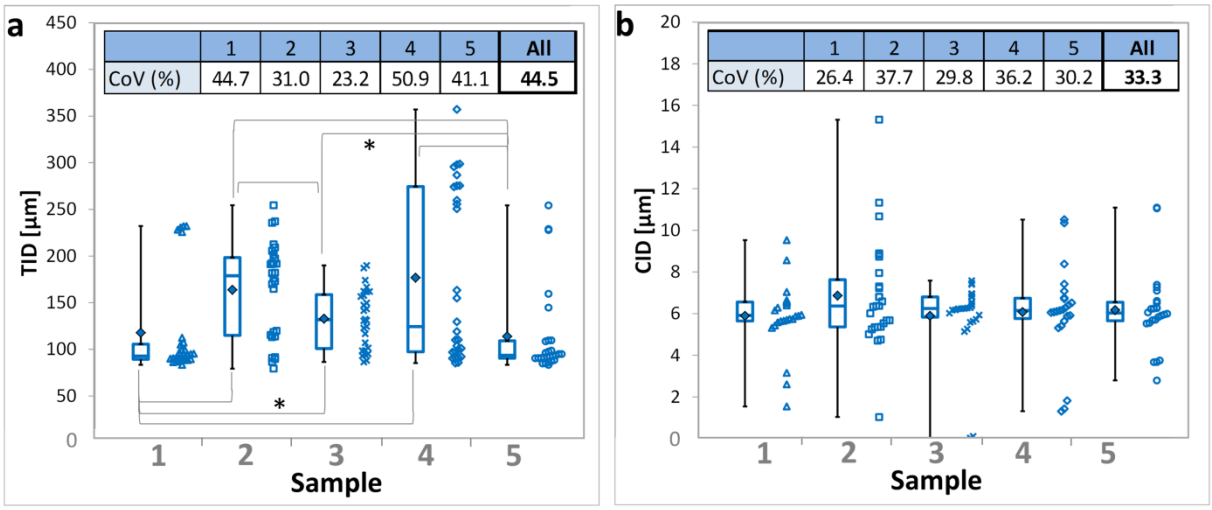

Figure 100 : The coefficient of variation (CoV) and distribution of repeat measurements in five bovine samples. a) TID and b) CID. The graphs display the individual measurements, a box plot (the median, upper quartile, lower quartile and range) and the mean (diamond). Differences between samples are displayed as significant (* p < 0.05) or close to significance (# p < 0.1, not applicable).

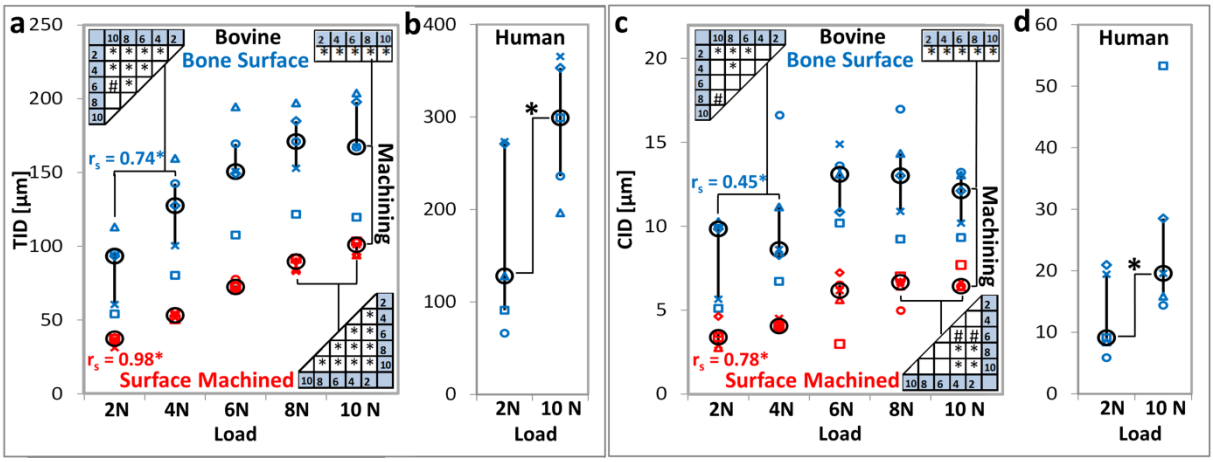

Figure 101 : Variation with maximum load on bovine bone (a and c) and on the human medial femoral head with the cartilage removed (b and d). a) and b) TID and c) and d) CID. Results are displayed as significant (* p < 0.05) or close to significance (# p < 0.1) and the graphs display mean values for each sample (each marker representing a different sample) as well as the median and interquartile range across the five samples. a) and c): r_s is the Spearman's correlation. The rectangular table displays the level of significance between the non-machined and machined bone at each different load. The triangular tables display the level of significance between the different loads for the bone's surface (top left) and machined surface (bottom right).

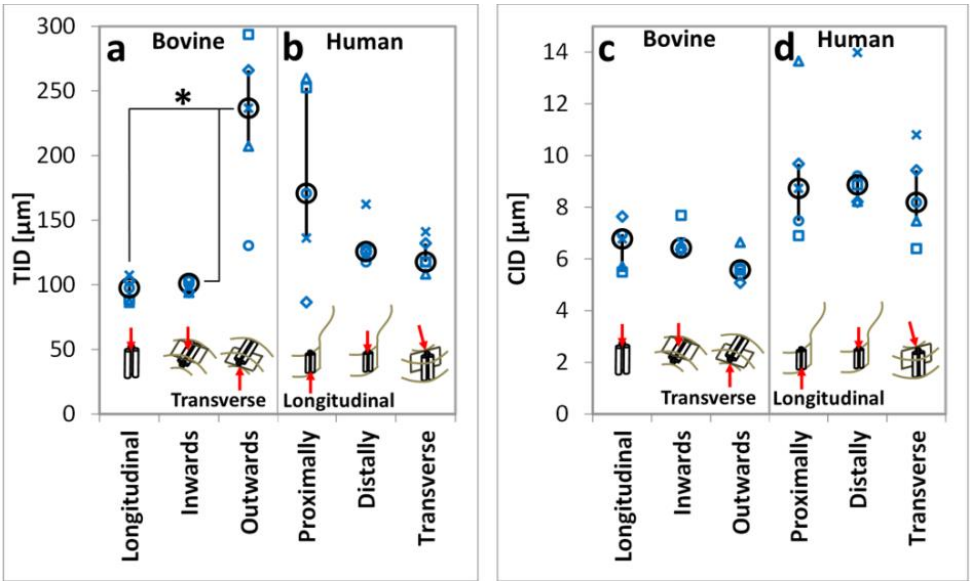

Figure 102: Variation with orientation on bovine bone within the longitudinal and transverse endosteal (inwards)/periosteal (outwards) directions (a and c) and on the human medial femoral neck in the transverse and distal/proximal longitudinal directions (b and d). a) and b) – TID and c) and d) – CID. Results are displayed as significant (* $p < 0.05$) or close to significance (# $p < 0.1$). The graphs display mean values for each sample (each marker representing a different sample) as well as the median and interquartile range across the five samples

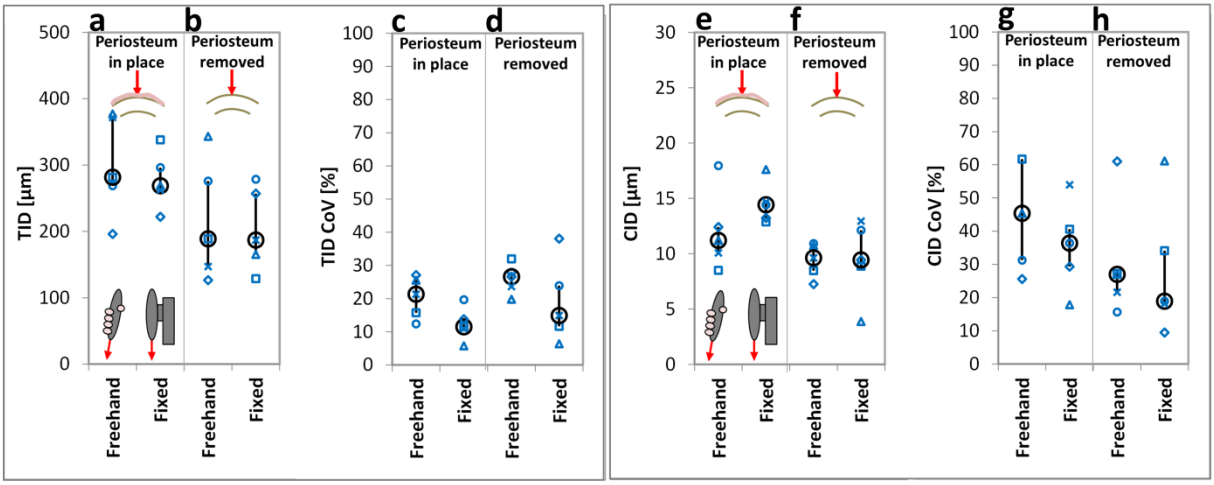

Figure 103: Variation with mode of use on bovine bone (a, b, e and f) and the coefficient of variation (CoV) of these measurements (c, d, g and h). a, b, c and d – TID and e, f, g and h – CID. Results are displayed as significant (* $p < 0.05$) or close to significance (# $p < 0.1$) and the graphs display mean values for each sample (each marker representing a different sample) as well as the median and interquartile range across the five samples.

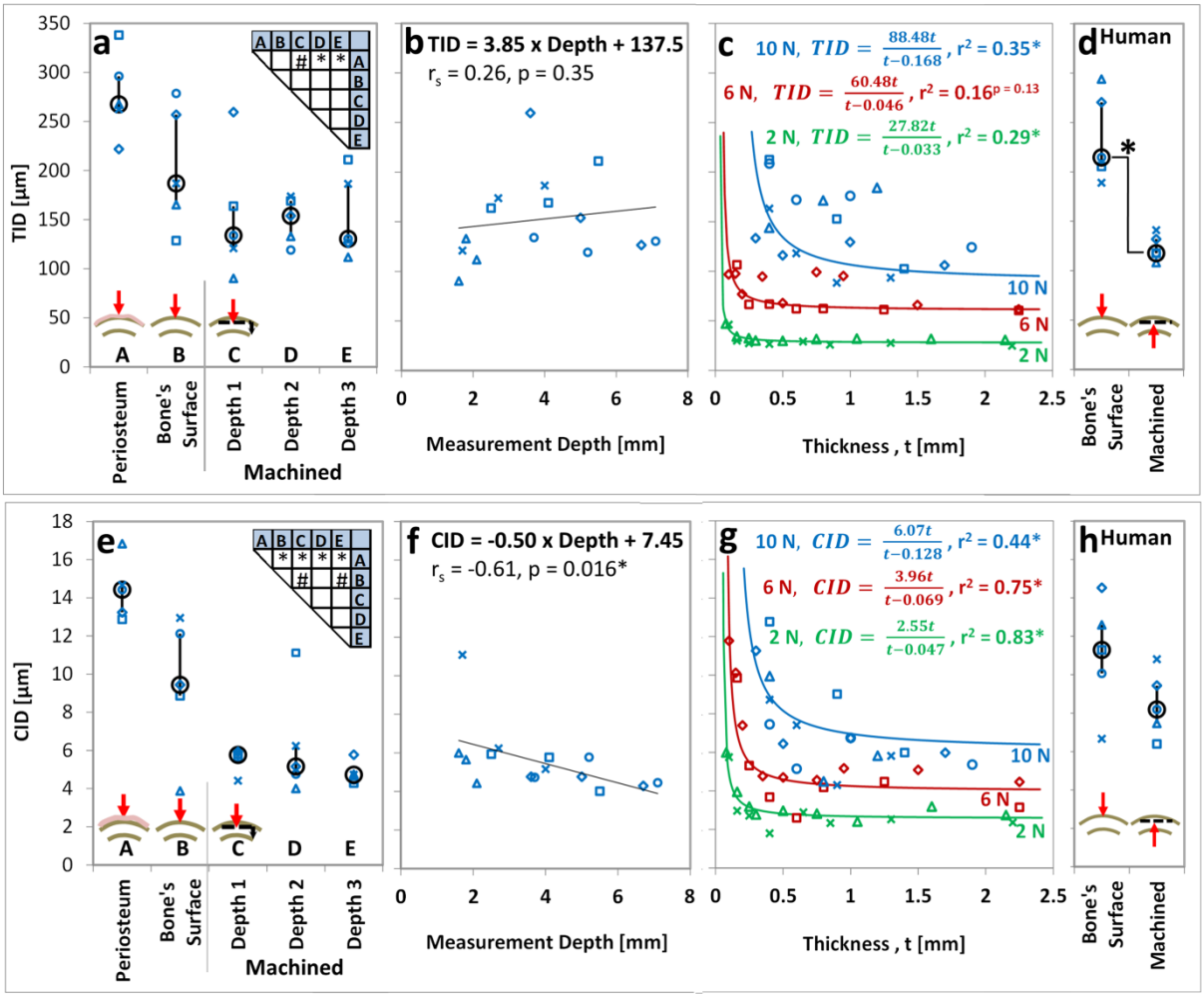

Figure 104: Variation with sample preparation (bovine bone) considering the removal of the periosteum and bone's surface (a and e), the depth the surface removed (b and f), the thickness of the sample (c and g) on bovine bone, and the removal of the surface on human bone (d and h). Upper (a, b, c and d) – TID and Lower (e, f, g and h) – CID. All figures display the mean values for each sample (each marker representing a different sample). a), d), e) and h) additionally show the median and interquartile range across the five samples and b), c), f) and g) display the Spearman's correlation (r_s) and adjusted correlation (r^2). Results are displayed as significant (* $p < 0.05$) or close to significance (# $p < 0.1$). The triangular table in a) and e) displays the level of significance between the different sample preparations. The equation in b) and f) are of the form IDI = m x Depth + C where IDI is in µm, depth is in mm, m is the gradient [µm/mm] and C is the y-intercept [µm]. The equations in c) and g are of the form IDI = P_1 x thickness/(thickness-P_2) where IDI is in µm, thickness is in mm, P_1 represents the horizontal asymptote [µm] and P_2 represents the vertical asymptote [mm].

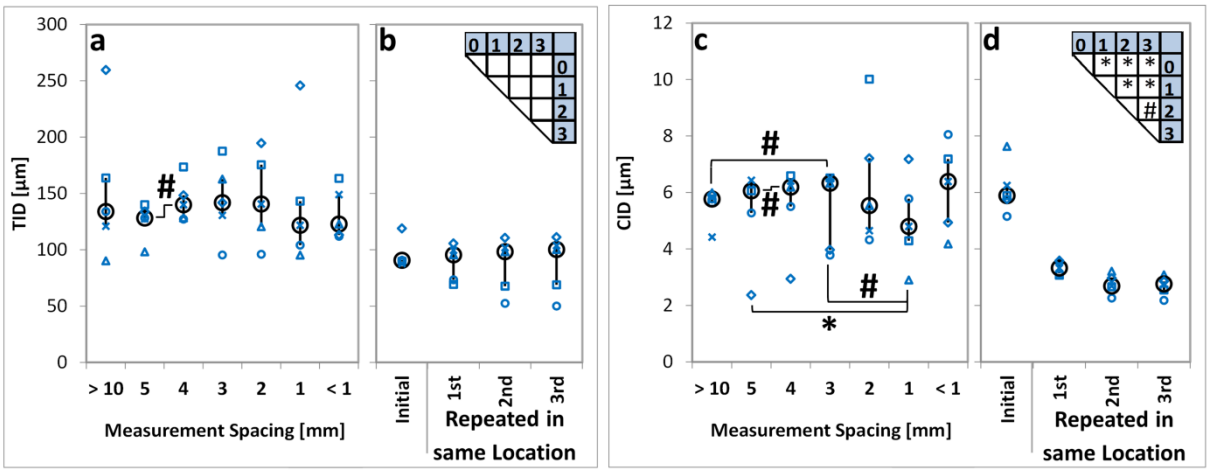

Figure 105: Variation with measurement spacing (a and c) and indentation repeated on the same location (b and d). a) and b) – TID and c) and d) – CID. Results are displayed as significant (* $p < 0.05$) or close to significance (# $p < 0.1$) and the graphs display mean values for each sample (each marker representing a different sample) as well as the median and interquartile range across the five samples. b) and d): The triangular table displays the level of significance between the different numbers of repeat measurements (with 0 representing the initial measurement, 1 the 1st repeat etc.)

9.4 Appendix 3 – Clinical Paperwork

9.4.1 Patient Information Sheet

OStEO Observational Study Examining Osteoporosis

University Hospital Southampton NHS
NHS Foundation Trust
UNIVERSITY OF Southampton

Investigating Fracture and Osteoporosis

Chief Investigator: Dr Philipp Thurner, Faculty of Engineering and the Environment, University of Southampton, SO17 1BJ Email: osteo@soton.ac.uk

R & D number: T&O0149 REC number: 12/SC/0325

Patient Information Sheet

Version 3.0 (29/11/12)

Introduction

We would like to invite you to take part in our research project. It is important that you know what is being done and why, so you can decide if you wish to be involved. Please take time to read and understand this information, talking to others if you wish, before deciding if you would like to take part. A researcher will go through the information sheet with you and you will have a chance to ask any questions before choosing to take part or not.

It is also important that you understand that you do not have to take part in this research. You are free to decline to enter or withdraw from the study at any time without giving a reason. This will not alter the standard of medical care that you receive.

Part 1 will tell you the study's purpose and what it will involve if you choose to take part. Part 2 gives you more detailed information about the conduct of the study.

Part 1 – why and what

Why is the research being done?

This research aims to test **new methods for diagnosing osteoporosis** and to increase the understanding of the disease. Osteoporosis is a bone disease that reduces the quality of bone, making it more likely to fracture. This **affects around 3 million people in the UK** leading to **230 000 fractures per year**. Patients who have had a hip replacement due to a fractured hip bone are being invited to join this study.

The study is being undertaken at University Hospital Southampton and the University of Southampton as part of a postgraduate project.

What does the research involve for me?

After you have had time to read this information you will be contacted by a researcher who will ask if you would like to take part. **Remember, you are free to say no or change your mind**. If you agree to take part you will be asked to sign a consent form. You will be given a copy of the form and a copy will be stored with your medical records and sent to your GP. The form asks for permission for us to:

- **Use bone** that has been removed as part of your hip operation.
- **Take blood and urine** samples to investigate factors relating to your osteoporosis and hip fracture (including genetic studies); these will not identify any individual genetic abnormalities or diseases.
- **Use information** from your medical records and to collect further information about you. This includes some blood test results and information on fracture risk factors and history.
- **Have bone density scans** (DEXA and pQCT scans).

For the bone density scan (DEXA and pQCT scans), you will be asked to return to the Southampton General Hospital approximately 1 month after you are discharged. You will be contacted to arrange the time and date of the appointment which will last less than 1 hour.

Are there any risks or benefits in taking part?

This study has **no major risks** for you. We will only use the bone that was removed for your operation: no additional bone is taken. Blood and urine samples are typically taken as part of your standard care. The DEXA and pQCT scans to measure your bone density will expose you to a very low dose of x-rays, similar to the level you would experience outside in a week

There is **likely to be no direct benefit** for being part of this research. However**, this research aims to help patients with osteoporosis** in the future. We will put these research findings onto the website (www.soton.ac.uk/osteo) but they will be completely anonymous The DEXA scan results will be available to your care team and GP (with your permission) and may help them with your treatment. You are asked to donate your tissue and be part of this research freely and will not receive any financial reward now or in the future. However, we do not want you to be out of pocket and can provide up to £20 toward travel if you need us to. To claim this, please bring travel receipts to the assessment session if possible.

Part 2 – detailed information

Is this confidential?

Any **personal information** that could identify you, such as name, contact details or NHS number will **only be stored on NHS computers**, being **strictly confidential**. All information stored outside of the hospital (i.e. at the University of Southampton) will be anonymous and the link to personal information will be coded. **All information will be stored securely and in accordance with the Data Protection Act**.

We will present the results at scientific meeting, publish them in journals and display them on the website (www.soton.ac.uk/osteo) to allow others to learn from our research but all results will be completely anonymous.

What will you do with the samples I donate?

The **bone samples will be tested at the University of Southampton to investigate new tools for diagnosing osteoporosis** and increase understanding of the disease. The bone tissue will be stored at the University for the length of the research. If any tissue remains at the end of this research, with your permission, the samples may be used for other research projects that have ethics approval. It is not yet known what these research projects involve.

What if something goes wrong?

We do not believe that there is any risk to you by taking part in this research. However, **if something does go wrong** due to someone's negligence, then **you may have grounds for legal action for compensation against University Hospital Southampton or the University of Southampton**. The normal NHS complaints system is also available to you and any complaint will be addressed.

Please initially raise your concerns with the Chief Investigator, Dr Philipp Thurner. If you wish to make a more formal complaint, please contact the hospital's Patient Advice and Liaison Service (PALS). Tel: 023 8079 8498, email: PALS@uhs.nhs.uk, write: PALS, C Level, Centre Block, University Hospital Southampton, Tremona Road, Southampton, SO16 6YD.

Who is involved with the research?

The research is being undertaken by students and staff at the University of Southampton but working with staff as University Hospital Southampton. This study is part of a Doctoral degree project at the University of Southampton for Tom Jenkins, supervised by Dr Philipp Thurner and Dr Nick Harvey and working with postdoctoral research fellow, Dr Louise Coutts. Dr Nicole Moss, a registrar at University Hospital Southampton, will also be undertaking the research.

The research is being funded by the Engineering and Physical Sciences Research Council (EPSRC). This study has been reviewed and approved by the National Research Ethics Service (NRES).

9.4.2 Consent Form

OStEO Observational Study Examining Osteoporosis

University Hospital Southampton NHS
NHS Foundation Trust
UNIVERSITY OF Southampton

Investigating Fracture and Osteoporosis

Dr Philipp Thurner, Faculty of Engineering and the Environment, University of Southampton, SO17 1BJ
R and D number: T&O0149 REC number: 12/SC/0325
Participant ID: _____ Participant DoB: _____

Informed Consent Form

Version 4.0 (13/03/13)

Thank you for reading the information about our research project. If you would like to take part, please read this form, initial the boxes on the right and sign at the bottom.

		Initial
1	I have read the Patient Information Sheet (version 3.0 dated 29/11/2012) for the study 'Investigating Fracture and Osteoporosis' and have been given a copy to keep. I have had the opportunity to consider the information, ask questions and have had these answered satisfactorily.	
2	I understand that my participation is voluntary and that I am free to withdraw at any time without giving any reason, without my medical care or legal rights being affected.	
3	I agree for the tissue removed as part of my hip operation to be used in this study.	
4	I am willing for further blood and urine samples to be taken for investigating factors relating to my osteoporosis and hip fracture. I understand that this will include genetic studies but will not identify any individual genetic abnormalities or diseases **(*Optional*).**	
5	I understand that sections of my medical notes and data collected during the study may be looked at by individuals from the University of Southampton, from regulatory authorities or from the NHS Trust, where it is relevant to my taking part in this research. I give permission for these individuals to have access to my records. I understand that the information will be kept secure and confidential.	
6	I am willing to return as an outpatient and undergo a bone density scan (DEXA and pQCT scans) (*Optional*).	
7	I understand that (my Doctor/my GP and/or I, as appropriate) may be informed of my participation in the research and any relevant test results.	
8	I understand that I will not benefit financially if this research leads to the development of a new treatment or test.	
9	I agree to participate in this study.	
10	I am interested in future research studies and give permission to be contacted. I understand that there will be a separate information sheet and separate consent form for my details to be kept on a research participant database (*Optional*).	
11	I give permission for my samples and data to be stored for possible use in future projects with Research Ethics Committee approval. I understand that my name or identifying details will not be linked to this data or samples (*Optional*).	

Name of Patient	Signature	Date

Researcher: I have discussed the study with this patient who has agreed to give informed consent.

Name of witness	Signature	Date

9.4.3 Personal Information Collection Form

Title of study:
Investigating Fracture and Osteoporosis

Name of Principal Investigator:
Dr Philipp Thurner

R and D Number: T&O0149

REC number: 12/SC/0325

PERSONAL INFORMATION FORM v1.0 (08/05/12)

INFORMATION NOT TO BE TRANSFERRED OUTSIDE NHS

NHS Number			
Date of Birth	DD	MM	YYYY
Title (Circle)	Mr/Mrs/Miss/Ms	Other:	
First Name			
Surname			
Sex (Circle)	Male/Female		
Ethnic Group (Circle)	A B C	White	British Irish Any other White Background
	D E F G	Mixed	White and Black Caribbean White and Black African White and Asian Any other Mixed Background
	H I J K	Asian and British Asian	Indian Pakistani Bangladeshi Any other Asian Background
	L M N	Black or Black British	Caribbean African Any other Black Background
	O P	Other Ethnic Group	Chinese Any other Ethnic Group

Address		
Email Address		
City		
Postcode		
Telephone numbers	Contact Name	Telephone Number
GP Name		
GP Address		

9.4.4 Assessment Form

OStEO Observational Study Examining Osteoporosis

University Hospital Southampton NHS
NHS Foundation Trust
UNIVERSITY OF Southampton

Investigating Fracture and Osteoporosis

Chief Investigator: Dr Philipp Thurner, Faculty of Engineering and the Environment, University of Southampton, SO17 1BJ Email: osteo@soton.ac.uk

R & D number: T&O0149 REC number: 12/SC/0325

Assessment Form

Version 2.1 (13/08/13)

Questionnaire to be completed in a researcher lead session. Any relevant details that are available in the medical notes should be used to complete any incomplete or uncertain questions (focussing on those marked with *'To be completed with aid of the medical notes'*).

 # Indicates information to be used for FRAX calculation

To be completed by the researcher
Participant ID:
Date of Birth:

SECTION ONE: FALLS AND INJURIES

Q1 Have you had any serious falls since the age of 45? No ☐ Yes ☐

a At what age did you first fall? ☐☐

b How many falls have you had in the last year? ☐☐

\# **c** Have you previously broken a bone? No ☐ Yes ☐

d Please mark on the drawing the location of any other broken bone(s) indicating the age at which you broke the bone(s) and annotating with the name of the bone(s) if known.

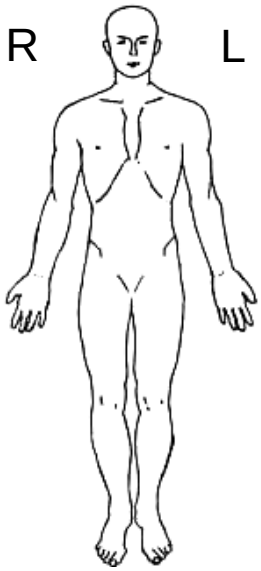

e How did you break bone? High trauma (fall from greater than standing height, car accident etc) ☐ Low trauma (fall from standing height or less) ☐

\# **f** Did either of your parents have a hip fracture? (if known) No ☐ Yes ☐

SECTION TWO: GENERAL WELL-BEING AND MEDICATION

Q2 Have the following issues started or become worse in the last year? Do you think any of these issues have caused a fall (particularly in those falls where a bone was broken)?

	Unchanged = 0 Worsened = 1	Cause a fall? No = 0, Yes = 1
i) Sudden loss of balance?	☐	☐
ii) Weakness in the arms or legs?	☐	☐
iii) Dizziness when standing up quickly?	☐	☐
iv) Unexplained weight loss?	☐	☐
v) Sudden attack of vision loss or blurred vision in one or both eyes?	☐	☐

 # d Have you ever had a diagnosis of rheumatoid arthritis? No ☐ Yes ☐

 # e Have you ever taken glucocorticoids? (greater than 5mg taken orally daily for more than 3 months) No ☐ Yes ☐

 # f Do you currently have any of the following disorders?

1 Type 1 (insulin dependent) diabetes	No ☐	Yes ☐
2 Type 2 (non-insulin dependent) diabetes	No ☐	Yes ☐
3 Osteogenisis Imperfecta (brittle bone disease)	No ☐	Yes ☐
4 Hyperparathyroidism	No ☐	Yes ☐
5 Hyperthyroidism (longstanding and untreated)	No ☐	Yes ☐
6 Hypogonadism or early menopause (before 45)	No ☐	Yes ☐
7 Chronic malnutrition or chronic liver disease	No ☐	Yes ☐

Q3a Have you had a previous diagnosis of Osteoporosis? No ☐ Yes ☐

To be completed with aid of the medical notes

b Do you currently or have you ever taken any medication for osteoporosis?

	Ever taken? (Yes – 1, No – 0)	Number of years and months taken for (yy.mm)	Currently taking? (Yes – 1, No – 0)	Number of years and months since last taken (yy.mm)
Alendronate				
Risedronate				
Raloxifene				
Denosumab				
Parathyroid Hormone				
Zolendronate				
Ibandronate				
Strontium Ralenate				
Other (please specify) _____				

c Do you currently taken any other medications? What conditions are these for?

Name of Medication	Reason for taking medication
1. _____	_____
2. _____	_____
3. _____	_____
4. _____	_____
5. _____	_____
6. _____	_____
7. _____	_____
8. _____	_____
9. _____	_____
10. _____	_____
11. _____	_____
12. _____	_____
13. _____	_____
14. _____	_____

Q4 EQ- 5D Quality of Life Assessment Tool

By placing a tick in one box in each group below, please indicate which statements best describe your own health state before you broke this bone.

Mobility

I have no problems in walking about ❑
I have some problems in walking about ❑
I am confined to bed ❑

Self-Care

I have no problems with self-care ❑
I have some problems washing or dressing myself ❑
I am unable to wash or dress myself ❑

Usual Activities (*e.g. work, study, housework, family or leisure activities)*

I have no problems with performing my usual activities ❑
I have some problems with performing my usual activities ❑
I am unable to perform my usual activities ❑

Pain/Discomfort

I have no pain or discomfort ❑
I have moderate pain or discomfort ❑
I have extreme pain or discomfort ❑

Anxiety/Depression

I am not anxious or depressed ❑
I am moderately anxious or depressed ❑
I am extremely anxious or depressed ❑

The scale below starts at 0, which is the worst health state you can imagine, and goes up to 100, which is the best health state you can imagine. We would like you to indicate on the scale how good or bad, in your own opinion, your own health was before you broke this bone.

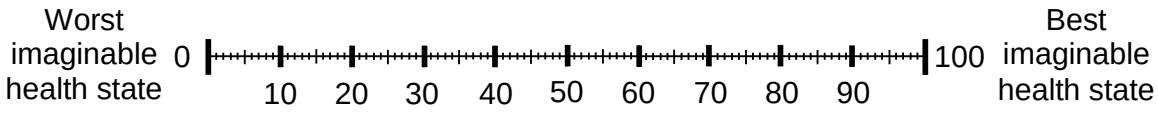

SECTION THREE: SOCIAL

Q5a Have you ever smoked regularly? (i.e. at least once a day for a year or more) No ☐ Yes ☐

If no, Go to Q6

\# **b** Do you still smoke regularly? No ☐ Yes ☐

c How old were you when you last smoked regularly? ☐☐

d Typically, how much do you smoke now?

Cigarettes/week ☐☐☐

Roll-up tobacco (per oz)	equivalent ~ 50 cigarettes
Cigars (1 cigar)	equivalent ~ 2 – 4 cigarettes
Pipe tobacco (per oz)	equivalent ~ 30 cigarettes

Q6 a Do you ever drink alcohol? No ☐ Yes ☐

If no, Go to Q7

\# **b** How many units do you normally drink per week? ☐☐

beer/cider	2 – 3 units per pint
wine (~12%)	1.5 units per small glass
	2 units per medium glass
	3 units per large glass
fortified wine (e.g. sherry/port ~ 20%)	1 unit per measure (50 ml)
spirits (~40%)	1 unit per single (25 ml) measure

SECTION FOUR: PHYSICAL ACTIVITY, HEIGHT AND WEIGHT

Q7 a On a typical day how long would you spend walking (in hours and minutes)? ☐☐

b How much time do you spend on exercise or physical activity in a typical week (give in approximate number of hours)? e.g. gardening, housework, exercise ☐☐

To be completed with aid of the medical notes

\# **c** What is your current weight (kg) ☐☐

\# **d** How tall are you (cm) ☐☐☐

SECTION FIVE: OESTROGEN

WOMEN ONLY. For men go to Q9

Q8 a At what age did your periods stop? ☐☐

To be completed with aid of the medical notes

b Have you had a hysterectomy (removal of the womb)?

No ☐ Yes ☐

c ***If yes*** how old were you? ☐☐

d Did the hysterectomy include removal of the ovaries?

No ☐ Yes ☐ Don't Know ☐

e Have you ever taken hormone replacement therapy?

No ☐ Yes ☐

f ***If yes,*** at what age did you start? ☐☐

g How long in total did you take it for (months)? ☐☐

h Have you ever taken an oral contraceptive pill?

No ☐ Yes ☐

i ***If yes,*** How long in total did you take it for (years and months)?

☐☐ Years ☐☐ Months

9.5 Appendix 4 – Matlab Algorithms

9.5.1 Calculation of Reference Point Indentation Parameters

```
%% Written by Tom Jenkins
% Code splits converted data (i.e. data with true force and displacement
% values - not raw that requires conversion) into cycle by cycle graphs.

% The user then deems if these graphs are suitable for calculation and,
if so,
% the code calculates output parameters

% This is repeated for all measurements within a folder of interest

close all
clear all
clc

%% Open file and get data from user
%Select file in folder (any)
[~, pathname] = uigetfile('*.txt','Select any file in the folder of
interest - note the naming convention and number of files - if there is
any missing files, ammend first');

directories = dir(strcat(pathname,'/*.txt'));
number = length(directories);

%% Load each data file (i.e. measurement) in the dataset in turn
for i=1:number;
clear cycledata fddata parameters
    dataname=strcat('\',directories(i).name);

% Save name in list
namelist{i,1} = directories(i).name;

%Open the file
filename=strcat(pathname,dataname);

%Load file
fddata=load(filename);

%Number of cycles
[size_data a]=size(fddata);
ncycles=10;

% % Smooth data - I believe they use a 10 point moving average?
for n=1:2
    fddata(:,n)=smooth(fddata(:,n),10,'lowess');
end

%Touchdown force - Approach to find a plateau region and hence the
%touchdown force (where there is no plateau this should still be robust)
TDF=0.1;

%1) Find the beginning of the linear region
%Based on linear fitting of curve between 5N and 9N
[p1,~,~] = find(fddata(:,2)>5);
[p2,~,~] = find(fddata(:,2)>9);
coeffs = polyfit(fddata(p1(1):p2(1),1), fddata(p1(1):p2(1),2), 1);
```

```
%Find deviation from that linearity
LoadDispl_short = fddata(1:p2(1),:);
LoadDispl_short(:,3) = coeffs(1)*LoadDispl_short(:,1)+coeffs(2);
LoadDispl_short(:,4) = abs((LoadDispl_short(:,2)-
LoadDispl_short(:,3))/max(LoadDispl_short(:,2)));
[p3,~,~] = find(LoadDispl_short(:,4)<0.1);

%2) find when displacement rate is +ve
LoadDispl_short(1:end-1,5)=LoadDispl_short(2:end,1)-
LoadDispl_short(1:end-1,1);
[p4,~,~] = find(LoadDispl_short(:,5)<-0.5);
if isempty(p4)==1
    p4=1;
end

%3) find where the curve plateaus for longest in this range
k=1;
lim = LoadDispl_short(p4(end),2);
findTD(k,1) = LoadDispl_short(p4(end),1);

for i1 = p4(end):p3
    if LoadDispl_short(i1,2)>lim
       findTD(k,2) = LoadDispl_short(i1,1);
       findTD(k,3) = lim;
       findTD(k,4) = findTD(k,2)-findTD(k,1);
       k=k+1;
       findTD(k,1) = LoadDispl_short(i1,1);
       lim=lim+0.1;
    end
end
[~, p5] = max(findTD(:,4));
InitialF = round(findTD(p5,3)*10)/10;

%4) Finally find the first point above this threshold load
    [q,~,~] = find(fddata(:,2)>InitialF+0.1);
    TD1 = q(1);
    % Initial touchdown force
    fddata(:,2) = fddata(:,2)-fddata(TD1,2);
    % Initial touchdown distance
    fddata(:,1) = fddata(:,1)-fddata(TD1,1);

%split cycles
thresh(1,1) = 1;
cyclecount=1;

for ncount = 2:length(fddata(:,2))
    if fddata(ncount,2)>0.5 && fddata(ncount-1,2)<0.5
       thresh(cyclecount,2) = ncount;

          [~,thresh(cyclecount,3)] =
min(fddata(thresh(cyclecount,1):thresh(cyclecount,2),2));
          thresh(cyclecount,3) = thresh(cyclecount,3) +
thresh(cyclecount,1) - 1;
          cyclecount = cyclecount+1;
    end

    if fddata(ncount,2)<0.5 && fddata(ncount-1,2)>0.5
       if max(fddata(thresh(cyclecount-1,1):ncount,2))>1.5
       thresh(cyclecount,1) = ncount;
       else
           cyclecount=cyclecount-1;
```

```
        end
    end

end

thresh(1,1) = 1;
thresh(1,3) = 1;
thresh(cyclecount,2) = ncount;
thresh(cyclecount,3) = ncount;
ncycles=cyclecount-1;

for n1=1:ncycles

point1=thresh(n1,3);
pointL=thresh(n1+1,3);

    cyclelength = pointL-point1+1;

    cycledata(1:cyclelength,2*n1-1)=fddata(point1:pointL,1);
    cycledata(1:cyclelength,2*n1)=fddata(point1:pointL,2);

    % Touchdown - Find initial force (have reset to 0,0)
    if n1==1
        parameters(1,n1) = 0;
        parameters(5,n1) = 0;
    else
    [p,~,~] = find(cycledata(1:cyclelength,2*n1)>cycledata(1,2*n1)+TDF);
    parameters(1,n1) = cycledata(p(1),2*n1-1);
    parameters(5,n1) = cycledata(p(1),2*n1);
    end

    %Peak - displacement when first within 0.03 of max force
    [maxforce, ~] = max(cycledata(1:cyclelength,2*n1));
    [s1,~,~] = find(cycledata(1:cyclelength,2*n1)>maxforce-0.03);
    parameters(2,n1) = cycledata(s1(1),2*n1-1);

    %Retraction - displacement when last within 0.03 of max force
    parameters(3,n1) = cycledata(s1(end),2*n1-1);

    %Liftoff: when last above threshold, TDF
    [p,~,~] = find(cycledata(1:cyclelength,2*n1)>cycledata(1,2*n1)+TDF);
    parameters(4,n1) = cycledata(p(end),2*n1-1);
    parameters(8,n1) = cycledata(p(end),2*n1);
    % Find the four forces of interest (touchdown, peak, retraction,
liftoff)
    %TDF - above

    %Peak force - force 1/3 of the way through cycle
    parameters(6,n1) = cycledata(s1(1),2*n1);
    %Retraction force - force 2/3 of the way through cycle
    parameters(7,n1) = cycledata(s1(end),2*n1);

    %Liftoff Force - above

    %avg max force
    parameters(9,n1)= mean(cycledata(s1(1):s1(end),2*n1));

    %Find 50% of loading slope
    [s2,~,~] = find(cycledata(1:s1(1),2*n1)>maxforce*0.5);
    parameters(10,n1) = cycledata(s2(1),2*n1-1);
```

```
    parameters(13,n1) = cycledata(s2(1),2*n1);

    %Find 95% and 40% of unloading slope
    % 95%
    [s3,~,~] = find(cycledata(s1(end):end,2*n1)>maxforce*0.95);
    parameters(11,n1) = cycledata(s3(end)+s1(end),2*n1-1);
    parameters(14,n1) = cycledata(s3(end)+s1(end),2*n1);
    % 40%
    [s4,~,~] = find(cycledata(s1(end):end,2*n1)>maxforce*0.4);
    parameters(12,n1) = cycledata(s4(end)+s1(end),2*n1-1);
    parameters(15,n1) = cycledata(s4(end)+s1(end),2*n1);

    parameters(16,n1) = (parameters(6,n1)-
parameters(13,n1))/(parameters(2,n1)-parameters(10,n1));
    parameters(17,n1) = (parameters(14,n1)-
parameters(15,n1))/(parameters(11,n1)-parameters(12,n1));

 end


%% Plot all cycles with approximate curves based on identified points
figure
%Maximize
%set(gcf, 'Position', get(0,'Screensize'));
 set(gcf, 'position', [1, 1, 1280, 908])
ygraphs = round(ncycles/2);

for ccount=1:ncycles
if ccount<=ygraphs
    subplot(ygraphs,2,2*ccount-1)
else
    subplot(ygraphs,2,2*(ccount-ygraphs))
end

plot(cycledata(:,2*ccount-
1),cycledata(:,2*ccount),parameters(1:4,ccount),parameters(5:8,ccount))
if ccount==1
cycletitle=strcat(dataname,{' Cycle '},num2str(ccount));
else
cycletitle=strcat({'Cycle '},num2str(ccount));
end
title(cycletitle)
ccount=ccount+1;

end

%% Get output measurements for this dataset

% Check if the data is representative and delete point if not
choice = questdlg('Are the selected points representative?', ...
    strcat(dataname,'Assess Graphs'), ...
    'Yes','No','Yes');
% Handle response
switch choice

    case 'Yes'

  %TID (1st-L) = RL -TDF1 [um]
        Measurement(i,1)= abs(parameters(3,end)-parameters(1,1));
        %IDI (1st-L) = PL - P1 [um]
```

```
            Measurement(i,2)= abs(parameters(2,end)-parameters(2,1));
            %CID (R-P) 1st cycle
            Measurement(i,3) = parameters(3,1)-parameters(2,1);
            %CID last cycle
            Measurement(i,4) = parameters(3,end)-parameters(2,end);
            %CID ratio: 1st/last
            Measurement(i,5) = Measurement(i,3)/Measurement(i,4);
            %avgCID
            Measurement(i,6) = mean(parameters(3,1:end)-parameters(2,1:end));
            %ID 1st
            Measurement(i,7) = parameters(3,1)-parameters(1,1);
            %Avg max force
            Measurement(i,8) = mean(parameters(9,1:end));
            %Touchdown
            Measurement(i,9) = 0-fddata(1,1);
            %avgLS
            Measurement(i,10) = mean(parameters(16,1:end));
            %avgUS
            Measurement(i,11) = mean(parameters(17,1:end));

        case 'No'
            % Delete point
            data2(i,:)=0;
            Measurement(i,:)=0;

end

close all;
end
```

9.5.2 The Whitening Front Tracking Method

```
% Algorithm written by Orestis Katsamenis (and published PlosONE (2013))
% Adaptations made my Tom Jenkins for increased automation

%Synchronise load-displacement-time with videography.
%Crop and register initial frame, subtract from all subsequent frames
%Automatically select whitening area from this subtraction image
%Use whitening extension, load and geometry to develop crack extension
%resistance curves and hence the crack growth and fracture toughness

%% Loading the video and the Load - Displacement Data
clear all
close all
clc

run FDanalysis2

%% Geometry

        prompt = {'Span (mm)',...
        'Width (mm)',...
        'Thickness (mm)',...
        'Pre-notch (mm)'...
        'Poisson Ratio'};
    title = 'Geometrical Parameters';
    numlines = 1;
    defaultanswer = {'6','1.25','0.75','0.4','0.33'};
    options.Resize='on';
    answer = inputdlg(prompt,title,numlines,defaultanswer,options);

        S = str2double(cell2mat(answer(1,1)));    %Span (mm)
        W = str2double(cell2mat(answer(2,1)));    %Width (mm)
        B = str2double(cell2mat(answer(3,1)));    %Thickness(mm)
        a0a = str2double(cell2mat(answer(4,1))); %Pre-notch (mm) - only
for guidance, leave as default if unknown
        v = str2double(cell2mat(answer(5,1)));    %Poisson's Ratio

%% Elasticity - calculate point of non-linearity
j=1;
for i=1:round(0.1*posmax):0.6*posmax
    rcoef =
corrcoef(LoadTime1(i:i+round(0.4*posmax),1),LoadTime1(i:i+round(0.4*posma
x),2));
    Rco(j,1)=i;
    Rco(j,2)=rcoef(1,2);
    j=j+1;
end

[~,Llim] = max(Rco(:,2));

%Convert to position
Lpos = Rco(Llim,1);
Upos = Lpos + round(0.4*posmax);

Ldisplim=Lpos/4000;
Udisplim=Upos/4000;

%Fit a line
coeffs = polyfit(LoadTime1(Lpos(1):Upos(1),1),
LoadTime1(Lpos(1):Upos(1),2), 1);
```

```
% Plot
fittedX = 0.5*Ldisplim:0.1*(1.5*Udisplim-0.5*Ldisplim):1.5*Udisplim;
fittedY = fittedX*coeffs(1)+coeffs(2);
fit_coef = coeffs;

% %Load and short LoadDispl curve in to LoadDispl_short
LoadDispl(:,1) = LoadTime1(:,1);
LoadDispl(:,2) = LoadTime1(:,2);
%
%
LoadDispl_short = sortrows(LoadDispl,1);
clear LoadDispl;

%linear part of Load-Displ data
    LoadDispl_short(:,3) = fit_coef(1)*LoadDispl_short(:,1)+fit_coef(2);

%difference between Load-Displ and Linear
    LoadDispl_short(:,4) = abs((LoadDispl_short(:,2)-
LoadDispl_short(:,3))/max(LoadDispl_short(:,2)));

    LoadDispl_short(:,5) = smooth(LoadDispl_short(:,4),51,'rlowess');

    errorthresh = max(LoadDispl_short(Lpos:Upos,5))*1.1;
    [rnonlin ~] =
find(LoadDispl_short(round(0.25*posmax):posmax,5)>errorthresh);

    PlasticRegInitiation =
LoadDispl_short(rnonlin(1)+round(0.25*posmax),1);

%Offset LoadDispl_short to generate Plastic Load-Line Displacement
    Plastic_LoadDisp(:,1) = LoadDispl_short(:,1)-PlasticRegInitiation;
    Plastic_LoadDisp(:,2) = LoadDispl_short(:,2);

    %Plot
    plot(LoadTime1(:,1),LoadTime1(:,2),'bo',[PlasticRegInitiation
PlasticRegInitiation],[0 LoadTime1(posmax,2)],'r');hold on;

plot(LoadDispl_short(1:round(1.2*(rnonlin(1)+0.25*posmax)),1),LoadDispl_s
hort(1:round(1.2*(rnonlin(1)+0.25*posmax)),3),'r','Linewidth',3)
    xlabel('Displacement [mm]');
    ylabel('Load [N]');

% Check if automatic selection has worked, otherwise manual
choice = questdlg('Has automatic linearity selection worked?', 'If No,
use manual selection', 'Yes','No','No');
% Handle response
switch choice
    case 'Yes'
          man(1) = 1;
    case 'No'
        man(1) = 2;
        close all
        string =[];
        string = {'First click the start of the linear portion of the
curve then the end'};
        waitfor (helpdlg(string,'Info'))
        plot(LoadTime1(:,1),LoadTime1(:,2),'o')
        xlabel('Displacement [mm]');
        ylabel('Load [N]');

        %Get upper and lower linearity limits
```

```
        [Ldisplim, ~] = ginput(1);
        [Udisplim, ~] = ginput(1);
        %Convert to position
        Lpos = find(LoadTime1(:,1)>Ldisplim);
        Upos = find(LoadTime1(:,1)>Udisplim);

        %Fit a line
        coeffs = polyfit(LoadTime1(Lpos(1):Upos(1),1),
LoadTime1(Lpos(1):Upos(1),2), 1);
        % Plot
        fittedX = 0.5*Ldisplim:0.1*(1.5*Udisplim-
0.5*Ldisplim):1.5*Udisplim;
        fittedY = fittedX*coeffs(1)+coeffs(2);
        fit_coef = coeffs;

        % %Load and short LoadDispl curve in to LoadDispl_short
        LoadDispl(:,1) = LoadTime1(:,1);
        LoadDispl(:,2) = LoadTime1(:,2);
        LoadDispl_short = sortrows(LoadDispl,1);
        clear LoadDispl;

        close all;

        %linear part of Load-Displ data
            LoadDispl_short(:,3) =
fit_coef(1)*LoadDispl_short(:,1)+fit_coef(2);

        %difference between Load-Displ and Linear
            LoadDispl_short(:,4) = abs((LoadDispl_short(:,2)-
LoadDispl_short(:,3))/max(LoadDispl_short(:,2)));

        %opens a window fot user to select X of Plastic Region Initiation
        string = {'Click where the curve deviates from linearity (when
linearity error deviates from 0)'};
        waitfor (helpdlg(string,'Info'))
            plot(LoadDispl_short(:,1),LoadDispl_short(:,4),'.');
            xlabel('Displacement [mm]');
            ylabel('Error in Linearity');

            [PlasticRegInitiation,~] = ginput(1);
            close all;

        %Offset LoadDispl_short to generate Plastic Load-Line
Displacement
            Plastic_LoadDisp(:,1) = LoadDispl_short(:,1)-
PlasticRegInitiation;
            Plastic_LoadDisp(:,2) = LoadDispl_short(:,2);
         %Plot
        plot(LoadTime1(:,1),LoadTime1(:,2),'bo',[PlasticRegInitiation
PlasticRegInitiation],[0
LoadTime1(posmax,2)],'r',LoadDispl_short(1:round(1.2*(rnonlin(1)+0.25*pos
max)),1),LoadDispl_short(1:round(1.2*(rnonlin(1)+0.25*posmax)),3),'r')
        xlabel('Displacement [mm]');
        ylabel('Load [N]');
end

%% Open tiff files
% Get pathname and image name
[imagename, pathname] = uigetfile('*.tif','Select the LAST image in the
sequence of the video');
```

```
    L = 8; %%%%%%%%%%%%%%%% EDIT
    L2 = 10; %%%%%%%%%%%%%%%% EDIT

    posL = findstr(pathname,'Loading');
    pathname2 = strcat(pathname(1:posL-1),'Videography\',dataname(1:end-
4),'\');


directories = dir(strcat(pathname2,'/*.tif'));
imagename = directories(end,1).name;

lastfile = str2double(imagename(L:L2));

nomefile=strcat(pathname2,imagename(1:L2-
4),'0000',imagename(L2+1:end)); %First image

    FrameRate = 1; %%%%%%%%%%%%%%%% EDIT
    Frame0= 1; %%%%%%%%%%%%%%%% EDIT
    FrameEnd=round(LoadTime1(posmax,3)*1.1); %%%%%%%%%%%%%%%% EDIT


Frame_Resolution = num2str(FrameEnd-Frame0);
FrameStep = 1;

FrameLin = round(LoadTime1(rnonlin(1)+round(0.25*posmax),3));

%% Calibration and Rotation
nomefile=strcat(pathname2,imagename(1:L2-
4),'0000',imagename(L2+1:end)); %First image
im0 = imread(nomefile);

 close all
string =[];
string = {'Set Scale: Click two points that define a known distance (i.e.
Click the span - first the left hand then right hand post)',...
    'Then, enter the known distance (in micrometres) and click',...
    ' "OK".'};
waitfor (helpdlg(string,'Info'));


imshow(im0);
[X1,Y1]=ginput(1);          % Select two points on the ruler for
converting
[X2,Y2]=ginput(1);          % pixels into physical units

prompt = {'Insert the known length (um)'};  % Insert the length (in um)
of the selected segment
Title = 'Calibration Length';
numlines = 1;
defaultanswer = {num2str(1000*S)};

answer = inputdlg(prompt,Title,numlines,defaultanswer);
Lmm = str2double(cell2mat(answer(1,1)));

Cal = Lmm/(sqrt((X2-X1)^2+(Y2-Y1)^2)); %convert pixels to um
angle = atan((Y2-Y1)/(X2-X1))*180/pi;
imR0=imrotate(im0,angle,'crop');  % Rotate the image (if needed change
"0" to desired angle in deg, or assign an variable to it);

[h0 w0] = size(imR0);
```

```
%%  ROI selection and
Crop %%%%%%%%%%%%%%%%%%%%%%%%%%%%%%%%%%%%%%%%%%%%%%%%%%%%%%%%

%Calculate transformed points of the base (rotated anti-clockwise about
%centre)

%Left point
radL = ((X1-w0/2)^2+(Y1-h0/2)^2)^0.5;
angL = atan((Y1-h0/2)/(w0/2-X1));
Y12 = radL*sin(angL+angle*pi/180)+h0/2;
X12 = w0/2-radL*cos(angL+angle*pi/180);

%Right point
radR = ((X2-w0/2)^2+(Y2-h0/2)^2)^0.5;
angR = atan((Y2-h0/2)/(X2-w0/2));
Y22 = radR*sin(angR-angle*pi/180)+h0/2;
X22 = w0/2+radR*cos(angR-angle*pi/180);

%Approx notch location (centre)
Cnotch = (X12+X22)/2;
Rnotch = (Y12+Y22)/2;

Rmin = round(Rnotch - 0.9*W*1000/Cal);
Rmax = round(Rnotch);
Cmin = round(Cnotch - 500/Cal);
Cmax = round(Cnotch + 500/Cal);

figure, imshow(imR0)
hold on
rectangle('Position',[Cmin,Rmin,Cmax-Cmin,Rmax-Rmin],'EdgeColor',[1 0
0]) %ROI, red - Top left, width, height
rectangle('Position',[X12,Y12-W*1000/Cal,X22-
X12,W*1000/Cal],'EdgeColor',[0 0 1]) %Beam, blue
hold off


string = {'Have the ROI and sample been correctly identified (i.e. red
line with an area including the notch and excluding the plunger and blue
line approximately including the top/bottom of the sample)?',...
    'If No - Click one point - the notch in line with the base of the
sample',...
       'Align with the centre of the plunger for improved registration or
the sharpened notch for improved whitening',...
        'The ROI is defined by the sample dimensions'};
choice = questdlg(string, 'If No - select notch manually',
'Yes','No','No');
% Handle response
switch choice
    case 'Yes'
        man(2)=1;
    case 'No'
        man(2)=2;
    [Cnotch,Rnotch]=ginput(1);   % Select the notch
end

%Crop limits
Rmin = round(Rnotch - 0.9*W*1000/Cal);
Rmax = round(Rnotch);
Cmin = round(Cnotch - 500/Cal);
Cmax = round(Cnotch + 500/Cal);
```

```
%Used to threshold notch (black area below notch)
RminT = round(Rnotch + 2);
RmaxT = round(Rnotch + 32);
CminT = round(Cnotch - 20);
CmaxT = round(Cnotch + 20);

threshold = imR0(RminT:RmaxT,CminT:CmaxT);


imRC0=imR0(Rmin:Rmax,Cmin:Cmax);    % Crop the image
close all

%% Define image processing variables

    gamma = 2.5;
    RresizeFactor = 1;
    level = 0.08; %Used in 'Evaluation of Damage' section
    oct = 6; %Used in 'Evaluation of Damage' section
    MagnFactor = 8; %Used in 'Evaluation of Damage' section

    clear prompt Title numlines defaultanswer options answer;

%% Process all frames in an iterative mode - apply image processing and
crop
j=1;

for i=Frame0:FrameStep:FrameEnd

    %get filename
    if i<10
        filename = strcat('000',num2str(i));
    else
        if i<100
            filename = strcat('00',num2str(i));
        else
            if i<1000
                filename = strcat('0',num2str(i));
            else
                filename = strcat(num2str(i));
            end
        end
    end

    nomefile=strcat(pathname2,imagename(1:L2-
4),filename,imagename(L2+1:end));
    im = imread(nomefile);

    im=im(:,:,1);
    imR=imrotate(im,angle,'crop');
    imRC=imR(Rmin:Rmax,Cmin:Cmax);
    %imRCF=imadjust(imRC,[0;0.9],[0;1],3);
    imRCF=imresize(imRC,RresizeFactor,'bilinear');
    imRCF=imadjust(imRCF,[],[],gamma);

    Images{j,1}=imRC;    %Save Cropped Images
    Images{j,2}=imRCF;   %Save Gamma corrected Images
    j=j+1;               %counter

    deltaind(j,1) = (i-Frame0)/60;    % Time variable
end
```

```
clear im imR imRC imRCF

[lengthImages, ~] = size(Images);

% Images{} Content :
% Images{:,1}   Images{:,2}
% Croped Image  Gamma Corr Im

%% Automatic selection of the notch
close all

rownotchb = (0.9*W+PlasticRegInitiation-a0a)*1000/Cal; %Based on
microscopy/input
rownotchc = (W-a0a)*1000/Cal;

[height width] = size(Images{1,1});
for i = 1:height
    rows(i,1:width)=height-i;
end

    threshval=3.5*sum(sum(threshold))/(31*41);
    IMBWL =(Images{FrameLin,1}>threshval);


    %Largest Element
NotchBW=~IMBWL;
CC = bwconncomp(NotchBW);
numPixels = cellfun(@numel,CC.PixelIdxList);
[biggest,idx] = max(numPixels);
NotchBW(CC.PixelIdxList{idx}) = 0;
IMBWL=~(NotchBW-~IMBWL);

%figure,imshow(IMBWL)
    heightmap = ~IMBWL.*rows;

    if max(max(heightmap)) ==0
        heightmap(1:height,1:width)=1;
    end

    rownotch = height-max(heightmap(:));
    [r c] = find(heightmap(rownotch,:));
    colnotch = round(c(1)+c(end))/2;

    % Check if user is happy with notch selection else click to select

    %Crop limits for sample image
RminN = round(Rnotch - W*1000/Cal);
RmaxN = round(Rnotch);
CminN = round(Cnotch - 500/Cal);
CmaxN = round(Cnotch + 500/Cal);
imRC0N=imR0(RminN:RmaxN,CminN:CmaxN);
YNotch0 =  rownotch-PlasticRegInitiation/Cal*1000;
[heightb widthb] = size(imRC0N);

clear title
% plot sample image and first image for notch identification
figure,

subplot(1,2,1);
```

```
imshow(Images{FrameLin,1},[])
 title('Sample image');
hold on
plot([1 width],[rownotch rownotch],'b')
plot([colnotch colnotch],[1 height],'b') %Detection
plot([1 width],[rownotchb rownotchb],'r') %Measurement
hold off


subplot(1,2,2);
%imshow(Images{1,1})
imshow(imRC0N,[])
 title('First image including base of sample');

hold on
plot([1 widthb],[YNotch0+0.1*W*1000/Cal YNotch0+0.1*W*1000/Cal],'b')
%plot([1 widthb],[YNotch0 YNotch0])
plot([colnotch colnotch],[1 heightb],'b') %Detection
plot([1 widthb],[rownotchc rownotchc],'r')  %Measurement
hold off

%Check if correctly identified
choice = questdlg('Has notch been correctly identified?', 'If No - select
notch manualy on left hand image', 'Yes','No','No');
% Handle response
switch choice
    case 'Yes'
    man(3)=1;
    case 'No'
    man(3)=2;
    [colnotch,rownotch]=ginput(1);
end

YNotch0 =  rownotch-PlasticRegInitiation/Cal*1000;
XNotch = colnotch;

a0 = (height-YNotch0+0.1*W)*Cal/1000;


  %%
  lrate = 0.001; %%%%%%%%%%%%%%%% EDIT

    %convert to pixels per frame
    imagelrate = lrate*FrameStep/FrameRate/Cal*1000;


close all
clear title



%Wait until Figure 1 is closed by user
clear xx xx2
cont=1;

    %Transform
      for i=1:lengthImages
          %Frame rate reg
          imshift = imagelrate*i;
```

```
            T = maketform('affine',[1 0 0; 0 1 0; 0 imshift 1]);    %#
represents translation
            Imagestemp{i,1} = imtransform(Images{1,2}, T, 'XData',[1
size(Images{i,2},2)], 'YData',[1 size(Images{i,2},1)]);

            %Auto registration
            xx = im2double(Images{i,2});    % Base Image
            yy = im2double(Images{1,2});    % Image To Be registered

            %Efficient subpixel image registration by cross-correlation
            [output Greg] = dftregistration(fft2(xx),fft2(yy),100);
            Imagestemp{i,2} = im2uint8(abs(ifft2(Greg))); %Save Registred
Images

            figure(1);
            subplot(1,3,1);
            imshow(Images{i,2},[]);
           title('Reference image, f(x,y)');

            subplot(1,3,2);
            imshow(Imagestemp{i,1},[]);
            title('Registered - Loading rate');

             subplot(1,3,3);
            imshow(Imagestemp{i,2},[]);
            title('Registered - Automatic');
      end

while cont==1
% Choose mode of registration
choice = questdlg('Select Registration method', 'Select Frame rate or
automatic registration', 'Replay','Loading Rate','Automatic','Frame
Rate');
% Handle response
switch choice
    case 'Loading Rate'
        man(4)=2;
        Images(:,3)=Imagestemp(:,1);
          cont = 0;
    case 'Automatic'
        man(4)=1;
        Images(:,3)=Imagestemp(:,2);
          cont = 0;
    case 'Replay'
      for i=1:lengthImages

            figure(1);
            subplot(1,3,1);
            imshow(Images{i,2},[]);
           title('Reference image, f(x,y)');

            subplot(1,3,2);
            imshow(Imagestemp{i,1},[]);
            title('Registered image - Frame rate');

             subplot(1,3,3);
            imshow(Imagestemp{i,2},[]);
            title('Registered image - Automatic');
      end
end
```

```
end

%%%%%%%%%%%%%%%%%%%%%%%%%%%%%%%%%%%%%%%%%%%%%%%%%%%%%%%%%%%%%%%%%%%%%%%%%%%%%%%%
% Images{} Content :
% Images{:,1}   Images{:,2}     Images{:,3}
% Croped Image  Gamma Corr Im   Registeres Im

%% Levels (subtraction)
for i = 1:lengthImages
    close all;
    [ResizeYX(1),ResizeYX(2)] = size (Images{i,3});
    clear ResizedIm ImComp ImEq
    ResizedIm = imresize(Images{i,2},[ResizeYX(1),ResizeYX(2)]);
    %ImComp = imcomplement(ResizedIm);
    ImComp = ResizedIm;
    ImEq = histeq(ImComp);
    ImEqNEw = imresize(ImEq,[ResizeYX(1),ResizeYX(2)]);


    Images{i,4} = imsubtract(ImEqNEw,histeq(Images{i,3}));
    Images{i,5} = imabsdiff(Images{i,4},Images{i,3});

end

%%%%%%%%%%%%%%%%%%%%%%%%%%%%%%%%%%%%%%%%%%%%%%%%%%%%%%%%%%%%%%%%%%%%%%%%%%%%%%%%
%%%%
% Images{} Content :
% Images{:,1}   Images{:,2} Images{:,3} Images{:,4} Images{:,5}
Images{:,6}
% Croped Image  Gamma Corr  Registered  Imsubtract  Imabsdiff   Leveled
Images{i,4}

%% Evaluation of Damage (MajorAxisLength - Centroid)
clear cx cy
%Max displacement (in pixels)
maxdisp = (ceil(lrate*FrameStep/FrameRate/Cal*1000*(FrameEnd-
Frame0))+1)*MagnFactor;

for i = lengthImages:-1:1

    xx=imresize(Images{i,4},MagnFactor);%,LevelThreshold/LevelOrder);
    se = strel('octagon',oct); %'arbitrary' 'octagon'
    xx2=im2bw(imopen(xx,se),level);
    xx2(1:maxdisp,:)=0;

% Find Largest Element (the whitening)
CC = bwconncomp(xx2);
BWlargest=xx2;
numPixels = cellfun(@numel,CC.PixelIdxList);
[biggest,idx] = max(numPixels);
xx2(CC.PixelIdxList{idx}) = 0;

    if isempty(biggest)==0 %not empty
    Images{i,7} = BWlargest - xx2;
    %figure,imshow(Images{i,7})
    %Find the centroid of the whitening
    % Find centre
    property = regionprops(Images{i,7}, 'Centroid');
    centre = property.Centroid;
    cxtemp = centre(:,1);
    cytemp = centre(:,2);
```

```
        if i<lengthImages
        %(check if first cycle)
        %Dist from previous 'valid' centre
        clear cxprev cyprev
        [~,~,cxprev] = find(cx);
        [~,~,cyprev] = find(cy);

        %Check the centre of the whitening is near previously detected
whitening
        %and is above a threshold size
        dist = sqrt((cxtemp-cxprev(1))^2+(cytemp-cyprev(1))^2);

            if dist>diststhresh || biggest < 50
                %If not close - try alternative methods of detection
                Images{i,7} = [];

                % Check if there is a 'large' whitening area near the
previous centre
                % point=ginput(1) (i.e. if the previous centre is within
a whitening area);
            %     if sum(point)>200
                  Images{i,7} = bwselect(xx2,cyprev(1),cxprev(1),4);
                  [~,~,v] = find(Images{i,7});
                  biggest = sum(v);

                  %If there isn't a whitening area close to prev centre -
then try second
                  %largest area

                      if biggest < 50
%
                        % Find Second Largest Element (xx2 is now the
whitening - largest
                        % element)
                        CC = bwconncomp(xx2);
                        BWlargest=xx2;
                        numPixels = cellfun(@numel,CC.PixelIdxList);
                        [biggest,idx] = max(numPixels);
                        xx2(CC.PixelIdxList{idx}) = 0;

                        if isempty(biggest)==0 %not empty
%
                        Images{i,7} = BWlargest - xx2;
                        %figure,imshow(Images{i,7})
                        % Find the centroid of the whitening
                        % Find centre
                        property = regionprops(Images{i,7}, 'Centroid');
                        centre = property.Centroid;
                        cxtemp = centre(:,1);
                        cytemp = centre(:,2);

                        dist = sqrt((cxtemp-cxprev(1))^2+(cytemp-
cyprev(1))^2);

                        %Check again if the whitening area is large
enough and close enough
                        % if not, erase
                            if dist>diststhresh || biggest < 50
                                Images{i,7} = [];
                            else
```

```
                                %Otherwise keep and record centre point
                                cx(i) = cxtemp;
                                cy(i) = cytemp;
                            end
                        else
                            Images{i,7}=[];
                        end
                    else
                        %Otherwise keep and record centre point
                        property = regionprops(Images{i,7}, 'Centroid');
                        centre = property.Centroid;
                        cxtemp = centre(:,1);
                        cytemp = centre(:,2);

                end

            else
                    %If initial method (largest element) works
                    property = regionprops(Images{i,7}, 'Centroid');
                    centre = property.Centroid;
                    cx(i) = centre(:,1);
                    cy(i) = centre(:,2);

            end


    else
        %First cycle find the distance threshold
        [height width] = size(Images{i,7});
        distthresh = round(0.1*sqrt(height^2+width^2));
        cx(i) = cxtemp;
        cy(i) = cytemp;
    end
%If empty - don't select a whitening area
end

end

clear xx xx2

%%
%  Extrema and offset %%%%%%%%%%%%%%%%%%%%%%%%%%%%%%%%%%%%%%%%%%%%%%%%%%%%%%%%
close all

Flag =0;
for i = 1:lengthImages

    %If there is no image, flag
    find(Images{i,7});
    if or(isempty(Images{i,7}),isempty(ans))
        Flag =1;
        continue
    end

    %The major axis (longest diagonal distance)
    Stat_Front = regionprops(Images{i,7},'Extrema');
    STAT_C = regionprops(Images{i,7},'Centroid');
    Centroid(i,1) = round(STAT_C.Centroid(1,1)*(1/MagnFactor));    %
Centroid X
    Centroid(i,2) = round(STAT_C.Centroid(1,2)*(1/MagnFactor));    %
Centroid Y
```

```
    tempFr1 = round(Stat_Front.Extrema(1,:)*(1/MagnFactor)); %Extrema
top-right
    tempFr2 = round(Stat_Front.Extrema(2,:)*(1/MagnFactor)); %Extrema
top-left

    if tempFr1(1,1) < 1
        tempFr1(1,1) = 1;
    end
     if tempFr1(1,2) < 1
        tempFr1(1,2) = 1;
     end
     if tempFr2(1,1) < 1
        tempFr2(1,1) = 1;
     end
     if tempFr2(1,2) < 1
        tempFr2(1,2) = 1;
    end


    if Flag==1

        Flag=0;
    else
        %if there isn't a flag (i.e. whitening image not empty) - find
the
        %displacement
        ElapsedTime =(i*FrameStep)/FrameRate;
        ii =1;
        %Find the corresponding displacement
        while LoadTime1(ii,3)<ElapsedTime
            ii =ii+1;
        end
        Displ = LoadTime1(ii,1);
        %Displacement offset plus notch position (in pixels)
        YNotch =YNotch0+Displ/Cal*1000;


    %Find if top left or top right is more extreme (pixels)
    Fr1 = sqrt((XNotch-tempFr1(1,1))^2+(YNotch-tempFr1(1,2))^2);
    Fr2 = sqrt((XNotch-tempFr2(1,1))^2+(YNotch-tempFr2(1,2))^2);

        if Fr1 >= Fr2
            Front(i,1) = (YNotch-tempFr1(1,2))*Cal; %in um (vertical
distance)
        else
            Front(i,1) = (YNotch-tempFr2(1,2))*Cal; %in um (vertical
distance)
        end

    ImagesFront{i,1} = zeros(size(Images{i,4}));
    ImagesFront{i,1} = Images{i,4};
    ImagesFront{i,1}(tempFr1(1,2),tempFr1(1,1)) = 255;
    ImagesFront{i,1}(tempFr1(1,2),tempFr2(1,1)) = 255;

    %Plot extreme points over image

ImagesFront{i,1}(round(Stat_Front.Extrema(3,2)*(1/MagnFactor)),ceil(Stat_
Front.Extrema(3,1)*(1/MagnFactor))) = 255 ; %right-top
```

```
ImagesFront{i,1}(ceil(Stat_Front.Extrema(4,2)*(1/MagnFactor)),ceil(Stat_F
ront.Extrema(4,1)*(1/MagnFactor))) = 255 ; %right-bottom

ImagesFront{i,1}(ceil(Stat_Front.Extrema(5,2)*(1/MagnFactor)),ceil(Stat_F
ront.Extrema(5,1)*(1/MagnFactor))) = 255 ; %bottom-right

ImagesFront{i,1}(ceil(Stat_Front.Extrema(6,2)*(1/MagnFactor)),ceil(Stat_F
ront.Extrema(6,1)*(1/MagnFactor))) = 255 ; %bottom-left

ImagesFront{i,1}(ceil(Stat_Front.Extrema(7,2)*(1/MagnFactor)),ceil(Stat_F
ront.Extrema(7,1)*(1/MagnFactor))) = 255 ; %left-bottom

ImagesFront{i,1}(ceil(Stat_Front.Extrema(8,2)*(1/MagnFactor)),ceil(Stat_F
ront.Extrema(8,1)*(1/MagnFactor))) = 255 ; %left-top


    Centroid(i,3) = sqrt((XNotch-Centroid(i,1))^2+(YNotch-
Centroid(i,2))^2); % Centroid Distance from notch
    Centroid(i,4) = Centroid(i,3)*Cal; %in um
    % 'MajorAxisLength'
end
end

%If there is no whitening image use original difference image
for i = lengthImages:-1:1
    if isempty(ImagesFront{i,1})
        ImagesFront{i,1} = Images{i,4};
    end
end
close all

%% Play sequence in a Video-like mode
close all
keep = 1;

while keep

    for i = 1:length(ImagesFront)

    scrsz = get(0,'ScreenSize');

    h3 = figure(3);
    %set(h2,'Position',[700 scrsz(4)/5 scrsz(3)-640 scrsz(4)-300]);
    imshow(ImagesFront{i,1},[],'InitialMagnification',
400) %title('Registered Image')
    fname =
strcat('DamageLocalization_',int2str(i),'_',int2str(lengthImages),'.tif');
    %imwrite(imresize(ImagesFront{i,1},3),fname,'tif');

    end

 keep = keep-1;
end


%% Calculate Whitening Diff
%%%%%%%%%%%%%%%%%%%%%%%%%%%%%%%%%%%%%%%%%%%%%%%%%%%%%%%%%%%%%%%%%%%%%%%%%%
WhitesCount = zeros(lengthImages,3);
```

```
%Whitening area (number of pixels)
for i = 1:lengthImages
WhitesCount(i,1) = (sum(sum(Images{i,7})))/MagnFactor^2; %Area in pixels
end

flag = 0;
startframe = 1;
% [~,MaxX] = max(LoadTime(:,4)); % MaxX : Index of Maximum Load
% FalureFrame = round(round(LoadTime(MaxX,3)*60)/FrameStep)

 while flag == 0
 WhitesCount(1,2) = FrameStep/FrameRate; %Frame

    for i = 2:lengthImages
        WhitesCount(i,2) =
(i*FrameStep)/FrameRate;                                    %60 = FPS - frame
number
        WhitesCount(i,3) = WhitesCount(i,1) - WhitesCount(i-
1,1);           %Diff From Previous Frame in Pixels (whitening size
difference)
        WhitesCount(i,4) = (WhitesCount(i,1) -
WhitesCount(startframe,1))*Cal^2*10^(-6);    %Diff From startframe in
mm^2 (whitening area)
    end

    [~, OffsetFrame] = min(WhitesCount(:,4));
    if WhitesCount(OffsetFrame,4) < -10
        startframe = OffsetFrame;
    else
        flag = 1;
    end

 end


for i = 1:lengthImages
    j = 1;

    % Finds the Load which corespond to the curent time frame
    while WhitesCount(i,2) >= LoadTime1(j,3)
        j = j+1;
    end

    if j == 1
        j=2;
    end

Centroid(i,5) = LoadTime1(j-1,1);    % Displacement  variable
% MA(i,3) = LoadTime1(j-1,1);          % Displacement  variable
WhitesCount(i,5) = LoadTime1(j-1,1); % Displacement  variable (mm)
WhitesCount(i,6) = LoadTime1(j-1,2); % Force variable (Newton)
WhitesCount(i,7) = LoadTime1(j-1,3); % Time variable (sec)
end

close all


%% max and min range (based on whitening area)
close all
[~,MaxX] = max(LoadTime1(:,2));
```

```
WhitesCount(:,8) = smooth(WhitesCount(:,4),11,'rlowess');

if max (WhitesCount(:,8)) ==0
    WhitesCount(:,8) = smooth(WhitesCount(:,4),3,'rlowess');
end
  areathresh = max(WhitesCount(1:round(0.25*length(WhitesCount)),8))*5;
  if areathresh>0.002
      areathresh=0.002;
  end
    [rarea ~] = find(WhitesCount(:,8)>areathresh);

    mindispa = WhitesCount(rarea(1),5);
    maxdispa = dmax;

    % Check if these max and min appear suitable

    figure();
    set(gcf, 'Position', get(0,'Screensize')); % Maximize figure.
    subplot(3,1,1)
    plot(WhitesCount(:,5),WhitesCount(:,4),'bo',[mindispa mindispa],[0
(max(WhitesCount(:,4))+max(WhitesCount(:,4))*0.055)],'r',[maxdispa
maxdispa],[0 (max(WhitesCount(:,4))+max(WhitesCount(:,4))*0.055)],'r');
    xlabel('Displacement (mm)');
    ylabel('Whitening Area (mm^2)');
    axis([0 (LoadTime1(MaxX,1)+LoadTime1(MaxX,1)*0.1) 0
(max(WhitesCount(:,4))+max(WhitesCount(:,4))*0.055)])
    %axis([0 (LoadTime1(MaxX,3)+LoadTime(MaxX,3)*0.1) -100 300])

    subplot(3,1,2)
    plot(WhitesCount(:,5),Front(:,1),'bo',[mindispa mindispa],[0
(max(Front(:,1)+100))],'r',[maxdispa maxdispa],[0
(max(Front(:,1)+100))],'r');
    xlabel('Displacement (mm)');
    ylabel('Front Distance from Notch (um)');
    axis([0 (LoadTime1(MaxX,1)+LoadTime1(MaxX,1)*0.1) 0
(max(Front(:,1)+100))])

    subplot(3,1,3)
    plot(LoadTime1(:,1),LoadTime1(:,2),'bo',[mindispa mindispa],[0
(max(LoadTime1(:,4))+max(LoadTime1(:,4))*0.055)],'r',[maxdispa
maxdispa],[0 (max(LoadTime1(:,4))+max(LoadTime1(:,4))*0.055)],'r')
    xlabel('Displacement (mm)');
    ylabel('Load (Newton)');
    axis([0 (LoadTime1(MaxX,1)+LoadTime1(MaxX,1)*0.1) 0
(max(LoadTime1(:,4))+max(LoadTime1(:,4))*0.055)])

            prompt = {'Minimum Displacement (i.e. when crack propagation
begins or Fd is nonlinear)',...
                strcat('Maximum Displacement (i.e. at max force
=',WhitesCount(end,5),'mm)')};
            Title = 'Displacement range';
            numlines = 1;
            defaultanswer = {num2str(mindispa),num2str(maxdispa)};
            options.Resize='on';
            answer =
inputdlg(prompt,Title,numlines,defaultanswer,options);

            mindisp = str2double(cell2mat(answer(1,1)));
            maxdisp = str2double(cell2mat(answer(2,1)));
```

```
            %Check if automatically calculated or manually changed
            if mindispa==mindispa
                if maxdispa==maxdispa
                    man(5)=1;
                else
                    man(5)=2;
                end
            else
                man(5)=2;
            end

    % Find these positions

    [~,minpos]=min(abs(WhitesCount(:,5)-mindisp));
    [~,maxpos]=min(abs(WhitesCount(:,5)-maxdisp));


%%  J Calculations for the Resistance Curve Test Method 1/2
%close all

%Calculate the effective stiffness based on prenotched sample (based on
%coefficients from FE analysis - Federico Quinci
    Ef = ((S^3*fit_coef(1))/(4*B*(W-a0)^3)); %for 3-point bending in MPa
    E = Ef -22.6*a0 -72.7*a0^2; %N/mm^2 (i.e. MPa)

for i = 1:length(WhitesCount)
    %As calculated in ASTM 1820-01  A1.4.1

    ai(i) = a0+ Front(i,1)*0.001;   % Total 'crack' length in (mm)
    f_ai_w_numerator(i) = 3*(ai(i)/W)^0.5*(1.99-(ai(i)/W)*(1-
(ai(i)/W))*(2.15-3.93*(ai(i)/W)+2.7*(ai(i)/W)^2));
    f_ai_w(i) = f_ai_w_numerator(i)/(2*(1+2*(ai(i)/W)*(1-
(ai(i)/W))^(3/2))); %Shape factor A1.3

    K(i) =((WhitesCount(i,6)*S)/(B*W^(3/2)))*f_ai_w(i); %A1.2 where B=Bn
for sample without side grooves (N/mm^3/2)
end

%%  J Calculations for the Resistance Curve Test Method 2/2
%close all;

%Calculate Apl
    for i = 1:length(Plastic_LoadDisp)

        if Plastic_LoadDisp(i,1)<0 %i.e. if in elastic zone
            Apl_raw(i,1) = 0;
        else
            if Plastic_LoadDisp(i,1)>LoadTime1(MaxX,1)-
PlasticRegInitiation; %i.e. after maximum load - post failure
                Apl_raw(i,1) = 0;
            else
                %Total area under plastic region of the curve - area of
                %this region added to previously calculated region
                Apl_raw(i,1) = Apl_raw(i-1,1) + trapz(Plastic_LoadDisp(i-
1:i,1),Plastic_LoadDisp(i-1:i,2));

            end
        end
    end
    %plot(Plastic_LoadDisp(:,1),Apl_raw)
```

```
%Find Apl value that correspond to displacement in whitening matrix
    %(i.e. down sample in accordance with videography)
for i = 1:length(WhitesCount(:,5))

    [c(i) index(i)] = min(abs(Plastic_LoadDisp(:,1)-(WhitesCount(i,5)-
PlasticRegInitiation)));
    Apl(i,1) = Apl_raw(index(i),1);

end

%Uncracked ligament length as a function of time
b(:,1) = W-ai(:);

%Calculate Jpl
Jpl(1,1) = 0;
J(1,1) = 0;

for i = 2:length(WhitesCount(:,5));
 Jpl(i,1) = (Jpl(i-1,1)+(2/b(i-1)*(Apl(i)-Apl(i-1))/B))*(1-(ai(i)-ai(i-
1))/b(i-1)); % ASTM A(1.7)
 test(i) = (ai(i)-ai(i-1))/b(i-1);
 %Apl(i)-Apl(i-1) is the area under this section i.e FIG A1.3 (or the
 %proportion initially calculated by trapz)
 %b is the uncracked ligament length  %B is the sample thickness
 %ai(i)-ai(i-1) is the crack propagation from the previous step (this is
 %close to 0 as increase in ai is not linearly increasing and close to
 %constant at b(i-1) is a function of ai.

 %Jpl: N/mm or KJ/m^2
end

%Only a rising R curve
[temp Flag] = max(Jpl);


%Calculate J and Keff
for i = 2:length(WhitesCount(:,5))
    if i <Flag
        %J=Jel+Jpl
        J(i,1) = ((K(i)^2)/E)+Jpl(i,1); %ASTM A(1.6)
        %J = (N/mm^3/2)^2/(N/mm^2) + N/mm (i.e. in N/mm or KJ/m^2)
        Jel(i,1) = ((K(i)^2)/E);

        %Jel=K^2/E
        Keff(i,1) = sqrt(E*J(i,1))*0.0316; %0.0316 (1000^3/2 x 10^-6) to
convert from N/mm^3/2 to MPa.sqrt(m)
    else
        J(i,1) = 0;
        Keff(i,1) = 0;
    end
end

%RCurveVals - Time, Disp, Load, Da, Keff, J

%Limit to rising portion of curve or maximum load
if maxpos>Flag-1
    maxpos=Flag-1;
end
clear RCurveVals
```

```
%Limit to previously identified span (i.e. rising r-curve)
ind = find(Front(minpos:maxpos,1))+minpos-1;

RCurveVals(:,1) = WhitesCount(ind,7); %Time
RCurveVals(:,2) = WhitesCount(ind,5); %Disp
RCurveVals(:,3) = WhitesCount(ind,6); %Load
RCurveVals(:,4) = Front(ind,1); %Whitening Offset, um
RCurveVals(:,5) = Keff(ind,1); %K
RCurveVals(:,6) = J(ind,1); %J

% J int: Fit a straight line
Jcoeffs = polyfit(RCurveVals(:,4),RCurveVals(:,6), 1);
JfittedX = [min(RCurveVals(:,4)),max(RCurveVals(:,4))];
JfittedY = JfittedX*Jcoeffs(1)+Jcoeffs(2); %JfittedY(1) is the initiation
toughness, JfittedY(2) is the fracture toughness and Jcoeffs(1) is the
crack growth resistan

% K eff: Fit a straight line
Kcoeffs = polyfit(RCurveVals(:,4),RCurveVals(:,5), 1);
KfittedX = [min(RCurveVals(:,4)),max(RCurveVals(:,4))];
KfittedY = KfittedX*Kcoeffs(1)+Kcoeffs(2);

%% Plot figures
figure();
    subplot(2,3,[1 3])
    plot(RCurveVals(:,4),RCurveVals(:,6),'bo',JfittedX, JfittedY, 'k-',
'LineWidth', 1);
    xlabel('Da (um)');
    ylabel('J (kJ/m^2)');
    axis([0 round(max(RCurveVals(:,4))*1.1) 0
ceil(max(RCurveVals(:,6))*11)/10])

    subplot(2,3,[4 6])
    plot(RCurveVals(:,4),RCurveVals(:,5),'ro',KfittedX, KfittedY, 'k-',
'LineWidth', 1);
    xlabel('Da (um)');
    ylabel('Keff (MPa.m^1/2)');
%     hold on;
%     plot(KfittedX, KfittedY, 'k-', 'LineWidth', 1);
   axis([0 round(max(RCurveVals(:,4))*1.1) 0
ceil(max(RCurveVals(:,5))*1.1)])

%% Export and save
% %% EXPORT
%close all
currentFolder = pwd;
ExportFilename=strcat(currentFolder,'\',dataname(1:end-4),'.xls');
ExportFilecsv1=strcat(currentFolder,'\',dataname(1:end-4),'graph','.csv');
ExportFilecsv2=strcat(currentFolder,'\',dataname(1:end-
4),'summary','.csv');
ExportFilecsv3=strcat(currentFolder,'\',dataname(1:end-
4),'manual','.csv');
savename = strcat(currentFolder,'\',dataname(1:end-4),'.mat');

%Save workspace variable
save(savename);

csvwrite(ExportFilecsv1,RCurveVals); % Rcurve csv

    %saveas(gcf, sprintf('Front Distance from Notch.tif'));
```

```
%%%%% Summary Value %%%%%%
 Output(:,1)=S;
Output(:,2)=W;
Output(:,3)=B;
Output(:,4)=a0;
Output(:,5)=KfittedY(1);
Output(:,6)=Kcoeffs(1);
Output(:,7)=KfittedY(2);
Output(:,8)=JfittedY(1);
Output(:,9)=Jcoeffs(1);
Output(:,10)=JfittedY(2);
Output(:,11)=E;

csvwrite(ExportFilecsv2,Output); % Rcurve csv
csvwrite(ExportFilecsv3,man); % Manual csv
% 1 is automatic, 2 is manual for - 1: Linearity selection, 2: ROI
% selection, 3: Notch selection, 4: Registration, 5: Max/Min Limits
```

9.5.3 Segmentation of Serial Section Fluorescence Microscopy Image Stack

9.5.3.1 Indent Segmentation

```
%% Written by Tom Jenkins

%% Semi-automatic segmentation of the indent
% Manually draw around the central indent then use this initial outline
to for refined automatic selection in the central and subsequent slices
close all
clear all
clc

% Get pathname and image name
[imagenameR, pathname] = uigetfile('*.tif','Select the red central
image:');

def = {num2str(imagenameR(end-5))};
answer = inputdlg(strcat('Distance of R from right hand side - default
shows location 6 from:',imagenameR),'R location',1,def);
Rlocation = str2double(answer{1});

%% Select image magnification
choice = questdlg('What is the image magnification', ...
    'Magnification', ...
    '10x','20x','50x','10x');
% Handle response
switch choice
    case '10x'
        res = 0.68;
        lim = 20;
    case '20x'
        res = 0.34;
        lim = 20;
    case '50x'
        res = 0.136;
        lim = 30;
end

%%
directories = dir(strcat(pathname,'/*.tif'));
number = length(directories);

%Split into R and G files
%Find selected central location
r=1;
g=1;
for i = 1:number
   tempname = directories(i).name;
   if tempname(end-Rlocation+1)=='R'
       if strcmp(tempname,imagenameR)==1
           centralloc = r;
       end
       Rnamelist{r} = tempname;
       r=r+1;
   end
   if tempname(end-Rlocation+1)=='G'
       Gnamelist{g} = tempname;
       g=g+1;
   end
end
```

```
% Loop through slices
%slice location central:end, central-1:end
sliceorder(1:length(Rnamelist)-centralloc+1) =
centralloc:length(Rnamelist);
sliceorder(length(Rnamelist)-centralloc+2:length(Rnamelist)) =
centralloc-1:-1:1;

choice = questdlg('Manual or automatic registration', ...
    'Registration', ...
    'Manual','Automatic','Automatic');
% Handle response
switch choice
    case 'Manual'
        man = 1;
        string = {'Click a repeatable point to register image'};
        waitfor (helpdlg(string,'Info'))

            for slices=1:length(sliceorder)
                slice = sliceorder(slices);
            %  slice=slice+1
            imagenameR = Rnamelist{slice};
            imagenameG=strcat(imagenameR(1:end-
Rlocation),'G',imagenameR(end-Rlocation+2:end));
            nomefileR=strcat(pathname,imagenameR);
            nomefileG=strcat(pathname,imagenameG);

            % Load R and G images and combine
            IR=imread(nomefileR);
            IR2 = IR(:,:,1);
            IG=imread(nomefileG);
            IG2 = IG(:,:,2);
            clear IRG
            IRG(:,:,1) = IR2;
            IRG(:,:,2) = IG2;
            IRG(:,:,3) = 0;

            figure,imshow(IRG);
            [xreg(slices),yreg(slices)]=ginput(1);
            close all
            end

            yreg2 = yreg(1)-yreg;
            xreg = xreg-xreg(1);

    case 'Automatic'
        man = 2;
end

slices=1;
cont = 1;
manualselect=0;

for slices=1:length(sliceorder)
    slice = sliceorder(slices);
if slice == centralloc-1
    cont=1;
end

imagenameR = Rnamelist{slice};
```

```
imagenameG=strcat(imagenameR(1:end-Rlocation),'G',imagenameR(end-
Rlocation+2:end));
    nomefileR=strcat(pathname,imagenameR);
    nomefileG=strcat(pathname,imagenameG);

%% Load R and G images and combine
IR=imread(nomefileR);
IR2 = IR(:,:,1);

IG=imread(nomefileG);
IG2 = IG(:,:,2);

clear IRG
IRG(:,:,1) = IR2;
IRG(:,:,2) = IG2;
IRG(:,:,3) = 0;

I=1;
if cont==1

if slices==1
%% Crop
IRcomb = IR2-IG2;

close all
string = {'Click the Left THEN Right hand point of the base of the
indent'};
waitfor (helpdlg(string,'Info'))
figure,imshow(IRG);
[x1,j1]=ginput(1);
[x2,j2]=ginput(1);
j= round(min(j1,j2));

%
close all
string = {'Click the point of the indent'};
waitfor (helpdlg(string,'Info'))
figure,imshow(IRG);
[col(I),row(I)]=ginput(1);
col(I)= round(col(I));
row(I) = round(row(I));

IRcrop = IRcomb(row(I)-100:j+50,round(x1)-150:round(x2)+150);
IRadapt = adapthisteq(IRcrop);
IR2b = medfilt2(IRadapt,[5 5]);
figure, imshow(IR2b) %%%%

string = {'Trace around the indent (left to right) then double click on
the selection'};
waitfor (helpdlg(string,'Info'))
h = imfreehand(gca);
position = wait(h);

%Split into Left and Right halves
ylimit = j+row(I)-100;

clear posL posLa posR posRa

[minval,minloc] = min(position(:,2));
posLa = position(1:minloc,:);
posRa = position(minloc+1:end,:);
```

```
indLpos = find(posLa(:,2)<ylimit);
posL(:,1:2) = posLa(indLpos,1:2);
indRpos = find(posRa(:,2)<ylimit);
posR(:,1:2) = posRa(indRpos,1:2);


else if manualselect==1

 %% Load R and G images and combine
 IRcomb2 = IR2-IG2;

        %Register images
        [optimizer,metric] = imregconfig('multimodal');
        optimizer.InitialRadius = optimizer.InitialRadius/3;
        optimizer.MaximumIterations = 200;

    if man==2

        registered = imregister(IRcomb2, IRcomb, 'translation', optimizer,
metric);
         IRcomb = registered;

     else

        IRcombtrans = imtranslate(IRcomb2,[0,yreg2(slices)]);
        IRcomb=IRcombtrans;
    end


 IRcrop = IRcomb(row(I)-100:j+50,round(x1)-150:round(x2)+150);
IRadapt = adapthisteq(IRcrop);
IR2b = medfilt2(IRadapt,[5 5]);

IRcrop = IRcomb(row(I)-100:j+50,round(x1)-150:round(x2)+150);
IRadapt = adapthisteq(IRcrop);
IR2b = medfilt2(IRadapt,[5 5]);
figure, imshow(IR2b) %%%%
string = {'Trace around the indent (left to right) then double click on
the selection'};
waitfor (helpdlg(string,'Info'))
h = imfreehand(gca);
position = wait(h);

%Split into Left and Right halves
ylimit = j+row(I)-100;

clear posL posLa posR posRa

[minval,minloc] = min(position(:,2));
posLa = position(1:minloc,:);
posRa = position(minloc+1:end,:);
indLpos = find(posLa(:,2)<ylimit);
posL(:,1:2) = posLa(indLpos,1:2);
indRpos = find(posRa(:,2)<ylimit);
posR(:,1:2) = posRa(indRpos,1:2);


    manualselect=0;
```

```
else if slice == centralloc-1
    %If in the middle slice
    imagenameR1 = Rnamelist{sliceorder(1)};
imagenameG1=strcat(imagenameR(1:end-Rlocation),'G',imagenameR(end-
Rlocation+2:end));
    nomefileR1=strcat(pathname,imagenameR1);
    nomefileG1=strcat(pathname,imagenameG1);

%% Load R and G images and combine
IR1=imread(nomefileR1);
IR21 = IR1(:,:,1);
IG1=imread(nomefileG1);
IG21 = IG1(:,:,2);
IRcomb = IR21-IG21;

    IRcomb2 = IR2-IG2;
        %Register images
        [optimizer,metric] = imregconfig('multimodal');
        optimizer.InitialRadius = optimizer.InitialRadius/3;
        optimizer.MaximumIterations = 200;

    if man==2

        registered = imregister(IRcomb2, IRcomb, 'translation', optimizer,
metric);
         IRcomb = registered;

    else

         IRcombtrans = imtranslate(IRcomb2,[0,yreg2(slices)]);
        IRcomb=IRcombtrans;
    end

    IRcrop = IRcomb(row(I)-100:j+50,round(x1)-150:round(x2)+150);
IRadapt = adapthisteq(IRcrop);
IR2b = medfilt2(IRadapt,[5 5]);

    clear posL posR posLa posRa
    previndent = IndentOutline{1,1};
[minval,minloc] = min(previndent(:,1));

posLa(:,2) = previndent(1:minloc,1)-row(I)+100;
posLa(:,1) = previndent(1:minloc,2)-round(x1)+150;
posRa(:,2) = previndent(minloc+1:end,1)-row(I)+100;
posRa(:,1) = previndent(minloc+1:end,2)-round(x1)+150;

indLpos = find(posLa(:,2)<ylimit);
posL(:,1:2) = posLa(indLpos,1:2);
indRpos = find(posRa(:,2)<ylimit);
posR(:,1:2) = posRa(indRpos,1:2);

posL=sortrows(posL,-2);
posR=sortrows(posR,-2);



    else
    IRcomb2 = IR2-IG2;

        %Register images
        [optimizer,metric] = imregconfig('multimodal');
```

```
        optimizer.InitialRadius = optimizer.InitialRadius/3;
        optimizer.MaximumIterations = 200;

    if man==2

        registered = imregister(IRcomb2, IRcomb, 'translation', optimizer,
metric);
         IRcomb = registered;

     else

        IRcombtrans = imtranslate(IRcomb2,[0,yreg2(slices)]);
        IRcomb=IRcombtrans;
    end


 IRcrop = IRcomb(row(I)-100:j+50,round(x1)-150:round(x2)+150);
IRadapt = adapthisteq(IRcrop);
IR2b = medfilt2(IRadapt,[5 5]);

    clear posL posR posLa posRa
    previndent = IndentOutline{slices-1,1};
[minval,minloc] = min(previndent(:,1));

posLa(:,2) = previndent(1:minloc,1)-row(I)+100;
posLa(:,1) = previndent(1:minloc,2)-round(x1)+150;
posRa(:,2) = previndent(minloc+1:end,1)-row(I)+100;
posRa(:,1) = previndent(minloc+1:end,2)-round(x1)+150;

indLpos = find(posLa(:,2)<ylimit);
posL(:,1:2) = posLa(indLpos,1:2);
indRpos = find(posRa(:,2)<ylimit);
posR(:,1:2) = posRa(indRpos,1:2);

posL=sortrows(posL,-2);
posR=sortrows(posR,-2);

    end
    end
end

%% Use as guideline to find real edge
 clear lefpos rightpos


%Left hand side
k=1;

for iL=length(posL):-1:1
    clear intensity

    intensity(:,1) = 1:2*lim+1;
    intensity(:,2) = IR2b(round(posL(iL,2)),round(posL(iL,1))-
lim:round(posL(iL,1))+lim);
    %smooth
    intensity(:,3) = smooth(intensity(:,1),intensity(:,2),10,'rloess');

    %Check if increasing or decreasing intensity
    if max(intensity(1:lim,3))>max(intensity(lim:end,3))
           %Find min (RHS) and max (LHS)
```

```
            [minthresh,minpos] = min(intensity(lim:end,3));
            [maxthresh,maxpos] = max(intensity(1:lim,3));
             %Threshold and select point
            thresh = minthresh*0.7+maxthresh*0.3;
            [abovethresh,~,~] = find(intensity(maxpos:minpos+lim-
1,3)>thresh);
            leftpos(k,1) = abovethresh(end)+maxpos+round(posL(iL,1))-lim-
2;

    else
           %Find min (LHS) and max (RHS)
            [minthresh,minpos] = min(intensity(1:lim,3));
            [maxthresh,maxpos] = max(intensity(lim:end,3));
             %Threshold and select point
            thresh = minthresh*0.3+maxthresh*0.7;
            [abovethresh,~,~] = find(intensity(minpos:maxpos+lim-
1,3)>thresh);
            leftpos(k,1) = abovethresh(1)+minpos+round(posL(iL,1))-lim-2;
    end

     leftpos(k,2) = round(posL(iL,2));

    k=k+1;
end

%Right hand side
k=1;

for iR=length(posR):-1:1
    clear intensity

    intensity(:,1) = 1:2*lim+1;
    intensity(:,2) = IR2b(round(posR(iR,2)),round(posR(iR,1))-
lim:round(posR(iR,1))+lim);
    %smooth
    intensity(:,3) = smooth(intensity(:,1),intensity(:,2),10,'rloess');

    %Check if increasing or decreasing intensity
    if max(intensity(lim:end,3))>max(intensity(1:lim,3))
        %Find min (LHS) and max (RHS)
        [minthresh,minpos] = min(intensity(1:lim,3));
        [maxthresh,maxpos] = max(intensity(lim:end,3));
        %Threshold and select point
        thresh = minthresh*0.7+maxthresh*0.3;
        [abovethresh,~,~] = find(intensity(minpos:maxpos+lim-1,3)>thresh);
        rightpos(k,1) = abovethresh(1)+minpos+round(posR(iR,1))-lim-2;
    else
        %Find min (RHS) and max (LHS)
        [minthresh,minpos] = min(intensity(lim:end,3));
        [maxthresh,maxpos] = max(intensity(1:lim,3));
        %Threshold and select point
        thresh = minthresh*0.3+maxthresh*0.7;
        [abovethresh,~,~] = find(intensity(maxpos:minpos+lim-1,3)>thresh);
        rightpos(k,1) = abovethresh(end)+maxpos+round(posR(iR,1))-lim-2;
    end

    rightpos(k,2) = round(posR(iR,2));

    k=k+1;

end
```

```
%Upper
clear upperpos
k=1;

%aspect ratio
iheight = posL(1,2)-posL(end,2);
iwidth = posR(1,1)-posL(1,1);
iAR = iwidth/iheight;

if iAR^0.75/12>0.4
    urange = round(iwidth*0.4);
else
    urange = round(iwidth*iAR^0.75/12);
end

for iU=posL(end,1)-urange:posL(end,1)+urange
    clear intensity

    intensity(:,1) = 1:2*lim+1;
    if iU<posL(end,1)
        [~,ypos]=min(abs(posL(:,1)-iU));
        intensity(:,2) = IR2b(round(posL(ypos,2))-
lim:round(posL(ypos,2))+lim,round(posL(ypos,1)));
    else
        [~,ypos]=min(abs(posR(:,1)-iU));
        intensity(:,2) = IR2b(round(posR(ypos,2))-
lim:round(posR(ypos,2))+lim,round(posR(ypos,1)));
    end

    %smooth
    intensity(:,3) = smooth(intensity(:,1),intensity(:,2),10,'rloess');

 %Check if increasing or decreasing intensity
    if max(intensity(1:lim,3))>max(intensity(lim:end,3))
        %Find min (RHS - i.e. lower) and max (LHS i.e. upper)
        [minthresh,minpos] = min(intensity(lim:end,3));
        [maxthresh,maxpos] = max(intensity(1:lim,3));
        %Threshold and select point
        thresh = minthresh*0.7+maxthresh*0.3;
        [abovethresh,~,~] = find(intensity(maxpos:minpos+lim-1,3)>thresh);
        threshpoint = abovethresh(end)+maxpos;
    else
        %Find min (LHS - i.e. upper) and max (RHS i.e. lower)
        [minthresh,minpos] = min(intensity(1:lim,3));
        [maxthresh,maxpos] = max(intensity(lim:end,3));
        %Threshold and select point
        thresh = minthresh*0.3+maxthresh*0.7;
        [abovethresh,~,~] = find(intensity(minpos:maxpos+lim-1,3)>thresh);
        threshpoint = abovethresh(1)+minpos;
    end

    if iU<posL(end,1)
        upperpos(k,1) = threshpoint+round(posL(ypos,2))-lim-2;
        upperpos(k,2) = iU;
    else
        upperpos(k,1) = threshpoint+round(posR(ypos,2))-lim-2;
        upperpos(k,2) = iU;
    end

    k=k+1;
```

```
end

%sort
leftpos=sortrows(leftpos,2);
rightpos=sortrows(rightpos,-2);
%smooth
leftpos(:,3) = smooth(leftpos(:,1),10,'rlowess');
rightpos(:,3) = smooth(rightpos(:,1),10,'rlowess');
upperpos(:,3) = smooth(upperpos(:,2),upperpos(:,1),10,'rlowess');

%% Combine
figure, imshow(IR2b);  hold on
plot(leftpos(:,3),leftpos(:,2),'g'); hold on
plot(rightpos(:,3),rightpos(:,2),'r');
plot(upperpos(:,2),upperpos(:,3),'b');
hold off

%Preliminary Combination of Left, Right and Upper
%Find uppermost point
[~,uminloc] = min(upperpos(:,3));
%Find where upper crosses left and right
[xil,yil] =
polyxpoly(leftpos(:,3),leftpos(:,2),upperpos(:,2),upperpos(:,3));
[xir,yir] =
polyxpoly(rightpos(:,3),rightpos(:,2),upperpos(:,2),upperpos(:,3));

%If they don't cross - find where they come closest
if isempty(xil)==1
    clear minLC
    for iLx = 1:urange;
        [~, minLC(iLx)] = min((leftpos(:,3)-
upperpos(iLx,2)).^2+(leftpos(:,2)-upperpos(iLx,3)).^2);
    end
    [lval,uval] = min(minLC);
    xil=0.5*(leftpos(lval,3)+upperpos(uval,2));
else
    xil=min(xil);
end

if isempty(xir)==1
    clear minRC
    for iRx = urange:2*urange+1;
        [~, minRC(iRx+1-urange)] = min((rightpos(:,3)-
upperpos(iRx,2)).^2+(rightpos(:,2)-upperpos(iRx,3)).^2);
    end
    [rval,uval] = min(minRC);
    xir=0.5*(rightpos(rval,3)+upperpos(uval,2));
else
    xir=max(xir);
end

%Find leftmost and rightmost intersections and there corresponsing points
%on left and right lines as well as the upper line
 [~,ulloc] = min(abs(xil - leftpos(:,3)));
 [~,ulmin] = min(abs(xil - upperpos(:,2)));

 [~,urloc] = min(abs(xir - rightpos(:,3)));
 [~,urmax] = min(abs(xir - upperpos(:,2)));

% Combine
```

```
%Left
%figure,plot(Combined(:,2),Combined(:,1))
Combined(1:length(leftpos)-ulloc+1,1:2)=leftpos(end:-1:ulloc,2:3);
%upper section weighted average with left and right
ldist = uminloc-ulmin;
rdist = urmax-uminloc;
for i=ulmin:urmax
    %Weighting depends on proximity to centre (max) point
    %For i = uminloc, 100% upper, for i=ulmin, 100% left, for i=urmax,
100%
    %right
    if i<uminloc
        %upperpos(i,2)<position(minloc,1)
       %combine with left
       [~,ulloc2] = min(abs(upperpos(i,3) - leftpos(:,2)));
       weight = ((uminloc-i)/ldist)^3;
       storeweight(i)=weight;
       comb(1:2) = leftpos(ulloc2,2:3);
    else
        %combine with right
        [~,urloc2] = min(abs(upperpos(i,3) - rightpos(:,2)));
        weight = ((i-uminloc)/rdist)^3;
        storeweight(i)=weight;
        comb(1:2) = rightpos(urloc2,2:3);
    end

      Combined(length(leftpos)-ulloc+2+i-ulmin,1:2)=(1-
weight)*upperpos(i,3:-1:2)+weight*comb(1:2);
end

%Right
Combined(length(leftpos)-ulloc+3+urmax-ulmin:length(leftpos)-
ulloc+2+urmax-ulmin+urloc,1:2)=rightpos(urloc:-1:1,2:3);


%make the lower points of the indent on the left and right side equal
limval=min(Combined(1,1),Combined(end,1));
comblim=find(Combined(:,1)<=limval);
Combined2 = Combined(comblim(1):comblim(end),:);
%plot(upperpos(:,2),upperpos(:,1),'r',upperpos(:,2),upperpos(:,3),'g');
% plot(leftpos(:,2),leftpos(:,1),'r');

% See if lines come close to crossing then round off
%Split in two (left and right)
[~,mincloc] = min(Combined2(:,1));
LeftComb = Combined2(1:mincloc,:);
RightComb = Combined2(mincloc+1:end,:);

clear proxLR

for ipl = 1:length(LeftComb)
    [~,ipr] = min(abs(LeftComb(ipl,1)-RightComb(:,1)));
    proxLR(ipl) = abs(LeftComb(ipl,2)-RightComb(ipr,2));
end


threshLR=proxLR(end);

if threshLR<1
   threshLR=1;
end
```

```
if threshLR>2
   threshLR=2;
end
threshLR=5*threshLR;

finalposL = find(proxLR<threshLR);

if isempty(finalposL)==1
    finalposL=length(proxLR);
end

Combined3(1:finalposL(1),:) = LeftComb(1:finalposL(1),:);
[~, startposR] = min(abs(RightComb(:,1)-LeftComb(finalposL(1),1)));
Combined3(finalposL(1)+1:finalposL(1)+length(RightComb)-startposR+1,:) =
RightComb(startposR:end,:);


%Binary Area enclose by line
IRb = IR(:,:,1); %figure,imshow(IRb)
[height,width]=size(IRb);
BWindent(1:height,1:width)=0;
BWindent = poly2mask(Combined3(:,2)+round(x1)-150,Combined3(:,1)+row(I)-
100,height,width);
%figure,imshow(BWindent)
%imopen
se = strel('disk', 1);
BW2 = imerode(BWindent,se);
%Only largest
BW3=BW2;
CC = bwconncomp(BW2);
numPixels = cellfun(@numel,CC.PixelIdxList);
[biggest,idx] = max(numPixels);
BW2(CC.PixelIdxList{idx}) = 0;
BW3 = BW3-BW2;
BW2 = imdilate(BW3,se);

%imclose
se = strel('disk', 5);
BW2 = imclose(BW2,se);


BW3=BW2;
CC = bwconncomp(BW2);
numPixels = cellfun(@numel,CC.PixelIdxList);
[biggest,idx] = max(numPixels);
BW2(CC.PixelIdxList{idx}) = 0;
BW2 = BW3-BW2;

%select largest

[BWR,BWC,~] = find(BW2);
kbo=1;
clear Lbo Rbo
if sum(sum(BW2))==0
    [BWR,BWC,~] = find(BWindent);
    BW2 = BWindent;
end

for ibo = max(BWR):-1:min(BWR)
   BWcol = find(BW2(ibo,:));
   Lbo(kbo,1) = ibo;
```

```
   Lbo(kbo,2) = BWcol(1);
   Rbo(kbo,1) = ibo;
   Rbo(kbo,2) = BWcol(end);
   kbo=kbo+1;
end
%

Combbo(1:length(Lbo),:) = Lbo;
Combbo(length(Lbo)+1:length(Lbo)+length(Rbo),:) = Rbo(end:-1:1,:);



if  sum(sum(BW2))<1000 || max(BWR)-min(BWR)<6
    cont=0;
end


end


   IRcomb2 = IR2-IG2;
%Register images
[optimizer,metric] = imregconfig('multimodal');
optimizer.InitialRadius = optimizer.InitialRadius/3;
optimizer.MaximumIterations = 200;

if cont==0
    if man==2
         registered = imregister(IRcomb2, IRcomb, 'translation',
optimizer, metric);

         IRcomb = registered;

    else
          IRcombtrans = imtranslate(IRcomb2,[0,yreg2(slices)]);
        IRcomb=IRcombtrans;
%        figure,imshow(IRcomb)
    end
end

IRadapt = adapthisteq(IRcomb);
 IRfilt = medfilt2(IRadapt,[5 5]);

if cont==0
   Combbo(:,1)=j-30;
   Combbo(:,2)=col(I);
end
% %Select largest element
h=figure,imshow(IRfilt); hold on

plot(Combbo(:,2),Combbo(:,1),'r')

hold off


%Check if this needs manual selection
choice = questdlg('Manual or automatic segmentation', ...
    'Segmentation', ...
    'Manual','Automatic','Automatic');
```

```
if strcmp(choice,'Manual')==1
    manualselect=1;
end

close all

%% Record variables

Image{slices,1} = IRcomb;
IndentOutline{slices,1} = Combbo;


clear Combined Combined2 Combined3 Combbo

end

%% Re-order
for nr = 1:length(sliceorder)
    [~,posnr] = min(abs(sliceorder-nr));
    IndentOutline2{nr,1} = IndentOutline{posnr,1};
    Image2{nr,1} = Image{posnr,1};
end

%% Playback
frate=2;

for iplay = 1:length(Image2)

    scrsz = get(0,'ScreenSize');

tempimage = Image2{iplay,1};
tempindent = IndentOutline2{iplay,1};

   h3 = figure();
imshow(tempimage,[],'InitialMagnification', 50) %title('Registered Image')
    hold on;
         plot(tempindent(:,2),tempindent(:,1),'r')
             hold off
                 pause(1/frate);

close all
end
```

9.5.3.2 Damage Segmentation

```
close all
baselinethresh =0.75;

% Indent/damage in last and/or final frame
figure,imshow(Image2{1,1})
pause(1)
figure,imshow(Image2{end,1})
pause(1)

choice = questdlg('No indent associated damage in:', ...
    'Baseline', ...
    'First','Final','Both','Both');
% Handle response
switch choice
    case 'First'
        Background1 = Image2{1,1};
        Background2 = Image2{1,1};
    case 'Final'
        Background1 = Image2{end,1};
        Background2 = Image2{end,1};
    case 'Both'
        Background1 = Image2{1,1};
        Background2 = Image2{end,1};
end

%% Baseline whitening (first and last frames)
  %Check images are the same size, if not make so
[height1, width1] = size(Background1);
[height2, width2] = size(Background2);


if height1<height2
    Background2=Background2(1:height1,:);
    heighta = height1;
else
    Background1=Background1(1:height2,:);
    heighta = height2;
end

if width1<width2
    Background2=Background2(:,1:width1);
    widtha = width1;
else
    Background1=Background1(:,1:width2);
    widtha = width2;
end


%% Find stain intensity baseline for the stack
for slices=1:length(Image2)
   %Load image
    currentslice = Image2{slices,1};
    currentslice = currentslice(1:heighta,1:widtha);

  %Find baseline/threshold
  clear counts x
  [counts(:,1),x] = imhist(currentslice(1:j,:));
  %exclude the 0s
  allloc = find(x);
```

```
  counts(allloc,2)=cumsum(counts(allloc,1));
  counts(allloc,3)=counts(allloc,2)/sum(counts(allloc,1));
  i1 = find(counts(:,3)>baselinethresh);
  baseline(slices) = x(i1(1));


end

absbaseline = mean(baseline);
clear bglevel
for slices=1:length(Image2)
   %Load image
  currentslice = Image2{slices,1};
  currentslice = currentslice(1:heighta,1:widtha);

  %Find background level
  bg = currentslice(currentslice >= absbaseline*0.25 & currentslice <
absbaseline*0.75);
  bglevel(slices,1) = sum(bg)/length(bg);

end

absbackground = mean(bglevel);
bglevel(:,2) = bglevel(:,1)/absbackground;


baseline1 = absbaseline*bglevel(1,2);
baseline2 = absbaseline*bglevel(end,2);
  %top 50% of image

    %Median value of top half (i.e. the baseline)

    stain1 = Background1>baseline1;
    stain2 = Background2>baseline2;

se1 = strel('disk',1);
staindil = imclose(stain1,se1);
stainfill = imfill(staindil,'holes');
se5 = strel('disk',10);
stainopen = imopen(stainfill,se5);
stainbg1 = bwareaopen(stainopen, 1000);

staindil = imclose(stain2,se1);
stainfill = imfill(staindil,'holes');

stainopen = imopen(stainfill,se5);
stainbg2 = bwareaopen(stainopen, 1000);


%Combine first and last to create baseline stain image
stainbaseline = stainbg1 + stainbg2;
stainbaseline2 = stainbaseline>0;

%air
air(1:height,1:width)=0;
air(j:height,1:width)=1;

centralindent = IndentOutline{1,1};
```

```
%% Loop through slices
for slices=1:length(Image2)
   %Load image
    currentslice = Image2{slices,1};
    currentslice = currentslice(1:heighta,1:widtha);
    currentindent = IndentOutline2{slices,1};

   %Correct baseline/threshold for background levels
  %Find background

  baseline = absbaseline*bglevel(slices,2);
  stainslice = currentslice>baseline;


%Dilate  - the stain for this image
staindil = imclose(stainslice,se1);
%stainfill = imfill(staindil,'holes');
stainopen = imopen(staindil,se5);
stainslice2 = bwareaopen(stainopen, 1000);

    %remove indent and base
    BWindent(1:height,1:width)=0;
    BWindent =
poly2mask(currentindent(:,2),currentindent(:,1),height,width);
    indentdamage = stainslice2-BWindent-air;
    indentdamage2 = indentdamage>0;


%Find damage close to indent
   %element closest to indent
    indentstain =
bwselect(indentdamage2,currentindent(:,2),currentindent(:,1));
    %if there is any stain directly next to indent, find closest
    if sum(sum(indentstain))==0
        indentstain =
bwselect(indentdamage2,centralindent(:,2),centralindent(:,1));
        if sum(sum(indentstain))==0
           indentstain(1:height,1:width) = 0;
        end
    end

 %Background only stain (everything except close to indent is background)
 bgonlystain = indentdamage2-indentstain;
 bgonlystain2=bgonlystain>0;

%Remove baseline from indentstain (is the stain close to indent there in
%first frame)
    indentonlystain = indentstain-stainbaseline2;
    indentonlystain2 = indentonlystain>0;

    %Check if what's left connects to the indent (is the stain still
close
    %to the indent)
    indentassociated =
bwselect(indentonlystain2,currentindent(:,2),currentindent(:,1));
    %if there is any stain directly next to indent, find closest
    if sum(sum(indentassociated))==0
        indentassociated =
bwselect(indentonlystain2,centralindent(:,2),centralindent(:,1));
        if sum(sum(indentassociated))==0
           indentassociated(1:height,1:width) = 0;
```

```
        end
    end

%Baseline indent stain (the stain close to the indent but part of the
%background)
    baselineindentstain = indentstain-indentassociated;
    baselineindentstain2 = baselineindentstain>0;

    %Outlines

    BB = bwboundaries(baselineindentstain2);
    BG = bwboundaries(bgonlystain2);
    BI = bwboundaries(indentassociated);

    BaselineIndent{slices,1} = BB;
    Background{slices,1} = BG;
    IndentDamage{slices,1} = BI;

    BaselineIndentBW{slices,1} = baselineindentstain2;
    BackgroundBW{slices,1} = bgonlystain2;
    IndentDamageBW{slices,1} = indentassociated;

end
```

9.5.3.3 Most Proximal Pore Segmentation and Quantification of the Indent and Damage

```
close all
frate=2;

%pos of depth labes
Rnamelist{1};
l1 = 5;
l2= 7;

%% Closest pore selection (playback to determine) and indent volume calc
   centralname = Rnamelist{centralloc};
   centraldepth = str2double(centralname(l1:l2));

for iplay = 1:length(Image2)

    scrsz = get(0,'ScreenSize');

    tempimage = Image2{iplay,1};

     temprname = Rnamelist{iplay};
     tempindent = IndentOutline2{iplay,1};

     BWindent(1:height,1:width)=0;
    BWindent = poly2mask(tempindent(:,2),tempindent(:,1),height,width);

    %calculate indent area and depth per slice
      indentvol(iplay,1)=str2double(temprname(l1:l2));
      indentvol(iplay,2)=sum(sum(BWindent));
      indentvol(iplay,3) = max(tempindent(:,1))-min(tempindent(:,1));


      %Find centrepoint of indent
      rowI = floor(min(tempindent(1,1),tempindent(end,1)));

      [~,column,~] = find(BWindent(rowI,:));

      if isempty(column)
          indentvol(iplay,4) = 0;
          indentvol(iplay,5) = 0;
      else
          indentvol(iplay,4) = sqrt(((max(column)-
col(I))*res)^2+(indentvol(iplay,1)-centraldepth)^2);
          indentvol(iplay,5) = sqrt(((col(I)-
min(column))*res)^2+(indentvol(iplay,1)-centraldepth)^2);
      end


    end



%% Pore Proximity
h=msgbox('Click the centre of the closest pore in the first and last
frame');
waitfor(h)
tempimage = Image2{1,1};
 figure,imshow(tempimage)
```

```
   [px1,py1] = ginput(1);
 tempimage = Image2{end,1};
 figure,imshow(tempimage)
    [pxe,pye] = ginput(1);
 close all

 stackheight = indentvol(end,1)-indentvol(1,1);
 clear porepos

h=msgbox('If the closest pore is identified click the top left of the
image, else click the closest part of the closest pore');
waitfor(h)
    for iplay = 1:length(Image2)
        tempimage = Image2{iplay,1};

        pxc = round((indentvol(iplay,1)-indentvol(1,1))*(pxe-
px1)/stackheight+px1);
        pyc = round((indentvol(iplay,1)-indentvol(1,1))*(pye-
py1)/stackheight+py1);

        porethresh = mean(mean(tempimage(pyc-25:pyc+25,pxc-25:pxc+25)));
        poreim = tempimage(pyc-200:pyc+200,pxc-200:pxc+200)>porethresh;

        se = strel('disk',2);
        poredil = imclose(poreim,se);
        porefill = imfill(poredil,'holes');
        poreopen = imopen(porefill,se);

        %Only largest
        pore=poreopen;
        CC = bwconncomp(poreopen);
        numPixels = cellfun(@numel,CC.PixelIdxList);
        [biggest,idx] = max(numPixels);
        poreopen(CC.PixelIdxList{idx}) = 0;
        pore = pore-poreopen;

          clear BoundoutP BoundoutP2

    BP = bwboundaries(pore);
    BoundoutP=BP{1,1};



    BoundoutP2(:,2)=BoundoutP(:,2)+pxc-200;
    BoundoutP2(:,1)=BoundoutP(:,1)+pyc-200;

      figure, imshow(tempimage); hold on
    plot(BoundoutP2(:,2),BoundoutP2(:,1)); hold off
    [p1,p2] = ginput(1);
    close all

    if p2>50
        clear BoundoutP2
       BoundoutP2 =  [p1,p2];
    end

    Pores{iplay,1}=BoundoutP2;

        [pr,pc,~] = find(pore);
        pr2 = pr+pyc-200;
```

```
        pc2 = pc+pxc-200;

        %close all
        porepos(iplay,1)=abs(indentvol(centralloc,1)-indentvol(iplay,1));
        porepos(iplay,2)=min(sqrt((pc2-col(I)).^2+(pr2-j).^2))*res;
        porepos(iplay,3)=sqrt(porepos(iplay,1)^2+porepos(iplay,2)^2);
    end

%% Playback and calculate indent and damage

    for iplay = 1:length(Image2)

    scrsz = get(0,'ScreenSize');

    %Load parameters
    tempimage = Image2{iplay,1};
    tempindent = IndentOutline2{iplay,1};

    tempbaselinestain = BaselineIndentBW{iplay,1};
    tempbg = BackgroundBW{iplay,1};
    tempindentdamage = IndentDamageBW{iplay,1};

    BB = BaselineIndent{iplay,1};
    BG = Background{iplay,1};
    BI = IndentDamage{iplay,1};

    temppores = Pores{iplay,1};
    temprname = Rnamelist{iplay};

    %Calculate parameters

    %baseline associated damage
    poredamvol(iplay,1)=str2double(temprname(l1:l2));
    poredamvol(iplay,2)=sum(sum(tempbaselinestain));

    %indent associated damage
    damvol(iplay,1)=str2double(temprname(l1:l2));
    damvol(iplay,2)=sum(sum(tempindentdamage));


    %Plot figure with overlay
    h3 = figure();
    imshow(tempimage,[],'InitialMagnification', 50) %title('Registered
Image')
    hold on;


    %background
    for iB = 1:length(BG)
        plottempBG = BG{iB};
       plot(plottempBG(:,2),plottempBG(:,1),'y')
    end

    %closest pore
    plot(temppores(:,2),temppores(:,1),'m')

    %baseline damage with indent
    for iB = 1:length(BB)
        plottempBB = BB{iB};
       plot(plottempBB(:,2),plottempBB(:,1),'c')
```

```
    end

    %indent damage
    for iI = 1:length(BI)
        tempstainC = BI{iI};
       plot(tempstainC(:,2),tempstainC(:,1),'b')
    end

    %indent
    plot(tempindent(:,2),tempindent(:,1),'r')


    hold off
    savename = strcat(pwd,'/',temprname(1:l2),'.tif');
    saveas(gcf,savename,'tif')

    pause(1/frate);

close all

    end

%% Plot

%area of indent - associated damage
figure(1)
plot(indentvol(:,1),indentvol(:,2),'ro',damvol(:,1),damvol(:,2)+indentvol
(:,2),'bo',poredamvol(:,1),poredamvol(:,2)+damvol(:,2)+indentvol(:,2),'co
')

%indent depth
figure(2)
plot(indentvol(:,1),indentvol(:,3),'ro')

%% Measurements summary
VolIndent = trapz(indentvol(:,1),indentvol(:,2))*res^2;
VolDepth = max(indentvol(:,3))*res;
VolDamage = trapz(damvol(:,1),damvol(:,2))*res^2;
VolPoreDamage = trapz(poredamvol(:,1),poredamvol(:,2))*res^2;
CentIndentArea = indentvol(centralloc,2)*res^2;
[~,~,di] = find(indentvol(:,4:5));
CentralDepth = indentvol(centralloc,3)*res;
CentralDiameter = indentvol(centralloc,4)+indentvol(centralloc,5);
MeanDiameter = mean(di)*2;
PoreProx = min(porepos(:,3));

% 1) Total volume of the indent, 3) The maximum depth of the indent,
% 3) The total volume of the damage, 4) the volume of the pore damage
% 5) The area of the central slice, 6) The depth of the central slice
% 7) The diameter of the  central slice, 7) The average diameter
% 8) The proximity to the closest pore

Summary = [VolIndent, VolDepth, VolDamage, VolPoreDamage, CentIndentArea,
CentralDepth, CentralDiameter, MeanDiameter, PoreProx];

ExportFilecsv1=strcat(pwd,'\',temprname(1:5),'summary','.csv');
csvwrite(ExportFilecsv1,Summary); % Rcurve csv
```

9.6 Appendix 5 – List of Publications

9.6.1 Core Work of the Thesis

9.6.1.1 Journal Publications

T. Jenkins, L. V. Coutts, D.G. Dunlop, R.O.C. Oreffo, C. Cooper, N.C. Harvey, P.J. Thurner and the OStEO group (N.K. Arden, J.M. Latham, P. Taylor, M. Baxter, N. Moss, C. Ball, K. Chan), *Variability in Reference Point Microindentation and Recommendations for Testing Cortical Bone: Maximum Load, Sample Orientation, Mode of Use, Sample Preparation and Measurement Spacing*, Journal of the Mechanical Behaviour of Biomedical Materials (2014), doi:10.1016/j.jmbbm.2014.09.030

T. Jenkins (joint first author), L. V. Coutts (joint first author), D.G. Dunlop, R.O.C. Oreffo, C. Cooper, N.C. Harvey, P.J. Thurner and the OStEO group (N.K. Arden, J.M. Latham, P. Taylor, M. Baxter, N. Moss, C. Ball, K. Chan, S. D'Angelo, J. Cushnaghan), *The Potential of Reference Point Microindentation for Improved Fracture Risk Assessment* (in preparation)

T. Jenkins, O. Andriotis, O. Katsamenis, L. V. Coutts, D.G. Dunlop, R.O.C. Oreffo, C. Cooper, N.C. Harvey, P.J. Thurner and the OStEO group (N.K. Arden, J.M. Latham, P. Taylor, M. Baxter, N. Moss, C. Ball, K. Chan), *Bone mechanics in health and disease: Investigation into the property assessed by Reference Point Microindentation* (in preparation)

9.6.1.2 Conference Articles

T. Jenkins, L.V. Coutts, R.O.C. Oreffo, D.G. Dunlop, C. Cooper, N.C. Harvey, P.J. Thurner, *The Potential of Reference Point Microindentation for Fracture Risk Assessment*, Podium at Bath Biomechanics Symposium, September 2014

T. Jenkins, L.V. Coutts, R.O.C. Oreffo, D.G. Dunlop, C. Cooper, N.C. Harvey, P.J. Thurner, *The Potential of Reference Point Microindentation as a Fracture Risk Assessment Tool*, Poster at the University of Southampton Postgraduate Conference, **Awarded Best Poster**, November 2013

T. Jenkins, L.V. Coutts, N.C. Harvey, R.O.C. Oreffo, D.G. Dunlop, C. Cooper, P.J. Thurner, *Reference Point Microindentation: Assessment of a Novel Fracture Risk Assessment Tool,* Poster at University of Southampton Ageing USRG Exhibition, September 2013

T. Jenkins, L.V. Coutts, N.C. Harvey, R.O.C. Oreffo, D.G. Dunlop, C. Cooper, P.J. Thurner, *Reference Point Indentation Trends of the Human Femoral Neck,* Poster at European Society of Biomechanics, August 2013

T. Jenkins, L.V. Coutts, O.L. Katsamenis, N.C. Harvey, P.J. Thurner, *Validation of Reference Point Indentation for Improved Fracture Risk Assessment*, Podium at University of Southampton postgraduate conference, November 2012

T. Jenkins, L.V. Coutts, O.L. Katsamenis, N.C. Harvey, P.J. Thurner, *Validation of Reference Point Indentation for Bone Fragility Assessment*, Podium at Bath Biomechanics Symposium, September 2012

9.6.2 Parallel and Collaborative Work

9.6.2.1 Journal Publications

O.L. Katsamenis, T. Jenkins, F. Quinci, S. Michopoulou, I. Sinclair, P.J. Thurner, *A Novel Videography Method for Generating Crack-Extension Resistance Curves in Small Bone Samples*, PLOSone, Volume 8, Issue 2, Article Number e55641, 2013

O.L. Katsamenis, T. Jenkins, P.J. Thurner, *Toughness and Damage Susceptibility in Human Cortical Bone is Proportional to Mechanical Inhomogeneity at the Osteonal Level*, Bone (Under Review)

L. V. Coutts, T. Jenkins, T. Li, D.G. Dunlop, R.O.C. Oreffo, C. Cooper, N.C. Harvey, P.J. Thurner and the OStEO group (N.K. Arden, J.M. Latham, P. Taylor, M. Baxter, N.Moss, C. Ball, K. Chan), *Reference Point Microindentation and Recommendations for Testing Cortical Bone: Location, Thickness and Orientation Heterogeneity*, Journal of the Mechanical Behaviour of Biomedical Materials (Under Review)

T. Li, T. Jenkins, S. Lanham, P.J. Thurner, R.O.C. Oreffo, *Effect of In Utero Vitamin D Deficiency on Rodent Offspring Skeletal Health in Adulthood*, Journal of the Royal Society Interface (Under Review)

L. V. Coutts, T. Jenkins, T. Li, D.G. Dunlop, R.O.C. Oreffo, C. Cooper, N.C. Harvey, P.J. Thurner and the OStEO group (N.K. Arden, J.M. Latham, P. Taylor, M. Baxter, N.Moss, C. Ball, K. Chan), *Comparison of Mechanical and Geometrical Properties with Mineral Density in Human Femoral Neck Cortical Bone* (In Preparation)

L. V. Coutts, T. Jenkins, T. Li, D.G. Dunlop, R.O.C. Oreffo, C. Cooper, N.C. Harvey, P.J. Thurner and the OStEO group (N.K. Arden, J.M. Latham, P. Taylor, M. Baxter, N.Moss, C. Ball, K. Chan), *Investigation into Variation of the Speed of Sound and the Correlation with Reference Point Micro-Indentation in the Human Femoral Neck* (In Preparation)

T. Jenkins, T. Li, S. Lanham , D.G. Dunlop, C. Cooper, N.C. Harvey, R.O.C. Oreffo, P.J. Thurner, *Application of the Whitening Front Tracking Method for Generating Crack-Extension Resistance Curves in Whole Animal Bones* (In Preparation)

9.6.2.2 Conference Articles

L.V. Coutts, T. Jenkins, R.O.C. Oreffo, D.G. Dunlop, C. Cooper, N.C. Harvey, P.J. Thurner, Comparison of Mechanical and Geometrical Properties with Mineral Density in Human Femoral Neck Cortical Bone, Poster at World Congress of Biomechanics, July 2014

T. Li, T. Jenkins, S. Lanham, P.J. Thurner, R.O.C. Oreffo, *Molecular Establishment and Micromechanical Assessment of Bone Quality*, Poster at Bone Research Society and British Orthopaedic Research Society Joint Meeting, September 2013

O.L. Katsamenis, T. Jenkins, F. Quinci, S. Michopoulou, I. Sinclair, P.J. Thurner, *Measuring Fracture Toughness of Small Bone Samples by Means of the "Whitening-Front Tracking" Method*, Podium at European Society of Biomechanics, August 2013

T. Li, T. Jenkins, R.O.C. Oreffo, P.J. Thurner, *Molecular Origins of Bone Micromechanics*, Podium at European Society of Biomechanics, August 2013

L.V. Coutts, T. Jenkins, N.C. Harvey, R.O.C. Oreffo, D.G. Dunlop, C. Cooper, P.J. Thurner, *Regional Variation in Reference Point Indentation in Healthy And Diseased Cortical Bone*, Poster at European Society of Biomechanics, August 2013

O.L. Katsamenis, T. Jenkins, S. Michopoulou, I. Sinclair, P.J. Thurner, *Multiscale Experimental Analysis of Human Bone Fracture Toughness: From the Osteonal up to the Tissue Leve*l, Podium at Orthopaedic Research Society, January 2013

T. Jenkins, O.L. Katsamenis, N.C. Harvey, S. Michopoulou, I. Sinclair, P.J. Thurner, *Whitening Front Tracking: A High-Speed Videography Method for Assessing Fracture Toughness of Small Bone Samples*, Poster at Orthopaedic Research Society, January 2013

O.L. Katsamenis, T. Jenkins (presenting author), S. Michopoulou, I. Sinclair, P.J. Thurner, *A Novel Method for Generating Crack Extension Resistance Curves in Small Bone Samples using High-Speed Videography*, Podium at European Orthopaedic Research Society, September 2012

10 References

1. NIH. *Osteoporosis Prevention, Diagnosis and Therapy*. NIH Consensus Development Program 2000 [cited 2011 26th October].
2. Kanis, J.A., *Assessment of Osteoporosis at the Primary Health Care Level*, 2007, World Health Organisation Collaborating Centre for Metabolic Bone Diseases: University of Sheffield. p. 339.
3. Melton, L.J., *Adverse Outcomes of Osteoporotic Fractures in the General Population.* Journal of Bone and Mineral Research, 2003. **18**(6): p. 1139-1141.
4. Woolf, A.D., Akesson, K., *Preventing Fractures in Elderly People.* British Medical Journal, 2003. **327**: p. 7.
5. Keene, G.S., M.J. Parker, and G.A. Pryor, *Mortality and Morbidity after Hip-Fractures.* British Medical Journal, 1993. **307**(6914): p. 1248-1250.
6. Harvey, N., S. Earl, and C. Cooper, *Epidemiology of Osteoporotic Fractures*, in *Primer of the Metabolic Bone Disease and Disorders of Mineral Metabolism*, M.J. Favus, Editor 2006, American Society for Bone and Mineral Research: Durham, USA. p. 244-248.
7. Hauselmann, H.J. and R. Rizzoli, *A Comprehensive Review of Treatments for Postmenopausal Osteoporosis.* Osteoporos Int, 2003. **14**(1): p. 2-12.
8. Deal, C.L., *Osteoporosis: Prevention, Diagnosis, and Management.* American Journal of Medicine, 1997. **102**(1 PART A): p. 35S-39S.
9. Kanis, J.A., *Diagnosis of Osteoporosis and Assessment of Fracture Risk.* The Lancet, 2002. **359**(9321): p. 1929-1936.
10. Siris, E.S., Y.T. Chen, T.A. Abbott, E. Barrett-Connor, P.D. Miller, L.E. Wehren, and M.L. Berger, *Bone Mineral Density Thresholds for Pharmacological Intervention to Prevent Fractures.* Archives of Internal Medicine, 2004. **164**(10): p. 1108-1112.
11. Schuit, S.C.E., M. van der Klift, A.E.A.M. Weel, C.E.D.H. de Laet, H. Burger, E. Seeman, A. Hofman, A.G. Uitterlinden, J.P.T.M. van Leeuwen, and H.A.P. Pols, *Fracture Incidence and Association with Bone Mineral Density in Elderly Men and Women: The Rotterdam Study.* Bone, 2004. **34**(1): p. 195-202.
12. Sheffield, U.o. *Who Fracture Risk Assessment Tool*. 2011 [cited 2013 28th June].
13. Tremollieres, F.A., J.-M. Pouilles, N. Drewniak, J. Laparra, C.A. Ribot, and P. Dargent-Molina, *Fracture Risk Prediction Using Bmd and Clinical Risk Factors in Early Postmenopausal Women: Sensitivity of the Who Frax Tool.* Journal of Bone and Mineral Research, 2010. **25**(5): p. 1002-1009.
14. Chappard, D., M.F. Basle, E. Legrand, and M. Audran, *New Laboratory Tools in the Assessment of Bone Quality.* Osteoporos Int, 2011. **22**(8): p. 2225-40.
15. Ritchie, R.O., *How Does Human Bone Resist Fracture?*, in *Skeletal Biology and Medicine*, M. Zaidi, Editor 2010, Blackwell Publishing: Oxford. p. 72-80.
16. Bouxsein, M.L., *Bone Quality: Where Do We Go from Here?* Osteoporosis International, 2003. **14**: p. S118-S127.
17. Rubin, C.D., *Emerging Concepts in Osteoporosis and Bone Strength.* Curr Med Res Opin, 2005. **21**(7): p. 1049-56.
18. Hernandez, C.J. and T.M. Keaveny, *A Biomechanical Perspective on Bone Quality.* Bone, 2006. **39**(6): p. 1173-81.
19. Diez-Perez, A., R. Guerri, X. Nogues, E. Caceres, M.J. Pena, L. Mellibovsky, C. Randall, D. Bridges, J.C. Weaver, A. Proctor, D. Brimer, K.J. Koester, R.O. Ritchie, and P.K. Hansma, *Microindentation for in Vivo Measurement of Bone Tissue Mechanical Properties in Humans.* J Bone Miner Res, 2010. **25**(8): p. 1877-85.
20. Randall, C., D. Bridges, R. Guerri, X. Nogues, L. Puig, E. Torres, L. Mellibovsky, K. Hoffseth, T. Stalbaum, A. Srikanth, J.C. Weaver, S. Rosen, H. Barnard, D. Brimer, A. Proctor, J. Candy, C. Saldana, S. Chandrasekar, T. Lescun, C.M. Nielson, E. Orwoll, D. Herthel, H. Kopeikin, H.T.Y. Yang, J.N. Farr, L. McCready, S. Khosla, A. Diez-Perez, and P.K. Hansma, *Applications*

of a New Handheld Reference Point Indentation Instrument Measuring Bone Material Strength. Journal of Medical Devices-Transactions of the Asme, 2013. **7**(4).

21. Gueerri-Fernandez, R.C., X. Nogues, J.M. Quesada Gomez, E. Torres del Pliego, L. Puig, N. Garcia-Giralt, G. Yoskovitz, L. Mellibovsky, P.K. Hansma, and A. Diez-Perez, *Microindentation for in Vivo Measurement of Bone Tissue Material Properties in Atypical Femoral Fracture Patients and Controls.* Journal of Bone and Mineral Research, 2013. **28**(1): p. 162-168.
22. Aref, M., M.A. Gallant, J.M. Organ, J.M. Wallace, C.L. Newman, D.B. Burr, D.M. Brown, and M.R. Allen, *In Vivo Reference Point Indentation Reveals Positive Effects of Raloxifene on Mechanical Properties Following 6months of Treatment in Skeletally Mature Beagle Dogs.* Bone, 2013. **56**(2): p. 449-53.
23. Allen, M.R., C.L. Newman, E. Smith, D.M. Brown, and J.M. Organ, *Variability of in Vivo Reference Point Indentation in Skeletally Mature Inbred Rats.* J Biomech, 2014. **47**(10): p. 2504-2507.
24. Katsamenis, O.L., T. Jenkins, and P.J. Thurner, *Toughness and Damage Susceptibility in Human Cortical Bone Is Proportional to Mechanical Inhomogeneity at the Osteonal Level.* Bone, 2015. **(under review)**.
25. Gallant, M.A., D.M. Brown, J.M. Organ, M.R. Allen, and D.B. Burr, *Reference-Point Indentation Correlates with Bone Toughness Assessed Using Whole-Bone Traditional Mechanical Testing.* Bone, 2013. **53**(1): p. 301-5.
26. Granke, M., A. Coulmier, S. Uppuganti, J.A. Gaddy, M.D. Does, and J.S. Nyman, *Insights into Reference Point Indentation Involving Human Cortical Bone: Sensitivity to Tissue Anisotropy and Mechanical Behavior.* J Mech Behav Biomed Mater, (0).
27. Carriero, A., E.A. Zimmermann, S.J. Shefelbine, and R.O. Ritchie, *A Methodology for the Investigation of Toughness and Crack Propagation in Mouse Bone.* J Mech Behav Biomed Mater, 2014. **39**: p. 38-47.
28. Milovanovic, P., Z. Rakocevic, D. Djonic, V. Zivkovic, M. Hahn, S. Nikolic, M. Amling, B. Busse, and M. Djuric, *Nano-Structural, Compositional and Micro-Architectural Signs of Cortical Bone Fragility at the Superolateral Femoral Neck in Elderly Hip Fracture Patients Vs. Healthy Aged Controls.* Experimental Gerontology, 2014. **55**: p. 19-28.
29. Hansma, P., P. Turner, B. Drake, E. Yurtsev, A. Proctor, P. Mathews, J. Lulejian, C. Randall, J. Adams, R. Jungmann, F. Garza-de-Leon, G. Fantner, H. Mkrtchyan, M. Pontin, A. Weaver, M.B. Brown, N. Sahar, R. Rossello, and D. Kohn, *The Bone Diagnostic Instrument Ii: Indentation Distance Increase.* Rev Sci Instrum, 2008. **79**(6): p. 064303.
30. Setters, A. and I. Jasiuk, *Towards a Standardized Reference Point Indentation Testing Procedure.* J Mech Behav Biomed Mater, 2014. **34**: p. 57-65.
31. Bridges, D., C. Randall, and P.K. Hansma, *A New Device for Performing Reference Point Indentation without a Reference Probe.* Review of Scientific Instruments, 2012. **83**(4).
32. Rasoulian, R., A. Raeisi Najafi, M. Chittenden, and I. Jasiuk, *Reference Point Indentation Study of Age-Related Changes in Porcine Femoral Cortical Bone.* J Biomech, 2013. **46**(10): p. 1689-1696.
33. Weiner, S. and H.D. Wagner, *The Material Bone: Structure Mechanical Function Relations.* Annual Review of Materials Science, 1998. **28**: p. 271-298.
34. Brandi, M.L., *Microarchitecture, the Key to Bone Quality.* Rheumatology (Oxford), 2009. **48 Suppl 4**: p. iv3-8.
35. Wolff, J., *The Law of Bone Remodeling (Translation of the German 1892 Edition)*, ed. Springer1986: Berlin Heidelberg New York.
36. Frost, H.M., *Bone's Mechanostat: A 2003 Update.* Anatomical Record Part a-Discoveries in Molecular Cellular and Evolutionary Biology, 2003. **275A**(2): p. 1081-1101.
37. Jang, I.G., I.Y. Kim, and B.M. Kwak, *Analogy of Strain Energy Density Based Bone-Remodeling Algorithm and Structural Topology Optimization.* Journal of Biomechanical Engineering-Transactions of the Asme, 2009. **131**(1).

38. Huiskes, R., H. Weinans, H.J. Grootenboer, M. Dalstra, B. Fudala, and T.J. Slooff, *Adaptive Bone-Remodeling Theory Applied to Prosthetic-Design Analysis.* J Biomech, 1987. **20**(11-12): p. 1135-1150.
39. McNamara, L.M. and P.J. Prendergast, *Bone Remodelling Algorithms Incorporating Both Strain and Microdamage Stimuli.* J Biomech, 2007. **40**(6): p. 1381-1391.
40. You, J., C.E. Yellowley, H.J. Donahue, Y. Zhang, Q. Chen, and C.R. Jacobs, *Substrate Deformation Levels Associated with Routine Physical Activity Are Less Stimulatory to Bone Cells Relative to Loading-Induced Oscillatory Fluid Flow.* Journal of Biomechanical Engineering-Transactions of the Asme, 2000. **122**(4): p. 387-393.
41. Bacabac, R.G., D. Mizuno, C.F. Schmidt, F.C. MacKintosh, J.J.W.A. Van Loon, J. Klein-Nulend, and T.H. Smit, *Round Versus Flat: Bone Cell Morphology, Elasticity, and Mechanosensing.* J Biomech, 2008. **41**(7): p. 1590-1598.
42. Burger, E.H. and J. Klein-Nulend, *Mechanotransduction in Bone - Role of the Lacuno-Canalicular Network.* Faseb Journal, 1999. **13**: p. S101-S112.
43. Verbruggen, S.W., T.J. Vaughan, and L.M. McNamara. *Computational Exploration of Loading-Induced Interstitial Fluid Flow in the Lacunar-Canalicular Network*. in *Orthopaedic Research Society*. 2013. San Antonio, Texas.
44. Nicolella, D.P., D.E. Moravits, A.M. Gale, L.F. Bonewald, and J. Lankford, *Osteocyte Lacunae Tissue Strain in Cortical Bone.* J Biomech, 2006. **39**(9): p. 1735-1743.
45. Reilly, G.C., *Observations of Microdamage around Osteocyte Lacunae in Bone.* J Biomech, 2000. **33**(9): p. 1131-1134.
46. Temiyasathit, S. and C.R. Jacobs, *Osteocyte Primary Cilium and Its Role in Bone Mechanotransduction*, in *Skeletal Biology and Medicine*, M. Zaidi, Editor 2010. p. 422-428.
47. You, J., G.C. Reilly, X.C. Zhen, C.E. Yellowley, Q. Chen, H.J. Donahue, and C.R. Jacobs, *Osteopontin Gene Regulation by Oscillatory Fluid Flow Via Intracellular Calcium Mobilization and Activation of Mitogen-Activated Protein Kinase in Mc3t3-E1 Osteoblasts.* Journal of Biological Chemistry, 2001. **276**(16): p. 13365-13371.
48. Klein-Nulend, J., P.J. Nijweide, and E.H. Burger, *Osteocyte and Bone Structure.* Current Osteoporosis Reports, 2003. **1**(1): p. 5-10.
49. Marotti, G., M. Ferretti, M.A. Muglia, C. Palumbo, and S. Palazzini, *A Quantitative-Evaluation of Osteoblast-Osteocyte Relationships on Growing Endosteal Surface of Rabbit Tibiae.* Bone, 1992. **13**(5): p. 363-368.
50. Martin, R.B., *Toward a Unifying Theory of Bone Remodeling.* Bone, 2000. **26**(1): p. 1-6.
51. Robinson, R.A., *An Electron-Microscopic Study of the Crystalline Inorganic Component of Bone and Its Relationship to the Organic Matrix.* J Bone Joint Surg Am, 1952. **34-A**(2): p. 389-passim.
52. Ziv, V. and S. Weiner, *Bone Crystal Sizes - a Comparison of Transmission Electron-Microscopic and X-Ray-Diffraction Line-Width Broadening Techniques.* Connective Tissue Research, 1994. **30**(3): p. 165-175.
53. Fratzl, P., H.S. Gupta, E.P. Paschalis, and P. Roschger, *Structure and Mechanical Quality of the Collagen-Mineral Nano-Composite in Bone.* Journal of Materials Chemistry, 2004. **14**(14): p. 2115-2123.
54. Guo, X. and H.J. Gao, *Bio-Inspired Material Design and Optimization*. Iutam Symposium on Topological Design Optimization of Structures, Machines and Materials: Status and Perspectives, ed. M.P. Bendsoe, N. Olhoff, and O. Sigmund. Vol. 137. 2006, Dordrecht: Springer. 439-453.
55. Gao, H.J., *Application of Fracture Mechanics Concepts to Hierarchical Biomechanics of Bone and Bone-Like Materials.* International Journal of Fracture, 2006. **138**(1-4): p. 101-137.
56. Gao, H.J., B.H. Ji, I.L. Jager, E. Arzt, and P. Fratzl, *Materials Become Insensitive to Flaws at Nanoscale: Lessons from Nature.* Proceedings of the National Academy of Sciences of the United States of America, 2003. **100**(10): p. 5597-5600.

57. Orlovskii, V.P., V.S. Komlev, and S.M. Barinov, *Hydroxyapatite and Hydroxyapatite-Based Ceramics.* Inorganic Materials, 2002. **38**(10): p. 973-984.
58. Viguet-Carrin, S., P. Garnero, and P.D. Delmas, *The Role of Collagen in Bone Strength.* Osteoporosis International, 2006. **17**(3): p. 319-336.
59. Kadler, K.E., C. Baldock, J. Bella, and R.P. Boot-Handford, *Collagens at a Glance.* Journal of Cell Science, 2007. **120**(12): p. 1955-1958.
60. Boedtker, H. and P. Doty, *The Native and Denatured States of Soluble Collagen.* Journal of the American Chemical Society, 1956. **78**(17): p. 4267-4280.
61. Miller, A., *Collagen - the Organic Matrix of Bone.* Philosophical Transactions of the Royal Society of London Series B-Biological Sciences, 1984. **304**(1121): p. 455-477.
62. Thompson, J.B., J.H. Kindt, B. Drake, H.G. Hansma, D.E. Morse, and P.K. Hansma, *Bone Indentation Recovery Time Correlates with Bond Reforming Time.* Nature, 2001. **414**(6865): p. 773-776.
63. Launey, M.E., M.J. Buehler, and R.O. Ritchie, *On the Mechanistic Origins of Toughness in Bone*, in *Annual Review of Materials Research, Vol 40*, D.R.R.M.Z.F. Clarke, Editor 2010. p. 25-53.
64. Gautieri, A., M.J. Buehler, and A. Redaelli, *Deformation Rate Controls Elasticity and Unfolding Pathway of Single Tropocollagen Molecules.* J Mech Behav Biomed Mater, 2009. **2**(2): p. 130-137.
65. Hunter, G.K., P.V. Hauschka, A.R. Poole, L.C. Rosenberg, and H.A. Goldberg, *Nucleation and Inhibition of Hydroxyapatite Formation by Mineralized Tissue Proteins.* Biochemical Journal, 1996. **317**: p. 59-64.
66. Chen, Y., B.S. Bal, and J.P. Gorski, *Calcium and Collagen Binding Properties of Osteopontin, Bone Sialoprotein, and Bone Acidic Glycoprotein-75 from Bone.* Journal of Biological Chemistry, 1992. **267**(34): p. 24871-24878.
67. McKee, M.D. and A. Nanci, *Osteopontin: An Interfacial Extracellular Matrix Protein in Mineralized Tissues.* Connective Tissue Research, 1996. **35**(1-4): p. 197-205.
68. Fantner, G.E., J. Adams, P. Turner, P.J. Thurner, L.W. Fisher, and P.K. Hansma, *Nanoscale Ion Mediated Networks in Bone: Osteopontin Can Repeatedly Dissipate Large Amounts of Energy.* Nano Letters, 2007. **7**(8): p. 2491-2498.
69. Zappone, B., P.J. Thurner, J. Adams, G.E. Fantner, and P.K. Hansma, *Effect of Ca2+ Ions on the Adhesion and Mechanical Properties of Adsorbed Layers of Human Osteopontin.* Biophysical Journal, 2008. **95**(6): p. 2939-2950.
70. Thurner, P.J., C.G. Chen, S. Ionova-Martin, L. Sun, A. Harman, A. Porter, J.W. Ager Iii, R.O. Ritchie, and T. Alliston, *Osteopontin Deficiency Increases Bone Fragility but Preserves Bone Mass.* Bone, 2010. **46**(6): p. 1564-1573.
71. Poundarik, A.A., T. Diab, G.E. Sroga, A. Ural, A.L. Boskey, C.M. Gundberg, and D. Vashishth, *Dilatational Band Formation in Bone.* Proceedings of the National Academy of Sciences, 2012. **109**(47): p. 19178-19183.
72. Bella, J., B. Brodsky, and H.M. Berman, *Hydration Structure of a Collagen Peptide.* Structure, 1995. **3**(9): p. 893-906.
73. Nyman, J.S., A. Roy, X.M. Shen, R.L. Acuna, J.H. Tyler, and X.D. Wang, *The Influence of Water Removal on the Strength and Toughness of Cortical Bone.* J Biomech, 2006. **39**(5): p. 931-938.
74. Ascenzi, A. and E. Bonucci, *The Tensile Properties of Single Osteons.* Anat Rec, 1967. **158-(4)**: p. 375-386.
75. Weiner, S. and W. Traub, *Bone-Structure - from Angstroms to Microns.* Faseb Journal, 1992. **6**(3): p. 879-885.
76. Gupta, H.S. and P. Zioupos, *Fracture of Bone Tissue: The 'Hows' and the 'Whys'.* Med Eng Phys, 2008. **30**(10): p. 1209-1226.
77. Alexander, B., T.L. Daulton, G.M. Genin, J. Lipner, J.D. Pasteris, B. Wopenka, and S. Thomopoulos, *The Nanometre-Scale Physiology of Bone: Steric Modelling and Scanning*

Transmission Electron Microscopy of Collagen-Mineral Structure. Journal of the Royal Society Interface, 2012. **9**(73): p. 1774-1786.

78. Gupta, H.S., J. Seto, W. Wagermaier, P. Zaslansky, P. Boesecke, and P. Fratzl, *Cooperative Deformation of Mineral and Collagen in Bone at the Nanoscale.* Proceedings of the National Academy of Sciences of the United States of America, 2006. **103**(47): p. 17741-17746.
79. Hardiman, M., T.J. Vaughan, and C.T. McCarthy, *The Effect of Fibre Constraint in the Nanoindentation of Fibrous Composite Microstructures: A Finite Element Investigation.* Computational Materials Science, 2012. **64**: p. 162-167.
80. Gregory, J.R. and S.M. Spearing, *Nanoindentation of Neat and in Situ Polymers in Polymer-Matrix Composites.* Composites Science and Technology, 2005. **65**(3-4): p. 595-607.
81. Buehler, M.J., *Molecular Nanomechanics of Nascent Bone: Fibrillar Toughening by Mineralization.* Nanotechnology, 2007. **18**(29).
82. Gupta, H.S., P. Messmer, P. Roschger, S. Bernstorff, K. Klaushofer, and P. Fratzl, *Synchrotron Diffraction Study of Deformation Mechanisms in Mineralized Tendon.* Physical Review Letters, 2004. **93**(15).
83. Saito, M. and K. Marumo, *Collagen Cross-Links as a Determinant of Bone Quality: A Possible Explanation for Bone Fragility in Aging, Osteoporosis, and Diabetes Mellitus.* Osteoporosis International, 2010. **21**(2): p. 195-214.
84. Knott, L. and A.J. Bailey, *Collagen Cross-Links in Mineralizing Tissues: A Review of Their Chemistry, Function, and Clinical Relevance.* Bone, 1998. **22**(3): p. 181-187.
85. Oxlund, H., M. Barckman, G. Ortoft, and T.T. Andreassen, *Reduced Concentrations of Collagen Cross-Links Are Associated with Reduced Strength of Bone.* Bone, 1995. **17**(4): p. S365-S371.
86. Buehler, M.J., *Nanomechanics of Collagen Fibrils under Varying Cross-Link Densities: Atomistic and Continuum Studies.* J Mech Behav Biomed Mater, 2008. **1**(1): p. 59-67.
87. Ritchie, R.O., J.H. Kinney, J.J. Kruzic, and R.K. Nalla, *A Fracture Mechanics and Mechanistic Approach to the Failure of Cortical Bone.* Fatigue & Fracture of Engineering Materials & Structures, 2005. **28**(4): p. 345-371.
88. Ager, J.W., G. Balooch, and R.O. Ritchie, *Fracture, Aging, and Disease in Bone.* Journal of Materials Research, 2006. **21**(8): p. 1878-1892.
89. Wagermaier, W., H.S. Gupta, A. Gourrier, M. Burghammer, P. Roschger, and P. Fratzl, *Spiral Twisting of Fiber Orientation inside Bone Lamellae.* Biointerphases, 2006. **1**(1): p. 1-5.
90. Wagermaier, W., H.S. Gupta, A. Gourrier, O. Paris, P. Roschger, M. Burghammer, C. Riekel, and P. Fratzl, *Scanning Texture Analysis of Lamellar Bone Using Microbeam Synchrotron X-Ray Radiation.* Journal of Applied Crystallography, 2007. **40**: p. 115-120.
91. Weiner, S., W. Traub, and H.D. Wagner, *Lamellar Bone: Structure-Function Relations.* Journal of Structural Biology, 1999. **126**(3): p. 241-255.
92. Ascenzi, A., E. Bonucci, and A. Simkin, *Approach to Mechanical Properties of Single Osteonic Lamellae.* J Biomech, 1973. **6**(3): p. 227-&.
93. Giraudguille, M.M., *Twisted Plywood Architecture of Collagen Fibrils in Human Compact-Bone Osteons.* Calcified Tissue International, 1988. **42**(3): p. 167-180.
94. Marotti, G., *A New Theory of Bone Lamellation.* Calcified Tissue International, 1993. **53**(0): p. S47-S56.
95. Rho, J.Y., P. Zioupos, J.D. Currey, and G.M. Pharr, *Variations in the Individual Thick Lamellar Properties within Osteons by Nanoindentation.* Bone, 1999. **25**(3): p. 295-300.
96. Braidotti, P., F.P. Branca, and L. Stagni, *Scanning Electron Microscopy of Human Cortical Bone Failure Surfaces.* J Biomech, 1997. **30**(2): p. 155-162.
97. Bigley, R.F., L.V. Griffin, L. Christensen, and R. Vandenbosch, *Osteon Interfacial Strength and Histomorphometry of Equine Cortical Bone.* J Biomech, 2006. **39**(9): p. 1629-1640.

98. Katsamenis, O.L., H.M.H. Chong, O.G. Andriotis, and P.J. Thurner, *Load-Bearing in Cortical Bone Microstructure: Selective Stiffening and Heterogeneous Strain Distribution at the Lamellar Level.* J Mech Behav Biomed Mater, 2013. **17**(0): p. 152-165.
99. Peterlik, H., P. Roschger, K. Klaushofer, and P. Fratzl, *From Brittle to Ductile Fracture of Bone.* Nature Materials, 2006. **5**(1): p. 52-55.
100. Ascenzi, A., P. Baschieri, and A. Benvenuti, *The Bending Properties of Single Osteons.* J Biomech, 1990. **23**(8): p. 763-&.
101. Ascenzi, A., P. Baschieri, and A. Benvenuti, *The Torsional Properties of Single Selected Osteons.* J Biomech, 1994. **27**(7): p. 875-&.
102. Ascenzi, A. and E. Bonucci, *Shearing Properties of Single Osteons.* Anatomical Record, 1972. **172**(3): p. 499-&.
103. Ascenzi, A. and E. Bonucci, *The Compressive Properties of Single Osteons Human Inst Micro Wave Micrometer Inst Electron Microscope.* Anatomical Record, 1968. **161**(3): p. 377-390.
104. Martin, R.B., V.A. Gibson, S.M. Stover, J.C. Gibeling, and L.V. Griffins, *Osteonal Structure in the Equine Third Metacarpus.* Bone, 1996. **19**(2): p. 165-171.
105. Burr, D.B., M.B. Schaffler, and R.G. Frederickson, *Composition of the Cement Line and Its Possible Mechanical Role as a Local Interface in Human Compact Bone.* J Biomech, 1988. **21**(11): p. 939-945.
106. Schaffler, M.B., D.B. Burr, and R.G. Frederickson, *Morphology of the Osteonal Cement Line in Human Bone.* The Anatomical record, 1987. **217**(3): p. 223-228.
107. Skedros, J.G., J.L. Holmes, E.G. Vajda, and R.D. Bloebaum, *Cement Lines of Secondary Osteons in Human Bone Are Not Mineral-Deficient: New Data in a Historical Perspective.* Anatomical Record Part a-Discoveries in Molecular Cellular and Evolutionary Biology, 2005. **286A**(1): p. 781-803.
108. Dong, X.N., X. Zhang, and X.E. Guo, *Interfacial Strength of Cement Lines in Human Cortical Bone.* Mechanics & chemistry of biosystems : MCB, 2005. **2**(2): p. 63-8.
109. Nalla, R.K., J.J. Kruzic, and R.O. Ritchie, *On the Origin of the Toughness of Mineralized Tissue: Microcracking or Crack Bridging?* Bone, 2004. **34**(5): p. 790-798.
110. Koester, K.J., J.W. Ager, and R.O. Ritchie, *The True Toughness of Human Cortical Bone Measured with Realistically Short Cracks.* Nature Materials, 2008. **7**(8): p. 672-677.
111. O'Brien, F.J., D. Taylor, and T.C. Lee, *The Effect of Bone Microstructure on the Initiation and Growth of Microcracks.* Journal of Orthopaedic Research, 2005. **23**(2): p. 475-480.
112. Nalla, R.K., J.S. Stolken, J.H. Kinney, and R.O. Ritchie, *Fracture in Human Cortical Bone: Local Fracture Criteria and Toughening Mechanisms.* J Biomech, 2005. **38**(7): p. 1517-1525.
113. Vashishth, D., *Hierarchy of Bone Microdamage at Multiple Length Scales.* International Journal of Fatigue, 2007. **29**(6): p. 1024-1033.
114. Nalla, R.K., J.J. Kruzic, J.H. Kinney, and R.O. Ritchie, *Mechanistic Aspects of Fracture and R-Curve Behavior in Human Cortical Bone.* Biomaterials, 2005. **26**(2): p. 217-231.
115. Seref-Ferlengez, Z., C. Philemon, O. Kennedy, and M.B. Schaffler. *Material Properties Losses from Diffuse Microdamage in Living Bone Recover without Bone Remodeling*. in *Orthopaedic Research Society*. 2013. San Antonio, Texas.
116. Boyce, T.M., D.P. Fyhrie, M.C. Glotkowski, E.L. Radin, and M.B. Schaffler, *Damage Type and Strain Mode Associations in Human Compact Bone Bending Fatigue.* Journal of Orthopaedic Research, 1998. **16**(3): p. 322-329.
117. Hazenberg, J.G., M. Freeley, E. Foran, T.C. Lee, and D. Taylor, *Microdamage: A Cell Transducing Mechanism Based on Ruptured Osteocyte Processes.* J Biomech, 2006. **39**(11): p. 2096-2103.
118. Zioupos, P., R.B. Cook, and J.R. Hutchinson, *Some Basic Relationships between Density Values in Cancellous and Cortical Bone.* J Biomech, 2008. **41**(9): p. 1961-1968.
119. Carter, D.R., G.H. Schwab, and D.M. Spengler, *Tensile Fracture of Cancellous Bone.* Acta Orthopaedica Scandinavica, 1980. **51**(5): p. 733-741.

120. Choi, K., J.L. Kuhn, M.J. Ciarelli, and S.A. Goldstein, *The Elastic-Moduli of Human Subchondral, Trabecular, and Cortical Bone Tissue and the Size-Dependency of Cortical Bone Modulus.* J Biomech, 1990. **23**(11): p. 1103-1113.
121. Szabo, M.E., J. Zekonyte, O.L. Katsamenis, M. Taylor, and P.J. Thurner, *Similar Damage Initiation but Different Failure Behavior in Trabecular and Cortical Bone Tissue.* J Mech Behav Biomed Mater, 2011. **4**(8): p. 1787-1796.
122. Keaveny, T.M., E.F. Morgan, G.L. Niebur, and O.C. Yeh, *Biomechanics of Trabecular Bone.* Annual Review of Biomedical Engineering, 2001. **3**: p. 307-333.
123. Grisso, J.A., J.L. Kelsey, B.L. Strom, G.Y. Chiu, G. Maislin, L.A. Obrien, S. Hoffman, and F. Kaplan, *Risk-Factors for Falls as a Cause of Hip Fracture in Women.* New England Journal of Medicine, 1991. **324**(19): p. 1326-1331.
124. Greenspan, S.L., E.R. Myers, L.A. Maitland, N.M. Resnick, and W.C. Hayes, *Fall Severity and Bone-Mineral Density as Risk-Factors for Hip Fracture in Ambulatory Elderly.* Jama-Journal of the American Medical Association, 1994. **271**(2): p. 128-133.
125. Riggs, B.L., S. Khosla, and L.J. Melton, *Sex Steroids and the Construction and Conservation of the Adult Skeleton.* Endocrine Reviews, 2002. **23**(3): p. 279-302.
126. Khosla, S., L.J. Melton, E.J. Atkinson, W.M. O'Fallon, G.G. Klee, and B.L. Riggs, *Relationship of Serum Sex Steroid Levels and Bone Turnover Markers with Bone Mineral Density in Men and Women: A Key Role for Bioavailable Estrogen.* Journal of Clinical Endocrinology & Metabolism, 1998. **83**(7): p. 2266-2274.
127. Frost, H.M., *On the Estrogen-Bone Relationship and Postmenopausal Bone Loss: A New Model.* Journal of Bone and Mineral Research, 1999. **14**(9): p. 1473-1477.
128. Westerlind, K.C., T.J. Wronski, E.L. Ritman, Z.P. Luo, K.N. An, N.H. Bell, and R.T. Turner, *Estrogen Regulates the Rate of Bone Turnover but Bone Balance in Ovariectomized Rats Is Modulated by Prevailing Mechanical Strain.* Proceedings of the National Academy of Sciences of the United States of America, 1997. **94**(8): p. 4199-4204.
129. Ilich, J.Z. and J.E. Kerstetter, *Nutrition in Bone Health Revisited: A Story Beyond Calcium.* Journal of the American College of Nutrition, 2000. **19**(6): p. 715-737.
130. Heaney, R.P., *Calcium, Dairy Products and Osteoporosis.* Journal of the American College of Nutrition, 2000. **19**(2): p. 83S-99S.
131. Cumming, R.G. and M.C. Nevitt, *Calcium for Prevention of Osteoporotic Fractures in Postmenopausal Women.* Journal of Bone and Mineral Research, 1997. **12**(9): p. 1321-1329.
132. Gallagher, J.C., B.L. Riggs, J. Eisman, A. Hamstra, S.B. Arnaud, and H.F. Deluca, *Intestinal Calcium-Absorption and Serum Vitamin-D Metabolites in Normal Subjects and Osteoporotic Patients - Effect of Age and Dietary Calcium.* Journal of Clinical Investigation, 1979. **64**(3): p. 729-736.
133. Chapuy, M.C., M.E. Arlot, F. Duboeuf, J. Brun, B. Crouzet, S. Arnaud, P.D. Delmas, and P.J. Meunier, *Vitamin-D(3) and Calcium to Prevent Hip-Fractures in Elderly Women.* New England Journal of Medicine, 1992. **327**(23): p. 1637-1642.
134. LeBoff, M.S., L. Kohlmeier, S. Hurwitz, J. Franklin, J. Wright, and J. Glowacki, *Occult Vitamin D Deficiency in Postmenopausal Us Women with Acute Hip Fracture.* Jama-Journal of the American Medical Association, 1999. **281**(16): p. 1505-1511.
135. Grant, A.M., F.H. Anderson, A. Avenell, M.K. Campbell, C. Cooper, C. Donaldson, R.M. Francis, W.J. Gillespie, C.M. Robinson, D.J. Torgerson, W.A. Wallace, G.C. McPherson, G.S. MacLennan, A.M. McDonald, M. Grant, and R.T. Grp, *Oral Vitamin D3 and Calcium for Secondary Prevention of Low-Trauma Fractures in Elderly People (Randomised Evaluation of Calcium or Vitamin D, Record): A Randomised Placebo-Controlled Trial.* Lancet, 2005. **365**(9471): p. 1621-1628.
136. Abrahamsen, B., T. Masud, A. Avenell, F. Anderson, H.E. Meyer, C. Cooper, H. Smith, A.Z. LaCroix, D. Torgerson, A. Johansen, R. Jackson, L. Rejnmark, J. Wactawski-Wende, K. Brixen, L. Mosekilde, J.A. Robbins, R.M. Francis, and D.V.D.I. Patien, *Patient Level Pooled*

Analysis of 68 500 Patients from Seven Major Vitamin D Fracture Trials in Us and Europe. British Medical Journal, 2010. **340**.

137. De Laet, C., J.A. Kanis, A. Oden, H. Johanson, O. Johnell, P. Delmas, J.A. Eisman, H. Kroger, S. Fujiwara, P. Garnero, E.V. McCloskey, D. Mellstrom, L.J. Melton, P.J. Meunier, H.A.P. Pols, J. Reeve, A. Silman, and A. Tenenhouse, *Body Mass Index as a Predictor of Fracture Risk: A Meta-Analysis.* Osteoporosis International, 2005. **16**(11): p. 1330-1338.
138. Johansson, H., J.A. Kanis, A. Oden, E. McCloskey, R.D. Chapurlat, C. Christiansen, S.R. Cummings, A. Diez-Perez, J.A. Eisman, S. Fujiwara, C.C. Gluer, D. Goltzman, D. Hans, K.T. Khaw, M.A. Krieg, H. Kroger, A.Z. LaCroix, E. Lau, W.D. Leslie, D. Mellstrom, L.J. Melton, T.W. O'Neill, J.A. Pasco, J.C. Prior, D.M. Reid, F. Rivadeneira, T. van Staa, N. Yoshimura, and M.C. Zillikens, *A Meta-Analysis of the Association of Fracture Risk and Body Mass Index in Women.* Journal of Bone and Mineral Research, 2014. **29**(1): p. 223-233.
139. Gunnes, M., E.H. Lehmann, D. Mellstrom, and O. Johnell, *The Relationship between Anthropometric Measurements and Fractures in Women.* Bone, 1996. **19**(4): p. 407-413.
140. Kanis, J.A., H. Johansson, O. Johnell, A. Oden, C. De Laet, J.A. Eisman, H. Pols, and A. Tenenhouse, *Alcohol Intake as a Risk Factor for Fracture.* Osteoporosis International, 2005. **16**(7): p. 737-742.
141. Kanis, J.A., O. Johnell, A. Oden, H. Johansson, C. De Laet, J.A. Eisman, S. Fujiwara, H. Kroger, E.V. McCloskey, D. Mellstrom, L.J. Melton, H. Pols, J. Reeve, A. Silman, and A. Tenenhouse, *Smoking and Fracture Risk: A Meta-Analysis.* Osteoporosis International, 2005. **16**(2): p. 155-162.
142. Kiel, D.P., D.T. Felson, M.T. Hannan, J.J. Anderson, and P.W.F. Wilson, *Caffeine and the Risk of Hip Fracture - the Framingham-Study.* American Journal of Epidemiology, 1990. **132**(4): p. 675-684.
143. Kanis, J.A., H. Johansson, A. Oden, O. Johnell, C. de Laet, L.J. Melton, A. Tenenhouse, J. Reeve, A.J. Silman, H.A.P. Pols, J.A. Eisman, E.V. McCloskey, and D. Mellstrom, *A Meta-Analysis of Prior Corticosteroid Use and Fracture Risk.* Journal of Bone and Mineral Research, 2004. **19**(6): p. 893-899.
144. Sambrook, P.N., *Glucocorticoid-Induced Osteoporosis*, in *Primer of the Metabolic Bone Disease and Disorders of Mineral Metabolism*, M.J. Favus, Editor 2006, American Society for Bone and Mineral Research: Durham, USA. p. 296-302.
145. Siris, E.S. and G.D. Roodman, *Paget's Disease of Bone*, in *Primer of the Metabolic Bone Disease and Disorders of Mineral Metabolism*, M.J. Favus, Editor 2006, American Society for Bone and Mineral Research: Durham, USA. p. 320-330.
146. Clines, G.A. and T.A. Guise, *Mechanisms of Bone Destruction and Formation by Metastatic Tumors*, in *Primer of the Metabolic Bone Disease and Disorders of Mineral Metabolism*, M.J. Favus, Editor 2006, American Society for Bone and Mineral Research: Durham, USA. p. 376-382.
147. Edwards, B.J., D.W. Raisch, V. Shankaran, J.M. McKoy, W. Gradishar, A.D. Bunta, A.T. Samaras, S.N. Boyle, C.L. Bennett, D.P. West, and T.A. Guise, *Cancer Therapy Associated Bone Loss: Implications for Hip Fractures in Mid-Life Women with Breast Cancer.* Clinical Cancer Research, 2011. **17**(3): p. 560-568.
148. Greenspan, S.L. and M.M. Luckey, *Evaluation of Postmenopausal Osteoporosis*, in *Primer of the Metabolic Bone Disease and Disorders of Mineral Metabolism*, M.J. Favus, Editor 2006, American Society for Bone and Mineral Research: Durham, USA. p. 268-272.
149. Cohen, A., P. Ebeling, S. Sprague, and E. Shane, *Transplantation Osteoporosis*, in *Primer of the Metabolic Bone Disease and Disorders of Mineral Metabolism*, M.J. Favus, Editor 2006, American Society for Bone and Mineral Research: Durham, USA. p. 302-309.
150. Kanis, J.A., O. Johnell, C. De Laet, H. Johansson, A. Oden, P. Delmas, J. Eisman, S. Fujiwara, P. Garnero, H. Kroger, E.V. McCloskey, D. Mellstrom, L.J. Melton, H. Pols, J. Reeve, A. Silman, and A. Tenenhouse, *A Meta-Analysis of Previous Fracture and Subsequent Fracture Risk.* Bone, 2004. **35**(2): p. 375-382.

151. Javaid, M.K. and C. Cooper, *Prenatal and Childhood Influences on Osteoporosis.* Best Practice & Research Clinical Endocrinology & Metabolism, 2002. **16**(2): p. 349-367.
152. Schonau, E., *The Peak Bone Mass Concept: Is It Still Relevant?* Pediatric Nephrology, 2004. **19**(8): p. 825-831.
153. Zamora, S.A., R. Rizzoli, D.C. Belli, D.O. Slosman, and J.P. Bonjour, *Vitamin D Supplementation During Infancy Is Associated with Higher Bone Mineral Mass in Prepubertal Girls.* Journal of Clinical Endocrinology & Metabolism, 1999. **84**(12): p. 4541-4544.
154. Cooper, C., J.G. Eriksson, T. Forsen, C. Osmond, J. Tuomilehto, and D.J.P. Barker, *Maternal Height, Childhood Growth and Risk of Hip Fracture in Later Life: A Longitudinal Study.* Osteoporosis International, 2001. **12**(8): p. 623-629.
155. Syddall, H.E., A.A. Sayer, S.J. Simmonds, C. Osmond, V. Cox, E.M. Dennison, D.J.P. Barker, and C. Cooper, *Birth Weight, Infant Weight Gain, and Cause-Specific Mortality - the Hertfordshire Cohort Study.* American Journal of Epidemiology, 2005. **161**(11): p. 1074-1080.
156. Dennison, E.M., H.E. Syddall, A.A. Sayer, H.J. Gilbody, and C. Cooper, *Birth Weight and Weight at 1 Year Are Independent Determinants of Bone Mass in the Seventh Decade: The Hertfordshire Cohort Study.* Pediatric Research, 2005. **57**(4): p. 582-586.
157. Javaid, M.K., S.R. Crozier, N.C. Harvey, C.R. Gale, E.M. Dennison, B.J. Boucher, N.K. Arden, K.M. Godfrey, C. Cooper, and G. Princess Anne Hosp Study, *Maternal Vitamin D Status During Pregnancy and Childhood Bone Mass at Age 9 Years: A Longitudinal Study.* Lancet, 2006. **367**(9504): p. 36-43.
158. Cockburn, F., N.R. Belton, R.J. Purvis, M.M. Giles, J.K. Brown, T.L. Turner, E.M. Wilkinson, J.O. Forfar, W.J.M. Barrie, G.S. McKay, and S.J. Pocock, *Maternal Vitamin-D Intake and Mineral Metabolism in Mothers and Their Newborn-Infants.* British Medical Journal, 1980. **281**(6232): p. 11-14.
159. Godfrey, K., K. Walker-Bone, S. Robinson, P. Taylor, S. Shore, T. Wheeler, and C. Cooper, *Neonatal Bone Mass: Influence of Parental Birthweight, Maternal Smoking, Body Composition, and Activity During Pregnancy.* Journal of Bone and Mineral Research, 2001. **16**(9): p. 1694-1703.
160. Richards, J.B., H.F. Zheng, and T.D. Spector, *Disease Mechanisms Genetics of Osteoporosis from Genome-Wide Association Studies: Advances and Challenges.* Nature Reviews Genetics, 2012. **13**(8): p. 576-588.
161. Kanis, J.A., H. Johansson, A. Oden, O. Johnell, C. De Laet, J.A. Eisman, E.V. McCloskey, D. Mellstrom, L.J. Melton, H.A.P. Pols, J. Reeve, A.J. Silman, and A. Tenenhouse, *A Family History of Fracture and Fracture Risk: A Meta-Analysis.* Bone, 2004. **35**(5): p. 1029-1037.
162. Burstein, A.H., D.T. Reilly, and M. Martens, *Aging of Bone Tissue - Mechanical-Properties.* Journal of Bone and Joint Surgery-American Volume, 1976. **58**(1): p. 82-86.
163. Nalla, R.K., J.J. Kruzic, J.H. Kinney, M. Balooch, J.W. Ager, III, and R.O. Ritchie, *Role of Microstructure in the Aging-Related Deterioration of the Toughness of Human Cortical Bone.* Materials Science & Engineering C-Biomimetic and Supramolecular Systems, 2006. **26**(8): p. 1251-1260.
164. Cefalu, C.A., *Is Bone Mineral Density Predictive of Fracture Risk Reduction?* Curr Med Res Opin, 2004. **20**(3): p. 341-9.
165. Vashishth, D., O. Verborgt, G. Divine, M.B. Schaffler, and D.P. Fyhrie, *Decline in Osteocyte Lacunar Density in Human Cortical Bone Is Associated with Accumulation of Microcracks with Age.* Bone, 2000. **26**(4): p. 375-380.
166. Qiu, S., D.S. Rao, S. Palnitkar, and A.M. Parfitt, *Age and Distance from the Surface but Not Menopause Reduce Osteocyte Density in Human Cancellous Bone.* Bone, 2002. **31**(2): p. 313-318.
167. Klein-Nulend, J., J.G.H. Sterck, C.M. Semeins, P. Lips, M. Joldersma, J.A. Baart, and E.H. Burger, *Donor Age and Mechanosensitivity of Human Bone Cells.* Osteoporosis International, 2002. **13**(2): p. 137-146.

168. Ehrlich, P.J. and L.E. Lanyon, *Mechanical Strain and Bone Cell Function: A Review.* Osteoporosis International, 2002. **13**(9): p. 688-700.
169. Dunstan, C.R., N.M. Somers, R.A. Evans, Rubin, Ott, Snyder, Davy, Schaffler, Parfitt, and Goldstein, *Osteocyte Death and Hip Fracture.* Calcified Tissue International, 1993. **53**: p. S113-S117.
170. Burr, D.B., *Bone Material Properties and Mineral Matrix Contributions to Fracture Risk or Age in Women and Men.* Journal of Musculoskeletal & Neuronal Interactions, 2002. **2**(3): p. 201-204.
171. Paschalis, E.P., F. Betts, E. DiCarlo, R. Mendelsohn, and A.L. Boskey, *Ftir Microspectroscopic Analysis of Normal Human Cortical and Trabecular Bone.* Calcified Tissue International, 1997. **61**(6): p. 480-486.
172. Paschalis, E.P., F. Betts, E. DiCarlo, R. Mendelsohn, and A.L. Boskey, *Ftir Microspectroscopic Analysis of Human Iliac Crest Biopsies from Untreated Osteoporotic Bone.* Calcified Tissue International, 1997. **61**(6): p. 487-492.
173. Paschalis, E.P., E. DiCarlo, F. Betts, P. Sherman, R. Mendelsohn, and A.L. Boskey, *Ftir Microspectroscopic Analysis of Human Osteonal Bone.* Calcified Tissue International, 1996. **59**(6): p. 480-487.
174. Grynpas, M.D., J.H. Tupy, and J. Sodek, *The Distribution of Soluble, Mineral-Bound, and Matrix-Bound Proteins in Osteoporotic and Normal Bones.* Bone, 1994. **15**(5): p. 505-513.
175. Saito, M., K. Marumo, K. Fujii, and N. Ishioka, *Single-Column High-Performance Liquid Chromatographic Fluorescence Detection of Immature, Mature, and Senescent Cross-Links of Collagen.* Analytical Biochemistry, 1997. **253**(1): p. 26-32.
176. Silva, M.J., *Biomechanics of Osteoporotic Fractures.* Injury, 2007. **38 Suppl 3**: p. S69-76.
177. Schaffler, M.B., K. Choi, and C. Milgrom, *Aging and Matrix Microdamage Accumulation in Human Compact Bone.* Bone, 1995. **17**(6): p. 521-525.
178. Mashiba, T., T. Hirano, C.H. Turner, M.R. Forwood, C.C. Johnston, and D.B. Burr, *Suppressed Bone Turnover by Bisphosphonates Increases Microdamage Accumulation and Reduces Some Biomechanical Properties in Dog Rib.* Journal of Bone and Mineral Research, 2000. **15**(4): p. 613-620.
179. Koester, K.J., H.D. Barth, and R.O. Ritchie, *Effect of Aging on the Transverse Toughness of Human Cortical Bone: Evaluation by R-Curves.* J Mech Behav Biomed Mater, 2011. **4**(7): p. 1504-1513.
180. Katsamenis, O.L., T. Jenkins, S. Michopoulou, I. Sinclair, and P.J. Thurner. *Multiscale Experimental Analysis of Human Bone Fracture Toughness: From the Osteonal up to the Tissue Level*. in *Orthopaedic Research Society*. 2013. San Antonio, Texas.
181. Bell, K.L., N. Loveridge, J. Power, N. Garrahan, B.F. Meggitt, and J. Reeve, *Regional Differences in Cortical Porosity in the Fractured Femoral Neck.* Bone, 1999. **24**(1): p. 57-64.
182. Poole, K.E.S., P.M. Mayhew, C.M. Rose, J.K. Brown, P.J. Bearcroft, N. Loveridge, and J. Reeve, *Changing Structure of the Femoral Neck across the Adult Female Lifespan.* Journal of Bone and Mineral Research, 2010. **25**(3): p. 482-491.
183. Keaveny, T.M. and O.C. Yeh, *Architecture and Trabecular Bone: Toward an Improved Understanding of the Biomechanical Effects of Age, Sex and Osteoporosis.* Journal of Musculoskeletal & Neuronal Interactions, 2002. **2**(3): p. 205-208.
184. Thurner, P.J. and O.L. Katsamenis, *The Role of Nanoscale Toughening Mechanisms in Osteoporosis.* Current Osteoporosis Reports, 2014. **12**(3): p. 351-6.
185. Dickenson, R.P., W.C. Hutton, and J.R.R. Stott, *The Mechanical-Properties of Bone in Osteoporosis.* Journal of Bone and Joint Surgery-British Volume, 1981. **63**(2): p. 233-238.
186. Reuters, T. *Web of Science*. 2014 [cited 2014 December].
187. Hans, D., P. DargentMolina, A.M. Schott, J.L. Sebert, C. Cormier, P.O. Kotzki, P.D. Delmas, J.M. Pouilles, G. Breart, and P.J. Meunier, *Ultrasonographic Heel Measurements to Predict Hip Fracture in Elderly Women: The Epidos Prospective Study.* Lancet, 1996. **348**(9026): p. 511-514.

188. Augat, P., T. Fuerst, and H.K. Genant, *Quantitative Bone Mineral Assessment at the Forearm: A Review.* Osteoporosis International, 1998. **8**(4): p. 299-310.
189. Marshall, D., O. Johnell, and H. Wedel, *Meta-Analysis of How Well Measures of Bone Mineral Density Predict Occurrence of Osteoporotic Fractures.* British Medical Journal, 1996. **312**(7041): p. 1254-1259.
190. Majumdar, S., T.M. Link, P. Augat, J.C. Lin, D. Newitt, N.E. Lane, and H.K. Genant, *Trabecular Bone Architecture in the Distal Radius Using Magnetic Resonance Imaging in Subjects with Fractures of the Proximal Femur.* Osteoporosis International, 1999. **10**(3): p. 231-239.
191. Formica, C.A., J.W. Nieves, F. Cosman, P. Garrett, and R. Lindsay, *Comparative Assessment of Bone Mineral Measurements Using Dual X-Ray Absorptiometry and Peripheral Quantitative Computed Tomography.* Osteoporosis International, 1998. **8**(5): p. 460-467.
192. Cummings, S.R., M.C. Nevitt, W.S. Browner, K. Stone, K.M. Fox, K.E. Ensrud, J.C. Cauley, D. Black, and T.M. Vogt, *Risk-Factors for Hip Fracture in White Women.* New England Journal of Medicine, 1995. **332**(12): p. 767-773.
193. Kanis, J.A., A. Oden, O. Johnell, H. Johansson, C. De Laet, J. Brown, P. Burckhardt, C. Cooper, C. Christiansen, S. Cummings, J.A. Eisman, S. Fujiwara, C. Gluer, D. Goltzman, D. Hans, M.A. Krieg, A. La Croix, E. McCloskey, D. Mellstrom, L.J. Melton, H. Pols, J. Reeve, K. Sanders, A.M. Schott, A. Silman, D. Torgerson, T. van Staa, N.B. Watts, and N. Yoshimura, *The Use of Clinical Risk Factors Enhances the Performance of Bmd in the Prediction of Hip and Osteoporotic Fractures in Men and Women.* Osteoporosis International, 2007. **18**(8): p. 1033-1046.
194. Sandhu, S.K., N.D. Nguyen, J.R. Center, N.A. Pocock, J.A. Eisman, and T.V. Nguyen, *Prognosis of Fracture: Evaluation of Predictive Accuracy of the Frax (Tm) Algorithm and Garvan Nomogram.* Osteoporosis International, 2010. **21**(5): p. 863-871.
195. Hillier, M.L. and L.S. Bell, *Differentiating Human Bone from Animal Bone: A Review of Histological Methods.* Journal of Forensic Sciences, 2007. **52**(2): p. 249-263.
196. Cook, R.B., C. Curwen, T. Tasker, and P. Zioupos, *Fracture Toughness and Compressive Properties of Cancellous Bone at the Head of the Femur and Relationships to Non-Invasive Skeletal Assessment Measurements.* Med Eng Phys, 2010. **32**(9): p. 991-7.
197. Unnanuntana, A., B.P. Gladnick, E. Donnelly, and J.M. Lane, *The Assessment of Fracture Risk.* J Bone Joint Surg Am, 2010. **92**(3): p. 743-53.
198. Chapurlat, R.D., P. Garnero, G. Breart, P.J. Meunier, and P.D. Delmas, *Serum Type I Collagen Breakdown Product (Serum Ctx) Predicts Hip Fracture Risk in Elderly Women: The Epidos Study.* Bone, 2000. **27**(2): p. 283-286.
199. Ross, P.D., B.C. Kress, R.E. Parson, R.D. Wasnich, K.A. Armour, and I.A. Mizrahi, *Serum Bone Alkaline Phosphatase and Calcaneus Bone Density Predict Fractures: A Prospective Study.* Osteoporosis International, 2000. **11**(1): p. 76-82.
200. Black, D.M., D.E. Thompson, D.C. Bauer, K. Ensrud, T. Musliner, M.C. Hochberg, M.C. Nevitt, S. Suryawanshi, S.R. Cummings, and F.I.T.R. Grp, *Fracture Risk Reduction with Alendronate in Women with Osteoporosis: The Fracture Intervention Trial.* Journal of Clinical Endocrinology & Metabolism, 2000. **85**(11): p. 4118-4124.
201. Chesnut, C.H., A. Skag, C. Christiansen, R. Recker, J.A. Stakkestad, A. Hoiseth, D. Felsenberg, H. Huss, J. Gilbride, R.C. Schimmer, P.D. Delmas, and V. Oral Ibandronate Osteoporosis, *Effects of Oral Ibandronate Administered Daily or Intermittently on Fracture Risk in Postmenopausal Osteoporosis.* Journal of Bone and Mineral Research, 2004. **19**(8): p. 1241-1249.
202. Black, D.M., P.D. Delmas, R. Eastell, I.R. Reid, S. Boonen, J.A. Cauley, F. Cosman, P. Lakatos, P.C. Leung, Z. Man, C. Mautalen, P. Mesenbrink, H.L. Hu, J. Caminis, K. Tong, T. Rosario-Jansen, J. Krasnow, T.F. Hue, D. Sellmeyer, E.F. Eriksen, S.R. Cummings, and H.P.F. Trial, *Once-Yearly Zoledronic Acid for Treatment of Postmenopausal Osteoporosis.* New England Journal of Medicine, 2007. **356**(18): p. 1809-1822.

203. Whitaker, M., J. Guo, T. Kehoe, and G. Benson, *Bisphosphonates for Osteoporosis — Where Do We Go from Here?* New England Journal of Medicine, 2012. **366**(22): p. 2048-2051.
204. Woo, S.-B., J.W. Hellstein, and J.R. Kalmar, *Systematic Review: Bisphosphonates and Osteonecrosis of the Jaws.* Annals of Internal Medicine, 2006. **144**(10): p. 753-761.
205. Black, D.M., M.P. Kelly, H.K. Genant, L. Palermo, R. Eastell, C. Bucci-Rechtweg, J. Cauley, P.C. Leung, S. Boonen, A. Santora, A. de Papp, D.C. Bauer, C. Fracture Intervention Trial, and H.P.F.T. Ste, *Bisphosphonates and Fractures of the Subtrochanteric or Diaphyseal Femur.* New England Journal of Medicine, 2010. **362**(19): p. 1761-1771.
206. Genazzani, A.R. and M. Gambacciani, *Hormone Replacement Therapy: The Perspectives for the 21st Century.* Maturitas, 1999. **32**(1): p. 11-17.
207. Girotra, M., M.R. Rubin, and J.P. Bilezikian, *The Use of Parathyroid Hormone in the Treatment of Osteoporosis.* Reviews in Endocrine & Metabolic Disorders, 2006. **7**(1-2): p. 113-121.
208. Cummings, S.R., J.S. Martin, M.R. McClung, E.S. Siris, R. Eastell, I.R. Reid, P. Delmas, H.B. Zoog, M. Austin, A. Wang, S. Kutilek, S. Adami, J. Zanchetta, C. Libanati, S. Siddhanti, and C. Christiansen, *Denosumab for Prevention of Fractures in Postmenopausal Women with Osteoporosis.* New England Journal of Medicine, 2009. **361**(8): p. 756-765.
209. Felson, D.T. and Y.Q. Zhang, *An Update on the Epidemiology of Knee and Hip Osteoarthritis with a View to Prevention.* Arthritis and Rheumatism, 1998. **41**(8): p. 1343-1355.
210. Woolf, A.D. and B. Pfleger, *Burden of Major Musculoskeletal Conditions.* Bulletin of the World Health Organization, 2003. **81**(9): p. 646-656.
211. Chen, A., C. Gupte, K. Akhtar, P. Smith, and J. Cobb, *The Global Economic Cost of Osteoarthritis: How the Uk Compares.* Arthritis, 2012. **2012**: p. 698709.
212. Goldring, M.B. and S.R. Goldring, *Osteoarthritis.* Journal of Cellular Physiology, 2007. **213**(3): p. 626-634.
213. Arden, N. and M.C. Nevitt, *Osteoarthritis: Epidemiology.* Best Practice & Research Clinical Rheumatology. **20**(1): p. 3-25.
214. Richette, P., M. Corvol, and T. Bardin, *Estrogens, Cartilage, and Osteoarthritis.* Joint Bone Spine, 2003. **70**(4): p. 257-262.
215. Spector, T.D. and A.J. MacGregor, *Risk Factors for Osteoarthritis: Genetics.* Osteoarthritis and cartilage / OARS, Osteoarthritis Research Society, 2004. **12 Suppl A**: p. S39-44.
216. Ganz, R., M. Leunig, K. Leunig-Ganz, and W.H. Harris, *The Etiology of Osteoarthritis of the Hip - an Integrated Mechanical Concept.* Clinical Orthopaedics and Related Research, 2008. **466**(2): p. 264-272.
217. Sowers, M.F., C. Hayes, D. Jamadar, D. Capul, L. Lachance, M. Jannausch, and G. Welch, *Magnetic Resonance-Detected Subchondral Bone Marrow and Cartilage Defect Characteristics Associated with Pain and X-Ray-Defined Knee Osteoarthritis.* Osteoarthritis and Cartilage, 2003. **11**(6): p. 387-393.
218. Bobinac, D., M. Marinovic, E. Bazdulj, O. Cvijanovic, T. Celic, I. Maric, J. Spanjol, and T. Cicvaric, *Microstructural Alterations of Femoral Head Articular Cartilage and Subchondral Bone in Osteoarthritis and Osteoporosis.* Osteoarthritis and Cartilage, 2013. **21**(11): p. 1724-1730.
219. Kellgren, J.H. and J.S. Lawrence, *Radiological Assessment of Osteo-Arthrosis.* Annals of the Rheumatic Diseases, 1957. **16**(4): p. 494-502.
220. Baker-LePain, J.C. and N.E. Lane, *Role of Bone Architecture and Anatomy in Osteoarthritis.* Bone, 2012. **51**(2): p. 197-203.
221. Rubinacci, A., D. Tresoldi, E. Scalco, I. Villa, F. Adorni, G.L. Moro, G.F. Fraschini, and G. Rizzo, *Comparative High-Resolution Pqct Analysis of Femoral Neck Indicates Different Bone Mass Distribution in Osteoporosis and Osteoarthritis.* Osteoporosis International, 2012. **23**(7): p. 1967-1975.

222. Sun, S.S., H.L. Ma, C.L. Liu, C.H. Huang, C.K. Cheng, and H.W. Wei, *Difference in Femoral Head and Neck Material Properties between Osteoarthritis and Osteoporosis.* Clinical Biomechanics, 2008. **23**: p. S39-S47.
223. Blain, H., P. Chavassieux, N. Portero-Muzy, F. Bonnel, F. Canovas, M. Chammas, P. Maury, and P.D. Delmas, *Cortical and Trabecular Bone Distribution in the Femoral Neck in Osteoporosis and Osteoarthritis.* Bone, 2008. **43**(5): p. 862-868.
224. Li, B.H. and R.M. Aspden, *Mechanical and Material Properties of the Subchondral Bone Plate from the Femoral Head of Patients with Osteoarthritis or Osteoporosis.* Annals of the Rheumatic Diseases, 1997. **56**(4): p. 247-254.
225. Neilson, M., A. White, U. Malik, E. Morrison, P.E. McGill, and S.W. McDonald, *Changes in Bone Architecture in the Femoral Head and Neck in Osteoarthritis.* Clinical Anatomy, 2004. **17**(5): p. 378-391.
226. Hunter, D.J. and D.T. Felson, *Osteoarthritis*. Vol. 332. 2006. 639-642.
227. Vestergaard, P., L. Rejnmark, and L. Mosekilde, *Osteoarthritis and Risk of Fractures.* Calcified Tissue International, 2009. **84**(4): p. 249-256.
228. Boutroy, S., N. Vilayphiou, J.P. Roux, P.D. Delmas, H. Blain, R.D. Chapurlat, and P. Chavassieux, *Comparison of 2d and 3d Bone Microarchitecture Evaluation at the Femoral Neck, among Postmenopausal Women with Hip Fracture or Hip Osteoarthritis.* Bone, 2011. **49**(5): p. 1055-1061.
229. Coutts, L.V., T. Jenkins, T. Li, D.G. Dunlop, R.O.C. Oreffo, C. Cooper, N. Harvey, and P.J. Thurner, *Reference Point Microindentation and Recommendations for Testing Cortical Bone: Location, Thickness and Orientation Heterogeneity.* Journal of the Mechanical Behaviour of Biomedical Materials, 2015 (under review).
230. Croft, P., C. Cooper, C. Wickham, and D. Coggon, *Defining Osteoarthritis of the Hip for Epidemiologic Studies.* American Journal of Epidemiology, 1990. **132**(3): p. 514-522.
231. Tanaka, S., K. Narusawa, H. Onishi, M. Miura, A. Hijioka, Y. Kanazawa, S. Nishida, S. Ikeda, and T. Nakamura, *Lower Osteocalcin and Osteopontin Contents of the Femoral Head in Hip Fracture Patients Than Osteoarthritis Patients.* Osteoporosis International, 2011. **22**(2): p. 587-597.
232. Lewis, G. and J.S. Nyman, *The Use of Nanoindentation for Characterizing the Properties of Mineralized Hard Tissues: State-of-the Art Review.* Journal of Biomedical Materials Research Part B-Applied Biomaterials, 2008. **87B**(1): p. 286-301.
233. Zhang, J., G.L. Niebur, and T.C. Ovaert, *Mechanical Property Determination of Bone through Nano- and Micro-Indentation Testing and Finite Element Simulation.* J Biomech, 2008. **41**(2): p. 267-275.
234. Zysset, P.K., *Indentation of Bone Tissue: A Short Review.* Osteoporosis International, 2009. **20**(6): p. 1049-1055.
235. Schwiedrzik, J.J. and P.K. Zysset, *The Influence of Yield Surface Shape and Damage in the Depth-Dependent Response of Bone Tissue to Nanoindentation Using Spherical and Berkovich Indenters.* Computer Methods in Biomechanics and Biomedical Engineering, 2015. **18**(5): p. 492-505.
236. Oliver, W.C. and G.M. Pharr, *An Improved Technique for Determining Hardness and Elastic-Modulus Using Load and Displacement Sensing Indentation Experiments.* Journal of Materials Research, 1992. **7**(6): p. 1564-1583.
237. Mullins, L.P., M.S. Bruzzi, and P.E. McHugh, *Measurement of the Microstructural Fracture Toughness of Cortical Bone Using Indentation Fracture.* J Biomech, 2007. **40**(14): p. 3285-8.
238. Kruzic, J.J., D.K. Kim, K.J. Koester, and R.O. Ritchie, *Indentation Techniques for Evaluating the Fracture Toughness of Biomaterials and Hard Tissues.* J Mech Behav Biomed Mater, 2009. **2**(4): p. 384-395.
239. Paietta, R.C., S.E. Campbell, and V.L. Ferguson, *Influences of Spherical Tip Radius, Contact Depth, and Contact Area on Nanoindentation Properties of Bone.* J Biomech, 2011. **44**(2): p. 285-290.

240. Hansma, P.K., P.J. Turner, and G.E. Fantner, *Bone Diagnostic Instrument.* Review of Scientific Instruments, 2006. **77**(7): p. 075105.
241. Li, S., E. Demirci, and V.V. Silberschmidt, *Variability and Anisotropy of Mechanical Behavior of Cortical Bone in Tension and Compression.* J Mech Behav Biomed Mater, 2013. **21**(0): p. 109-120.
242. Farr, J.N., M.T. Drake, S. Amin, L.J. Melton, L.K. McCready, and S. Khosla, *In Vivo Assessment of Bone Quality in Postmenopausal Women with Type 2 Diabetes.* Journal of Bone and Mineral Research, 2014. **29**(4): p. 787-795.
243. Hammond, M.A., M.A. Gallant, D.B. Burr, and J.M. Wallace, *Nanoscale Changes in Collagen Are Reflected in Physical and Mechanical Properties of Bone at the Microscale in Diabetic Rats.* Bone, 2014. **60**: p. 26-32.
244. Carriero, A., J.L. Bruse, K.J. Oldknow, J.L. Millán, C. Farquharson, and S.J. Shefelbine, *Reference Point Indentation Is Not Indicative of Whole Mouse Bone Measures of Stress Intensity Fracture Toughness.* Bone, 2014. **69C**(Article): p. 174-179.
245. Chen, J. and S.J. Bull, *On the Relationship between Plastic Zone Radius and Maximum Depth During Nanoindentation.* Surface & Coatings Technology, 2006. **201**(7): p. 4289-4293.
246. Chen, J.J. and S.J. Bull, *Approaches to Investigate Delamination and Interfacial Toughness in Coated Systems: An Overview.* Journal of Physics D-Applied Physics, 2011. **44**(3).
247. Kruzic, J.J. and R.O. Ritchie, *Comments on "Measurement of the Microstructural Fracture Toughness of Cortical Bone Using Indentation Fracture".* J Biomech, 2008. **41**(6): p. 1379-1380.
248. Quinn, G.D. and R.C. Bradt, *On the Vickers Indentation Fracture Toughness Test.* Journal of the American Ceramic Society, 2007. **90**(3): p. 673-680.
249. Hoffler, C.E., X.E. Guo, P.K. Zysset, and S.A. Goldstein, *An Application of Nanoindentation Technique to Measure Bone Tissue Lamellae Properties.* Journal of Biomechanical Engineering-Transactions of the Asme, 2005. **127**(7): p. 1046-1053.
250. O'Brien, F.J., D. Taylor, G.R. Dickson, and T.C. Lee, *Visualisation of Three-Dimensional Microcracks in Compact Bone.* Journal of Anatomy, 2000. **197**: p. 413-420.
251. Lee, T.C., S. Mohsin, D. Taylor, R. Parkesh, T. Gunnlaugsson, F.J. O'Brien, M. Giehl, and W. Gowin, *Detecting Microdamage in Bone.* Journal of Anatomy, 2003. **203**(2): p. 161-172.
252. Mohsin, S., F.J. O'Brien, and T.C. Lee, *Microcracks in Compact Bone: A Three-Dimensional View.* Journal of Anatomy, 2006. **209**(1): p. 119-124.
253. Wasserman, N., B. Brydges, S. Searles, and O. Akkus, *In Vivo Linear Microcracks of Human Femoral Cortical Bone Remain Parallel to Osteons During Aging.* Bone, 2008. **43**(5): p. 856-861.
254. Frisch, T., M.S. Sorensen, and P. Bretlau, *Recognition of Basic Fuchsin Prestained Microfissures of Intravital Origin with Fluorescence Microscopy: Validation of a Shortcut.* European Archives of Oto-Rhino-Laryngology, 2001. **258**(2): p. 55-60.
255. ASTM, *Standard Test Method for Measurement of Fracture Toughness*, in *E1820*2001: West Conshohocken.
256. Katsamenis, O.L., T. Jenkins, F. Quinci, S. Michopoulou, I. Sinclair, and P.J. Thurner, *A Novel Videography Method for Generating Crack-Extension Resistance Curves in Small Bone Samples.* Plos One, 2013. **8**(2).
257. Thurner, P.J., B. Erickson, R. Jungmann, Z. Schriock, J.C. Weaver, G.E. Fantner, G. Schitter, D.E. Morse, and P.K. Hansma, *High-Speed Photography of Compressed Human Trabecular Bone Correlates Whitening to Microscopic Damage.* Engineering Fracture Mechanics, 2007. **74**(12): p. 1928-1941.
258. Hardisty, M.R., T.C. Garcia, S. Choy, J. Dahmubed, S.M. Stover, and D.P. Fyhrie, *Stress-Whitening Occurs in Demineralized Bone.* Bone, 2013. **57**(2): p. 367-374.
259. Ritchie, R.O., R.K. Nalla, J.J. Kruzic, J.W. Ager, G. Balooch, and J.H. Kinney, *Fracture and Ageing in Bone: Toughness and Structural Characterization.* Strain, 2006. **42**(4): p. 225-232.

260. de Riese, C., *Osteoporosis: Are We Measuring What We Intend to Measure? In Search of the Ideal Bone Strength Study.* 2006. **6078**: p. 607825-607825-11.
261. Sturtridge, W., B. Lentle, and D.A. Hanley, *The Use of Bone Density Measurement in the Diagnosis and Management of Osteoporosis.* Canadian Medical Association Journal, 1996. **155**(7): p. 924-929.
262. Blake, G.M. and I. Fogelman, *The Role of Dxa Bone Density Scans in the Diagnosis and Treatment of Osteoporosis.* Postgraduate Medical Journal, 2007. **83**(982): p. 509-517.
263. Technology, N.I.o.S.a. *Physical Measurement Laboratory - Table of X-Ray Mass Attenuation Coefficeints*. 2014 [cited 2015 7th January].
264. Kanis, J.A., O. Johnell, A. Oden, H. Johansson, and E. McCloskey, *Frax (Tm) and the Assessment of Fracture Probability in Men and Women from the Uk.* Osteoporosis International, 2008. **19**(4): p. 385-397.
265. Kanis, J.A., E.V. McCloskey, H. Johansson, O. Strom, F. Borgstrom, A. Oden, and G. Natl Osteoporosis Guideline, *Case Finding for the Management of Osteoporosis with Frax (R) - Assessment and Intervention Thresholds for the Uk.* Osteoporosis International, 2008. **19**(10): p. 1395-1408.
266. Lee, T.C., E.R. Myers, and W.C. Hayes, *Fluorescence-Aided Detection of Microdamage in Compact Bone.* Journal of Anatomy, 1998. **193**: p. 179-184.
267. Burr, D.B. and M. Hooser, *Alterations to the En-Bloc Basic Fuchsin Staining Protocol for the Demonstration of Microdamage Produced in-Vivo.* Bone, 1995. **17**(4): p. 431-433.
268. O'Brien, F.J., D. Taylor, and T.C. Lee, *An Improved Labelling Technique for Monitoring Microcrack Growth in Compact Bone.* J Biomech, 2002. **35**(4): p. 523-526.
269. Dall'Ara, E., C. Karl, H. Richter, and P. Zysset, *Sample Preparation for Nanoindentation: Comparison of Four Different Techniques*, 2010, TUWien: ILSB Internal Report.
270. Schneider, P., P. Hansma, C. Randall, and R. Muller, *Quantitative 3d Microcrack Imaging for Weak and Strong Bones Assessed by Reference Point Indentation*, in *ASBMR*2013: Baltimore, Maryland.
271. Landis, E.N. and D.T. Keane, *X-Ray Microtomography.* Materials Characterization, 2010. **61**(12): p. 1305-1316.
272. Ketcham, R.A. and W.D. Carlson, *Acquisition, Optimization and Interpretation of X-Ray Computed Tomographic Imagery: Applications to the Geosciences.* Computers & Geosciences, 2001. **27**(4): p. 381-400.
273. Cooper, D.M.L., J.R. Matyas, M.A. Katzenberg, and B. Hallgrimsson, *Comparison of Microcomputed Tomographic and Microradiographic Measurements of Cortical Bone Porosity.* Calcified Tissue International, 2004. **74**(5): p. 437-447.
274. Muller, R., H. Van Campenhout, B. Van Damme, G. Van Der Perre, J. Dequeker, T. Hildebrand, and P. Ruegsegger, *Morphometric Analysis of Human Bone Biopsies: A Quantitative Structural Comparison of Histological Sections and Micro-Computed Tomography.* Bone, 1998. **23**(1): p. 59-66.
275. Schneider, P., M. Stauber, R. Voide, M. Stampanoni, L.R. Donahue, and R. Muller, *Ultrastructural Properties in Cortical Bone Vary Greatly in Two Inbred Strains of Mice as Assessed by Synchrotron Light Based Micro- and Nano-Ct.* Journal of Bone and Mineral Research, 2007. **22**(10): p. 1557-1570.
276. Landrigan, M.D., J.L. Li, T.L. Turnbull, D.B. Burr, G.L. Niebur, and R.K. Roeder, *Contrast-Enhanced Micro-Computed Tomography of Fatigue Microdamage Accumulation in Human Cortical Bone.* Bone, 2011. **48**(3): p. 443-450.
277. Leng, H.J., X. Wang, R.D. Ross, G.L. Niebur, and R.K. Roeder, *Micro-Computed Tomography of Fatigue Microdamage in Cortical Bone Using a Barium Sulfate Contrast Agent.* J Mech Behav Biomed Mater, 2008. **1**(1): p. 68-75.
278. Meyer, E., *Atomic Force Microscopy.* Progress in Surface Science, 1992. **41**(1): p. 3-49.
279. Jenkins, T., L.V. Coutts, D.G. Dunlop, R.O.C. Oreffo, C. Cooper, N.C. Harvey, and P.J. Thurner, *Variability in Reference Point Microindentation and Recommendations for Testing Cortical Bone: Maximum Load, Sample Orientation, Mode of Use, Sample*

Preparation and Measurement Spacing. J Mech Behav Biomed Mater, 2015. **42**(0): p. 311-324.
280. Manilay, Z., E. Novitskaya, E. Sadovnikov, and J. McKittrick, *A Comparative Study of Young and Mature Bovine Cortical Bone.* Acta Biomaterialia, 2013. **9**(2): p. 5280-5288.
281. Liu, D., H.D. Wagner, and S. Weiner, *Bending and Fracture of Compact Circumferential and Osteonal Lamellar Bone of the Baboon Tibia.* Journal of Materials Science-Materials in Medicine, 2000. **11**(1): p. 49-60.
282. Skedros, J.G., M.W. Mason, and R.D. Bloebaum, *Modeling and Remodeling in a Developing Artiodactyl Calcaneus: A Model for Evaluating Frost's Mechanostat Hypothesis and Its Corollaries.* Anatomical Record, 2001. **263**(2): p. 167-185.
283. Mori, R., T. Kodaka, and Y. Naito, *Histological Comparison of Long-Bone Cortex between 11-Year-Old Giant Cow with Dermal Dysplasia and the Child Cow Aged 8.5 Years.* Journal of Veterinary Medical Science, 2012. **74**(2): p. 197-200.
284. Yan, J., K.B. Clifton, J.J. Mecholsky Jr, and R.L. Reep, *Fracture Toughness of Manatee Rib and Bovine Femur Using a Chevron-Notched Beam Test.* J Biomech, 2006. **39**(6): p. 1066-1074.
285. Aerssens, J., S. Boonen, G. Lowet, and J. Dequeker, *Interspecies Differences in Bone Composition, Density, and Quality: Potential Implications for in Vivo Bone Research.* Endocrinology, 1998. **139**(2): p. 663-670.
286. Kaye, B., C. Randall, D. Walsh, and P. Hansma, *The Effects of Freezing on the Mechanical Properties of Bone.* The Open Bone Journal, 2012. **4**: p. 6.
287. Hamer, A.J., J.R. Strachan, M.M. Black, C.J. Ibbotson, I. Stockley, and R.A. Elson, *Biomechanical Properties of Cortical Allograft Bone Using a New Method of Bone Strength Measurement - a Comparison of Fresh, Fresh-Frozen and Irradiated Bone.* Journal of Bone and Joint Surgery-British Volume, 1996. **78B**(3): p. 363-368.
288. van Haaren, E.H., B.C. van der Zwaard, A.J. van der Veen, I.C. Heyligers, P.I. Wuisman, and T.H. Smit, *Effect of Long-Term Preservation on the Mechanical Properties of Cortical Bone in Goats.* Acta Orthopaedica, 2008. **79**(5): p. 708-716.
289. Johansson, H., J.A. Kanis, A. Oden, O. Johnell, and E. McCloskey, *Bmd, Clinical Risk Factors and Their Combination for Hip Fracture Prevention.* Osteoporosis International, 2009. **20**(10): p. 1675-1682.
290. Coats, A.M., P. Zioupos, and R.M. Aspden, *Material Properties of Subchondral Bone from Patients with Osteoporosis or Osteoarthritis by Microindentation Testing and Electron Probe Microanalysis.* Calcified Tissue International, 2003. **73**(1): p. 66-71.
291. Cummings, S.R., J.L. Kelsey, M.C. Nevitt, and K.J. Odowd, *Epidemiology of Osteoporosis and Osteoporotic Fractures.* Epidemiologic Reviews, 1985. **7**: p. 178-208.
292. Kruzic, J.J., S.J. Kuskowski, and R.O. Ritchie, *Simple and Accurate Fracture Toughness Testing Methods for Pyrolytic Carbon/Graphite Composites Used in Heart-Valve Prostheses.* Journal of Biomedical Materials Research Part A, 2005. **74A**(3): p. 461-464.
293. Thurner, P.J., B. Erickson, P. Turner, R. Jungmann, J. Lelujian, A. Proctor, J.C. Weaver, G. Schitter, D.E. Morse, and P.K. Hansma, *The Effect of Naf in Vitro on the Mechanical and Material Properties of Trabecular and Cortical Bone.* Advanced Materials, 2009. **21**(4): p. 451-457.
294. Fischer-Cripps, A.C., *Review of Analysis and Interpretation of Nanoindentation Test Data.* Surface & Coatings Technology, 2006. **200**(14-15): p. 4153-4165.
295. Jepsen, K.J., *The Aging Cortex: To Crack or Not to Crack.* Osteoporosis International, 2003. **14**: p. S57-S62.
296. Zioupos, P. and J.D. Currey, *Changes in the Stiffness, Strength, and Toughness of Human Cortical Bone with Age.* Bone, 1998. **22**(1): p. 57-66.
297. Brown, C.U., Y.N. Yeni, and T.L. Norman, *Fracture Toughness Is Dependent on Bone Location - a Study of the Femoral Neck, Femoral Shaft, and the Tibial Shaft.* Journal of Biomedical Materials Research, 2000. **49**(3): p. 380-389.

298. Yeni, Y.N. and T.L. Norman, *Fracture Toughness of Human Femoral Neck: Effect of Microstructure, Composition, and Age.* Bone, 2000. **26**(5): p. 499-504.
299. Center, J.R., T.V. Nguyen, N.A. Pocock, and J.A. Eisman, *Volumetric Bone Density at the Femoral Neck as a Common Measure of Hip Fracture Risk for Men and Women.* Journal of Clinical Endocrinology & Metabolism, 2004. **89**(6): p. 2776-2782.
300. Carbonare, L.D., F. Bertoldo, M.T. Valenti, S. Zenari, M. Zanatta, S. Sella, S. Giannini, and V. Lo Cascio, *Histomorphometric Analysis of Glucocorticoid-Induced Osteoporosis.* Micron, 2005. **36**(7-8): p. 645-652.
301. Martin, D.E., A.E. Severns, and J.M. Kabo, *Determination of Mechanical Stiffness of Bone by Pqct Measurements: Correlation with Non-Destructive Mechanical Four-Point Bending Test Data.* J Biomech, 2004. **37**(8): p. 1289-1293.
302. Pluijm, S.M.F., W.C. Graafmans, L.M. Bouter, and P. Lips, *Ultrasound Measurements for the Prediction of Osteoporotic Fractures in Elderly People.* Osteoporosis International, 1999. **9**(6): p. 550-556.
303. Gregg, E.W., A.M. Kriska, L.M. Salamone, M.M. Roberts, S.J. Anderson, R.E. Ferrell, L.H. Kuller, and J.A. Cauley, *The Epidemiology of Quantitative Ultrasound: A Review of the Relationships with Bone Mass, Osteoporosis and Fracture Risk.* Osteoporosis International, 1997. **7**(2): p. 89-99.
304. Yi-Xian, Q., X. Yi, L. Wei, E. Mittra, C. Rubin, and B. Gruber, *Noninvasive Ultrasound Imaging for Bone Quality Assessment Using Scanning Confocal Acoustic Diagnosis, Muct, Dxa Measurements, and Mechanical.* Medical Biometrics. Proceedings 7th International Conference, ICMB 2008. (Lecture Notes in Computer Science vol. 4901), 2007.
305. Moayyeri, A., S. Kaptoge, N. Dalzell, R.N. Luben, N.J. Wareham, S. Bingham, J. Reeve, and K.T. Khaw, *The Effect of Including Quantitative Heel Ultrasound in Models for Estimation of 10-Year Absolute Risk of Fracture.* Bone, 2009. **45**(2): p. 180-184.
306. Bouxsein, M.L. and E. Seeman, *Quantifying the Material and Structural Determinants of Bone Strength.* Best Practice & Research Clinical Rheumatology, 2009. **23**(6): p. 741-753.
307. Melton, L.J., B.L. Riggs, T.M. Keaveny, S.J. Achenbach, P.F. Hoffmann, J.J. Camp, P.A. Rouleau, M.L. Bouxsein, S. Amin, E.J. Atkinson, R.A. Robb, and S. Khosla, *Structural Determinants of Vertebral Fracture Risk.* Journal of Bone and Mineral Research, 2007. **22**(12): p. 1885-1892.
308. Boskey, A.L., E. DiCarlo, E. Paschalis, P. West, and R. Mendelsohn, *Comparison of Mineral Quality and Quantity in Iliac Crest Biopsies from High- and Low-Turnover Osteoporosis: An Ft-Ir Microspectroscopic Investigation.* Osteoporosis International, 2005. **16**(12): p. 2031-2038.
309. Morris, M.D. and G.S. Mandair, *Raman Assessment of Bone Quality.* Clinical Orthopaedics and Related Research, 2011. **469**(8): p. 2160-2169.
310. Matousek, P. and N. Stone, *Emerging Concepts in Deep Raman Spectroscopy of Biological Tissue.* Analyst, 2009. **134**(6): p. 1058-1066.
311. Djokoto, C., G. Tomlinson, S. Waldman, M. Grynpas, and A.M. Cheung, *Relationship among Mrta, Dxa, and Qus.* Journal of Clinical Densitometry, 2004. **7**(4): p. 448-456.